Australian National University

Variation in human rib and femoral histology: A study of ancient and modern humans

Tahlia J Stewart

January 2026

A thesis submitted for the degree of Doctor of Philosophy of
The Australian National University

© Copyright by Tahlia J Stewart 2026
All Rights Reserved

Declaration

This thesis contains no material which has been accepted for the award of any other degree or diploma in any university. To the best of the author's knowledge, it contains no material previously published or written by another person, except where due reference is made in the text.

Tahlia Jade Stewart

January 2026

Acknowledgements

I am enormously grateful to my chair of panel Laura Wilson, primary supervisor Justyna Miszkiewicz, and panel advisers Eline Schotsmans, Patrick Mahoney and Robert Paine, for their continuous support and guidance. I would like to thank Eline and Patrick in particular for facilitating access to samples during a global pandemic and all of my panel for not losing faith in me when the pandemic, health issues and life kept getting in the way of my PhD completion. And thank you for reading through this momentous document to provide such valuable and thoughtful feedback. My dissertation was greatly improved thanks to your guidance and advice.

Justyna, thank you for sticking by me throughout the years, for helping me piece together a project when the world shut down and my project fell apart (multiple times). Your unwavering support and constant pep talks have kept me going when there have been so many times I've almost given up.

The School of Archaeology and Anthropology for supporting me through to my third iteration of this project, as well as through many health issues…and the extensions that came with that.

My colleagues at the Trauma and Orthopaedic Research Unit for patiently listening to my PhD (mis)adventures. I hope to officially use my qualifications to support TORU research soon.

To my friends for sticking with me and listening to my concerns about *all* of my studies over *many* years. Adam for the barrage of 'you should be at uni' in my late teens and early twenties. You believed in me when I thought no one did and I wouldn't have had the courage to apply to sit the mature-age entry exam in secret without your words echoing in my head. Gone, never forgotten, and forever grateful. Alannah for helping me with perspective. Your understanding, support and close friendship has gotten me through some pretty hard times, and I'll never forget it. Sophie for starting a Facebook conversation with me back in about 2013 and just never stopping. You've been there for me every part of my journey, sending flowers at research milestones – or just before them to help pick me up when I was spiralling. You've been by my side through all the major life changes since we met, and I wouldn't have made it through this one, or any of the others without you.

My godbrother Stuart who asked about my research every time we spoke and enjoyed talking about all things archaeology – particularly Ancient Egypt, an era he loved. I hope you can see this now I wish you were here for me to tell you all about it in person.

My in-laws who have always understood and supported Mitch and I when I needed to go into hermit mode. When Mitch has been looking after me, you've been looking after him and I appreciate you all immensely. Thank you for supporting us and understanding when I've had to bring my laptop with me everywhere. Thank you, Kim, for becoming my sister-in-law and also one of my closest friends. I'm so grateful to have had your support throughout my program.

My furbaby Finn for keeping me company while working on this research for literally his *entire life* and even spent a good portion of time as a new puppy running around my old office in the Banks Building – sorry maintenance team. You've earned an honorary dog-torate in my eyes.

My brothers who have always been there to listen or advise when things weren't going to plan. You have always understood when I've missed major milestones, being unable to visit Perth during particularly stressful times during my program and university career since moving to Canberra. Thank you for visiting us when I've been unable to fly and making yourselves available whenever I've been able to.

My parents for supporting my university career from the beginning, even though I was 22 when it started, and embracing me and my ambitions enough to let me go when I wanted to move to the opposite side of the country to pursue higher degree research. Thank you for encouraging me to keep going each time I needed it. Thank you for always being there for me through the ups and downs, and always having us to stay when we come to Perth. Thank you for always coming to watch me dress up like I'm at Hogwarts and walk across a stage. I *promise* this will be the last one.

My husband Mitch – who has never known me to *not* be working on my doctorate. I'm forever grateful that we found each other. Thank you for your unwavering support throughout the ups and downs and total collapses of my project. For picking up the slack when I was inundated with full-time work and PhD life, for never losing faith that I would finish this thing and being a sounding board for all of my findings and ramblings down academic rabbit holes. Thank you for keeping me (and Finn) fed and watered, and cared for during the times where PhD life took over everything else, and when my health has also taken priority. I love you and I couldn't have done this or *survived this* without you.

Finally, to my high school vice-principal, who told me I wasn't university material and should drop out in year 12. This one is for you.

This research was supported by an Australian Government Research Training Program (RTP) Scholarship.

Abstract

Remodelling is a process of bone renewal occurring throughout the human lifespan. Remodelling evidence is retained in bone microstructure (histology) in modern and ancient samples, providing a rich source of knowledge about human health and behaviour. However, we do not fully understand how age, biological sex, social status, and anatomical form of bones, influence human femoral and rib histology, particularly in Australia. To date, only one study examined Australian human femoral and rib histology, but none have compared Australian to medieval British samples to explore ancestral indicators of remodelling. This thesis aimed to investigate how different factors influence human rib and femoral histology, particularly in largely unexplored modern Australian samples compared to medieval British samples as a more widely studied ancestral population.

Four questions were identified: (1) does human rib and femoral bone histology vary with age, sex and social status in samples of English ancestry?; (2) do modern and medieval human bone histology comparisons indicate more sedentary modern lifestyle? (3); is there variation in histological variables between serial rib sections? (4); does cortical bone histology vary in the femur and rib with distinct bone metabolic activities? The methods in this thesis were bone histomorphometry and cross-sectional geometry, where secondary osteons, Haversian canals, porosity, and cortical bone were quantified and analysed using univariate and multivariate statistics.

The first thesis question found that secondary osteon densities were higher in older than middle aged adults in the rib, but not in the femur. Females had higher rib and femoral osteon and Haversian canal area than males. Modern ribs had higher secondary osteons densities than the medieval samples, except for the anterior femur, where this applied only to modern versus medieval low status. Rib porosity was higher in medieval low status samples, except in the anterior femur where it was higher in modern samples. Modern samples had lower rib cortical width than medieval samples. For thesis question two, a discriminant function analysis based on multivariate comparisons successfully separated medieval and modern rib and femoral bone, but there was no conclusive evidence that modern humans were more sedentary than medieval humans. Results from analyses addressing thesis question three found that there were correlations between serial pairs of rib cross-sections in most histological variables, except porosity and osteon and Haversian canal densities, suggesting that sampling ribs in different shaft areas may render different histological results depending on variables observed. For the final thesis question four it was discovered that femoral secondary osteons and Haversian canals were larger than in the rib, but they did not necessarily vary in shape,

though nuances in the shape variables used were evident. A reduced major axis regression determined secondary osteon and Haversian canal isometry in the rib but positive allometry in the femur, suggesting different constraints in secondary osteon formation.

This thesis concludes that bone histology, a product of remodelling, is in a complex relationship with age, sex, and social status (determining diet, health and access to resources) and that it changes depending on whether the femur or rib are investigated, and also on the rib sectioning location. It appears that rib and femur remodelling in modern Australia has remained similar to English medieval times. However, there is an allometric constraint on histology, which means that future rib and femur studies should account for bone size when examining histology. These results suggest that rib and femoral microstructure is influenced differently by different factors. This thesis is the first comprehensive study of bone histology applying multivariate and allometric analyses that includes modern Australian alongside medieval English samples.

List of Abbreviations

Table 0.1 List of Abbreviations.	
Acronym	**Definition**
%Ct.Ar	Percent Cortical Area
AAD	Age-At-Death
Abn	Abnormal
Adol	Adolescent (12 – 19 years old)
AFTER	The Australian Facility for Taphonomic Experimental Research
ANK	Ankyloses Protein
ANU	Australian National University
ARC	Australian Research Council
BMD	Bone Mineral Density
BMP	Bone Morphogenic Proteins
BMU	Basic Metabolic Unit
BSP	Bone Sialoproteins
CBFA1	Core Binding Factor Alpha-1
COPD	Chronic Obstructive Pulmonary Disease
CSA	Total Cross-Section Area
CSF-1	Colony Stimulating Factor-1
Ct.Ar	Cortical Area
Ct.ArA	Absolute Cortical Area
Ct.Po	Cortical Porosity
Ct.Wi	Mean Cortical Width
DF	Degrees of Freedom
DFA	Discriminant Function Analysis
DISH	Diffuse Idiopathic Skeletal Hyperostosis
DNA	Deoxyribonucleic Acid
DPX	Dibutylphthalate Polystyrene Xylene
ECM	Extracellular Matrix
Es.Ar	Endosteal Area
FGF	Fibroblast Growth Factor
Fg.OPD	Fragmentary Osteon Population Density
GAG	Glycosaminoglycan
H.Ar	Haversian canal Area
H.AsRa	Haversian canal Aspect Ratio
H.Circ	Haversian canal Circularity
H.Dm	Haversian canal Diameter
H.Pm	Haversian canal Perimeter
H.Rn	Haversian canal Roundness
H.Sd	Haversian canal Solidity
HREC	Human Research Ethics Committee
ICAM-1	Intercellular Adhesion Molecule 1
IGF-1	Insulin-like Growth Factor-1
IGF-2	Insulin-like Growth Factor-2
KS	Kolmogorov-Smirnov Test
LEH	Linear Enamel Hypoplasia
LiDAR	Light Detection And Ranging
LIEF	Linkage Infrastructure, Equipment and Facilities
MA	Middle Adult (35 – 49 years old)
M-CSF	Macrophage Colony-Stimulating Factor
MedHigh	Medieval High Socioeconomic Status Group
MedLow	Medieval Low Socioeconomic Status Group
MES	Minimum Effective Strain

MIA	Multiple Image Alignment
ModCon	Modern Contemporary Socioeconomic Status Group
Nor	Normal
N.Po	Number of Porosities
NPP1	Nucleotide Pyrophosphatase Phosphodiesterase-1
NSW	New South Wales
OA	Older Adults (50+ years old)
OHI	Oxford Histological Index
On.Ar	Osteon Area
On.AsRa	Osteon Aspect Ratio
On.Circ	Osteon Circularity
On.Dm	Osteon Diameter
On.Pm	Osteon Perimeter
On.Rn	Osteon Roundness
On.Sd	Osteon Solidity
OPD	Osteon Population Density
OPG	Osteoprotegrin
PMI	Post-Mortem Interval
Po.Ar	Mean Porosity Area
PTH	Parathyroid Hormone
RANK	Receptor Activator of Nuclear Factor Kappa-Beta
RANKL	Receptor Activator of Nuclear Factor Kappa-Beta Ligand
RMA	Reduced Major Axis Regression
RPM	Rotations Per Minute
ROI	Region of Interest
SASF	Surgical and Anatomical Science Facility
SES	Socio-Economic Status
SIBLINGs	Small Integrin-Binding Ligand N-Linked Glycoproteins
SLRPs	Small Leucine-Rich Proteoglycans
SW	Shapiro-Wilk Test
TGF-β1	Transforming Growth Factor-Beta 1
TGF-β2	Transforming Growth Factor-Beta 2
TGF-β3	Transforming Growth Factor-Beta 3
TNAP	Tissue-Nonspecific Alkaline Phosphatase
Tt.Po.Ar	Total Porosity Area
UK	United Kingdom
USA	United States of America
UTS	University of Technology, Sydney
VEGF	Vascular Endothelial Growth Factor
VIFM	Victorian Institute of Forensic Medicine
Wnt	Wingless-related Integration Site
YA	Young Adult (20 – 34 years old)

Table of Contents

Declaration ii
Acknowledgements iii
Abstract v
List of Abbreviations vii
Table of Contents ix
List of Tables xiv
List of Figures xvi
Chapter 1 Introduction 1
1.1 Study Context 1
1.1.1 Research Question 1 2
1.1.2 Research Question 2 3
1.1.3 Research Question 3 4
1.1.4 Research Question 4 5
1.2 Research Design 6
1.3 Research Significance 7
1.4 Thesis Structure 9
Chapter 2 Skeletal Biology 10
2.1 Gross Skeletal Anatomy 10
2.1.1 Skeletal Anatomy Regions 10
2.1.2 Planes of Reference 11
2.1.3 Directional Terms 11
2.2 Human Skeletal Tissue Types 12
2.3 Macrostructure of Bone 13
2.3.1 Periosteum 13
2.3.2 Bone Tissue Types 14
2.3.3 Endosteum 16
2.3.4 Marrow Cavities 17
2.3.5 Cartilage 17
2.4 Microstructure of Bone 17
2.4.1 Inorganic Components of the ECM 18
2.4.2 Organic Components of the ECM 21
2.4.3 The Cellular Matrix 26
2.5 Bone Remodelling 32

2.5.1 The BMU 32
2.6 Osteons 36
2.6.1 Primary Osteons 36
2.6.2 Secondary Osteons 37
2.6.3 Variations of the Secondary Osteon 39
2.7 Bone Growth and Development 41
2.7.1 Intramembranous Ossification 43
2.7.2 Endochondral Ossification 43
2.8 Intrinsic and Extrinsic Effects on Bone 45
2.8.1 Biomechanical Loading 46
2.8.2 Age 50
2.8.3 Biological Sex and Endocrine Homeostasis 52
2.8.4 Genetic Background and Ancestry 55
2.8.5 Disease 57
2.8.6 Intra-Skeletal Variability 62
Chapter 3 Literature Review 65
3.1 Histology, A History 65
3.1.1 Early Applications of Microscopy and Bone 65
3.1.2 Histological Applications in Bioarchaeology 67
3.2 Histology of the Rib and Femur 69
3.2.1 Archaeological Evidence 69
3.2.2 Anatomical Evidence 82
3.2.3 Animal Models 91
3.3 The Research Gap 97
3.4 Restatement of Research Questions and Hypotheses 102
Research Question 1 102
Research Question 2 103
Research Question 3 103
Research Question 4 104
Chapter 4 Materials 105
4.1 Sample Sources 105
4.1.1 Australian Facility for Taphonomic Experimental Research (AFTER) 105
4.1.2 St. Gregory's Priory and Cemetery Osteological Collection 119
Chapter 5 Methods 138
5.1 Sample Selection, Collection and Transfer to the ANU 138

5.1.1 St. Gregory's Priory and Cemetery Osteological Collection 138
5.1.2 AFTER Samples 140
5.2 Laboratory Based Methods 141
5.2.1 Embedding, decalcification and staining 141
5.2.2 Reducing embedded samples 144
5.2.3 Glass Slide Mounting 145
5.2.4 Further Reduction and Polishing 145
5.2.5 Cleaning, Dehydrating and Clearing 146
5.2.6 Cover-Slipping 147
5.3 Slide and Sample Storage 147
5.4 Data Collection 147
5.4.1 Imaging 148
5.4.2 Image Storage 151
5.5 Image Analysis 151
5.5.1 Rib Cross-Sectional Geometry Data 151
5.5.2 Secondary Osteon and Haversian Canal Data 154
5.6 Data Storage 155
5.7 Data Analysis 155
5.7.1 Data Cleaning and Formatting 155
5.7.2 Data Normality and Intra-Observer Error Testing 155
5.7.3 Data Analysis 157
5.7.4 Data Analysis by Research Question 157
5.7.5 Summary of Statistical Tests 173
5.8 Research Question Results 175
Chapter 6 Results 176
6.1 Data normality and intra-observer error test results 176
6.2 Descriptive Summary of all Observed Variables 180
6.3 Research Question 1 182
6.3.1 Descriptive Trends: Age-At-Death 182
6.3.2 Inferential Statistics: Age-At-Death 186
6.3.3 Hypotheses Results: Age-At-Death 190
6.3.4 Descriptive Trends: Sex 191
6.3.5 Inferential Statistics: Sex 194
6.3.6 Hypotheses Results: Sex 196
6.3.7 Descriptive Trends: Socioeconomic Group 197

6.3.8 Inferential Statistics: Socioeconomic Status Group 200
6.3.9 Hypotheses Results: Socioeconomic Status Group 204
6.4 Research Question 2 205
6.4.1 Descriptive Trends 205
6.4.2 Inferential Statistics 208
6.4.3 Multivariate Statistics 210
6.4.4 Hypotheses Results 214
6.5 Research Question 3 217
6.5.1 Descriptive Trends 217
6.5.2 Inferential Statistics 220
6.5.3 Hypothesis Results 221
6.6 Research Question 4 222
6.6.1 Descriptive Trends 222
6.6.2 Inferential Statistics 230
6.6.3 Multivariate Statistics 241
6.6.4 Hypotheses Results 248
6.7 Results Summary 251
6.7.1 Research Question 1 251
6.7.2 Research Question 2 251
6.7.3 Research Question 3 252
6.7.4 Research Question 4 252
Chapter 7 Discussion 254
7.1 Research Question 1 254
7.1.1 Age-At-Death and Bone Remodelling 254
7.1.2 Sex and Bone Remodelling 256
7.1.3 Socioeconomic Status and Bone Remodelling 258
7.1.4 Differences Between Rib and Femoral Bone Remodelling 261
7.2 Research Question 2 263
7.2.1 Contemporary and Medieval Bone Differences 263
7.2.2 Contemporary Sedentary Lifestyle 264
7.3 Research Question 3 266
7.3.1 Rib Cross-Sectional Intra-Element Variation 266
7.4 Research Question 4 268
7.4.1 Osteon and Haversian Canal Size in the Rib and Femur 269
7.4.2 Osteon and Haversian Canal Shape in the Rib and Femur 272

7.4.3 Rates of Osteonal and Haversian Canal Growth in the Rib and Femur 278
Chapter 8 Conclusion 283
8.1 Key Findings 283
8.1.1 Research Question 1 283
8.1.2 Research Question 2 285
8.1.3 Research Question 3 286
8.1.4 Research Question 4 286
8.2 Limitations 288
8.2.1 Sample Demographics 288
8.2.2 Methodological Limitations of Histology 288
8.2.3 Skeletal Element Selection 289
8.2.4 Taphonomy of Archaeological Samples 289
8.3 Future Directions 289
8.4 Research Significance 290
8.5 Research Achievements 293
Chapter 9 References 294

List of Tables

Table 3.1: Table 3.1 Histological studies of Archaeological Human Ribs and Femora. 70
Table 3.2: Table 3.2 Histological studies of Anatomical Human Ribs and Femora. 82
Table 3.3: Histological studies of Non-Human Ribs and Femora. 91
Table 4.1: Individuals sampled from the AFTER Donors. 117
Table 4.2: Individuals sampled from the St. Gregory's Priory and Cemetery Skeletal Collection. 134
Table 5.1: Cross-Sectional Geometry measurements observed. 153
Table 5.2: Secondary osteon and Haversian canal measurements observed. 154
Table 5.3: Hypothesis Testing Guidelines (Elliott and Woodward 2007). 157
Table 5.4: Log-transformation equations applied by variable. 164
Table 5.5: RMA analyses and sub-analyses conducted. 172
Table 6.1: Results from data normality tests. 176
Table 6.2: Intra-observer Error Testing: paired correlations and paired samples t-test results. 177
Table 6.3: Intra-observer Error Testing: Bland-Altman plot data. 178
Table 6.4: Sample summary. 180
Table 6.5: Descriptive statistics for all variables observed. 181
Table 6.6: Descriptive statistics for all variables observed in AAD analysis. 183
Table 6.7: Age-At-Death Correlations (Spearman's Rho). 186
Table 6.8: Age-At-Death Correlations (Spearman's Rho): Corrected by stature. 186
Table 6.9: Age-At-Death Categories (Kruskal-Wallis). 187
Table 6.10: Age-At-Death: Post-hoc pairwise comparisons. 188
Table 6.11: Age-At-Death Categories (Kruskal-Wallis): Corrected by stature. 189
Table 6.12: Age-At-Death: Corrected by Stature: Post-hoc Kruskal-Wallis pairwise. 190
Table 6.13: Descriptive statistics for all variables observed in Sex analysis. 192
Table 6.14: Sex differences (Mann-Whitney U). 194
Table 6.15: Sex differences (Mann-Whitney *U*): Corrected by stature. 195
Table 6.16: Descriptive statistics for all variables observed in SES analysis. 197
Table 6.17: Differences between SES Groups (Kruskal-Wallis). 200
Table 6.18: SES Groups: Post-hoc Kruskal-Wallis pairwise comparisons. 202
Table 6.19: Differences between SES Groups (Kruskal-Wallis): Corrected by stature. 203
Table 6.20: SES Groups: Corrected by Stature: Post-hoc Kruskal-Wallis pairwise comparisons. 204
Table 6.21: Descriptive statistics for all variables observed in research question 2. 206
Table 6.22: Medieval to Modern bone differences (Mann-Whitney U). 209
Table 6.23: Medieval to Modern bone differences (Mann-Whitney U): Corrected by stature. 210
Table 6.24: Medieval to Modern bone: Discriminant Function Analysis of the Rib. 211
Table 6.25: Medieval to Modern bone: Discriminant Function Analysis of the Anterior Femur. 212
Table 6.26: Medieval to Modern bone: Discriminant Function Analysis of the Rib: Corrected by Stature. 213
Table 6.27: Medieval to Modern bone: Discriminant Function Analysis of the Anterior Femur: Corrected by Stature. 214

Table 6.28: Descriptive statistics for all variables observed in research question 3. 217
Table 6.29: Serial rib differences (Spearman's Rho). 220
Table 6.30: Serial rib differences: Wilcoxon signed rank test results. 221
Table 6.31: Descriptive statistics for all variables observed in research question 4. 223
Table 6.32: Descriptive statistics for independent sample sub-group observed in research question 4. 227
Table 6.33: Descriptive statistics for related sample sub-group observed in research question 4. 229
Table 6.34: Mann-Whitney U results: Independent sample sub-group. 231
Table 6.35: Friedman's results: Related sample sub-group: Triple Datapoints. 232
Table 6.36: Wilcoxon Signed Rank Test results: Related sample sub-group: Rib/Anterior Femur Pairs. 233
Table 6.37: Wilcoxon Signed Rank Test results: Related sample sub-group: Rib/Posterior Femur Pairs. 234
Table 6.38: Wilcoxon Signed Rank Test results: Related sample sub-group: Anterior Femur/Posterior Femur Pairs. 235
Table 6.39: Mann-Whitney U results: Independent sample sub-group: Corrected by Stature. 236
Table 6.40: Friedman's results: Related sample sub-group: Triple Datapoints: Corrected by Stature. 237
Table 6.41: Wilcoxon Signed Rank Test results: Related sample sub-group: Rib/Anterior Femur Pairs: Corrected by stature. 238
Table 6.42: Wilcoxon Signed Rank Test results: Related sample sub-group: Rib/Posterior Femur Pairs: Corrected by stature. 239
Table 6.43: Wilcoxon Signed Rank Test results: Related sample sub-group: Anterior Femur/Posterior Femur Pairs: Corrected by stature. 240
Table 6.44: Reduced Major Axis Regression Results for the Rib. 243
Table 6.45: Reduced Major Axis Regression Results for the Anterior Femur. 246
Table 6.46: Reduced Major Axis Regression Results for the Posterior Femur. 248

List of Figures

Figure 2.1: The anatomical position with anatomical directional terms labelled. 11
Figure 2.2: Cross section of a proximal femur (femoral head). 13
Figure 2.3: Woven versus lamellar bone. 16
Figure 2.4: The crystalline structure of hydroxyapatite. 18
Figure 2.5: Diagrammatic structure of collagen amino acids. 21
Figure 2.6: Diagrammatic structure of congregated tropocollagen. 22
Figure 2.7: Developmental cell lines in osteoblastogenesis and osteoclastogenesis. 26
Figure 2.8: Bone resorbing osteoclast. 27
Figure 2.9: Cellular pathway for a mature osteoblast. 28
Figure 2.10: Cell line development from a mesenchymal stem cell (1) to mature osteoblast (4). 29
Figure 2.11: Osteocyte structure. 30
Figure 2.12: The Bone Multicellular Unit cutting cone shape. 33
Figure 2.13: Differences in the creation and appearance of primary and secondary osteons. 37
Figure 2.14: Illustration of a secondary osteon in longitudinal cross-section. 38
Figure 2.15: Illustration of a secondary osteon in transverse cross-section. 39
Figure 2.16: Bone mass trajectory throughout human lifespan by sex. 51
Figure 3.1: Map of key studies of human rib and femur histology in archaeological and modern anatomical remains. 69
Figure 4.1: The location of the AFTER facility, northwest of Sydney, at the base of the Blue Mountains. 106
Figure 4.2: The location of St Gregory's Priory and cemetery in Canterbury, United Kingdom. 119
Figure 4.3: St Gregory's Church and surrounds, approximately 1084 AD. 120
Figure 4.4: St Gregory's Church, prior to the 1145 fire. 121
Figure 4.5: Archbishop Theobold's St Gregory's Priory, c. 1181. 122
Figure 4.6: St Gregory's Priory following renovations and additions, ~1400 AD. 123
Figure 4.7: The burials excavated from within the Priory grounds, labelled by SK#. 126
Figure 5.1: Laboratory methods undertaken. 144
Figure 5.2: Left: Femur slide ES_HB04_1602. Right: Femur sample ES_HB09_1618. 149
Figure 5.3: Human rib cross-section. Light microscopy, 10x magnification. 150
Figure 5.4: Example of rib cross-sectional geometry area definitions. 152
Figure 5.5: Secondary osteon with external cement line indicated in red and the Haversian canal perimeter in green. 154
Figure 5.6: RMA investigation of the allometric relationship between the chela (oversized claw) and body size of the male fiddler crab. 171
Figure 6.1: Bland-Altman Plots for intra-observer error. 180
Figure 6.2: Scatterplots of key age-at-death variables. 184
Figure 6.3: Boxplots of key age-at-death variables. 185
Figure 6.4: Boxplots of key biological sex variables. 194
Figure 6.5: Boxplots of key socioeconomic status variables. 200
Figure 6.6: Boxplots of key era variables. 208
Figure 6.7: Scatterplots of standard rib histology variables. 219

Figure 6.8: Boxplots of key osteon and Haversian canal variables. 226
Figure 6.9: Reduced major axis regression plots of the rib data. 243
Figure 6.10: Reduced major axis regression plots of the anterior femur data. 245
Figure 6.11: Reduced major axis regression plots of the posterior femur data. 247

Chapter 1 Introduction

This chapter introduces the research topic, outlining project context, research objectives, questions and hypotheses to form a foundation for the background and literature review chapters that follow. It then outlines the thesis structure, providing a brief description of all main chapters and broader thesis direction.

1.1 Study Context

In bioarchaeology and skeletal biology, we are interested in reconstructing human health, behaviour and condition based upon evidence rendered from human remains (Buikstra et al. 2022; Goodman and Martin 2002). Rooted in human osteology, the anatomical study of human skeletal remains (Larsen 2002), traditional bioarchaeological methods have included macroscopic analysis of bones and teeth, examining lesions as disease markers (Goodman and Martin 2002; Keenleyside 1998; Lambert 1993; Ubelaker and Pap 1998; van Gerven et al. 1995), skeletal muscle attachment site size as (entheseal) markers of physical exertion, strength and athleticism (Hawkey and Merbs 1995; Mariotti et al. 2007; Robb 1998), tooth wear for markers of subsistence strategy (Kaifu et al. 2003; Lovejoy 1985), bone morphology and morphometry for estimations of biological sex (Konigsberg and Hens 1998; Phenice 1969) and age-at-death (Lovejoy et al. 1985; Mulhern and Jones 2005; Wescott 2015). Some bioarchaeologists with backgrounds in skeletal biology have turned to examining human bone microscopically (Burr et al. 1990; Cho and Stout 2011; Drew et al. 2021; Ericksen 1980; Lazenby and Pfeiffer 1993; Martin and Armelagos 1979; 1985; Miszkiewicz and Mahoney 2016; Miszkiewicz et al. 2020; 2021; 2022a; b; c; Mulhern 2000; Mulhern and van Gerven 1997; Pfeiffer 1998; Pfeiffer et al. 2006; Richman et al. 1979; Robling and Stout 2003; Snoddy et al. 2022; Stout and Lueck 1995; Thompson and Gunness-Hey 1981; Thompson et al. 1981; Walker et al. 2023a; b), which is known to differ from what is macroscopically visible (Rabey et al. 2015) and can provide insight into bone biological processes, such as bone loss (Agnew and Stout 2012) and metabolic changes (McCarthy 2016), that cannot be observed in detail without microscopic intervention. Additionally, a recent call was made by many high profile bioarchaeologists to steer away from purely traditional methods, listed above, and moving towards multi-disciplinary approaches to expand the use of scientific techniques from other disciplines (Buikstra et al. 2022).

However, while this shift towards the application of microscopy in bioarchaeology and skeletal biology has occurred in Europe and America increasingly since the 1970s (Absolonova et al. 2013; Agnew and Stout 2012; Baccino et al. 1999; Burr et al. 1990; Cho and Stout 2011; Cole

et al. 2022; Crowder and Rosella 2007; Crowder et al. 2022; De Gruchy et al. 2024; Dominguez and Agnew 2016; Drew et al. 2021; Eleazer and Jankauskas 2016; Ericksen 1980; Fahy et al. 2017; García-Donas et al. 2016; Karydi et al. 2022; Lazenby and Pfeiffer 1993; Lagacé et al. 2019; Maat et al. 2006; Mavroudas et al. 2022; Miszkiewicz and Mahoney 2016; Paine and Brenton 2006; Pfeiffer 1998; Pfeiffer et al. 2006; 2019; Reid 1986; Richman et al. 1979; Robling and Stout 2003; Stewart et al. 2015; Stout and Lueck 1995; Thompson and Gunness-Hey 1981; Thompson et al. 1981), relatively little is known about human bone microstructure in an Australian context where few studies have been conducted to observe Australian human bone microstructure (Maggio 2022; Maggio and Franklin 2019; 2021; Pedersen et al. 2024).

1.1.1 Research Question 1

Does human rib and femur histology vary with age-at-death, sex and systemic health and physical activity (as inferred by socioeconomic status) in samples of English ancestry?

1.1.1.1 Age-At-Death Hypotheses

$H0_a$: There is no monotonic relationship between absolute (chronological) age-at-death (AAD) and either observed variable; osteon population density (OPD), fragmentary (Fg) OPD, cortical porosity (Ct.Po), or cortical width (Ct.Wi).

$H0_b$: Each of the observed variables (OPD, Fg.OPD, Ct.Po or Ct.Wi) have a similar distribution across AAD categories.

$H0_c$: Each of the observed variables (OPD, Fg.OPD, Ct.Po or Ct.Wi) have a similar distribution across the rib and the femur.

1.1.1.2 Biological Sex Hypotheses

$H0_a$: Each of the observed variables, OPD, Fg.OPD, osteon area (On.Ar), Haversian canal area (H.Ar), Ct.Po and Ct.Wi have a similar distribution in male and female groups.

$H0_b$: Each of the observed variables, OPD, Fg.OPD, On.Ar, H.Ar and Ct.Po have similar distributions between the rib and femur.

1.1.1.3 Socioeconomic Status Hypotheses

$H0_a$: Each of the observed variables, OPD, osteon circularity (On.Circ), porosity area (Po.Ar), Ct.Po, Ct.Wi and % cortical area (%Ct.Ar) have a similar distribution across the three

socioeconomic status (SES) groups; medieval lower class, medieval upper class and contemporary.

$H0_b$: Each of the observed variables, OPD, On.Circ, Po.Ar and Ct.Po have similar distributions between the rib and femur.

The rib and femur have often been selected for observation in histological studies in contemporary anatomical (rib only: Absolonova et al. 2013; Agnew and Stout 2012; Crowder and Rosella 2007; Crowder et al. 2022; Dominguez and Agnew 2016; García-Donas et al. 2016; Kim et al. 2007; Pfeiffer et al. 2016; femur only: Lagacé et al. 2019; Maat et al. 2006; Maggio and Franklin 2021; both rib and femur: Baccino et al. 1999; Cole et al. 2022; Jowsey 1966; Mavroudas et al. 2022; Pedersen et al. 2024; Reid 1986; Stewart et al. 2015) and archaeological contexts (rib only: Mulhern 2000; Paine and Brenton 2006; Pfeiffer et al. 2019; Stout and Lueck 1995; femur only: De Gruchy et al. 2024; Burr et al. 1990; Ericksen 1980; Lazenby and Pfeiffer 1993; Martin and Armelagos 1979; Miszkiewicz and Mahoney 2016; Richman et al. 1979; Thompson and Gunness-Hey 1981; Thompson et al. 1981; both rib and femur: Cho and Stout 2011; Eleazer and Jankauskas 2016; Fahy et al. 2017; Karydi et al. 2022; Miszkiewicz et al. 2022b; Pfeiffer 1998; Pfeiffer et al. 2006; Robling and Stout 2003). Reasons for the selection of the rib and femur are due to the different functional adaptations of the femur as a weight-bearing and rib as a non-weight-bearing bone, with the underlying premise that their metabolisms differ due to these adaptations (Agnew and Stout 2012; Crowder and Rosella 2007; Dominguez and Agnew 2016; Karlson 1998; Paine and Brenton 2006; Seeman et al. 1992; 2000; Stewart et al. 2021; Tommerup et al. 1993). However, there is still much we do not know about how lifestyle factors such as physical activity, systemic health, socioeconomic status, advancing age and sex can affect rib and femur microstructure, and how these effects may present differently between the two bones.

1.1.2 Research Question 2

Is there a trend of bone quality “deteriorating” in contemporary individuals to reflect generally more sedentary lifestyles than their medieval ancestral population?

$H0_a$: Each of the observed variables, OPD, On.Circ, On.Ar, %Ct.Ar, Po.Ar and Ct.Po have a similar distribution between medieval and modern era individuals.

$H0_b$: Medieval and modern ribs and anterior femora cannot be separated using discriminant function analysis (DFA), based on the variables OPD, On.Circ, On.Ar, Po.Ar and Ct.Po.

$H0_c$: There is no evidence of a more sedentary lifestyle influencing modern individuals as compared to medieval individuals in either observed variable; OPD, On.Circ, On.Ar, %Ct.Ar, Po.Ar and Ct.Po.

There have been no studies investigating differences in bone histology between an archaeological and modern population, using samples that share the same ancestry. As contemporary European Australians are mostly descendants of English migrants (Australian Bureau of Statistics 2021), here, for the first time, bone histology from contemporary Australians, of European descent, and their ancestral medieval British individuals can be observed and compared.

Contemporary lifestyles, globally (Ding et al. 2016) and in Australia (Ding et al. 2015; Owen and Bauman 1992; Tremblay et al. 2010) are considered to be more sedentary (Dyer 2000; Judd and Roberts 1999; Zvi 1981), with easier access to food and sufficient nutrition (Hull 1989; Roberts and Manchester 2005) and healthcare (Clegg and Reed 1994; Harvey 2002; Theilmann 1987) than in medieval Britain, though some nutritional deficiencies are present in the contemporary Australian population, such as calcium and vitamin D (Dunlop et al. 2023; Shlisky et al. 2022; see also Chapter 4: Materials). In addition to comparing medieval and contemporary bone histology broadly, evidence of the modern sedentary lifestyle is sought, observing selective histological variables that would demonstrate increased sedentism in an individual, based on existing literature and skeletal biology. Many studies have reported on patterns of physical activity and behaviour in populations, in Europe (Mariotti et al. 2007; Miszkiewicz and Mahoney 2016; Pfeiffer 1998; Pfeiffer et al. 2006) and America (Burr et al. 1990; Ericksen 1980; Hawkey and Merbs 1995; Robb 1998), but these have been in past populations rather than looking at how contemporary lifestyles have impacted upon human bone metabolism as compared to medieval ancestors. While studies in bioarchaeology have identified variation in individuals consistent with limb disuse due to medical conditions, these are necessarily restricted to case studies of individuals (Lazenby and Pfeiffer 1993; Miszkiewicz et al. 2020; Schlecht et al. 2012; Snoddy et al. 2022; Walker et al. 2023b) and no studies have been identified in the literature where evidence of population sedentism has been identified using human bone histology.

1.1.3 Research Question 3

Is there variation in standardised histological variables between serial cross-sections from the human rib midshaft?

$H0_a$: There is no monotonic relationship in either observed variable; Ct.Ar, Ct.Wi, absolute cortical area (Ct.ArA), Po.Ar, On.Ar, H.Ar, Ct.Po, OPD, Fg.OPD and On.Circ between paired serial histological sections of the rib, approximately 1cm apart in the rib shaft.

$H0_b$: Each of the observed variables; Ct.Ar, Ct.Wi, Ct.ArA, Po.Ar, On.Ar, H.Ar, Ct.Po, OPD, Fg.OPD and On.Circ have a similar distribution between paired serial histological sections of the rib, approximately 1cm apart in the rib shaft.

Skeletal biology principles dictate that, on a microstructural scale, bone adapts locally to biomechanical loading, or to pressures from weight-bearing behaviours, rather than resulting in even distribution of remodelled tissue throughout an entire bone (Biewener and Bertram 1993; Lanyon et al. 1982; Stout et al. 2019; see also Chapter 2: Skeletal Biology). It is based upon this premise that we know that intra-skeletal variation, or variation within the same bone, exists. However, this has not been investigated within an Australian context and was restricted to just two variables common in estimations of age-at-death to assess the implications of sampling location in age-at-death estimation research (Dominguez et al. 2020). While understanding intra-element variation is incredibly important to inform sampling methods for estimating age-at-death using histology, it holds biological importance as well, to better understand how microstructures within bone, and the overall shape of the bone itself, ebb and flow throughout the diaphysis, or midshaft and so analysis of more variables would be beneficial. In addition to few examples of intra-element variability in the literature, Dominguez et al. (2020) observed three cross-sections taken at the anterior, midshaft and posterior regions of the rib. Here, common bone histological variables of microstructures and the key cross-sectional geometry variables of overall bone shape are compared within serial rib cross-sections, sampled approximately 1 cm apart within the midshaft to understand how these variables change between even closely sampled locations within the same bone.

1.1.4 Research Question 4

Does cortical bone histology vary between bones of different levels of metabolic activity, such as the femur and the rib?

$H0_a$: Each of the observed osteon and Haversian canal size variables, On.Ar, H.Ar, osteon diameter (On.Dm), Haversian canal diameter (H.Dm), osteon perimeter (On.Pm) and Haversian canal perimeter (H.Pm), have a similar distribution across the rib and the femur.

$H0_b$: There is no difference in the osteon and Haversian canal shape variables, On.Circ, Haversian canal circularity (H.Circ), osteon roundness (On.Rd), Haversian canal roundness (H.Rd), osteon aspect ratio (On.AsRa), Haversian canal aspect ratio (H.AsRa), osteon solidity (On.Sd) and Haversian canal solidity (H.Sd) between the rib and the femur.

$H0_c$: There is no difference in the osteon and Haversian canal growth rates, (1) between osteons and Haversian canals, and (2) between the rib and the femur.

Finally, differences in cortical bone metabolism between the rib and femur are explored, to understand bone microstructure shape and size differences within these two differently adapted bones due to their functional differences (Agnew and Stout 2012; Crowder and Rosella 2007; Dominguez and Agnew 2016; Karlson 1998; Paine and Brenton 2006; Seeman et al. 1992; 2000; Stewart et al. 2021; Tommerup et al. 1993). Previous studies have identified intra skeletal variation, or differences between bone microstructure variables measured between different bones from within the same individual (Fahy et al. 2017; Stewart et al. 2021). The most common size variables measured within bone histology are measured to compare between these two metabolically different bones. Additionally, four different ways of measuring shape (Zdilla et al. 2016) are used to investigate patterns of bone microstructure geometric properties between the rib and femur, two of which have not been employed in bone histology until now, to provide novel and nuanced ways of observing and interpreting shape data in bone histology. Finally, a novel method is tested to explore bone metabolic differences between the rib and femur, by calculating bone microstructure growth and scaling relationships through allometric regressions (Shingleton 2010). This method has been employed elsewhere in bone histology to look at the scaling effect of cortical bone size on bone microstructures (Miszkiewicz and Mahoney 2019). Additionally, it has been used to measure Haversian perimeter against osteon area in human and non-human ribs and limb bones (Skedros et al. 2013a). However, it has not been used to look at the differences in scaling relationships of area between osteons and their paired Haversian canals to look at the scaling geometric relationship of these two related structures, how that differs between two metabolically distinct bones, and how donor demographic factors may impact the geometric relationship.

1.2 Research Design

This project compares human rib and femur shaft cross-sections from two human osteological samples. One sample is of a forensic nature, comprised of contemporary Australian donors, whose bodies were donated to The Australian Facility for Taphonomic Experimental Research (AFTER). This sample is unique as it is well documented having known age-at-death, sex, and

select medical history and cause of death contextual information. Samples collected from these 18 donors include two serial rib mid-shaft cross-sections of the third rib, as well as 1x1 cm^2 samples from the upper third margin of the anterior femur. The second sample is archaeological, comprised of individuals excavated from a late medieval site (11^{th} – 16^{th} century AD) located in Canterbury, United Kingdom. This sample comes with estimated age-at-death and sex data, as well as socio-economic status inferred from burial arrangement and positioning within a churchyard of St Gregory's Priory in Canterbury, UK. Samples collected from these 63 individuals include two serial rib mid-shaft cross-sections from a middle rib (3^{rd} – 6^{th}), and 1x1 cm^2 samples from the anterior and posterior midshaft of the femur, depending on preservation and availability. The total sample set had 81 individuals, with 2 serial rib cross-sections from 48 individuals, paired rib and femur samples from 61 individuals, and paired anterior and posterior femur samples from 9 individuals, for a grand total of 200 histological slides.

Samples were embedded in epoxy resin using disciplinary standards for undecalcified hard tissues (An and Martin 2003; Ascenzi and Fabry 1959; Bancroft and Gamble 2002; Beauchesne and Saunders 2006; Frost 1958; Grupe and Garland 1993; Horobin 2002; Maat et al. 2001; Maggio et al. 2019; Paine 2007; Sanderson 1994; Von Hagens 1979). Slides were imaged using an Olympus BX53 Semi-Motorised Fluorescence Microscope with an attached DP74 inverted camera and cellSens® standard life science imaging software. Slides were imaged at 10x magnification, which is standard in bone histology to assess the necessary variables observed in this research (Crowder and Stout 2011). Image analysis and data collection was conducted using Fiji ImageJ (Schindelin et al. 2012). Secondary osteons and their Haversian canals were measured for size (Dempster et al. 2013; Doube et al. 2010) and shape (Doube et al. 2010; Zdilla et al. 2016), and cross-sectional geometry and porosity (Agnew and Stout 2012) data measured the proportion of cortical bone. Data were then analysed according to research questions outlined below.

1.3 Research Significance

The findings reported in this thesis will make significant contributions to the disciplines of bioarchaeology, forensic and biological anthropology, and skeletal biology, especially to Australian audiences. The contributions advance our current knowledge of bone remodelling and metabolism with age-at-death, biological sex and socioeconomic status, which is historically associated with restrictions in dietary quality and nutrition access (Bhote 2004; Dyer 2000; Rogers and Waldron 2001), levels of physical activity (Jordan 2001; Zvi 1981) and general health and wellbeing (Covey 2001; Manchester and Roberts 1989; see also

Miszkiewicz and Mahoney 2016). Specifically, this research will improve the understanding of how the rib and the femur respond to these factors differently, due to their differing functional adaptations (Agnew and Stout 2012; Crowder and Rosella 2007; Dominguez and Agnew 2016; Karlson 1998; Paine and Brenton 2006; Seeman et al. 1992; 2000; Stewart et al. 2021; Tommerup et al. 1993), and how these factors manifest in their bone microstructure (Baccino et al. 1999; Cho and Stout 2011; Cole et al. 2022; Eleazer and Jankauskas 2016; Fahy et al. 2017; Jowsey 1966; Karydi et al. 2022; Mavroudas et al. 2022; Miszkiewicz et al. 2022b; Pedersen et al. 2024; Pfeiffer 1998; Pfeiffer et al. 2006; Reid 1986; Robling and Stout 2003; Stewart et al. 2015). Additionally, typifying the key differences in bone histology variables between modern and medieval human bone can both inform methodological practice of categorising bone based on temporal age of a sample, as well as demonstrate the vast differences between these two populations of the same ancestry. Furthermore, intra-element variation can inform sampling methods as well as improve our understanding of bone micro anatomy. In addition, novel methods of measuring osteonal and Haversian canal rates of growth can observe and quantify bone metabolic processes in a new way (Shingleton 2010), while morphometric measures of these microstructures can suggest new ways of measuring shape in bone histology (Doube et al. 2010; Zdilla et al. 2016).

These findings have broad implications across bioarchaeology, forensic and biological anthropology, and skeletal biology, offering new insights into how bone microstructure and morphology respond to demographic and functionally adaptive factors. Bioarchaeologists can refine sampling strategies and explore population differences through histological variables (Buikstra et al. 2022; Larsen 2002; Roberts and Gowland 2018), while forensic and biological anthropologists may improve age-at-death and sex estimations, as well as fragment identification, by incorporating observed microstructural and geometric variation (Biehler-Gomez et al. 2024; Lemos et al. 2024; Pilli et al. 2025; Spradley 2016). At the same time, skeletal biology benefits from the improved understanding of localised microstructural adaptation within skeletal biology (Biewener and Bertram 1993; Lanyon et al. 1982; Stout et al. 2019), and differences in osteonal and Haversian canal morphometrics between the rib and femur provide insight into patterns of bone metabolism in two differently metabolically active bones with differing functional adaptations (Agnew and Stout 2012; Crowder and Rosella 2007; Dominguez and Agnew 2016; Karlson 1998; Paine and Brenton 2006; Seeman et al. 1992; 2000; Stewart et al. 2021; Tommerup et al. 1993). The introduction of novel shape measures beyond circularity (e.g., roundness, aspect ratio, solidity) (Doube et al. 2010; Zdilla et al. 2016) further enhances the capacity to interpret bone behaviour and activity patterns (Keenan et al.

2017; Skedros 2024), while the novel recognition of scaling relationships between osteons and Haversian canals provides a new perspective on bone metabolism and growth dynamics.

1.4 Thesis Structure

This thesis contains nine main chapters, with two additional chapters for bibliographic references referred to intext, and appendices of supplemental information and images. The research context, key research questions, and hypotheses are outlined in **Chapter One: Introduction**. **Chapter Two: Skeletal Biology** provides the background explanation of what is meant by bone physiology and microstructure and describe the natural processes and key external influences on human skeletal biology. **Chapter Three: Literature Review** narrows the research focus broadly described in the previous chapter, to focus on the key literature that has informed this research, and synthesises known literature from the archaeological, anatomical and experimental non-human evidence. The populations from which the samples observed in this project are derived, are outlined and described in **Chapter Four: Materials**, to provide further contextual information for the sample sets and to understand what population-specific factors might influence or explain results. **Chapter Five: Methods** outlines the methodological techniques employed and sequential steps that were taken to answer the research questions, from sample acquisition and preparation, through to data analysis. **Chapter Six: Results** provides answers to the above research questions, detailing results of each statistical analysis performed, proving or disproving the hypotheses made prior to analysis. Key results will be thoroughly disseminated, discussed and explored in **Chapter Seven: Discussion**, to provide explanations and interpretations of all results, giving meaning and context to this dissertation. Key research outcomes and inferences will be summarised in **Chapter Eight: Conclusion**.

Chapter 2 Skeletal Biology

This chapter introduces human skeletal biology. Properties of basic human skeletal anatomy, comprised of the four categories of skeletal tissues are defined and described briefly before focusing on bone biology, which is the premise upon which this dissertation is formed. Bone macrostructural and microstructural components, appearance and variation are discussed. The process of bone growth and development, as well as similar processes of bone maintenance and repair are described. Factors regulating bone growth, health, repair and maintenance are outlined. Finally, intra-skeletal differences in bone metabolism are introduced, comparing differences between and within skeletal elements so that the underpinnings of this dissertation and its associated research can be understood and situated within the literature.

2.1 Gross Skeletal Anatomy

The average adult human skeleton is comprised of 206 bone elements, but this number reduces from approximately 350 following the fusion of some skeletal elements during juvenile growth and development (Clarke 2008). The study of the human skeleton uses standard terminology for clarity and consistency in recording and reporting of anatomical features and characteristics (e.g. Dempster et al. 2013; Parfitt et al. 1987). As such, these terms must remain consistent to ensure unambiguous communication across the discipline. Of interest to this thesis are skeletal anatomical regions, planes of references used when describing the location of a bone or area of interest, and directional and motional terms.

2.1.1 Skeletal Anatomy Regions

Analysis of the human skeleton needs to be proceeded by arranging the available skeletal elements into a standard anatomical position (Figure 2.1). Skeletal elements need to be laid out as to reflect the individual standing with their feet flat, but pointing forward, arms to their sides with their palms forward and thumbs pointing away from their body and their head straight, looking forward. In this position, no long bones are crossed or obscured from view, allowing left and right siding to be undertaken.

‘Cranial’ anatomy refers to that of the skull, whilst the ‘postcranial’ refers to the remainder of the skeleton. The skeleton is also classified as ‘axial’ and ‘appendicular’. The axial skeleton refers to the bones of the human torso, including vertebrae, sacrum, ribs and sternum, while the appendicular refers to the limbs, including the shoulder and pelvic girdles (Bass et al. 2002; White and Folkens 2005).

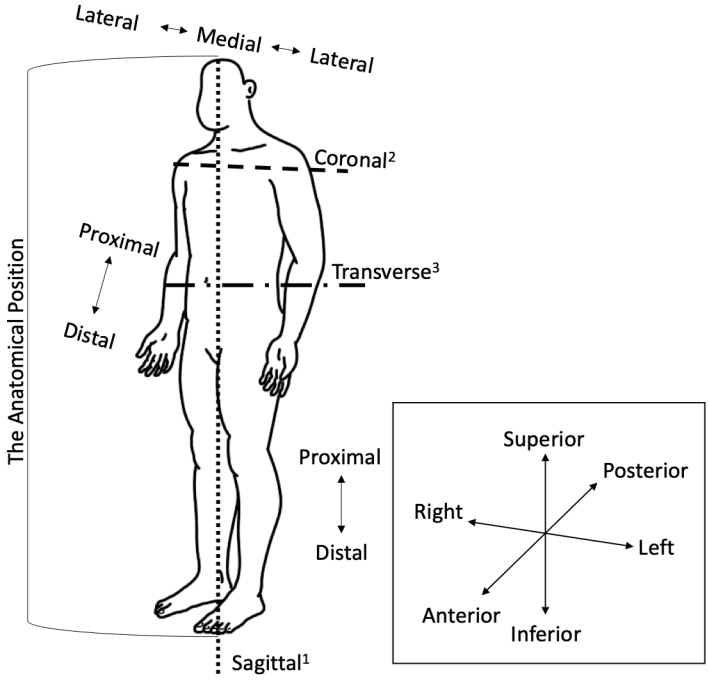

Figure 2.1: The anatomical position with anatomical directional terms labelled.

1) A sagittal section divides the body into a left and right side. Further a mid-sagittal section divides the body into halves in this way. 2) A coronal section divides the body into front and back portions. 3) A transverse section divides the body into top and bottom portions. Adapted from White and Folkens (2005:70).

2.1.2 Planes of Reference

Planes of reference divide the human body into portions to aid in the description of interior structures (Figure 2.1) The sagittal plane, also called the midsagittal plane, runs along the body's midline, dividing the individual into symmetrical left and right portions. Planes that run parallel to the sagittal plane are called parasagittal planes. Coronal, or frontal, planes are at a right angle to sagittal planes, dividing the body into anterior and posterior sections. Transverse, or horizontal, planes separate the body into upper and lower sections and can pass through the body at any height.

2.1.3 Directional Terms

Humans are bipedal animals. Directional terms are specific to the human body as they are placed in an upright standing position. Directionality can be stated in terms of body region or specific skeletal elements (Figure 2.1). If a structure is described as anterior to another, it means it lays towards the front of the individual, whilst if it is posterior, it lays towards the back.

If a structure is medial to another, it means it lays towards the midline of the body, whilst if it is lateral, it lays further away from the midline. The terms proximal and distal are usually used in reference to the limb bones. Proximal means closer to the axial skeleton while distal means further away from the axial skeleton. The terms external and internal refer to structures that are on the outer or inner of another structure. For example, the cranial vault is external to the brain. However, in this instance, these terms differ from the terms endocranial and ectocranial, which refer specifically to the inner and outer surface of the cranial vault, respectively. The terms superficial, deep and subcutaneous are usually used in reference to softer structures. Superficial refers to a structure that is closer to the surface. Deep is the opposite of superficial, referring to a structure further from the surface. Subcutaneous is specific to skin, meaning immediately below the skin, but some skeletal elements can be described in this way, such as the anteromedial tibial surface, just inferior to the knee. Palmar refers to the inner palm surface of the hand, including the fingerprint region of the fingertips. Plantar is the equivalent term for the foot, referring to the sole of the foot, or the surface that rests on the ground while standing. The term dorsal can be used for both the hands and feet, referring to the backs of the hands, which also stretches to the fingernail region of the fingertips and toenails of the toes.

2.2 Human Skeletal Tissue Types

There are four categories of mineralized tissues in vertebrates: dentine, enamel, bone and cartilage. Despite being generally considered dental tissues, dentine and enamel, like bone, have evolutionary origins as components of the exoskeleton in primitive vertebrates (Hall 2003; 2005; Wagner and Aspenberg 2011). In fact, cartilage is the only skeletal tissue that has evolutionary origins in the endoskeleton (Hall 2003; 2005; Wagner and Aspenberg 2011). These evolutionary histories of skeletal tissues extend approximately 750 million years into our past (Hall 2003; 2005). Each skeletal tissue type has its own distinctive evolutionary history, components, characteristics and features which perform different functions in human skeletal anatomy and biology. Here, bone is covered in detail, and cartilage covered in section 2.2.6. Dentine and enamel are not covered in this dissertation as no teeth were observed as part of this research.

Bone is aerobic, meaning that it consumes a high level of oxygen and is specific to vertebrates (Hall 2005). Bone is a crucial part of the musculoskeletal system, providing protection and support for soft tissue elements, such as muscles, ligaments and tendons, due to its mineralised structure (Hall 2005; Ross and Pawlina 2011). The elements of the bony skeleton also act as levers for these softer tissues to produce movement (Ross and Pawlina 2011; Seeman 2008). Additionally, bones perform a crucial role in human biology, as blood cell

production, fat storage centres, as reservoirs for important nutrients, such as calcium, and for haematopoiesis in the marrow cavities (Clarke 2008; Taichman 2005). Calcium and phosphate levels can also be regulated and maintained by the bone matrix as required (Datta et al. 2008; Hall 2005; Ross and Pawlina 2011).

2.3 Macrostructure of Bone

Here, the macroscopic structure of bone is described; beginning with the outer topography of bone, including the periosteum, which covers the outer surface of bone. Next, bone cavities are described, including the endosteum, which lines the inner surface of bone, and marrow cavities. The final part of this section introduces the two main types of bone tissue: trabecular and cortical bone. A schematic cross-section of a femoral head is in Figure 2.2 to demonstrate the key macroscopic components of human bone, visible in a cross-section.

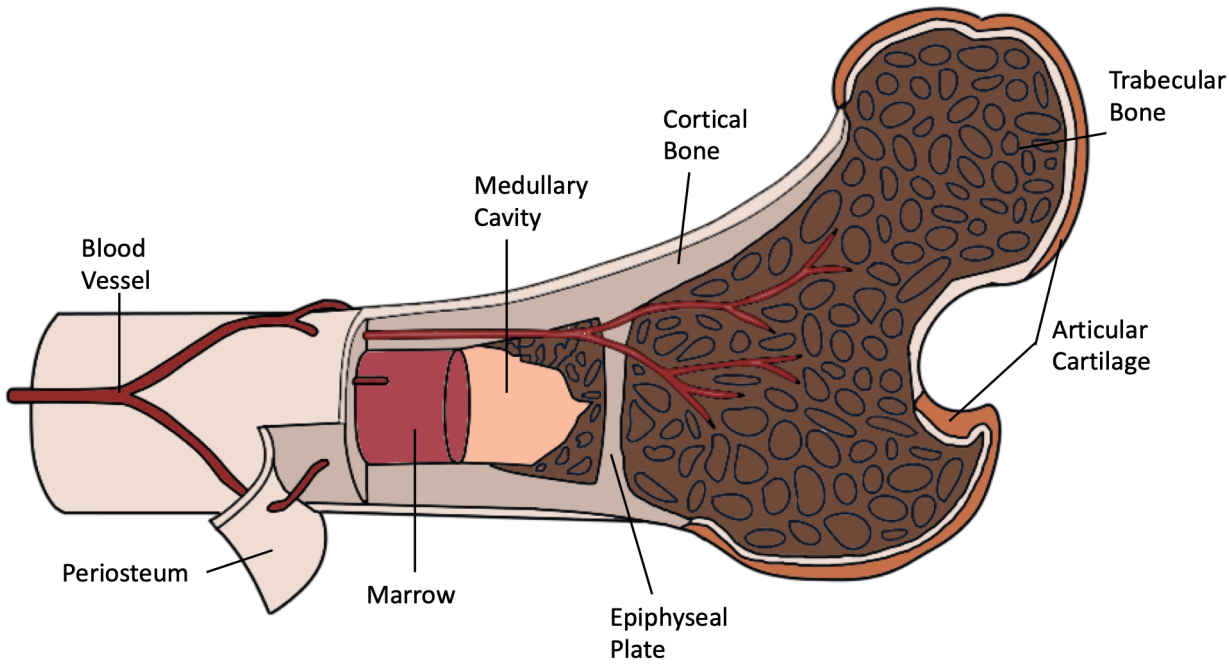

Figure 2.2: Cross section of a proximal femur (femoral head).
Image by Tahlia J Stewart (adapted from Pbroks13 2008).

2.3.1 Periosteum

The outer surface of bone, with the exception of articular surfaces, is covered with periosteum, which is a dense fibrous connective tissue (Clarke 2008; Li and Fennessy 2021; Ross and Pawlina 2011). If a bone is growing, the periosteum will contain a thick cellular layer of osteoprogenitor cells (Section 2.3.3), but if no active growth is occurring, the fibrous layer will make up the primary component of the periosteum (Li and Fennessy 2021; Ross and Pawlina

2011). Periosteal cells which line the periosteum, can undergo division to develop into osteoblasts (Section 2.3.3) (Chang and Knothe Tate 2012; Ross and Pawlina 2011). The fibrous layer of the periosteum is made up of collagen fibers which run parallel to the bone surface, encapsulating the bone, with the exception of articular surfaces and muscle, ligament and tendon attachment sites (Clarke 2008; McBride et al. 2011; Ross and Pawlina 2011). At these sites, collagen fibers will run directly from these structures into the extracellular matrix of the bone tissue, connecting with Sharpey's collagen fibers that reside there (Aaron 2012; Ross and Pawlina 2011). The periosteum plays a crucial role in appositional growth and bone repair, but increased rates of bone formation in comparison to bone resorption lead to an increased bone diameter with age (Clarke 2008; Colnot 2009).

2.3.2 Bone Tissue Types

There are two main bone types found in the human skeleton; cortical, or compact bone, and trabecular, or spongy bone, which make up 80% and 20% of the average adult human skeleton respectively (Aloia 1994; Clarke 2008; Ross and Pawlina 2011). These bone types are structurally and functionally different, but also share some characteristic similarities. Cortical bone is dense and solid, encompassing the marrow cavity, while trabecular bone has a 'latticework' structure of plates and rods intermingled in the marrow cavity (Clarke 2008). However, both bone tissue types contain osteons (Clarke 2008).

Cortical bone is located in long bone shafts and the outer layers of vertebral bodies and is deposited in concentric layers of collagen fibrils around osteons or Haversian systems, which facilitate blood flow, and house lymphatics, connective tissue and nerves (Aloia 1994; Datta et al. 2008). Within these lamellar layers, are lacunae, which contain osteocytes; a cell responsible for crucial functions pertaining to bone modelling and remodelling (Datta et al. 2008). Cortical osteons measure approximately 400 mm long and 200 mm wide and are a cylindrical branching network that reside in the cortical tissue (Clarke 2008; Eriksen et al. 1994). Healthy adult humans are estimated to have 21 x 106 cortical osteons, equating to an area of ~3.5m^2 (Clarke 2008). The main function of cortical bone is to protect the structurally less robust trabecular bone and the marrow within, but its microstructures are unique in a way to facilitate necessary bone processes; modelling and remodelling (Aloia 1994; Brickley and Ives 2008; Datta et al. 2008; Martin et al. 1998). Cortical bone is generally less influenced by metabolic changes than trabecular bone in humans, and its porosity is <5%, subject to the ratio of secondary osteons that are actively remodelling to those that are not (Clarke 2008). However, even healthy adult humans are subject to cortical thinning and increasing intracortical porosity with advanced age (Clarke 2008).

Trabecular bone is located within vertebrae, in flat bones and in the centre of long bones (Aloia 1994; Datta et al. 2008; Ralston 2021). Trabecular bone has mineralised spicules, plates and rods, which are organised along mechanical force lines and frequently intersect, both obliquely and transversely (Aloia 1994; Clarke 2008). The voids within this 'latticework' structure hold marrow and blood vessels during life (Brickley and Ives 2008; Ralston 2021; Ross and Pawlina 2011). Trabecular bone may only account for 20% of an individual's total bone mass, but due to these voids and close contact with marrow and blood, it has a greater surface area than cortical bone and is more reactive to hormonal changes and fluctuating mineral homeostasis (Aloia 1994; Ralston 2021). Trabecular osteons are referred to as 'packets', and are a semilunar shape, ~35mm thick, comprised of concentric layers of lamellar bone (Clarke 2008). The healthy adult human is estimated to have 14 x 106 packets, equating to a total area of ~7m^2 (Clarke 2008).

In addition to these two key bone tissue types, bone tissue can be categorized according to whether it is woven (also called immature) or lamellar (also called mature) bone (Clarke 2008; Eriksen et al. 1994; Figure 2.3). Cortical and trabecular bone are usually deposited in a lamellar fashion, meaning collagen fibrils are deposited by osteoblasts in interchanging orientations (Eriksen et al. 1994). The underlying skeletal mechanism by which this lamellar pattern is adhered to by osteoblasts has not yet been identified, but this arrangement of collagen fibrils does significantly increase the strength of bone, as compared to woven deposition patterns (Clarke 2008). This underlying skeletal mechanism has been speculated to be connected to an as-yet unidentified biorhythm, potentially linked to mammalian body size and organism life history patterns, but lamellar deposition has been correlated with enamel deposition, thus defining lamellar bone as an incremental tissue (Bromage et al. 2009; 2011; 2012; 2016a; 2016b; Bromage and Janal 2014; Mahoney et al. 2016a; 2017; 2018). Woven bone is usually deposited in the process of primary bone formation, but may also be present due to pathological interference, such as Paget's disease or hyperparathyroidism, and is usually associated with excessive bone formation (Clarke 2008; Kobayashi et al. 2003; Lindsay et al. 2006; Ubara et al. 2003; 2005).

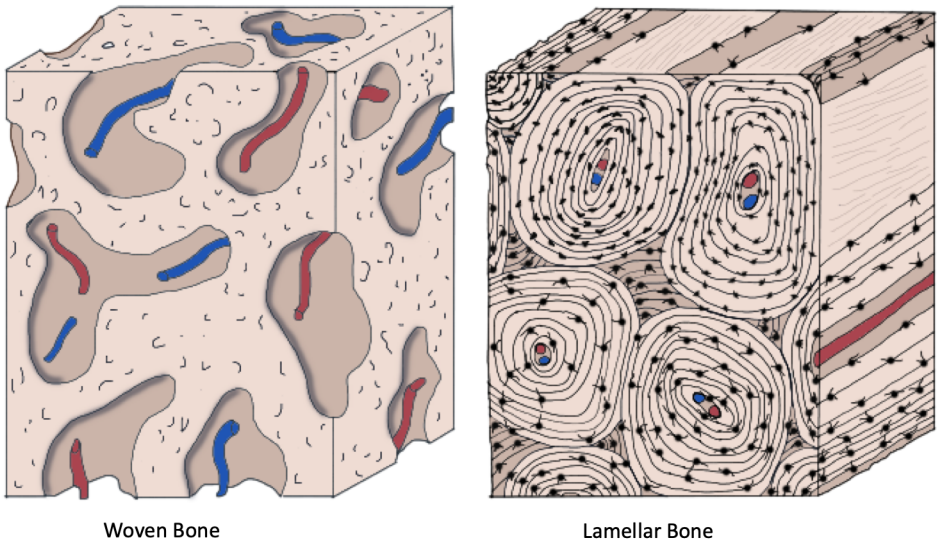

Figure 2.3: Woven versus lamellar bone.
Image by Tahlia J Stewart (adapted from Safadi et al. 2009).

2.3.3 Endosteum

The inner surface of bone is important because bone cavities are where bone tissue interacts with marrow cavities and metabolism associated with bone turnover and mineral storage (Tuckermann and Adams 2021). The way a bone behaves within its inner cavity can be diagnostic in terms of health, diet and metabolic processes (Tuckermann and Adams 2021). The inner surface of bone cavities is lined with endosteum, which is similar in structure to the periosteum, as a layer of connective tissue, holding osteoprogenitor cells (Langen et al. 2017; Ross and Pawlina 2011). The endosteum lines the inner layer of cortical bone, the trabecular bone within the marrow cavity, and the blood vessel canals (also called Volkman's canals) (Clarke 2008; Neagu et al. 2016; Ross and Pawlina 2011). Often just one cellular layer thick, the osteoprogenitor cells can undergo division into either osteoblasts or bone-lining cells, the latter of which can be difficult to differentiate from osteoprogenitor cells, even at a microscopic level (Neagu et al. 2016; Ross and Pawlina 2011). This is due to visual similarities between the two, including their flattened shape, elongated nuclei and virtually identical cytoplasmic characteristics (Neagu et al. 2016; Ross and Pawlina 2011). For this reason, and due to their location within the endosteum, they are often simply referred to as endosteal cells to avoid misidentification (Neagu et al. 2016; Ross and Pawlina 2011). The endosteal surface typically has a total surface area of 0.5m^2 and has a higher bone remodelling rate than the periosteal surface, which has been suggestively linked to increased biomechanical influence or cytokine exposure from the neighbouring marrow cavity (Clarke 2008). In contrast to the periosteum,

the endosteum has a higher rate of bone resorption than bone formation, leading to an increased marrow cavity with age (Clarke 2008; Langen et al. 2017).

2.3.4 Marrow Cavities

Marrow cavities are a storage space for bone marrow, in addition to the voids within trabecular bone (Fazeli et al. 2013; Ross and Pawlina 2011). Red bone marrow contains blood cells at varying developmental phases, as well as a complex system of reticular fibres and cells to support developing blood vessels and cells (Ross and Pawlina 2011; Wang et al. 2018). The rate of blood cell development decreases with age, reducing the amount of red bone marrow, and increasing the amount of fat cells, becoming yellow marrow (Ross and Pawlina 2011; Wang et al. 2018). Under certain circumstances, such as rapid blood loss, yellow marrow can return to red marrow, which, in adults, is usually confined to the voids in trabecular bone, as well as in selective skeletal elements such as the sternum and iliac crest (Liu et al. 2011; Ross and Pawlina 2011; Wang et al. 2018).

2.3.5 Cartilage

There are three types of cartilage found in the human body, hyaline, elastic and fibrocartilage. Hyaline cartilage is the most common type of cartilage found in adult skeletons, located at the ventral end of ribs, in the circular rings of the trachea and on synovial joint surfaces whereby it is better known as articular cartilage (Armiento et al. 2019). The growth plates of growing, sub-adult, skeletons are also comprised of hyaline cartilage (Martin et al. 2015). Elastic cartilage is mostly found in the anatomy of the outer ear and the eustachian tube, which connects the middle-ear to the nasal-sinus cavities (Krishnan and Grodzinsky 2018). Additionally, the epiglottis is comprised of elastic cartilage, which is a piece of anatomy activated during swallowing to prevent excess food from entering the airway (Krishnan and Grodzinsky 2018). Fibrocartilage can be found in intervertebral discs, the pubic symphysis, menisci and in the bony anchors of some tendons and ligaments (Armiento et al. 2019). Fibrocartilage has also been identified forming at sites where hyaline cartilage has acquired significant damage, exposing the subchondral plate (Armiento et al. 2019). The microstructure of cartilage will be discussed in section 2.3.2 following the discussion of collagen and proteins.

2.4 Microstructure of Bone

Bone is a connective tissue, with an extracellular matrix (ECM), consisting of organic and inorganic components. Inorganic components include calcium phosphate, which is present in the form of hydroxyapatite [$Ca_{10}(PO_4)_6(OH)_2$] (Datta et al. 2008; Hall 2005; Ross and Pawlina

2011). Organic components of the ECM include type I collagen and non-collagenous proteins such as osteocalcin, osteopontin and osteonectin (Hall 2005). Here, each of these microscopic components are described.

2.4.1 Inorganic Components of the ECM

Human bone ECM contains up to 65% inorganic materials in the form of minerals and other inorganic components (Rosa et al. 2022). The mineral component of bone is nanocrystalline, and called hydroxyapatite, a type of calcium phosphate and insoluble salt (Bala et al. 2013). Here, hydroxyapatite is introduced and described, followed by other trace minerals found in human bone and what benefits or detriments they can induce.

2.4.1.1 Hydroxyapatite

Hydroxyapatite is denoted by the chemical formula $Ca_{10}(PO_4)_6(OH)_2$ and is arranged in a hexagonal construct (Figure 2.4). Approximately 40% of hydroxyapatite is comprised of calcium and 18% of phosphorous, with a subsequent ratio of 1.67 of calcium to phosphorous (Habibah et al. 2022).

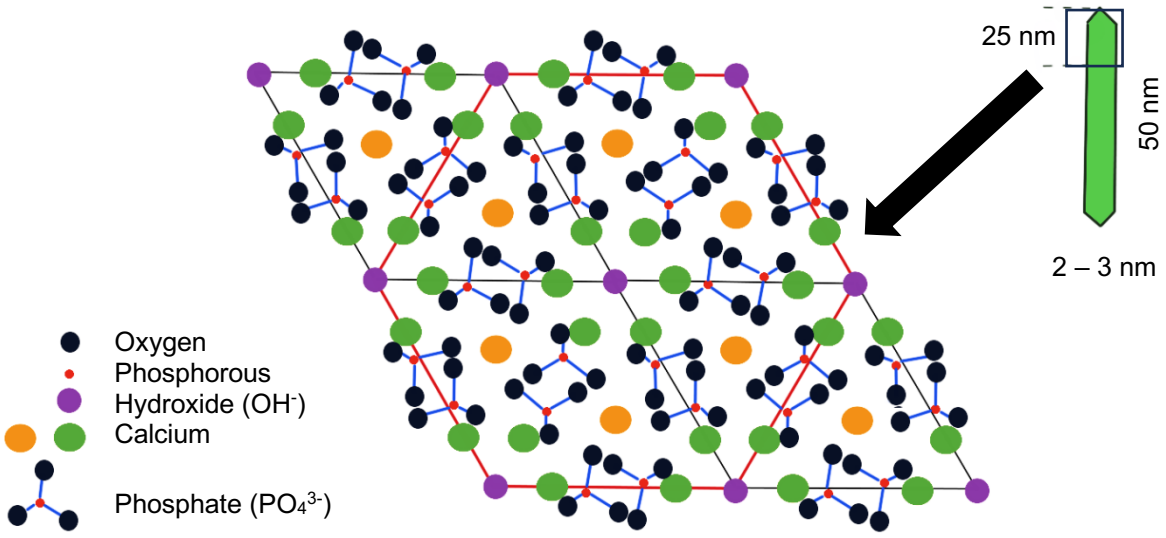

Figure 2.4: The crystalline structure of hydroxyapatite.
Image by Tahlia J Stewart (adapted from Wallace 2019:137).

Hydroxyapatite is produced by the mineralisation of Type I collagen to increase stiffness of bone by approximately five times over, but simultaneously increasing fracture risk by up to 300% (Currey 2002). On its own, hydroxyapatite is brittle, but strong, providing bone with the necessary rigidity and hardness to support the body whilst weightbearing (Boivin et al. 2008;

Gupta et al. 2006). Hydroxyapatite is often considered ‘impure’ with other trace minerals infiltrating its matrix, such as magnesium, strontium, sodium and potassium which take the place of the calcium ions, carbonate which takes the place of the phosphate groups, and chloride and fluoride which take the place of the hydroxide ions (Rosa et al. 2022).

Other trace minerals can be found within bone including boron, iron, zinc, magnesium and copper, but the amounts and ratios of each vary between individuals in response to dietary and environmental differences (Akiva et al. 2016; Darrah et al. 2013; Dey et al. 2010; Gaffney-Stomberg 2019; Grynpas and Omelon 2007). These trace elements are initially found in dietary components such as fruit and vegetables, but also in water supplies, saturating local crops and leading to a cyclical uptake in local inhabitants and resulting in geographically unique patterns in these trace elements within human (and animal) bone (Darrah et al. 2013; Gaffney-Stomberg 2019). Boron, iron, zinc, magnesium and copper have shown to be beneficial to bone health in a variety of ways.

2.4.1.2 Boron

Boron is osteogenic, increasing bone metabolism and growth (Hunt 2012). By activating vitamin D production, boron supports bone mineralisation and sufficient dietary boron has been associated with improved trabecular and cortical bone structure (Hakki et al. 2013; Nielsen and Stoecker 2009).

2.4.1.3 Iron

Iron stimulates the production of the bone matrix by activating lysyl hydroxylase, which is necessary for collagen stabilization (Zofková et al. 2017). Additionally, iron activates 25-hydroxycholecalciferol hydroxylase, which converts non-bioactive vitamin D to bioactive vitamin D, and assists in the bone matrix mineralisation process (Zofková et al. 2017). Iron deficiency can lead to poor mineralisation of the bone matrix, femoral and tibial cortical thinning, pathologies of the trabecular microstructure in the vertebrae, and more broadly a loss of bone strength (Madeiros et al. 2004; Parelman et al. 2006).

2.4.1.4 Magnesium

Magnesium aids in the production of hydroxyapatite and is discharged from the apatite crystals during the bone resorption process (Aina et al. 2012; Zofková et al. 2017). Additionally, magnesium supports vitamin D production and the mineralisation of bone marrow stromal cells, which are progenitor cells for skeletal tissues including bone and cartilage (Yoshizawa

et al. 2014; Zofková et al. 2017). Osteoblast population density and activity reduce with magnesium deficiency, resulting in increased bone resorption and loss and decreased bone deposition (Kanazawa et al. 2007).

2.4.1.5 Copper

Copper is a crucial element in the regulation of bone growth and development by stimulating lysyl oxidase activation and allowing the development of lysine crosshatches in collagen and elastin (Zofková et al. 2017). Copper also destroys free radicals which are located in bone and upregulate osteoclastic activity and downregulates osteoclastic bone resorption directly (Kubiak et al. 2010; Li and Yu 2007).

2.4.1.6 Zinc

Zinc promotes osteoblastic activity and the collagen production, whilst prohibiting osteoclastic resorption of bone (Zofková et al. 2017). Zinc deficiency can prevent intestinal calcium absorption, crucial for healthy bone metabolism (Suzuki et al. 2015). Zinc has demonstrated to play a crucial role during skeletal growth and development for bone mineralisation, matrix formation and modelling (Hadley et al. 2010). Additionally, zinc can reduce the detrimental effects on osteoblasts of toxicity caused by the exposure to trace elements such as cadmium, lead and chromium, which are associated with industrial areas and activities such as mining and heavy metal refinery (Brzóska et al. 2007; Jamieson et al. 2006; Zofková et al. 2013; 2017).

2.4.1.7 Cadmium

Cadmium has been described as a strong carcinogenic element, capable of causing oxidative stress, abnormal DNA methylation, altering cellular proliferation and differentiation activity, preventing DNA repair processes and destabilising DNA structure (Bishak et al. 2015). In the skeletal environment, cadmium can cause bone loss and compromise bone quality, leading to a loss of BMD, increased fracture risk and higher incidence of osteoporosis (Akesson et al. 2006; Engström et al. 2012; Sadeghi et al. 2014).

2.4.1.8 Lead and Chromium

Lead and chromium are heavy metals which can accrue in the body over extended periods of time, usually leaching into the body through industrial pollution. Lead has primarily been associated with compromising osteoblastogenesis, leading to cortical thinning and lower BMD due to reduced bone growth (Bier et al. 2015; Tsai et al. 2016; Wong et al. 2015). Chromium

has been found to cause oxidative stress to osteoblasts, leading to early apoptosis, stimulating osteoclastogenesis (Andrews et al. 2011; Zijlstra et al. 2012). This results in an imbalance in bone remodelling with bone resorption outweighing new bone deposition, leading to bone loss, cortical thinning and decreased BMD.

2.4.2 Organic Components of the ECM

The organic components of the ECM are primarily produced by osteoblasts and secreted into the extracellular space (Mansour et al. 2017). Up to 90% of the organic components of the ECM is type I collagen, with the remaining 10% made up of collagen types III and IV, and an assortment of non-collagenous proteins including osteocalcin, osteonectin, osteopontin, laminin, fibronectin, vitronectin and bone sialoprotein (Shekaran and García 2011). Here, each of these organic structures are described.

2.4.2.1 Collagens

The key purpose of collagen is to provide mechanical support for the bone and body, and a framework for bone cells to reside within (Saito and Marumo 2015). Type I collagen is made up of three key amino acids; glycine, proline and hydroxyproline, which form three α chains, and together form a triple-helix shaped tropocollagen unit (Van Gulick et al. 2019; Figure 2.5).

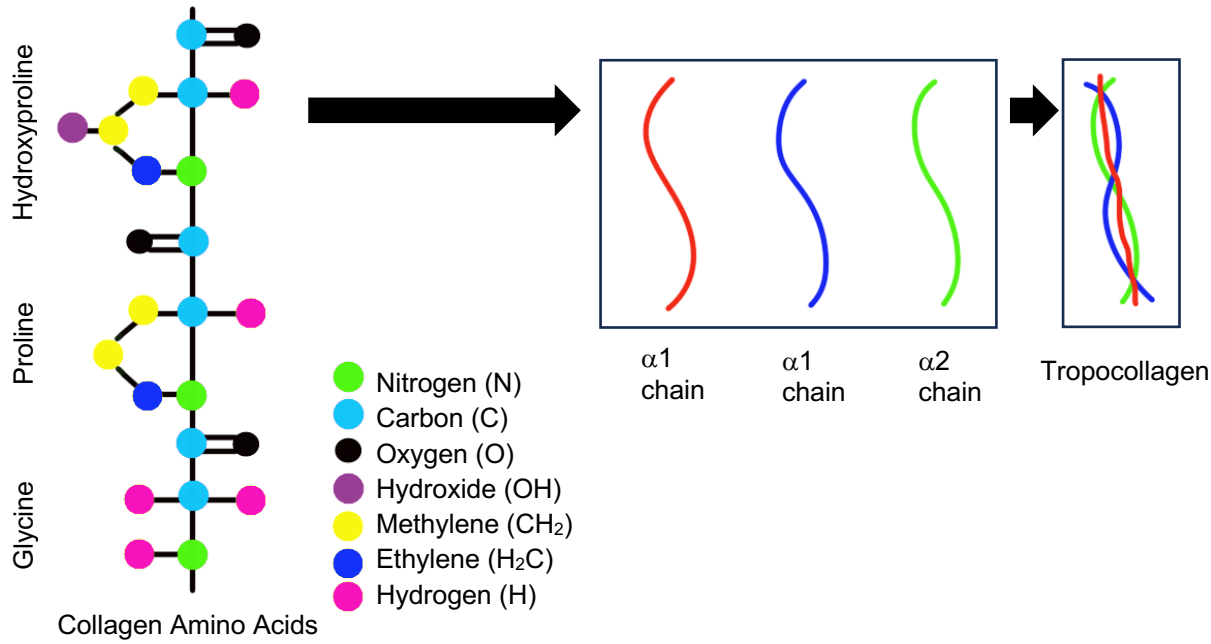

Figure 2.5: Diagrammatic structure of collagen amino acids.

Figure 2.5 demonstrates how collagen amino acids form the α chains, and subsequently how the α chains then comprise the tropocollagen. These tropocollagen then form collagen fibrils

which make up the collagen fibres, see Figure 2.6 below. Image by Tahlia J Stewart (adapted from Rosa et al. 2022).

Type I collagen is cross-linked with hydroxyapatite, its own flexibility and resilience complimenting the strength and rigidity of the hydroxyapatite to support weightbearing but reduce fracture risk (Currey 2002). It does this at the nanostructural level with the tropocollagen units congregating, along with the crystallised minerals of hydroxyapatite, to form mineralised collagen fibrils, which when bundled together, form collagen fibres (Rosa et al. 2022; Van Gulick et al. 2019; Varma et al. 2016; Figure 2.6).

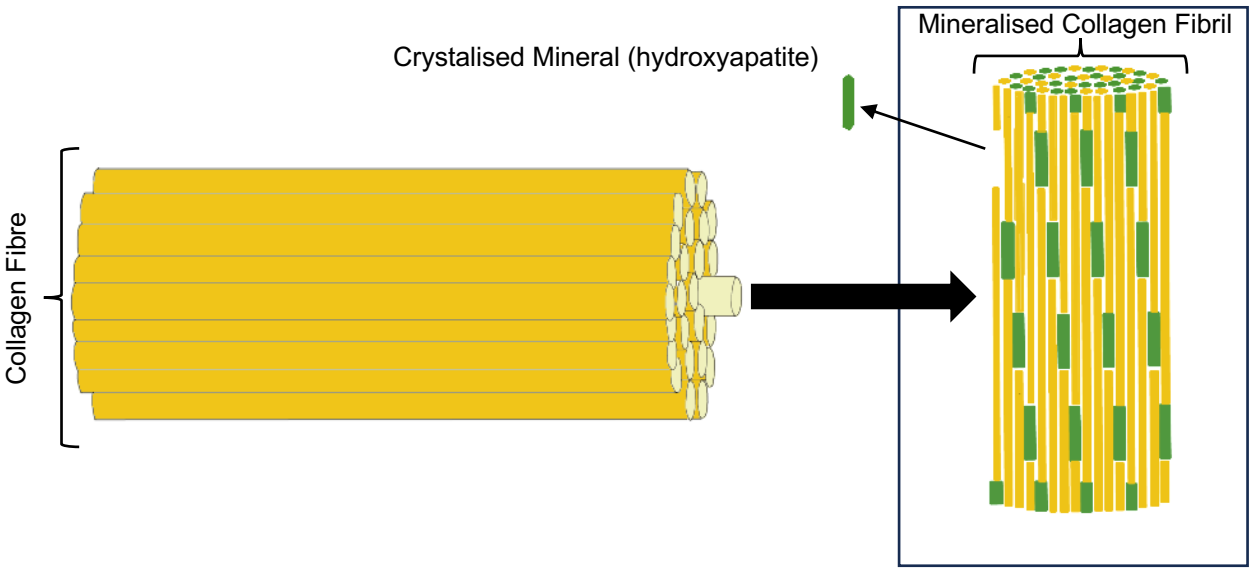

Figure 2.6: Diagrammatic structure of congregated tropocollagen.
Together with the crystallised mineral hydroxyapatite, the tropocollagen forms collagen fibrils which make up the larger collagen fibres. Image by Tahlia J Stewart (adapted from Rosa et al. 2022).

Much smaller amounts of type III and V collagen are located in the extra cellular space, particularly that of osteocytes, and these collagen types are believed to assist with the ECM organisation and make up, collagen fibre size regulation, as well as type I collagen synthesis (Garnero 2012; 2015; Olsen 1995).

2.4.2.2 Proteins

There are four groups of non-collagenous proteins found in bone; proteoglycans,y-carboxyglutamate-containing proteins, glycoproteins and small integrin-binding ligands N-linked glycoproteins (SIBLINs) (Paiva and Granjeiro 2017).

Proteoglycans

These proteins are defined by the glycosaminoglycan deposits covalently bound to its core. Of particular importance to bone are biglycan, decorin, keratocan and asporin, which regulate cellular behaviours via cellular surface receptors and cytokine networks (Lin et al. 2020). This includes during vital processes such as cell proliferation, osteogenesis, mineralisation and mineral deposition, bone remodelling, bone formation, collagen fibrillogenesis and mineralisation, bone matrix deposition (Coulson-Thomas et al. 2015; Kalamajski et al. 2009; Kirby and Young 2018; Moorehead et al. 2019).

y-Carboxyglutamate-Containing Proteins

This group includes osteocalcin, matrix Gla protein and periostin, and are located in the bone matrix (Finkelman and Butler 1985; Wen et al. 2018). Osteocalcin is secreted by osteoblasts during osteogenesis and regulates calcium metabolism within hydroxyapatite (Lin et al. 2020). During bone resorption, osteocalcin is discharged into the circulatory system, where it has been identified as a biochemical marker of bone formation (Mizokami et al. 2017). Matrix Gla protein knockout mice have undergone early bone mineralisation and matrix Gla protein saturated mice exhibit compromised intramembranous bone mineralisation suggesting that matrix Gla protein plays a significant role in the disruption of osteogenesis and mineralisation inhibition (Luo et al. 1997). In the long bones, periostin is largely expressed by osteoblasts and their precursory cells and primarily performs cellular adhesion functions, such as binding to cellular surface receptors to assist in aggregation, proliferation, adhesion and differentiation of osteoblasts (Merle and Garnero 2012; Wen et al. 2018). Additionally, periostin assists in collagen folding and the production of collagen fibrils, contributing to matrix production and optimizing bone strength (Wen et al. 2018).

Glycoproteins

Glycoproteins characteristically fasten carbohydrate molecules to their protein chain in a variety of ways, the most noteworthy in bone is osteonectin, which is secreted in large quantities by osteoblasts (Lin et al. 2020). Osteonectin plays a crucial role in calcium release regulation by binding collagen and hydroxyapatite mineral crystals and monitoring the mineralisation of collagen during osteogenesis (Rosset and Bradshaw 2016). In vivo experimentation has proven that osteonectin knockout mice have demonstrably reduced collagen type I, lower bone mineral density, and reduced osteoblast and osteoclast population densities, as well as demonstrated lower biomechanical properties of their bone (Delany et al. 2000). This evidence suggests that osteonectin plays a significant role in maintaining optimal bone metabolism and mass.

Small Integrin-Binding Ligand N-Linked Glycoproteins (SIBLINGs)

This group of glycophosphoproteins, hereafter referred to as SIBLINGs, include sialoprotein, osteopontin and matrix extracellular phosphoglycoprotein (Bellahcène et al. 2008). Sialoprotein is secreted at the start of mineralisation, and plays a crucial role in osteoblastogenesis and bone matrix mineralisation (Marinovich et al. 2016). Osteopontin is highly secreted by osteoblasts and osteocytes, and plays a major role in osteogenesis, bone mineralisation and remodelling (Singh et al. 2018). More specifically, osteopontin monitors osteoclastogenesis and osteoclastic activity in bone turnover, contributing to bone resorption patterns (Singh et al. 2018). Matrix extracellular phosphoglycoprotein is expressed by mature osteoblasts and plays important roles in phosphate regulation, bone mineralisation and remodelling (Zelenchuk et al. 2015).

2.4.2.3 Cartilage Microstructure

Cartilage, similar to bone, is a form of connective tissue, but dissimilar to bone it is avascular, aneural and alymphatic (Krishnan and Grodzinsky 2018). All three types of cartilage, introduced in Section 2.2.6, have a low cellular density by comparison to bone (Stockwell 1967). The main cells contained in cartilage are called chondrocytes and they produce the key components of the ECM within cartilage (Naba et al. 2016). These key components of the cartilage ECM include proteoglycans, supported by a very hydrated network of collagen fibrils so as to perform the required biomechanical functions providing mechanical support and resistance to shape malformation (Krishnan and Grodzinsky 2018). The ratios, densities and types of collagens and proteoglycans differ between the three types of cartilages, and result in their different appearances and functionalities.

Hyaline Cartilage

Hyaline cartilage has a sheeny, glass-like appearance and provides a lubricating surface for synovial joints to move smoothly (Unsworth et al. 1975). As much as 85% of the weight of living hyaline cartilage is comprised of water (Mow et al. 1992). While multiple different collagen types are found in hyaline cartilage, it is type II collagen that makes up the main structure of the collagen fibrillar network, with type IX collagen covalently linked to the type II collagen molecules surfaces and type XI collagen forming the more intricate inner filamentous template (Eyre et al. 2006). In living tissue, there is <100nm between the collagen fibrils, ensuring tensile and shear strength of the tissue (Han et al. 2011). The type IX collagen is capable of sensory interactions with other collagen fibrils and other ECM molecules (Olsen

1997). Type IV collagen is also found in the ECM nearest chondrocytes and performs a sensory role in order to adapt to changes in the nearby ECM and allowing a chondrocytic response if warranted (Alford et al. 2015; Melrose et al. 2016). Collagen types III, X, XII and XIV are also found in hyaline cartilage (Eyre et al. 2006). The main proteoglycan in hyaline cartilage is aggrecan, which is composed of a central protein with >100 chondroitin sulfate glycosaminoglycan (GAG) chains and fewer keratan sulfate chains stemming from it (Dudhia 2005). The central protein is ~450nm long while the GAG chains are ~40nm long, with spaces between GAG chains ~3nm (Lee et al. 2013; Ng et al. 2003). This close distance between GAG chains results in increased compressive strength and allows the hyaline cartilage to better support joints, particularly weightbearing joints such as the hip and knee (Krishnan and Grodzinsky 2018). In addition to aggrecan, other proteoglycans found in hyaline cartilage include versican, perlecan and small leucine-rich proteoglycans (SLRPs) (Gubbiotti et al. 2017; Paracuellos et al. 2017). SLRPs perform sensory and signaling roles, assisting in collagen fibril regulation, interactions with other ECM molecules, and the regulation of cellular signaling junctions via binding growth factors, cytokines and external ECM structures (Melrose et al. 2016). Larger molecules within the ECM, termed macromolecules, also perform cellular signaling and mechanosensory roles (Ringer et al. 2017). Lubricin is found in the most superficial layers of articular cartilage where it aids in friction reduction for the synovial joint surfaces (Jay and Waller 2014).

Fibrocartilage

Type I collagen is the primary collagen type found within fibrocartilage, which is the reason for its increased tensile strength (Krishnan and Grodzinsky 2018). Type VI collagen can be found in the ECM nearest the chondrocytes, but compared to hyaline cartilage, fibrocartilage has comparatively less type II collage and proteoglycans in the ECM (Wachsmuth et al. 2006).

Elastic Cartilage

Elastic cartilage ECM is primarily comprised of type II collagen, proteoglycans and elastin fibers (Wachsmuth et al. 2006). Elastic cartilage has a somewhat yellow appearance compared to the other cartilage types, and this is due to the presence of the elastin fibers (Krishnan and Grodzinsky 2018). The presence of the elastin fibers also result in a much higher elasticity of elastic cartilage than the other cartilage types (Krishnan and Grodzinsky 2018).

2.4.3 The Cellular Matrix

In addition to the ECM, bone contains a cellular matrix, comprised primarily of 4 distinct cell types to undergo processes of bone metabolism and maintenance on a cellular level; osteoclasts, osteoblasts, osteocytes and lining cells. These can be distinguished into two main types of cell lines; hematopoietic (osteoclasts) and mesenchymal (osteoblasts, osteocytes and lining cells) (Figure 2.7).

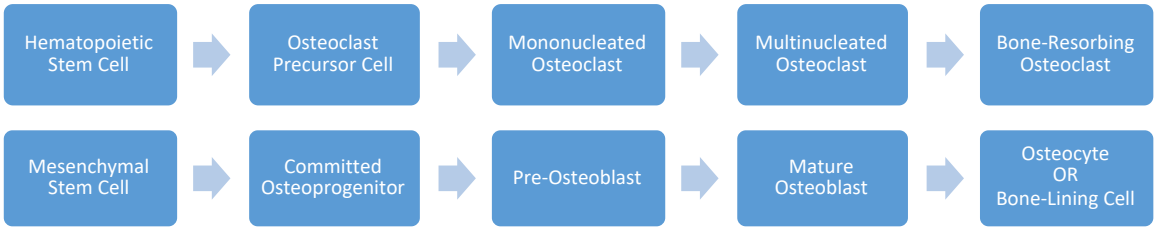

Figure 2.7: Developmental cell lines in osteoblastogenesis and osteoclastogenesis.

2.4.3.1 Osteoclasts

While other bone cells can influence and effect bone resorption indirectly, osteoclasts are the only cells known to directly resorb bone (Clarke 2008). Osteoclasts derive from mono-nuclear precursor cells within the monocyte-macrophage lineage; specifically, those within the bone marrow (Boyle et al. 2003; Clarke 2008). Two cytokines are crucial for osteoclastogenesis, RANKL and macrophage CSF (M-CSF), which are expressed largely by marrow bound stromal cells and both membrane-bound and soluble osteoblasts (Clarke 2008; Teitelbaum and Ross 2003). Both stromal cells and osteoblasts are required to be present in the bone marrow for osteoclastogenesis to occur (Teitelbaum and Ross 2003).

Osteoclasts are multi-nucleated, and their cytoplasm contains highly developed organelles including mitochondria, endoplasmic reticulum, Golgi apparatus, transport secretory vesicles and microtubule arrays, to facilitate the metabolic activity required for efficient bone resorption (Figure 2.8; Šromová et al. 2023). A key characteristic of the osteoclast is its ruffled border which has developed for a very specific function, with its membrane of many folds to produce multiple finger-like structures to adhere to the bone surface. Osteoclasts secrete adhesion molecules called integrins to further help form a seal within which the osteoclast can begin to form a bone resorption bay (Šromová et al. 2023).

During osteoclast differentiation, the differentiating osteoclast will attach itself to the bone surface with the ruffled border which is lined with proton pumps, creating a sealed zone. The proton pumps release protons into the resorptive bay formed by the sealed zone, creating an

acidic environment and facilitating further breakdown of the bone tissue (Šromová et al. 2023). The broken-down tissue is absorbed into the osteoclast via transcytosis, and carried by transport vesicles through the cellular matrix until they are released from the exposed cellular

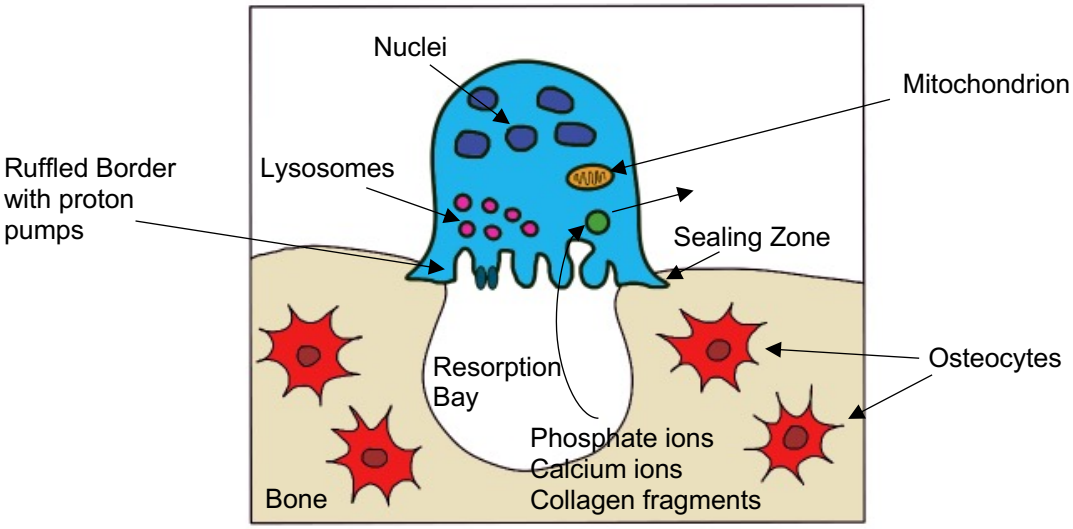

Figure 2.8: Bone resorbing osteoclast.
Image by Tahlia J Stewart (adapted from Šromová et al. 2023).

membrane into the ECM. Additionally, the lysosomes within the osteoclast release an enzyme called tartrate-resistant acid phosphate which assists to breakdown bone tissue in the resorption process (Šromová et al. 2023). Osteoclasts also secrete an enzyme called cathepsin K, which assists to digest the protein components within the bone matrix (Boyle et al. 2003). Bone resorption occurs locally, directly beneath the ruffled border of the osteoclast, penetrating the bone surface.

2.4.3.2 Osteoprogenitor Cells

Osteoprogenitor cells are spindle-shaped cells that derive from mesenchymal stem cells that reside in the bone marrow (Clarke 2008). Osteoprogenitor cells are of the osteoblast cell lineage, giving rise to and sustaining osteoblasts as they produce and deposit new bone matrix at bone formation sites (Clarke 2008). Additionally, they work to maintain neighbouring osteocytes within existing and new bone deposits near bone formation sites (Clarke 2008). The differentiation of mesenchymal stem cells into osteoprogenitor cells requires the canonical Wnt/β-catenin pathway and related proteins (Logan and Nusse 2004). This pathway is therefore necessary for embryonic and fetal skeletal formation and development, and adult bone remodelling (Boyden et al. 2002). Osteoprogenitor cells also sustain populations of bone-

lining cells that cover the surface of inactive bone, and line active bone formation sites (Clarke 2008).

2.4.3.3 Osteoblasts

Osteoblasts are single-nuclear cells and have an enlarged Golgi apparatus to facilitate the processing and storage of bone ECM proteins, including osteocalcin and collagen prior to their adhering to hydroxyapatite crystals, and have a rough endoplasmic reticulum which plays a secretory vesicle role and a part in protein synthesis (Clarke 2008; Kim et al. 2020; Figure 2.9).

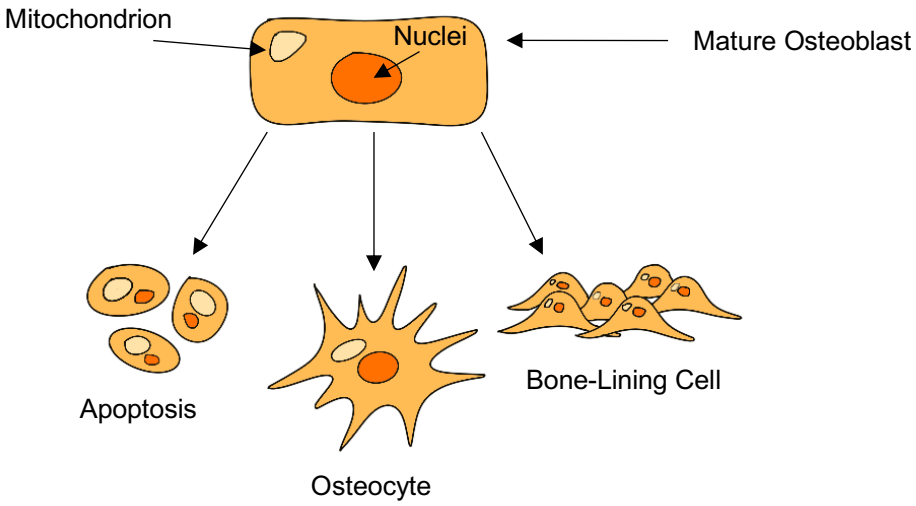

Figure 2.9: Cellular pathway for a mature osteoblast.
Image by Tahlia J Stewart (adapted from Šromová et al. 2023).

Osteoblasts are located in the vicinity of bone-lining cells, linked by adherens junctions, a cell junction where the cytoplasm of one cell is linked to the fibrillar actin cytoskeleton of another (Clarke 2008; Figure 2.10). Pre-osteoblasts located in proximity to already functioning osteoblasts, can be identified due to their alkaline phosphatase expression; an enzyme that is a definitive feature of osteoblasts (Clarke 2008). Different populations of osteoblasts are complimentarily heterogenous, meaning that osteoblasts will express distinctive genes, which leads to regional variation between bone formation sites (Clarke 2008). Osteoblasts are specialized bone-forming and storing cells that can also regulate osteoclast behaviour (Katsimbri 2017). Osteoblasts firstly conduct bone matrix formation, which involves the formation and deposition of osteoid, an unmineralised material, and secondly mineralise the osteoid, whereby the osteoid is strengthened (Caetano-Lopes et al. 2007; Kim et al. 2020; Figure 2.10). Mature osteoblasts are responsible for the secretion of bone matrix proteins, including type I collagen, the main bone matrix protein, onto the surface of the bone formation site (Clarke 2008; Katsimbri 2017). Osteoblasts assist in mineralization by the localised release

of phosphates via osteoblastic matrix vesicles, housed in the osteoid (Katsimbri 2017). The osteoblastic matrix vesicles combine with calcium deposits located in the extracellular matrix and leads to the crystallization of hydroxyapatite and hardens the bone (Katsimbri 2017).

After completing bone formation and a lifespan of approximately 3 months in humans, osteoblasts can have either of four outcomes (Manolagas 2000). Osteoblasts may become dormant osteoblasts or bone-lining cells, undergo apoptosis (cell death), or differentiate into cartilage cells (Franz-Odendaal et al. 2006; Manolagas 2000; Parfitt 1990; Figure 2.9). As the newly deposited bone mineralizes, some mature osteoblasts will become embedded within the mineralised bone matrix, becoming osteocytes.

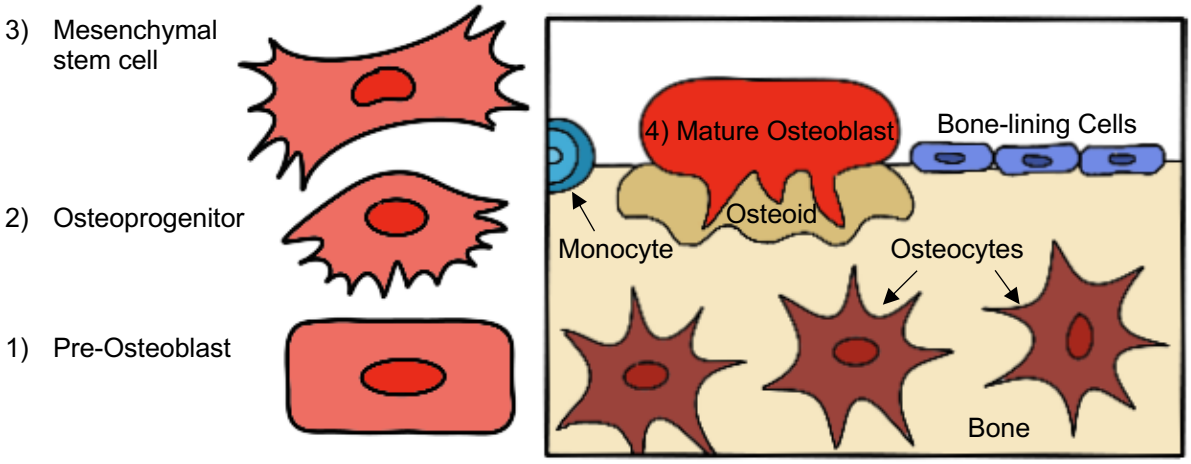

Figure 2.10: Cell line development from a mesenchymal stem cell (1) to mature osteoblast (4). A mature osteoblast (4) produces osteoid on the surface of bone. Image by Tahlia J Stewart (adapted from Šromová et al. 2023).

2.4.3.4 Osteocytes

Osteocytes make up approximately 90-95% of the bone cell population in the mammalian skeleton, with approximately 20,000 – 80,000 cells per mm^3 (Bach-Gansmo et al. 2015; Buenzli and Sims 2015; Currey et al. 2017; Dong et al. 2014; Franz-Odendaal et al. 2006; Gegenbaur 1864; Stein and Werner 2013). It has been suggested that there are roughly ten times the number of osteocytes than osteoblasts in any one bone (Franz-Odendaal et al. 2006; Parfitt 1990). Osteocytes are formed from mesenchymal stem cells via mature osteoblast differentiation, becoming embedded within the osteoid tissue matrix, which eventually become mineralized as the osteocyte matures (Bonewald 2011; Currey et al. 2017; Kerschnitzki et al. 2011; Uda et al. 2017).

Osteocytes have a distinct morphology, with long dendritic processes extending from the cell to communicate with other cells or vessels or to facilitate the transfer of waste or nutrients to or from the cell (Schaffler and Kennedy 2012; Figure 2.11). Osteocytes have a large nucleus, taking up almost half of the cellular space and they reside within bony voids known as lacunae, while canaliculi house their dendritic processes as they reach for neighbouring structures (Tresguerres et al. 2020; Figure 2.11).

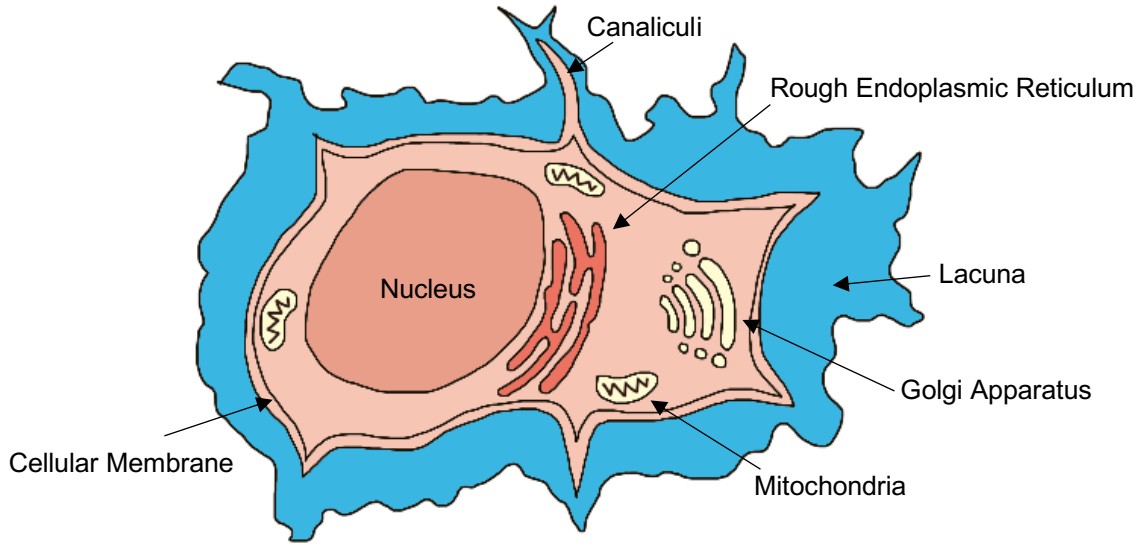

Figure 2.11: Osteocyte structure.
Image by Tahlia J Stewart (adapted from Cusabio Technology 2024).

Each osteocyte has approximately 50 dendritic processes, which extend through canalicular passages of the bone tissue, connecting to a network of other osteocytes, osteoblasts, endosteal bone-lining cells and ultimately the medullary cavity's vascular network for blood supply (Currey et al. 2017; Kerschnitzki et al. 2011; Seeman 2008; Uda et al. 2017). The communication occurs through this lacuna-canalicular network via gap junctions on the dendritic processes (Uda et al. 2017). It has been further suggested that osteocytes are capable of signalling distant cells and organs through factors they release into the medullary cavity, or directly into the blood stream (Fulzele et al. 2017; Uda et al. 2017). Parfitt (2002a) postulated that the dense arrangement of osteocytes ensures that there are never more than a few microns of bone tissue without a lacuna and its osteocyte, and implies that osteocytes play a role in bone compositional and structural integrity (Currey et al. 2017; Uda et al. 2017).

Osteocytes play a crucial role in the natural processes of bone modelling and remodelling (Bonewald 2011; Currey et al. 2017; Qiu et al. 2002; Seeman 2008; Uda et al. 2017). Their precise role within these processes is still hotly debated (Currey et al. 2017). General

consensus is that osteocytes are capable of sensing and measuring bone tissue strain through the constant identification and assessment of microdamage in the bone tissue, to their dendritic processes, or the canalicular passages that their processes reside in (Burr 2014; Frost 1960; Verborgt et al. 2000). Once damage reaches a pre-determined amount, the osteocytes will initiate the process of bone remodelling to remove the damaged tissue and replace it with newly deposited bone (Burr et al. 2002; Currey et al. 2017; Klein-Nulend et al. 2013; Stern and Nicolella 2013). There are multiple signalling pathways through which osteocytes have been proposed to govern osteoblastic and osteoclastic behaviour. For example, sclerostin is a protein responsible for the regulation of osteoblast function and is almost exclusively secreted by osteocytes (Currey et al., 2017; Kim et al. 2017; McClung et al. 2014; Tu et al. 2015).

2.4.3.5 Bone-Lining Cells

Bone-lining cells are flattened cells of the osteoblast lineage, that makeup the endosteum on both trabecular and endosteal surfaces and lay beneath the periosteum on bone's mineralized surface (Clarke 2008; Parfitt 2001a). Initially believed to be derived from the endothelium, bone-lining cells are now suggested to be dormant osteoblasts, due to their expression of osteoblastic indicators including alkaline phosphatase, osteocalcin, osteonectin, IGF-1 and IGF-2, TGF-β1, TGF-β2 and TGF-β3, and FGF (Eriksen et al. 2007; Everts et al. 2002; Hauge et al. 2001; Parfitt 2001a). Bone-lining cells have been identified as 'smoothing' cells; each cell enwrapping, sometimes multiple, collagen fibrils that protrude from the bone surface (Everts et al. 2002). This activity has been identified at both sites where osteoclasts had already performed bone resorption, but had left behind uneven collagen fibrils, and at sites where osteoclasts had not yet been, where both mineralized and non-mineralized collagen fibrils were present and enwrapped by bone-lining cells (Everts et al. 2002). Everts et al. (2002) believes that after the osteoclasts have withdrawn from the resorptive bay, bone-lining cells will enter and clean the base, which they believe to be a prerequisite for bone deposition (Wein 2017). Bone-lining cells only enwrap collagen fibrils on the bone surface, and so are believed to be capable of distinguishing between collagen protruding from the bone surface and collagen that makes up the periosteal layer (Everts et al. 2002; Wein 2017). Once the resorptive bay is cleaned of protruding collagen fibrils, the bone-lining cells deposit a proline-rich protein layer, which contains osteopontin and makes up the lamina limitans (also known as the cement line), where bone formation initiates (Everts et al. 2002). In addition to this direct role in bone resorption and formation, bone-lining cells may also play an indirect role by modulating osteoclastogenesis as they express ICAM-1, which is a protein known to assist in osteoclast differentiation and proliferation (Everts et al. 2002).

2.5 Bone Remodelling

Bone undergoes modelling and remodelling, often referred to as bone turnover, which occurs in response to a variety of physiological or mechanical pressures or conditions (Datta et al. 2008; Katsimbri 2017). Bone modelling is the constructive process of bone formation to change bone morphology, both size and shape, by osteoblasts, that can take place with or without prior bone resorption (Seeman 2008). During infancy, the skeleton will undergo vigorous bone modelling, to form and shape bone, and, to a lesser extent, remodelling, to replace and renew existing bone (Katsimbri 2017; Seeman 2008). Bone remodelling is the process of the resorption of existing bone tissue by osteoclasts, followed by the deposition of new bone in the same location by osteoblasts (Seeman 2008). Bone remodelling continues beyond growth cessation into adulthood as a lifelong process, while bone modelling significantly decreases, largely restricted to a physiological response to trauma or pathological intervention (Katsimbri 2017; Kobayashi et al. 2003). This dissertation examines adult individuals and focuses on microstructural markers of remodelling. As such, modelling and further discussion of skeletal growth will not be undertaken as part of this thesis. Rather, this section will discuss remodelling at length and the structures that are created during this process and therefore used as markers or proxies of this remodelling, secondary osteons.

2.5.1 The BMU

Bone remodelling, in its simplest of terms, is the ‘turnover’ of layers of bone, which under usual circumstances happens without significant changes in bone quantity, shape or size, and is a continuous, life-long process (Frost 1969). The key purposes of this remodelling in adulthood are to maintain bone strength by removing impaired bone tissue and replacing it with new bone, and to govern calcium and phosphate homeostasis (Katsimbri 2017; Seeman 2008). In adults, cortical bone remodelling, which is the main physiological process examined in this dissertation, occurs at a rate of 2 – 3 % each year, is considered sustainable in terms of maintaining its biomechanical strength (Katsimbri 2017). Together osteoblasts and osteoclasts make up the basic metabolic unit (BMU; Figure 2.12), which governs bone remodelling on three endosteal surfaces (endcortical, intracortical and trabecular), as well as on the periosteal surface (Bliziotes et al. 2006; Orwoll 2003; Seeman 2008). Bone remodelling in trabecular bone is faster, suggesting that it plays a crucial role in mineral metabolism and homeostasis; thus, instigating more BMU sites when more calcium or phosphate are required (Katsimbri 2017). This is because newly formed bone is better at facilitating ion exchange with extracellular fluid (Katsimbri 2017). Bone remodelling in adult life, leads to increased periosteal bone deposition, but simultaneous cortical and trabecular thinning with advanced age

(Katsimbri 2017). This occurs because the periosteal bone balance is slightly positive, meaning more bone is deposited than resorbed, but endosteal and trabecular bone balances are slightly negative, with more resorption than deposition (Katsimbri 2017).

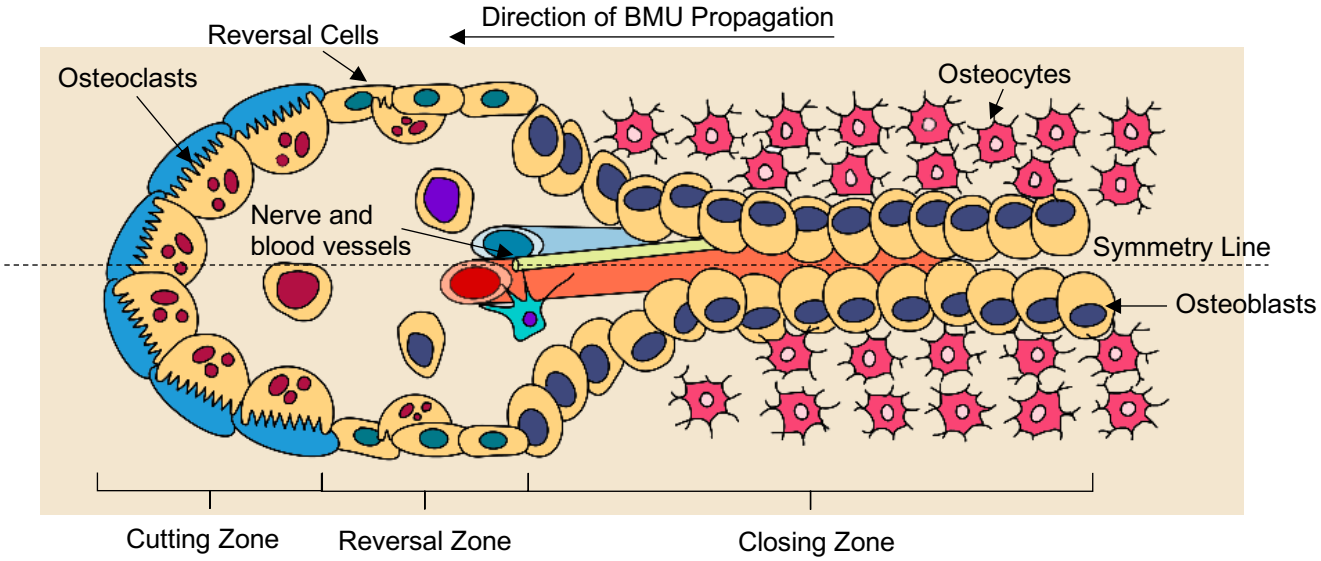

Figure 2.12: The Bone Multicellular Unit cutting cone shape.
Image by Tahlia J Stewart (adapted from Bolamperti et al. 2022).

Underlying mechanisms in bone enable it to locate and assess the scale of damage, resorb the damaged tissue and replace it with new bone tissue to repair its physical composition, micro- and macro-structure (Parfitt 2001b; 2002b). The term 'bone resorption' intuitively sounds disadvantageous, but the resorptive stage of the remodelling process plays a crucial role in the maintenance of bone health (Seeman 2008). However, excessive, non-specific or suppressed bone resorption can lead to an accumulation of damaged bone tissue, slowed healing, or unchecked excessive bone deposition (Mashiba et al. 2010; Odvina et al. 2005). Bone formation is the second key stage in the remodelling process, restoring bone volumetric bone mineral density to its previous state, provided the that an equal amount of new bone is deposited to that which was resorbed (Seeman 2008). Many internal and external factors can encourage or inhibit the bone remodelling process, which will be discussed later in this chapter. Here, the normal, healthy, bone remodelling process is introduced, describing each of the four phases, first described by Frost (1969); activation, resorption, reversal and formation.

2.5.1.1 Activation

The activation phase is referred to as the activation phase as it is defined by the appearance of osteoblast-derived osteoclasts at the location of the BMU, prompted – or activated – by biomechanical or systemic influences recognized by their osteoblast-derived 'sister' cells,

osteocytes (Bolamperti et al. 2022). Before the activation phase begins, bone is said to be in a ‘quiescent’ state (Katsimbri 2017). Osteocytes, as described previously, are believed to be signal-sensitive; able to receive signals from elsewhere in the bone tissue and external to the bone organ, to stimulate the activation process (Bonewald 2011). Osteocytes can be activated by the production of cytokine colony stimulating factor 1 (CSF-1), which then stimulates osteocyte multiplication and differentiation into osteoclast precursors, that then migrate to the location of the BMU initiation via the peripheral bloodstream (Bolamperti et al. 2022; Pettit et al. 2008). Other stimuli include hormonal; linked with estrogen or parathyroid hormone (PTH) in response to systemic changes in bone homeostasis; or associated with mechanical strain on or micro-damage to bone tissue (Katsimbri 2017). When one of these signals is received, bone lining cells will withdraw, collagenase will consume the endosteal membrane, and osteoclast precursors are recruited from the circulation and their differentiation into osteoclasts will begin as they migrate (Katsimbri 2017). Once the larger, multinucleated osteoclasts migrate to the BMU site, they affix to the outer surface of bone and begin the resorption process by expressing hydrogen ions and enzymes, such as cathepsin K (Katsimbri 2017).

2.5.1.2 Resorption

During the resorption phase, osteoclasts work together to remove bone, creating a cavity that is recognizable in histological analyses, that is referred to as a ‘resorptive bay’ or ‘cutting cone’ in cortical bone, or as a ‘hemi-cone’ in trabecular bone (Bolamperti et al. 2022; Parfitt 2002a). The resorption phase will last approximately 2-4 weeks (Katsimbri 2017). Osteoclasts first express hydrogen ions to lower the BMU site pH to approximately 4.5, to facilitate the mobilization of the bone mineral (Katsimbri 2017). Once the pH is lowered, the osteoclasts will secrete enzymes, metalloproteinase and cathepsin K and others, to consume the organic matrix of bone (Katsimbri 2017). Osteoclasts will follow a pathway in the direction of mechanical strain, which is proximal-distally for most long bones (Bolamperti et al. 2022; van Oers et al. 2008a). The resorptive bay produced by the osteoclasts usually reaches a diameter of between 150 – 350 μm, which defines the size of the histological feature, a BMU or osteon, as viewed in cross-section (Bolamperti et al. 2022). Average rates of bone resorption is ~20 μm per day (Bolamperti et al. 2022; Martin et al. 1998). As the osteoclasts progress the advancing BMU, a growing capillary nourishes the tissue, to stimulate the arrival of more osteoclast precursors to assist in bone resorption (Bolamperti et al. 2022). After the resorption phase is complete, the multinucleated osteoclasts will go through apoptosis (Katsimbri 2017).

2.5.1.3 Reversal

The reversal phase is short, by comparison to the resorption and formation phases, and is defined by the lining of the resorptive bay with mononucleic cells (called monocytes), and the migration of osteocytes and osteoblast precursor cells to the BMU site, which are recruited in preparation for the bone formation phase (Bolamperti et al. 2022; Katsimbri 2017). The precise purpose of the monocytes has yet to be determined, but some evidence suggests that they prepare the rough resorbed surface of the resorptive bay for the deposition of a 'reversal line'; a thin matrix layer that is mineral-deficient and sulphur-rich, separating the BMU from surrounding interstitial lamellae (Bolamperti et al. 2022; Everts et al. 2002; Robling et al. 2006). During this reversal phase, the bone-lining cells are believed to facilitate the coupling, or transition, between the resorption and formation phases (Bolamperti et al. 2022; Everts et al. 2002; Tang et al. 2009). One of these coupling signals is the expression of transforming growth factor (TGF)-beta1, derived from the bone matrix (Bolamperti et al. 2022; Bonewald and Mundy 1990; Katsimbri 2017; Tang et al. 2009). The level of TGF-β1 in the bone matrix is related to serum osteocalcin and bone-specific alkaline phosphatase, which are known bone turnover indices, and related to osteoblast proteins, and potentially are by-products of collagenesis (Ducy et al. 1996; Katsimbri 2017). TGF- β1 may also be the driving force behind the mobilisation of osteoblastic precursor, stromal and mesenchymal stem cells to the resorptive bay before formation (Bolamperti et al. 2022; Tang et al. 2009). TGF- β1 also inhibits osteoblastic RANKL production, which also decreases osteoclastic bone resorption, slowing the resorption phase to a halt for the transition to the formation phase (Bonewald 2011; Bonewald and Johnson 2008; Katsimbri 2017; Locklin 1999; Martin and Sims 2005). The migration and differentiation of these cell types take 2-3 days, but the entire of the reversal phase of BMU remodelling is approximately 9 days in duration (Bolamperti et al. 2022; Martin et al. 1998; Moreira and Dempster 2019).

2.5.1.4 Formation

After the completion of the reversal phase, the osteoblasts commence osteoid secretion; bone's organic matrix component comprised of type I collagen and non-collagenous proteins, proteoglycans and water (Bolamperti et al. 2022; Marks and Odgren 2002; Martin et al. 1998). Osteoblasts deposit the osteoid into the cavities formed by the osteoclasts (Katsimbri 2017). The osteoid matrix contributes to approximately 50% of an individual's bone volume, and 40% of their bone weight (Katsimbri 2017). The bone formation phase can last from 4 – 6 months,

with an approximate 10-day delay between osteoid deposition and mineralisation, which occurs through the expression of calcium phosphate crystals (Katsimbri, 2017; Martin et al. 1998). This delay means that a ~7 μm osteoid layer can be found between the osteoid-depositing osteoblasts and any newly mineralised bone (Bolamperti et al. 2022; Pirok et al. 1966). Increased or decreased thickness of this layer can be indicative of pathological conditions and has been found to be associated with osteomalacia (Monier-Faugere et al. 1998). The mineralisation site is called the 'mineralisation front', where osteoblasts will produce and deposit the calcium phosphate crystals necessary for mineralisation of the osteoid matrix into new bone (Bolamperti et al. 2022; Katsimbri 2017; Šromová et al. 2023). This process is controlled by pyrophosphate, preventing atypical calcification (Bolamperti et al. 2022). The quantity of pyrophosphate is in turn controlled by nucleotide pyrophosphatase phosphodiesterase 1 (NPP1) and ankyloses protein (ANK), which both increase pyrophosphate and nonspecific alkaline phosphatase (TNAP) (Bolamperti et al. 2022). Additionally, the osteopontin protein assists in mineralisation, and its quantity often correlates with pyrophosphate (Johnson et al. 2003; Katsimbri 2017).

After fulfilling their roles, between 50 – 70% of osteoblasts will undergo apoptosis (cell death), while the rest will differentiate into one of two possible cell types; osteocytes or bone lining cells (Bolamperti et al. 2022; Katsimbri 2017). Osteoblasts can become embedded inside the mineralized bone matrix before differentiating into osteocytes or flatten to become the bone lining cells that coat bone tissue surfaces (Bolamperti et al. 2022; Šromová et al. 2023).

2.6 Osteons

The main type of osteon referred to in this work is the secondary osteon, which is a product of bone remodelling and turnover, and is used as a proxy for bone turnover rate (Fahy et al. 2017). However, there are also primary osteons, described briefly here first for context as they are unrelated to secondary osteons and will not be discussed further within this dissertation. Finally, secondary osteons are described, followed by a description of their various forms.

2.6.1 Primary Osteons

Primary osteons, also called primary vascular canals, are blood vessels located in the periosteal layer of bone, which are superimposed by primary lamellar diaphyseal apposition, and are usually longitudinally oriented (Currey 2002; Weiner and Wagner 1998). This can lead to their visual confusion with secondary osteons while examining a transverse section of bone using a light microscope, but despite their visual similarities, primary osteons are not related

to secondary osteons in origin, function or form. Primary osteons form without bone resorption, or subsequent formation and deposition of new bone (Currey 2002). Usually, primary osteons will be located between external lamellae, but do not include any lamellae within their structure (Currey 2002). Primary osteons are more abundant in primary bone, forming in sub-adult bone during the folding of bone layers during appositional growth and are uncommon in adult individuals (Chang and Liu 2022; Figure 2.13). As the individuals observed in this dissertation are adults, primary osteons will not be observed and so will not be further discussed here.

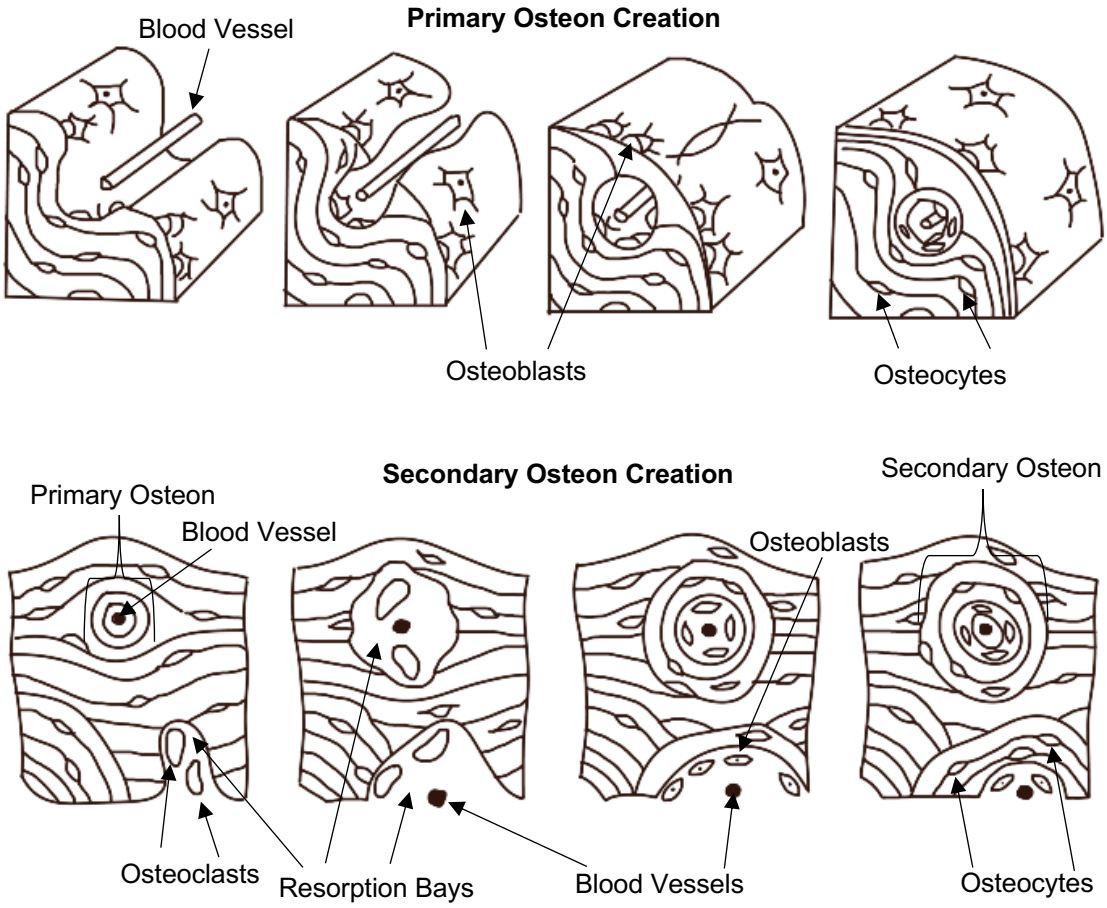

Figure 2.13: Differences in the creation and appearance of primary and secondary osteons. Image by Tahlia J Stewart (adapted from Zylberberg 2004).

2.6.2 Secondary Osteons

Secondary osteons form within preexisting compact bone via the bone remodelling process (Section 2.4.1), and as such, will be the main type of osteon discussed in this research (Ross and Pawlina 2011; Weiner and Wagner 1998; Figure 2.12; 2.13; 2.14). This process begins with osteoclasts forming a tunnel-like structure through compact bone, around an existing vascular canal, also called a Haversian canal, which creates an outer border (Ascenzi and Roe 2012; Ross and Pawlina 2011). This tunnel is then populated with blood vessels and

connective tissues, including osteoblasts, which work to deposit new bone on the inner walls of the osteonal tunnel (Ross and Pawlina 2011). The opposing functions of the osteoclast's resorption and the osteoblast's deposition of bone tissue is termed a bone remodelling unit (Ross and Pawlina 2011). This unit creates two distinguishable behaviours of bone tissue; an advancing a 'cutting cone' (Figure 2.12), which widens and extends the osteonal tunnel (also called a resorption canal), and a 'closing cone', which follows and narrows the tunnel again by depositing new layers of lamellar bone, generally coaxial with the orientation of the vascular canal they are formed around (Ascenzi and Roe 2012; Ross and Pawlina 2011; Weiner and Wagner 1998). This process discontinues once the tunnel is almost refilled, with the exception of the central canal, which serves as a main blood vessel, and smaller canals that radiate from the centre, called canaliculi, which house osteocyte dendritic projections (Weiner and Wagner 1998). When viewed longitudinally, osteons are cylindrical and usually several millimeters in length (Figure 2.13), but for histological analyses it is best to view them horizontally (Figure 2.14) to view the microstructural features present within the osteon (Ascenzi et al. 1973; Ascenzi and Bonucci 1967; 1968; Ascenzi and Fabry 1959; Eriksen et al. 1994).

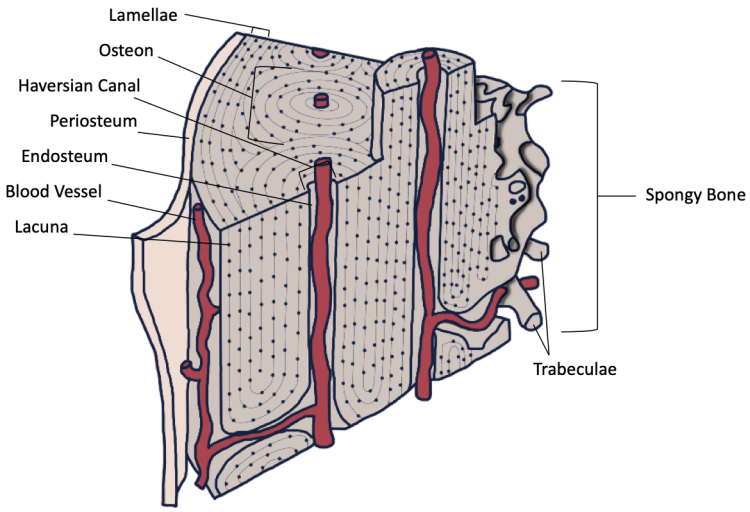

Figure 2.14: Illustration of a secondary osteon in longitudinal cross-section.
Image by Tahlia J Stewart (adapted from Chahal et al. 2019).

In a horizontal section, osteons appear like nested circular layers of lamellar bone, separated by thin layers of cementum in between, which present like dark rings (Ascenzi and Bonucci 1972; Weiner and Wagner 1998). In healthy, young adults, osteons are approximately 84 – 300 microns in diameter, with the central canal approximately 11 – 68 microns in diameter, separated by lamellae between 2 – 16 microns thick, but morphometrics are dependent on the location of the resorption canal within the skeleton, and external and internal factors that can

alter the remodelling process and thus, osteon formation, which will be introduced in section 2.7 (Ascenzi and Roe 2012; Pfeiffer et al. 2006). Secondary osteons can be categorized into types; type I, also called common osteons, described above, but additionally type II (also called embedded osteons), double zonal osteons, completed zonal osteons, sealed osteons and drifting osteons.

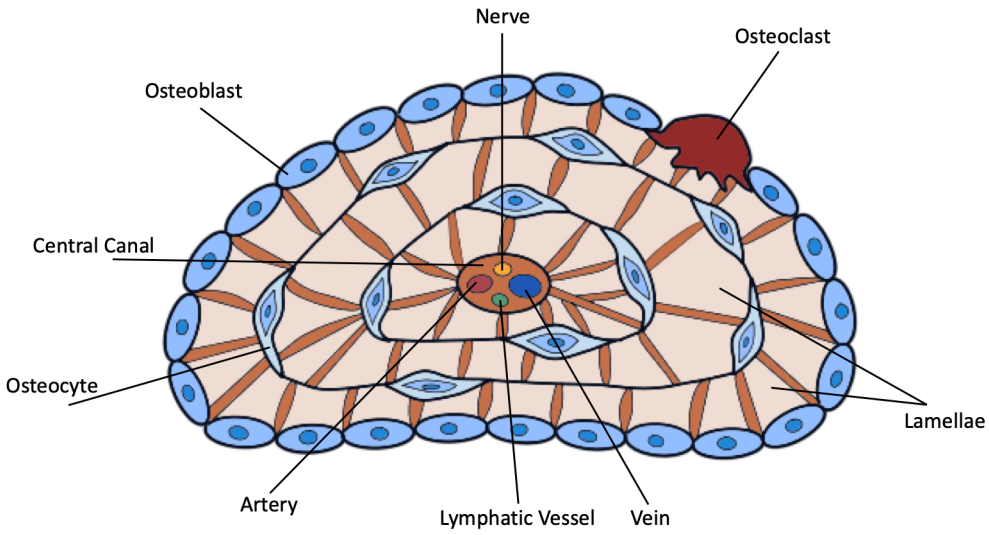

Figure 2.15: Illustration of a secondary osteon in transverse cross-section.
Image by Tahlia J Stewart (adapted from Designua 2014).

2.6.3 Variations of the Secondary Osteon

Sealed osteons are a variation of secondary osteons, categorized by a central canal filled with bone tissue (Skedros et al. 2018). Researchers have postulated that the presence, in particular excess presence of sealed osteons is indicative of reduced bone quality (Congiu and Pazzaglia 2011; Pazzaglia et al. 2015). The derivation of sealed osteons has been speculated over in recent years but has yet to be identified (Congiu and Pazzaglia 2011; Maggiano et al. 2016; Pazzaglia et al. 2015; Skedros et al. 2018). Skedros et al. (2018) suggest that sealed, or partially sealed osteons are a byproduct of the remodelling process in some individuals and may represent the closing cone of secondary osteons and do not represent a pathology, merely an increased plasticity and unusual response to a normal biological process. In cross-section, sealed osteons may appear to have a pale Haversian canal, being void of blood and rather, filled with a continuation of bone tissue but not in an organised layer like the lamellae of the osteon itself (Skedros et al. 2018).

Drifting osteons are another variation of secondary osteons, best viewed longitudinally through the bone cortex (Robling and Stout 1999). There are three key identifying features of drifting

osteons; approximately 90% displacement of transverse drift along the longitudinal axis, changes in concentric morphology and direction of transverse drift at various cross-sections throughout the length of the osteon (Robling and Stout 1999). The transverse drift occurs due to unevenly occurring resorption and formation during remodelling of the BMU, usually continuous resorption and formation on opposite sides of the osteon (Frost 1964; Robling and Stout 1999; Skedros et al. 2007). In addition to the three key features defined above, drifting osteons usually have a non-centrally aligned Haversian canal (Robling and Stout 1999). Two main hypotheses on the origin of drifting osteons exist; complex strain patterns and metabolic disruption, but both of these theories have flaws as associations with differential loading patterns haven't been identified (Currey 2002; Robling and Stout 1999; Skedros et al. 2007). Additionally, there have been no relationships identified between the presence of drifting osteons and general health and/or societal status (Cooke et al. 2022). Thus, the origins of drifting osteons are still unclear.

Embedded osteons are also called type II osteons, and are smaller variations of the common, or type I, osteons that develop within the confines of, but don't cross, the cement line border of an already existing secondary osteon (Robling and Stout 1999; Skedros et al. 2007). Double zonal osteons are difficult to distinguish from embedded osteons, as they are defined by osteons with a hypercalcified ring within the lamellae and can appear as if there is an additional osteon within the confines of another due to the presence of one hypercalcified ring within another, however, embedded osteons will usually have a more ruffled outer cement line, while a hypercalcified ring will appear thick but smooth (Skedros et al. 2007). Double zonal osteons are believed to form when bone formation is disrupted or its mineral density is altered (Robling and Stout 1999; Skedros et al. 2007). Embedded osteons tend to increase with advancing age as osteons will remodel over each other indiscriminately, creating fragmented osteons, which are those that have been partially obscured or remodeled over by younger osteons (Maggiano et al. 2016).

Additional morphologies of secondary osteons have been identified in recent years. Elongated osteons have diameters which are twice as long in one axial plane as the other (Skedros et al. 2007). Connected singlet osteons contain two or multiple connected central canals within the same cement line border (Skedros et al. 2007). Dumbbell osteons have two or multiple separate central canals within the same cement line border, and a band of constriction in the middle; while connected dumbbell osteons are similar, they instead have two or multiple connected central canals (Skedros et al. 2007). A connected doublet osteon occurs when two secondary osteons overlap, thus having multiple separate central canals, but do not have a

dumbbell shape (Skedros et al. 2007). Multiple osteons are defined as an osteon with multiple separate central canals (Skedros et al. 2007). Finally, recently deposited secondary osteons can appear as darker in appearance than other osteons, due to their poor or incomplete mineralization, and can have incomplete closure (Skedros et al. 2007). These additional secondary osteon variants described by Skedros et al. (2007), were not found to have an association with biomechanical loading and their origin is still unknown.

Osteon banding is an anomaly that occurs in modelling and remodelling, leading to the development of five or more linearly arranged osteons (Andronowski et al. 2017). This anomaly can affect both primary and secondary osteons, but until recently was thought to be a characteristic of non-human bone, particularly common in young individuals of a rapid growing species (Dominguez and Crowder 2012; Hillier and Bell 2007; Mulhern and Ubelaker 2001). As such, it has been suggested that osteon banding is a strong indicator of distinguishing non-human from non-human bone, based on its respective presence or absence (Dominguez and Crowder 2012; Hillier and Bell 2007; Mulhern and Ubelaker 2001). This is despite osteon banding having been identified in sub-adult humans, but the general consensus is that this anomaly does not persist or occur into human adulthood (Dominguez and Crowder 2012; Hillier and Bell 2007; Mulhern and Ubelaker 2001). However, Andronowski et al. (2017), have recently identified the presence of osteon banding in healthy human adult males aged 47 – 69 years. Osteon banding was identified in multiple skeletal elements, including the temporal, parietal, occipital, frontal, clavicle, mandible, femur, tibia, sacrum, ulna and the second metatarsal (Andronowski et al. 2017). Andronowski et al. (2017) speculate over osteon banding being a byproduct of ossification that occurs during growth and may indeed persist into some adults, but further research is needed to assess normal, healthy variation of this phenomenon in humans. While it is important to identify and understand the different variants of osteons and their origins, where known, osteon variants will not be recorded as part of this dissertation. Rather, this dissertation is interested in type I secondary osteons.

2.7 Bone Growth and Development

Before moving into what factors can influence bone remodelling, it is important to understand the process of bone growth and development to fully appreciate how these factors can also influence how bone is formed during these early phases of human life. There are some similarities in these processes to those described above during bone remodelling, especially bone formation and deposition, but there are key differences also.

Bone is formed from both the embryological mesoderm and neural crest germ layers in two stages (Hall 2005). The first stage of bone formation is the deposition of osteoid; an unmineralised but 'bone-like' matrix and in the second stage, this osteoid is permeated by hydroxyapatite to form mineralized bone (Hall 2005). During this process, osteoid is separated from bone by the lamina limitans, a thin organic layer (Hall 2005; Scherft 1978). The cells responsible for bone deposition are osteoblasts, which stop dividing when they develop into osteocytes, but will continue to deposit bone (Hall 2005).

Bone formation that occurs during human growth, is generally categorized as either intramembranous or endochondral ossification (Ross and Pawlina 2011). Endochondral ossification is when bone formation begins with a cartilaginous model, in which cartilage serves as a predecessor for bone (Ross and Pawlina 2011). While intramembranous ossification is when bone formation occurs without this cartilaginous predecessor (Ross and Pawlina 2011). However, some complexities exist, such as the long bones, which are initially formed via endochondral ossification, but their continued growth also shares elements of intramembranous ossification, assisted by the periosteum (Ross and Pawlina 2011).

The process of bone formation, or skeletogenesis, begins with the three primary germ layers of the developing human embryo; the ectoderm (outer layer), mesoderm (middle layer) and endoderm (inner layer) (Ross and Pawlina 2011). Of these three primary germ layers, only the ectoderm and mesoderm are relevant in skeletogenesis (Ross and Pawlina 2011). Different regions of the ectoderm and mesoderm will migrate and cluster to form specific parts of the human skeleton. The skull's anterior, including dentin of the teeth and connective tissues, bone and cartilage of the face, will form from migrating neural crest cells from the closing neural tube which rises from the ectoderm (Berendsen and Olsen 2015). The cartilages and bones of the skull's posterior will form from prechordal cells, while somites (or paraxial mesodermal cells), fuse to form the axial skeleton, and mesodermal cells from the lateral plate form the appendicular skeleton (Berendsen and Olsen 2015). After migration to the sites of their respective future bones and cartilage, these cells, now mesenchymal cells begin the process of skeletogenesis, forming specific, predetermined skeletal elements (Berendsen and Olsen 2015; Hall and Miyake 1992). This initiates with the selective differentiation of these mesenchymal cells into either chondrocytes to undergo endochondral bone formation, or osteoblasts to undergo intramembranous bone formation (Berendsen and Olsen 2015). Here, both the intramembranous and endochondral ossification processes are described, with an additional examination of endochondral bone throughout continued growth.

2.7.1 Intramembranous Ossification

Beginning at approximately 8 weeks gestation in humans, intramembranous ossification initiates with the differentiation of mesenchymal cells into osteoprogenitor cells, releasing Cbfa1 transcription factor, which is crucial for osteoblast differentiation, and necessary gene expression (Ross and Pawlina 2011). Bone formation sites vascularise, and the osteoprogenitor cells undergo structural changes to differentiate into osteoblasts (Ross and Pawlina 2011). These changes include growing larger and rounder in shape, cytoplasmic changes from eosinophilic (acidic) to basophilic (basic), and the formation of a well-defined Golgi apparatus (Ross and Pawlina 2011). The newly differentiated osteoblasts will express collagens and proteins necessary for intramembranous bone formation, largely type I collagen, but also bone sialoproteins (BSP), osteocalcin, and other structural components of osteoid (Ross and Pawlina 2011).

As the osteoid matrix grows, osteoblasts will disperse but remain connected by cytoplasmic processes, and are transformed into osteocytes (Ross and Pawlina 2011; Scheuer and Black 2000). The osteoid matrix will then calcify, and the cytoplasmic processes between osteocytes will come to reside within canaliculi and the osteocytes will settle in lacunae (Ross and Pawlina 2011; Scheuer and Black 2000). Throughout this process, mesenchymal cells will increasingly populate sites of bone formation, undergoing this process of differentiation, and leading to increased bone formation site area as the matrix grows (Ross and Pawlina 2011). The initial bone spicules formed, become sites for osteoprogenitor cells to begin a process called appositional growth, whereby these spicules will grow centrifugally from the centre of ossification, and fuse to form a network of trabecular bone (Ogden 1987; Ross and Pawlina 2011; Scheuer and Black 2000; Weinmann and Sicher 1947). With continued division, osteoblast populations will increase to facilitate the growth of new trabecular bone spicules and begin to deposit layers of woven bone; an immature bone tissue categorized by voids containing connective tissues and blood vessels (Ross and Pawlina 2011). Intramembranous ossification is restricted to regions of the skull, mandible and the clavicle, and is a somewhat straightforward process compared to endochondral ossification, which is both more common and complex in human skeletogenesis (Berendsen and Olsen 2015; Kronenberg 2003; Ross and Pawlina 2011).

2.7.2 Endochondral Ossification

Endochondral ossification occurs within the majority of human skeletal elements, largely those of the appendicular skeleton, and weight-bearing regions of the axial skeleton, such as the

vertebrae (Berendsen and Olsen 2015; Kronenberg 2003; Ross and Pawlina 2011). Similar to intramembranous ossification, endochondral ossification begins at approximately 8 weeks gestation in humans and begins with the migration and congregation of mesenchymal cells at sites of bone formation (Berendsen and Olsen 2015; Hall and Miyake 1992; Kronenberg 2003; Ross and Pawlina 2011). The mesenchymal cells, stimulated by a variety of bone morphogenic proteins (BMPs) and FGFs, will begin to produce type II collagen and subsequently, differentiate into cartilage matrix forming chondrocytes, the key cell type of cartilage formation (Berendsen and Olsen 2015; Gosman 2011). The perichondrium is formed by cells on the perimeter of the condensation of chondrocytes (Gosman 2011). The chondrocytes will then secrete type II collagen, proteoglycan aggrecan and transcription factors to increase chondrocyte proliferation and cartilage matrix formation (Gosman 2011; Kronenberg 2003). As chondrocyte populations proliferate and the cartilage matrix expands, the cartilage template, called the anlagen, elongates (Gosman 2011; Kronenberg 2003;). Chondrocytes at the centre of the cartilage matrix will halt proliferation and undergo hypertrophy (cellular enlargement) and begin the production of cartilage type X, ECM and the secretion of angiogenic factors to stimulate angiogenesis in the perichondrium (Gosman 2011; Kronenberg 2003). This leads to blood vessel formation, which facilitates the migration of osteoblasts, osteoclasts and hematopoietic cells, creating the centre of primary ossification (Gosman 2011; Kronenberg 2003). This also stimulates the migration of chondroclasts to the centre of ossification, and perichondrial cells to differentiate into osteoblasts, which will produce a bone collar of cortical bone to protect the primary centre of ossification (Gosman 2011; Kronenberg 2003). Following this, the hypertrophic chondrocytes will undertake apoptosis, leaving behind the prototype of the forming skeletal element for the osteoblasts to populate the cartilage and begin to deposit bone matrix, forming the primary spongiosa – what will become trabecula bone (Gosman 2011; Kronenberg 2003).

Despite the cellular death of hypertrophic chondrocytes, the bone prototype continues to enlarge and elongate with the ongoing proliferation of chondrocytes (Gosman 2011; Kronenberg 2003). The marrow cavity is formed and filled, by hematopoietic stem cells coordinating with the stroma (Gosman 2011; Kronenberg 2003). Under the direction of both the hypertrophic and typical chondrocytes, the skeletal element will grow and change morphology based on the predetermined element that is being formed (Gosman 2011; Kronenberg 2003). In the long bones, once the skeletal element reaches a large enough size, secondary centres of ossification will form at one or both epiphyses of the cartilage, resulting in the formation and continuation of a cartilage growth plate between the epiphyses and diaphysis, even once they have been reconstructed by true bony tissue (Gosman 2011;

Kronenberg 2003). Endochondral development of the growth plates and eventual fusion of the long bone's epiphyses, is a slow process, only finishing during adolescence, following pubertal growth (Gosman 2011; Kronenberg 2003; Mackie et al. 2011). As such, the fusion of the growth plates is often used to estimate age-at-death in sub-adults (Cunningham et al. 2016). In the following section, the development of the growth plates is described.

2.7.2.1 Development of the Growth Plate

Chondrocytes within the growth plate continue the process of proliferation, production of the ECM and undergoing hypertrophy (Mackie et al. 2011). These three phases will alternate in dominance, depending on the stage of growth, skeletal element involved, and age and species of the individual (Wilsman et al. 1996). The deposition of ECM within the growth plate contributes to growth, and is populated by densely packed aggrecan, glycosaminoglycan hyaluronan and fibrils of collage type II, improving the mechanical stability and compression capacity of the developing bone (Mackie et al. 2011). The hypertrophic chondrocytes change their genetic expression to better modify existing configuration and composition of the ECM and cartilage of the growth plate to adjust as the skeletal element grows and changes (Mackie et al. 2011). Hydroxyapatite crystals will form within the ECM, surrounding mature hypertrophic chondrocytes as the cartilage growth plate will begin to mineralize (Mackie et al. 2011). Osteoclasts will migrate to the growth plate to degrade the cartilage matrix, followed by the migration of osteoblasts and bone marrow cells to begin depositing true bony tissue (Mackie et al. 2011). These contribute to the ossification of the growth plate in preparation for fusion epiphyseal fusion, and gradually, the ossification activity will outweigh that of chondrocyte proliferation, resulting in the disappearance of the growth plate cartilage, joining of the primary and secondary centres of ossification, and epiphyseal fusion is complete (Mackie et al. 2008; 2011). However, when bone growth occurs at a growth plate or an ossification centre, it is not sufficient to produce the complex adult morphology of skeletal elements, which requires a coupled process of bone formation and resorption via modelling and remodelling, throughout the bone tissue and on the periosteal and endosteal envelopes (Gosman 2011). Similar to bone remodelling, bone growth and development can be affected by intrinsic and extrinsic factors that may inhibit or facilitate these processes. The following section will introduce some of the most prevalent and most widely accepted of these intrinsic and extrinsic factors.

2.8 Intrinsic and Extrinsic Effects on Bone

There are a variety of intrinsic and extrinsic factors that have an impact upon bone tissue, leading to changes at a macro- and microscopic level. Here, age-related changes, differences

between the biological sexes, patterns associated with biomechanical loading and physical activity, genetic predisposition to bone strength and quality, the manifestation of disease and intra-skeletal differences between skeletal elements will be discussed, with particular relevance to how these manifests in terms of bone histology.

2.8.1 Biomechanical Loading

Bones act as levers in locomotion, manoeuvring the body against gravitational pull. This form of biomechanical stress, also termed loading, imparts energy to the bone, which cannot disappear, but must be stockpiled or dispersed (Currey 2002; Seeman 2008). Thus, bone has to be flexible enough to withstand and absorb the energy, and it does so by changing its morphology; shortening and widening in response to compression, and lengthening and narrowing in response to torsion, without becoming damaged through cracking or fracturing (Currey 2002; Seeman 2008). However, bone must also be lightweight for efficient locomotion and mobility (Seeman 2008; Zebaze et al. 2007). To achieve this compromise between strength and flexibility, bone is elastic, but if the bone is subjected to excessive loading which surpasses the bone's ability to morphologically adapt, plastic, irreversible damage will occur, leading to abnormal shape and the accumulation of micro-cracks to release the excess energy (Currey 2002; Lanyon and Baggott 1976; Seeman 2008; Turner 2006). To an extent, this micro-cracking is favourable, as opposed to fracturing, and can be repaired through bone natural processes, such as modelling and remodelling, but excessive accumulation of micro-cracks compromise bone strength and can increase fracture risk (Burr et al. 1998). As such, bone is under a constant pressure to be strong but lightweight in its structural composition; optimizing strength but minimalizing mass (Wang et al. 2005; 2009). In load-bearing tubular bones, such as the tibia and femur, bone will maintain strength by having a thicker layer of cortical bone, around the exterior, which also serves to protect the marrow cavity inside (Ruff and Hayes 1988; Seeman 2008). To ensure bone remains lightweight for optimal mobility and efficient locomotion, trabecular bone makes up much of the bone's interior around the marrow cavity; a porous type of bone (Seeman 2008).

Biomechanical stress associated with physical activity, affects skeletal elements differently, changing based on their capacity to bear weight and participate in physical activity (Tommerup et al. 1993). Furthermore, there is variation even within the same skeletal elements dependent on the distribution of weight during physical activity (Robling et al. 2006). Generally speaking, biomechanical stress increases the bone remodelling rate, which increases bone mass and density (Aloia 1994). This relationship also occurs inversely, meaning that when physical activity is reduced, the rate of bone remodelling decreases, which in turn decreases bone mass

and density (Aloia 1994). These effects are also reflected in bone microstructure. Frost (1997a) proposed an inverse relationship between increasing strain magnitude, or biomechanical load, and osteon diameter. He identified that both osteons and Haversian canals were smaller in the periosteal cortex, where bone formation rates increased to accommodate increasing strain, which has been replicated elsewhere (Britz et al. 2009; Burr et al. 2002; Burr and Martin 1993; Frost 1987a; 1997; Robling and Stout 2003; Skedros et al. 1994; 2001; Young et al. 1986). Generally speaking, increasing densities of both osteons and osteocytes are also consistent with increased biomechanical load and increased levels of physical activity and/or repeated strain activities (Miszkiewicz 2016; Raab et al. 1991; Skedros 2005; Skedros et al. 2005; Tommerup et al. 1993). This is because the increased new bone formation rates associated with locomotion and biomechanical loading, leads to an increase in osteon and osteocyte densities (Miszkiewicz 2016; Raab et al. 1991; Skedros 2005; Skedros et al. 2005; Tommerup et al. 1993). This association between exercise induced biomechanical stress and bone modelling and remodelling, has been shown in human applications, investigating handedness in tennis players (Bass et al. 2002; Haapasalo et al. 2000). Contrariwise, histological analysis of human immobilised limbs have demonstrated a decrease in density variables of bone microstructure (Schlecht et al. 2012). The histological responses of bone tissue to biomechanical load, have been theorized about for well over 100 years, adapting as our understanding improves.

2.8.1.1 Wolff's Law

Wolff was an orthopaedic surgeon who first proposed 'Wolff's Law' in 1892, theorising that the internal and external structure of bone reflected the direction and nature of mechanical loads applied to the bone itself (Bertram and Swartz 1991; Cole et al. 2023; Ruff et al. 2006; Wolf 1986). Wolff's Law is described in a translation of his work in 1986, p. 1;

> *"[…] the law of bone remodelling is the law according to which alterations of the internal architecture clearly observed and following mathematical rules, as well as secondary alterations of the external form of the bone following the same mathematical rules, occur as a consequence of primary changes in the shape and stressing or in the stressing of the bones."*

Wolff's Law assumes that bone responds to load in the same manner whether it is a static or dynamic applied load (Cole et al. 2023). However, Roux (1885) later observed that bone could adapt to dynamic loads, but not to static loads (Lee and Taylor 1999; Roesler 1987).

2.8.1.2 A Mechanostat Theorem and the Utah Paradigm

A mechanostat theorem was proposed by Frost (1987a), who reimagined Wolff's Law to encompass contemporary findings to better understand mechanisms behind bone metabolism and the bone response to biomechanical loading. Frost (1987a) proposed a mechanism, or mechanisms, that monitors and controls bone growth, modelling and remodelling, which all directly determine acquired bone mass. In addition, this mechanism(s), Frost (1987a) proposed how bone responds to biomechanical load through detecting musculoskeletal usage, signaling a bone response and beginning bone growth, modelling and/or remodelling to accommodate biomechanical load and keeping them within an equilibrium as much as possible. The mechanostat model allows load bone to remodel to within a set range (termed the Adapted window, see below) (Frost 1987a). However, if bone were to remodel extending beyond this range, termed the minimum effective strain (MES) and measured experimentally by a strain gauge (by the unit με), it would venture into one of three alternative windows;

1. Disuse: whereby resorption happens more rapidly than new bone formation and deposition (MES<50με).

2. Adapted: whereby bone resorption and formation occur in equilibrium above the remodelling limit (MESr = 50 – 100με).

3. Mild Overload: whereby excess bone formation occurs at the modelling limit (MESm = 1,000 – 1,500με) and bone remodelling is inhibited.

4. Pathological Overload: whereby microdamage accumulates at a rate faster than bone remodelling can occur, above the microdamage limit (MESp = 3,000με). Bone can fail entirely at a strain gauge in excess of >25,000με in young adult individuals (Cole et al. 2023; Frost 1987a).

It is important to note that these thresholds for each window vary between and even within individuals, dependent on external and intrinsic factors, some of which are discussed in this section. The Utah Paradigm of skeletal physiology is the most current, and even still, continuously evolving, understanding of bone biology (Frost 2000; Cole et al. 2023). It encompasses multidisciplinary evidence and understanding, primarily about bone as a material and organ, but also neighbouring tissues such as ligaments, tendons and fascia, as well as skeletal joints (Frost 2000). A bone's strength is determined by four characteristics; (1) bone stiffness, (2) ratios of bone types present in a cross-section, such as woven, lamellar,

plexiform, compact and trabecular, (3) the size, shape and distribution of bone tissue types, and (4) the presence or amount of microdamage (Frost 2000). Additionally, modelling and remodelling are two key biological factors in bone strength; increasing bone mass in response to biomechanical loading via modelling and increased bone formation; or decreasing bone mass in response to a lack of biomechanical loading via remodelling and increased resorption (Frost 2000).

There are four driving principles of bone functional adaptation, identified by a variety of bone biologists over several related disciplines and based upon an accumulated knowledge:

1. Bone adapts to dynamic strains, such as intermittent load and respond with appositional growth, rather than static strains which will still result in bone loss (Hert et al. 1971).

2. Bone responds locally to strain, not to strain as a whole bone entity. This means that regionally distributed strain will cause preferential modelling at periosteal sites of increased strain, rather than an even distribution of periosteal modelling about the bone surface (Lanyon et al. 1982). Additionally, >70% of longitudinal forces acting upon a bone are not uniform, leading to uneven distribution of forces between regions of a cross-section and between cross-sections, contributing to the vast variation seen at the microstructural level between histology slides even within the same skeletal element (Biewener and Bertram 1993; Stout et al. 2019).

3. Bone can still adapt in response to low strain if applied at high frequencies. This applies even in strain <10με at frequencies between 20-50hz (Rubin et al. 2002).

4. Bone can become immune to strain loading cycles after approximately 40 per day (Rubin and Lanyon 1984; Turner 1998). This is believed to be due to the oversaturation of the osteocytic network, which overproduces fluids pertaining to overstrain and reduces the osteocytic mechano-sensory response (Scheiner et al. 2016). Bone only requires approximately 4 loading cycles per day to remove the risk of disuse bone loss occurrence and having a rest period of approximately 15 seconds in between loading cycles improves the bone adaptive response dramatically (Meakin et al. 2014; Rubin and Lanyon 1984).

Initially, consensus was that body weight played a major role in the amount of biomechanical load subjected to weight-bearing bones, but as we now know, experimental evidence indicates

that instead this is attributed to muscle force, mass and strength (Martin et al. 1998). We know that non-mechanical elements can influence bone modelling and remodelling, including hormones, nutrition, microdamage and genetics (Frost 2000). Genetics and biomechanical load combine to influence bone remodelling rates with the MES range defined by Frost (2000). The MES is genetically determined and reflects threshold of biomechanical load that when levels of strain fall below it, mechanically stimulated bone remodelling halts, or is induced when strain levels exceed it (Frost 2000). As a result, the MES varies between individuals, subject to their genetic makeup and other influences on their bone biology such as those discussed herein.

2.8.2 Age

Age related changes to bone occurs at both the macroscopic and microscopic level. Loro et al. (2000) found that 60-90% of the adulthood variance in cortical thickness, volumetric bone mineral density and vertebral and femoral shaft cross-sectional areas was accounted for by variance at the pre-pubertal stage. Similar results have been replicated elsewhere (Emaus et al. 2005; 2006; Garn et al. 1992; Wang et al. 2009). This reinforces that bone health during growth and development is important for attained bone health in adulthood. During pre-pubertal growth, bone mass increases in close association with height, but this relationship reduces in adolescence, with bone mass continuing to increase past adult attained height (Bonjour et al. 1991; Glastre et al. 1990). The rate of bone mass decreases in females post-menarche, and in males at approximately 17 years of age, but male timing is closely associated with pubertal stage and androgen levels (Krabbe et al. 1979; Theintz et al. 1992). Bone mass continues to increase, but at a slower rate, with both males and females reaching peak bone mass in the third decade (Bonjour et al. 1991; Parsons et al. 1996; Recker et al. 1992). However, it appears that bone mass does not necessarily continue to increase in the third decade in all individuals, with some studies unable to identify any increase in bone mass past the age of 20 (Hui et al. 1985; Matković et al. 1979; Nilas et al. 1988). From the third to fifth decade of life, bone mass in both males and females will plateau, but bone mass in females will begin to decrease at approximately age 40, and males at approximately age 45 (Figure 2.15; Jones et al. 1994; Mazess 1982; Mazess et al. 1987; Riggs et al. 1981; 1982; Rodin et al. 1990; Warming et al. 2002). However, the age at onset of bone mass reduction appears to vary between individuals, with seemingly healthy, pre-menopausal females showing decreases in bone mass (Citron et al. 1995). In females, menopause is associated with an increase in the rate of bone mass reduction, but menopause duration is not well-defined and can vary from 5 – 10 years (Elders et al. 1988; Hui et al. 1987). Despite individual differences

in onset of bone mass reduction, both males and females, generally, will continue this reduction throughout the rest of their life (Jones et al. 1994; Mazess 1982; Mazess et al. 1987; Riggs et al. 1981; 1982; Rodin et al. 1990; Warming et al. 2002). However, this continuous bone loss, through decreased bone formation and deposition and simultaneously increased bone resorption, makes histological analyses of bone remodelling problematic as it introduces an asymptote, or threshold for the histological recording of bone remodelling events.

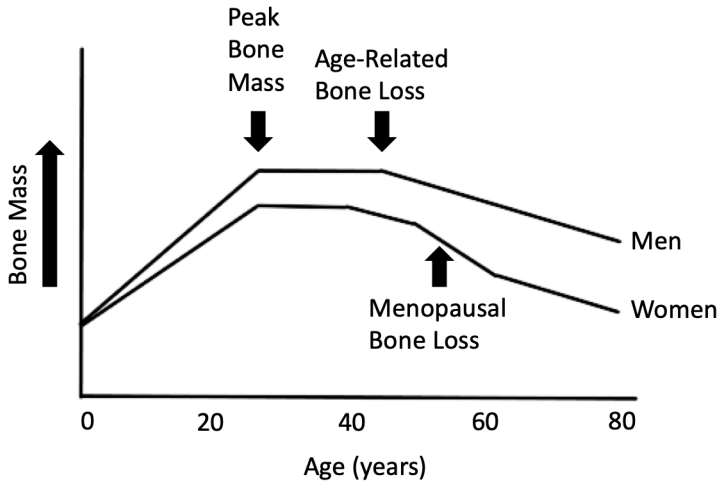

Figure 2.16: Bone mass trajectory throughout human lifespan by sex.
Image by Tahlia J Stewart (adapted from Compston 2001: 426).

2.8.2.1 Asymptote

The asymptote theory has been postulated to occur sometime after an individual reaches approximately 50 years of age (Crowder and Rosella 2007). Continuous bone remodelling throughout life, leads to the creation of fragmentary osteons, and can completely remove all evidence of already accumulated osteons as the production of new osteons overlays previous ones (Crowder and Rosella 2007; Stout and Paine 1994). Equations developed by Frost (1987b), have attempted to use predictive modelling to estimate the values of 'missing' osteons when measuring osteon population density (OPD). It is based on this premise that forensic methods of identification have been produced to estimate an individual's age-at-death using OPD (Stout and Paine 1992; 1994; Streeter 2011), methods of which have been tested and modified over the years (Crowder and Rosella 2007; Goliath et al. 2016; Paine and Brenton 2006). Although, it has been identified that age estimations based on histology are problematic as other factors, such as diet, can negatively impact both result accuracy and precision, especially when samples come from bone tissue or types that are known to be more prone to metabolic influence such as trabecular bone tissue, or elements such as the ribs or the clavicle

rather than the femur or humerus (Crowder and Rosella 2007; Dominguez and Agnew 2016; Paine and Brenton 2006).

2.8.2.2 Age-Related Changes in Remodelling

Faster rates of bone remodelling and an increased bone resorption with reduced bone formation and deposition have been identified in individuals of advanced age (Corrado et al. 2020). This is believed to be due to poorer osteoblast differentiation and activity, paired with increased osteoclast differentiation and activity which subsequently results in a reduced bone mass and mineral density and an increased risk of fracture (Kenkre and Bassett 2018). Additionally, individuals of advanced age tend to have reduced populations of osteocytes, leading to a reduced mechano-sensation and therefore reduced moderation of the bone adaptive response and homeostasis (Bach-Gansmo et al. 2016; Gaudio et al. 2010; Hemmatian et al. 2017; Javaheri and Pitsillides 2019). These changes to the bone remodelling process are largely due to this intrinsic change in cellular differentiation and activity patterns which modify bone tissues metabolic response to the same influences. This also equates to changes on the macroscopic scale, such as decreases in trabecular and cortical bone density, cortical thinning, and increased bone porosity (Corrado et al. 2020; Ebbesen et al. 1999; Kenkre and Bassett 2018; Parfitt et al. 1995). A literature review of age-related changes in bone histology will be provided in Chapter 3.

2.8.3 Biological Sex and Endocrine Homeostasis

Albright et al. (1941) reported on their discovery that estrogen deficiency was associated with the development of postmenopausal osteoporosis. In addition to providing a foundation for estrogen replacement therapy as a potential treatment for the condition, this prompted investigations into how estrogen and other hormones affect bone tissue.

2.8.3.1 Sex Steroids

Sex steroids have been identified as important regulators of bone maintenance, health and metabolism throughout life, with deficiencies having adverse effects on both males and females at all ages (Bhattarai et al. 2020; Frenkel et al. 2010; Ortona et al. 2023). Sex steroids are the key proponents in human sexual dimorphism, which transpires with puberty, leading to a larger bone size in males (Clarke and Khosla 2009; Compston 2001; Handelsman et al. 2018). Even after applying height and weight controls, males typically have increased long bone diameter and cortical thickness than females (Clarke and Khosla 2009; Compston 2001; Handelsman et al. 2018). This larger bone size and cortical thickness is believed to be

associated with biomechanical benefits and could help to explain the higher fracture risk in females than males (Compston 2001; Handelsman et al. 2018). Hypogonadism, or the decreased or complete lack of gonad hormone secretion, can adversely affect the age of attained peak bone mass in both sexes.

Estrogen

Estrogen receptors are secreted by osteoclasts and osteoblasts and the hormone itself regulates the lifespan length of bone cells by instigating apoptosis in osteoclasts and their precursor cells, and simultaneously prevents apoptosis of osteoblasts and osteocytes (Frenkel et al. 2010; Krum et al. 2008; Riggs et al. 2002). This results in the inhibition of excess bone resorption (Krum et al. 2008). Additionally, estrogen prevents osteoclast formation by inhibiting RANKL and osteoprotegrin (OPG) production by osteoblasts and osteocytes (Krum et al. 2008). This helps to explain why post-menopausal women, who have reduced estrogen levels, have an increased amount of bone resorption (Krum et al. 2008). Deficient levels of estrogens, such as 17ß-estradiol, is a key contributing factor in menopause-related bone loss and post-menopausal osteoporosis in females (Compston 2001). Clinical administration of estrogen during and after menopause can increase bone mineral density and reduce fracture risk by up to 24% (Cauley et al. 2003; Khosla and Hofbauer 2017).

Estrogen has also been identified as a crucial component in normal growth plate closure in both males and females, with deficiencies associated with delayed bone age and height attainment (Khosla 2008; Smith et al. 1994). Late menarche and premenopausal amenorrhea have been associated with low bone mass and density, with even asymptomatic ovulation disruptions leading to reduced bone mass in the spine (Biller et al. 1989; Prior et al. 1990; Rigotti et al. 1984; Rosenthal et al. 1989; Sowers et al. 1992). In addition, an individual who experiences early onset menopause has a significantly higher risk of osteoporosis (Bagur and Mautalen 1992). Estrogen has multi-factorial pathways to effecting bone tissue mechanics in both sexes; including genomic ligand/receptor interaction, ligand/plasma membrane interactions, osteoblast and osteoclast differentiation and activity and to assist in the expression of RANKL in bone-lining cells (Kelly et al. 2017; Lee et al. 2018; Lin et al. 2019; Streicher et al. 2017).

Androgens

In males, androgens, such as testosterone, are believed to play a pivotal role in pubertal skeletal growth. Late pubertal onset or androgen deficiency in males can lead to lower bone

mineral density and reduced adulthood peak bone mass, with reported increases in bone mineral density following testosterone treatment (Bertelloni et al. 1995; Compston 2001; Finkelstein et al. 1987; 1992; Frenkel et al. 2010). Testosterone treatment has also been associated with increased bone calcium, and if administered during growth prior to epiphyseal fusion, can increase attained peak bone mass (Finkelstein et al. 1989; Mauras et al. 1994). Additionally, estrogen and androgens have been identified as active components in bone mineral density and mass in their opposing biological sexes; with estrogen deficiency adversely effecting males during adolescent growth (Khosla 2008; Smith et al. 1994). Androgen deficiencies in females can delay the attainment of adulthood peak bone mass, while excessive androgen levels can lead to higher bone mineral density (Buchanan et al. 1988a; 1988b; Daniel et al. 1992; Dixon et al. 1989). Androgen receptors have been identified in osteoblasts and osteocytes, epiphyseal chondrocytes and growth plate cartilage cells, and endothelial cells in blood vessels located within bone marrow (Abu et al. 1997; Carrascosa et al. 1990; Compston 2001; Frenkel et al. 2010). These receptors in the growth plate appear to be the same between males and females and are present in all strata of the growth plate, throughout development (Ben-Hur et al. 1997; Carrascosa et al. 1990). Castration in males, which results in androgen deficiency, leads to rapid bone loss and increased rates of bone turnover (Stěpán et al. 1985). As androgens convert to estrogen, it is unclear whether it is the lack of androgens or the lack of androgen-converted-estrogens, such as 17ß-estradiol, that causes these adverse effects in bone density (Clarke and Khosla 2009).

Progesterone

Progesterone remains under-researched compared to estrogens and androgens (Prior 2018). High levels of progesterone have been associated with increased stimulation of osteoblast proliferation and differentiation due to their expression of progesterone receptors (Canalis and Raisz 1978; Klein-Hitpass et al. 1998). In contrast, females who experience a short luteal phase or anovulation in their menstrual cycle and these have been associated with diminished bone mineral density of the spine (Prior et al. 1990). These females tend to have reduced progesterone production, but normal serum estradiol concentrations, which implies that progesterone deficiency can lead to reduced bone mineral density (Prior et al. 1990). Progesterone is also used as a preventative treatment for bone loss in women, and in cyclic therapy to ensure regular menstrual cycles and healthy luteal phase ovulation (Dennerstein et al. 1985). P4, the type of progesterone used in this treatment, is osteoblastic, increasing osteoblast maturation and differentiation, and it is suggested that P4 is a potential anti-resorptive treatment due to these characteristics (Prior 2018; Verhaar et al. 1994).

Parathyroid Hormone (PTH)

PTH plays a crucial role in calcium homeostasis and is expressed by the parathyroid gland as a reaction to poor levels of serum calcium (Bhattarai et al. 2020; Jüppner et al. 1991; Katsimbri 2017). In addition to bone tissue, PTH also performs a direct role in the kidneys and an indirect role in the intestine which can aid in the metabolic absorption of necessary nutrients for optimal bone quality such as calcium and vitamin D (Bhattarai et al. 2020; Jüppner et al. 1991). In bone tissue, PTH will bind to receptors on the surfaces of osteoblasts and stromal cells, stimulating the secretion of M-CSF and RANKL, which assist to stimulate osteoclastogenesis in the remodelling activation phase (Bhattarai et al. 2020; Jüppner et al. 1991).

RANK/RANKL/OPG System

The RANK/RANKL/OPG system regulates osteoclastogenesis, thus impacting on bone resorption rates (De Leon-Oliva et al. 2023; Frenkel et al. 2010; Udagawa et al. 2021). As they circulate through the blood stream, the osteoclast precursors will produce the receptor activator, RANK, which RANKL binds, creating a crucial signal for osteoclastogensis (De Leon-Oliva et al. 2023; Frenkel et al. 2010; Udagawa et al. 2021). OPG is a cytokine that inhibits osteoclastogenesis, while the binding of RANKL to RANK receptors stimulates it (De Leon-Oliva et al. 2023; Frenkel et al. 2010; Udagawa et al. 2021). All three components of this system are produced by osteoblastic cells; stromal and bone-lining cells (De Leon-Oliva et al. 2023; Frenkel et al. 2010; Udagawa et al. 2021). A review of the literature will be conducted in Chapter 3 to outline the evidence of sex differences in bone histological microstructures.

2.8.4 Genetic Background and Ancestry

In addition to heritable traits that can influence bone metabolism, regional variance exists, which despite similarities in ethnicity, can be attributed to region-specific environmental factors, rather than ancestry or genetics (Norris et al. 2013). Scandinavia has the highest hip fracture risk in the world at 920 per 100,000 per year, while the lowest is just 4.1 per 100,000 found in Cameroon, Africa (Cheng et al. 2011; Dhanwal et al. 2010). This regional variation could be multi-causal, due to genetic or ancestral sources, environmental influence due to location of residence during early development or current location of residence; or a reflection of an individual's socio-economic status (Chantler et al. 2012; Dhanwal et al. 2010; Lauderdale et al. 1998). After puberty, higher trabecular bone density and thickness has been identified in African-American individuals (Han et al. 1996). The underlying mechanisms that cause this variance have not yet been identified but are believed to also account for a lower remodelling

rate as the increased trabecular thickness means a decrease in existing surface for remodelling (Han et al. 1996). Other US studies in adult bone health have identified faster bone remodelling rates in African-Americans over Caucasians, but others have found no variance, or even the opposite, supporting a multi-causal origin of this regional and perhaps superficial ancestral variation (Finkelstein et al. 2002; Kleerekoper et al. 2009; Perry et al. 1996). However, calcium absorption, serum vitamin D levels and urinary calcium have been found to vary between ethnic groups in sub-adults (Abrams et al. 1995; 1999; Braun et al. 2007; Bryant et al. 2003; Poopedi et al. 2011; Weaver et al. 2008). These factors can influence the calcium retention capacity of bone, for example, if an individual has a genetic predisposition for increased calcium absorption and lower urinary calcium excretion, they will have a higher calcium retention that an individual without these genetic traits (Norris et al. 2013).

Genetics and ancestry have been identified as large proponents in attained adult bone mass, with as much as 60 – 80% of variance attributed to, probably many, heritable polymorphisms (Christian et al. 1989; Dequeker et al. 1987; Havill et al. 2013; Kelly et al. 1990; Pocock et al. 1987; Seeman et al. 1996; Solomon 1968; Thandrayen et al. 2009). One polymorphism identified at the collagen 1A1 gene locus, which is also a recognition site for transcription factor Sp1, is associated with the regulation of bone mass and fracture risk (Compston 2001; Grant et al. 1996; Uitterlinden et al. 1998). Other genetic proponents of bone mass believed to play a role are linked to the vitamin D, estrogen and calcium receptor genes, as well as genes associated with cytokines and growth factors (Clark and Duncan 2015). A previous study by Richards et al. (2009) identified 9 genes associated with BMD of the femoral neck, or the lumbar spine, and an additional 4 genes with fracture risk, independent of BMD. The vitamin D receptor gene has been widely studied in an effort combat rising global frequencies of osteoporosis, and it has been suggested that 80% of variance in BMD is due to genetic variants in vitamin D receptor alleles (Morrison et al. 1994). However, it has been stated that before this can be accepted, these results must be confirmed in a genome-wide study (Clark and Duncan 2015).

Gene knockout studies in mice have identified genes that are linked to weak but flexible (Bbx, Cadm1, Fam73b), weak but brittle (Prpsap2, Slc38a10, Sparc) and strong but brittle bones (Asxl1, Setdb1, Spns2, Trim45) (Bassett et al. 2012). This means that these genes directly lead to either weakened BMD or strengthened BMD, but stronger BMD does not necessarily equate to superior bone structure, with brittleness increasing fracture risk (Bassett et al. 2012). The Bbx gene is largely linked with cartilage expression and the regulation of skeletal development, bone formation and mineralization (Ammann and Rizzoli 2003). Cadm1 appears

to be associated with the nasal bones, but not cartilage, while Fam73b is associated with cartilage, but not bone, but leads to skeletal abnormalities such as decreased body size and BMD in females, but abnormal dental morphologies in males (Bassett et al. 2012; Bernard 2003). In addition to low BMD, Prpsap2 is potentially osteocarcinogenic, or bone cancer-causing (MacDonald et al. 2009). Slc38a10 is associated with decreased body size and lowered BMD (Luyten et al. 2009). Sparc is a collagen regulator during bone formation and turnover, osteoclast maturation and activity (Boskey et al. 2003). Asxl1 has been suggested as a regulator of skeletal development and is homozygously lethal due to sever craniofacial deformity, while heterozygous individuals have minor deformities of the lumbar and sacral vertebrae (Giangreco et al. 2012). Setdb1 is suggested to be associated with osteoblast lineage and differentiation, while Spns2 regulates osteoblast and osteoclastic recruitment and migration, as well as S1P secretion; a protein involved in the coupling of bone formation and resorption (Both et al. 2012; Ito et al. 2008). Trim45, in cooperation with the protein AP-1, assists in osteoblast differentiation and bone formation (Li et al. 2008). Given the roles of these genes, it is evident that variants in them can lead to skeletal abnormalities, BMD deficiencies, increased fracture risk or abnormal bone turnover processes. Additionally, some genetically inherited traits that compromise bone metabolism, can lead to genetic disease.

2.8.5 Disease

There are four main categories of disease; genetic, degenerative, infectious and metabolic. Each of these types can be reflected in the human skeleton due to their capacity to disrupt or alter the bone remodelling process. Traditionally, research applications of ancient health and disease of these conditions have been identified due to the macroscopic presence of skeletal deformities, lesions or other abnormalities (Ortner 2003). It has been discovered that what is happening at a macroscopic level, does not always relate to what was happening at a microscopic level, it has been suggested that bone microstructure may be more accurate when ascertaining whether an individual suffered from a pathological condition (Rabey et al. 2015). Specific diseases identified or reported in the individuals or populations observed as part of this thesis are described in Chapter 4: Materials, but here, some common forms of osteological disease are discussed.

As considered in section 2.7.2, bone changes occur with advancing age, and this can result in the manifestation of degenerative diseases such as osteoporosis and osteoarthritis. These diseases have been identified in ancient humans and unfortunately remain prevalent today (Hernigou et al. 2024).

2.8.5.1 Osteoporosis

Osteoporosis is categorized as bone loss and is defined by a BMD >2.5 standard deviations below a person's expected BMD and is associated with a decrease in hydroxyapatite, per unit of bone (Aaron et al. 1987; Aloia 1994; Hui et al. 1987; Huijbregts 2001; Jones et al. 1994; Mazess 1982; Nilas et al. 1988; Riggs et al. 1982; Sözen et al. 2017; Waldron 2008; Warming et al. 2002). The process by which this loss of hydroxyapatite happens is when bone resorption exceeds bone formation and deposition (Shapovalov and Musiienko 2021). Osteoporosis can be defined as primary or secondary (Huijbregts 2001). Idiopathic, postmenopausal and senile osteoporosis are considered primary forms of osteoporosis, while secondary osteoporosis occurs as a byproduct of medication or another health condition, such as osteogenesis imperfecta (Huijbregts 2001; Waldron 2008). Senile osteoporosis affects both sexes after age 70 and is characterized by the loss of both trabecular and cortical bone, which occurs via a decrease in bone formation but maintained, or even increased resorption, in conjunction with reduced osteoblast density (Huijbregts 2001; Waldron 2008). Osteoporotic bone appears far more porous than healthy bone, with trabecular bone lacunae broader and infiltrating deeper into the cortices, widening the marrow cavity, contributing to a phenomenon called cortical thinning, whereby the layer of cortical bone reduces (Adejuyigbe et al. 2023).

2.8.5.2 Osteoarthritis

Osteoarthritis (OA) is a degenerative bone disease of the joints that is most common in weight-bearing joints such as the hips or knees (Austin 2017; Luyten et al. 2009; Tomsová and Schierová 2016; van Hove et al. 2009). Second to dental disease, OA is the most common affliction seen in human skeletal remains (Waldron 2008). Due to its degenerative nature, OA is often related to advanced age, but lifestyle factors such as excessive physical activity, joint stress, trauma, and obesity can increase an individual's predisposition (Luyten et al. 2009; van Hove et al. 2009). Any animals with synovial joints can be afflicted by OA, as it is categorized as the progressive erosion of articular cartilage over three phases of severity (Aigner and McKenna 2002; Waldron 2008). During the first phase, chondrocyte metabolism is reduced, and enzymes that erode the cartilage are released at a rate that enzyme inhibitors are unable to cope with (Aigner and McKenna 2002; Waldron 2008). The second phase is categorized by the disorganised formation of the cartilage matrix, and the fragmentation of collagen and proteoglycan, which dissipates into the joint cavity (Waldron 2008). The final phase induces an inflammatory response in the synovial membrane, due to the presence of the dispersed fragments and erosion of the articular cartilage (Lohmander et al. 1994; Waldron 2008). Following this, the synovium will increase blood flow to the area by releasing vascular

endothelial growth factor (VEGF), which facilitates new blood vessel formation (Haywood et al. 2003). Bone tissue will also attempt repair by increasing bone formation, producing osteophytes, or bony protrusions, along the joint margins (Waldron 2008). Bone formation is increased on the articular surface, but over time this can also erode to form first pitting or holes in surface topography, and eventually eburnation, or the polishing of the articular surface (Waldron 2008). As the severity of OA increases, the joint can become malformed, with the flattening and widening of the articular surfaces (Waldron 2008).

2.8.5.3 Dietary Deficiency and Metabolic Disease

Ancient and clinical skeletal research has identified several conditions linked with metabolic disease and dietary deficiencies that negatively impact skeletal tissues (Aaron et al. 1992; Appelman-Dijkstra and Papapoulos 2018; Brickley and Ives 2008; Corral-Gudino et al. 2013; de Boer and van der Merwe 2016; Ferrari et al. 2015; Gallagher 2013; Goltzman 2018; Lips et al. 2013; Lu et al. 2017; Mays 2014; Ortner 2003; Rolvien et al. 2017; Schultz 2001; Shore and Chesney 2013a; 2013b; Waldron 2008). Dietary deficiencies are often referred to as metabolic disease, as they interrupt a body's metabolism, including that of skeletal tissues (Brickley and Ives 2008). Here, several vital vitamin and mineral deficiencies are introduced briefly.

Calcium

As described previously, calcium makes up a large component of hydroapoxyapatite, Ca10(PO4)6(OH)2, which comprises the mineral component of bones and teeth and contains 99% of a human body's calcium stores. For this reason, calcium has been identified as a crucial element of nutritional importance for bone health (Bonjour et al. 1991). Supplementation of calcium as a prevention and treatment for osteoporosis has been recommended in the clinical realm, with supplementation reducing and decelerating bone loss, reducing fracture risk and increasing BMD in elderly sufferers of osteoporosis (Bonjour et al. 1991; Chapuy et al. 1992; Dawson-Hughes et al. 1997; Friedman et al. 2016; Jackson et al. 2006; Prince et al. 2006).

Childhood calcium deficiency leads to the development of rickets, which arises when the bone matrix fails to undergo normal processes of calcification (Shore and Chesney 2013a; 2013b). Vitamin D deficiency can also lead to rickets, as vitamin D is required for healthy intestinal calcium absorption (Shore and Chesney 2013a; 2013b). Advanced rickets results in distinct macroscopically observable morphological changes in bone, including bowed lower limbs, which curve outward laterally, shorter attained adult height due to reduced length and curvature of the lower limb bones, and square shaped skull and chest cavity deformities (Shore

and Chesney 2013a; 2013b). If this condition goes untreated throughout growth and development, these changes can be permanent and persist into adulthood (Shore and Chesney 2013a; 2013b). As adult bones are less pliable and have a stronger ability to withstand such severe morphological change, vitamin D and calcium deficiency in adults instead leads to osteomalacia, which is a defect in bone mineralization that leads to increased bone fragility and fracture risk (Bonjour et al. 1991). While osteomalacia and rickets are less frequent in most contemporary Western societies, they remain common in many developing countries where nutrition is inadequate.

Phosphorus

Similar to calcium, phosphorus makes up a part of the normal mineralized bone component, but unlike calcium, phosphorus is commonly found in most foodstuffs, such as dairy, meat, eggs, cereals and vegetables (Bonjour et al. 1991; Kraft 2015). In addition, many highly processed foods contain phosphate additives, meaning that the amount of phosphorus in the western diet in increasing, and this increase has been associated with decreased BMD. As such, insufficient dietary phosphorus and the need to resort to supplements are rare (Bonjour et al. 1991). However, tricalcium phosphate has been used as an effective supplement to reduce the risk of hip fracture, but the phosphate component was mainly used to stabilize the calcium-phosphate ratio during calcium supplementation (Chapuy et al. 1992). Excess phosphorus in the diet has been found to have adverse effects on bone remodelling and increase the risk of osteomalacia, largely due to its tendency to inhibit calcium and vitamin D absorption, and its association with hyperparathyroidism; all of which negatively affect bone quality (Chapuy et al. 1992).

Vitamin D Deficiency

Vitamin D is essential for osteoid mineralization, mineral absorption via the intestines and renal regulation of calcium and phosphorus absorption and secretion (Goltzman 2018). It can be synthesized into the skin by sunlight exposure or absorbed from dietary components such as eggs and fish (Shore and Chesney 2013a; 2013b). In adults, a vitamin D deficiency can lead to osteopenia (Holick 2002). Adequate vitamin D is required for the healthy uptake of calcium and phosphorus from the diet (Gallagher 2013). Thus, severe vitamin D deficiency leads to decreased serum levels of calcium and phosphorus, which halts mineralization of newly deposited bone, and systemic manifestations of unmineralized osteoid (Holick 2002). The unmineralized osteoid is weak and predisposes an individual to fracture, and can lead to

skeletal malformations in children (rickets), or osteomalacia in adults (Brickley and Ives 2008; Lips et al. 2013).

Microscopically, vitamin D deficient bone, including both rickets and osteomalacia, are categorized by insufficient cartilage and cortical bone mineralisation, with a prevalence of unmineralised osteoid (Goltzman 2018). Sufferers often also develop secondary hyperparathyroidism, which leads to an increase in bone resorption, and an over representation of Howship's lacunae, filled with many active osteoclasts (Lips et al. 2013). These characteristics are systemic, appearing throughout the skeletal elements (Goltzman 2018). While rickets and osteomalacia appear similar microscopically, there are large differences in macroscopic appearances between affected children and adults. This is because during growth, children are far more susceptible to skeletal deformities due to the lack of mineralization of osteoid, cartilage and cortical bone (Shore and Chesney 2013a; 2013b). As such, the younger an individual is at the time a vitamin D deficiency establishes, the more severe and long-lasting the manifestations are. Malformations suffered by some children due to rickets, can appear so severe to medical professionals, that it has been recognised that it can be difficult to attribute lesions and deformities to rickets or child abuse related fractures (Rolvien et al. 2017).

Vitamin C

Humans are one of the few animals unable to synthesise vitamin C from dietary glucose (Ferrari et al. 2015). Instead, sourcing vitamin C solely from dietary intake of fresh fruit and vegetables (Ferrari et al. 2015). The concentrated form of vitamin C, ascorbic acid, plays an essential role in mature cartilage synthesis, which can lead to reduced integrity of blood vessels, when their collagenic walls become compromised (Ferrari et al. 2015). Scurvy is a nutritional disease caused by a vitamin C deficiency (Brickley and Ives 2008; Ferrari et al. 2015; Mays 2014). Soft tissue manifestations of scurvy include increased bleeding, failure to heal wounds, reduced inflammatory response, cutaneous lesions due to hyperkeratosis or follicular deposition of keratin, bleeding of the gums, ante-mortem tooth loss, and alopecia (Ferrari et al. 2015; Francescone and Levitt 2005; Hirschmann and Raugi 1999; Mays 2014; Ortner 2003). Additionally, the musculoskeletal system can be affected, with 80% of scurvy patients suffering from myalgia (muscle pain) and arthralgias (joint pain) (Fain 2005). Synovitis of the joints, particularly lower joints, is rare, but can manifest in scurvy patients (Ferrari et al. 2015). Microscopically, the synovial membrane will show interstitial bleeding, with over-sized fibroblasts but reduced collagen density, as well as disorganized vascular basement

membrane (Bevelaqua et al. 1976). Clinical studies with animal models have identified the role of vitamin C in osteoclastogenesis and osteoblastogenesis, thus mediating matrix deposition and the amount and quality of collagen formed (Finck et al. 2014). While generalised bone pain is frequently reported in scurvy patients, x-rays typically fail to identify abnormalities, but inconsistent reports of bone conditions have been reported, such as cortical thinning, increased fractures, osteopenia, and if the spine and pelvis are affected, symptoms and appearance can mimic axial spondyloarthritis (Mertens and Gertner 2011; Pazzola et al. 2013).

2.8.6 Intra-Skeletal Variability

Lastly, it is important to consider that these extrinsic and intrinsic factors can impact different bones in a variety of ways and to different extents, even within the same individual. Here, the concept of intra-skeletal variation is introduced, which underpins a major component of this thesis. In-depth literature review of this concept will be discussed in Chapter 3.

Intra-skeletal variation refers to differences between skeletal elements within the same individual (Fahy et al. 2017; Stewart et al. 2021). Perhaps the most reported reason for intra-skeletal differences is that bones are subject to different patterns of biomechanical loading pressures depending on their location within the body and functional adaptation whether on an individual or evolutionary scale (Agnew and Stout 2012; Crowder and Rosella 2007; Dominguez and Agnew 2016; Karlson 1998; Paine and Brenton 2006; Stewart et al. 2021; Tommerup et al. 1993). One of the key driving principles of bone functional adaptation described in section 2.7.1, describes how bone responds locally to strain (Frost 2001; Lanyon et al. 1982). It is by this governing principle that different bones, even within the same individual, will result in vastly different patterns of biomechanical loading, which results in likewise different microstructural appearances. Additionally, bone is anisotropic, subject to many different load thresholds on a variety of directional planes, which makes for a multitude of possible combinations of biomechanical loading patterns across each skeletal element within a skeleton (Rittweger 2011; Doblaré and Garcia 2002; Iyo et al. 2004; Frankel and Nordin 2012). In fact, patterns of biomechanical loading can be influenced by just about infinite forms of human habitual behaviours, ranging from cyclical, low-force activities such as walking or running, to infrequent sudden high force activities such as jumping or more specifically landing, or changing direction at speed (Hart et al. 2020). However, as these activities trigger a local response in the bones subject to the subsequent biomechanical load patterns they involve, it automatically suggests that some bones are more frequently subject to such activities and therefore load patterns than others. For example, the activities described above; walking, running, jumping, changing direction at speed, impact upon weightbearing bones, but

would not trigger a response in non-weightbearing bones at all, as bone triggers a local response (Lanyon et al. 1982). However, seated weightlifting activities, such as bicep curls, would impact upon the upper limb bones, but would not trigger a response in other bones (Tommerup et al. 1993). As most physical activity undertaken by humans involves the long bones, these are the most impacted by biomechanical loading and are the strongest load-bearing bones in the human skeleton (Hart et al. 2020).

In addition, different bones are subject to different rates of bone remodelling, which further influences the appearance and densities of bone microstructures (Amprino and Marotti 1964; Fahy et al. 2017; Mulhern 2000; Skedros et al. 2003; 2013a; Stewart et al. 2021; Vajda et al. 1999; Wilson et al. 1998). Bone remodelling rates vary greatly between cortical and trabecular bone, and between bone types themselves, associated with the surface: volume ratio differences between bone shapes and sizes (Parfitt 2002b). Even when just considering cortical bone of the differences bone of the skeleton, there is a great variety in bone remodelling rates (Katsimbri 2017). For example, due to constant loading from the surrounding musculature from respiration, the ribs are never totally at rest, and the cortical bone in ribs remodels relatively fast, at 4% annually in adults >50 years of age (Frost 1969; Skedros et al. 2013a). Femoral cortical bone is much denser than cortical bone observed in the rib and is believed to have a comparatively slow remodelling rate (Frost 1969; Skedros et al. 2013a; Tommerup et al. 1993).

Variability can even occur within a single skeletal element (Stout et al. 2019). This is once again due to the principle of bone functional adaptation that stipulates that bone responds locally (Lanyon et al. 1982). This may prove problematic for histology, which takes a single slice of bone to observe microscopically. When considering which bones to observe for this research, a pilot study was conducted looking at intra-skeletal variation, to see which bones were subject to the most amounts of biomechanical loading and thus, which weren't and therefore might be best representative of systemic health (Stewart et al. 2021). From these results, it was clear that the femur and the rib were suitable choices, and while this was the hypothesis based upon the literature, it had yet to be experimentally demonstrated within an intra-skeletal model (Stewart et al. 2021). The rib is a good histological measure for inter-individual observation, as it is more 'controlled' than the femur with less variation due to biomechanical loading (Lanyon et al. 1982; Skedros et al. 2013a; Stewart et al. 2021; Tommerup et al. 1993). Thus, by examining rib histology as opposed to the femur, it allows us to control for individual differences in biomechanical pressures and physical activity where the femur would not. Further, by selecting the femur as the secondary bone to observe as part of

this research meant that it was also possible to still observe those nuances the rib might overlook, such as individual patterns of behaviour and physical activity (Skedros et al. 2013a; Stewart et al. 2021; Tommerup et al. 1993).

It is still poorly understood how the extrinsic and intrinsic factors introduced in this chapter influence bone microstructure, particularly between two bones inherently different metabolisms and within the same skeletal element. Thus, a major component of this dissertation focuses on how two bones of different metabolic patterns respond to a variety of factors including age-at-death, biological sex, physical activity and systemic health. Another component of this dissertation looks closely at intrinsic differences between the two bones in terms of osteon and Haversian canal sizes and shapes and how these differ between a bone that is subject to varied patterns of biomechanical loading versus one that is subjected to constant, stable biomechanical loading. An additional component focuses on intra-skeletal variation and looks at changes within the same rib to answer methodological questions of sampling for histological analysis, but also to inform upon bone biology and improve our understanding of intra-skeletal variation. Chapter Three will engage with the literature, exploring the evidence relevant for each research question in turn.

Chapter 3 Literature Review

This chapter reviews the literature on human rib and femur histology by paying particular attention to these two different bones' metabolic activity and how it relates to their histology. Studies comparing the femur and rib intra- and inter-skeletally are discussed, as well as studies assessing each bone separately. Ancient, modern, and animal specimens are discussed to review what is known about bone histology in these two bones across anthropological, archaeological, clinical/biomedical, and animal experimental research. A brief introduction to the history of histological approaches in anthropology and archaeology is provided at the start of the chapter to introduce the technique and highlight its rarity in application in these fields.

3.1 Histology, A History

Histology is the microscopic study of tissue and cellular structure from living organisms (Guo et al. 2020). In the clinical realm, histology is the gold standard in the assessment of tissues or cells for diagnosis of a range of conditions and diseases (Guo et al. 2020). Its use in bone is generally limited in a clinical context due to the invasive nature of sample collection (De Boer et al. 2013; Nicolau et al. 2025). However, in academic, clinical and scientific research, bone histology, and specifically bone histomorphometry, the measurement of bone microstructure size, shape and density, is extremely valuable as a tool to reconstruct patterns of bone structure and metabolism (Dalle Carbonare et al. 2021; Hughes-Austin et al. 2025; Kulak and Dempster 2010; Miller 2008; Nicolau et al. 2025). Bone histology is not a new concept. Beginning in the anatomical sciences, the study of human bone tissue and its microstructural organisation was first conducted in 1691 by Clopton Havers (1657-1702), who is also the namesake of the Haversian canal, a structure he first identified (Havers 1691). The development of histology as a disciplinary tool, was only made possible with the invention of the microscope, which interestingly owes credit for its invention to the field of optometry.

3.1.1 Early Applications of Microscopy and Bone

The first microscope was invented in 1590 by an early optometrist Hans Jansen, who discovered that a pair of spectacle lenses inside a long tube were capable of magnifying incredibly small objects (Genung 1942). Over the next 30 years, several other individuals made this same discovery, leading to the development of a more complex model in the 1620s, complete with a rotating platen and height adjustable stage which was capable of magnifying objects up to 50,000 times (Barellus 1665; Genung 1942). Along with instructions on how to use the stage and platen, Petrus Barellus stated that the microscope should be used in full sunlight to best illuminate the sample being observed, perhaps a rudimentary, pre-electric form

of light microscopy (Barellus 1665; Genung 1942). Following these rudimentary models, inventors focused their efforts on simplifying designs into singular lenses and increasing magnification potential (Hooke 1665). However, the majority of users were still driven primarily by curiosity rather than scientific profession and it would be many years before anatomists or biologists saw the value in microscopy and this slowed technological advancement during this time (Genung 1942). Problems with these earlier models included chromatic aberration, which was not rectified until 1811, when Bernardino Marzoli, an Italian optician created an achromatic objective allowing clearer imaging resolution (Genung 1942; Mayall 1890).

The application of the microscope in the anatomical sciences became more systematic in the 18th century and greatly expanded in the 1830s with the technological improvements made with the compound microscope and development of singular achromatic lenses which improved the microscope's resolution further (Barbero and Raynaud 2023). It was due to these technological improvements that Theodor Schwann and Matthias Jakob Schleidon first identified in 1837 that cells are the basic organisational unit in all organic organisms (Aminoff and Daroff 2003: 215-217; Aszmann 2000; Thomas 2017). Thin sections of highly transparent tissues and other specimens became a necessity for observation under light microscopy, requiring the development of advanced dissection techniques and the invention of specialised equipment such as microtomes to produce thin sections of specimens (Abd El-Aziz et al. 2025; Quekett 1848). Biologists began experimenting with synthetic dyes to better observe and distinguish between microstructures by staining tissues a variety of colours (Bracegirdle 2002). By the end of the 19th century, the production of thin sections and staining for viewing under the microscope had become gold standard in the anatomical sciences, and the fields of histology and cytology; the study of cells, had been well established (Diamantis et al. 2013), with clinicians using histology and cytology to diagnose their patients (Krönig 1887; Menetrier 1886).

By the mid-20th century, Harold Frost, an orthopaedic surgeon, and Lent Johnson, a pathologist, were leading the field on the principles of bone biology, functional adaptation and structure (Frost 1964; Webster 2005). It was around this time that Milch et al. (1958) first employed a quantitative analysis of bone histology, which previously was largely used in a descriptive, or qualitative manner. Alan Boyde and colleagues had also begun using the newly developed Scanning Electron Microscope (SEM) to identify more complex fine structures within bone microtissues (Boyde and Hordell 1968; Boyde and Jones 1968).

3.1.2 Histological Applications in Bioarchaeology

The first application of histology in past humans was conducted by a clinician JN Czermak in 1879, where an Egyptian mummy was diagnosed with arteriosclerosis, a condition characterised by the thickened and hardened arterial walls (Aufderheide 2003; Aufderheide and Rodríguez-Martin 1998; Denton 2008). In 1891, bone histology was first applied in archaeological human bone by pathologist Theopfil Mitchell Prudden (Garland 1993). Prudden identified periostitis and osteomyelitis from the histology of two tibiae from a prehistoric adult excavated in Colorado, believing it to be evidence of a possible syphilis case (Garland 1993). Extensive histological analysis was conducted by Ruffer (1921) on several organs of Egyptian mummies, with illustrations and photographs published to assist in their description. However, despite these earlier studies, Wilhelm Graf (1949) was the first to define paleohistology as "the examination of microscopic sections of ancient human beings and the recognising of tissues and cells in such sections". (Graf 1949: 236).

In the 1960s and 1970s, bone histology grew within bioarchaeology and biological anthropology, looking at human bone microstructure in past humans (Ahlqvist and Damsten 1969; Kerley 1965; Kerley and Ubelaker 1978; Martin and Armelagos 1979; Richman et al. 1979; Stout 1976). These applications primarily looked at patterns in relation to age-at-death (Ahlqvist and Damsten 1969; Kerley 1965; Kerley and Ubelaker 1978), dietary patterns and patterns relating to physical activity and lifestyle (Martin and Armelagos 1979; Richman et al. 1979). Over the following 40-50 years, studies of human bone histology in bioarchaeology and biological anthropology have further studied the effects on human bone tissue with advancing age (Stout and Paine 1992; Stout and Lueck 1995; Cho et al. 2006), and how bone tissue is influenced by repeated physical activities and behaviours with varying mechanical load (Bridges 1990; Larsen and Ruff 1990; Robling and Stout 2008; Ruff 1992; Ruff and Hayes 1983a; 1983b; Ruff et al. 2006; Shaw and Stock 2009a; 2009b; Weiss 2005). However, still today, there are few studies that investigate intra-skeletal differences within and/or between individuals (e.g. Peck and Stout 2007; Stewart et al. 2015; 2021). This is due to a variety of reasons, but largely due to a lack of expertise available and thus training provided to students in most archaeology and biological anthropology courses, including in-depth understanding of sex and age-at-death estimation techniques (Paine 2007). Additionally, histology has traditionally required access to prohibitively expensive laboratory equipment, consumables (Maggio et al. 2019; Paine 2007) and access to samples is limited due to the irreversible and invasive nature of the technique (de Boer et al. 2013; Nicolau et al. 2025). However, there has been development and publication of inexpensive materials (García-Donas et al. 2017; Maggio

et al. 2019; Paine 2007), and a push from biological anthropologists and bioarchaeologists alike to expand into neighbouring disciplines to employ novel techniques (Buikstra et al. 2022), such as the application of geographic information systems (GIS) in spatial studies of bone histology (Mallouchou et al. 2020; Rose et al. 2012). In addition, there has been a very recent expansion of bone histology begin within the southern hemisphere, particularly into the Oceania and Asia Pacific Region (Maggio 2022; Maggio and Franklin 2019; 2021; Miszkiewicz et al. 2020; 2021; 2022a; b; Pedersen et al. 2024; Snoddy et al. 2022; Walker et al. 2023a; 2023b).

Prior to the last few years, many of the studies conducted on human bone have been limited to European and American samples, with very little conducted within Australia and the wider Pacific region until recent years, particularly involving intra-skeletal studies of the rib and femur (Miszkiewicz et al. 2022; Pederson et al. 2024; Figure 3.1). Figure 3.1 illustrates the scarcity of studies comparing both the rib and the femur on a global scale, with 16 conducted around the world, but only one of which observed an Australian sample (Pederson et al. 2024). As such, there is a large gap in the literature based upon the geographical region alone and a need to improve our understanding of bone metabolism and intra-skeletal variation within the Australian population and wider Pacific region. It is important to expand focus into individuals within the Australian and wider Pacific region because genetics and population history are known to impact bone metabolism (Christian et al. 1989; Dequeker et al. 1987; Havill et al. 2013; Kelly et al. 1990; Pocock et al. 1987; Seeman et al. 1996; Solomon 1968; Thandrayen et al. 2009), and so different populations can have variation in their histology. This has implications for biomedical research in trauma and orthopaedics (Austin et al. 2024; Jha et al. 2019; Weiss et al. 2017) and for anthropological/bioarchaeological approaches to reconstructing past bone biology and behaviour (e.g. Burr et al. 1990; Eleazer and Jankauskas 2016; Miszkiewicz and Mahoney 2016). Further, no studies have directly compared contemporary Australian samples to ancestral British samples to better contextualise Australian bone metabolism and intra-skeletal variation in the broader literature.

In the section below, the key literature is discussed, beginning with studies that conducted human bone histology on both the rib and femur in archaeological humans, followed by studies that observed bone microstructure in either the rib or the femur separately. The literature is then expanded to included anatomical donors, and lastly, animal experimental studies.

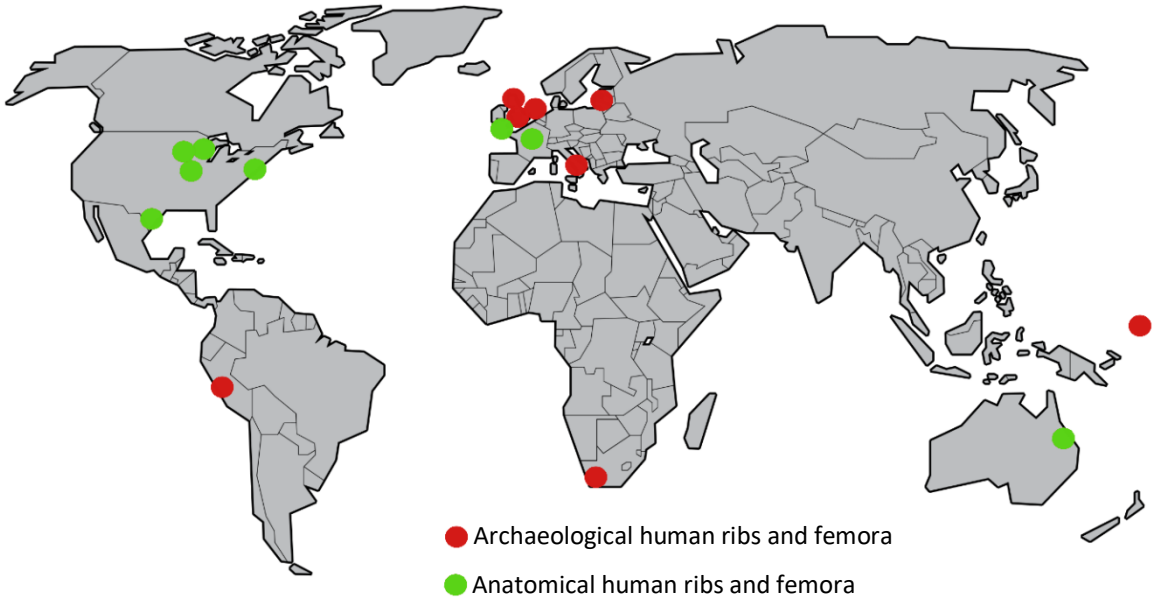

Figure 3.1: Map of key studies of human rib and femur histology in archaeological and modern anatomical remains.

3.2 Histology of the Rib and Femur

Literature documenting bone microstructure of the rib and femur can be separated into archaeological, anatomical human, and animal model experimental evidence. Here, the archaeological evidence is discussed first since it relates directly to the thesis research questions. Specifically, studies comparing rib and femoral histology are focussed on, followed by the anatomical human evidence, whereby rib and femoral histology of contemporary or cadaveric humans have been examined. Lastly, the experimental or animal evidence is explored, whereby studies have observed rib and femoral histology using an animal model in either an observational or experimental study design. The literature review is presented chronologically because histology techniques have advanced with time, so the more recent publications present more detail in terms of results. From the literature covered within, key areas of focus and research gaps will be identified, and at the end of this chapter, the research questions will be stated and their corresponding hypotheses formulated.

3.2.1 Archaeological Evidence

The histological studies of archaeological human ribs and femora are listed in Table 3.1, outlining where the individuals originated from, and which histological variables were examined. Additional studies have observed histological variation in the femur and rib separately, investigating intra-element variation (femur: de Gruchy et al. 2024), inter-

populational variation (rib: Stout and Lueck 1995; femur: Burr et al. 1990; Ericksen 1980; Thompson and Gunness-Hey 1981), effects of limb disuse (femur: Lazenby and Pfeiffer 1993), socioeconomic status (femur: Miszkiewicz and Mahoney 2016), effects with dietary differences (rib: Paine and Brenton 2006; femur: Richman et al. 1979; Thompson and Gunness-Hey 1981), age-at-death and sex (rib: Pfeiffer et al. 2019; Mulhern 2000; femur: Martin and Armelagos 1979; Thompson et al. 1981).

Table 3.1: Table 3.1 Histological studies of Archaeological Human Ribs and Femora.

Publication	**Sample**	**Histomorphometry/Cross-Sectional Geometry Variables**
Pfeiffer 1998	Spitalfields (England) *n* = 20 St. Thomas (Canada) *n* = 21	Osteon Area Haversian canal Area
Robling and Stout 2003	Paloma *n* = 48	Osteon Population Density
Pfeiffer et al. 2006	South Africa *n* = 44 Spitalfields *n* = 20 St. Thomas *n* = 20	Osteon Area Haversian canal Area
Cho and Stout 2011	Imperial Romans *n* = 149	Osteon Population Density Osteon Area Total Subperiosteal Area Cortical Area Endosteal Area Relative Cortical Area
Eleazer and Jankauskas 2016	Lithuanian Alytus *n* = 30, sub-adults <7 years old	Osteon Area Osteonal Bone Area Cortical Porosity Total Cross-Section Area Endosteal Area Cortical Area %Cortical Area
Fahy et al. 2017	St. Gregory's *n* = 10	Osteon Population Density
Karydi et al. 2022	St. Peter's *n* = 14	Cortical Area Intact Osteon Number Fragmented Osteon Number Intact Osteon Density Fragmented Osteon Density Osteon Population Density Osteon Area Relative Cortical Area Osteon Circularity Percentage Osteonal Bone
Miszkiewicz et al. 2022	Marshall Islands *n* = 1	Haversian canal Density Haversian canal Area

The first study to observe cortical bone of the femur and rib histologically in archaeological humans was by Pfeiffer (1998). Pfeiffer (1998) set out to quantify osteon and Haversian canal area in a variety of recent, but still archaeological, human populations, and to determine the natural human range of these measurements. At that time, very little existed in the literature about cortical osteon geometry and so this paper greatly expanded knowledge in osteon and

Haversian canal area variation (Evans 1976; Stout 1976; Stout and Teitelbaum 1976). One sample included in this study are from the Spitalfields skeletal collection, an 18thC population excavated from a crypt in Spitalfields, London who died between 1756-1835 (Pfeiffer 1998). Within this sample there are 9 females and 11 males, all with known age-at-death (ranging from 25-50 years) and represented by paired rib and femur sections (Pfeiffer 1998). The sample termed St. Thomas were sourced from a 19thC settler population excavated from St. Thomas Church in Ontario, Canada (Pfeiffer 1998). Within this sample there are 7 females and 14 males, all with known age-at-death (ranging from 17-81 years) and represented by paired rib and femur sections (Pfeiffer 1998). Pfeiffer (1998) was interested to identify to what extent microstructural variability could be attributed to factors such as biological sex, age-at-death and population or geo-location. The femoral osteon area was significantly larger than that of the rib in the Spitalfields and St. Thomas samples, as well as when the samples were combined. However, the difference was not as pronounced in the St. Thomas samples (Pfeiffer 1998). When Pfeiffer (1998) looked at this relationship within individuals, there were only two of 40 individuals with larger osteon and Haversian canal area in the rib than femur and these were both females from the St. Thomas sample set. Haversian canal area was statistically significantly larger in the femur than the rib both overall and in the Spitalfields sample, but there was no significant difference in the St. Thomas sample (Pfeiffer 1998). Additionally, femoral osteons had a range in size of approximately 10,000μm^2, while osteons in the rib only ranged in size approximately 4,000μm^2 (Pfeiffer 1998). No significant difference between the sexes were identified, but osteon area was frequently smaller in females than males in the femur, while Haversian canal area was no different either in trend or significance (Pfeiffer 1998).

However, Pfeiffer (1998) did identify significant positive relationships between femoral osteon and Haversian canal area and age-at-death in the Spitalfields sample, but not in the samples from St. Thomas. Similar to the femoral osteons, osteon area in the rib was larger in females than males for both the Spitalfields and St. Thomas samples, but this was not statistically significant (Pfeiffer 1998). There were no relationships identified between osteon or Haversian canal area and age-at-death in either sample (Pfeiffer 1998). However, this study was limited as the only variables collected were osteon and Haversian canal area and so no density or shape variables were collected as part of this research. Additionally, other cross-sectional geometry variables could have provided insight into age-related changes, such as cortical width or endosteal area to observe the cortical thinning phenomena (Agnew and Stout 2012).

In contrast to Pfeiffer (1998) who was focused on osteonal geometry for more broad remodelling inferences, Robling and Stout (2003) were interested in reconstructing

remodelling rates and thus collected osteon population density (OPD). Robling and Stout (2003) examined human bone histology on ribs and femora from a sample of the archaeological Paloma skeletal sample. The Paloma date from 7800 – 4600 BP and were located on an ancient archaeological site on the central coast of Peru approximately 65km south of Lima (Robling and Stout 2003). Throughout site occupation, the inhabitants included in this study initially participated in an almost exclusive hunter-gatherer subsistence strategy, requiring significant physical activity as they would travel across the Andes foothills (Robling and Stout 2003). By the end of the time period investigated, they subscribed to a settled maritime-based economy which was increasingly sedentary by comparison, requiring far less movement (Robling and Stout 2003). The authors believed this would enable a good sample with which to investigate the effects of shifting levels of physical activity through time in a genetically and environmentally similar population (Robling and Stout 2003). Femoral OPD was regressed against rib OPD using a reduced major axis regression (Robling and Stout 2003). This demonstrated that some individuals had elevated remodelling in the femur while others had decreased remodelling as compared to the rib, then should be expected based on rib remodelling rates as inferred by the OPD as well as body size alone (Robling and Stout 2003). Robling and Stout (2003) interpreted this to mean that individuals with increased femoral remodelling over the rib was evidence that they partook in higher levels of physical activity and therefore increased biomechanical loading than those who had decreased femoral remodelling as compared to the rib. We now know that osteon size and circularity also hold valuable information regarding biomechanical load that could have been missed from this study by excluding these variables. For example, van Oers et al. (2008a; 2008b) identified that osteons with a smaller area were associated with areas of increased strain and Schlecht et al. (2012) and Lazenby and Pfeiffer (1993) demonstrated that limb disuse will result in large as well as fewer osteons. Additionally, compression or tensile loading tends to result in more circular shaped osteons, while torsion may result in elliptical shaped osteons which are less resistant to bending (Rothschild and Panza 2007).

Pfeiffer et al. (2006) followed up Pfeiffer's 1998 study by the addition of another archaeological sample of human femora and ribs, and continued with a re-analysis of osteon and Haversian canal area. This newly sampled population was from Later Stone Age foragers from a variety of archaeological sites spread throughout the south and west margins of the South African Cape (Pfeiffer et al. 2006). The 44 individuals (19 males, 25 females) examined were dated to approximately 6000-800 BP, but unlike the previously examined individuals from Spitalfields and St. Thomas, the samples from South Africa were largely not pair matched femora and ribs (Pfeiffer et al. 2006). Only four of the 44 individuals had both a femoral and rib sample provided

for the study (Pfeiffer et al. 2006). Similar to Pfeiffer's 1998 work, osteon and Haversian canal area were the focus variables and the new data from the South African individuals were added to the original 1998 analysis (Pfeiffer et al. 2006). With osteon data from all three populations pooled, rib osteon area was found to be significantly smaller than that of femoral osteons, but sex and age-at-death were not found to be significant factors in osteon size (Pfeiffer et al. 2006). Haversian canal area was not significantly different between the rib and femur and neither sex nor age-at-death were significant factors in Haversian canal size variability (Pfeiffer et al. 2006). Osteon area was significantly smaller in the rib than femur for all three populations when examined separately, but Haversian canal area was not significantly different between the rib and femur and did not have a significant relationship with age-at-death or sex (Pfeiffer et al. 2006). The authors then calculate the median osteon and Haversian canal area femur:rib ratio which demonstrated a large amount of variability between the three populations (Pfeiffer et al. 2006). Femoral osteon area to rib osteon area ratio was largest in the Spitalfield individuals, followed by the St. Thomas and lastly by the South African individuals (Pfeiffer et al. 2006). While femoral Haversian canal area to rib Haversian canal area ratio was also largest in the Spitalfield individuals, they were followed by the South African individuals and the St. Thomas individuals had larger Haversian canals in the ribs than the femur (Pfeiffer et al. 2006). The intra-skeletal comparison of paired rib and femora identified several individuals that did not fit the normal pattern of larger osteon and Haversian canal area in the femur (Pfeiffer et al. 2006). Two individuals in the South African population sampled, two of 20 in the Spitalfields population sampled and two of 20 in the St. Thomas population sampled had the same size or larger structures in the rib (Pfeiffer et al. 2006). The authors state that convention suggests that smaller femoral osteon size in the South African individuals might imply a high level of physical activity but the females from the St. Thomas population have smaller femoral osteon area than the South African individuals and historical documentation and archaeological evidence does not agree with this (Pfeiffer et al. 2006). As such, the authors conclude by stating that secondary osteon and Haversian canal area should not be used to infer behavioural patterns of physical activity in past humans at this time (Pfeiffer et al. 2006).

Similarly, Pfeiffer and colleagues (2006) stated that osteon and Haversian canal area also does not play a logical role in age-at-death estimation or estimation of sex based on their results. Based on the results on their study and the particular samples they used, this may be correct, but it is important to investigate these relationships further with larger sample sizes, using paired rib and femur samples wherever possible, in individuals of known age-at-death and known sex and in individuals from the same or similar genetic and/or environmental background in order to control for as many aspects of potential variation as possible. It may

be true that there is no relationship between osteon and Haversian canal area, age-at-death, biological sex and physical activity patterns, but this study was in a limited sample of three archaeological populations of different environmental and genetic ancestry, with 84 individuals when pooled, but some subgroups of less than ten (Pfeiffer et al. 2006). A similar study conducted by Ericksen (1980) observed differences in femoral bone microstructures in three Native American populations and identified significant differences between each population, which they associated with different subsistence and labour strategies between them. Similarly, Thompson and Gunness-Hey (1981) also identified differences in femoral human bone microstructure between 3 Inuit populations and a Caucasian population from the US, which they stated could be related to different subsistence strategies, patterns in repeated activities and dietary components. Ericksen (1980) also identified significant increases in osteon population density with advancing age-at-death. A possible explanation for the lack of inter-populational differences found by Pfeiffer et al. (2006), could be related to hierarchical differences within populations which could be masking true differences. Miszkiewicz and Mahoney (2016) identified differences within a single population based on socio-economic status, which has been historically documented as determining an individual's level and type of physical activity (as well as diet quality, see Richman et al. 1979; Paine and Brenton 2006, for histological effects of diet on femoral and rib histology respectively) and therefore, biomechanical loading patterns visible in their femoral microstructure. It is important to state that Pfeiffer et al. (2006) was a landmark paper with the most comprehensive work at that time in osteon and Haversian canal geometrics in the rib and femur.

Cho and Stout (2011) were the first histological study of the femur and rib to measure OPD and osteon size, as well as cross-sectional geometry variables. They examined human femoral and rib bone remodelling in an Imperial Roman sample excavated from the Isola Sacra necropolis approximately 23km west of Rome. These 149 individuals are dated to approximately 1700 BP and were of the middle-class from an urban society who's lives and livelihoods centred around the local harbor (Cho and Stout 2011; Garnsey 1999; Meiggs 1973). Only adult individuals were included in the analysis and age-at-estimation was conducted based on cranial suture closure, dentition wear pattern, pubic symphysis and auricular surface morphology (Cho and Stout 2011; Prowse et al. 2004). Sex estimation was conducted based on cranial and pelvic morphology as well as long bone metrics (Cho and Stout 2011; Prowse et al. 2004). Of the 149 individuals, 114 were paired samples of rib and femur cross-sections (Cho and Stout 2011). In the rib, mean OPD had a significant positive relationship with age-at-death and females had significantly larger OPD than males (Cho and Stout 2011). Contrary to Pfeiffer et al. (2006), Cho and Stout found that osteon area in the rib had a significant negative

relationship with age-at-death, and that males had significantly larger mean osteon area in the rib than females (Cho and Stout 2011). Conversely, in the femur, there were no statistically significant relationships identified between OPD or osteon area and age-at-death and sex (Cho and Stout 2011). In the rib, Cho and Stout (2011) identified significant positive linear relationships between body mass and total cross-section area, cortical area and endosteal area. Males had statistically significantly larger mean total cross-section area than females (Cho and Stout 2011). In female ribs, cortical area decreased with age-at-death, but in males, cortical area decreased in mid-life and then increased in individuals with age-at-death >50 years old (Cho and Stout 2011). This contrasts with findings by Pfeiffer et al. (2019) who determined that there was a significant decrease in cortical area with advancing age in pooled sexes. Cho and Stout (2011) also found that males have a significantly larger endosteal area than females (Cho and Stout 2011). Mean cortical area and total cross-section area both decrease with increasing age-at-death (Cho and Stout 2011). In the femur, there was also a significant positive linear relationship between body mass and total cross-section area, cortical area and endosteal area (Cho and Stout 2011). Femoral total cross-section area increased with advanced age-at-death and males had a significantly higher mean total cross-section area than females (Cho and Stout 2011). Femoral cortical area in males was significantly larger than females, but age-related changes in cortical area were not statistically significant (Cho and Stout 2011). Cho and Stout (2011) found that femoral mean endosteal area significantly increased with age-at-death, which agrees with prior literature published by Martin and Armelagos (1979) who identified that both males (4.9%) and females (10.7%) suffered significant net loss of femoral cortical bone (Cho and Stout 2011). Intra-skeletal analysis of paired rib and femoral samples identified that cortical area and total cross-section area of the femur are larger that the rib, but mean OPD in the rib was higher than in the femur (Cho and Stout 2011). Mean osteon area did not significantly differ between the femur and rib (Cho and Stout 2011). Female cortical area and total cross-section area decrease with advancing age in both the femur and rib (Cho and Stout 2011). However, in males the cortical area and total cross-section area decrease with advancing age was higher in the femur than the rib (Cho and Stout 2011). There were no statistically significant relationships between age-at-death or sex and OPD in the femur or rib, which echoes results by Stout and Lueck (1995) who failed to identify any significant difference in OPD between sexes (Cho and Stout 2011).

Similar to Cho and Stout (2011), Eleazer and Jankauskas (2016) also used a combination of cross-sectional geometry and histomorphometry to examine the femur, humerus and rib, bones of different patterns in loading regimes and under different metabolic pressure. The samples were collected from late medieval humans from a Lithuanian cemetery which dated

to the 14th – 18th century (Eleazer and Jankauskas 2016). The authors chose to use a single population sample to reduce individual variation in physical activity levels, dietary differences and geographical and temporal differences (Eleazer and Jankauskas 2016). Historical documentation records common occurrence of disease, malnutrition and traumatic injury at this site (Jankauskas 1994; 1998; Jankauskas and Urbanavičius 1998), leading to a high level of population stress in the individuals interred here (Eleazer and Jankauskas 2016; Jankauskas 1994; 1998; Jankauskas and Urbanavičius 1998). Populations within this region, including the population examined by Eleazer and Jankauskas (2016), also had reduced adult attained stature and slowed growth rates in sub-adults (Šereikienė and Jankauskas 2002; 2004). The individuals examined in Eleazer and Jankauskas (2016) could not be categorised into socio-economic groups based on grave-goods as this was not a common practice in Alytus culture. Despite this, social class divides were large in this region, which was a Feudal society during the time of the Alytus culture, and suggests a range of social classes present in the Alytus population (Eleazer and Jankauskas 2016).

Eleazer and Jankauskas (2016) observed cortical bone microstructure in 30 sub-adult (<7 years old based on age-at-death estimation methods) individuals, separated into a group with skeletal lesions present and another without skeletal lesions. Skeletal lesions observed in the study included cribra orbitalia, periostitis, porotic hyperostosis and enamel hypoplasia which have all been associated with a range of chronic, fatal and non-fatal health conditions, ranging from nutritional deficiency to osteomyelitis, but generally assumed to have lived long enough with their condition to have formed a skeletal lesion (Buikstra and Ubelaker 1994; Goodman and Rose 1990; Ortner 2003). The group without skeletal lesions present were assumed to either have no-stress, meaning they died by either violent or accidental death, or had an acute condition whereby they died before a skeletal lesion could develop (Eleazer and Jankauskas 2016). Eleazer and Jankauskas (2016) observed cortical bone at the rib midshaft to observe bone metabolism, femoral midshaft to observe patterns in biomechanical loading, and the humeral midshaft as an intermediate between the other two elements.

Histomorphometry variables observed included intact osteon area (On.Ar), osteonal bone area (On.B.Ar) which is the accumulative total area of bone inhabited by intact and fragmented osteons and cortical porosity (Ct.Po) which is the total area of bone inhabited by porosities such as resorption spaces and Haversian canals (Eleazer and Jankauskas 2016). Cross-sectional geometry variables observed included total cross-section area (CSA), endosteal area (Es.Ar), cortical area (Ct.Ar) and % cortical area (%Ct.Ar) (cortical area/total cross-section area) (Eleazer and Jankauskas 2016). Eleazer and Jankauskas's (2016) results demonstrated

that there was no statistically significant difference in any of the cross-sectional geometry variables in either of the long bones between the lesion and non-lesion groups. However, all cross-sectional geometry variables in the rib were larger in the lesion group, which Eleazer and Jankauskas (2016) attribute to endosteal bone loss, leading to an increased endosteal area, but periosteal bone gain, leading to increased cortical and total cross-section area. However, the authors state that most of their geometric results were not statistically significant and fail to include *p*-values for any of their numerical results, which makes it difficult to interpret which results are significant (Eleazer and Jankauskas 2016). There were general trends suggesting that consistent increases in all cross-sectional geometry variables are associated with skeletal lesion presence, which was strongest in the rib but still the case in the humerus and femur as well to a lesser degree; for example Es.Ar was ~23% larger in the lesion presence ribs, 11% larger in the femora and 9% larger in the humerii (Eleazer and Jankauskas 2016). Additionally, there were no statistically significant results in the histomorphometry variables between the lesion and non-lesion groups, but non-statistically significant trends are reported (Eleazer and Jankauskas 2016). The lesion group individuals had marginally higher On.Ar and On.B.Ar in the femur, but these were lower in the rib and humerus (Eleazer and Jankauskas 2016). Lesion individuals had 4% higher porosity in the femur and 17% higher porosity in the humerus, which appeared to be related to the presence of more and larger resorption spaces, but in the rib, porosity was 9% lower in the lesion individuals, which the authors believed reflected levels of biomechanical stress (Eleazer and Jankauskas 2016).

Eleazer and Jankauskas (2016) state that the systemic stress associated with the lesion individuals disrupted the expectation that the rib has the lowest porosity and the femur the most due to the increased level of biomechanical stress in the femur, and instead, in the lesion group, the humerus had the highest porosity, but the rib still had the lowest. The results described by Eleazer and Jankauskas (2016) agree with the notion in the literature that axial skeletal elements such as the rib, are more susceptible to systemic and metabolic fluctuations than appendicular skeletal elements, such as the long bones (Agnew and Stout 2012; Crowder and Rosella 2007; Dominguez and Agnew 2016; Karlson 1998; Paine and Brenton 2006; Seeman et al. 1992; 2000; Stewart et al. 2021; Tommerup et al. 1993). This reinforces that elements like the rib are much more valuable for investigations of systemic health and bone metabolism. The lack of statistically significant results between the lesion and non-lesion group also suggests that the relationship between what is visible at the macroscopic level, may not be reflective of what is visible at the microscopic level. Whether this is due to our general lack of understanding of this relationship or suggests that although an individual lives long enough to develop a skeletal lesion in response to a chronic or sub-acute health condition, this may

not mean it is long enough to impact upon bone microstructures and broader metabolism. Additionally, it could also mean that despite the absence of a macroscopic skeletal lesion, bone microstructures can be impacted by factors skeletally invisible to the naked eye and *vice versa*, a concept which has been suggested elsewhere (Ortner and Aufderheide 1991; Schlecht 2012; Wood et al. 1992).

Similar to Robling and Stout (2003), Fahy et al.'s (2017) primary focus was on OPD and how carbon and nitrogen isotope ratios can be influenced differently between bones of differing metabolism and remodelling rates. Their study observed 10 medieval adult individuals from the St Gregory's Cemetery and sampled anterior midshaft of the tibia and humerus, the femoral posterior midshaft, a section from the occipital and complete transverse cross-sections from the midshaft of a metacarpal, radius, left 5th rib, and clavicle (Fahy et al. 2017). OPD was calculated within the cortical bone from all samples and Fahy et al. (2017) used a region of interest (ROI) sampling strategy for all sections, with 5 ROIs selected for each bone. For most bones, the ROIs were located adjacent to the periosteal border in the cortex on the anterior aspect, except for the femur whereby the ROIs were in the posterior aspect, and the occipital and rib whereby the ROIs were in the external aspect (Fahy et al. 2017).

As these were medieval individuals, age-at-death and sex were estimated using skeletal profiling methods (Fahy et al. 2017). Individuals were estimated to be between 25-35 years of age-at-death and there were 5 males and 5 females (Fahy et al. 2017). OPD was highest in the metacarpal, humerus and rib, and lowest in the occipital, with the femur and tibia falling in between (Fahy et al. 2017). Females had higher OPD than males but this relationship was not fully understood by Fahy et al. (2017) and they suggested it could be due to sex-based occupation differences or the robusticity of the selected bones, which it appears they did not control for via the application of a robusticity index or stature estimation (Stock and Shaw 2007) as has been done to account for bone size differences elsewhere (Stewart et al. 2021). Fahy et al.'s (2017) results did not agree with literature elsewhere that the femur has a slower remodelling rate than the rib, as there was no significant difference between OPD in the two bones (Cox and Sealy 1997; Hedges et al. 2007). However, a recent study by de Gruchy et al. (2024) identified significant regional differences in femoral bone remodelling rates, with slowed remodelling in the periosteal region, mid-range remodelling in the mid-cortical region and higher remodelling rates in the endosteal region, but this general pattern did vary within 6 of 16 individuals. This suggests that femoral remodelling depends on ROI placements within the cortex and not just aspect such as anterior versus posterior aspect.

In 2022, Karydi et al. measured the largest number of variables across osteon and Haversian canal size, shape and density, and cross-sectional geometry in a study of ribs and femora to date. The primary purpose of this paper was to validate several established age-at-death estimation techniques using the rib (Cho et al. 2002; Goliath et al. 2016; Stout et al. 1994; Stout and Paine 1992) and femur (Ahlqvist and Damsten 1969; Goliath et al. 2016; Kerley 1965; Kerley and Ubelaker 1978). Karydi et al. (2022) observed a sample of 14 individuals from the 19th century St Peter's cemetery in Blackburn, England, who died between 1839 – 1857 at known ages and sexes (except for 1 individual of unknown sex). Samples were taken at the middle-third of the 6th rib (n = 11) and the femur (n = 5), but only 1 rib and femur sample were paired from the same individual (Karydi et al. 2022). Two individuals were infants, aged 1.5 and 2.8 years, while the rest ranged from young to old adults (Karydi et al. 2022). Additionally, two individuals were recorded as pathological with bony overgrowths, which could mean remodelling rates were abnormal in these elements (Hillier and Bell 2007; Karydi et al. 2022). As they were testing several age-at-death estimation techniques in the rib and femur, Karidyi et al. (2022) observed many variables; cortical area (Ct.Ar), intact osteon number (N.On), fragmented osteon number (N.On.Fg), intact osteon density (OPDI), fragmented osteon density (OPDF), osteon population density (OPD), osteon area (On.Ar), relative cortical area (Ct.Ar/Tt.Ar), osteon circularity (On.Cr) and percentage osteonal bone (%On.B). Karydi et al. (2022) identified significant correlations for all histomorphometric variables and age-at-death, except for On.Ar where the relationship was a weak negative decrease with advancing age-at-death. Of particularly high significance was OPD and OPDF, which agrees with research by Crowder et al. (2022) that found looking at OPDF independently was more valuable than OPD or OPDI. This is because OPDF is more likely to be directly associated age-at-death due to the accumulation of osteons over time and reaching the age asymptote whereby intact osteons are remodelled over with ageing, leading to increased OPDF (Crowder et al. 2022).

Karydi et al. (2022) also demonstrated that males had higher On.Ar (in contrast to Burr et al. 1990 where female femoral osteon area was higher), On.Cr and Ct.Ar.Tt.Ar than females but differences were not statistically significant after controlling for age-at-death. Results of the rib age-at-death method validation found that the age-at-death of younger individuals were routinely over-estimated, and older individuals were routinely under-estimated, with differences in known age-at-death and estimated age-at-death being as high as 57.9 years using the Goliath et al. (2016) method. This is similar to results of Paine and Brenton (2006), whereby the age-at-death of older individuals were also routinely underestimated, postulated by the authors to be due to poor diet slowing osteonal remodelling. Estimations using the Stout

et al. (1994) and Goliath et al. (2016) methods consistently over-estimated age-at-death (Karydi et al. 2022). The authors report that the lowest inaccuracy was recorded using the Stout et al. (1994) method, which over- or under-estimated age-at-death by an average of 10.68 years (Karydi et al. 2022). However, despite this, Karydi et al. (2022) also stated that age-at-death estimates done using the Stout et al. (1994) and Goliath et al. (2016) methods were statistically significantly different from the known age-at-death. Karydi et al. (2022) decided that Cho et al. (2002) provided the overall best age-at-death estimation based on human rib histomorphometry. Results of the femoral age-at-death method validation determined that On.Cr had a statistically significantly positive relationship with age-at-death, but the other variables were not statistically significant (Karydi et al. 2022). Non-statistically significant trends were identified, such as OPDI, OPD and %On.B increased, and On.Ar decreased with advancing age-at-death (Karydi et al. 2022). In contrast to the rib results, OPDF did not have any trending or statistically significant relationship with age-at-death in the femur (Karydi et al. 2022). This could be partially due to the extreme levels of biomechanical loading and strain that the femur is subjected to in comparison to the rib, which several other studies have agreed (Agnew and Stout 2012; Crowder and Rosella 2007; Dominguez and Agnew 2016; Karlson 1998; Paine and Brenton 2006; Seeman et al. 1992; 2000; Stewart et al. 2021; Tommerup et al. 1993). Similar to the rib, age-at-death of younger individuals were routinely over-estimated, and older individuals were routinely under-estimated, with differences in known age-at-death and estimated age-at-death being as high as 62.5 years using the Ahlqvist and Damsten (1969) method (Karydi et al. 2022). Further, estimations using the Ahlqvist and Damsten (1969) method consistently over-estimated age-at-death (Karydi et al. 2022). The authors report that the lowest inaccuracy and bias were recorded using the Kerley (1965) method, which over- or under-estimated age-at-death by an average of 18.1 years (Karydi et al. 2022). Karydi et al. (2022) found that only age-at-death estimates done using the Ahlqvist and Damsten (1969) method was statistically significantly different from the known age-at-death.

Finally, Karydi et al. (2022) looked at differences in OPD, On.Cr and On.Ar between the rib and the femur and found that as a non-statistically significant trend, femoral values were higher than rib values, but the only statistically significant result of this analysis was higher On.Ar in the femur compared to the rib. Given the variability of the results rendered by Karydi et al. (2022), rather than validating age-at-death estimation equations created based on microstructural appearance in geographically separate populations, it may instead be more useful to focus on known skeletal biology changes that occur within human bone as humans age, and instead focus on those variables, such as OPD, OPDF which increase with advancing

age (Crowder and Rosella 2007; Stout and Paine 1994), Ct.Wi, which decreases via cortical thinning and Ct.Po, which increases with advancing age (Corrado et al. 2020; Ebbesen et al. 1999; Kenkre and Bassett 2018; Parfitt et al. 1995). A similar study conducted by Lagacé et al. (2019) in the human femur, found that the Goliath et al. (2016) method was also inadequate at estimating age-at-death in all but 4 of their 29 individuals. However, they did identify statistically significant increases of osteon circularity and osteon population density and decreases of osteon area with advancing known age-at-death (Lagacé et al. 2019).

Miszkiewicz et al. (2022) conducted an intra-skeletal study on an individual who had been dated to ~1720 years BP and was excavated on Ebon Islet, Ebon Atoll, in the Marshall Islands. Age-at-death and biological sex were estimated via standard methods, and the individual was estimated to be 30-49 years old and a probable male (Buikstra and Ubelaker 1994). Sampling strategy was decided based on biomechanical landmarks and bone fragment availability due to skeletal fragmentation and included the distal humerus, proximal radius, posterior femur, and a fragment of an unsided, unnumbered rib (Miszkiewicz et al. 2022). While this sampling strategy is good for targeting biomechanical research questions, the differences in sampling locations between each bone is not well-suited for a broader analysis of intra-skeletal differences, whereby consistent sampling strategies would better identify differences in bone remodelling between each element, i.e. at the midshaft of each bone (Miszkiewicz et al. 2022). Microstructural variables observed included Haversian canal density (H.Dn) and Haversian canal area (H.Ar), along with macroscopic measurements to demonstrate robusticity differences between elements, which included shaft diameter and cortical thickness (femur only due to posterior aspect sample) (Miszkiewicz et al. 2022). As this was a case study (n = 1), no inferential statistics could be run, and so only descriptive statistics were provided (Miszkiewicz et al. 2022). H.Dn was highest in the rib, followed by the humerus and radius, with the femur having the lowest H.Dn values (Miszkiewicz et al. 2022). Trends in H.Ar were in the same order as H.Dn but reversed, with the rib having the smallest H.Ar values and the femur having the largest (Miszkiewicz et al. 2022). Despite the rib having the smallest mean H.Ar and smallest minimum H.Ar, it also had the highest maximum recorded H.Ar suggesting wider variability in H.Ar than any other element in the rib (Miszkiewicz et al. 2022).

As has been demonstrated in the literature above, there is a clear inconsistency in the histological results of comparisons between the femur and the rib. The studies discussed above observed archaeological samples of estimated age-at-death and biological sex, but inclusion of documented samples, such as anatomical donors, could assist in correcting any observations made on the ancient samples. The anatomical evidence is thus reviewed next.

3.2.2 Anatomical Evidence

Table 3.2 documents which anatomical papers have looked at differences between the rib and femur and details where the individuals originated from, and which histological variables were measured in each study. Additional studies have observed histological variation in the femur and rib separately, investigating changes with age-at-death (rib: Absolonova et al. 2013; Kim et al. 2007; García-Donas et al. 2016; Pfeiffer et al. 2016; femur: Lagacé et al. 2019; Maat et al. 2006), osteon and Haversian canal size and density (femur: Maggio and Franklin 2021), porosity (rib: Agnew and Stout 2012), to propose more specific definitions of histological variables (rib: Crowder et al. 2022), identify factors impacting osteons size (rib: Dominguez and Agnew 2016) and differences within and between ribs based on their position within the rib cage (Crowder and Rosella 2007).

Table 3.2: Table 3.2 Histological studies of Anatomical Human Ribs and Femora.

Publication	**Sample**	**Histomorphometry/Cross-Sectional Geometry Variables**
Jowsey 1966	Autopsy *n* = 26, Minnesota, USA	Osteon Perimeter (On.Pm) Haversian Canal Perimeter (H.Pm) Cortical Thickness (Ct.Wi)
Reid 1986	Forensic cases *n* = 4, London, UK	Osteon Lamellar Thickness (Lm.Wi)
Stewart et al. 2015	Autopsy *n* = 16, Missouri, USA	Total Subperiosteal Area (Tt.Ar) Cortical Area (Ct.Ar) Endosteal Area (Es.Ar) Relative Cortical Area (Ct.Ar/Tt.Ar)
Cole et al. 2022	Paired rib & long bones *n* = 9, Missouri, USA	**Cross-Sectional Geometry Variables:** Total Area (Tt.Ar) Endosteal Area (Es.Ar) Cortical Area (Ct.Ar) % Cortical Area (Ct.Ar/Tt.Ar x 100) % Bone Area Total Porosity ((Ct.Ar-Tt.Po.Ar)/Tt.Ar x 100) % Bone Area Cortical Porosity ((Ct.Ar-Ct.Po.Ar)/Tt.Ar x 100) % Endosteal Area (Es.Ar/Tt.Ar x 100) **ROI Variables:** Cortical Area (Ct.Ar) % Cortical Area (Ct.Ar/Tt.Po.Ar x 100) Bone Area (Ct.Ar-Tt.Po.Ar) % Bone Area ((Ct.Ar-Tt.Po.Ar)/Tt.Ar x 100) % Porosity (Tt.Po.Ar/Ct.Ar x 100) Pore Density (N.Po/Ct.Ar) Total Pore Number (N.Po) Total Pore Area (Tt.Po.Ar) Mean Pore Area (Calculated by ImageJ) Mean Pore Perimeter (Calculated by ImageJ) Mean Pore Circularity (Calculated by ImageJ = 4π x (Ar/Pm^2)) Mean Pore Aspect Ratio (Calculated by ImageJ = Major Axis/Minor Axis)

		Mean Pore Roundness (Calculated by ImageJ = 4 x Ar/π x Major Axis^2) Mean Pore Solidity (Calculated by ImageJ = Area/Convex Area)
Mavroudas et al. 2022	Cadaveric donors *n* = 6, Texas, USA	Osteon Area (On.Ar) Haversian Canal Area (H.Ar) Intact Osteon Population Density (In.OPD) Fragmentary Osteon Population Density (Fg.OPD) Anterior Femoral Width (Ant.Wi)
Pedersen et al. 2024	Cadaveric donors *n* = 17 Queensland, Australia	Osteon Population Density (OPD) Intact Osteon Population Density (In.OPD) Fragmentary Osteon Population Density (Fg.OPD) Osteon Area (On.Ar) Haversian Canal Area (H.Ar)

Jowsey (1966) conducted the first histomorphometric study of contemporary adult human ribs and femora, in 26 individuals (aged 20-90 years) at autopsy in Minnesota, USA. Jowsey (1966) aimed to define osteonal characteristics in a variety of animals, as well as humans, and determine how osteonal characteristics changed with age-at-death in humans. The observed individuals had all died of sudden trauma or heart attack but were determined to be skeletally "normal" and were physically active at their time of death (Jowsey 1966). Femora were sampled at the mid-shaft and ribs anywhere from 8-20cm from the spine (Jowsey 1966). Sampling at inconsistent locations within the rib could be problematic as some research has demonstrated that histomorphology and histomorphometry can vary even within the same skeletal element (Lanyon et al. 1982; Stout et al. 2019). Jowsey (1966) identified that histomorphometric measures increase relatively consistently with body size, in both non-human and human mammals, suggesting that analysis should be tempered with statistical accounting for body size variation. When comparing histomorphometric results with age-at-death, Jowsey (1966) determined that femoral osteon perimeter does not change with advanced age, but Haversian canal perimeter increased significantly. These results contrast with Lagacé et al. (2019), where they identified statistically significantly smaller osteons with advancing age in the femur. In the rib, osteon perimeter decreased with advancing age, but results were not statistically significant, while Haversian canal perimeter remained similar, at approximately 165µm, throughout human life (Jowsey 1966). Cortical width in the rib decreased with advancing age and results were statistically significant (Jowsey 1966). Cortical width also decreased in the femur, but results were not statistically significant (Jowsey 1966).

Jowsey (1966) explains that in these samples, it appears that femoral cortical width decreased with advancing age as endosteal bone became increasingly infiltrated with vascular spaces, however in the rib, there was extensive loss of endosteal bone which led to a more significant decrease in cortical width with advanced age. These results in the femur disagree with earlier

research by Currey (1964), whose results suggested that femoral osteons decreased in size with advancing age, while Haversian canal size did not change. However, Currey (1964) measured the smallest diameter of osteons and their Haversian canals and included elongated osteons, while Jowsey (1966) only measured rounded osteons and Haversian canals which were captured longitudinally in cross-section, and this could have led to these differing results. Jowsey (1966) also identified that osteon perimeter seemed to reach a maximum of 250μm regardless of body size across any species they observed, including humans. Jowsey (1966) believed that the increasing femoral Haversian canal size while femoral osteons remained a similar size, contributes to the increase in cortical porosity that is evident with advancing age (Jowsey 1960).

Reid (1986) observed rib cross-sections in 6 individuals who were sampled at autopsy, 4 of which were sub-adults ranging from neonate to adolescent, as well as femoral cross-sections from 2 adult individuals from a local forensic osteological collection. All individuals were from London, UK, but it is unclear where the cross-sections were taken from within the skeletal elements (Reid 1986). The analysis was largely qualitative in nature, looking broadly at collagen orientation, but also included measurement of osteon lamellar thickness (Reid 1986). Reid (1986) stated that there were few femoral osteons suitable for measurement as they were not running longitudinally in the transverse cross-section and appeared elongated or oblique. Reid (1986) defined osteon lamellar thickness as half of the interlamellar separation (as defined in Frost 1962), which is calculated by the measure of half the distance between the middle of two adjacent transverse lamellae. This measure averaged 2.94μm in the femur, but the overall average was not reported for the rib as the individuals were of a varied age, including neonates, and the measure was reported differently for the adult individuals (Reid 1986). In the adult rib samples, the inner lamellae and outer lamellae of osteons were reported separately, and results seemed to suggest that the outer lamellae are thinner than the inner lamellae in both individuals (Reid 1986). The differences between the inner and outer lamellae were statistically significant, and the femoral osteon lamellae were more similar in size to the inner lamellae of the rib, which averaged 2.78 and 3.09μm, compared to the outer lamellae which averaged 1.93 and 2.11μm (Reid 1986). Frost (1962) found that outer lamellae were thicker than the inner lamellae in the ribs of human adult individuals, which is the opposite to Reid's (1986) findings.

Due to the small sample size, Reid (1986) did not run more complex statistics to look at the relationship between age-at-death and osteonal lamellae thickness. Reid (1986) states that generally their results suggest that average lamellae thickness in the rib is lower in younger

individuals and increases with advancing age. However, this relationship cannot be linear as the average lamellae thickness was lowest in the oldest individual (43 years old) at the outer lamellae level, and highest in the second oldest individual (39 years old) at the inner lamellae level (Reid 1986). In the sub-adult individuals, which ranged in age from 2 months to 13 years, the lowest average lamellae thickness was in a 5-month-old, and the highest was in a 10-year-old individual (Reid 1986). No analysis with outputs of statistical significance was undertaken.

Stewart et al. (2015) conducted the first study of cross-sectional geometry variables of contemporary adult human ribs and femora. They observed paired rib and femoral cortical bone in 16 individuals at autopsy in Missouri, USA and aimed to measure intraskeletal variability between long bones and ribs (Stewart et al. 2015). Measured variables included total subperiosteal area, cortical area and endosteal area to calculate relative cortical area (Stewart et al. 2015). The individuals included in this study had documented age-at-death, ancestry, sex and cause of death (Stewart et al. 2015). The femur had a larger relative cortical area than the rib (femur mean relative cortical area = 0.656, rib mean relative cortical area = 0.353), but the rib had more variation with a larger standard deviation from the mean (femur standard deviation = 0.112, rib standard deviation = 0.140) (Stewart et al. 2015). Females had lower relative cortical area in the rib than males, but a higher relative cortical area than men in the femur (Stewart et al. 2015). However, while there were statistically significant differences within each individual between the different bones, there were no statistically significant relationships with either biological sex or age-at-death, which suggests that differences between the bones occurs independently of those variables (Stewart et al. 2015). The femur and the rib had a statistically significant relationship in terms of their relative cortical area (r = 0.543, p <0.05) (Stewart et al. 2015). However, a Pearson's r of 0.543 is fairly weak and this suggests that there are differing factors that define relative cortical area in the rib compared to the femur which could potentially relate to different patterns of biomechanical load and susceptibility to systemic health between the bones (Agnew and Stout 2012; Crowder and Rosella 2007; Dominguez and Agnew 2016; Karlson 1998; Paine and Brenton 2006; Seeman et al. 1992; 2000; Stewart et al. 2015; 2021; Tommerup et al. 1993).

Cole et al. (2022) conducted the first study combining cross-sectional geometry and histomorphometry variables of paired femora and ribs from 9 individuals donated to two local universities in Missouri, USA. The cross-sectional geometry variables they observed included total, endosteal and cortical areas, which were used to calculate % cortical area, % total porosity, % cortical porosity and % endosteal area (Cole et al. 2022). The histomorphometry analysis was conducted using mapped quadrants of the femora at each aspect; anterior,

posterior, medial and lateral, and the rib was divided into the pleural and cutaneous cortices (Cole et al. 2022). Variables observed in these ROIs included cortical area, bone area, total porosity number and area, to calculate % cortical area, % bone area, % porosity and pore density (Cole et al. 2022). Further measures were calculated by Fiji ImageJ including mean porosity area, perimeter, circularity, aspect ratio, roundness and solidity (Cole et al. 2022). Circularity, aspect ratio, roundness and solidity are different ways of calculating how round or circular an object might be, based on different calculations, which are not often all observed within the same study, and have not been applied in the measurement of osteons or Haversian canals (Cole et al. 2022; Doube et al. 2010; Zdilla et al. 2016). Circularity determines how close a structure is to a perfect circle, roundness is similar but ignores slight deviations or irregularities in a structure's perimeter, solidity defines how convex versus concave a structure is and aspect ratio considers whether the major and minor axes suggest an elongated shape (rectangular) or round shape (square) (Zdilla et al. 2016).

Cole et al. (2022) determined that when cortical porosity was accounted for, cortical bone area was significantly reduced, by up to 66.8%. The femur was statistically significantly larger than the rib in total cross-section, endosteal and cortical area, but also in relative measurement % cortical area, % bone area after accounting for porosity (Cole et al. 2022). Despite this, the femur still had higher cortical porosity than the rib, and the rib had higher % endosteal area than the femur which suggests that the overall cortical thickness was larger enough in the femur than rib to compensate for the increased cortical porosity (Cole et al. 2022). Total porosity area was not significantly different between the femur and rib, but cortical porosity was statistically significantly higher in the femur than rib, but this was reversed in trabecular porosity (Cole et al. 2022). Total pore density was higher in the rib than femur when considering both cortical and trabecular porosity, which suggests that trabecular pore density was high enough in the rib to compensate for the lower cortical pore density as compared to the femur (Cole et al. 2022). Porosities were significantly more circular and smaller in the rib than femur and this trend continued for the diameter and perimeter pore measures (Cole et al. 2022). With respect to cortical porosity and pore measures, the femur demonstrated no variation between the quadrants, but the rib had statistically significant differences in cortical pore measures, with higher values in the cutaneous sector, and a significantly higher pore density in the pleural sector (Cole et al. 2022). This suggests that while ROIs are likely suitable for application in histological porosity analysis in the femur, this may not be the case for the rib whereby whole cross-sections should be observed.

Cole et al (2022) suggest that the higher density of porosities in the rib as compared to the femur in their results is associated with generally higher remodelling in the rib, demonstrated via higher OPD values elsewhere (Cho and Stout 2011; Fahy et al. 2017; Mulhern 2000; Mulhern and van Gerven 1997; Skedros et al. 2003; Vajda et al. 1999; Wilson et al. 1998). Elsewhere, it has also been stated that the decreased strain impact on stochastic remodelling (Frost 1990); higher susceptibility to metabolically stimulated resorption (Skedros et al. 2013a); and a higher frequency of targeted microdamage remodelling associated with breathing (Cho and Stout 2011; Skedros et al. 2003) have also led to higher remodelling rates in the rib compared to the femur. However, a limitation of Cole et al. (2022) is that they do not define, nor seem to control for, the age-at-death of the individuals in their study. Age-at-death has been repeatedly demonstrated to be associated with increased cortical porosity, cortical thinning and overall substantial decrease in cortical bone area due to endosteal resorption in excess of periosteal formation (Agnew and Stout 2012; Sedlin 1964; Pirok et al. 1966; Pavón et al. 2010). Age-related cortical thinning occurs with a phenomenon known as trabecularisation of the cortex, whereby endocortex porosities do not infill and eventually broaden the endosteal area (Zebaze et al. 2010). Without stating or controlling for age-at-death in the study sample, it is difficult to determine whether the porosity results in Cole et al. (2022) are impacted by advanced age-at-death.

Mavroudas et al. (2022) observed the effects of burning on histological age-at-death in the rib and femur, sampling 6 individuals from Texas, USA. Key variables observed include osteon area, Haversian canal area, intact osteon population density, fragmentary osteon population density and anterior femoral width (Mavroudas et al. 2022). While no associations were made regarding the effects of burning on the bone, their results in terms of age-at-death estimation and differences between the rib and femur were valuable. Mavroudas et al. (2022) state that irrespective of the method used to estimate age-at-death, all methods were based on two guiding principles, the increase in presence of osteons with advancing age-at-death, and the reduction of cortical bone area. Thus, methods revolve around observing to what extent a cross-section is occupied by osteons, whether they be intact or fragmentary. While all individuals in this study were of known age-at-death and sex, they were all in the older adult age-at-death category (Buikstra and Ubelaker 1994) aged 61-84 and all but one were female (Mavroudas et al. 2022).

Mavroudas et al. (2022) demonstrated that both femoral osteon and Haversian canal area were higher than the rib across all individuals, both before and after burning. There did not appear to be any relationship in the rib with OPD and age-at-death although the sample size

of 6 is restrictive in terms of statistical analysis (Mavroudas et al. 2022). However, the femoral results were not reported individually by variable, and rather, were reported as an age-at-death estimate based upon the variables collectively and so comparison between age-related in the variables with age-at-death was not possible (Mavroudas et al. 2022). Mavroudas et al. (2022) reported that while age-at-death estimation using histology was possible on burned remains, the femoral estimates rendered more accurate age-at-death estimation than the rib, but only when anterior femoral width was included. However, there are several limitations associated with this study.

Firstly, Mavroudas et al. (2022) were primarily looking at the effects of burning and assessing whether histological examination for the purpose of estimating age-at-death was still possible, rather than looking specifically at age-related changes in the rib and femur. Thus, variables were measured but reported in terms of the age-at-death estimation methods used, rather than individually. Secondly, there was no observation of cortical width conducted in the rib, which is known to exhibit the phenomenon of cortical thinning due to increased porosity and trabecularisation (Sedlin 1964; Pirok et al. 1966; Pavón et al. 2010; Zebaze et al. 2010). Thirdly, the sample size was too small to conduct anything more than descriptive statistics, which makes it difficult to identify if there is a relationship between variables (osteon area, Haversian canal area, intact and fragmentary osteon population density and anterior femoral width) and factors (such as age-at-death and sex). As described in Chapter Two, there have been reported histological differences in cortical bone with age-at-death (Jones et al. 1994; Mazess 1982; Mazess et al. 1987; Riggs et al. 1981; 1982; Rodin et al. 1990; Warming et al. 2002) and biological sex (Clarke and Khosla 2009; Compston 2001; Handelsman et al. 2018), especially with increasing age and menopause associated bone loss (Cauley et al. 2003; Khosla and Hofbauer 2017; Krum et al. 2008). A larger sample size, with more evenly distributed sex and age-at-death groups would assist in a more thorough analysis.

Pedersen et al. (2024) observed differences in age-at-death and intra-skeletal variability in 17 individuals from Queensland, Australia, the first intra-skeletal study in Australia. Variables observed include osteon population density, intact and fragmentary osteon population density, osteon and Haversian canal area (Pedersen et al. 2024). When data were pooled, there were no associations with age-at-death and either histological variable identified, but when observing the male group separately, this changed. Male femoral osteon population density and rib porosity had positive statistically significant relationships with age-at-death (Pedersen et al. 2024). Haversian canal area in the rib significantly increased with advancing age-at-death (Pedersen et al. 2024). In terms of intra-skeletal variability, male osteon population density in

the rib was statistically significantly higher than in the femur and osteonal and Haversian canal area was statistically significantly smaller in the rib than femur (Pedersen et al. 2024). Once a robusticity index was applied to control for bone size differences in the femur, results were no longer statistically significant, but there was no robusticity index applied to the rib values and so a comparison between the femur and rib could not be made (Pedersen et al. 2024). This demonstrates that bone size or individual body size might account for a large portion of the differences in histological variation in the femur. However, without applying the robusticity index to the rib, it is difficult to say whether this is due to an increased biomechanical load in the femur with increasing body size which could be masking true differences between the skeletal elements (Miszkiewicz 2016; Stock and Shaw 2007). This could be tested by applying a control for bone or body size to the rib and femur together, and then looking at intra-skeletal variability.

Elsewhere, Maggio and Franklin (2021) failed to identify any significant strong correlations with chronological age-at-death and osteon or Haversian canal morphometric measures relating to size or density in the femur. Rather, they identified significant differences between age-at-death groups, separating young adults (18-34 years), middle adults (35-49 years), older adults (50 – 74 years) and elder adults (75+ years) (Maggio and Franklin 2021). At the anterior femur aspect, osteon area was significantly difference between young and middle adults, while Haversian canal area was significantly different between young, middle and older adults (Maggio and Franklin 2021). Young adults had significantly different Haversian canal perimeter to all three of the other age-at-death groups (Maggio and Franklin 2021). At the posterior femur aspect, young adults had significantly different osteon count to middle adults, osteon size was significantly different between young and older adults and osteon and Haversian canal size as well as osteon population density were significantly different between young and elderly adults (Maggio and Franklin 2021). However, Absolonova et al. (2013) who observed age-at-death trends in the rib, identified statistically significant positive relationships between age-at-death and intact osteon density, osteon circularity, Haversian canal perimeter/osteon perimeter and Haversian canal diameter/osteon diameter, as well as statistically significant negative relationships between age-at-death and cortical bone width, % total osteon area, osteon area, osteon circumference, maximal and minimal Haversian canal and osteon axis, Haversian canal and osteon diameter, Haversian canal and osteon feret diameter, osteon compactness and Haversian canal perimeter. Further, Agnew and Stout (2012) identified significant intracortical bone loss and increased porosity in an elderly donor sample and Dominguez and Agnew (2016) observed a similar phenomenon in their study of the human rib whereby cortical area had a statistically significant negative relationship, and porosity area had a statistically

significant positive relationship with age-at-death. An earlier study of the human rib by Kim et al. (2007) identified a statistically significant increase in osteon population density with advancing age-at-death, but decrease in osteon and Haversian canal area, as well as cortical area.

More recently, Crowder et al. (2022) proposed that osteon population density should be separated into intact and fragmentary osteons to look at their densities separately as well as together in their study of the human rib. They determined that the accuracy of age-at-death estimates relying on combined osteon population density, as well as intact osteon population density, seemed to plateau at approximately 55 years of age, whereas those relying on fragmentary osteon population density did not (Crowder et al. 2022). This could be explained by the asymptote, which was explained in Chapter 2 (Section 2.8.2.1) (Crowder et al. 2022). A lifetime of continuous bone remodelling leads to an increased population of fragmentary osteons, remodelling over osteons that came before, and can mean a greater population density of fragmentary osteons compared to intact ones (Crowder and Rosella 2007; Stout and Paine 1994). Thus, fragmentary osteon population density could be a better measure of age-at-death as these will accrue at a higher rate than intact osteons with advancing age (Crowder and Rosella 2007; Stout and Paine 1994). The reason for the stronger and more numerous relationships identified in the rib rather than the femur, could relate to the rib being less skewed due to the patterns associated with highly variable biomechanical loading that is observed in the femur. If each individual had differing levels and patterns of physical activity, the microstructural variation of these differences between individuals could be masking any age-related changes in the bone microstructure (Tommerup et al. 1993).

Despite all of these results, there is still no age-at-death estimation formulae that can work accurately across multiple populations, based upon regional differences whether due to societal ways of life, socio-economic status, dietary differences or genetic influences. Rather, García-Donas et al. (2016) possibly provided some solid insight, stating that peer-reviewed, *population specific* standards are urgently needed to improve accuracy of histological estimation of -age-at-death. However, this has also been disputed with attempts to build a population-specific equation for age-at-death estimation using the clavicle having been hindered by individual variation due to diet and systemic health influences which are difficult to predict in an unknown sample and to control for in a documented sample (Kranioti et al. 2020).

While some common themes occur between anatomical, or contemporary humans and archaeological humans, there is either inconsistency in histological results or a broad variation in results between studies. better understand this observation, we will now turn to animal models.

3.2.3 Animal Models

Table 3.3 documents which experimental studies using animal models have assessed differences between the rib and femur. The majority of these studies observe bone histology in quadrupedal species (High 1987; Nganvongpanit et al. 2017; Raab et al. 1991; Tommerup et al. 1993; Vajda et al. 1999), one study observing the mixed-modal macaque (Lad et al. 2019) and another a bipedal hopping macropod (Stewart et al. 2021).

Table 3.3: Histological studies of Non-Human Ribs and Femora.

Publication	**Sample**	**Histomorphometry/Cross-Sectional Geometry Variables**
High 1987	Dogs *n* = 32	Ratio of Cortical to Total Cortical Bone Areas Ratio of No. of Bone Resorbing to No. of Bone Forming Foci % of Bone Forming Sites with Single Labels % of Bone Forming Sites with Double Labels Radial Closure Rate (mm/year) Osteonal Bone Formation Rate (mm^2/mm^2/year) Osteonal Formation Time (years) Osteonal Resorption Time (years) Osteonal Activation Frequency Foci (no./mm^2/year)
Tommerup et al. 1993 (ribs)/ Raab et al. 1991 (femora)	Sows *n* = 20	% of Forming Surface Density of Forming Osteons Interlabel Width
Vajda et al. 1999	Dogs *n* = 11	Total Cross-section Area Cortical Bone Area Porosity No. of Resorption Osteons No. of Reversal Osteons No. of Single Labelled Osteons No. of Double Labelled Osteons Mineral Apposition Rate Volume-Referent Bone Formation Rate Osteon Diameter Haversian Canal Diameter Mean Wall Thickness Osteon Formation Time
Nganvongpanit et al. 2017	Asian Elephants *n* = 5	Osteon Diameter Haversian Canal Diameter Osteon Area

		Haversian Canal Area Lacunae Area Cortical Width Trabecular Width Bone Diameter
Lad et al. 2019	Macaque *n* = 5	Total Cross-Section Area No. of Intact Osteons No. of Fragmentary Osteons Osteon Area Osteon Population Density % Haversian Bone
Stewart et al. 2021	Kangaroo *n* = 1	Maximum Bone Length Midshaft Circumference Cortical Width Vascular Canal Density Total Vascular Density Cortical Width Robusticity Index Midshaft Circumference Robusticity Index Vascular Canal Density per Cortical Width Robusticity Index Vascular Canal Density per Midshaft Circumference Robusticity Index

High (1987) conducted an experimental study on 32 beagles (16 males and 16 females), aged 19 – 35 months old. The study aim was to investigate the effects of prostaglandin E2 on cortical bone remodelling in the 9th rib and femur, which were sectioned at the mid-diaphysis (High 1987). Variables observed include ratio of cortical to total cortical bone areas, ratio of number of bone resorbing to number of bone forming foci, % of bone forming sites with single labels, % of bone forming sites with double labels, radial closure rate (mm/year), osteonal bone formation rate (mm^2/mm^2/year), osteonal formation time (years), osteonal resorption time (years), osteonal activation frequency foci (no./mm^2/year) (High 1987). Results indicated that supplemented prostaglandin E2 can stimulate bone remodelling, but that results were dependent on the dosage of prostaglandin E2 administers, the sex of the beagle and which bone was being observed (High 1987). The primary indicator that prostaglandin 32 induced bone remodelling was by the femoral deposition of new subperiosteal, circumferential, fibrous-lamellar bone (High 1987). However, there were no reversal lines present, which suggested the new bone deposition was occurring without prior resorption at the site via the stimulation of osteoblast recruitment (High 1987). Additionally, there was a statistically significant increase in the deposition of Haversian bone in both the femur and rib, similarly with no evidence of reversal lines (High 1987).

However, High (1987) does not report the numerical results between the femur and rib separately and so it is difficult to fully understand to what extent they differ in microstructural features. High's (1987) results suggest that values of almost all variables were higher in male

than female beagles, except for osteon formation rate and osteon resorption rate, which appeared to be faster in females than males. Despite the primary objective of this paper being the comparison of prostaglandin E2 in 3 different dosages and a control, these differences between the biological sexes occur separately across every dosage group observed by High (1987), which means that the differences between the sexes cannot be a result of the different dosage groups. However, as sex differences were not an objective of the paper, it is uncertain whether these differences were statistically significant. Additionally, there were no controls factored into the analysis for differences in body size, which has been closely associated with the size of osteons and Haversian canals (Miszkiewicz 2016; Pedersen et al. 2024; Stock and Shaw 2007).

Raab et al. (1991; femora) and Tommerup et al. (1993; ribs) conducted the first experimental study which focused on the differences in histological features between weight-bearing and non-weight-bearing bones to investigate whether weight-bearing activities also induced non-weight-bearing bones. The model used 3-year-old female pigs and had 3 experimental groups; 6 basal sows were sacrificed at the start of the study, 7 control sows did not undergo any behavioural change, and 7 trained sows undertook treadmill exercise at 5km/hour, for 20 minutes/day, 5 times/week at a 5% incline (Raab et al. 1991; Tommerup et al. 1993). The control and trained groups were sacrificed after 20 weeks, and the left 7^{th} rib and left femur were sampled at the mid-shaft from each animal (Raab et al. 1991; Tommerup et al. 1993). Variables observed included % of forming surface, density of forming osteons and inter-label width (Raab et al. 1991; Tommerup et al. 1993). Tommerup et al. 1993 failed to identify any effects of exercise on either the periosteal or endocortical percentage double-labelled surface, osteonal remodelling frequency, or mineral apposition rate in either of the bone envelopes within the rib.

When we consider the femoral data from the same experiment, reported by Raab et al. (1991), results determined that walking induced femoral periosteal remodelling, and that periosteal surface formation and mineral apposition rate were higher in the trained group compared to the control group, but they did not identify any effects of walking on the endosteal surface. Likewise, walking did not lead to increased intracortical remodelling (Raab et al. 1991). There was also no difference between groups in the number of labelled osteons, however, osteonal mineral apposition rate was faster in the trained group compared to the control (Raab et al. 1991). The changes observed within the trained group femora were not enough to stimulate macroscopic gross increases in bone robusticity, mineral density or cortical width, but the increased remodelling at the periosteal surface suggested to be driven by increased

osteoblastic activation (Raab et al. 1991). Additionally, there were no significant differences in periosteal, endosteal or osteonal remodelling between the control and trained group in the rib (Tommerup et al. 1993). Thus, Tommerup et al. (1993) deduces that weight-bearing activities may increase femoral periosteal bone formation and deposition, but that is not a systemic effect across all skeletal elements. Rather, the effects are localised to the weight-bearing bones. As discussed in Chapter Two, Section 2.8.1, this has been demonstrated elsewhere in the literature and makes up one of the key principles of bone functional adaptation (Lanyon et al. 1982). In fact, as Biewener and Bertram (1993) and Stout et al. (2019) determined, >70% of forces acting on bone do not occur uniformly, which suggests that there is an uneven distribution of both force and microstructural tissue response to that force, amongst different regions of a cross-section and between sequential cross-sections within the same skeletal element. However, the extent of these differences and how they occur within an element such as the rib which is not weight-bearing, is not understood and has not been addressed in the literature in the context of examining intra-element variation.

Vajda et al. (1999) were primarily interested in investigating the effects of lactation on cortical bone in the rib and femur, using a beagle model. Cross-sectional geometry data, including total cross-section area, cortical bone area and porosity; as well as microstructural variables including number of resorption, reversal, single labelled and double labelled osteons, mineral apposition rate, volume-referent bone formation rate, and osteon formation time, and; osteon morphometrics including osteon and Haversian canal diameter and mean wall thickness. Vajda et al. (1999) had a control group which were unmated (n = 6), and a lactating group (n = 5, 3 = mid- and 2 = post-lactation), all of which were not old enough to experience age-related bone loss or osteopenia.

Results demonstrated statistically significant differences between the control and lactating groups, as well as statistically significant differences between how the rib and femur responded within the experimental groups (Vajda et al. 1999). Rib intracortical remodelling activity was 12 times higher than the femur, evident in the volume-referent bone remodelling rate (Vajda et al. 1999). Further indication that higher intracortical remodelling in the rib, was the higher number of single and double labelled osteons, reversal and resorption osteons and bone multicellular unit (BMU) activation frequency (Vajda et al. 1999). Lactating group ribs had 160% higher number of resorption osteons and 100% higher number of reversal osteons (Vajda et al. 1999). Lactating group femora had a significantly reduced cortical bone area, increased BMU activation frequency, and number of single labelled, reversal and resorption osteons, compared to controls (Vajda et al. 1999). Ribs and femora from post-lactating individuals had

significantly higher rates of bone formation and mineral apposition, which could suggest that following cessation of lactation, an individual is able to recoup during a “recovery” phase, which has been identified elsewhere in the literature in studies of the lumbar spine (Kalkwarf and Specker 1995) and ilium (Grizzo et al. 2020), but no such human study has been conducted on the rib or femur (Vajda et a. 1999). It is unknown if the recovery phase witnessed here in beagles in the rib and femur is similar for humans.

Nganvongpanit et al. (2017) investigated long bone and rib morphology, observing femora and the 5th rib at the midshaft in 5 Asian elephants, the heaviest land-dwelling mammal on Earth, to see how mammalian bone tissue adapted to carrying such large load. The cross-sectional geometry variables were measured in 2 individuals and include cortical and trabecular width, and bone diameter (Nganvongpanit et al. 2017). Microstructural variables were measured in 3 individuals and include osteon and Haversian canal diameter and area, as well as osteocyte lacunae area (Nganvongpanit et al. 2017). Key differences in bone morphology between Asian elephants and humans include the lack of open medullary cavities in all bones, which instead were filled with trabecular bone, and increased density of cortical bone in the elephant compared to human (Nganvongpanit et al. 2017). Femoral bone diameter, trabecular and cortical bone width was significantly higher than the rib, which is similar to most mammalian species, including humans (Nganvongpanit et al. 2017). Rib osteons and Haversian canals were significantly larger, both in diameter and area, than those in the femur, but osteocyte lacunae area was significantly larger in the femur compared to those in the rib (Nganvongpanit et al. 2017). However, density of lacunae and osteons were similar between the rib and femur, which given that the rib is smaller overall than the femur, but also has significantly larger osteons, it is interesting that a similar number of them can reside within the same amount of bone tissue (Nganvongpanit et al. 2017).

Lad et al. (2019) conducted a histological study of differential mechanical loading between the lower limb bones and ribs of 5 macaques. The femora and ribs were both sampled at the mid-shaft and variables measured include total cross-section area, number of intact and fragmentary osteons, osteon area and population density and % Haversian bone (Lad et al. 2019). Femora osteon population density (OPD) was lowest at 5.40/mm^2 while rib OPD was highest at 17.39/mm^2 (Lad et al. 2019). Percent Haversian bone was lowest in the femur at 11.43% and highest in the rib at 28.01% (Lad et al. 2019). Osteon area was lowest in the rib at 0.0171mm^2 and higher in the femur at 0.0215mm^2, but this was highest in the tibia at 0.0236mm^2 (Lad et al. 2019). OPD and osteon area were statistically significantly different between the femur and rib, but % Haversian bone was not significantly different between

elements, suggesting that this may be relative to bone size (Lad et al. 2019). A key conclusion from Lad et al. (2019) is that remodelling is impacted to a greater extent by strain frequency rather than magnitude, which would explain the increased OPD, % Haversian bone area and higher osteon area in the rib, which all suggest a higher remodelling rate in the rib (Hert et al. 1971; Miszkiewicz 2016; Rubin et al. 2002; Skedros et al. 2005). Elsewhere, smaller osteons have been associated with localised compression activities while larger osteons have been associated with localised tension activities (Skedros et al. 1994; 1997; van Oers et al. 2008b). This could also reflect the differences in osteon size between the rib, primarily under compression load, with little tension load, associated with respiration, and femur, which is under compression, but also extremely variable tension load associated with dynamic movement patterns (Agnew and Stout 2012; Crowder and Rosella 2007; Lad et al. 2019; Pfeiffer et al. 2006; Skedros et al. 1994; 1997; 2013b; van Oers et al. 2008b). The trends identified in Lad et al. (2019), could be more similar to human results as macaques are more closely related to humans as a species than animals used in the previously discussed studies, such as pigs, dogs and elephants, and also have a more similar mode of locomotion, occasionally using bipedalism for short stints (Kimura 1985).

Stewart et al. (2021) conducted a similar study to Lad et al. (2019), but using an eastern grey kangaroo to look at intra-skeletal variability between the long bones and ribs within the same individual. The key focus of this paper was to categorise differences in microstructural variables between the included skeletal elements, measuring maximum bone length, cortical width and midshaft circumference to apply robusticity indexes to raw data to account for differences in bone size prior to analysis (Stewart et al. 2021). Microstructural variables observed include vascular canal density per mm^2 of bone and total vascular canal density which was the summed vascular density of each region of interest in each bone, i.e. vascular density per $12mm^2$ (Stewart et al. 2021). In using multiple skeletal elements from one individual, Stewart et al. (2021) avoided biases associated with inter-individual differences that influence the bone remodelling process and the proxies by which we observe this process histologically, such as genetics (e.g. Bassett et al. 2012), sex (e.g. Ortona et al. 2023), physical activity patterns (e.g. Robling et al. 2006), disease (e.g. Rabey et al. 2015) and age (e.g. Goliath et al. 2016).

Results of Stewart et al. (2021) indicated that the rib was significantly more highly vascularised than the femur, whether corrected for robusticity based on bone midshaft circumference and bone length, or cortical width. While most of the bones included in this study were statistically significantly different from each other, the femur and rib were the most statistically significantly

different example of a weight-bearing versus non-weight-bearing bone, in terms of vascular canal density (Stewart et al. 2021). The significantly higher vascularity of the rib than femur has been described in humans (Frost 1969). Results of Stewart et al. (2021) suggest that the rib may be more metabolically susceptible than other skeletal elements, with the exception of the fibula, which may be a kangaroo locomotion byproduct of angled repeated activity associated with jumping to change direction quickly, similar to patterns identified in some human athletes (Goh et al. 1992; Hopwood and Butterfield 1990; Miller et al. 2017; Takebe et al. 1984). Fatima et al. (2019) has suggested that kangaroos are useful as experimental models for humans in studies of biomechanics and bone adaption due to many similarities in bipedal locomotion and shared biomechanical load distribution patterns. Thus, the results described in Stewart et al. (2021) may provide some context to the results that are revealed in this research. Particularly in light of human-based studies, such as that by Cho and Stout (2011), who identified significantly higher OPD in the rib compared to the femur. This further reinforces prior literature in suggesting that femoral weight-bearing load is significantly higher and is more irregularly distributed than the rib (Cho and Stout 2011; Pfeiffer et al. 2006).

As it can be seen from the literature discussed above, using animal models to investigate intra-skeletal remodelling differences between the rib and femur have repeatedly identified differences in how these two bones respond under a variety of experimental factors, including the administration of hormones (High 1987), differential weight-bearing patterns (Lad et al. 2019; Nganvongpanit et al. 2017; Raab et al. 1991; Stewart et al. 2021; Tommerup et al. 1993), and the effects of lactation (Vajda et al. 1999). However, it is important to consider whether results determined in an animal experimental model are replicable in a human study, such as when observing patterns based on weight-bearing activities in quadrupedal or mix-modal species.

3.3 The Research Gap

The literature described above provides context for the research questions that have been answered before, which populations have been studied and give rise to this research. A common theme woven throughout the archaeological and anatomical evidence, as well as evidence from experimental animal models, is that population is an important variable, whether due to environmental, genetic or behavioural patterns. Few studies have observed individuals from Australia (Maggio 2022; Maggio and Franklin 2019; 2021; Pedersen et al. 2024) and the wider Pacific Region (Miszkiewicz et al. 2020; 2021; 2022a; 2022b; Snoddy et al. 2022; Walker et al. 2023a; 2023b). Here, there is an opportunity to study contemporary Australian donors, which have been understudied (Maggio 2022; Maggio and Franklin 2019; 2021; Pedersen et

al. 2024), are difficult to access in large numbers and usually are associated with older age-at-death averages and a skew towards male donors (Jiang et al. 2020). This research has the unique opportunity to expand the available sample size and demographic range of age-at-death and sex distributions by also observing medieval British individuals, which are a genetically ancestral population of the vast majority of contemporary Caucasian Australians (Australian Bureau of Statistics 2021).

As few studies have conducted histological analysis of Australian human bone, it is important to investigate histological variation with age-at-death and biological sex within this understudied population, which has been advocated for in the literature (García-Donas et al. 2016). Maggio and Franklin (2021) identified increasing osteon population density (OPD) with advancing age-at-death, but did not measure fragmentary OPD, which more recently has been postulated as a more accurate measure of age-at-death as fragmentary OPD increases exponentially more so than intact OPD (Crowder et al. 2022). Pedersen et al. (2024) identified increasing OPD and fragmentary OPD with advancing age-at-death. Advancing age has also been associated with intracortical bone loss and increased porosity (Agnew and Stout 2012; Dominguez and Agnew 2016).

Biological sex of samples investigated for histology is an important factor because females and males have different hormonal activity underlying bone remodelling (Bhattarai et al. 2020; Frenkel et al. 2010; Ortona et al. 2023), with females experiencing estrogen loss around the time of menopause (Cauley et al. 2003; Compston 2001; Frenkel et al. 2010; Khosla and Hofbauer 2017; Krum et al. 2008; Riggs et al. 2002). Dominguez and Agnew (2016) did not identify any associations between biological sex and osteon area in the human rib, however, Kim et al. (2007) identified statistically significant differences between Korean male and female ribs, with males having higher OPD, and females having higher osteon area. Young females had higher Haversian canal area than males, but as they progressed beyond menopause, males quickly overtook them and had statistically significantly higher Haversian canal area (Kim et al. 2007). There were no significant difference in cortical area between the sexes (Kim et al. 2007). However, skeletal biology demonstrates that females will be subjected to increased cortical bone loss via trabecularisation of the cortex as they age, resulting in increased cortical porosity and decreased cortical width (Cauley et al. 2003; Compston 2001; Frenkel et al. 2010; Khosla and Hofbauer 2017; Krum et al. 2008; Riggs et al. 2002). Thus, it is important to investigate these variables when observing histological sex differences in human bone.

It is becoming increasingly clear that human social and economic status has a genuine impact on the risk of developing bone metabolic issues, such as osteoporosis and osteopenia (Brennan-Olsen et al. 2016; Courtney et al. 2023; Syddall et al. 2012). However, very few studies of bone histology include socioeconomic status in their study design (Miszkiewicz and Mahoney 2016). Socioeconomic status would be a useful application as the literature documents statistically significant differences in human femoral cortical bone microstructural geometry and proliferation between individuals of differing socioeconomic status (Miszkiewicz and Mahoney 2016). However, we do not know how socioeconomic status impacts upon human rib cortical bone as this has not been investigated. The literature demonstrates that microstructures in the rib are more likely to reflect systemic change or influence within an individual than the femur as the rib is not subject to inter-individual differences in biomechanical loading (Agnew and Stout 2012; Crowder and Rosella 2007; Dominguez and Agnew 2016; Karlson 1998; Paine and Brenton 2006; Stewart et al. 2021; Tommerup et al. 1993). Thus, by looking at human rib microstructure through the lens of socioeconomic status, we may see more pronounced effects of diet, nutrition and general health which are highly influenced by an individual's socioeconomic status and access to resources as a result of their status (Chantler et al. 2012; Lauderdale et al. 1998). Key variables to observe differences in socioeconomic status might target differing patterns of physical activity and biomechanical loading, such as OPD (Miszkiewicz 2016; Raab et al. 1991; Skedros 2005; Skedros et al. 2005; Tommerup et al. 1993) and osteon circularity (Rothschild and Panza 2007), as well as porosity and bone loss variables which may be associated with poor general health and nutrition (Aaron et al. 1992; Appelman-Dijkstra and Papapoulos 2018; Brickley and Ives 2008; Corral-Gudino et al. 2013; de Boer and van der Merwe 2016; Ferrari et al. 2015; Gallagher 2013; Goltzman 2018; Lips et al. 2013; Lu et al. 2017; Mays 2014; Ortner 2003; Rolvien et al. 2017; Schultz 2001; Shore and Chesney 2013a; 2013b; Waldron 2008).

It is also important to interpret differing results in the effects of age-at-death, biological sex and socioeconomic status between the rib and femur to better understand how bones, even within the same individuals, may be differently impacted by extrinsic and intrinsic factors due to their functional adaptation and different primary purpose (weight-bearing femur versus the protective rib) and subsequent different metabolic patterns (Agnew and Stout 2012; Crowder and Rosella 2007; Dominguez and Agnew 2016; Karlson 1998; Paine and Brenton 2006; Stewart et al. 2021; Tommerup et al. 1993). Few studies that have observed both the rib and the femur, have discussed the meaning behind how these bones were differently impacted by the factors they were investigating, especially in terms of skeletal biology. However, this

provides important context for understanding the mechanisms behind why the femur and rib respond in the ways they do to these factors.

There have been no previous studies that have compared a medieval to a contemporary population with shared ancestry. Previous work by Pfeiffer (1998) has looked at temporal change broadly, but between populations of different ancestry and from vastly different geographical regions, England, Canada and South Africa, enabling factors such as genetic influence and geographical and societal impacts upon human behaviour to go unchecked or unaccounted for. There is a commonly held perception that contemporary humans are more sedentary in modern Western societies than in the past, where during medieval times humans engaged in more physically laborious roles in their day-to-day life (Dyer 2000; Judd and Roberts 1999; Zvi 1981). The literature has demonstrated that sedentism, inactivity and limb disuse result in compromised bone quality and metabolism (Aloia 1994; Burr 2010; Frost 2000; Robling et al. 2006; Schlecht et al. 2012; Zebaze et al. 2010). In underactive people you would expect to see lower bone remodelling rates, and thus lower OPD (Miszkiewicz 2016; Raab et al. 1991; Schlecht et al. 2012; Skedros 2005; Skedros et al. 2005; Tommerup et al. 1993), more circular osteons with reduced angular strain which contributes to elongated osteons (Frost 1964; Keenan et al. 2017; Nareliya Mishra et al. 2022; Skedros 2024), larger osteons associated with reduced remodelling rates (Schlecht et al. 2012; Skedros et al. 2001; Tuckermann and Adams 2021; van Ooers et al. 2008a; 2008b), increased cortical thinning and cortical porosity due to understimulated bone failing to reach upper limits of bone rocusticity (Aloia 1994; Frost 2000; Robling et al. 2006). Additionally, it may be useful to identify which variables may be diagnostically different between medieval and contemporary humans, which has not been achieved before, in order to differentiate methodologically between temporal populations from the same site or region. Overall, it is important that we draw conclusion for modern populations from ancient samples, only after direct comparison of both.

Histomorphometric methods need to improve in conjunction with our disciplinary understanding. With studies now focusing on intra-skeletal differences between bones (e.g. Pedersen et al. 2024) and intra-element differences (e.g. de Gruchy et al. 2024) within the same bone, it is important to understand how these impact sampling strategies in histology. De Gruchy et al. (2024) recently measured intra-element variation in the femur, focussing on the periosteal versus endosteal surfaces within the same cross-section. The endosteal surface was found to have higher osteon population density, while the periosteal surface had the lowest and mid-cortical region fell in the middle (de Gruchy et al. 2024). However, only the difference between the endosteal and periosteal surfaces were statistically significant. This

was not the case across each of the 16 individuals sampled in the study, with 2 of them having the opposite, with highest OPD in the periosteal region and lowest in the endosteal region, while 6 individuals had lower OPD in the mid-cortical region than both the periosteal and endosteal regions (de Gruchy et al. 2024). This work suggests that intra-element variation can occur even within the same cross-section, but did not look at differences between two neighbouring cross-sections to see if histological variables change as you traverse the length of a bone shaft. De Gruchy et al. (2024) only looked at the femur, and no previous studies have compared histology between two neighbouring serial cross-sections within the rib to ascertain whether sampling location can impact upon results.

Further, several studies have now looked at differences in femoral and rib microstructure and metabolism, but few have controlled for inter-individual differences. Paired analysis approaches of rib and femur histology is imperative to properly understand functional adaptational differences in these two bones, to control for differences between individuals such as body size, genetics, biological sex, age-at-death, socioeconomic status and systemic health. Additionally, due to size and robusticity differences between the bones, even within the same individuals, cortical bone histological variables should focus on osteon morphometrics to compare 'like-for-like' structures, such as osteon and Haversian canal area, diameter and perimeter for osteonal size comparisons (Dempster et al. 2013), and osteon and Haversian canal circularity, roundness, aspect ratio and solidity for measures of osteonal shape (Dempster et al. 2013; Doube et al. 2010; Zdilla et al. 2016). To date, no one has looked at the rates of growth of osteons and their paired Haversian canals to confirm if this differs or occurs proportionally to each other, or if this can differ between the rib and the femur. This measurement of comparative growth rates has been applied to related biological structures elsewhere in zoology (Shingleton 2010), but has not been applied in a human context to look at rates of growth of the two key bone microstructures observed in human bone histology.

There are significant benefits in working with human skeletal samples as opposed to both modern cadaveric human samples and experimental animal samples. Firstly, despite experimental animal models playing a crucial role in our understanding of bone adaptation (Bassett et al. 2007; Biewener and Bertram 1994; Bourrin et al. 2000; Goren 2023; Grandhi et al. 1986; High 1987; Jowsey 1966; Lad et al. 2019; Lanyon and Rubin 1984; Nganvongpanit et al. 2017; Rott et al. 2022; Singh et al. 1974; Stewart et al. 2021; Tommerup et al. 1993; Vajda et al. 1999), no animal model is able to imitate the human interaction of physical activity and bone metabolism due to the unique patterns in bone metabolism and locomotive biomechanics. Secondly, there are inconsistent results between experimental animal models

and human skeletal studies, which could be partially due to differences in timing of growth spurts and differences in overall growth rates between species, as well as a general lack of cortical bone remodelling in non-human species except for under tremendous load (Erben 1996; Forwood 2008; Martin 2007; Yao et al. 1999). Thirdly, skeletal samples enable histological analysis rather than relying on radiological techniques which subject living humans to large doses of radiation and provide sub-par remodelling data. Lastly, skeletal histological samples as opposed to cadaveric samples allow for a larger sample size, giving greater statistical power and therefore greater weight to interpretation of results.

3.4 Restatement of Research Questions and Hypotheses

The following research questions with associated hypotheses have been formulated based on the literature reviewed above.

Research Question 1

Does human rib and femur histology vary with age-at-death, sex and systemic health and physical activity (as inferred by socioeconomic status) in samples of English ancestry?

Age-At-Death

$H0_a$: There is no monotonic relationship between absolute (chronological) age-at-death (AAD) and either observed variable; OPD, Fg.OPD, Ct.Po or Ct.Wi.

$H0_b$: Each of the observed variables (OPD, Fg.OPD, Ct.Po or Ct.Wi) have a similar distribution across AAD categories.

$H0_c$: Each of the observed variables (OPD, Fg.OPD, Ct.Po or Ct.Wi) have a similar distribution across the rib and the femur.

Biological Sex

$H0_a$: Each of the observed variables, OPD, Fg.OPD, On.Ar, H.Ar, Ct.Po and Ct.Wi have a similar distribution in male and female groups.

$H0_b$: Each of the observed variables, OPD, Fg.OPD, On.Ar, H.Ar and Ct.Po have similar distributions between the rib and femur.

Socioeconomic Status

$H0_a$: Each of the observed variables, OPD, On.Circ, Po.Ar, Ct.Po, Ct.Wi and %Ct.Ar have a similar distribution across the three socioeconomic status (SES) groups; medieval lower class, medieval upper class and contemporary.

$H0_b$: Each of the observed variables, OPD, On.Circ, Po.Ar and Ct.Po have similar distributions between the rib and femur.

Research Question 2

Is there a trend of bone quality "deteriorating" in contemporary individuals to reflect generally more sedentary lifestyles than their medieval ancestral population?

$H0_a$: Each of the observed variables, OPD, On.Circ, On.Ar, %Ct.Ar, Po.Ar and Ct.Po have a similar distribution between medieval and modern era individuals.

$H0_b$: Medieval and modern ribs and anterior femora cannot be separated using discriminant function analysis (DFA), based on the variables OPD, On.Circ, On.Ar, Po.Ar and Ct.Po.

$H0_c$: There is no evidence of a more sedentary lifestyle influencing modern individuals as compared to medieval individuals in either observed variable; OPD, On.Circ, On.Ar, %Ct.Ar, Po.Ar and Ct.Po.

Research Question 3

Is there variation in standardised histological variables between serial cross-sections from the human rib midshaft?

$H0_a$: There is no monotonic relationship in either observed variable; Ct.Ar, Ct.Wi, Ct.ArA, Po.Ar, On.Ar, H.Ar, Ct.Po, OPD, Fg.OPD and On.Circ between paired serial histological sections of the rib, approximately 1cm apart in the rib shaft.

$H0_b$: Each of the observed variables; Ct.Ar, Ct.Wi, Ct.ArA, Po.Ar, On.Ar, H.Ar, Ct.Po, OPD, Fg.OPD and On.Circ have a similar distribution between paired serial histological sections of the rib, approximately 1cm apart in the rib shaft.

Research Question 4

Does cortical bone histology vary between bones of different levels of metabolic activity, such as the femur and the rib?

$H0_a$: Each of the observed osteon and Haversian canal size variables, On.Ar, H.Ar, On.Dm, H.Dm, On.Pm and H.Pm, have a similar distribution across the rib and the femur.

$H0_b$: There is no difference in the osteon and Haversian canal shape variables, On.Circ, H.Circ, On.Rd, H.Rd, On.AsRa, H.AsRa, On.Sd and H.Sd, between the rib and the femur.

$H0_c$: There is no difference in the osteon and Haversian canal growth rates, (1) between osteons and Haversian canals, and (2) between the rib and the femur.

Chapter 4 Materials

Here, the two key sample sets from the St. Gregory's Priory and Cemetery Osteological Collection and the AFTER are described. Previous research using the individuals studied here and other individuals from these same sources is detailed. The demographics and contextual information recorded at the time of body donation (AFTER), and sample collection (St. Gregory's Priory and Cemetery Osteological Collection) are presented to fully describe the materials used in this research.

4.1 Sample Sources

Two sample sets were examined as part of this research. One is comprised of contemporary humans (donors) and includes known age-at-death and sex, and some medical history. The second is archaeological with estimated age-at-death, sex and social status, based on standard anthropological biological profiling methods. Here, both of their respective governing institutions, provenance, and contextual information for each are described.

4.1.1 Australian Facility for Taphonomic Experimental Research (AFTER)

Taphonomy is the study of the decomposition and/or fossilisation process undergone by organisms, as well as changes in the environmental surrounds of the organism's remains and can involve observing this phenomenon at either a macro- or microscopic scale (Bell 2012; Varlet et al. 2020; Voss et al. 2020). This field largely has roots in the forensic discipline, to better understand the events surrounding human decomposition processes in victims of murder, war or similar, particularly in a variety of environmental and other conditions unique to a body deposition site (Schotsmans et al. 2020; Varlet et al. 2020). Research in this area has traditionally involved the study of decomposition in laboratory animals, especially those with larger surface areas, more similar to humans, such as pigs (Hewadikaram and Goff 1991; Payne et al. 1968; Shean et al. 1993; Varlet et al. 2020). While previously, controlled animal taphonomy studies took place within laboratories, many forensic institutions have begun conducting semi-controlled experiments in outdoor locations, and on-site purpose-built facilities (Forbes 2017; Varlet et al. 2020). This allows investigation into the effects of a variety of environmental factors unique to the local geographic region and has also allowed for the development of human body donation programs whereby individuals can choose to donate their body to forensic science in the event of their death. The world's first 'body farm' was opened in 1981 in Knoxville Tennessee, USA and since then, similar facilities have opened elsewhere in the US (n = 8; Connor et al. 2024; George et al. 2022; Gocha et al. 2022; Jantz and Jantz 2008), Canada (n = 1; Pecsi et al. 2020), The Netherlands (n = 1; Oostra et al. 2020)

and Australia (*n* = 1; Forbes 2017), with some discussion of one being established in the United Kingdom (Williams et al. 2020) (Forbes 2017; Vidoli et al. 2017). These facilities are often established as joint ventures between universities and forensic bodies for both research and industry-led training purposes.

4.1.1.1 The AFTER Facility

The Australian Facility for Taphonomic Experimental Research (AFTER) was established in January 2016 by the University of Technology, Sydney (UTS), jointly funded by an Australian Research Council (ARC) Linkage Infrastructure, Equipment and Facilities (LIEF) grant and by affiliated academic, police and forensic organisations (Schotsmans et al. 2024; University of Technology Sydney 2017). The main purpose of the AFTER facility is the study of taphonomy, to better understand the biological, physical, and chemical processes of decomposition (University of Technology Sydney 2017). Structurally within the UTS, AFTER is situated in the Centre for Forensic Sciences and the Surgical and Anatomical Science Facilities, but is physically located approximately 50km northwest of Sydney, in Hawkesbury, NSW, Australia on a remote bushland property (33° 38' S, 150° 39' E) (Figure 4.1) (Barton et al. 2020).

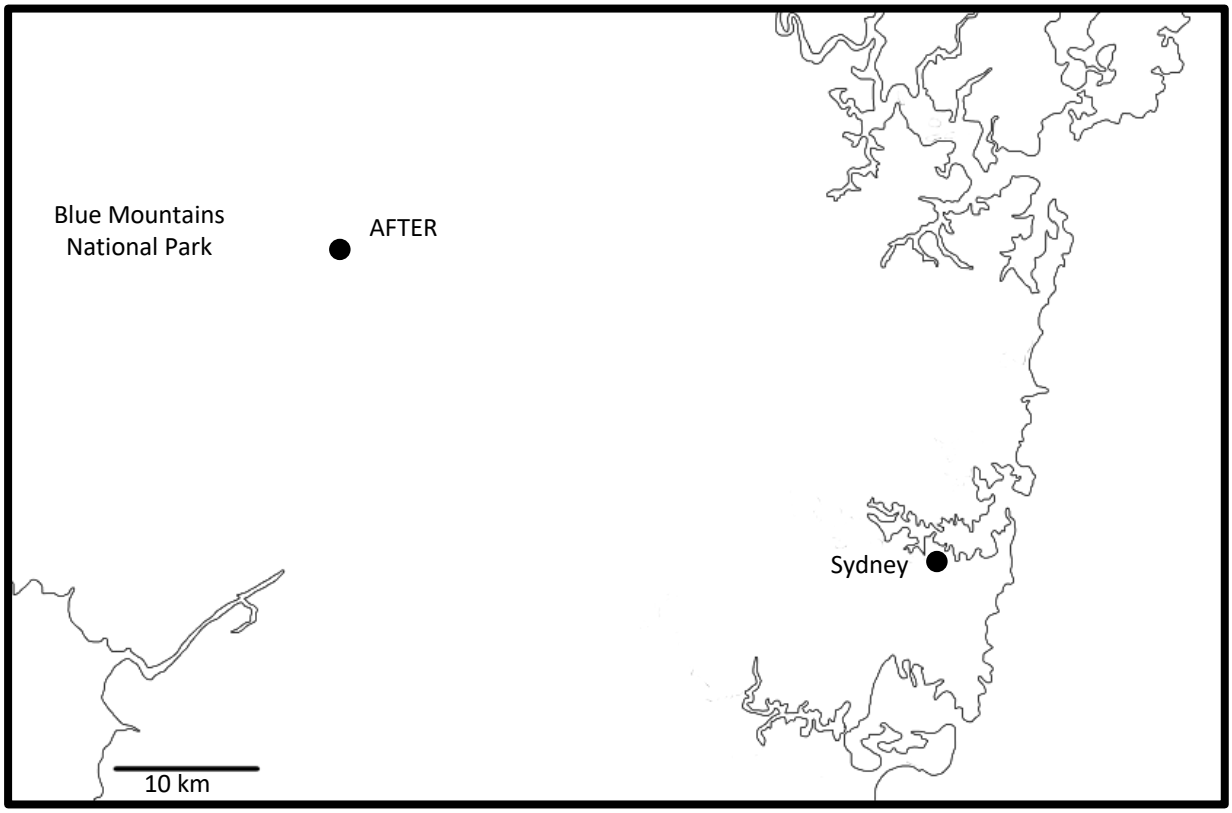

Figure 4.1: The location of the AFTER facility, northwest of Sydney, at the base of the Blue Mountains.

AFTER and its surrounding property extends for 4.86 hectares, with a variety of natural environments replicated on the grounds for decomposition simulation (Barton et al. 2020; Schotsmans et al. 2024). This part of south-east Australia has been categorised by the Köppen Climate Classification System as a moist, mid-latitude climate, which has summers ranging from warm – hot and experiences mild winters (University of Technology Sydney 2017). The facility is closed to the public and is considered “maximum security” (University of Technology Sydney 2017). The broader region is characterised as Cumberland Dry Sclerophyll Eucalyptus Forest with soils ranging from sandy clay loam to gravelly sandy clay (Barton et al. 2020; Knobel et al. 2019; Luong et al. 2018). Topsoil is dark brown and organic-rich to an approximate depth of 15cm, with a lower horizon of mostly sands, with some silt inclusions extending to approximately 30cm deep (Barton et al. 2020; Luong et al. 2018). The topsoil has been described as acidic with a pH level of 5.5 with an average electrical conductivity level of 80.9□S/cm (Schotsmans et al. 2024; Watson et al. 2020). The subsoil has been characterised as comprised of minor clays, coloured yellow, brown and grey to a depth of approximately 80cm (Barton et al. 2020; Luong et al. 2018). The subsoil has also been described as acidic, with a pH level of 5.8, and an average electrical conductivity level of 58.8μS/cm (Watson et al. 2020). Soil composition is particularly relevant to this research as multiple of the individuals observed histologically in this study spent time buried within AFTER and surrounds prior to sampling, which will be further described below.

4.1.1.2 AFTER Research

AFTER facilitates collaboration between a variety of institutions conducting research on human burials and is the first of its kind in the southern hemisphere (Forbes 2017). Many studies conducted at AFTER have focused on using pig carcasses as a proxy for human decomposition processes (Barton et al. 2020; Dawson et al. 2020; Knobel et al. 2019; Marhoff-Beard et al. 2018; Menzies 2021; Ueland et al. 2018; 2019). However, there has been extensive research conducted on the human donors, including many of the same individuals observed in this research, largely focused on outcomes related to the decomposition process (Barton et al. 2020; Blau et al. 2018; Dawson et al. 2020; Deo et al. 2019; Knobel et al. 2019; Luong et al. 2018; Marhoff-Beard et al. 2018; Menzies 2021; Skopyk et al. 2021; Ueland et al. 2021a; 2021b; Watson et al. 2020; Wilson et al. 2020). This also includes, more recently, taphonomic degradation of bone microstructures using histology as the main method of investigation (Schotsmans et al. 2024). Here, the previous research on AFTER donors is described.

AFTER researchers have conducted the first Australian-climate specific studies on how the decomposition process influences body surrounds, such as soil chemical composition (Barton et al. 2020; Luong et al. 2018). Luong et al. (2018) determined that in human decomposition studies in Australia, burial plots must be at least 5x5m^2 as lateral leaching of cholesterols from the body could infiltrate the soils to this extent. In addition, sediment substrate was also affected up to 49cm below the body (Luong et al. 2018). Barton et al. (2020) identified increased soil moisture, electrical conductivity, as well as higher levels of nitrate, ammonium and phosphorus in the region directly under a cadaver, up to 30cm below the body, and that these levels persisted up to 700 days. The presence of nitrate, ammonium and phosphorus may lead to increased rates of diagenesis at localised points in bone histology at regions of pooling beneath the body, as described by Barton et al. (2020). However, the AFTER individuals were sampled at the sternal third margin of the rib, and at the anterior femur, both of which are superior facing when a body is laying in the supine position. Additionally, it can be expected that if the presence of these biochemicals is consistent between individuals, that results will also be consistent based on localised histological diagenesis between individuals.

Wilson et al. (2020) used time-lapse photography to track body positioning and movement in AFTER donors throughout the decomposition process over a 16-month period. Results demonstrated that there was significant movement in all limbs, with the most amount of movement occurring in the lower limbs overall, but with the furthest displacement occurring in the right radius at the styloid process, which moved >51cm (Wilson et al. 2020). Additionally, results showed that most post-mortem limb movement occur in advanced decomposition, during the mummification phase (Wilson et al. 2020). While these results are important for the forensics field, it is not expected that differences in limb movement will influence histological results.

There is a large body of research focusing on cadaveric odor detection, with a particular focus on cadaver dogs. AFTER has facilitated research into volatile organic compound profiles which are by- and end-products of the decomposition process, and form the scent picked up by cadaver dogs (Deo et al. 2019; Knobel et al. 2019; Ueland et al. 2021a). These studies have focused on building a profile of these volatile organic compounds, which are unique to both our Australian temperate climate generally, and seasonal variability within the region (Deo et al. 2019). Studies of the post-mortem interval (PMI) have also been conducted at AFTER, within paper outputs as well as a PhD dissertation (Marhoff-Beard et al. 2018; Menzies 2021). Marhoff-Beard et al. (2018) tested internationally recognized standard methods for estimating time since death, also called the PMI, for the first time in an Australian context (Megyesi et al.

2005; Vass 2011). Their results demonstrated that the Megyesi et al. (2005) method overestimated whilst the Vass (2011) method underestimated the PMI in an Australian context, indicating that the Australian climate and other environmental factors are different to those overseas and require further research. Thus, Menzies (2021) conducted an extensive review of estimating PMI in an Australian context at AFTER, using AFTER donors. Menzies identified significant changes that occurred with PMI, including weight loss, skeletal bleaching rate, the growth and/or retreat of mold/algae species, insect species appearance and/or disappearance as well as their lifecycles at any point in time, and lastly significant weather events or sudden weather changes (Menzies 2021). While Menzies (2021) conducted their research in just one donor, it suggests that many extrinsic factors contribute to the decomposition process, which may differ between burials, even when deposited at the same broader site, due to seasonal change. This is something to consider as a limitation as the AFTER donors observed in this research were deposited at different times and had been deposited for a variety of lengths of time when sampled for histology (Table 4.1).

AFTER has facilitated research into novel ways to locate human burials, using technological advancements in remote sensing, soil topography micro-anomalies, and patterns in below-ground temperature and ground-based weather data (Blau et al. 2018; Watson et al. 2020). Blau et al. (2018) found that topographical mass grave structure was still visible even 18 months after deposition when using light detection and ranging (LiDAR) surveys, but a single grave was not. Additionally, Blau et al. (2018) identified warmer temperatures in graves associated with higher oxygen levels early in the decomposition process, followed by cooler temperatures with oxygen depletion which occurs in late-stage decomposition. Watson et al. (2020) measured the length of time during which gravesites are recognisably distinct from their surrounds by observers based on changes in soil topography. Results indicated that three years after burial, vegetation redistribution remained significantly less than the surrounding area, but at just a brief glance, after approximately 20 months, smaller graves were difficult to detect by sight alone due to leaf litter redistribution (Watson et al. 2020). Insect activity and decomposition stages have long been used in the field of forensics to ascertain time since death but understanding of these is relatively newer in an Australian context (Voss et al. 2009). AFTER has facilitated research comparing these processes between humans and pigs to assess the use of pigs as proxies for humans in such research (Dawson et al. 2020). Dawson et al. (2020) observed that decomposition rates in pigs are faster than humans in both summer and winter climates, with human remains undergoing desiccation or mummification rather than skeletonization in later stages of decomposition, in contrast to pigs. Additionally, the range of insect species present during the first two weeks of decomposition ranged from 2-5 times

higher in pigs than humans, which the authors deducted could be due to differences in body mass, microbiomes, diet and/or medical history, all of which influence the process of decomposition in terms of speed, comparative length of phases and signals to insect species when phases end or begin (Dawson et al. 2020). Skopyk et al. (2021) explored differences in decomposition process and insect colonisation between human individuals and identified that no two individuals underwent identical processes, suggesting that both extrinsic and intrinsic factors influence the decomposition process. Previous research has stated that histological integrity of bone can be compromised in soil after 8-14 years, however, none of the AFTER individuals have spent that long buried prior to sampling for histology (Table 4.1; Astolphi et al. 2019). Further, more recent research, conducted on AFTER donors, suggests that there is no evidence of histological diagenesis in these samples at all, despite undergoing putrefaction, which will be further discussed below (Schotsmans et al. 2024).

Ueland et al. (2021b) observed the effects of fresh versus frozen environments on AFTER donors, identifying differences in the majority of fatty acid analytes between the fresh and frozen specimens. Additionally, the fresh donor demonstrated more distinct phases throughout the decomposition process in both the fatty acids and sterol compounds than the frozen donor (Ueland et al. 2021b). The effects of fresh versus frozen environments on human bone histology are not fully understood. Recently, Schotsmans et al. (2024) used the Oxford Histological Index (OHI), put forward by Hedges et al. (1995) and modified by Millard (2001) to assess the histological effects of diagenesis on fresh versus frozen AFTER donors. Schotsmans et al. (2024) failed to identify any significant differences in OHI scores between fresh and frozen donor human bone histology. Thus, it is not expected that differences in bone histology will be identified in this research based on whether the donor was fresh or frozen prior to their deposition at the AFTER facility.

4.1.1.3 The Donor Samples

The University of Technology Sydney (UTS) Body Donation program is coordinated by the UTS Surgical and Anatomical Sciences Facility. Donor consent was collected, giving permission for their remains to be used for research purposes at AFTER, under the *NSW Anatomy Act 1977*. All use of donor material and contextual information provided by the next of kin and AFTER documentation, was covered by the UTS Human Research Ethics Committee Program Approval (UTS HREC Ref No. ETH15#8208;0029, ETH18#8208;2999), as well as the Australian National University (ANU) Human Research Ethics Committee (Protocol: 2019/041), and is in compliance with legislated and ethical protocols associated with the use of human material in research. All data associated with the 18 AFTER donors included

in this research were provided already anonymised and minimal health and cause of death data were included as considerations when observing bone metabolic processes and individual differences.

The fresh donor remains are refrigerated at 4°C and frozen donors were stored at -28°C within 48 hours post-mortem. Upon arrival at AFTER, donors are placed in designated plots on the grounds to replicate a variety of decomposition scenarios. Cages are placed over external individuals to prevent disturbance by scavengers (Barton et al. 2020; Dawson et al. 2020; Knobel et al. 2019; Watson et al. 2020). Donor associated data typically include individual demographics, some health data, and body processing information.

All donors sampled for this research were of Caucasian Australian ethnicity, and European ancestry. As such, here is a brief background of what we know of modern Australian bone health based on the clinical and medical literature which is of relevance to this research. Australians on average consume approximately 800-900 mg of calcium per day, which falls short of the recommended 1000 mg per day (Australian Bureau of Statistics 2023; Balk et al. 2017). Vitamin D is on average approximately 70.2 nmol/L while recommended levels are > 75 nmol/L (Center et al. 1999). However, when looking on a global scale, these numbers are comparable to the US (calcium: Fulgoni et al. 2015; vitamin D: Looker et al. 2002), Canada (calcium: Sacco and Tarasuk 2009; vitamin D: Langlois et al. 2010) and the UK (calcium: Allen et al. 2013; vitamin D: MacDonald et al. 2008). This suggests that while most Australians are likely not reaching the recommended daily intake of calcium and vitamin D, this is not a uniquely Australian experience. Rather, this appears to be a byproduct of the modern western diet and lifestyle (Dunlop et al. 2023; Shlisky et al. 2022). However, more recent evidence has uncovered that as much as 95% of Australians do not get the recommended daily intake of 10□g per day of vitamin D, and that as many at 1 in 4 Australians >25 years of age could have a serum vitamin D deficiency (<50 nmol/L) (Dunlop et al. 2023). This contrasts greatly with the earlier evidence provided by the International Osteoporosis Foundation and Balk et al. (2017) and could suggest a considerable shift in lifestyle and diet attitudes in Australia over the past decade. How this might manifest in the AFTER individuals would be as osteomalacia, with reduced mineralization of osteoid and reduced osteoblastic activity (Bell et al. 2010). This may appear in histology as slowed bone deposition, larger but fewer osteons due to malnourishment (Bell et al. 2010; Paine and Brenton 2006).

Despite Australian experts recommending approximately 300 active minutes per week, or 60 minutes per day, of physical activity (Johnson et al. 2021), only 25% of Australian adults

reportedly achieve this (Australian Bureau of Statistics 2022a). Furthermore, as these data were self-reported it is estimated that true values are likely to be even lower than this (Johnson et al. 2021). Partially because of low physical activity, rates of obesity in Australia are high, with 35.7% of adults being overweight (body mass index 25-29.9 kg/m^2), with 31.3% of these individuals being obese (body mass index 30 kg/m^2) (Australian Bureau of Statistics 2022a). While some studies suggest that increased body mass index has a positive relationship with bone mineral density, obesity is believed to negatively impact upon key drivers of bone homeostasis and metabolism, by inhibiting vitamin D absorption (Rajakumar et al. 2008; Wortsman et al. 2000); promoting cytokine production via inflammation pathways, which causes bone loss and lower bone mineral density (Lucas et al. 2012; Ouchi et al. 2011); and by lowering osteocalcin, which subsequently inhibits osteoblastic activity (Holecki et al. 2007; Yerlikaya and Onmaz 2022). From the limited health information associated with the AFTER donors, there isn't any information about weight or obesity status, however, several of the co-morbidities listed can be associated as obesity related conditions (Table 4.1). Should any of the AFTER donors have been obese, this might present in their histology as slowed bone remodelling, with larger, and fewer osteons, perhaps evident of less physical activity.

Approximately 924,000 Australians (3.4%) are living with osteoporosis, which is a chronic bone condition whereby an individual has insufficient bone mineral density and thus increased risk of fracture, or osteopenia, which is a precursor to osteoporosis (Australian Institute of Health and Welfare 2024a). However, this increases exponentially with advanced age, with 20% of Australians aged >75 years having osteoporosis and osteopenia (Australian Institute of Health and Welfare 2024a). Although we have cause of death information for each of the donors, we have no health information and so do not know if any of the donors had been diagnosed with osteoporosis or osteopenia during life. Histologically, osteoporotic bone displays interrupted bone metabolism, with bone resorption rates overtaking rates of bone deposition and reduced microstructural population (Henry and Bordoni 2023, further described in Chapter 2). It is expected that the rate of donors affected by osteoporosis or osteopenia would be no more than representative of a modern Australian sample aged >59 years. There are some other health conditions listed in conjunction with their cause of death information which may provide some indication of bone health and/or quality, which are described below.

Donor 1602 had hypertension, also known as high blood pressure (Table 4.1). There have been links drawn between systemic hypertension and decreased rates of bone remodelling, possibly associated with lower levels of osteocalcin and 25-hydroxy vitamin D (Hu et al. 2021). Elevated blood pressure can also raise intraosseous pressure, causing hypoxia (Ching et al.

2021), which is characterised by insufficient oxygen flow to tissues and other structures (Bhutta et al. 2022). This can lead to homeostasis, or localised metabolic interruption and interfere with bone metabolism, triggering periosteal bone remodelling and even altering Wnt–β-catenin signalling (described in Chapter 2) to further reduce bone formation (Ching et al. 2021; Vlashi et al. 2023).

A number of the AFTER donors included in this research experienced cardiac failure in the time before their death, which may or may not have been chronic prior to death (donors affected include 1603, 1718, 1719; Table 4.1). Several experimental studies have identified a significant loss of bone mineral density in heart failure patients versus patients without heart failure (Bozic et al. 2010; Jankowska et al. 2009; Kenny et al. 2006; Majumdar et al. 2012; Terrovitis et al. 2012). However, the relationship between this decreased bone mineral density and heart failure is not fully understood. Heart failure patients tend to have reduced mobility and poor physical activity levels, which could lead to less outdoor time and decreased vitamin D levels; a well-known necessary ingredient for good bone quality (Bhattarai et al. 2020; Loncar et al. 2020). Additionally, decreased biomechanical loading will increase bone loss with reduction in applied geospatial mechanical forces (Zengin et al. 2017). Furthermore, heart failure often involves long-term reliance on diuretics, which can lead to malabsorption of vitamin D and other critical micronutrients for optimal bone health, and even resulting in secondary hyperparathyroid complications (Hagström et al. 2010). However, there has also been a suggest pathophysiological link between osteoporosis and chronic heart failure via the sympathetic nervous system, which is hyperactivated in heart failure and multiple receptors for which are located within bone tissue (Guan et al. 2023). When hyperactivated, the sympathetic nervous system increases osteoclast differentiation, promoting bone resorption and ultimately leading to bone loss (Baek et al. 2017; Guan et al. 2023). Thus, in the AFTER donors affected by heart failure, there may be evidence of more advanced bone loss such as decreased osteon population density, cortical thinning and/or increased porosity.

Renal failure and kidney impairment is listed as a health condition for several AFTER donors (1603, 1718, 1719, 1722, 1804, 1805; Table 4.1). The kidney plays a key role in bone metabolism, as a regulating organ of calcium and phosphorus homeostasis maintenance (Cannata-Andía et al. 2020; Hsu et al. 2020). With the reduced kidney function which comes with renal failure and chronic kidney disease, the metabolic balances of calcium, phosphorous and other key minerals and hormones change, including calcidiol and calcitriol, vitamin D hormones, leading to complications such as increased risk of fracture, significant bone loss and vascular calcification (Cannata-Andía et al. 2020; Hsu et al. 2020). Similar to those who

experienced heart failure in life, we might expect to see more evidence of bone loss and slowed bone remodelling in AFTER donors who experienced renal failure or kidney disease, such as decreased osteon population density, cortical bone thinning, with increased cortical porosity.

A number of the AFTER donors observed in this research were affected by a form of cancer (donors 1617, 1621, 1705, 1717, 1721, 1803, 1805; Table 4.1). Cancer cells can directly impact bone, but cancer treatments can also harm bone health on a cellular level, amplifying the negative effects on bone metabolism (Drake 2014). As a results, many cancer patients are now treated with anti-resorptive therapies to reduce bone resorption which is often elevated by cancer treatments (Drake 2014). However, bone is the most common site of metastases, as cancerous cells can stimulate osteoblasts and osteoclasts to produce cancerous growth factors, quickly proliferating and spreading the cancer (Coleman et al. 2014; Roodman 2004). Stomach cancer patients (such as donor 1617) are at a further increased risk of experiencing bone loss if they undergo a gastrectomy due to acidity reduction post-surgery and lacking the necessary acidification for optimal calcium absorption (Lim et al. 2012). Prostate cancer patients (such as donor 1621) often undergo testosterone suppression inducing therapies as part of their cancer treatments (Drake 2014; Smith 2007). This testosterone suppression reduces the bioavailability of estradiol and can increase fracture incidence in this population by >70% due to bone loss (Drake 2014; Zhumkhawala et al. 2013). Whether their cancer diagnoses place them at an increased risk of bone loss or not, will depend on the treatment trajectories the AFTER donors underwent during life, but there could be more evidence of bone loss in these donors than those who did not have cancer diagnoses.

Two AFTER donors observed in this research (donors 1706, 1717) are listed as having liver disease (Table 4.1). The biggest contributor to bone loss in liver disease patients is reduced bone formation, however there can be an additional, but less pronounced increase in bone resorption as well (Danford et al. 2020; Jeong and Kim 2019). Histological studies have identified suppressed osteoblastogenesis and increased rates of early osteoblast apoptosis, or cellular death, both of which contribute to reduced new bone deposition (Guichelaar et al. 2002). Similar effects are seen in individuals who drink to excess, such as donor 1804. 34% of alcoholics have osteoporosis (Peris et al. 1992). However, while it may seem intuitive that alcoholics also have increased rates of osteoporosis due to their alcoholism via liver disease, it is unknown whether this relationship is due to liver disease or if it relates to malnutrition or other lifestyle habits common in this population (Danford et al. 2020; Jeong and Kim 2019; Ke et al. 2023). Similar to the above conditions, in the AFTER donors with liver disease and

alcoholism, there may be additional signs of bone loss, resulting from more bone resorption than bone deposition.

AFTER donor 1716 had Alzheimer's disease, a degenerative neurological disorder characterised by a progressive decline in patient cognition (Kumar et al. 2021; Loskutova et al. 2009) (Table 4.1). Up to 52% of Alzheimer's patients also have osteoporosis, however the disease pathophysiology is not fully understood (Kumar et al. 2021). The strongest contender for the link between these two diseases, is the abnormal expression of amyloid depositions, which in Alzheimer's disease, involves the deposition of lesions in the brain, and when deposited in bone tissue, may interfere with RANKL signaling (discussed in Chapter 2), causing increased osteoclastic activity and bone resorption (Chen and Lo 2017). It has also been suggested that bone mineral density is most susceptible to Alzheimer's disease pathways in the earliest stages of the disease (Loskutova et al. 2009). Based on the literature described here, donor 1716 may have increased evidence of bone loss visible in their histology than other AFTER donors.

Chronic obstructive pulmonary disease (COPD) is a multi-factorial progressive condition characterised by persistent airflow restriction due to inflammatory responses (Liao et al. 2024; Sarkar et al. 2015). Four of the AFTER donors observed as part of this research had COPD at the time of their death (donors 1618, 1717, 1719, 1806; Table 4.1), which is present in 7% of Australians aged over 65 years (Australian Bureau of Statistics 2022b). COPD patients often have several generalized risk factors for osteoporosis as a co-morbidity, such as having reduced physical activity due to their poor lung function, and the literature clearly demonstrates that regular exercise supports healthy bone metabolism (Li et al. 2022; Santos et al. 2017). Additionally, many COPD patients will be low weight due to hypoxia, or lack of sufficient oxygen to support peripheral tissues which leads to wasting of the muscles and may experience reduced appetite and malnutrition due to lack of activity (Li et al. 2022). This can also equate to reduced mechanical loading pressure being applied to their bones and a subsequent loss of bone mass (Rosen and Klibanski 2009). However, there are also disease-specific risk factors, such as systemic inflammation (Li et al. 2022). The cytokines produced in the systemic inflammation associated with COPD, are key instigators of osteoclastogenesis, in both in-vivo and in-vitro experimental studies, leading to increased rates of bone resorption and equating to bone loss (Bai et al. 2011; Liang and Feng 2012). Furthermore, glucocorticoids are a common treatment for COPD and are known to increase the risk of fracture as they cause a reduction in bone mineral density (Amiche et al. 2016; Sarkar et al. 2015). Glucocorticoids cause early osteoblast apoptosis by altering the Wnt signaling pathway (see Chapter 2) and

prevent osteobastogenesis and maturation via cytokine production (Li et al. 2022; Sarkar et al. 2015; Seckl 2004). It could therefore be expected that these AFTER donors may display evidence of bone loss in their histology due to their COPD diagnoses, similar to the conditions described above.

Donor 1803 (Table 4.1) had been diagnosed with Parkinson's disease, a degenerative neurological condition characterised by progressive neuron loss in the basal ganglia, causing motor and mobility symptoms such as tremors, instability and body rigidity (Burch and Sheerin 2005; Kalia and Lang 2015). It has been acknowledged that Parkinson's disease and bone loss are often co-morbidly linked in patients, however this relationship is not fully understood (Figueroa and Rosen 2020; Liguori et al. 2024). A common byproduct of disease progression is a loss of bodyweight, which could contribute to a reduction in bone mass (Chen et al. 2003). Additionally, a common medication associated with the disease, levodopa, has been linked with reducing bone mineral density (Gao et al. 2015). Of great concern is the increased falls risk associated with Parkinson's disease, which is particularly unsafe in individuals also of increased risk of fracture due to reduced bone mineral density (Tan et al. 2014). Donor 1803 may exhibit evidence of bone loss in their histology due to the Parkinson's disease diagnosis.

Despite many of the previous conditions suggesting that the AFTER donors may exhibit signs of advanced bone loss. It is important to state that they are a representative sample of an advanced age group in a modern Australian context. The above conditions are more common with advancing age, and so it is to be expected that these donors would have been diagnosed with age-related conditions such as those described here. In addition, as outlined in Chapter 2, age-related bone loss occurs in conjunction with these age-related conditions and so it is to be expected that some evidence of bone loss is likely to be encountered during this research. It is rare to gain access to young, modern forensic samples as generally speaking, those who donate their bodies to science have lived to a more advanced age. This is an unfortunate, but necessary to disclose limitation of this research that the donors sampled range in age from 59-93 years of age, and only four of the 18 donors observed in this study were female. This is a common demographic problem encountered by donor collections around the world, skewing in favour of older and male donors (Jiang et al. 2020). However, this research is the first conducted on samples from AFTER using histology to look at bone metabolism variation between individuals, and the first using modern Australian samples to compare rib and femur bone metabolism.

Table 4.1: Individuals sampled from the AFTER Donors.

Donor ID	Samples Collected	Sample Details	Death Date	Placement Date	Days Deposited at time of sampling	Age-At-Death	Sex	Stature (cm)*	Cause of Death	Fresh or Frozen; Clothed or Unclothed; Supine or Prone
1602	ES-HB03 ES-HB04	Right rib Right femur	19/01/2016	02/02/2016	1238	64	M	185	Cardiac arrest, intracranial haemorrhage, occlusive thrombus of abdominal aorta, hypertension	Frozen Unclothed Supine
1603	ES-HB05 ES-HB06	Left femur Right rib	30/01/2016	02/02/2016	1238	76	M	170	End stage cardiac failure, acute on chronic renal failure	Fresh Unclothed Supine
1617	ES-HB07 ES-HB08	Right femur Right rib	29/06/2016	27/07/2016	1062	64	M	172	Weight loss, suspected stomach cancer	Frozen Unclothed Supine
1618	ES-HB09 ES-HB10	Right femur Right rib	04/07/2016	27/07/2016	1063	77	M	172	Hospital acquired pneumonia, pulmonary emboli, pulmonary diseases	Fresh Unclothed Supine
1619	ES-HB11 ES-HB12	Left femur Right rib	26/07/2016	02/08/2016	1057	59	M	152	Aspiration pneumonia	Fresh Unclothed Supine
1621	ES-HB15 ES-HB16	Right femur Right rib	15/11/2016	18/11/2016	949	77	M	171	Metastatic prostate cancer	Fresh Unclothed Supine
1705	ES-HB13 ES-HB14	Right femur Right rib	09/03/2017	11/03/2017	836	69	F	168	Diffuse large B-cell lymphoma, segmental left pulmonary embolus	Fresh Unclothed Supine
1706	ES-HB33 ES-HB34	Right femur Right rib	13/03/2017	17/03/2017	830	74	M	180	Septicaemia, bowel perforation, obstructive chronic hernia, chronic liver disease, rapid atrial fibrillation	Fresh Unclothed Supine
1716	ES-HB17 ES-HB18	Right femur Right rib	23/06/2017	30/06/2017	725	91	M	167	Pneumonia, Alzheimers Disease	Fresh Unclothed Supine

1717	ES-HB23 ES-HB24	Right femur Right rib	04/07/2017	07/07/2017	718	67	F	167	Acute liver failure, liver metastases, metastatic non-small cell lung carcinoma, asthma, COPD	Fresh Unclothed Supine
1718	ES-HB21 ES-HB22	Right rib Right femur	06/07/2017	08/07/2017	717	74	M	176	Sepsis, cellulitis & pneumonia, heart failure, acute on chronic renal failure	Fresh Unclothed Supine
1719	ES-HB35 ES-HB36	Right femur Right rib	07/07/2017	11/07/2017	714	89	M	163	Acute exacerbation COPD, COPD, congestive cardiac failure, chronic kidney disease	Fresh Unclothed Supine
1721	ES-HB25 ES-HB26	Right femur Right rib	31/10/2017	19/03/2018	463	74	M	180	Mesothelioma, prostate cancer	Frozen Clothed Supine
1722	ES-HB19 ES-HB20	Left femur Left rib	25/11/2017	19/03/2018	463	80	M	175	Acute kidney injury, dehydration	Frozen Clothed Prone
1803	ES-HB37 ES-HB38	Right femur Right rib	07/01/2018	10/01/2018	531	87	M	172	Community acquired pneumonia, non-Hodgkin's lymphoma, Parkinson's Disease, Walderstrom's macroglobulinemia	Fresh Unclothed Supine
1804	ES-HB31 ES-HB32	Right femur Right rib	05/02/2018	09/02/2018	501	75	M	168	Haemorrhagic pancreatitis complicated by multiorgan failure, acute chronic kidney disease, alcohol excess	Unknown
1805	ES-HB27 ES-HB28	Right femur Right rib	01/02/2018	19/03/2018	463	93	F	156	Non-ST elevation myocardial infarction, acute renal impairment, metastatic cancer	Frozen Clothed Supine
1806	ES-HB29 ES-HB30	Right femur Right rib	10/02/2018	19/03/2018	463	73	M	164	Pneumothroax pneumonia, exacerbation of COPD, progressive interstitial lung disease, probable secondary to myostasis, scleroderma overlap	Frozen Clothed Supine

*Estimated by the next of kin at the time of body donation.

4.1.2 St. Gregory's Priory and Cemetery Osteological Collection

Canterbury is a historic city, with archaeological evidence dating as far back as the Iron Age (750 BC – 43 AD), and in the 6th Century, became an Archbishop's ecclesiastical jurisdiction, with daily life largely led by religion (Gernay 2015). The St. Gregory's Priory and Cemetery Osteological Collection is part of a British Late Medieval population, held and widely researched at the Skeletal Biology Research Centre at the University of Kent's School of Conservation and Archaeology. This collection is one of the top 5 most well-documented skeletal collections in Britain (Roberts and Mays 2011). The skeletal collection was excavated from St. Gregory's Priory, and neighbouring cemetery in Canterbury, UK (Figure 4.2; Miszkiewicz and Mahoney 2016). The Priory operated in the 11th-16th centuries, and burials from both the Priory and cemetery sites date to this period (Hicks and Hicks 2001a). Priors, their families and high status, wealthy locals were interred within the Priory grounds, while parish members of St Gregory's and neighbouring St Mary and Northgate, as well as the deceased from St John's hospital for the 'poor and infirm' were interred in the St Gregory's cemetery (Dawson 2014; Gernay 2015).

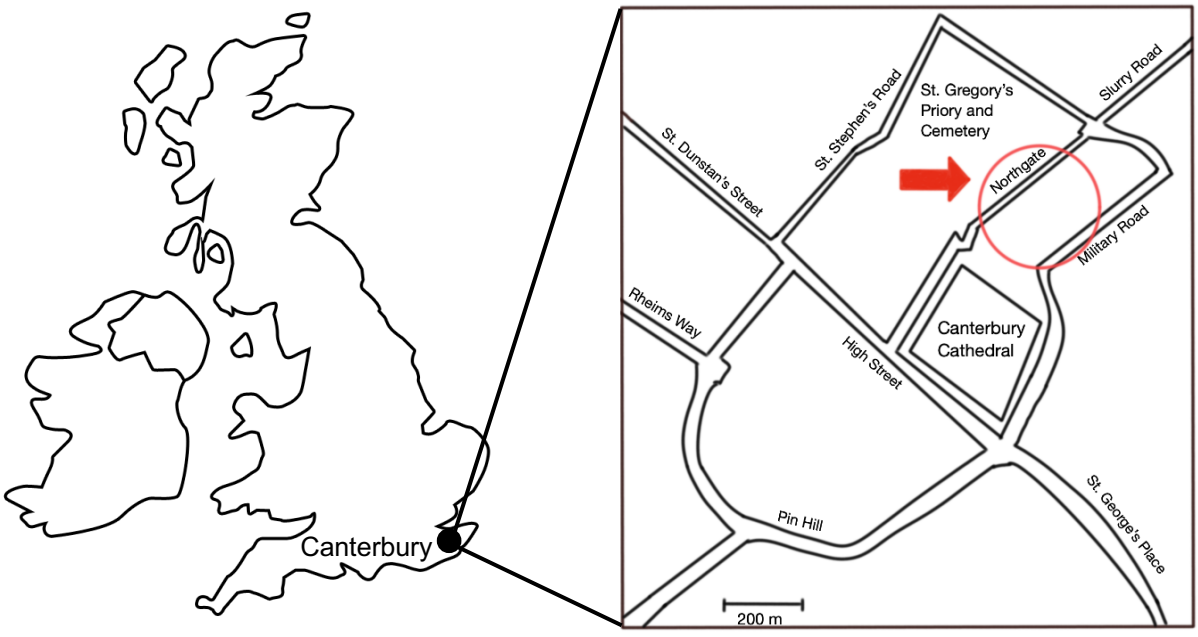

Figure 4.2: The location of St Gregory's Priory and cemetery in Canterbury, United Kingdom. Image by Tahlia J Stewart (adapted from Miszkiewicz and Mahoney 2016).

4.1.2.1 The Archaeological Site

St Gregory's cemetery, church, and later, priory, were excavated in the 1980s by archaeological teams from the Canterbury Archaeological Trust following the discovery of

burials and building foundations during the City construction of a sewer trench at the site (Frere et al. 1990; Hicks and Hicks 2001a; Youngs and Clark 1981). The site has undergone extensive re-building since prior to the establishment of the St. Gregory's Priory. Multiple structures have been built and demolished on site, subsequently overlapping structures that came before. As such, the site's stratigraphy can be difficult to interpret with many overlapping foundations and some instances of grave cuts dividing earlier burials (Hicks and Hicks 2001a). St Gregory's Church and cemetery were established in approximately 1084, by the then Archbishop of Canterbury, Lanfranc (Barlow 1979; Burton 2005). The church was constructed to support 18 priests and clerks who provided pastoral care and administered rites to the sick and dying, performing baptisms, taking confession and burying local people of low socio-economic status free of charge (Burton 2005; Hicks and Hicks 2001a). The church is believed to have been the first structure on what had previously been open, vacant land, comprised of brown loamy soil, extending up to 60cm deep into the stratigraphy of the site. Ceramic inclusions suggest that this stratigraphical layer dates as far back as the late Saxon period (AD 850 – 1066). This early structure was comprised of a long, rectangular building with a clergy room (also called a chancel) beyond the altar at the eastern end of the church and graveyard to the south (Figure 4.3).

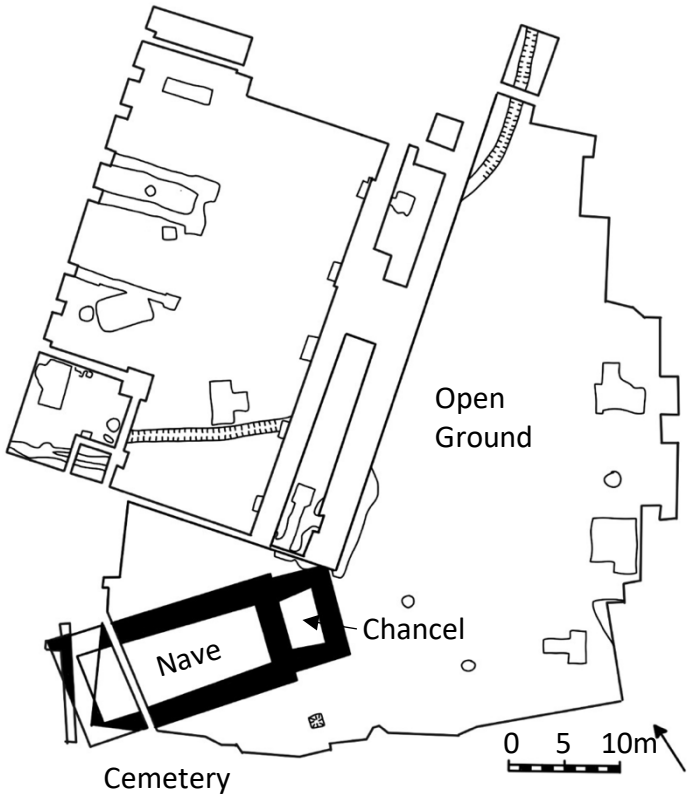

Figure 4.3: St Gregory's Church and surrounds, approximately 1084 AD.
(Image: Adapted from Hicks and Hicks 2001a:2).

St Gregory's Church transitioned to Priory in ~1133 AD, with the appointment of a Prior and his twelve Augustinian Canons, who were followers of St Augustine of Hippo. St Augustine were much more flexible with regards to the types of foods and drink they were allowed than the previous Benedictine clergy, being able to overindulge, which will be elaborated on below. With the transformation to Priory, more construction began at the St Gregory's site (Gaimster et al. 1990). The chancel was extended to transform into a choir and a new chancel was installed, extending the church further east. The main section of the church was expanded to create north and south transepts, with smaller chapels at their eastern ends. Temporary structures to accommodate construction work has been uncovered on the site, including wells, a cesspit and storage pits, as well as short-term accommodation for labourers (Figure 4.4).

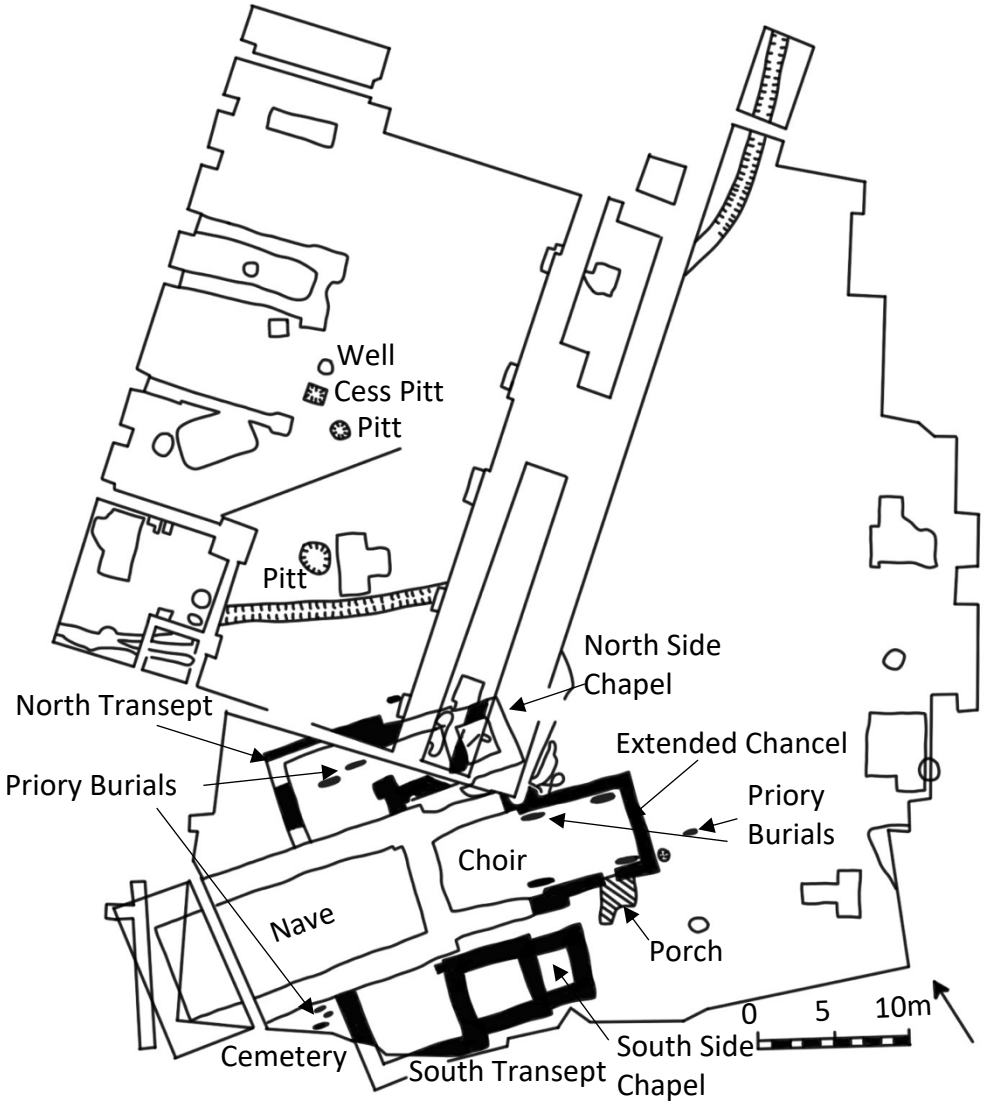

Figure 4.4: St Gregory's Church, prior to the 1145 fire.

(Image: Adapted from Hicks and Hicks 2001a:16).

In 1145, much of the St Gregory's Priory burned down, which lead to its reconstruction with a significantly more grandiose structure, planned under the leadership of Archbishop Theobold (died ~1161) who didn't live to see it fully constructed (completed ~1181). The new Priory had more elaborate multipurpose rooms, including a Prior's lodge, library, refectory, kitchen, cellar, day room, undercroft, chapter house, pentice, an infirmary cloister, multiple lodgings for resident Canons, and multiple courtyards (Figure 4.5) (Gaimster et al. 1990). The new building had sophisticated plumbing infrastructure, capable of bringing piped water into the Priory.

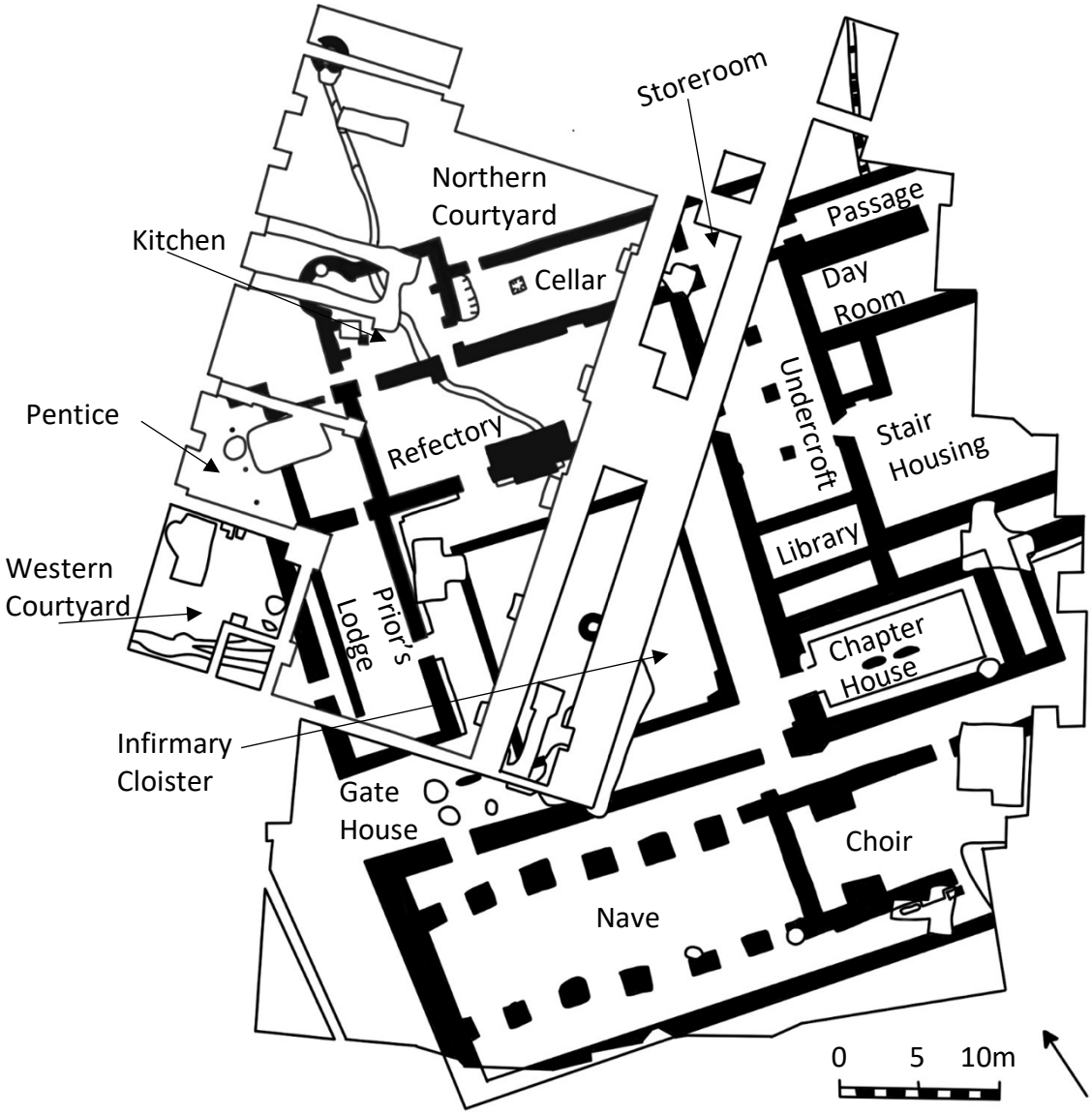

Figure 4.5: Archbishop Theobold's St Gregory's Priory, c. 1181.
(Image: Adapted from Hicks and Hicks 2001a:25).

It has been suggested that St Gregory's Priory was in its 'golden age' and thriving during this period following the rebuild. Decorative murals spanned the walls and artefacts from as far as Egypt were found amongst the priory sedimentary layers (Samuel and Blows 2001),

suggesting importation of more expensive and elaborate items and materials took place during this time. Following a well-documented earthquake in 1382, St Gregory's sustained some damages and again underwent a remodel to repair and improve existing structures. This included further reinforcing of the external walls of the church and the addition of a tower between the Prior's lodgings and church (Hicks and Hicks 2001a). The refectory was also completed retiled at approximately this time, with brand new, elaborate tiles installed, while prior to this time, tiles elsewhere in the Priory had often been removed and reused as needed. Hicks and Hicks (2001a) suggest that there appears to have been an influx of wealth around this time. Renovations of the main cloister, the construction of a 'Lady Chapel' usually associated with an altar to honour the Virgin Mary (Sumpter 2008), and addition of new kitchen infrastructure such as a new oven also occurred around this time (Figure 4.6).

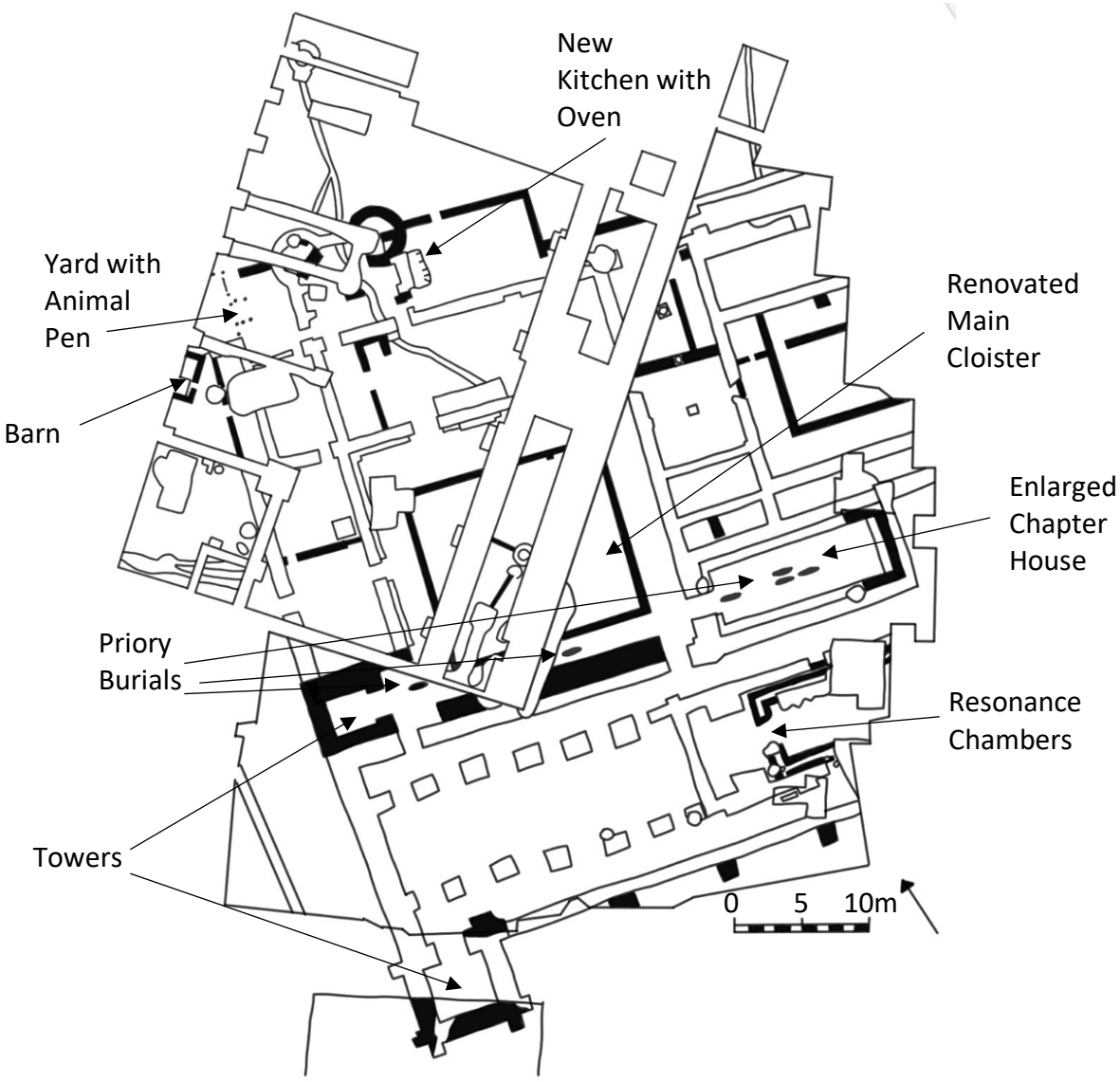

Figure 4.6: St Gregory's Priory following renovations and additions, ~1400 AD.
(Image: Adapted from Hicks and Hicks 2001a:31).

Residents of the Priory had access to sophisticated technologies for the time, such as plumbing and cooling stores, which were essentially pits dug into the ground and lined with timber, intended to keep the contents stored within at a cooler temperature. It has been suggested that such pits could have been used to store oysters and beer, which were common at the Priory (Hicks and Hicks 2001a). There is evidence of ebbs and flows in wealth availability at the Priory, with alternating trends in reusing and importing new materials for renovations, but there does seem to be periods of exorbitant and luxurious spending habits on elaborate food and drink. Animal remains consistent with diet suggest that Priors and other residents ate a large amount of mutton, lamb and pork, specifically 'suckling pig', in addition to wild birds and saltwater fish, all consistent with protein saturated diet and frequent access to high-quality food (Powell et al. 2001). In addition to frequent access to rich, varied foods, residents of the Priory had access to a plumbed water supply (Clarke 1901). Clarke (1901) describes the accidental excavation in 1807 by the military of a pipeline which ran through the St Gregory's gardens, providing water to residents. Once excavated, the pipe was said to be in 'fine condition'. However, it has been suggested that sanitation and hygiene is not really understood at the site as no latrines or 'reredorters' have been identified or excavated. Due to the evidence of piped water entering the Priory, it can be assumed they had the knowledge and means to construct similar infrastructure for cess removal, but no evidence of this has been found.

In 1537, St Gregory's Priory ceased operations and was converted into accommodations for Richard Neville of Nottinghamshire. The Priory remained a residential building for almost 300 years, passing between prominent historical, political and religious figures (Gentles 1980), but in ~1848, it was demolished when the military barracks was constructed on the site. Sometime afterwards, this too was demolished (Bone and Seary 2015) and terraced homes were constructed on top of the foundations, but these were lost in bombings during World War II. From 1961, the site was occupied by multiple high density residential dwellings and a general post sorting office (Wilson and Hurst 1959). These final buildings were demolished in the 1980s, shortly prior to the excavations undertaken by the Canterbury Archaeological Trust in 1988 and 1991, led by Hicks and Hicks, the editors of the key site report and findings (2001b).

4.1.2.2 St Gregory's Burials: Priory and Cemetery

A total of 1,342 graves with interred, articulated skeletons were excavated from the site (Figure 4.7). Generally, skeleton condition and completeness was recorded as being of considerably good quality, with 40% of individuals being at least 75% complete (Anderson and Andrews 2001). All individuals were buried in the supine position, though upper-limb positioning appeared to vary. Approximately 80% of female adults and 75% of sub-adults had their arms

outstretched at their sides, whereas approximately 33% of male adults had their hands resting on their pelvis or chest. 89% of individuals were interred without a coffin and only 2 interments held multiple individuals: a pair of sub-adults and an adult male and female (Anderson and Andrews 2001). Although there were sub-adult individuals excavated from the sites associated with the St Gregory's Priory and surrounds, only adult individuals were observed as part of this research. As such, from herein, only information pertaining to the adult individuals will be included. Though it should be stated that the presence of sub-adults and females inside the Priory has been suggested to indicate the burial of Priors and their families rather than only those directly associated with the Priory (Anderson and Andrews 2001).

The majority of adults (~80%) excavated from the cemetery were male and <10% were older than 40-45 years of age. Burials were not separated according to sex, with male and female burials neighbouring. Similarly, in the Priory, 70% of adult individuals excavated were male and 30% were female. This high male:female ratio is common elsewhere at other monastic and ecclesial excavation sites (Lambrick 1985; Poulton and Woods 1984; Mays 1991; Ward 1990). It has been stated that there is little evidence of burials being opened at a later stage to inter family members or spouses (Anderson and Andrews 2001). Elsewhere, it has been stated that only the 'sacrist', a term referencing a church appointed official, decided where an individual would be buried (Knowles and Brooke 1951), which may suggest that individuals were not able to choose to be buried near those known or related to them.

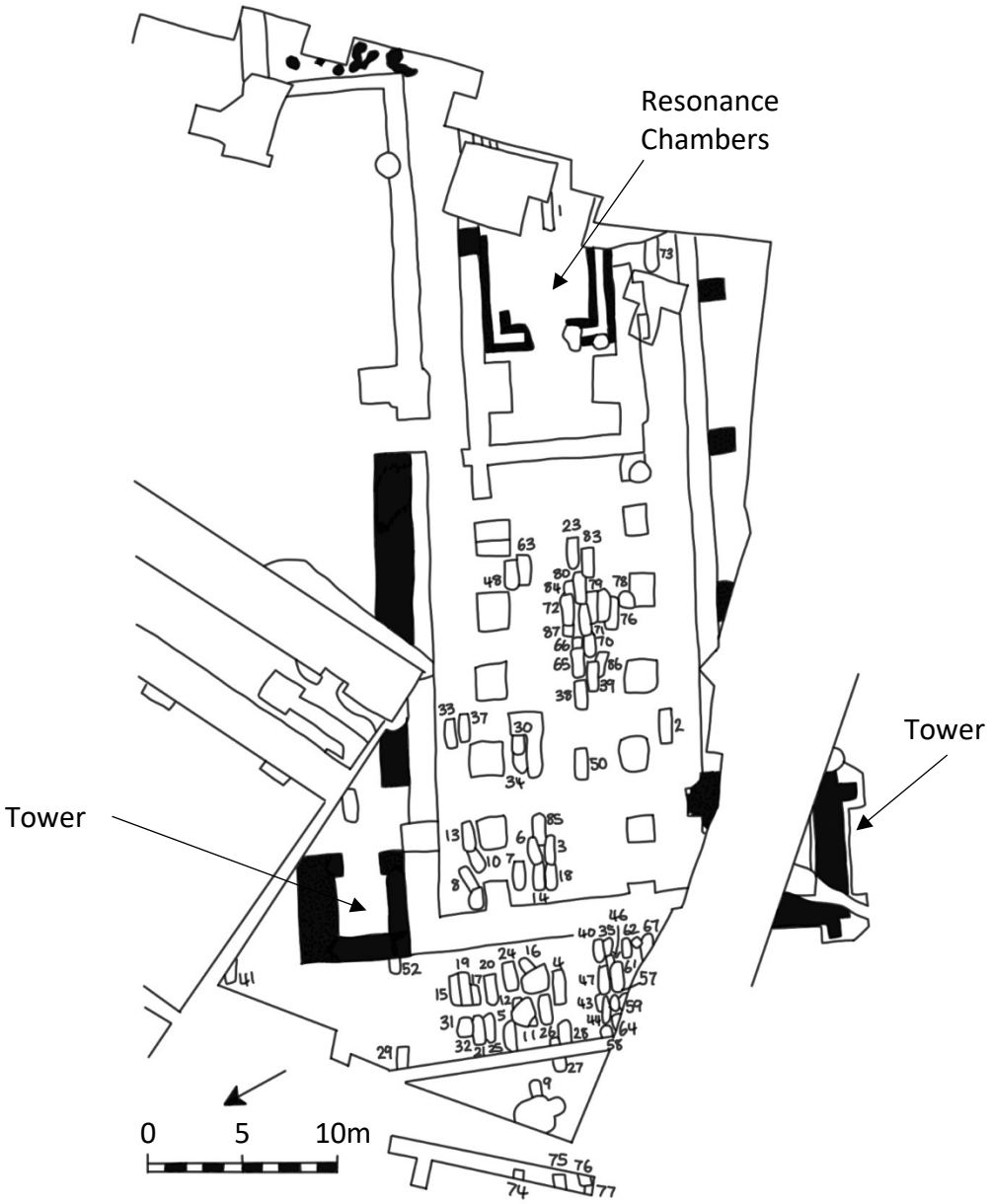

Figure 4.7: The burials excavated from within the Priory grounds, labelled by SK#.
(Image: Adapted from Hicks and Hicks 2001a:44).

4.1.2.3 Palaeopathology and Population Health

There were manifestations of skeletal disease and conditions identified on some individuals within both the Priory and Cemetery groups. One case of a congenital skeletal condition was an adult male with a cleft lip and palate, which was the first such archaeological evidence of this condition within Britain (Anderson 1994). This individual had no evidence of any other bony abnormalities, but did have an 'odontome', which is an odontogenic tumour, arising from the dental lamina as a cluster of odontogenic cells to form a mass of 'tooth-like' structures

(Anderson 1994; Singh et al. 2010). In 390 AD China, surgical intervention had been attempted in similar cases (Bhattacharya et al. 2009), however while there was no evidence of surgical treatment in the St Gregory's case, this individual lived into adulthood (40 – 50 years old; Anderson 2002) suggesting he was cared for. Additional evidence of care for an individual with a skeletal deformity at St Gregory's, is a case of Madelung's deformity of the right wrist in an elderly male individual (Anderson and Carter 1995). This individual had greatly reduced mobility of the right elbow due to the significant shortening of the ulna and radius which occurred to the early fusion of the growth plate during youth (Anderson and Carter 1995).

Other congenital skeletal conditions identified in the St Gregory's Skeletal Collection include arthrogryposis multiplex congenita in 35 – 45-year-old male (Anderson 2002; Anderson and Thomas 1997), a condition whereby multiple joints have severely reduce range of movement and may appear deformed (Sucuoglu et al. 2015). This individual was excavated from a burial in the cemetery, indicating they are of low socio-economic status, and had a host of skeletal abnormalities, including osteoarthritis (OA), bilateral hip dysplasia and bilateral 'club-foot' featuring a deformed and fused calcaneus, talus and navicular junction holding the foot in a hyperflexed position (Anderson and Thomas 1997). Additionally, there is a case of partial aplasia of the spinous process in a female 30 – 35-year-old (Anderson 2002) and 7 individuals presented with varying degrees of a paracondylar process; 2 sub-adults and 4 adults with evidence of a tubercle at the site, and 1 adult with one fully formed fully formed (Anderson 1996). A paracondylar process is categorized as when bony overgrowth, forming a tubercle, protrudes from the lateral process, posteriorly to the occipital condyle, to create a 'occipital vertebrae' of sorts and is considered even in modern day to be a rare condition (Anderson 1996; Nolet et al. 1999). Of these seven individuals, just one sub-adult had been interred within the Priory and was therefore classified as high status (Anderson 1996). Several benign tumours were identified; an enchondroma in a 35 – 45-year-old male, which derives from the hyaline cartilage (Biondi et al. 2024), and two osteoid osteomas, which derive from bone tissue (Tepelenis et al. 2021), in two separate 40 – 50-year-old males (Anderson 2002). A metastatic carcinoma, believed to be evidence of prostate cancer, was identified in an elderly male, however it is not recorded whether this individual was buried within the Priory or in the general population cemetery, however it should be noted that diagnosing cancer types based on the presence of skeletal lesions is difficult (Castoldi et al. 2018; Wakely et al. 1995).

A case of congenital dislocation of the hip was identified in a young adult female (20-25 years old). The right acetabulum presented with an almost totally remodelled surface, indicative of a chronic condition rather than a trauma-related injury (Waldron 2008). A makeshift acetabulum

had formed superior on the ilium, presenting as a slight concavity with evidence of eburnation and increased porosity which are associated with osteoarthritis (Myszka et al. 2020; Waldron 2008). Other cases of arthritis-related conditions were identified in the St. Gregory's Priory and Cemetery skeletal collections. Primary osteoarthritis (OA), is, even today, extremely common especially in those of advanced age, affecting approximately 80% of people over 75 years old (Aboulenain and Saber 2022). Commonly affected joints include hips, knees and hands, but joints all over the body can be impacted (GBD 2017). OA was also extremely common in ancient humans, believed to have been prevalent since Palaeolithic times (MacLennan 1999), and the St. Gregory's Priory and Cemetery skeletal collection is no exception. Primary OA is a multi-factorial disease, with links to genetics (Aubourg et al. 2021), physical activity patterns and traumatic injury (Jiménez et al. 2018). In archaeological research, it is most frequently attributed to repeated, occupational stress, however, in the clinical literature, OA is well-documented as having a multi-factorial aetiology (Waldron 2008; 2019). In the St Gregory's skeletal collection, the most common site of OA is the spine, with evidence of eburnation and osteophyte formation in vertebrae. >50% of mature adult individuals and >25% of all adults in the sample display evidence of OA, however, there is no reported difference in rates of OA between the Priory and Cemetery individuals (Anderson and Andrews 2001). In addition to the spine, there was evidence of degenerative joint disease of the temporo-mandibular joint, shoulder, elbow, wrist and hand, knee, ankle and foot. Only one individual had evidence of multiple sites of OA; a mature adult female interred in the cemetery who had osteoarthritic evidence of the left shoulder, elbow and wrist, her right hand and bilateral knees. However, males were disproportionately affected by OA with three times as many males presenting evidence of OA than females (Anderson and Andrews 2001).

As previously mentioned, vertebral degeneration was the most common form of osteoarthritic evidence observed in the St. Gregory's skeletal collection. Males were disproportionately affected by vertebral degeneration (>58%) than females (>35%), however frequencies were similar between the mature and older adult individuals, which Anderson and Andrews (2001) suggest could be indicative of earlier onset than other medieval sites. The cervical spine was the most affected region of the spine affected, which based on studies of the thoracic and lumbar regions, may suggest compression loading from load-bearing , but rather than from the upper limb, originating from load-bearing upon the back of the neck or the top of the head (Barrett et al. 2020; Bruno et al. 2017). However, osteophyte formation was far more common than vertebral degeneration in the St. Gregory's skeletal collection with >79% of adults (>93% of males and >52% of females) having evidence of osteophyte formation. Regions most affected by vertebral osteophyte formation were the lower cervical, mid-lower thoracic and

lower lumbar, which is consistent with the literature that states regions of increased curvature are most commonly affected (Anderson and Andrews 2001; Bruno et al. 2017; Cooper et al. 1992; Ismail et al. 1999; Melton et al. 1993; Siminoski et al. 2012). In the clinical literature, osteophyte formation is most commonly attributed to increased biomechanical load, or repeated strain activity in osteoarthritis (Hsia et al. 2017), however it has also been associated with diseases such as ankylosing spondylitis (Schett and Rudwaleit 2010), Reiter's syndrome (Kim et al. 1999), and diffuse idiopathic skeletal hyperostosis (DISH) (Miyamoto et al. 2009).

Schmorl's nodes are described as rounded concavities which can form in the superior or inferior surfaces of vertebral bodies and were also identified in >64% of adult individuals (Anderson and Andrews 2001). Schmorl's nodes are commonly associated with extreme strain, as they tend to form when a vertebral disc ruptures due to excessive compression load bearing (Azzouzi and Ichchou 2022). Schmorl's nodes are more likely to form during adolescence, while the skeleton is more plastic and pliable (Williams et al. 2007). Mid-lower thoracic (superior surface) and upper lumbar (inferior surface) vertebrae were most affected, and males were disproportionately affected than females, which is consistent with the archaeological literature, a trend which has continued into modern populations (Azzouzi and Ichchou 2022; Brayda-Bruno et al. 2018; Hilton et al. 1976; Knowles 1983; Stroud and Kemp 1993; Yin et al. 2015; Zehra et al. 2017).

4.1.2.4 Socio-Economic Status Groups

Medieval Britain was largely governed by feudalism, with the Church wielding a lot of power and leading to a strong distinction between socioeconomic status groups (Clark 1982; Harvey 2002; Hull 1989). An individual's socioeconomic status was often reflected in their individual and population health due to increased frequencies of infectious disease and limited accessibility to high-quality food and clean water in low socioeconomic status individuals and communities (Hull 1989; Roberts and Manchester 2005). The wealthy lived comfortably, with access to formal education, managing expansive properties, partaking in political decision-making and discussions, and enjoying leisurely activities such as attending dances, feasts and game hunting expeditions (Dyer 2000; Holt 1972). Religious Clergy, similar to those residing within the St Gregory's Priory, managed the spiritual needs of their communities, performing religious rites and ceremonies for parishioners, participating in pilgrimages to neighbouring communities and attending to the ill and infirmed at local hospitals and those unable to afford medical care (Clegg and Reed 1994; Harvey 2002; Theilmann 1987). In contrast, the lives of the everyday people of low socioeconomic status, such as those living in the surrounds of St Gregory's Priory and interred at the cemetery, was largely situated around physical labour

(Dyer 2000). As St Gregory's was situated in a township but was also categorized as a market town (Gernay 2015), local low status individual careers could have included; servant, craftsperson, blacksmith, wood- or leather-worker, miller, crop planter, harvester, plougher or domesticated animal rearer (Dyer 2000; Judd and Roberts 1999; Zvi 1981). All of these roles involve hard physical labour, carrying heavy goods and long periods of time on their feet (Judd and Roberts 1999).

In addition to contrasting levels of daily physical activity and stress between the two socio-economic groups represented in the St Gregory's Skeletal Collection, there is additional evidence to support contrasting diet between the two groups. Medieval British socioeconomic status influenced the resources available to an individual, including food sources (Hull 1989; Roberts and Manchester 2005). High status individuals ate a varied diet of different meats, including duck, pig, chicken, pigeon, swan, beef, venison, fresh- and salt-water fish, water-dwelling mammals and crustaceans (Dyer 2000; Jotischky 2011; Powell et al. 2001; Rogers and Waldron 2001; Serjeantson and Woolgar 2006). Additionally, high status individuals often had access to a variety of dairy foods, including milk, cream, cheese and butter, as well as wine and ale (Dyer 2000; Rogers and Waldron 2001). It has been stated that the daily caloric intake for a high-status monastic individual, such as those residing within St Gregory's Priory, would have been roughly 300% of what is recommended for modern individuals (Miszkiewicz and Mahoney 2016). In contrast to this, low status medieval individuals primarily subsisted on cereals, eggs and cheese (Dyer 2000), a common meal was a dish named 'pottage', a stew-like meal consisting of oats, green beans and peas (Dyer 2000). Low status individuals had very limited opportunity for meat and fish (Van der Veen 2003).

With this disparity in physiological stress levels and differing accessibility to high quality foods, it is unsurprising that there is also a disparity in disease and general health and wellbeing between the two socio-economic groups represented in the St Gregory's Skeletal Collection. Infectious diseases were more common in medieval low status communities, with higher frequencies of tuberculosis and leprosy (Manchester and Roberts 1989). With few opportunities for high-quality foods, low status individuals were also more susceptible to malnutrition, leading to conditions such as iron-deficiency anaemia, Paget's disease, osteopenia and osteoporosis (Miszkiewicz and Mahoney 2016). However, the high status individuals were not necessarily resistant to disease, suffering similar frequencies during pandemics of the plague, as well as conditions associated with high caloric diets and too little physical activity, such as diffuse idiopathic skeletal hyperostosis (also known as DISH) (Rogers and Waldron 2001).

Linear Enamel Hypoplasia (LEH) is a well-documented condition whereby growth arrests occur in the enamel of the teeth in periods of high stress during growth, presenting as a horizontal line (Griffin and Donlon 2009; Hillson and Bond 1997; Miszkiewicz 2015a). Elsewhere, LEH has been observed to assess broad population health due to its non-specific aetiology (Goodman and Armelagos 1985; Larsen 1997; Roberts and Manchester 2005). It has been suggested that contributing factors to the formation of LEH include significant episodes of infectious disease, malnutrition, exposure to toxic or poisonous materials, and even periods of psychological stress (Goodman and Armelagos 1985; Larsen 1997; Roberts and Manchester 2005). Miszkiewicz (2015) observed significantly higher frequencies of LEH in individuals excavated from the St Gregory's cemetery than those excavated from the Priory, suggesting the low status individuals had higher incidence of systemic physiological stress, disease and generally poorer wellbeing than their high status counterparts.

Cribra orbitalia, porosity of the orbital roof, has been identified in ~7% of the adult individuals from the Canterbury cemetery, but much more prolific (~46%) in the sub-adult individuals (Gernay 2015). Cribra orbitalia has long been believed to be associated with chronic iron-deficiency anaemia (Carlson et al. 1974). However more recently, it has been suggested to only occur with particular forms of iron-deficiency anaemia, such as those also associated with renal disfunction, protein deficiency and other forms of endocrine disease (Rivera and Lahr 2017; Walker et al. 2009). Despite the uncertainty related to the disease-specific aetiology of cribra orbitalia, it is a condition known to be associated with malnutrition and disease, which suggests that these were issues, particularly in children, faced by individuals interred at the St Gregory's cemetery. The same research observed respiratory disease in ~64% of the individuals from St Gregory's cemetery, with evidence of periostitis of the maxillary sinuses and periosteal rib lesions (Gernay 2015). This has been interpreted as evidence of air pollution rather than disease, although Gernay (2015) does note that these two conditions are rarely seen in the same individual, which is suggestive of different aetiologies or perhaps multi-factorial aetiologies.

In a study conducted by Miszkiewicz and Mahoney (2016), observed OPD and osteon and Haversian canal area values in femoral cortical bone were significantly higher in the upper compared to lower socio-economic class individuals in the Canterbury Collection. The authors suggest that these differences could relate to lifestyle characteristics, such as the increased level of biomechanical stress due to physical activity and high levels of manual labour in the lower-class individuals, as well as due to dietary components, which contextual evidence records vastly higher protein levels in the high socioeconomic status group (Miszkiewicz and

Mahoney 2016). In the clinical realm, it has been suggested that high protein consumption, when combined with regular calcium or dairy ingestion, corresponds with healthier bone, but upon surpassing an optimal amount of protein, too much can be detrimental to bone health and strength (Pasiakos et al. 2015; Richman et al. 1979). The upper class individuals had access to an extremely protein-rich diet including meat, fats and dairy, in comparison to the lower class group, whose daily diet would have been much lower in protein, being largely grain based with little diet variation and little to no meat or dairy (Miszkiewicz and Mahoney 2016; Powell et al. 2001; Rogers and Waldron 2001). A similar study conducted by Pitfield et al. (2019), identified a similar pattern in sub-adult humeral cortical bone from the St Gregory's Skeletal Collection. Until approximately age 7, high and low status sub-adults had similar OPD, and osteonal size and shape metrics, however, after this age, high status sub-adults displayed a higher OPD, larger osteonal size and higher osteon circularity (Pitfield et al. 2019). Documentary evidence states that children generally entered the workforce at approximately age 8 (Hanawalt 1977), which reinforces the interpretation that low socio-economic status children were beginning laborious tasks at this stage, carrying increased loads, which resulted in a slowed remodelling rate and smaller osteon size metrics (Pitfield et al. 2019). Additionally, increased load bearing is also associated with lower osteon circularity, due to irregular patterns in microstructural strain (Skedros et al. 2013b), which could explain the higher osteon circularity in the high status sub-adults. Similar to their adult counterparts, the increased OPD in high status sub-adults from St Gregory's Priory, perhaps is indicative of their easier access to high protein foods (Pasiakos et al. 2015; Pitfield et al. 2019; Richman et al. 1979). This perhaps reinforced by additional research which observed differences in dental microwear and dental abrasion, and did not find significant differences in patterns between the two socioeconomic groups in sub-adults aged 1 – 8 years old from the St Gregory's Skeletal Collection (Dawson and Brown 2013; Mahoney et al. 2016b). Additional research observed fast bone remodelling via increased OPD in adult females than males in the St Gregory's Skeletal Collection, however the socioeconomic status for these individuals is unknown (Fahy et al. 2017).

Despite these differences in dietary subsistence and patterns in physical activity between the socio-economic classes, it doesn't appear that there was a difference in birth rates (White et al. 2022). Additionally, they identified that in spite of the aforementioned lifestyle differences, low status sub-adults had significantly higher survivorship than high status sub-adults, and that low status adult males had significantly lower mortality rates than high status females (White et al. 2022). The authors suggest this could be due to the high risk of mortality for all women, associated with pregnancy and childbirth during the medieval period (White et al. 2022; see

Ward 2006 for a background on women's health during the Medieval period). However, as there is no statistically significant result regarding mortality for the sub-adults, and likewise no statistically significant results regarding survivorship for the adults, it is unclear how biologically significant these differences are, despite the statistical significance.

4.1.2.5 Sample Description

The sample examined in this research was a selection of individuals from the St. Gregory's Priory (*n* = 31) and Cemetery (*n* = 32) skeletal collection. A total of 63 individuals were sampled for this research, with a rib cross-section and/or an anterior and/or posterior femur sample collected. Peripheral data included estimated age-at-death and sex, as well as femoral length for stature estimations (Table 4.2). Methods employed to obtain peripheral data are detailed in Chapter 5.

Table 4.2: Individuals sampled from the St. Gregory's Priory and Cemetery Skeletal Collection.

Individual ID	Samples Collected	Sample Details	Burial Location	Age-At-Death Category	Sex	Femoral Length (cm)
SK6	Rib x 2 Femur	Left rib – midshaft; 2 x cross-sections 1 cm apart Posterior	Priory	Mature Adult (35-50yo)	Female	45.60*
SK7	Rib x 2 Femur	Unknown rib – highly fragmented – midshaft; 2 x cross-sections 1 cm apart Posterior	Priory	Older Adult (50+yo)	Male	49.80*
SK10	Rib	Left rib – midshaft	Priory	Adolescent (12-20yo)	-	41.70^
SK12	Femur	Posterior	Priory	-	-	45.00#
SK13	Rib Femur	Left rib – midshaft Posterior	Priory	-	Female	47.50#
SK14	Rib Femur	Left rib – midshaft Posterior	Priory	-	Female	43.50*
SK15	Rib x 2 Femur	Left rib – midshaft; 2 x cross-sections 1 cm apart Posterior	Priory	Young Adult (20-35yo)	Female	46.00#
SK18	Rib x 2 Femur x 2	Left rib – midshaft; 2 x cross-sections 1 cm apart Anterior, Posterior	Priory	-	Male	47.10*
SK19	Rib x 2 Femur	Left rib – midshaft; 2 x cross-sections 1 cm apart Posterior	Priory	-	Female	45.60+
SK20	Rib x 2	Left rib – midshaft; 2 x cross-sections 1 cm apart	Priory	-	Female	39.70#
SK24	Femur x 2	Anterior, Posterior	Priory	-	-	48.00*
SK33	Rib x 2 Femur	Left rib – midshaft; 2 x cross-sections 1 cm apart Posterior	Priory	-	-	45.70*
SK37	Rib x 2 Femur x 2	Left rib – midshaft; 2 x cross-sections 1 cm apart Anterior, Posterior	Priory	Mature Adult (35-50yo)	Male	50.10*
SK39	Rib Femur x 2	Left rib – midshaft Anterior, Posterior	Priory	Older Adult (50+yo)	Female	44.60#
SK47	Rib x 2 Femur x 2	Left rib – midshaft; 2 x cross-sections 1 cm apart Anterior, Posterior	Priory	Young Adult (20-35yo)	Male	48.90#
SK48	Rib x 2 Femur	Left rib – midshaft; 2 x cross-sections 1 cm apart Posterior	Priory	-	Female	43.70#
SK50	Rib x 2 Femur	Left rib – midshaft; 2 x cross-sections 1 cm apart Posterior	Priory	-	Female	41.10#
SK51	Femur x 2	Anterior, Posterior	Priory	-	-	46.90*

SK52	Rib	Left rib – midshaft	Priory	Young Adult (20-35yo)	Female	52.00⁺
SK53	Rib	Left rib – midshaft	Priory	-	Male	46.80#
SK55	Femur	Posterior	Priory	-	-	46.20*
SK56	Femur	Posterior	Priory	-	-	48.30*
SK63	Rib Femur x 2	Left rib – midshaft Anterior, Posterior	Priory	Older Adult (50+yo)	Male	49.30*
SK65	Femur	Posterior	Priory	-	-	44.00*
SK66	Rib x 2 Femur	Left rib – midshaft; 2 x cross-sections 1 cm apart Posterior	Priory	-	-	46.60#
SK71	Rib Femur	Unknown rib – highly fragmented – midshaft Posterior	Priory	Mature Adult (35-50yo)	Female	45.20#
SK72	Rib x 2	Left rib – midshaft; 2 x cross-sections 1 cm apart	Priory	-	Male	43.80#
SK79	Rib Femur	Left rib – midshaft Posterior	Priory	-	Female	42.10*
SK80	Rib x 2 Femur	Left rib – midshaft; 2 x cross-sections 1 cm apart Posterior	Priory	Mature Adult (35-50yo)	Male	42.10#
SK85	Femur	Posterior	Priory	-	Female	48.50*
SK91	Rib x 2	Left rib – midshaft; 2 x cross-sections 1 cm apart	Priory	-	Male	45.10*
SK132	Rib x 2 Femur	Left rib – midshaft; 2 x cross-sections 1 cm apart Posterior	Cemetery	Mature Adult (35-50yo)	Female	47.30#
SK167	Rib x 2 Femur	Right rib – no left available – midshaft; 2 x cross-sections 1 cm apart Posterior	Cemetery	Mature Adult (35-50yo)	Male	49.60#
SK191	Rib Femur	Left rib – midshaft Posterior	Cemetery	Mature Adult (35-50yo)	Male	47.70#
SK198	Femur	Posterior	Cemetery	Mature Adult (35-50yo)	Female	40.60#
SK237	Femur	Posterior	Cemetery	Mature Adult (35-50yo)	Male	44.80#
SK446	Rib x 2 Femur	Left rib – midshaft; 2 x cross-sections 1 cm apart Posterior	Cemetery	Mature Adult (35-50yo)	Male	47.10#
SK531	Rib x 2 Femur	Left rib – midshaft; 2 x cross-sections 1 cm apart Posterior	Cemetery	Mature Adult (35-50yo)	Female	42.70#
SK573	Rib x 2 Femur	Left rib – midshaft; 2 x cross-sections 1 cm apart Posterior	Cemetery	Mature Adult (35-50yo)	Male	50.30#
SK612	Rib x 2 Femur	Left rib – midshaft; 2 x cross-sections 1 cm apart Posterior	Cemetery	Mature Adult (35-50yo)	Female	45.70#
SK614	Rib	Right rib – midshaft	Cemetery	Mature Adult (35-50yo)	Female	40.80*

	Femur	Posterior				
SK644	Rib x 2 Femur	Right rib – approximately at the neck third margin; 2 x cross-sections 1 cm apart Posterior	Cemetery	Mature Adult (35-50yo)	Male	44.70[v]
SK650	Rib Femur	Right rib – midshaft Posterior	Cemetery	Mature Adult (35-50yo)	Female	42.00[#]
SK667	Rib Femur x 2	Left rib – midshaft Anterior, Posterior	Cemetery	-	Male	44.00[#]
SK700	Rib x 2 Femur	Left rib – midshaft; 2 x cross-sections 1 cm apart Posterior	Cemetery	Mature Adult (35-50yo)	Female	37.70[#]
SK735	Rib	Left rib – midshaft	Cemetery	-	Female	44.20[#]
SK750	Femur	Posterior	Cemetery	-	-	39.00[#]
SK840	Rib Femur	Left rib – midshaft Posterior	Cemetery	Mature Adult (35-50yo)	Female	42.40[#]
SK880	Rib Femur	Left rib – midshaft Posterior	Cemetery	Mature Adult (35-50yo)	Male	44.60[#]
SK901	Rib	Left rib – midshaft	Cemetery	-	Female	39.80*
SK905	Femur	Posterior	Cemetery	-	-	42.60*
SK954	Rib x 2 Femur	Left rib – midshaft; 2 x cross-sections 1 cm apart Posterior	Cemetery	Mature Adult (35-50yo)	Male	-
SK967	Rib x 2 Femur	Left rib – approximately at the sternum third margin – midshaft; 2 x cross-sections 1 cm apart Posterior	Cemetery	Mature Adult (35-50yo)	Male	48.60[#]
SK985	Rib x 2 Femur x 2	Left rib – midshaft; 2 x cross-sections 1 cm apart Anterior, Posterior	Cemetery	Mature Adult (35-50yo)	Male	-
SK1054	Rib x 2 Femur	Left rib – approximately at the neck third margin – midshaft; 2 x cross-sections 1 cm apart Posterior	Cemetery	Mature Adult (35-50yo)	Male	43.90[#]
SK1104	Rib Femur	Left rib – midshaft Posterior	Cemetery	Mature Adult (35-50yo)	Male	44.00[#]
SK1105	Rib Femur	Left rib – midshaft Posterior	Cemetery	Mature Adult (35-50yo)	Male	41.30[#]
SK1122	Rib x 2	Left rib – midshaft; 2 x cross-sections 1 cm apart	Cemetery	-	Female	39.10[#]
SK1123	Femur	Posterior	Cemetery	-	-	45.60^
SK1161	Rib x 2 Femur x 2	Left rib – midshaft; 2 x cross-sections 1 cm apart Anterior, Posterior	Cemetery	Mature Adult (35-50yo)	Male	49.60*

SK1167	Femur	Posterior	Cemetery	Mature Adult (35-50yo)	Female	42.30[#]
SK1230	Rib x 2 Femur x 2	Left rib – midshaft; 2 x cross-sections 1 cm apart Anterior, Posterior	Cemetery	Mature Adult (35-50yo)	Male	48.60*

*Estimated from Jacobs 1992 formula. ^Estimated from F1 region of Jacobs 1992 formula. [#]Intact femur measured. [+]Estimated from F2 region of Jacobs 1992 formula. [v]Estimated from F4 region of Jacobs 1992 formula.

Chapter 5 Methods

This chapter describes all methods undertaken on samples, including contextual data collection such as age-at-death and biological sex estimation techniques, sample collection, sample processing, slide production, secure storage, slide imaging, data collection, data organisation and storage, and analysis. All slide preparation procedures were undertaken using protocols based on discipline-wide standard methodologies and informed by the literature. Some deviations were made, as required, to troubleshoot sample specific issues experienced as detailed within.

5.1 Sample Selection, Collection and Transfer to the ANU

5.1.1 St. Gregory's Priory and Cemetery Osteological Collection

The curator of St. Gregory's Priory and Cemetery osteological collection (hereafter: Canterbury Skeletal Collection) the University of Kent granted permission for *n* = 53 rib cross-section samples to be collected, and for access to *n* = 64 already existing histological slides from the posterior and anterior femur. Local ethics advisory board at the University of Kent (November 2010) approved the use of these samples for histological analyses. Sample selection had an even sex ratio at 50 individuals, and a further three individuals were added to increase representation of high socio-economic individuals. Sample selection attempted to represent a reasonable sample spread, with good age-at-death category, sex and socio-economic status representation, but this was dependent on preservation of the correct skeletal elements and whether the individual was available for histological sampling, which is a destructive sampling method.

Estimations of biological sex and age-at-death were based on standardised methods in anthropology outlined by Buikstra and Ubelaker (1994). Sex estimation methods analysed morphological variation of the skull and pelvis, as well as measured post-cranial joint surfaces. Age-at-death was estimated based on known morphological changes that happen throughout growth and ageing. These assessments were conducted on closure and eventual obliteration of the cranial sutures, dental eruption and wear and changes to the pubic symphysis and auricular surface of the pelvis. Rather than an age-at-death estimate being stated, each set of skeletal remains were assigned to age-at-death categories defined by Buikstra and Ubelaker (1994); adolescent 12-20 years, young adult 20-35, middle adult 35-50 years and older adult 50+ years.

Fifty-three rib samples were collected at the University of Kent School of Anthropology and Conservation, using a Dremel® handheld rotary saw with attached diamond blade, which is standard practice. However, due to increased fragility of the rib fragments, these were sometimes easily fractured by the vibrations from the handheld saw. Thus, some samples were left as whole fragments of rib shafts, rather than small cross-sections. A mid-shaft section of the left rib was selected for sampling where possible, but if the left rib was unavailable, or no rib shaft fragment was properly sided and identified, a right rib may have been selected. An exact number rib was not possible to determine due their fragmentary nature. Previous work has determined that mid-thoracic ribs (ribs 3 – 8) are relatively biomechanically constrained bones, meaning they are naturally controlled for differential loading patterns between individuals compared to weight-bearing bones such as the femur (Dominguez et al. 2020; Stewart et al. 2021; Tommerup et al. 1993). Additionally, while the left sixth rib has previously been referred to as the 'standard' rib to use in histological analysis (Stout and Paine 1992), reasoning behind this has evolved since the 3rd to 5th and 7th to 8th ribs offer similar osteon and Haversian canal microstructural data to the sixth rib (Crowder and Rosella 2007). As such, mid-thoracic ribs were selected, avoiding osteological landmarks that suggested a fragment may be sourced from an upper or lower rib.

Samples were secured in polyethylene bags, labelled with the identifying SK number, rib side and number of the rib sampled. These were sealed within a plastic container and shipped to the ANU via secure, tracked, express international courier. Included in the shipping parcel were manifests documenting each rib sample (Table 4.2). Australian biosecurity procedures and standards were adhered to, to ensure the samples were safely shipped into the country via the correct channels and with the necessary permissions (Department of Agriculture, Fisheries and Forestry 2015).

The femoral samples from the Canterbury Skeletal Collection that were observed in this thesis were sectioned and produced into histological slides as part of a previous PhD thesis (Miszkiewicz 2014). These slides were stored at the ANU on loan with approval from the University of Kent and new images were captured for this thesis following methods described in Section 5.4.1. Where paired femur images were unavailable for the SK#s represented by the rib samples, individuals from the same burial section within either the priory or cemetery were used, who were also of a comparable age-at-death (AAD) and sex. There were some instances where this was not possible, and in these situations, individuals of unknown AAD and/or sex, but from the same burial section were used. A manifest of femoral samples is included in Table 4.2.

5.1.2 AFTER Samples

Modern rib and femur samples were sourced through the Australian Facility for Taphonomic and Experimental Research (AFTER), NSW. The donors from whom the samples were sourced were acquired via the Body Donation Program, which is located within the Surgical and Anatomical Science Facility (SASF) at the University of Technology Sydney (UTS). Donor consent was given for the use of their remains in AFTER research, as per the *Anatomy Act 1977* (New South Wales Government 2018). These samples were collected from the AFTER facility as part of a larger project led by Dr Eline Schotsmans into which the present thesis was integrated under the following ethic clearance: University Technology Sydney Ethics ETH15-0029 and ETH18-2999; and Australian National University Ethics protocol 2019/041). Donation and sampling methods complied with all legal and ethical standards associated with the use of human remains in scientific research. Eighteen donors were included, with anterior femur and rib pair-matched samples from each donor. The rib cross-sections were collected as part of another project, and were taken from the right 3rd rib, sawing a complete cross-section of the rib shaft from approximately 2 cm from the sternal end. Despite a different rib being sampled in the AFTER donors, observations are believed to be comparable to the UK archaeological rib samples as previous research has determined similar microstructural features and patterns in biomechanical load pressures in ribs 3 – 8 (Crowder and Rosella 2007; Dominguez et al. 2020; Tommerup et al. 1993). Rib cross-sections were taken using a Ryobi saw (R18MT, Type 2).

Femora were cut at the proximal third margin of the right femur (left was used where the right was compromised, e.g. the donor had undergone a total hip replacement), and a 3-5cm segment of the diameter (measured superior-inferiorly) was removed. Using a Dremel® 8220 multi-tool with a diamond blade, a small ~1cm2 sample was then cut from the inferior end of the segment, from the anterior periosteal border to the inner trabecular border as part of this research, while the remainder of the sample went to the Victorian Institute of Forensic Medicine (VIFM), Melbourne. All AFTER samples used in this research were cut from the donor remains in June 2019. Individuals are of known age and sex, with some additional stature estimations from next of kin, health and cause of death information available (Table 4.1). Both the anterior femur and rib samples were hand-delivered to the ANU from the AFTER facility by Dr Eline Schotsmans, once ethics permissions for the transfer and storage of the samples at the ANU had been approved.

5.2 Laboratory Based Methods

Each sample underwent a series of laboratory-based procedures to create a glass histological slide. Here, those methods are described. All samples used in this research were stored within the secure hard tissue histology laboratory at the ANU's School of Archaeology and Anthropology in Canberra, Australia.

5.2.1 Embedding, decalcification and staining

All rib and femur samples were embedded in epoxy resin prior to being reduced for slide production. There is some discourse in the literature about whether dry bone needs to be embedded in resin prior to being reduced for slide production, with some researchers opting to leave their samples unembedded, but others encouraging embedding (Cho 2012; Martin et al. 1998; Paine and Godfrey 1997; Rubin and Lanyon 1984). Ultimately, all samples in this study were embedded due to their fragility, in particular the archaeological samples, which were at high risk of fracturing when sawn prior to embedding. The process of embedding in plastics is based on the premise of catalytic homopolymerisation, which is the binding of many single-molecule structures into less multi-molecule structures, which ultimately makes an object more stable, both structurally and chemically (Horobin 2002). Two types of plastic are often used in skeletal histology, methy- or polymethyl-methacrylate, and epoxy resin (Luft 1961; Richardson et al. 1960). However, there are clear distinctions between which materials are used by which research disciplines. Methy- or polymethyl-methacrylate are usually used in medical research on fresh bone samples (Erben 1997; for examples see Emmanual et al. 1987; Raab et al. 1991). Using methacrylate plastics for histology involve extensive procedures and require more technical equipment, such as clinical incubators, and the sample to be fixed in formalin (a common preservative) and 70% ethanol beforehand (Erben 1997). While this results in exceptional histological slides with well-preserved, and easily identifiable microstructures, this process is unnecessary in archaeological applications on dry bone, when more affordable consumables with shorter slide production times are available (see further inexpensive histology suggestions Maggio et al. 2019). Epoxy resins are the hardest type of resin plastics and facilitate histological slide production suitable for light and electron microscopy (Sanderson 1994). Epoxy resins are commonly used in archaeological studies of skeletal histology since Von Hagens (1979) identified that bone tissue was easily permeated by resin for histological analysis (Drapeau and Streeter 2006; Mulhern 2000; Pfeiffer et al. 2006; Skedros et al. 2001; 2004; 2011; Miszkiewicz 2015b; 2016; Miszkiewicz and Mahoney 2016; 2017). Other resin types available include acrylic and polyester resins, but epoxy resins are more durable, set faster and are suitable for use under light and electron microscopes

(Sanderson 1994). Additionally, epoxy resins are affordable and do not require strict temperature controls for fast-curing (Maggio et al. 2019; Sanderson 1994).

Decalcification is the process of demineralisation and is often completed using formic, hydrochloric and nitric acids, undertaken prior to embedding (Callis 2002; Cho 2012; Sanderson 1994). However, the harsh process of demineralisation can damage archaeological or other dry bone samples, by destroying the micro-architecture within. Staining, conducted during the embedding process, assists in the microstructural identification of histopathological structures (Floyd 2002; Horobin 2002; Villanueva 1988). However, staining is not necessary for histomorphometrical and histomorphological analyses, as relevant structures are visible on unstained osteons and Haversian canals and broader bone structure. Thus, for this study, these samples were not subject to staining or decalcification processes, which range from unnecessary to potentially destructive to the dry nature of all samples included in this research.

Embedding protocols were formulated from standards in biological anthropology (An and Martin 2003; Ascenzi and Fabry 1959; Bancroft and Gamble 2002; Beauchesne and Saunders 2006; Cho 2012; Frost 1958; Grupe and Garland 1993; Maat et al. 2001; Miszkiewicz 2015b; 2016; Miszkiewicz and Mahoney 2016; 2017; Paine 2007). These protocols were created purposefully for historical and archaeological skeletal samples, although with minimal modifications, described below where applicable, they were able to be applied to the modern AFTER samples. This is because the AFTER samples had been deposited in surface decomposition contexts whereby the donor skeletons had become dry and macerated through decomposition processes, and hence embedding protocols for archaeological dry bone samples were still suitable.

Usually, sample reduction via handheld Dremel® rotary saw is done prior to embedding, so that a sample can be entirely encased in resin. However, for the medieval samples in this study, many fractured easily when this was done prior to embedding, and so these ribs were embedded as whole rib fragments, with the end protruding from the resin solution (Figure 5.1A). Femoral samples (1cm^2) and modern ribs were smaller in size (~1cm thick segment of the rib mid-shaft), and so were fully encased in resin solution.

Twenty-five mm diameter Buehler® SamplKups were used and were coated with a layer of Buehler® Release Agent (20-8186-004) on the inside of the SamplKup before the sample was placed inside, with the inferior, horizontal section face down. A 15ml glass vial was tared to 0g on an AND Company Ltd.® digital scale (FX-3000i). Approximately 8g of Buehler® Epoxicure II Epoxy Resin (20-3430-064) was poured into the vial, the weight measured and recorded to

two decimal places. The ratio of resin to Buehler® Epoxicure II Epoxy Hardener (20-3432-016) used was 4:1, and so the necessary amount of hardener for the already poured amount of resin was added to the vial in order to maintain this ratio (~2g). The vial was tilted and stirred with a glass stirring wand for two minutes, with a stopwatch set as a reminder, until the mixture blended with no discernible layers of either solution and the consistency was clear. The mixture was poured into the appropriate mold to coat the sample in resin. SamplKups were placed on an A3 piece of paper, with the relevant SK numbers labelled underneath each mold. Buehler® Epoxicure II Epoxy Resin requires 6 – 8 hours at room temperature 20° Celsius (Buehler® 2019). Once set, embedded samples were extracted from the molds so that they could be reused for the next batch of samples embedding.

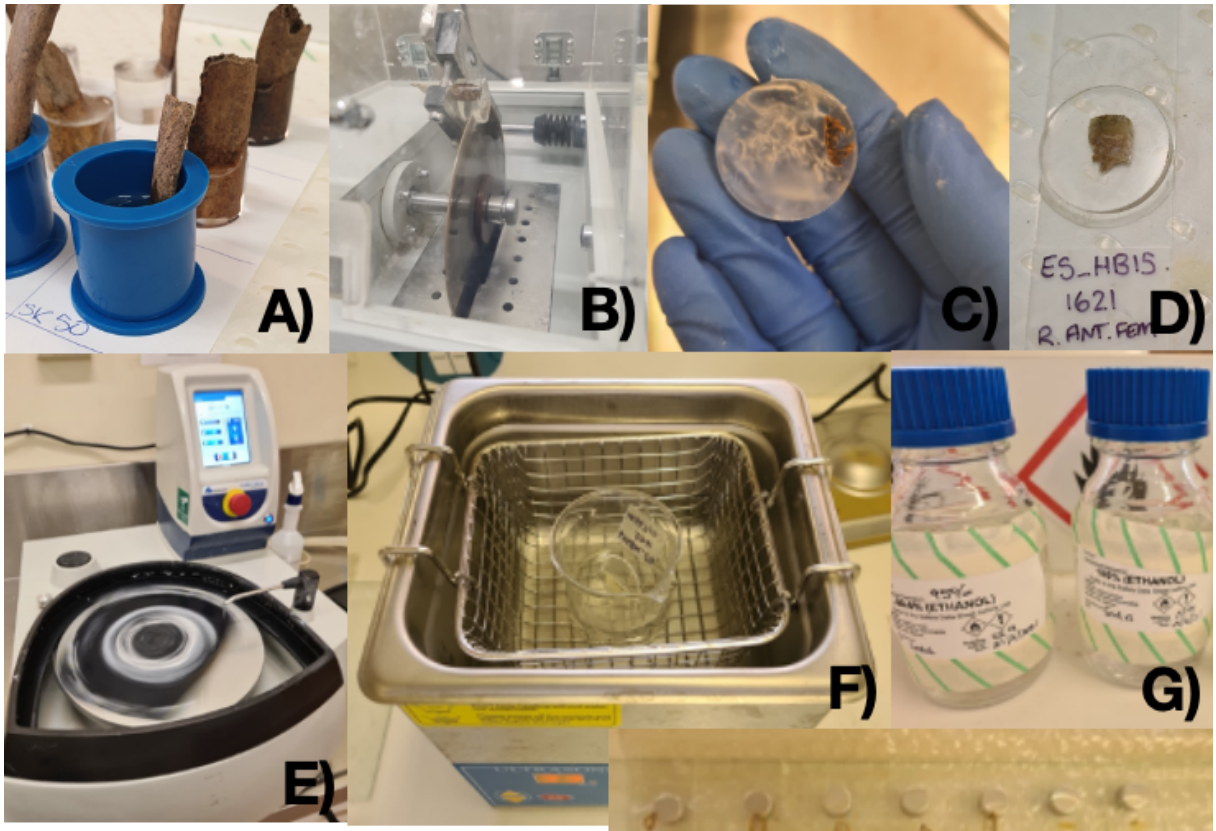

Figure 5.1: Laboratory methods undertaken.

A) Whole rib fragments embedded in epoxy resin. B) Kemet tabletop saw. C) Transverse rib cross-section prior to glass slide mounting. D) Sample following glass slide mounting. E) Buehler® 300 Grinder-Polisher. F) Ultrasonic cleaner used for removing micro-debris. G) 95% Ethanol and 100% Ethanol concentrates. H) Slides after cover slipping. Images: Tahlia J Stewart.

5.2.2 Reducing embedded samples

The medieval ribs needed to have their rib shafts trimmed that were protruding from the resin prior to mounting in the tabletop saw. Rib shafts were trimmed using a handheld Dremel® Rotary Tool 4000. A flexible shaft attachment was used to reduce vibrations and thus minimise the chance of sample shattering. The rotary tool was fitted with a Dremel® EZ545 Diamond Cut Wheel (38.1mm). All embedded samples, including the UK rib and AFTER rib and femoral samples, were cut into histological slices using a Kemet MICRACUT® 151 Precision Cutter fitted with a diamond blade (150mm diameter) (hereafter referred to as a Kemet tabletop saw), to expose clean cross-sections for slide mounting. Where possible, two slices were taken per rib to produce two slides per sample, but this wasn't possible for the AFTER femoral samples due to their small (<1cm^2) size. The Kemet tabletop saw was set to 250 rotations per minute

(RPM) and slices were taken transversely through the sample, to expose either a complete rib cross-section, or a transverse section of the anterior femur sample.

Where medieval rib samples were embedded on an angle due to being embedded as whole rib shaft fragments, they were positioned in the chuck for the Kemet tabletop saw on such an angle as to facilitate a cleanly transverse cut. For some samples, this meant they had to be ground down first, using a Buehler® EcoMet 300 grinder polisher, to remove excess resin and enable the samples to be placed securely in the chuck so that at least one transverse cut could be made through the sample (Figure 5.1B). After the slice(s) was made, the sectioned surface was smoothed using a 400-grit grinding pad to ensure the mounted surface is free from scratches that can result from the cutting process. The samples were then dried with a paper towel and left to air-dry overnight prior to mounting on glass slide.

5.2.3 Glass Slide Mounting

The dried, sectioned samples were placed on clean glass microscope slides to prepare for mounting. Sections were attached to Thermo Scientific® frosted microscope slide using Stuk® Epoxy Glue. Stuk® Epoxy Glue is quick setting, dries clear, is solvent free to prevent damage to more delicate samples, and is water resistant so it does not dissolve during the remainder of the slide production process (Glauert and Glauert 1958; Glauert et al. 1956). Additionally, Stuk® Epoxy Glue is packaged in a double-headed syringe containing both epoxy and hardener, which are dispensed equally onto a clean disposable surface, mixed for approximately 15 seconds and then applied to the sectioned surface of the sample. The sample was then pressed to the glass slide, sliding back and forth smoothly to prevent and/or remove any bubbles from forming in the adhesive, which can obstruct microstructures during image analysis (Glauert and Glauert 1958; Glauert et al. 1956). Although Stuk® Epoxy Glue is fast drying, the slides were left to airdry overnight to ensure they were completely dry before beginning sample reduction so to reduce the risk of sample movement or removal from the slide.

5.2.4 Further Reduction and Polishing

Standards indicate that histological slide samples should be approximately 100μm thick for best visibility of microstructures (Crowder and Stout 2011). However, some of the UK rib slides had to be up to 150μm thick to prevent sample loss during the reduction process due to poor preservation. Slide appearance under 10x magnification using a BX53 microscope was assessed periodically, and slide thickness was measured with a pair of Links® high precision

stainless steel digital callipers. This was done to assess and optimise slide thickness and microstructure visibility throughout slide reduction. Slides were reduced in thickness using a Buehler® Eco-Met 300 Grinder-Polisher.

First stages of reduction were done using 320 grit Buehler® silicon carbide abrasive paper with the platen set to 400RPM. Once samples were approximately 2mm thick, the abrasive paper was switched to 400 grit, at 0.5mm thick, the abrasive paper was switched to 800 grit, and once reaching 0.25mm thick, the abrasive paper was switched to 1200 grit. The increasing grit rating of the abrasive paper meant that scratches were gradually buffed out, and sample reduction slowed down as the process moves gradually from grinding to polishing. Once all large scratches were ground away through grinding, polishing was conducted to remove micro-scratches and even out the ground sample surface to optimize microstructure visibility. Polishing was done using the Buehler® Eco-Met 300 Grinder-Polisher but equipped with a Buehler® polishing cloth, dampened with water and sprinkled with Buehler® MicroPolish II 0.3□m Powder. Slides were polished until the resin surrounding the sample appeared glassy clear, with no visible scratches on the surface. The slide was periodically checked under a BX53 microscope to ensure the elimination of micro-scratches before setting aside for slide dehydrating and clearing.

5.2.5 Cleaning, Dehydrating and Clearing

Ultrasonic bathing was carried out to remove micro-debris from the slides (Williams 1994). Slides were rinsed with water and dried to remove larger debris from the grinding and polishing processes. Each slide was placed in a 200ml glass beaker, filled with water deep enough to cover the sample. The beaker was placed in an ultrasonic cleaner, which was also ¼ filled with water.

The ultrasonic cleaner ran a cycle for 2 minutes, with the heating off (at room temperature, which ranged from 15 - 20°C), which has been demonstrated to remove micro-debris from the sample and clean the sample using ultrasonic vibrations (Williams 1994). Samples were then dried with paper towel and left to airdry under a heat lamp. The water in the beaker was emptied and refilled after each sample to remove suspended micro-debris particles and to reduce the risk of increased water temperature. The process of ultrasonic bathing gradually warms the water with ultrasonic vibrations, and so the water in the ultrasonic cleaner tub was also emptied if it warmed to a point of 22°C to prevent sample heating. Dehydration is necessary to remove residual water from the sample, which can infiltrate a thin section

obscuring microstructure visibility, and, if left not removed, can lead to untimely taphonomic degradation (Mendelow and Hamilton 1950).

Slides were dipped three times into 95% ethanol and left to airdry, before being submerged three times in 99-100% ethanol and being left to airdry. 95% ethanol was used first to prevent over drying and rapid shrinkage of samples if suddenly exposed to higher concentrates of ethanol. Clearing is undertaken to remove alcohol from the sample and clear the sample for optimal histological analysis. Slides were submerged in Xylene twice, inside a chemical fume-hood, before being left to airdry overnight.

5.2.6 Cover-Slipping

Cover-slipping involves the adhesion of a glass cover to the sample, completely encasing the sample in glue, resin and glass, assisting to preserve the sample for as long as possible. Slides were cover slipped in either 18 x 18 mm^2, 22 x 22 mm^2 or 22 x 40 mm^2 cover slips, depending on sample size. Cover slips were attached using Thermofisher® dibutylphthalate polystyrene xylene (DPX) mounting media glue, and left to dry overnight at room temperature. DPX glue is clear, will not discolour with time and once dry, forms a similar reflective index to glass, suitable for light electron microscopy (Thermo Scientific® 2015).

5.3 Slide and Sample Storage

Slides were stored in plastic slide storage boxes, affixed with labels containing ethical clearance information to help ensure their safety and security within the histological laboratory. Samples from the UK University of Kent and AFTER Facility were separated and each slide was clearly labelled with the relevant individual and sample ID in permanent marker to ensure positive identification was maintained throughout slide analysis and storage. Leftover sample residuals were kept in labelled polyethylene bags in case further slides were required and/or eventual return to the originating facility, either the University of Kent or the AFTER facility.

5.4 Data Collection

Following slide preparation, the slides were digitally imaged for data collection to occur. Here, the imaging methodologies and region of interest (ROI) selection protocols are described, based on discipline standards. Then, the methods of image storage and analysis, data collection by variable are described and data collation and storage are detailed.

5.4.1 Imaging

Imaging was undertaken using an Olympus BX53 Semi-Motorised Fluorescence Microscope with an attached DP74 inverted camera. The cellSens® standard life science imaging software package was used for all imaging. Slides were placed on the microscope stage and viewed using the live function in cellSens®. 10x magnification is standard in bone histology to assess the necessary variables observed in this research (Crowder and Stout 2011). Set to 10x magnification, the focus was adjusted for optimal clarity of microstructures before images were taken using the 'snap' features to capture a single image measuring 1.972mm^2. Whole cross-section or whole sample images were taken using the manual multiple image alignment (MIA) tool, which automatically stitches screen captures of the live slide view together into one seamless image as the user manually moves the stage platform that the slide sits on. Captures were taken in both polarised and light microscopy. Scales were burned into the final image outputs to facilitate feature measuring during data collection. These whole cross-section images of the rib samples were used in cross-sectional geometry analysis, described below. Whole sample images of the femoral samples were used for region of interest (ROI) mapping (similar sampling strategy to Eleazer and Jankauskas 2016). Imaging protocols differed between the femora and ribs because the femur samples were partial samples rather than entire cross-sections. Here, imaging techniques and protocols are described for the femora and ribs.

5.4.1.1 Femora

Femoral samples were imaged at 10x magnification, with both light and polarized images taken, which is standard in skeletal histology for the assessment of osteons and Haversian canals, which are the smallest structures observed in this research (Crowder and Stout 2011). Assigning ROIs using consistent methodology is necessary for experiment replication. ROIs have been used for analysis portions of femoral cortical bone histology elsewhere, due to sample availability, localised diagenesis and large cross-section size of femora (Crowder 2013; Gocha and Agnew 2016; Maggio and Franklin 2021; Matsuo et al. 2019; Miszkiewicz et al. 2022; Miszkiewicz and Mahoney 2016). The midpoint of each femoral sample was visually assessed under 10x magnification prior to ROI mapping to ensure the targeted area still represented sub-periosteal cortical bone.

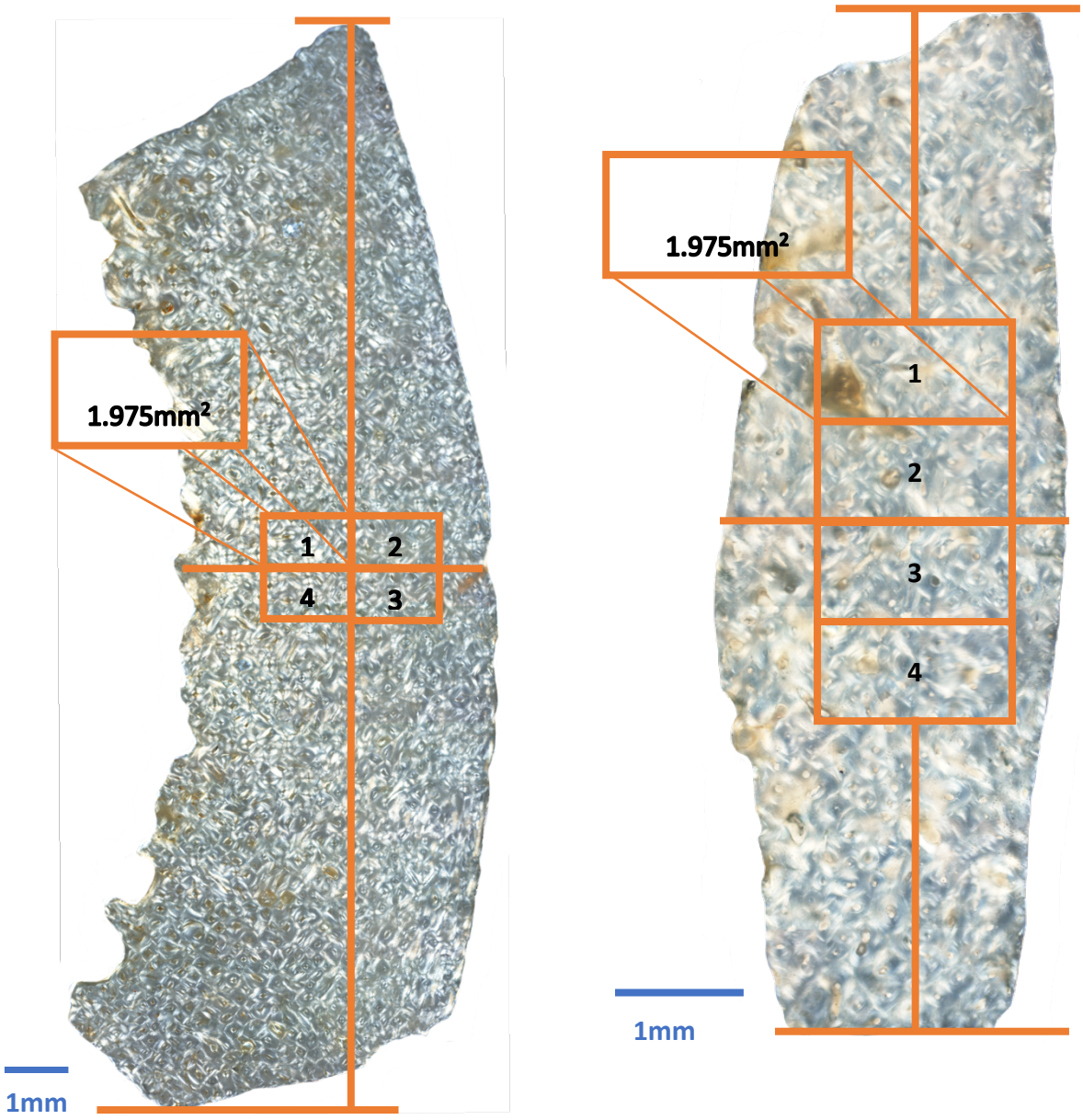

Figure 5.2: Left: Femur slide ES_HB04_1602. Right: Femur sample ES_HB09_1618.
Polarised images taken at 10x magnification, with 4 ROIs mapped at midpoints. Image by Tahlia J Stewart.

The femoral samples were imaged in their entirety to assist in ROI mapping. Once the initial image of the entire sample has been taken, a crosshair was applied to locate the midpoint both on the periosteal to endosteal and medial to lateral axes. The midpoint was calculated as the junction between the furthermost medial and lateral points, and the furthermost periosteal and endosteal points. At the midpoint, a microstructural landmark was selected. Microstructural landmarks could be anything from a Haversian canal to an air bubble or foreign artefact as it just needed to be a pivot point between all four ROIs. Four ROIs were imaged in a rotation

around this landmark, numbered in a clockwise order (Figure 5.2, Left). Each ROI was 1.975mm^2, which is the largest single snapshot possible while set to 10x magnification using the CellSens® software. This equated to a total of 7.9mm^2 of femoral bone analysed for each individual. However, some samples were too narrow for ROIs to fit in this arrangement and so this method had to be adjusted to facilitate imaging. For these samples, the 4 ROIs were taken along the midpoint, with ROIs 1 and 2 above the junction between the furthermost medial and lateral points, and the furthermost periosteal and endosteal points, and ROIs 3 and 4 below this junction (Figure 5.2, Right). This equated to the same amount of bone analysed, 7.9mm^2, for each individual. For each femur sample, the image of the complete sample was retained for future reference and analysis, and the 4 ROIs from each sample were analysed for this research.

5.4.1.2 Ribs

Similar to the femur samples, ribs were imaged in their entirety at 10x magnification and in both light and polarized microscopy, as is standard in bone histology for measuring the smallest structures observed in this research, osteons and Haversian canals (Crowder and Stout 2011). The whole cross-section images were used to collect cross-sectional geometry data, which assesses geometrical shape and size properties of a cross-section and measures the distribution of cortical bone and medullary cavity (Agnew and Stout 2012). Full cross-section analysis of microstructural variables was also completed rather than ROI analysis. Human rib histological studies often will analyse the entire cross-section instead of applying ROI methods (Dominguez and Agnew 2016; García-Donas et al. 2022; Qiu et al. 2003) due to

Figure 5.3: Human rib cross-section. Light microscopy, 10x magnification.
Image by Tahlia J Stewart.

the much smaller cross-section size and difficulty to apply ROIs to the narrower margins of cortical bone in the human rib, especially when compared to the human femur.

5.4.2 Image Storage

Images were stored on a WD Elements 1.5TB Portable Hard Drive and uploaded to the ANU's One Drive Online Storage System for additional backup of data. During data analysis, each image was stored temporarily to the desktop of the PI's MacBook Air for smoother software processing. Images were secure in these locations and only shared via the One Drive Online Storage System with individuals included by name in relevant Ethics Approvals. Images are to be stored in this secure manner for 5 years after thesis submission, or as long as Ethics Approval allows, whichever is first, to ensure their availability for any necessary follow-up research or to answer any queries resulting from thesis dissemination or subsequent publications.

5.5 Image Analysis

Image analysis was conducted using the open-source software, Fiji ImageJ (Schindelin et al. 2012). Three main forms of data were collected: cross-sectional geometry data for the ribs, and porosity and secondary osteon data for both the rib and femur samples. Here, the image analysis protocols for each type of data collected are described.

5.5.1 Rib Cross-Sectional Geometry Data

Rib cross-sectional geometry has been used to investigate the proportion of cortical versus trabecular bone and medullary space within a rib cross-section (Agnew and Stout 2012; Holcombe et al. 2019; Holcombe and Huang 2023; Murach et al. 2017). Images were exported as TIFF files from cellsSens® software and imported to Fiji ImageJ. The scale was set using measurements acquired and burnt into the TIFF image via cellSens® at the time of imaging. The line of the scale was measured using the line tool in Fiji, followed by the set scale tool. For cross-sectional geometry images, millimetres were the preferred unit of measure, due to the larger size of features measured. Thus, burnt in scales that were measured in micrometres (μm or μm^2), were converted to millimetres (mm or mm^2).

The premise of cross-sectional geometry is to separate the cortical bone from the trabecular bone and medullary, or endosteal, cavity in a given cross-section to assess proportions of the different components of a bone cross-section (Figure 5.4). Trabecular bone lacks the

comparatively dense osteonal structure that we see in cortical bone, with sparser looking matrix and increased porosity (Agnew and Stout 2012; Frost 1997). Thus, the border between cortical and trabecular bone was delineated using the polygon selection tool, tracing around and thus identifying the endosteal area pictured below (Figure 5.4).

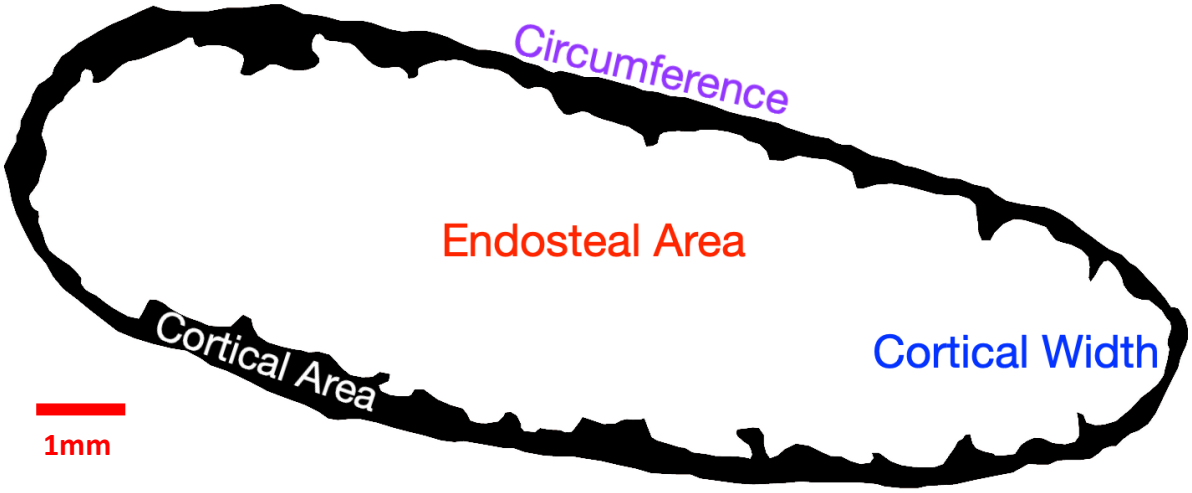

Figure 5.4: Example of rib cross-sectional geometry area definitions.
Image by Tahlia J Stewart.

Each rib cross-section image, such as that in Figure 5.3, was transformed into that pictured in Figure 5.4 to facilitate cross-sectional geometry analysis. Measurements of endosteal area and perimeter were recorded and the endosteal area was deleted from the image, replaced with black background fill. Then the outer circumference, or the periosteal border, was delineated using the polygon selection tool. The measurements of periosteal circumference and total cross-section area were recorded and then the external space in the surrounding image was deleted and also replaced with black background fill, leaving a ring of cortical bone. Image type was changed to 16-bit, to adjust to a flattened greyscale image. Using the threshold tool, the greyscale image was then converted to a solid black image representing the cortical bone (Figure 5.4). Once a rib cross-section was reduced to an outer rim of solid black cortical bone, the BoneJ Slice Geometry tool was used to measure total cross-section area (CSA), endosteal area (Es.Ar), cortical area (Ct.Ar) and mean cortical width (Ct.Wi). Where a rib cross-section was incomplete due to breakage, it was excluded from the cross-sectional geometry analysis as the whole cross-section could not be observed.

5.5.1.1 Porosity Data

Cross-sectional geometry studies of the rib often incorporate measurements of porosity, to more accurately measure cortical bone in a cross-section by removing voids, or porosities in its structure (Agnew and Stout 2012; Holcombe et al. 2019; Holcombe and Huang 2023; Murach et al. 2017). Each area of cortical porosity was measured using the polygon selection tool to trace the perimeter and measured in millimetres (mm^2) to match other cross-sectional geometry data. Porosity measurements were subtracted from the rib cross-section cortical area to account for voids in cortical bone and exclude from cortical area measurements (Agnew and Stout 2012). Porosities in the cortical bone included those pertaining to vascularity or resorption, but not including canaliculi or osteocyte lacunae as these are considered to substantially contribute to mechanical properties (Agnew and Stout 2012; Martin 1984). Porosity data collected included, mean porosity area (Po.Ar) and number of porosities (N.Po). These measurements were utilised in calculated variables, as detailed in Table 5.1 below.

Table 5.1: Cross-Sectional Geometry measurements observed.

Measurement	Abbreviation[1]	Unit	Definition
Cross-Section Area[2,3]	CSA	mm^2	Total area within the periosteal border of a cross-section (rib only) (CSA = Ct.Ar + Es.Ar).
Cortical Area[2,4]	Ct.Ar	mm^2	Area of cortical bone within a slide (rib and femur) (RIB: Ct.Ar = CSA – Es.Ar; FEMUR: This was recorded as the area of cortical bone in a given ROI).
Endosteal Area[2,4]	Es.Ar	mm^2	Area of the medullary cavity or endosteal area within a cross-section (rib only) (Es.Ar = CSA – Ct.Ar).
% Cortical Area[2]	%Ct.Ar	%	Percentage of a cross-section occupied with cortical bone (rib only) (%Ct.Ar = (Ct.Ar/CSA) x 100).
Absolute Cortical Area[2]	Ct.ArA	mm^2	Area of cortical bone accounting for voids or porosities in the cortical bone (rib and femur) (Ct.ArA = Ct.Ar – Tt.Po.Ar).
Mean Cortical Width[3,4]	Ct.Wi	mm	Average width of cortical bone in a cross-section. Calculated via the BoneJ Slice Geometry plugin for Fiji (rib only).
Mean Porosity Area[2,4]	Po.Ar	mm^2	Average area of a porosity in a slide (rib and femur) (Po.Ar = Tt.Po.Ar/#Po).
Number of Porosities	N.Po	Count	Count of the number of porosities present in a slide or ROI (rib and femur).
Total Porosity Area[2,4]	Tt.Po.Ar	mm^2	Sum of all porosities in a slide or ROI (rib and femur).
Cortical Porosity[2,4]	Ct.Po	%	Percentage of a cross-section or ROI occupied by cortical porosity (rib and femur) (Ct.Po = (Tt.Po.Ar/Ct.Ar) x 100).

[1] Abbreviations followed naming conventions defined by Dempster et al. 2013. [2] Agnew and Stout 2012. [3] Doube et al. 2010. [4] Dempster et al. 2013.

5.5.2 Secondary Osteon and Haversian Canal Data

Using Fiji ImageJ, secondary osteons and Haversian canals were traced using the polygon selection tool in all ROIs for both femur and rib samples (Figure 5.5). Using the Analyse Set Measurements tool, measurements observed include those defined below in Table 5.2. Only osteon and Haversian canal area were manually measured using the polygon selection tool. From these manual measurements, Fiji ImageJ automatically measured and recorded perimeter, diameter, circularity, aspect ratio, roundness and solidity for both osteons and Haversian canals. These data were collected in pairs, recording secondary osteons and their paired Haversian canals. Area, perimeter and diameter were collected in μm^2 and µm due to their small scale, while circularity, aspect ratio, roundness and solidity are indexed.

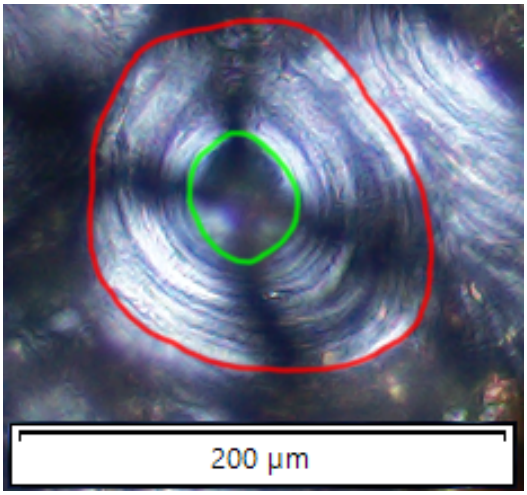

Figure 5.5: Secondary osteon with external cement line indicated in red and the Haversian canal perimeter in green.

The borders were traced around using the polygon selection tool to measure perimeter and then to automatically calculate other measurements listed in Table 5.2. Image by Tahlia J Stewart, Polarised microscopy, 10x magnification.

Table 5.2: Secondary osteon and Haversian canal measurements observed.

Measurement	Abbreviation[1]		Unit	Definition
Area[2,3]	On.Ar	H.Ar	μm^2	The area within the external osteonal lamellar border
Perimeter[2,3]	On.Pm	H.Pm	µm	The length of the external osteonal lamellar border
Diameter[2,3]	On.Dm	H.Dm	µm	The longest distance between two opposite points along the external osteonal lamellar border
Circularity[2]	On.Circ	H.Circ	Calculated	= $(4\pi \times Ar)/Pm^2$. A value ranging from 0.0, indicating an oval shape, to 1.0, indicating a perfect circle
Aspect ratio[2]	On.AsRa	H.AsRa	Calculated	= Major Axis/Minor Axis. Ratio of the longest point to the shortest point of the feature

Roundness[2]	On.Rn	H.Rn	Calculated	= 4 x Ar/(π x major axis^2). Also known as the inverse AR
Solidity[2]	On.Sd	H.Sd	Calculated	= Ar/convex area.
Osteon Population Density[3,4]	OPD		Calculated	= #On/1mm^2. Number of osteons per mm^2.
Fragmentary Osteon Population Density[4]	Fg.OPD		Calculated	=#Fg.On/1mm^2. Number of fragmentary osteons per mm^2.

[1] Abbreviations followed naming conventions defined by Dempster et al. 2013. [2] Doube et al. 2010. [3] Dempster et al. 2013. [4] Karydi et al. 2022.

5.6 Data Storage

Data were stored across multiple locations and mediums including Microsoft Excel and IBM SPSS (v. 24) to prevent data loss or file corruption. Storage locations were on private or secure hard drives and servers to prevent data theft or being compromised, as per ethics protocols. All data collected and images taken will be kept for a period of 5 years from completion of this dissertation in case required for follow-up after submission, publication or dissemination of findings.

5.7 Data Analysis

Data analysis was performed in stages pertaining to data preparation, descriptive data, and inferential, univariate and multivariate analysis as defined and required by the research questions, described below.

5.7.1 Data Cleaning and Formatting

Data were screened in Microsoft Excel to remove duplicates and irrelevant data points. Some outliers were identified via descriptive range of values, but were validated via re-measurement and so none were removed. Missing datapoints were coded as such during analysis so as to not falsely skew data towards zero. Variable names and shorthand were formatted to standardised nomenclature (Dempster et al. 2013), and all data units were validated to ensure uniform formatting throughout. All data were then copied to a main data sheet in IBM SPSS (v. 24) and separated into sub-data sheets; one for each research question, and sub-question if necessary, to facilitate differing statistical analysis plans.

5.7.2 Data Normality and Intra-Observer Error Testing

Tests of normality were applied to each variable in the whole sample to inform inferential analysis according to standard statistical convention. Those where sample size was $n \geq 50$,

the Kolmogorov-Smirnov test of normality was applied, and for those where sample size was $n < 50$, the Shapiro-Wilk test of normality was applied (Mishra et al. 2019). Normality values were recorded to inform whether inferential statistical analyses should be parametric or non-parametric, according to statistical convention (Orcan 2020). p significance was defined as <0.05, and a significant p-value indicated abnormal distribution, while insignificant p-values indicated normal distribution. Whereby a variable's dataset was determined to be normally distributed, parametric statistical testing could be used, while abnormally distributed variable datasets were tested using non-parametric statistical tests.

Intra-observer error testing was conducted to ascertain consistency in data collection (Lynnerup et al. 1998; Villa and Lynnerup 2010). For bone histology studies, intra-observer error testing involves a portion of the histology images being re-analysed and data re-collected at least 2 months following initial data collection (Lynnerup et al. 1998; Miszkiewicz and Mahoney 2016; Villa and Lynnerup 2010). Previous studies have re-analysed approximately 10% of their sample (Lynnerup et al. 1998; Miszkiewicz and Mahoney 2016; Villa and Lynnerup 2010). Here, 20 images were re-analysed, collecting repeated data approximately 4 months following completion of data collection, representing ~25% of the individuals observed in this study. Images chosen for re-analysis were selected at random, using a random sample selection code in Microsoft Excel. This involves the application of an INDEX function, which can then select a sample at random from a list of, in this case individual IDs, defined by a RANDBETWEEN function. The individual IDs listed included all individuals from the UK and AFTER samples. When a duplicate individual ID was selected, the function was re-run until a new individual ID was selected. This was repeated until a total of 20 unique individual IDs were selected. From there, a list of image IDs was produced for each individual, and the INDEX and RANDBETWEEN function process was repeated to randomly select 1 image for re-analysis for each individual. Each of the 20 images were re-analysed following methods described in section 5.4.5, re-counting secondary and fragmentary osteons, and re-measuring osteon and Haversian canal area, perimeter, diameter, circularity, aspect ratio, roundness, and solidity.

Repeated data collected were compared to that collected initially via paired correlations (parametric Pearson's r or non-parametric Spearman's rho depending on variable normality or abnormality), Bland-Altman graphs (Bland and Altman 1986), and paired samples t-tests for normally distributed variables, or Wilcoxon signed rank tests for abnormally distributed variables. This is as per conventions in bone histology (Lynnerup et al. 1998; Miszkiewicz and Mahoney 2016). Pearson's *r* and Spearman's *rho* were run in SPSS and the r, r^2 and *p*-values were recorded. Paired sample *t*-tests and Wilcoxon signed rank tests were run in SPSS and

the *t*, degrees of freedom and *p*-values were recorded for the *t*-tests, and *Z* and *p*-values were recorded for the Wilcoxon signed rank tests. Bland-Altman plots were created in SPSS, by first calculating the difference between observation 1 and observation 2, called the 'difference variable', and the average of the two datapoints. A one-sample *t*-test was run for each 'difference variable'. The Bland-Altman plots were created, and *y*-axis reference lines were added to demarcate the mean, 95% confidence interval lower and upper margins, and +/- 2 standard deviations from the mean (Lynnerup et al. 1998; Villa and Lynnerup 2010).

5.7.3 Data Analysis

Descriptive data were extracted, ascertaining mean, minimum and maximum values, and standard deviation for all variables. The number of slides and the number of individuals represented in each variable's dataset, was summed. Each research question employed sub-groups of relevant variables from the rib, anterior and posterior femur. As such, for each research question, these sub-groups were re-observed via descriptive statistics, and tests of normality were re-conducted for each variable within each bone/bone region sub-group to guide further parametric or non-parametric statistical analysis.

5.7.4 Data Analysis by Research Question

Here, the inferential and, where applicable, multivariate statistical analysis methods are described for each research question and sub-question, to test their respective hypotheses. Null hypothesis testing was guided by the protocol outlined in Table 5.3.

Table 5.3: Hypothesis Testing Guidelines (Elliott and Woodward 2007).

Decision	**Outcome**	
	H_0 True	*H_0 False*
Reject H_0	Type I error (α)	Correct decision ($1 - \beta$)
Do not reject H_0	Correct decision ($1 - \alpha$)	Type II error (β)

5.7.4.1 Research Question 1: Does human rib and femur histology vary with age-at-death, sex and systemic health and physical activity (as inferred by socioeconomic status) in samples of English ancestry?

To answer this research question, there are three sub-questions, to separately observe differences in bone histology through the lens of (a) age-at-death, (b) sex and (c) socio-economic status, and within each of these sub-questions, there are multiple hypotheses to be tested to identify not only variations in human bone histology with AAD, biological sex and SES, but also how these variations manifest in the femur as compared to the rib. Here, each

of these sub-questions and their respective hypotheses are listed, along with descriptions of the statistical methods employed to answer them.

1a) Age-At-Death (AAD)

Key variables observed in this part of research question 1 included; OPD, Fg.OPD, Ct.Po and Ct.Wi.

$H0_a$: There is no monotonic relationship between absolute (chronological) age-at-death (AAD) and either observed variable; OPD, Fg.OPD, Ct.Po or Ct.Wi.

This question required the testing of a relationship between the absolute known AAD for the AFTER individuals, and each of the variables. Due to small sample sizes in the sub-groups analysed for testing this hypothesis (n = 17), the non-parametric Spearman's *Rho* was run rather than the parametric Pearson's r (Mishra et al. 2019; Orcan 2020). The assumptions of the Spearman's *Rho* test were upheld, such as having paired observations of absolute known AAD and each continuous variable (Elliott and Woodward 2007). Spearman's *Rho* is not sensitive to outliers, which can easily cause misclassification in histomorphometric datasets due to the measurements of such small structures (Lagacé et al. 2020). The Spearman's *Rho* was then repeated, accounting for individual body size variation between individuals via the application of a stature correction. The stature correction involved multiplying each variable's datapoint by the stature measurement of the AFTER individual and dividing by 100 where necessary to prevent exceedingly high values. This is a technique similar to robusticity indices applied elsewhere (Miszkiewicz and Mahoney 2019; Stock and Shaw 2007). Both sets of results were reported, firstly not accounting for individual body size variation, and secondly accounting for individual body size variation, to examine how the application of this stature index affected the outcome. The Bonferroni Correction was applied to account for multiple p-values being produced simultaneously, to reduce the risk of a type 1 error in hypothesis testing (Abdi 2007; Bonferroni 1936; Elliott and Woodward 2007; Haynes 2013).

$H0_b$: Each of the observed variables (OPD, Fg.OPD, Ct.Po or Ct.Wi) have a similar distribution across AAD categories.

This question required the testing of differences in distribution between the AAD categories for each of the variables. Due to small sub-group sizes, adolescent (n = 1) and young adult (n = 3) AAD categories had to be excluded from further statistical analysis. Due to small sub-group sizes (n <30) in the remaining middle adult (n = 26) and old adult (n = 17) categories, non-

parametric Mann-Whitney *U* tests were run rather than the two-sample *t*-test (Mishra et al. 2019; Orcan 2020). Additionally, the Mann-Whitney *U* test is not sensitive to outliers, which can easily cause misclassification in histomorphometric datasets due to the measurements of such small structures (Lagacé et al. 2020). Mann-Whitney *U* test assumptions were upheld, including independent datapoints and ordinal data classifications (Elliott and Woodward 2007). To ensure datapoints were independent, data collected from paired rib sections of the same individuals were averaged prior to inclusion. Mann-Whitney *U* tests were run separately for each bone (rib, anterior femur and posterior femur), and so data collected from multiple bones of the same individual were still considered independent as they were not tested simultaneously. The Mann-Whitney *U* was then repeated, accounting for individual body size variation between individuals via the application of a stature correction. The stature correction involved multiplying each variable's datapoint by the stature measurement of the individual, and dividing by 100 to prevent exceedingly high values, similar to robusticity indices applied elsewhere (Miszkiewicz and Mahoney 2019; Stock and Shaw 2007). Both sets of results were reported, firstly not accounting for individual body size variation, and secondly accounting for individual body size variation, to examine how the application of this stature index affected the outcome. The Bonferroni Correction was applied to account for multiple *p*-values being produced simultaneously, to reduce the risk of a type 1 error in hypothesis testing (Abdi 2007; Bonferroni 1936; Haynes 2013).

$H0_c$: Each of the observed variables (OPD, Fg.OPD, Ct.Po or Ct.Wi) have a similar distribution across the rib and the femur.

This question required the testing of differences in distribution between the AAD categories for each of the variables separately within the rib, anterior and posterior femur. While in $H0_b$ results were separated by bone and bone region to control for intrinsic bone differences in these variables, in $H0_c$, these differences in the results between bones were specifically assessed. As such, $H0_c$ did not require additional statistical testing, and thus, statistical methods are the same as above. However, rather than taking the results from differences between AAD categories for each variable, for this hypothesis, results from the differences between AAD categories for each variable as compared between the rib, anterior and posterior femur were used to test this hypothesis.

1b) Biological Sex

Key variables observed in this part of research question 1 included; OPD, Fg.OPD, On.Ar, H.Ar, Ct.Po or Ct.Wi.

$H0_a$: Each of the observed variables, OPD, Fg.OPD, On.Ar, H.Ar, Ct.Po and Ct.Wi have a similar distribution in male and female groups.

This question required the testing of differences in distribution between male and females for each of the variables. Due to small sample size in the female sub-group (n = 4), the anterior femur was excluded from this analysis. Additionally, all other sub-groups were small (n <30) and so Mann-Whitney U tests were run rather than the two-sample t-test (Mishra et al. 2019; Orcan 2020). Mann-Whitney U test assumptions were upheld, including independent datapoints and ordinal data (Elliott and Woodward 2007). Data collected from paired rib sections of the same individuals were averaged prior to inclusion to ensure independence. Mann-Whitney U tests were run separately for each bone (rib, anterior femur and posterior femur), and so data collected from multiple bones of the same individual were still considered independent as they were not tested simultaneously. Additionally, the Mann-Whitney U test is not sensitive to outliers, which can easily cause misclassification in histomorphometric datasets due to the measurements of such small structures (Lagacé et al. 2020). The Mann-Whitney U was repeated, accounting for individual body size variation between individuals via the application of a stature correction. The stature correction involved multiplying each variable's datapoint by the stature measurement of the individual, and dividing by 100 to prevent exceedingly high values, similar to robusticity indices applied elsewhere (Miszkiewicz and Mahoney 2019; Stock and Shaw 2007). Both sets of results were reported, firstly not accounting for individual body size variation, and secondly accounting for individual body size variation, to examine how the application of this stature index affected the outcome. The Bonferroni Correction was applied to account for multiple p-values being produced simultaneously, to reduce the risk of a type 1 error in hypothesis testing (Abdi 2007; Bonferroni 1936; Haynes 2013).

$H0_b$: Each of the observed variables, OPD, Fg.OPD, On.Ar, H.Ar and Ct.Po have similar distributions between the rib and posterior femur.

This question required the testing of differences in distribution between males and females for each of the variables separately within the rib and posterior femur. While in $H0_a$ results were separated by bone and bone region to control for intrinsic bone differences, in $H0_b$, these differences in the results between bones were specifically assessed. As such, $H0_b$ didn't require additional analysis, and thus, statistical methods are the same as above. However, rather than inferring the results from differences between males and females for each variable,

for this hypothesis, results from the differences between males and females for each variable as compared between the rib and posterior femur were used to test this hypothesis.

1c) Socioeconomic Status (SES)

Key variables observed in this part of research question 1 included; OPD, On.Circ, Po.Ar, Ct.Po Ct.Wi or %Ct.Ar.

$H0_a$: Each of the observed variables, OPD, On.Circ, Po.Ar, Ct.Po, Ct.Wi and %Ct.Ar have a similar distribution across the three socioeconomic status (SES) groups; medieval lower class, medieval upper class and contemporary.

This question required the testing of differences in distribution between medieval lower and upper class, and modern contemporary groups for each of the variables. The anterior femur was excluded from this analysis due to small medieval sample sizes (medieval high status n = 6, medieval low status n = 2). Remaining sub-groups were small (n <30) and so Kruskal-Wallis H tests were run rather than the one-way analysis of variance (ANOVA) test (Mishra et al. 2019; Orcan 2020). Kruskal-Wallis H test assumptions were upheld, including a minimum of three groups of data, independent datapoints and ordinal data (Elliott and Woodward 2007). Data collected from paired rib sections of the same individuals were averaged prior to inclusion to ensure independence. Kruskal-Wallis H tests were run separately for each bone (rib, anterior femur and posterior femur), and so data collected from multiple bones of the same individual were still considered independent as they were not tested simultaneously. Additionally, the Kruskal-Wallis H test is not sensitive to outliers, which can easily cause misclassification in histomorphometric datasets due to the measurements of such small structures (Lagacé et al. 2020). The Kruskal-Wallis H test was repeated, accounting for individual body size variation between individuals via the application of a stature correction. The stature correction involved multiplying each variable's datapoint by the stature measurement of the individual, and dividing by 100 to prevent exceedingly high values, similar to robusticity indices applied elsewhere (Miszkiewicz and Mahoney 2019; Stock and Shaw 2007). Both sets of results were reported, firstly not accounting for individual body size variation, and secondly accounting for individual body size variation, to examine how the application of this stature index affected the outcome. The Bonferroni Correction was applied to account for multiple p-values being produced simultaneously, to reduce the risk of a type 1 error in hypothesis testing (Abdi 2007; Bonferroni 1936; Haynes 2013).

$H0_b$: Each of the observed variables, OPD, On.Circ, Po.Ar and Ct.Po have similar distributions between the rib and posterior femur.

This question required the testing of differences in distribution between SES groups for each of the variables separately within the rib and posterior femur. While in $H0_a$ results were separated by bone to control for intrinsic bone differences, in $H0_b$, these differences in the results between bones were specifically assessed. As such, $H0_b$ didn't require additional analysis, and thus, statistical methods are the same as above. However, rather than inferring the results from differences between SES groups for each variable, for this hypothesis, results from the differences between SES groups for each variable as compared between the rib and posterior femur were used to test this hypothesis.

5.7.4.2 Research Question 2: Is there a trend of bone quality "deteriorating" in contemporary individuals to reflect generally more sedentary lifestyles than their medieval ancestral population?

Key variables observed as part of this research question included; OPD, On.Circ, On.Ar, %Ct.Ar, Po.Ar and Ct.Po.

$H0_a$: Each of the observed variables, OPD, On.Circ, On.Ar, %Ct.Ar, Po.Ar and Ct.Po have a similar distribution between medieval and modern era individuals.

This question required the testing of differences in distribution between medieval and modern individuals for each of the variables. There were no posterior femur samples collected from the modern (AFTER) individuals, and so the posterior femur was excluded from this analysis. Additionally, sample sizes between modern and medieval sub-groups were vastly different (medieval rib $n = 51$, modern rib $n = 15$; medieval anterior femur $n = 8$, modern anterior femur $n = 15$) and so Mann-Whitney *U* tests were run rather than the two-sample *t*-test (Mishra et al. 2019; Orcan 2020). Mann-Whitney *U* test assumptions were upheld, including independent datapoints and ordinal data (Elliott and Woodward 2007). Data collected from paired rib sections of the same individuals were averaged prior to inclusion to ensure independence. Mann-Whitney *U* tests were run separately for each bone (rib and anterior femur), and so data collected from multiple bones of the same individual were still considered independent as they were not tested simultaneously. Additionally, the Mann-Whitney *U* test is not sensitive to outliers, which can easily cause misclassification in histomorphometric datasets due to the measurements of such small structures (Lagacé et al. 2020). The Mann-Whitney *U* was repeated, accounting for individual body size variation between individuals via the application of a stature correction. The stature correction involved multiplying each variable's datapoint by

the stature measurement of the individual, and dividing by 100 to prevent exceedingly high values, similar to robusticity indices applied elsewhere (Miszkiewicz and Mahoney 2019; Stock and Shaw 2007). Both sets of results were reported, firstly not accounting for individual body size variation, and secondly accounting for individual body size variation, to examine how the application of this stature index affected the outcome. The Bonferroni Correction was applied to account for multiple *p*-values being produced simultaneously, to reduce the risk of a type 1 error in hypothesis testing (Abdi 2007; Bonferroni 1936; Haynes 2013).

$H0_b$: Medieval and modern ribs and anterior femora cannot be separated using discriminant function analysis (DFA), based on the variables OPD, On.Circ, On.Ar, Po.Ar and Ct.Po.

DFA uses a combination of independent variables to create a new, linear variable called a function. Variables are assigned a coefficient value and individuals and their datapoints are classified into a group, in this case either medieval or modern, based on the function that is created (Elliott and Woodward 2007). Elsewhere, this has been conducted in an archaeological context to discriminate differences in human bone microstructure between two medieval socioeconomic groups (Miszkiewicz and Mahoney 2016). Individuals can be more accurately classified into sub-groups if a function is statistically significant, but that is not to say that statistical significance is indicative of successful classification, and so Eigen values and canonical correlation values were recorded to guide analysis and interpretation (Elliott and Woodward 2007). Wilks's *lambda* and *chi*-square values were recorded to test group mean equality. DFA assumptions include normality, removal of outliers, lineariy, mulicolinearity/singularity, and nil variance-covariance matrices heterogeneity (Elliott and Woodward 2007). These assumptions were addressed prior to analysis. Variable independence was addressed similarly to above, with paired rib cross-sectional data being averaged so that each individual had just one set of averaged data for each variable. Paired rib and anterior femur datapoints were acceptable as the rib and anterior femur were tested separately. There were no significant outliers that required removal prior to DFA. Assessment of data linearity was performed using scatterplots and correlation matrices were performed in conjunction with the DFA, included in the DFA SPSS outputs. Box's *M* tests were also performed in conjunction with the DFA and included in the DFA SPSS outputs to assess variance-covariance matrix homogeneity. SPSS outputs automatically presented DFA results as separate covariance matrices if heterogeneity was observed, rather than pooled covariance matrices. Prior to discriminant function analyses (DFA), OPD, On.Circ, On.Ar, Po.Ar and Ct.Po data were log-transformed to address assumptions of normality in DFA testing. Equations applied to each variable for log-transformation are described in Table 5.4 below.

Table 5.4: Log-transformation equations applied by variable.	
Variable	**Equation**
OPD	logOPD = Lg10(OPD)
On.Circ	logOn.Circ = Lg10(On.Circ)
On.Ar	logOn.Ar = Lg10(On.Ar)
Po.Ar	logPo.Ar = Lg10(Po.Ar)
Ct.Po	logCt.Po = Lg10(Ct.Po)

Seven DFAs were performed with era (medieval or modern) as the dependent variable. Four were performed for the rib data, and three for the anterior femur data. For the rib analyses, predictor variables included OPD, On.Circ, On.Ar, Po.Ar and Ct.Po for the entire sample (*n* = 71) and then divided into demographic sub-groups to explore variation when controlling for biological sex and age-at-death (AAD). Due to small sample sizes in the other AAD categories, only old adults (OA, age 50+) could be included as an AAD sub-group. OPD, On.Circ, On.Ar, Po.Ar and Ct.Po were listed as predictor variables (*n* = 21). The entire sample was then split by biological sex, and OPD, On.Circ, On.Ar, Po.Ar and Ct.Po were listed as predictor variables (male *n* = 45, female *n* = 32). Small sub-group sizes prevented statistically robust analysis from being conducted while controlling for more than one demographic variable simultaneously, i.e., female OAs.

For the anterior femur analyses, predictor variables included OPD, On.Circ, On.Ar, Po.Ar and Ct.Po for the entire sample (*n* = 28) and then divided into demographic sub-groups to explore variation when controlling for biological sex and AAD. Due to small sample sizes in the other AAD categories, only OA (age 50+) could be included as an AAD sub-group. OPD, On.Circ, On.Ar, Po.Ar and Ct.Po were listed as predictor variables (*n* = 20). The entire sample was then split by biological sex, and OPD, On.Circ, On.Ar, Po.Ar and Ct.Po were listed as predictor variables (male *n* = 21). The female subgroup was too small to be included as a separate sub-group for analysis (*n* = 5). Similar to the rib DFA, small sub-group sizes prevented statistically robust analysis from being conducted while controlling for more than one demographic variable simultaneously, i.e., male OAs.

The Bonferroni correction was applied to all *p*-values generated to reduce the risk of false significance (Abdi 2007; Bonferroni 1936; Haynes 2013). Other results output included Eigen-values, which guided results interpretation, canonical correlation, function *chi*-square, degrees of freedom (*df*), loading matrix and the classification output, which provided a percentage of correctly classified datapoints (as either modern or medieval) based on the predictor variables. Where a variable failed the tolerance test, it was removed as a predictor variable and a function was calculated based on the remaining variables.

The DFAs were then repeated with data which were corrected by the application of a stature correction to account for individual variation in body size which may skew the results. The stature correction involved multiplying each variable's datapoint by the stature measurement of the individual and dividing by 100 where necessary to prevent exceedingly high values. This is a technique similar to robusticity indices applied elsewhere (Miszkiewicz and Mahoney 2019; Stock and Shaw 2007). For this part of the analysis, seven further DFAs were performed with era (medieval or modern) as the dependent variable. Four were performed for the rib data, and three for the anterior femur data. For the rib analyses, predictor variables included OPD, On.Circ, On.Ar, Po.Ar and Ct.Po for the entire sample (n = 66) and then divided into demographic sub-groups to explore variation when controlling for biological sex and age-at-death (AAD). Due to small sample sizes in the other AAD categories, only old adults (OA, age 50+) could be included as an AAD sub-group. Predictor variables included OPD, On.Circ, On.Ar, Po.Ar and Ct.Po (n = 18). The entire sample was then split by biological sex, and predictor variables for this sub-analysis included OPD, On.Circ, On.Ar, Po.Ar and Ct.Po (male n = 40, female n = 32). Small sub-group sizes prevented statistically robust analysis from being conducted while controlling for more than one demographic variable simultaneously, i.e., female OAs. For the anterior femur analyses, predictor variables included OPD, On.Circ, On.Ar, Po.Ar and Ct.Po for the entire sample (n = 23) and then divided into demographic sub-groups to explore variation when controlling for biological sex and AAD. Due to small sample sizes in the other AAD categories, only OA (age 50+) could be included as an AAD sub-group. Predictor variables for this sub-analysis included OPD, On.Circ, On.Ar, Po.Ar and Ct.Po (n = 17). The entire sample was then split by biological sex, and predictor variables included OPD, On.Circ, On.Ar, Po.Ar and Ct.Po (male n = 17). The female subgroup was too small to be included as a separate sub-group for analysis (n = 5). Similar to the rib DFA, small sub-group sizes prevented statistically robust analysis from being conducted while controlling for more than one demographic variable simultaneously, i.e., male OAs.

$H0_c$: There is no evidence of a more sedentary lifestyle influencing modern individuals as compared to medieval individuals in either observed variable; OPD, On.Circ, On.Ar, %Ct.Ar, Po.Ar and Ct.Po.

This null hypothesis does not require any further statistical tests, rather, the previous tests run to test the previous two hypotheses can be assessed for evidence of sedentary lifestyles in contemporary individuals compared to the medieval sample. If the rib and anterior femur of contemporary individuals do reflect a more sedentary lifestyle by comparison to medieval individuals, it is expected that their bone histology would include reduced OPD and increased

On.Ar due to slower remodelling (Schlecht 2012), increased On.Circ, with less skewing which is often caused by repeated strain activity (Frost 1990; Skedros et al. 2014), and evidence of cortical thinning (reduced %Ct.Ar) and increased porosity (increased Po.Ar and Ct.Po) due to inactivity-associated bone loss (Frost 1990; 1997; Schlecht 2012).

5.7.4.3 Research Question 3: Is there variation in standardised histological variables between serial cross-sections from the human rib midshaft?

Key variables observed as part of this research question included; Ct.Ar, Ct.Wi, Ct.ArA, Po.Ar, On.Ar, H.Ar, Ct.Po, OPD, Fg.OPD and On.Circ.

$H0_a$: There is no monotonic relationship in either observed variable; Ct.Ar, Ct.Wi, Ct.ArA, Po.Ar, On.Ar, H.Ar, Ct.Po, OPD, Fg.OPD and On.Circ between paired serial histological sections of the rib, approximately 1cm apart in the rib shaft.

Data were arranged by individual, with paired observations recorded for slides 1 and 2. Each variable, except Ct.Wi (n = 11; due to few unbroken rib cross-sections for cross-sectional geometric analysis), had a dataset of 48 individuals, each with a pair of observations for each variable. Descriptive statistics were recorded, including n, minimum, maximum, mean and standard deviation for each variable. Bivariate scatterplots were created to visualise relationships between the paired datapoints for each variable, with datapoints from slide 1 on the *y*-axis and those from slide 2 on the *x*-axis. Trend lines were applied. Two-tailed Spearman's *rho* tests were run for each variable in SPSS. Results outputs included Spearman's r (correlation coefficient), the coefficient of determination (r^2) and the p-value. Statistical significance was defined as $p < 0.05$. The r-value was to determine if there was a relationship between data extracted from an individual's slide 1, as compared to what was extracted from slide 2, while the r^2-value was to ascertain how much of the data extracted from one slide, could be explained by the data extracted from the other. This research question was further addressed via a second null hypothesis.

$H0_b$: Each of the observed variables; Ct.Ar, Ct.Wi, Ct.ArA, Po.Ar, On.Ar, H.Ar, Ct.Po, OPD, Fg.OPD and On.Circ have a similar distribution between paired serial histological sections of the rib, approximately 1cm apart in the rib shaft.

While the previous null hypothesis was centered on observing any relationship between data extracted from one slide compared to data extracted from another from the same individual, this null hypothesis instead looks at differences in distribution of the data extracted, between the paired slides. As such, a Wilcoxon Signed Rank test was run, with slide 1 being one group,

and slide 2 being the other. Results outputs included a test statistic and the asymptotic (two-sided) *p*-value, which indicated either statistically significant differences (p <0.05) between slide 1 and slide 2 groups, or no statistically significant differences (p >0.05) between slide 1 and slide 2 groups. The Bonferroni correction was applied to each *p*-value to reduce the risk of false statistical significance (Abdi 2007; Bonferroni 1936; Haynes 2013).

Using the combined results of the two tests described above, the research question can be addressed, not only based on relationships between the paired data for each observed variable, but also by any observed differences between the two pairs of data.

5.7.4.4 Research Question 4: Does cortical bone histology vary between bones of different levels of metabolic activity, such as the femur and the rib?

Key variables observed as part of this research question included; On.Ar, H.Ar, On.Dm, H.Dm, On.Pm, H.Pm, On.Circ, H.Circ, On.Rd, H.Rd, On.AsRa, H.AsRa, On.Sd and H.Sd.

$H0_a$: Each of the observed osteon and Haversian canal size variables, On.Ar, H.Ar, On.Dm, H.Dm, On.Pm and H.Pm, have a similar distribution across the rib and the femur.

For this analysis, the dataset was separated into independent and dependent samples, for osteon and Haversian canal size to be tested appropriately. For the independent paired rib and posterior femur samples, non-parametric testing was used due to small sample size (rib n = 9, posterior femur n = 7). Thus, to test for differences in size variable distribution across two bones, an independent-samples Mann-Whitney *U* test was performed. Data outputs recorded included the Mann-Whitney *U* score, the associated *p*-value and the mean rank for each bone within each size variable to compare mean differences between bones. Where the *p*-value was <0.05, the result was deemed statistically significant and the null hypothesis was rejected, indicating that there were statistically significant differences in the distribution of that size variable between the rib and posterior femur. Where the *p*-value was >0.05, the result was deemed not statistically significant and the null hypothesis was retained, indicating that there were no statistically significant differences in the distribution of that size variable between the rib and posterior femur. The asymptotic two-sided, significance was recorded, and the Bonferroni correction was applied to reduce the risk of false statistical significance when running multiple tests simultaneously (Abdi 2007; Bonferroni 1936; Haynes 2013). The independent samples Mann-Whitney *U* test was repeated on the same dataset (rib n = 9, posterior femur n = 7), after the application of a stature correction to control for differences in individual body size. Results of both analyses were recorded.

There was a total of *n* = 8 individuals, from whom a rib, anterior femur and posterior femur sample was sourced. To test for differences in osteon and Haversian canal size metrics between the three bones, a related-samples Friedman's two-way analysis of variance by ranks test was performed. Data outputs recorded included the Friedman's test score, the associated p-value and the mean rank for each bone within each size variable to compare mean differences between bones. Where the *p*-value was <0.05, the result was deemed statistically significant and the null hypothesis was rejected, indicating that there were statistically significant differences in the distribution of that size variable between the three groups. Where the *p*-value was >0.05, the result was deemed not statistically significant and the null hypothesis was retained, indicating that there were no statistically significant differences in the distribution of that size variable between the three groups. The asymptotic two-sided, significance was recorded, and the Bonferroni correction was applied to reduce the risk of false statistical significance when running multiple tests simultaneously (Abdi 2007; Bonferroni 1936; Haynes 2013). Post-hoc pairwise comparisons isolated differences between pairs of the three variables, to investigate differences between groups. The Friedman's two-way analysis of variance by ranks test was repeated on the same dataset (*n* = 8), after the application of a stature correction to control for differences in individual body size. Results of both analyses were recorded.

There were a number of individuals, from whom either a paired rib and anterior femur sample (*n* = 26), or a paired rib and posterior femur sample (*n* = 44), or a paired anterior and posterior femur sample (*n* = 10) was sourced. As such, these individuals were split into three groups for separate, related samples analysis. For each of these three sub-groups, a non-parametric (due to *n* <50 sample size) related-samples Wilcoxon signed rank test was performed. Data outputs recorded included the Wilcoxon signed-rank test statistic, the associated *p*-value and the mean for each bone within each size variable to compare mean differences between bones. Where the *p*-value was <0.05, the result was deemed statistically significant and the null hypothesis was rejected, indicating that there were statistically significant differences in the distribution of that size variable between the two bones being tested. Where the *p*-value was >0.05, the result was deemed not statistically significant and the null hypothesis was retained, indicating that there were no statistically significant differences in the distribution of that size variable between the two bones being tested. The asymptotic two-sided, significance was recorded, and the Bonferroni correction was applied to reduce the risk of false statistical significance when running multiple tests simultaneously (Abdi 2007; Bonferroni 1936; Haynes 2013). The related-samples Wilcoxon signed rank test was repeated on the same three datasets, after the

application of a stature correction to control for differences in individual body size. Results of both analyses were recorded.

$H0_b$: There is no difference in the osteon and Haversian canal shape variables, On.Circ, H.Circ, On.Rd, H.Rd, On.AsRa, H.AsRa and On.Sd, between the rib and the femur.

For this analysis, the dataset was separated into independent and dependent samples, for the shape variables to be tested appropriately. For the independent paired rib and posterior femur samples, non-parametric testing was used due to small sample size (rib n = 9, posterior femur n = 7). Thus, to test for differences in variable distribution across two bones, an independent-samples Mann-Whitney U test was performed. Data outputs recorded included the Mann-Whitney U score, the associated p-value and the mean rank for each bone within each variable to compare mean differences between bones. Where the p-value was <0.05, the result was deemed statistically significant and the null hypothesis was rejected, indicating that there were statistically significant differences in the distribution of that shape variable between the rib and posterior femur. Where the p-value was >0.05, the result was deemed not statistically significant and the null hypothesis was retained, indicating that there were no statistically significant differences in the distribution of that shape variable between the rib and posterior femur. The asymptotic two-sided, significance was recorded and the Bonferroni correction was applied to reduce the risk of false statistical significance when running multiple tests simultaneously (Abdi 2007; Bonferroni 1936; Haynes 2013). The independent samples Mann-Whitney U test was repeated on the same dataset (rib n = 9, posterior femur n = 7), after the application of a stature correction to control for differences in individual body size. Results of both analyses were recorded.

There was a total of n = 8 individuals, from whom a rib, anterior femur and posterior femur sample was sourced. To test for differences in osteon and Haversian canal shape metrics between the three bones, a related-samples Friedman's two-way analysis of variance by ranks test was performed. Data outputs recorded included the Friedman's test score, the associated p-value and the mean rank for each bone within each variable to compare mean differences between bones. Where the p-value was <0.05, the result was deemed statistically significant and the null hypothesis was rejected, indicating that there were statistically significant differences in the distribution of that variable between the three groups. Where the p-value was >0.05, the result was deemed not statistically significant and the null hypothesis was retained, indicating that there were no statistically significant differences in the distribution of that shape variable between the three groups. The asymptotic two-sided, significance was

recorded and the Bonferroni correction was applied to reduce the risk of false statistical significance when running multiple tests simultaneously (Abdi 2007; Bonferroni 1936; Haynes 2013). Post-hoc pairwise comparisons isolated differences between pairs of the three variables, to investigate differences between groups. The Friedman's two-way analysis of variance by ranks test was repeated on the same dataset (n = 8), after the application of a stature correction to control for differences in individual body size. Results of both analyses were recorded.

There were a number of individuals, from whom either a paired rib and anterior femur sample (n = 26), or a paired rib and posterior femur sample (n = 44), or a paired anterior and posterior femur sample (n = 10) was sourced. As such, individuals were split into three groups for separate, related samples analysis. For each of these three sub-groups, a non-parametric (due to n <50 sample size) related-samples Wilcoxon signed rank test was performed. Data outputs included the Wilcoxon signed-rank test statistic, associated p-value and the mean for each bone within each variable to compare mean differences in osteon and Haversian canal shape between bones. Where the p-value was <0.05, the result was deemed statistically significant and the null hypothesis was rejected, indicating that there were statistically significant differences in the distribution of that shape variable between the two bones being tested. Where the p-value was >0.05, the result was deemed not statistically significant and the null hypothesis was retained, indicating there were no statistically significant differences in the distribution of that shape variable between the two bones being tested. The asymptotic two-sided, significance was recorded, and the Bonferroni correction applied to reduce the risk of false statistical significance when running multiple tests simultaneously (Abdi 2007; Bonferroni 1936; Haynes 2013). The related-samples Wilcoxon signed rank test was repeated after applying a stature correction to control for individual body size differences. Results of both analyses were recorded.

$H0_c$: There is no difference in the osteon and Haversian canal growth rates, (1) between osteons and Haversian canals, and (2) between the rib and the femur.

This part of research question 4 investigates differential growth rates in osteons and Haversian canals, using reduced major axis regression (RMA). RMA is frequently used in biology and zoology research, investigating differential rates of growth of biological structures within an organism (Shingleton 2010; Figure 5.6). Here, it is performed to investigate differential rates of growth between osteons and Haversian canals. The nature of osteons, which encase the central Haversian canal, dictates that osteons will be of a larger dimension than Haversian

canals which nest inside them (Robling and Stout 1999). However, there is much we do not understand about rates of growth differences between the osteon and Haversian canal.

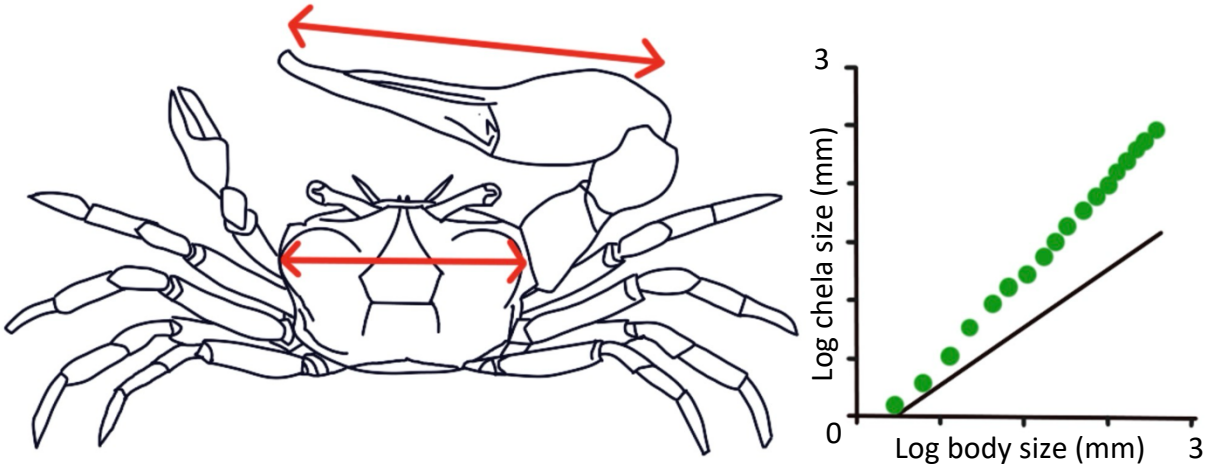

Figure 5.6: RMA investigation of the allometric relationship between the chela (oversized claw) and body size of the male fiddler crab.

Image: Adapted from Shingleton 2010.

RMA is a suitable test of the relationship between osteon and Haversian canal growth for multiple reasons. Firstly, RMA does not require a defined mutual relationship between the two variables being tested. Secondly, RMA minimizes the sum of areas by using vertical and horizontal distances of data points around the line of best fit, while other regressions look at the sum of squares (Harper 2016). Thus, the RMA handles residual data with more robusticity than alternative regression tests. Thirdly, the RMA is symmetrical, which reduces deviations between the *x*- and *y*-values (Harper 2016). In combination, this makes the RMA a good fit for histological applications as it allows for errors in data, which is common in histomorphometry due to the measurement of such minute structures. Despite its suitability, to the best of my knowledge, an RMA has never been applied to investigate differential growth rates in osteons and Haversian canals.

The RMA was performed using Past4 (ver. 4.15), a statistics software with a paleontological focus, and was performed on osteon and Haversian canal area data from the rib, anterior femur and posterior femur separately, so as to compare differential growth rates between the rib and femur, and femoral regions. Sub-analyses were conducted in sample demographic groups, to see if the relationship between osteonal and Haversian growth rates differed between sample sub-sets, where sample size allowed (Table 5.5). Data were log10

transformed, using the equations logOn.Ar = Lg10(On.Ar) and logH.Ar = Lg10(H.Ar), to meet the RMA assumption of normality.

Table 5.5: RMA analyses and sub-analyses conducted.

Rib		**Anterior Femur**		**Posterior Femur**	
Sample	*n*	**Sample**	***n***	**Sample**	***n***
Entire Sample	71	Entire Sample	28	Entire Sample	53
Medieval	53	Medieval	10	Males	21
Modern	18	Modern	18	Females	19
Males	39	Males	22	Middle Adults	28
Females	25	Old Adults	20	Male Middle Adults	17
Middle Adults	28	Male Old Adults	16	Female Middle Adults	10
Old Adults	21	Modern Old Adults	18		
Male Middle Adults	17	Modern Males	15		
Male Old Adults	17				
Female Middle Adults	11				
Medieval Middle Adults	28				
Medieval Males	24				
Medieval Females	22				
Modern Old Adults	18				
Modern Males	15				

RMA outputs included the slope (*b*), the coefficient of determination (r^2), 95% confidence interval (CI) slope, intercept and *p*-value. Where $b > 1$, the structures undergo positive allometry, whereby the structure on the *x*-axis (osteon area) grows faster than the structure on the *y*-axis (Haversian canal area). Where $b < 1$, the structures undergo negative allometry, whereby the structure on the *y*-axis (Haversian canal area) grows faster than the structure on the *x*-axis (osteon area). Where $b = 1$, the structures undergo isometric growth, whereby both structures grow at the same rate. When isometry is at play, the growth ratio between the variables is constant, which means there is likely a dimensional or proportionate anatomical effect. However, allometry means that the growth between variables is not constant, which means that one structure will grow at a proportionally faster or slower rate than the other (Harper 2016; Shingleton 2010). Where the *b*-value was undiagnostic, the 95% CI slope was considered in addition to the *b*-value. Scattergrams were also created to visualize the strength of the relationships investigated. For each analysis, a determination of the relationship as either positive allometry, negative allometry or isometric growth was made, dependent on the *b*, 95% CI slope and the associated *p*-value.

5.7.5 Summary of Statistical Tests

Table 5.6: Summary of Statistical Analysis by Research Question and Hypothesis.

Research Question 1a) Age at Death	**Tests Applied**
$H0_a$: There is no monotonic relationship between absolute (known) age-at-death (AAD) and either observed variable; OPD, Fg.OPD, Ct.Po or Ct.Wi.	• Spearman's *Rho* (Mishra et al. 2019; Orcan 2020). • Spearman's *Rho* repeated with stature correction applied (Stock and Shaw 2007). • Bonferroni Correction applied to both tests (Bonferroni 1936).
$H0_b$: Each of the observed variables (OPD, Fg.OPD, Ct.Po or Ct.Wi) have a similar distribution across AAD categories.	• Mann Whitney *U* (Mishra et al. 2019; Orcan 2020). • Mann Whitney *U* repeated with stature correction applied (Stock and Shaw 2007). • Bonferroni Correction applied to both tests (Bonferroni 1936).
$H0_c$: Each of the observed variables (OPD, Fg.OPD, Ct.Po or Ct.Wi) have a similar distribution across the rib and the femur.	• No additional statistical tests performed. • Interpretation of above results to look at differences between bone and bone regions rather than with age-at-death.
Research Question 1b) Biological Sex	
$H0_a$: Each of the observed variables, OPD, Fg.OPD, On.Ar, H.Ar, Ct.Po and Ct.Wi have a similar distribution in males and females.	• Mann Whitney *U* (Mishra et al. 2019; Orcan 2020). • Mann Whitney *U* repeated with stature correction applied (Stock and Shaw 2007). • Bonferroni Correction applied to both tests (Bonferroni 1936).
$H0_b$: Each of the observed variables, OPD, Fg.OPD, On.Ar, H.Ar and Ct.Po have similar distributions between the rib and posterior femur.	• No additional statistical tests performed. • Interpretation of above results to look at differences between bone and bone regions rather than with biological sex.
Research Question 1c) Socioeconomic Status	
$H0_a$: Each of the observed variables, OPD, On.Circ, Po.Ar, Ct.Po, Ct.Wi and %Ct.Ar have a similar distribution across the three socioeconomic status (SES) groups; medieval lower class, medieval upper class and contemporary.	• Kruskal Wallis *H* (Mishra et al. 2019; Orcan 2020). • Kruskal Wallis *H* repeated with stature correction applied (Stock and Shaw 2007). • Bonferroni Correction applied to both tests (Bonferroni 1936).
$H0_b$: Each of the observed variables, OPD, On.Circ, Po.Ar and Ct.Po have similar distributions between the rib and femur.	• No additional statistical tests performed. Interpretation of above results to look at differences between bone and bone regions rather than with socioeconomic status.
Research Question 2: Medieval vs Contemporary	
$H0_a$: Each of the observed variables, OPD, On.Circ, On.Ar, %Ct.Ar, Po.Ar and Ct.Po have a similar distribution between medieval and contemporary era individuals.	• Mann Whitney *U* (Mishra et al. 2019; Orcan 2020). • Mann Whitney *U* repeated with stature correction applied (Stock and Shaw 2007).

	• Bonferroni Correction applied to both tests (Bonferroni 1936).
$H0_b$: Medieval and modern ribs and anterior femora cannot be separated using discriminant function analysis (DFA), based on the variables OPD, On.Circ, On.Ar, Po.Ar and Ct.Po.	• Log10-transformation applied. • Discriminant Function Analysis and Box's *M* (Elliott and Woodward 2007). • Discriminant Function Analysis and Box's *M* repeated with stature correction applied (Stock and Shaw 2007). • Bonferroni Correction applied to both tests (Bonferroni 1936).
$H0_c$: There is no evidence of a more sedentary lifestyle influencing modern individuals as compared to medieval individuals in either observed variable; OPD, On.Circ, On.Ar, %Ct.Ar, Po.Ar and Ct.Po.	• No additional statistical tests performed. Interpretation of above results to assess whether there is evidence of the contemporary individuals being more sedentary than the medieval individuals based on the literature and skeletal biology.
Research Question 3: Intra-Element Variation	
$H0_a$: There is no monotonic relationship in either observed variable; Ct.Ar, Ct.Wi, Ct.ArA, Po.Ar, On.Ar, H.Ar, Ct.Po, OPD, Fg.OPD and On.Circ between paired serial histological sections of the rib, approximately 1cm apart in the rib shaft.	• Spearman's *Rho* of paired serial sections (Mishra et al. 2019; Orcan 2020). • Bonferroni Correction applied (Bonferroni 1936).
$H0_b$: Each of the observed variables; Ct.Ar, Ct.Wi, Ct.ArA, Po.Ar, On.Ar, H.Ar, Ct.Po, OPD, Fg.OPD and On.Circ have a similar distribution between paired serial histological sections of the rib, approximately 1cm apart in the rib shaft.	• Wilcoxon Signed Rank test with slide 1 in one group, and slide 2 in the other (Mishra et al. 2019; Orcan 2020). • Bonferroni Correction applied (Bonferroni 1936).
Research Question 4: Femur vs Rib	
$H0_a$: Each of the observed osteon and Haversian canal size variables, On.Ar, H.Ar, On.Dm, H.Dm, On.Pm and H.Pm, have a similar distribution across the rib and the femur.	Independent Datasets: • Mann Whitney *U* (Mishra et al. 2019; Orcan 2020). • Mann Whitney *U* repeated with stature correction applied (Stock and Shaw 2007). • Bonferroni Correction applied to both tests (Bonferroni 1936). Related Samples Dataset (3 bones, same individual): • Friedman's two-way analysis of variance by ranks (Mishra et al. 2019; Orcan 2020). • Friedman's two-way analysis of variance by ranks repeated with stature correction applied (Stock and Shaw 2007). • Bonferroni Correction applied to both tests (Bonferroni 1936). Related Samples Datasets (2 bones, same individual):

	• Wilcoxon Signed Rank test (Mishra et al. 2019; Orcan 2020). • Wilcoxon Signed Rank test repeated with stature correction applied (Stock and Shaw 2007). • Bonferroni Correction applied (Bonferroni 1936).
$H0_b$: There is no difference in the osteon and Haversian canal shape variables, On.Circ, H.Circ, On.Rd, H.Rd, On.AsRa, H.AsRa and On.Sd, between the rib and the femur.	Independent Datasets: • Mann Whitney *U* (Mishra et al. 2019; Orcan 2020). • Mann Whitney *U* repeated with stature correction applied (Stock and Shaw 2007). • Bonferroni Correction applied to both tests (Bonferroni 1936). Related Samples Datasets (3 bones, same individual): • Friedman's two-way analysis of variance by ranks (Mishra et al. 2019; Orcan 2020). • Friedman's two-way analysis of variance by ranks repeated with stature correction applied (Stock and Shaw 2007). • Bonferroni Correction applied to both tests (Bonferroni 1936). Related Samples Datasets (2 bones, same individual): • Wilcoxon Signed Rank test (Mishra et al. 2019; Orcan 2020). • Wilcoxon Signed Rank test repeated with stature correction applied (Stock and Shaw 2007). • Bonferroni Correction applied (Bonferroni 1936).
$H0_c$: There is no difference in the osteon and Haversian canal growth rates, (1) between osteons and Haversian canals, and (2) between the rib and the femur.	• Log10-transformation applied. • Reduced Major Axis regression (Harper 2016; Shingleton 2010).

5.8 Research Question Results

Following dissemination of the hypothesis testing results, a brief summary for each research question, summarizing the key results and answers to each research question will be provided in the Results Chapter (Chapter 6). Deeper interpretation of results will occur in the Discussion Chapter (Chapter 7).

Chapter 6 Results

This chapter reports the results from the data collection and analysis conducted in this thesis. It begins by reporting the results of data normality tests and intra-observer error test. It then outlines each research question and their relevant null hypotheses for testing, followed by the descriptive and inferential statistical results. The results of each null hypothesis test are outlined, and each research question is answered based upon the results of the descriptive and inferential statistical results. Finally, a summary of all key research findings for each research question is outlined to prepare for the Discussion chapter.

6.1 Data normality and intra-observer error test results

A Kolmogorov-Smirnov (KS) test of normality was used where n individuals >50. Shapiro-Wilk (SW) test of normality was used where n individuals <50. p significance was defined as <0.05. The majority of variables (17/22) were not normally distributed, based on their KS and SW tests of normality results (Table 6.1).

Table 6.1: Results from data normality tests.

Variable	*n*. Slides/ Individuals	KS/SW *p*	Outcome	Action
Normally Distributed				
Ct.Wi (mm)	41 / 30	0.147	Normal distribution	Parametric tests where sample size permits
Po.Ar (mm^2)	200 / 81	0.095	Normal distribution	
%Ct.Ar (%)	44 / 31	0.281	Normal distribution	
H.Circ	200 / 81	0.200	Normal distribution	
H.Rd	200 / 81	0.200	Normal distribution	
Skewed Distribution				
AAD	50 / 17	**0.012***	Skewed distribution	Non-parametric tests and log transformation where relevant
Ct.Ar (mm^2)	200 / 81	**<0.001*****	Skewed distribution	
Ct.ArA (mm^2)	200 / 81	**<0.001*****	Skewed distribution	
Ct.Po (%)	200 / 81	**<0.001*****	Skewed distribution	
On.Ar (μm^2)	200 / 81	**<0.001*****	Skewed distribution	
H.Ar (μm^2)	200 / 81	**<0.001*****	Skewed distribution	
OPD (#/mm^2)	200 / 81	**<0.001*****	Skewed distribution	
Fg.OPD (#/mm^2)	200 / 81	**0.007***	Skewed distribution	
On.Circ	200 / 81	**<0.001*****	Skewed distribution	
On.Pm (μm)	200 / 81	**<0.001*****	Skewed distribution	
On.Dm (μm)	200 / 81	**<0.001*****	Skewed distribution	
On.AsRa	200 / 81	**0.011***	Skewed distribution	
On.Rd	200 / 81	**0.014***	Skewed distribution	
On.Sd	200 / 81	**<0.001*****	Skewed distribution	
H.Pm (μm)	200 / 81	**<0.001*****	Skewed distribution	
H.Dm (μm)	200 / 81	**<0.001*****	Skewed distribution	
H.AsRa	200 / 81	**0.028***	Skewed distribution	
H.Sd	200/81	**<0.001*****	Skewed distribution	

N.: number of slides; KS: Kolmogorov-Smirnov test; SW: Shapiro-Wilk test. Statistically significant results are shown in bold.

Those variables that were normally distributed included Ct.Wi (SW, p = 0.147), Po.Ar (KS, p = 0.095), %Ct.Ar (SW, p = 0.281), H.Circ (KS), p = 0.200) and H.Rd (KS, p = 0.200). All other variables were not normally distributed (KS or SW, p <0.05) and this required non-parametric testing or log transformation for inclusion in inferential univariate, bivariate, or multivariate statistical analysis.

Intra-observer error testing using paired correlations identified acceptable to excellent reliability for the majority of variables. However, measures of circularity, aspect ratio and solidity were poorly correlated (Table 6.2). When paired samples *t*-tests were run, the only instance where secondary observations were significantly different from the first observations, were in the number of fragmented osteons (Table 6.2).

Table 6.2: Intra-observer Error Testing: paired correlations and paired samples t-test results.

	1st and 2nd observation correlated				**Paired samples *t*-test**		
Variable	***n***	***r***	***r²***	***p***	***t*#/*Z*^**	**df**	***p***
On.Ar (μm²)	20	0.887	0.787	**<0.001*** **	-0.187^	-	0.852
H.Ar (μm²)	20	0.880	0.774	**<0.001*** **	-0.112^	-	0.911
N.On (#)	20	0.997	0.994	**<0.001*** **	0.000^	-	1.000
N.Fg.On (#)	20	0.977	0.955	**<0.001*** **	-2.066^	-	**0.039***
On.Circ	20	0.602	0.362	**0.005****	-0.037^	-	0.970
On.Pm (μm)	20	0.884	0.782	**<0.001*** **	-0.336^	-	0.737
On.Dm (μm)	20	0.886	0.785	**<0.001*** **	-0.523^	-	0.601
On.AsRa	20	0.695	0.483	**<0.001*** **	-0.149^	-	0.881
On.Rd	20	0.717	0.514	**<0.001*** **	-0.336^	-	0.737
On.Sd	20	0.021	0.000	0.931	-0.020^	-	0.984
H.Pm (μm)	20	0.863	0.745	**<0.001*** **	-0.896^	-	0.370
H.Circ	20	0.568	0.323	**0.009****	0.853#	19	0.404
H.Dm (μm)	20	0.860	0.740	**<0.001*** **	-1.269^	-	0.204
H.AsRa	20	0.740	0.548	**<0.001*** **	-0.485^	-	0.627
H.Rd	20	0.707	0.500	**<0.001*** **	0.213#	19	0.834
H.Sd	20	-0.232	-0.054	0.325	-1.700^	-	0.089

Intra-observer agreement was also evaluated using a Bland-Altman analysis to assess the consistency between the two sets of measurements. For most variables, the mean difference (bias) fell within the bands of the 95% confidence interval and no statistically significant differences between the first and second sets of collected data were identified. However, the number of fragmentary osteons was an exception, with the mean (-0.450) falling outside of the 95% confidence interval (-0.865 - -0.035) and a significant difference between the two datasets (p = 0.035) (Table 6.3; Figure 6.1). These results indicate a generally good agreement between the repeated measurements, with the observed bias and limits of agreement being acceptable, except for the number of fragmentary osteons.

Table 6.3: Intra-observer Error Testing: Bland-Altman plot data.

Variable	Descriptives *n*	Mean	Std. Dev.	95% Confidence Interval (lower, upper)	Single sample *t*-test *t*	df	*p*
On.ArDIF	20	-593.542	4699.645	-2793.043, 1605.960	-0.565	19	0.579
H.ArDIF	20	-51.367	495.928	-283.468, 180.735	-0.463	19	0.648
N.OnDIF	20	0.000	0.459	-0.215, 0.215	0.000	19	1.000
N.Fg.OnDIF	20	-0.450	0.887	-0.865, -0.035	-2.269	19	**0.035***
On.CircDIF	20	-0.001	0.023	-0.011, 0.010	-0.097	19	0.923
On.PmDIF	20	-11.923	61.912	-40.899, 17.053	-0.861	19	0.400
On.DmDIF	20	-5.113	24.117	-16.400, 6.175	-0.948	19	0.355
On.AsRaDIF	20	0.006	0.124	-0.052, 0.064	0.221	19	0.827
On.RdDIF	20	-0.001	0.059	-0.028, 0.027	-0.039	19	0.970
On.SdDIF	20	0.000	0.006	-0.003, 0.003	0.030	19	0.976
H.PmDIF	20	-5.650	21.456	-15.692, 4.392	-1.178	19	0.254
H.CircDIF	20	0.004	0.018	-0.005, 0.012	0.853	19	0.404
H.DmDIF	20	-2.287	7.681	-5.882, 1.308	-1.331	19	0.199
H.AsRaDIF	20	0.003	0.082	-0.036, 0.041	0.148	19	0.884
H.RdDIF	20	0.002	0.033	-0.014, 0.017	0.213	19	0.834
H.SdDIF	20	-0.001	0.004	-0.003, 0.001	-0.980	19	0.340

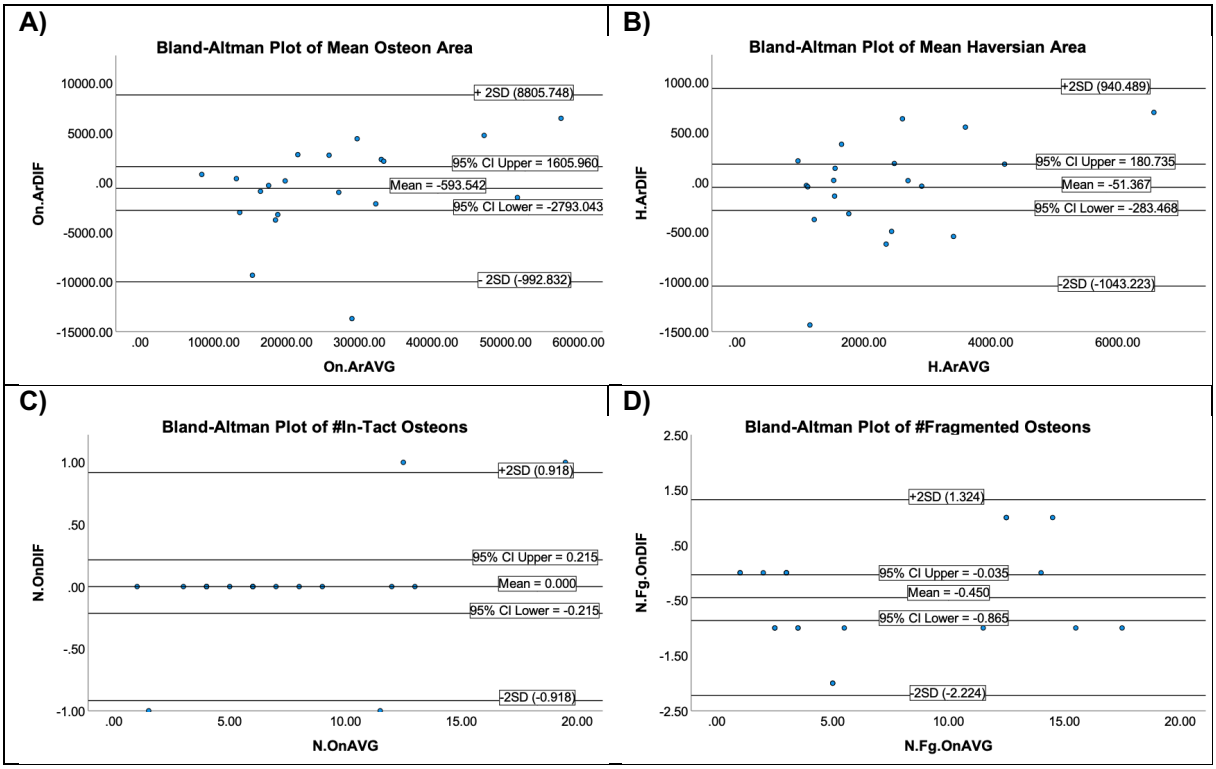

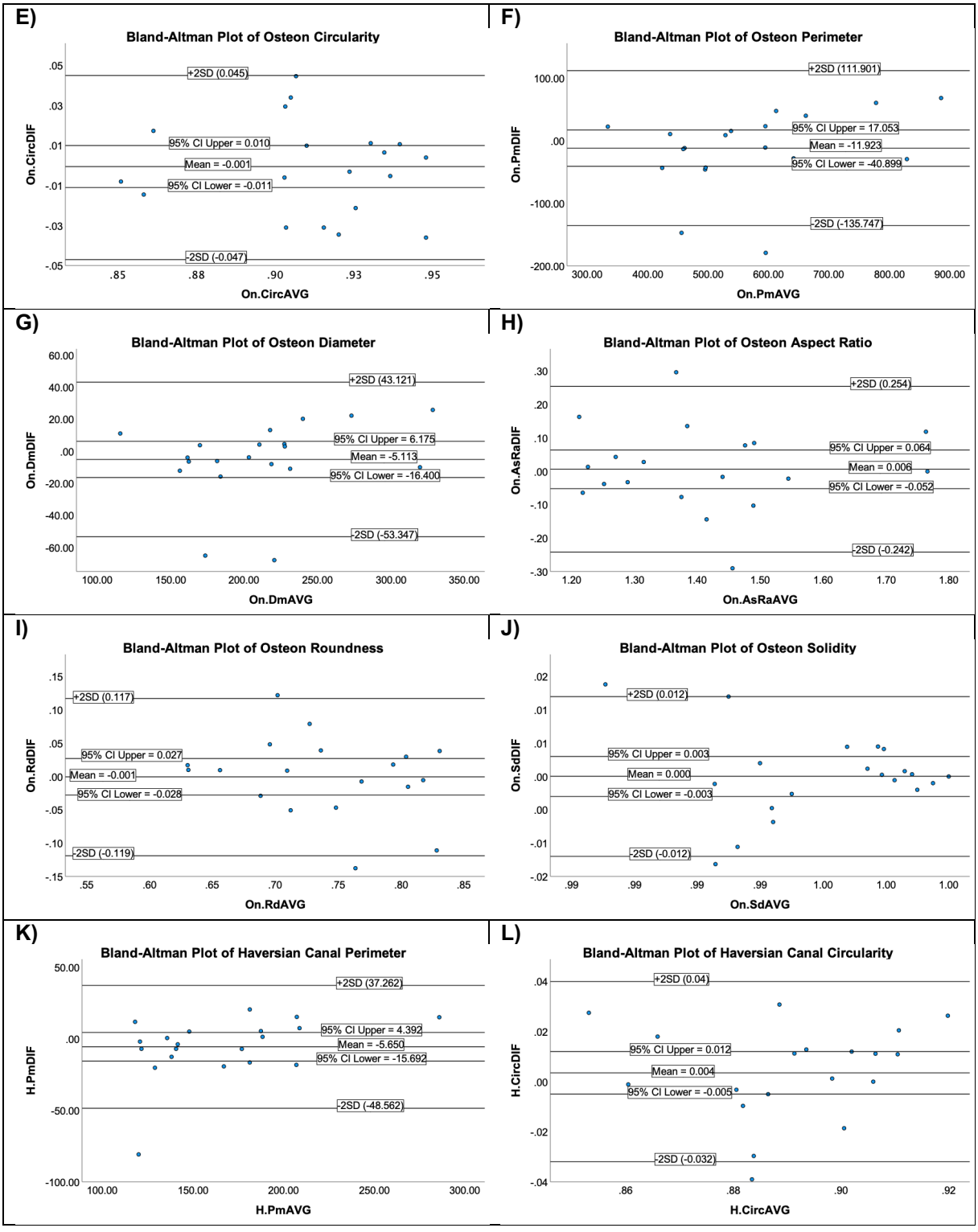
E)
Bland-Altman Plot of Osteon Circularity
On.CircDIF
On.CircAVG
+2SD (0.045)
95% CI Upper = 0.010
Mean = -0.001
95% CI Lower = -0.011
-2SD (-0.047)
F)
Bland-Altman Plot of Osteon Perimeter
On.PmDIF
On.PmAVG
+2SD (111.901)
95% CI Upper = 17.053
Mean = -11.923
95% CI Lower = -40.899
-2SD (-135.747)
G)
Bland-Altman Plot of Osteon Diameter
On.DmDIF
On.DmAVG
+2SD (43.121)
95% CI Upper = 6.175
Mean = -5.113
95% CI Lower = -16.400
-2SD (-53.347)
H)
Bland-Altman Plot of Osteon Aspect Ratio
On.AsRaDIF
On.AsRaAVG
+2SD (0.254)
95% CI Upper = 0.064
Mean = 0.006
95% CI Lower = -0.052
-2SD (-0.242)
I)
Bland-Altman Plot of Osteon Roundness
On.RdDIF
On.RdAVG
+2SD (0.117)
95% CI Upper = 0.027
Mean = -0.001
95% CI Lower = -0.028
-2SD (-0.119)
J)
Bland-Altman Plot of Osteon Solidity
On.SdDIF
On.SdAVG
+2SD (0.012)
95% CI Upper = 0.003
Mean = 0.000
95% CI Lower = -0.003
-2SD (-0.012)
K)
Bland-Altman Plot of Haversian Canal Perimeter
H.PmDIF
H.PmAVG
+2SD (37.262)
95% CI Upper = 4.392
Mean = -5.650
95% CI Lower = -15.692
-2SD (-48.562)
L)
Bland-Altman Plot of Haversian Canal Circularity
H.CircDIF
H.CircAVG
+2SD (0.04)
95% CI Upper = 0.012
Mean = 0.004
95% CI Lower = -0.005
-2SD (-0.032)

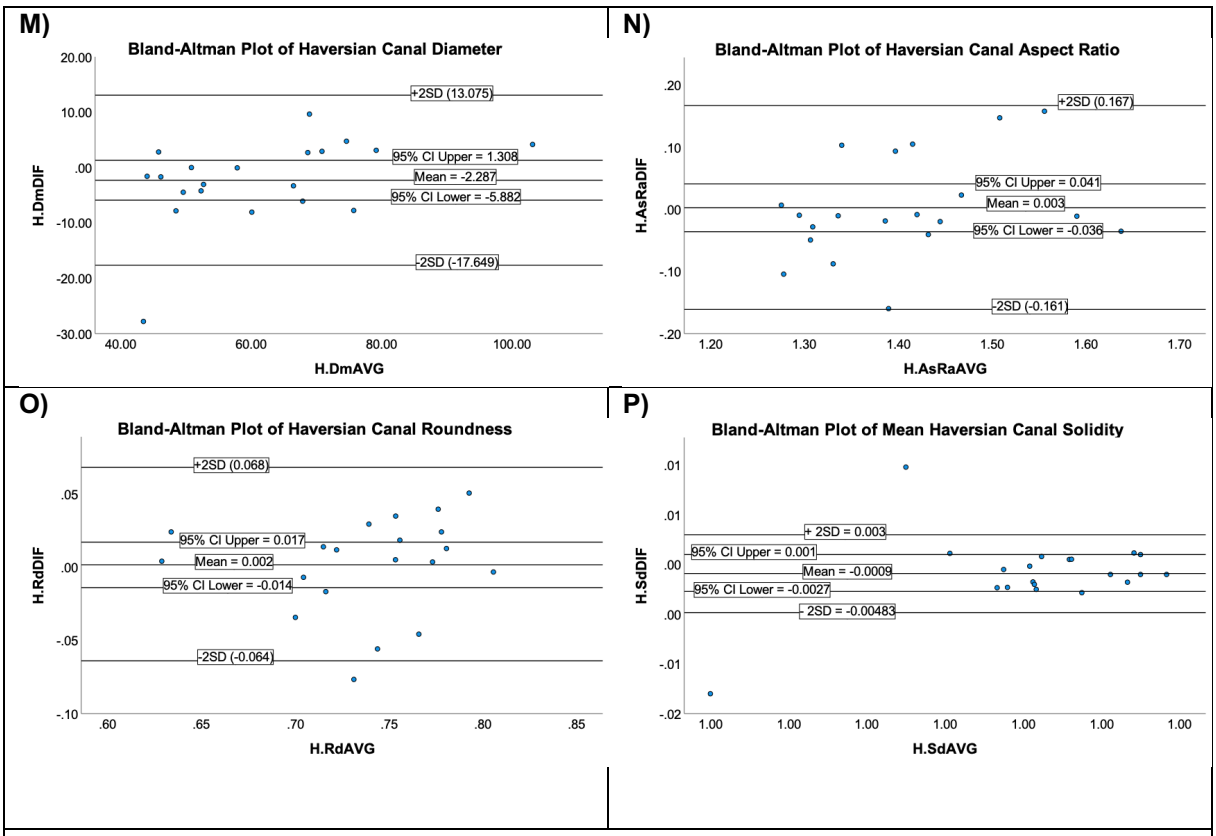

Figure 6.1: Bland-Altman Plots for intra-observer error.

A) Mean Osteon Area. **B)** Mean Haversian Canal Area. **C)** Number of In-tact Osteons. **D)** Number of Fragmented Osteons. **E)** Osteon Circularity. **F)** Osteon Perimeter. **G)** Osteon Diameter. **H)** Osteon Aspect Ratio. **I)** Osteon Roundness. **J)** Osteon Solidity. **K)** Haversian Canal Perimeter. **L)** Haversian Canal Circularity. **M)** Haversian Canal Diameter. **N)** Haversian Canal Aspect Ratio. **O)** Haversian Canal Roundness. **P)** Haversian Canal Solidity.

6.2 Descriptive Summary of all Observed Variables

Table 6.4: Sample summary.

Bone	*n*. Individuals	% of Individuals	*n*. Slides	% of Slides
Rib	71	43.8	119	59.5
Anterior Femur	28	17.3	28	14.0
Posterior Femur	63	38.9	53	26.5
Total	**162***	**100.0**	**200**	**100.0**

* The sample comprised a total of 81 different individuals; with 2 serial rib slides from 48 individuals, paired rib and femur slides from 61 individuals, and paired anterior and posterior femur slides from 9 individuals.

A summary of the number of rib histological slides versus femur histological slides, delineated further by the anterior and posterior aspects of the femur, is shown in Table 6.4. Descriptive statistics for each variable observed are shown in Table 6.5.

Table 6.5: Descriptive statistics for all variables observed.

Variable	*n*. Slides/ Individuals	Min.	Max.	Mean	St.D.
AAD	50 / 17	59	93	76.12	9.030
Ct.Ar (mm^2)	200 / 81	6.194	44.946	14.187	7.984
Ct.Wi (mm)	41 / 30	0.316	1.662	0.758	0.299
Ct.ArA (mm^2)	200 / 81	4.430	43.776	13.094	8.344
Po.Ar (mm^2)	200 / 81	0.000	0.091	0.027	0.014
Ct.Po (%)	200 / 81	0.000	43.839	11.508	11.244
On.Ar (μm^2)	200 / 81	11,270.171	221,634.582	29,076.472	19,118.101
H.Ar (μm^2)	200 / 81	860.955	12,541.433	2,609.523	1,886.271
OPD (#/mm^2)	200 / 81	3.930	22.693	11.602	3.621
Fg.OPD (#/mm^2)	200 / 81	0.970	10.776	4.676	2.113
On.Circ	200 / 81	0.818	0.941	0.910	0.020
%Ct.Ar (%)	44 / 31	15.191	63.257	36.858	11.822
On.Pm (μm)	200 / 81	381.71	954.46	584.284	111.128
On.Dm (μm)	200 / 81	137.03	348.65	212.497	39.717
On.AsRa	200 / 81	1.030	1.598	1.380	0.072
On.Rd	200 / 81	0.667	0.971	0.749	0.034
On.Sd	200 / 81	0.950	1.066	0.993	0.010
H.Pm (μm)	200 / 81	104.74	333.64	165.144	42.467
H.Circ	200 / 81	0.842	0.932	0.891	0.017
H.Dm (μm)	200 / 81	39.27	125.13	61.254	16.248
H.AsRa	200 / 81	1.089	1.745	1.407	0.095
H.Rd	200 / 81	0.628	0.918	0.745	0.037
H.Sd	200/81	0.989	1.000	0.999	0.002

Average age-at-death (AAD) was 76.12 years. In terms of bone structural measures, cortical area (Ct.Ar) was on average 14.187mm^2, cortical width (Ct.Wi) was on average 0.758mm, absolute cortical area (Ct.ArA) was on average 13.094mm^2 and percent cortical area (%Ct.Ar) was on average 36.858%.

When considering the histological measures of porosity, mean porosity area (Po.Ar) was 0.027mm^2, and cortical porosity (Ct.Po) had an average of 11.508%. Of the osteon variables mean osteon area (On.Ar) was on average 29,076.472μm^2, osteon population density (OPD) was on average 11.602/mm^2, fragmented osteon population density (Fg.OPD) averaged 4.676/mm^2, mean osteon circularity (On.Circ) averaged 0.910, mean osteon perimeter (On.Pm) averaged 584.284µm, mean osteon diameter (On.Dm) averaged 212.497µm, mean osteon aspect ratio (On.AsRa) averaged 1.380, mean osteon roundness (On.Rd) averaged 0.749, and mean osteon solidity (On.Sd) averaged 0.993.

Of the Haversian canal measurements mean Haversian canal area (H.Ar) averaged 2,609.523μm^2, mean Haversian canal perimeter (H.Pm) averaged 165.144μm, mean Haversian canal circularity (H.Circ) averaged 0.891, mean Haversian canal diameter (H.Dm) averaged 61.254μm, mean Haversian canal aspect ratio (H.AsRa) averaged 1.407, mean Haversian canal roundness (H.Rd) averaged 0.745 and mean Haversian canal solidity (H.Sd) averaged 0.999.

6.3 Research Question 1

Does human rib and femur histology vary with age-at-death, sex and systemic health and physical activity (as inferred by socioeconomic status) in samples of English ancestry?

6.3.1 Descriptive Trends: Age-At-Death

There are three key steps, and thus three hypotheses to test in order to address this research question. The first tests if there is a relationship between chronological AAD and the four key variables; OPD, Fg.OPD, Ct.Po and Ct.Wi in both the rib and femur separately. The second tests if there are differences between the AAD categories for each of the targeted variables. The final hypothesis tests if there is a difference in how these effects, if identified in $H0_a$ and/or $H0_b$, manifest differently between the rib and femur. Therefore, the null hypotheses for this part of research question 1 are as follows:

$H0_a$: There is no monotonic relationship between absolute (chronological) age-at-death (AAD) and either observed variable; OPD, Fg.OPD, Ct.Po or Ct.Wi.

$H0_b$: Each of the observed variables (OPD, Fg.OPD, Ct.Po or Ct.Wi) have a similar distribution across AAD categories.

$H0_c$: Each of the observed variables (OPD, Fg.OPD, Ct.Po or Ct.Wi) have a similar distribution across the rib and the femur.

Table 6.6: Descriptive statistics for all variables observed in AAD analysis.

Variable	Bone/Region	AAD Category	*n*.	Min.	Max.	Mean	St.D.
AAD	Rib	OA	17	59	93	76.41	9.368
	Anterior Femur	OA	17	59	93	76.41	9.368
Stature (cm)	Rib	Adol	1	158.88	158.88	158.88	-
		YA	3	167.72	183.86	176.457	8.152
		MA	26	147.22	181.12	167.115	9.100
		OA	17	152.00	185.00	169.996	8.562
	Anterior Femur	YA	1	177.79	177.79	177.79	-
		MA	3	177.08	180.65	179.063	1.818
		OA	16	152.00	185.00	169.375	8.438
	Posterior Femur	YA	2	167.72	177.79	172.755	7.121
		MA	26	147.22	181.12	167.115	9.100
		OA	3	164.26	179.93	174.310	8.724
Ct.Wi (mm)	Rib	Adol	1	1.057	1.057	1.057	-
		YA	2	1.021	1.069	1.045	0.034
		MA	12	0.559	1.662	0.907	0.278
		OA	9	0.316	0.753	0.492	0.173
Ct.Po (%)	Rib	Adol	1	4.150	4.150	4.150	-
		YA	3	0.869	8.046	3.581	3.897
		MA	28	0.369	10.480	3.557	2.379
		OA	20	0.272	8.270	2.897	2.501
	Anterior Femur	YA	1	16.519	16.519	16.519	-
		MA	4	17.875	25.165	20.782	3.492
		OA	19	12.348	42.051	28.755	7.988
	Posterior Femur	YA	2	13.210	18.966	16.088	4.070
		MA	28	8.747	28.867	21.517	5.100
		OA	3	19.587	32.264	25.714	6.349
OPD (#/mm^2)	Rib	Adol	1	9.062	9.062	9.062	-
		YA	3	7.000	9.660	8.450	1.346
		MA	28	4.056	12.908	8.808	1.975
		OA	20	6.398	19.611	13.646	3.759
	Anterior Femur	YA	1	12.677	12.677	12.677	-
		MA	4	8.367	14.579	11.695	2.836
		OA	19	9.762	22.693	15.493	3.016
	Posterior Femur	YA	2	10.142	11.663	10.903	1.076
		MA	28	6.212	19.777	12.469	3.426
		OA	3	8.494	14.579	11.114	3.129
Fg.OPD (#/mm^2)	Rib	Adol	1	3.927	3.927	3.927	-
		YA	3	1.367	2.723	2.101	0.685
		MA	28	0.970	5.535	3.242	1.425
		OA	20	1.935	8.089	5.065	1.566
	Anterior Femur	YA	1	6.339	6.339	6.339	-
		MA	4	1.775	7.226	4.627	2.578
		OA	19	5.705	10.776	7.600	1.566
	Posterior Femur	YA	2	3.550	4.944	4.247	0.986
		MA	28	2.028	9.381	5.560	2.014
		OA	3	1.395	9.001	4.986	3.821

Variables observed to assess changes in femur and rib histology with AAD included OPD, Fg.OPD, Ct.Wi and Ct.Po. Descriptive results for the anterior femur identified an increase in OPD with AAD category (middle-adult (MA; 35-49 years), m = 11.695/mm^2; old-adult (OA; 50+

years), *m* = 15.493/mm^2), while in the posterior femur OPD increased in MA (*m* = 12.469/mm^2) individuals, and then decreased in OA (*m* = 11.114/mm^2) individuals, and in the rib, OPD was similar in young-adult (YA; 20-34 years), *m* = 8.450/mm^2 and MAs (*m* = 8.808/mm^2), but higher in OAs (*m* = 13.646/mm^2) (Table 6.6). Similar trends were observed in Fg.OPD in the anterior femur (MA *m* = 4.627/mm^2; OA *m* = 7.600/mm^2), posterior femur (YA *m* = 4.247/mm^2; MA *m* = 5.560/mm^2; OA *m* = 4.986/mm^2) and rib (YA *m* = 2.101/mm^2; MA *m* = 3.242/mm^2; OA *m* = 5.065/mm^2) (Table 6.6). Ct.Po appears to increase with AAD category in both the anterior femur (MA *m* = 20.782%; OA *m* = 28.755%) and posterior femur (YA *m* = 16.088%; MA *m* = 21.517%; OA *m* = 25.714%), but remains fairly stable, and with lower values than observed in the femur, throughout age in the rib (YA *m* = 3.581%; MA *m* = 3.557%; OA *m* = 2.897%) (Table 6.6). There was a marked decrease in rib Ct.Wi with AAD category (YA *m* = 1.045mm; MA *m* = 0.907mm; OA *m* = 0.492mm) (Table 6.6).

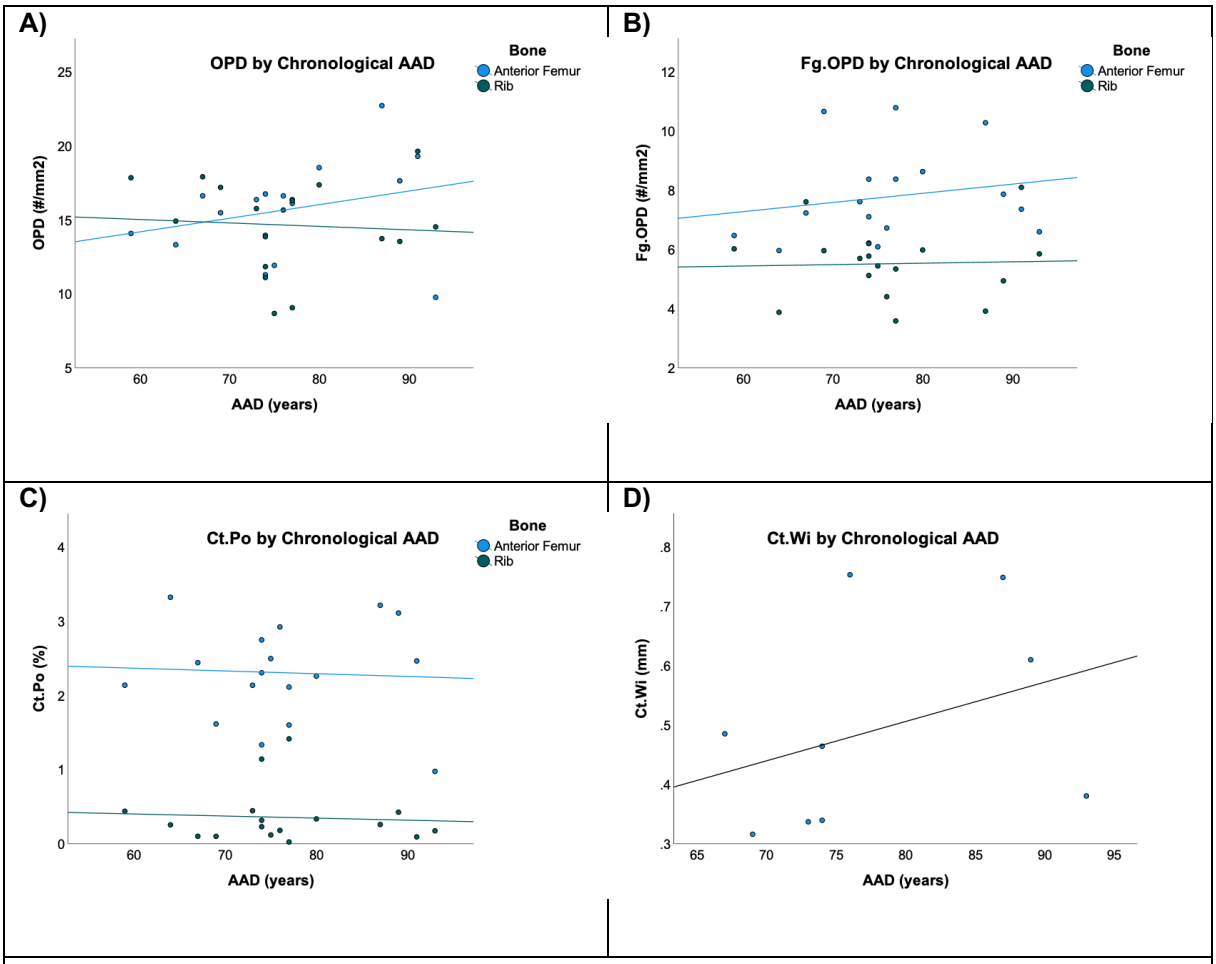

Figure 6.2: Scatterplots of key age-at-death variables.

A) Osteon Population Density (OPD) by Chronological Age-At-Death (AAD). **B)** Fragmented OPD (Fg.OPD) by Chronological AAD. **C)** Cortical Porosity (Ct.Po) by Chronological AAD. **D)** Cortical Width by Chronological AAD.

Scatterplots were created of known chronological AAD with OPD, Fg.OPD and Ct.Po for the anterior femur and rib, as well as Ct.Wi of the rib, to identify trends in descriptive values (Figure 6.2). Broad trends indicated that OPD increased with chronological AAD in the anterior femur but decreased with chronological AAD in the rib. Additionally, Fg.OPD appears to increase with chronological AAD in the anterior femur but decrease with chronological AAD in the rib. However, Ct.Po appears to decrease with chronological AAD in both the anterior femur and the rib, but these relationships appear weak as the trendlines are close to horizontal. Ct.Wi seems to increase with chronological AAD in the rib (Figure 6.2).

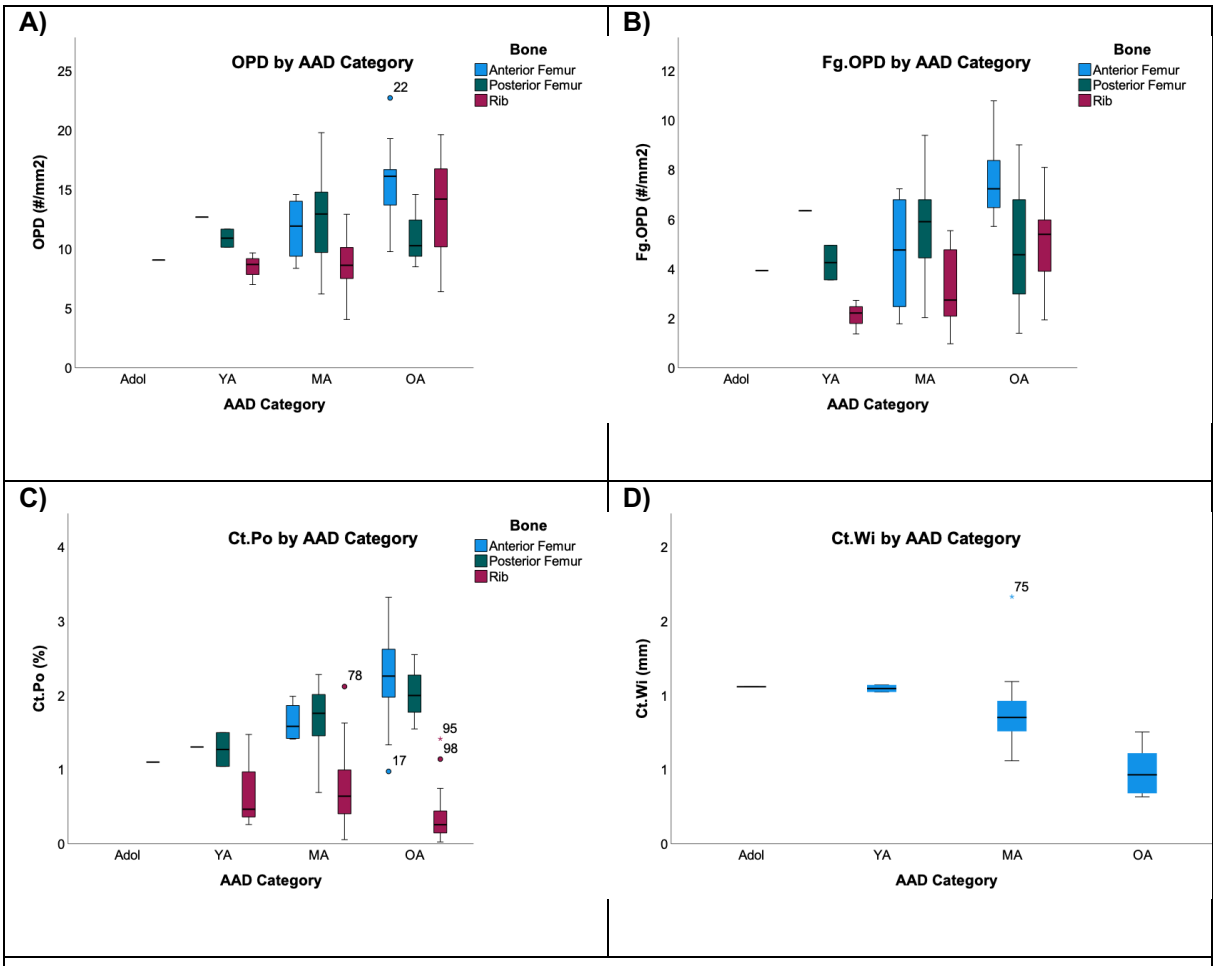

Figure 6.3: Boxplots of key age-at-death variables.

A) Osteon Population Density (OPD) by Age-At-Death (AAD) Category. **B)** Fragmented OPD (Fg.OPD) by AAD Category. **C)** Cortical Porosity (Ct.Po) by AAD Category. **D)** Cortical Width (Ct.Wi) by AAD Category.

Variables observed to assess changes in femur and rib histology with AAD included OPD, Fg.OPD, Ct.Wi and Ct.Po. Boxplots suggest an increase in OPD with AAD category in the

anterior femur and rib, but OPD appeared to peak in middle-aged adults (MA; 35-49 years) at the posterior femur (Figure 6.3A). Similar trends were observed in Fg.OPD (Figure 6.3B). Ct.Po appears to increase with AAD category in both the anterior femur and posterior femur but in the rib remains fairly stable throughout young adulthood (YA; 20-34 years) and MA, before dropping off in older adulthood (OA; 50+ years) (Figure 6.3C). Additionally, the rib appears to have lower values than both femoral regions (Figure 6.3C). There was a marked decrease in rib Ct.Wi with AAD category (Figure 6.3D).

6.3.2 Inferential Statistics: Age-At-Death

Spearman's *Rho* correlations rendered no statistically significant results in either the rib or anterior femur, between OPD, Fg.OPD, Ct.Po or Ct.Wi and known chronological AAD (Table 6.7). There were no known AAD values for individuals from whom the posterior femur samples were derived so correlations could not be performed for this bone region.

Table 6.7: Age-At-Death Correlations (Spearman's Rho).

Variable	Bone	*n*. Individuals	Spearman's *Rho*	*p*-value
OPD	Rib	17	-0.177	0.371
	Anterior Femur	17	0.360	0.156
Fg.OPD	Rib	17	-0.128	0.625
	Anterior Femur	17	0.314	0.219
Ct.Po	Rib	17	-0.133	0.611
	Anterior Femur	17	-0.015	0.955
Ct.Wi	Rib	9	0.452	0.222

* Significance values have been adjusted by the Bonferroni Correction for multiple tests.

Once OPD, Fg.OPD, Ct.Po and Ct.Wi values were corrected by stature (eg. (OPD/Stature) x 100; see Chapter 5: Methods), Spearman's *Rho* results did not render any statistically significant relationships between known chronological AAD and either variable (Table 6.8).

Table 6.8: Age-At-Death Correlations (Spearman's Rho): Corrected by stature.

Variable	Bone	*n*. Individuals	Spearman's *Rho*	*p*-value
OPD	Rib	14	-0.053	0.858
	Anterior Femur	14	0.293	0.309
Fg.OPD	Rib	14	-0.046	0.875
	Anterior Femur	14	0.286	0.321
Ct.Po	Rib	14	-0.152	0.604
	Anterior Femur	14	0.015	0.958
Ct.Wi	Rib	9	0.306	0.504

* Significance values have been adjusted by the Bonferroni Correction for multiple tests.

Results of the Kruskal-Wallis *H* test indicate that OPD (*H* = 18.347, df = 3, *p* <0.001), Fg.OPD (*H* = 16.767, df = 3, *p* <0.001) and Ct.Wi (*H* = 14.511, df = 3, *p* = 0.002) are statistically significantly different between AAD categories in the rib. While Ct.Po (*H* = 6.031, df = 2, *p* = 0.049) was statistically significantly different between AAD categories in the anterior femur (Table 6.9). However, only one adolescent was included in the entire sample, and only the rib was observed for this individual, which reduces the ability to observe patterns across the full spectrum of AAD Categories, and between bones.

Table 6.9: Age-At-Death Categories (Kruskal-Wallis).

Variable	Bone	AAD Category	*n*. Individuals	Mean Rank	Kruskal-Wallis *H*	df	*p*-value
OPD	Rib	Adol	1	24.00	18.347	3	**<0.001****
		YA	3	18.00			
		MA	28	19.39			
		OA	20	37.85			
	Anterior Femur	Adol	-	-	4.864	2	0.088
		YA	1	6.00			
		MA	4	6.38			
		OA	19	14.13			
	Posterior Femur	Adol	-	-	1.009	2	0.604
		YA	2	13.00			
		MA	28	17.71			
		OA	3	13.00			
Fg.OPD	Rib	Adol	1	29.00	16.767	3	**<0.001****
		YA	3	11.00			
		MA	28	20.64			
		OA	20	36.90			
	Anterior Femur	Adol	-	-	4.580	2	0.101
		YA	1	7.50			
		MA	4	6.25			
		OA	19	14.08			
	Posterior Femur	Adol	-	-	1.463	2	0.481
		YA	2	10.00			
		MA	28	17.79			
		OA	3	14.33			
Ct.Po	Rib	Adol	1	38.00	2.453	3	0.484
		YA	3	11.00			
		MA	28	20.64			
		OA	20	36.90			
	Anterior Femur	Adol	-	-	6.031	2	**0.049***
		YA	1	2.00			
		MA	4	6.75			
		OA	19	14.26			
	Posterior Femur	Adol	-	-	3.749	2	0.153
		YA	2	6.00			
		MA	28	17.14			
		OA	3	23.00			
Ct.Wi	Rib	Adol	1	21.00	14.511	3	**0.002****
		YA	2	21.00			
		MA	12	15.42			
		OA	9	5.78			

* Significance values have been adjusted by the Bonferroni Correction for multiple tests.

Results of the post-hoc pairwise comparisons identified which AAD Category pairings were statistically significantly different from each other. For OPD in the rib, OA individuals had statistically significantly higher values than MA individuals (-18.457, p <0.001). There was no statistically significant difference between any other AAD categories in the rib. For Fg.OPD in the rib, OA individuals had statistically significantly higher values than MA (-16.257, p = 0.001) and YA (-25.900, p = 0.035) individuals. For Ct.Wi in the rib, OA individuals had statistically significantly lower values than MA individuals (9.639, p = 0.0012). There was no statistically significant difference between any AAD category for Ct.Po in the Anterior Femur.

Table 6.10: Age-At-Death: Post-hoc pairwise comparisons.

Variable	Bone	AAD Category 1 – AAD Category 2	Test Statistic	*p*-value*
OPD	Rib	MA – YA	-1.393	1.000
		MA – Adol	4.607	1.000
		MA – OA	-18.457	**<0.001****
		YA – Adol	6.000	1.000
		YA – OA	-19.850	0.206
		Adol – OA	-13.850	1.000
Fg.OPD	Rib	MA – YA	-9.643	1.000
		MA – Adol	8.357	1.000
		MA – OA	-16.257	**0.001****
		YA – Adol	18.000	1.000
		YA – OA	-25.900	**0.035****
		Adol – OA	-7.900	1.000
Ct.Po	Anterior Femur	MA – YA	-4.750	1.000
		MA – OA	-7.513	0.160
		YA – OA	-12.263	0.273
Ct.Wi	Rib	MA – YA	5.583	1.000
		MA – Adol	5.583	1.000
		MA – OA	9.639	**0.012***
		YA – Adol	0.000	1.000
		YA – OA	15.222	**0.035***
		Adol – OA	15.222	0.247

* Significance values have been adjusted by the Bonferroni Correction for multiple tests.

Once OPD, Fg.OPD, Ct.Po and Ct.Wi were corrected by stature to account for individual variation in body size, results of the Kruskal-Wallis H test changed. OPD (H = 13.022, df = 3, p = 0.005), Fg.OPD (H = 11.790, df = 3, p = 0.008) and Ct.Wi (H = 12.863, df = 3, p = 0.005) were statistically significantly different between AAD categories in the rib (Table 6.11. However no statistically significant differences in any variable between AAD categories were identified in either femoral aspect (Table 6.11).

Table 6.11: Age-At-Death Categories (Kruskal-Wallis): Corrected by stature.							
Variable	**Bone**	**AAD Category**	***n.* Individuals**	**Mean Rank**	**Kruskal-Wallis *H***	**df**	***p*-value**
OPD	Rib	Adol	1	28.00	13.022	3	**0.005****
		YA	3	16.33			
		MA	26	18.60			
		OA	17	33.38			
	Anterior Femur	YA	1	6.00	4.783	2	0.092
		MA	3	4.33			
		OA	16	11.94			
	Posterior Femur	YA	2	11.00	1.194	2	0.550
		MA	26	16.77			
		OA	3	12.67			
Fg.OPD	Rib	Adol	1	28.00	11.790	3	**0.008***
		YA	3	9.83			
		MA	26	20.02			
		OA	17	32.35			
	Anterior Femur	YA	1	6.00	4.783	2	0.092
		MA	3	4.33			
		OA	16	11.94			
	Posterior Femur	YA	2	9.50	1.485	2	0.476
		MA	26	16.81			
		OA	3	13.33			
Ct.Po	Rib	Adol	1	35.00	3.953	3	0.267
		YA	3	21.00			
		MA	26	26.96			
		OA	17	19.35			
	Anterior Femur	YA	1	2.00	4.038	2	0.133
		MA	3	6.67			
		OA	16	11.75			
	Posterior Femur	YA	2	6.50	3.220	2	0.200
		MA	26	16.12			
		OA	3	21.33			
Ct.Wi	Rib	Adol	1	21.00	12.863	3	**0.005****
		YA	2	19.25			
		MA	12	13.21			
		OA	7	5.00			

* Significance values have been adjusted by the Bonferroni Correction for multiple tests.

Statistically significant differences between AAD categories were identified in post-hoc Kruskal-Wallis pairwise testing, once corrected by individual stature. The OA category had significantly higher OPD than the MA AAD category (-14.786, p = 0.003). Fg.OPD was significantly higher in the OA than MA (-12.334, p = 0.024) AAD categories. In Ct.Wi, the OA category was statistically significantly lower than both the MA (8.208, p = 0.047) and YA (14.250, p = 0.037) AAD categories (Table 6.12).

Table 6.12: Age-At-Death: Corrected by Stature: Post-hoc Kruskal-Wallis pairwise.				
Variable	**Bone**	**AAD Category 1 – AAD Category 2**	**Test Statistic**	***p*-value***
OPD	Rib	MA – YA	-2.263	1.000
		MA – Adol	9.404	1.000
		MA – OA	-14.786	**0.003****
		YA - Adol	11.667	1.000
		YA – OA	-17.049	0.282
		Adol – OA	-5.382	1.000
Fg.OPD	Rib	MA – YA	-10.186	1.000
		MA – Adol	7.981	1.000
		MA – OA	-12.334	**0.024***
		YA - Adol	18.167	1.000
		YA – OA	-22.520	0.052
		Adol – OA	-4.353	1.000
Ct.Wi	Rib	MA – YA	6.042	1.000
		MA – Adol	7.792	1.000
		MA – OA	8.208	**0.047***
		YA - Adol	1.750	1.000
		YA – OA	14.250	**0.037***
		Adol – OA	16.000	0.126

* Significance values have been adjusted by the Bonferroni Correction for multiple tests.

6.3.3 Hypotheses Results: Age-At-Death

$H0_a$: There is no monotonic relationship between absolute (chronological) age-at-death (AAD) and either observed variable; OPD, Fg.OPD, Ct.Po or Ct.Wi.

Scatterplots marking chronological age-at-death and each variable were created, but lines of best fit demonstrated that all relationships were relatively weak, many being almost horizontal (Figure 6.2A-D). This was further reinforced when Spearman's *Rho* correlations were run and no statistically significant relationships were identified between any variable and chronological AAD, in either bone (Table 6.7). These results were replicated when measures were controlled by stature to account for differences in stature, as a proxy for individual body size (Table 6.8). However, testing was limited as chronological AAD was only known for the 17 contemporary individuals, and so further tests were run to identify any significant differences between AAD categories: Adol, YA, MA and OA.

These results suggest that there is no statistically significant relationship between known AAD and either variable, in either the rib or femur. This upholds the null hypothesis.

$H0_b$: Each of the observed variables (OPD, Fg.OPD, Ct.Po or Ct.Wi) have a similar distribution across AAD categories.

Initial descriptive statistics presented in boxplots were suggestive of trends between bones, with OPD and Fg.OPD increasing from MA to OA in the anterior femur and the rib but decreasing from MA to OA in the posterior femur (Figure 6.3A-B). Additionally, Ct.Po increased from MA to OA in the anterior femur, and from YA to MA to OA in the posterior femur, but values were much lower in the rib, increasing from YA to MA and decreasing steeply in OA individuals (Figure 6.3C).

Inferential statistics demonstrated that OA individuals had statistically significantly higher OPD and Fg.OPD than MA individuals in the rib. However, OPD and Fg.OPD was not statistically significantly different between other AAD categories in the rib (Table 6.10; 6.12). Ct.Wi was statistically significantly lower in OA individuals than both MA and YA individuals, with YA individuals having the highest Ct.Wi of these three AAD categories in the rib (Table 6.10; 6.12). There were no statistically significant differences between either AAD category, for either variable, in the anterior or posterior femur (Table 6.10; 6.12).

These results reject the null hypothesis, confirming statistically significant differences in several of the targeted variables between AAD categories.

$H0_c$: Each of the observed variables (OPD, Fg.OPD, Ct.Po or Ct.Wi) have a similar distribution across the rib and the femur.

Inferential testing of chronological AAD with each of the targeted variables did not render any statistically significant results for either the anterior femur or the rib. Thus, in this instance, there were no differences between the femur and rib in how chronological AAD presented in OPD, Fg.OPD or Ct.Po. While the rib had statistically significant differences in OPD, Fg.OPD and Ct.Wi between AAD categories, the anterior and posterior femur did not.

This suggests differences in the distribution of these variables between the rib and femur with AAD category and rejects the null hypothesis.

6.3.4 Descriptive Trends: Sex

There are two key steps, and thus two hypotheses to test in order to address this research question. The first will test if there is a relationship between biological sex and the key variables; OPD, Fg.OPD, On.Ar, H.Ar, Ct.Po and Ct.Wi in both the rib and femur separately. The second asks if there is a difference in how these effects, if identified in $H0_a$, manifest differently between the rib and femur. Therefore, the null hypotheses for this part of research question 1 are as follows:

$H0_a$: Each of the observed variables, OPD, Fg.OPD, On.Ar, H.Ar, Ct.Po and Ct.Wi have a similar distribution in male and female groups.

$H0_b$: Each of the observed variables, OPD, Fg.OPD, On.Ar, H.Ar and Ct.Po have similar distributions between the rib and posterior femur.

Variables observed to assess changes in femur and rib histology with sex included OPD, Fg.OPD, On.Ar, H.Ar, Ct.Po and Ct.Wi.

Table 6.13: Descriptive statistics for all variables observed in Sex analysis.

Variable	Bone/ Region	Sex	*n*.	Min.	Max.	Mean	St.D.
OPD (#/mm^2)	Rib	Female	16	7.934	17.893	10.744	3.280
		Male	30	6.996	17.829	11.176	3.313
	Anterior Femur	Female	4	9.762	16.608	13.819	3.005
		Male	22	8.367	22.693	14.879	3.162
	Posterior Femur	Female	20	9.001	16.481	11.701	2.500
		Male	22	6.212	19.777	12.326	3.515
Fg/OPD (#/mm^2)	Rib	Female	16	2.002	7.603	4.120	1.669
		Male	30	1.264	6.195	3.823	1.514
	Anterior Femur	Female	4	6.466	10.649	7.733	1.972
		Male	22	1.775	10.776	6.886	1.954
	Posterior Femur	Female	20	2.155	9.381	5.521	1.886
		Male	22	1.395	8.240	5.232	2.025
On.Ar (μm^2)	Rib	Female	16	14203.431	82811.746	27478.853	16749.060
		Male	30	14231.013	39804.916	21163.687	6246.260
	Anterior Femur	Female	4	32932.432	42447.368	38257.677	3940.926
		Male	22	24310.345	57525.000	35333.299	9657.177
	Posterior Femur	Female	20	27109.375	56945.946	37237.620	6949.480
		Male	22	13800.000	61666.667	32514.232	11900.479
H.Ar (μm^2)	Rib	Female	16	1225.071	5561.523	2441.975	1119.199
		Male	30	935.334	3786.061	1729.005	598.343
	Anterior Femur	Female	4	2390.000	2970.000	2722.683	273.108
		Male	22	1310.000	7901.495	3311.790	1696.303
	Posterior Femur	Female	20	1625.375	11450.903	3834.727	2246.104
		Male	22	1220.000	8423.926	3042.495	2141.997
Ct.Po (%)	Rib	Female	16	0.792	10.480	3.395	2.688
		Male	30	0.272	8.270	2.846	1.981
	Anterior Femur	Female	4	12.348	30.895	22.667	8.118
		Male	22	16.519	42.051	27.620	7.651
	Posterior Femur	Female	20	14.845	28.486	22.582	3.947
		Male	22	8.747	32.264	21.044	5.751
Ct.Wi (mm)	Rib	Female	11	0.316	1.662	0.809	0.394
		Male	15	0.337	1.092	0.718	0.248

Descriptive results identified mild sex differences in OPD for the anterior femur (Female *m* = 13.819/mm^2; Male *m* = 14.879/mm^2), posterior femur (Female *m* = 11.701/mm^2; Male *m* = 12.326/mm^2) and rib (Female *m* = 10.744/mm^2; Male *m* = 11.176/mm^2), with highest overall

values in the anterior femur, and lowest overall values in the rib (Table 6.13; Figure 6.4A). Similar trends were observed in Fg.OPD in the anterior femur (Female *m* = 7.733/mm^2; Male *m* = 6.886/mm^2), posterior femur (Female *m* = 5.521/mm^2; Male *m* = 5.232/mm^2) and rib (Female *m* = 4.120/mm^2; Male *m* = 3.823/mm^2) (Table 6.13; Figure 6.4B). On.Ar appeared slightly larger in females in the anterior femur (Female *m* = 38,257.677/µm^2; Male *m* = 35,333.299/µm^2), posterior femur (Female *m* = 37,237.620/µm^2; Male *m* = 32,514.232/µm^2) and rib (Female *m* = 27,478.853/µm^2; Male *m* = 21,163.687/µm^2), with overall larger On.Ar values in the anterior femur, and smaller On.Ar values in the rib (Table 6.13; Figure 6.4C). H.Ar was slightly higher in males in the anterior femur (Female *m* = 2,722.683/µm^2; Male *m* = 3,311.790/µm^2), but higher in females in the posterior femur (Female *m* = 3,834.727/µm^2; Male *m* = 3,042.495/µm^2) and rib (Female *m* = 2,441.975/µm^2; Male *m* = 1,729.005/µm^2). Overall, for females, values were higher in the posterior femur, and lower in the rib, but for males, values were higher in the anterior femur and lower in the rib (Table 6.13; Figure 6.4D). Males appear to have higher Ct.Po at the anterior femur (Female *m* = 22.667%; Male *m* = 27.620%), but females have higher Ct.Po at the posterior femur (Female *m* = 22.582%; Male *m* = 21.044%) and in the rib (Female *m* = 3.395%; Male *m* = 2.846%) (Table 6.13; Figure 6.4E). Rib Ct.Wi was higher in females (Female *m* = 0.809 mm; Male *m* = 0.718 mm) (Table 6.13; Figure 6.4F).

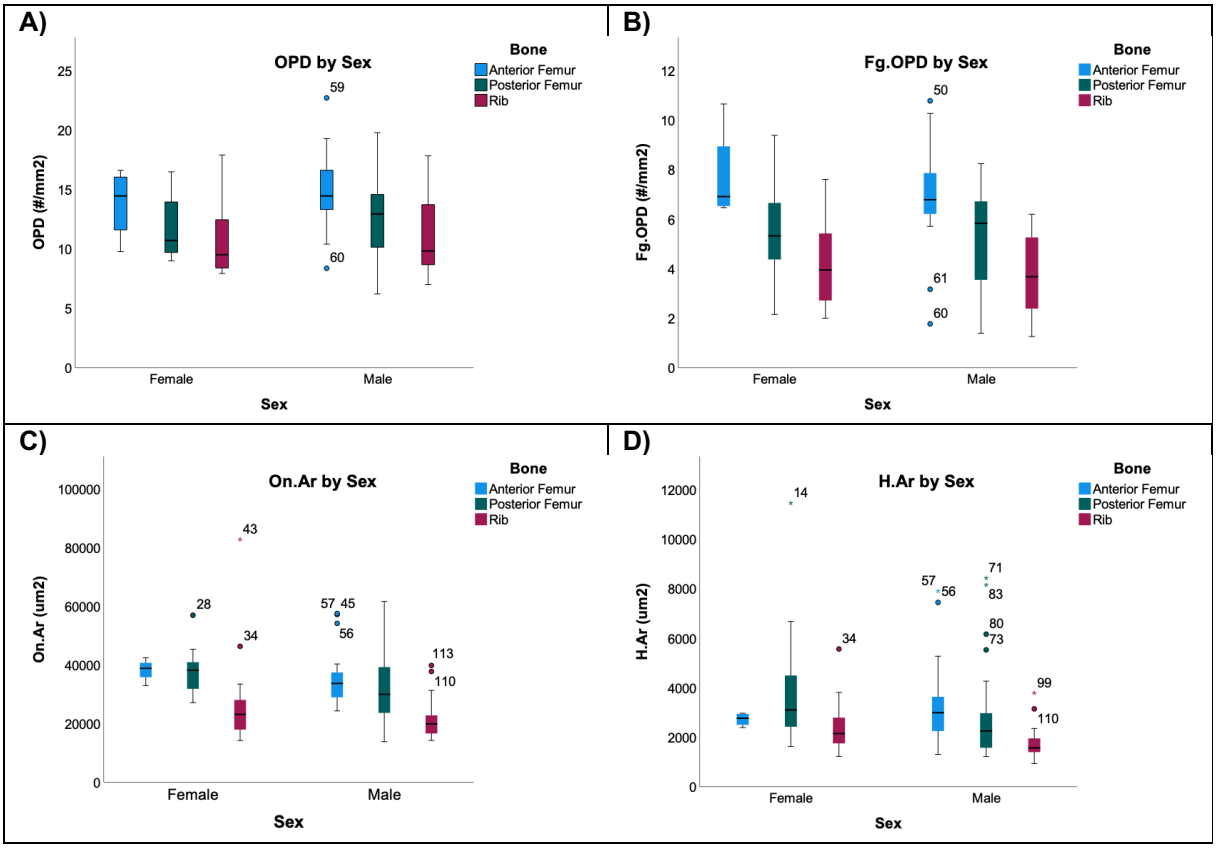

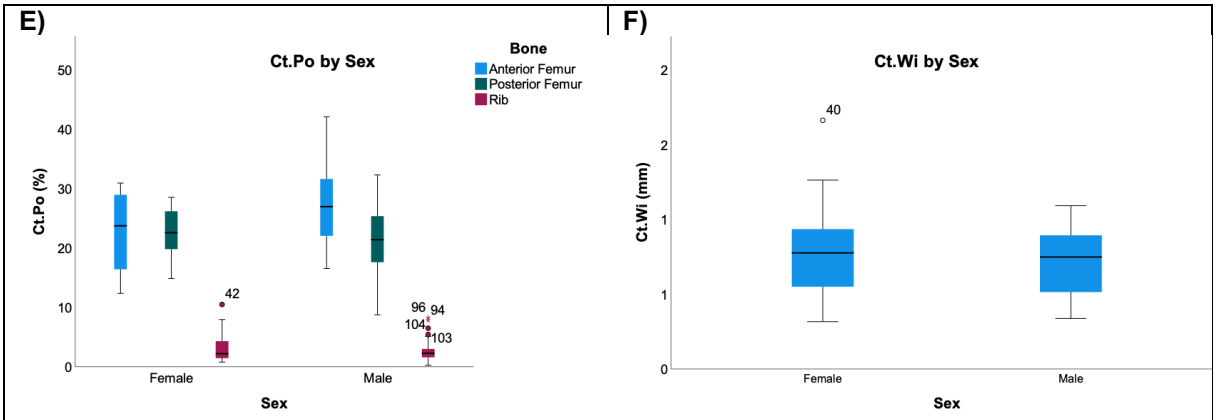

Figure 6.4: Boxplots of key biological sex variables.

A) Osteon Population Density (OPD) by Sex. **B)** Fragmented OPD by Sex. **C)** Mean Osteon Area (On.Ar) by Sex. **D)** Mean Haversian Canal Area (H.Ar) by Sex. **E)** Cortical Porosity Area (Ct.Po) by Sex. **F)** Cortical Width (Ct.Wi) by Sex.

6.3.5 Inferential Statistics: Sex

Results of the Mann-Whitney *U* test indicate that there is no statistically significant difference in OPD, Fg.OPD, Ct.Po or Ct.Wi between females and males as observed in the rib, anterior or posterior femur. H.Ar was statistically significantly higher in females than males in the rib (U = 133.000; z = -2.468, p = 0.014). On.Ar was also statistically significantly higher in females than males in the posterior femur (U = 137.000; z = -2.090, p = 0.037). There were no statistically significant differences identified between females and males in any variable within the anterior femur (Table 6.14). However, it is important to note that only 4 females, compared to 22 males, were available for sampling the anterior femur.

Table 6.14: Sex differences (Mann-Whitney U).

Variable	Bone	Sex	*n*. Individuals	Mean Rank	Mann-Whitney *U*	*z*-value	*p*-value
OPD	Rib	Female	16	22.81	229.000	-0.254	0.800
		Male	30	23.87			
	Anterior Femur	Female	4	11.75	37.000	-0.498	0.619
		Male	22	13.82			
	Posterior Femur	Female	20	20.27	195.500	-0.617	0.537
		Male	22	22.61			
Fg.OPD	Rib	Female	16	25.06	215.000	-0.577	0.564
		Male	30	22.67			
	Anterior Femur	Female	4	16.00	34.000	-0.712	0.477
		Male	22	13.05			
	Posterior Femur	Female	20	21.43	218.500	-0.038	0.970
		Male	22	21.57			
On.Ar	Rib	Female	16	27.44	177.000	-1.453	0.146

		Male	30	21.40			
	Anterior Femur	Female	4	19.00	22.000	-1.563	0.118
		Male	22	12.50			
	Posterior Femur	Female	20	25.65	137.000	-2.090	**0.037***
		Male	22	17.73			
H.Ar	Rib	Female	16	30.19	133.000	-2.468	**0.014***
		Male	30	19.93			
	Anterior Femur	Female	4	11.00	34.000	-0.711	0.477
		Male	22	13.95			
	Posterior Femur	Female	20	25.35	143.000	-1.939	0.052
		Male	22	18.00			
Ct.Po	Rib	Female	16	24.00	232.000	-0.185	0.854
		Male	30	23.23			
	Anterior Femur	Female	4	10.25	31.000	-0.924	0.356
		Male	22	14.09			
	Posterior Femur	Female	20	23.20	186.000	-0.856	0.392
		Male	22	19.95			
Ct.Wi	Rib	Female	11	14.14	17.500	-0.363	0.716
		Male	15	13.03			

* Significance values have been adjusted by the Bonferroni Correction for multiple tests.

Once OPD, Fg.OPD, On.Ar, H.Ar, Ct.Po and Ct.Wi were corrected by stature to account for individual body size differences, results of the Mann-Whitney *U* test changed and additional statistically significant differences were identified. In the rib, On.Ar (U = 126.000; z = -1.978, p = 0.048) and H.Ar (U = 97.000; z = -2.753, p = 0.006) were statistically significantly higher in females than males. In the posterior femur, On.Ar (U = 96.000; z = -2.813, p = 0.005) and H.Ar (U = 126.000; z = -2.002, p = 0.045) were statistically significantly higher in females than males (Table 6.15). There were no statistically significant sex differences in the anterior femur.

Table 6.15: Sex differences (Mann-Whitney *U*): Corrected by stature.

Variable	Bone	Sex	*n*. Individuals	Mean Rank	Mann-Whitney *U*	*z*-value	*p*-value
OPD	Rib	Female	16	20.50	180.000	-0.535	0.593
		Male	25	20.50			
	Anterior Femur	Female	4	12.00	34.000	-0.170	0.865
		Male	18	11.39			
	Posterior Femur	Female	20	18.50	200.000	0.000	1.000
		Male	20	22.50			
Fg.OPD	Rib	Female	16	21.90	151.000	-1.310	0.190
		Male	25	19.10			
	Anterior Femur	Female	4	14.75	23.000	-1.107	0.268
		Male	18	10.78			
	Posterior Femur	Female	20	19.95	172.000	-0.757	0.449
		Male	20	21.05			
On.Ar	Rib	Female	16	25.70	126.000	-1.978	**0.048***
		Male	25	15.30			
	Anterior Femur	Female	4	15.50	20.000	-1.362	0.173
		Male	18	10.61			
		Female	20	23.20	96.000	-2.813	**0.005****

	Posterior Femur	Male	20	17.80			
H.Ar	Rib	Female	16	24.20	97.000	-2.753	**0.006***
		Male	25	16.80			
	Anterior Femur	Female	4	10.00	30.000	-0.511	0.610
		Male	18	11.83			
	Posterior Femur	Female	20	22.90	126.000	-2.002	**0.045***
		Male	20	18.10			
Ct.Po	Rib	Female	16	24.00	183.000	-0.454	0.650
		Male	25	17.00			
	Anterior Femur	Female	4	9.25	27.000	-0.766	0.444
		Male	18	12.00			
	Posterior Femur	Female	20	21.25	130.000	-1.894	0.058
		Male	20	19.75			
Ct.Wi	Rib	Female	11	12.91	67.000	-0.261	0.794
		Male	13	12.15			

* Significance values have been adjusted by the Bonferroni Correction for multiple tests.

6.3.6 Hypotheses Results: Sex

$H0_a$: Each of the observed variables, OPD, Fg.OPD, On.Ar, H.Ar, Ct.Po and Ct.Wi have a similar distribution in male and female groups.

Descriptive data presented in boxplots demonstrated mild differences in distributions of OPD, Fg.OPD, Ct.Po and Ct.Wi, as well as less subtle differences in On.Ar and H.Ar between male and female groups in the rib and femoral regions (Figure 6.4). However, Mann-Whitney U tests demonstrated that there was no statistically significant difference in OPD, Fg.OPD, Ct.Po or Ct.Wi between males and females in either bone (Table 6.14; 6.15). Only On.Ar and H.Ar were statistically significantly higher in females in the posterior femur and rib respectively.

These results reject the null hypothesis, identifying statistically significant differences in the distribution of On.Ar and H.Ar data between male and female groups in the rib and posterior femur, with females having statistically significantly larger osteons and Haversian canals than males.

$H0_b$: Each of the observed variables, OPD, Fg.OPD, On.Ar, H.Ar and Ct.Po have similar distributions between the rib and femur.

In the descriptive data presented in Table 6.13 and Figure 6.4, there appeared to be mild sex differences identified in all variables in the rib and femoral aspects. However, the Mann-Whitney U test results only identified statistically significant differences in On.Ar and H.Ar were significantly higher in females in the posterior femur and rib respectively, and no statistically significant sex differences were identified in the anterior femur (Table 6.14; 6.15).

These results suggest that although some differences in the way sex differences impact the rib and femoral regions were identified in descriptive statistics, these were largely found to be not statistically significant through inferential testing. Once accounting for body size variation, only On.Ar and H.Ar in the rib and posterior femur proved significantly different between males and females and no statistically significant differences were identified in the anterior femur. However, this rejects the null hypothesis as On.Ar appears to be more impacted by sex differences in the posterior femur, while H.Ar appears to be more impacted by sex differences in the rib.

6.3.7 Descriptive Trends: Socioeconomic Group

There are two key steps, and thus two hypotheses to test that address this research question. The first tests if there is a relationship between socioeconomic status (SES) group and the key variables; OPD, On.Circ, Po.Ar, Ct.Po, Ct.Wi and %Ct.Ar in both the rib and femur separately. The second asks if there is a difference in how these effects, if identified in $H0_a$, manifest differently between the rib and femur. Therefore, the null hypotheses for this part of research question 1 are as follows:

$H0_a$: Each of the observed variables, OPD, On.Circ, Po.Ar, Ct.Po, Ct.Wi and %Ct.Ar have a similar distribution across the three socioeconomic status (SES) groups; medieval lower class, medieval upper class and contemporary.

$H0_b$: Each of the observed variables, OPD, On.Circ, Po.Ar and Ct.Po have similar distributions between the rib and femur.

Variables observed to assess changes in femur and rib histology with systemic health and physical activity (as inferred by socioeconomic group), included OPD, On.Circ, Po.Ar, Ct.Po, Ct.Wi, and %Ct.Ar.

Table 6.16: Descriptive statistics for all variables observed in SES analysis.

Variable	Bone/Region	SES Group	*n.*	Min.	Max.	Mean	St.D.
OPD (#/mm^2)	Rib	MedHigh	25	6.398	11.228	8.922	1.273
		MedLow	28	4.056	13.672	9.147	2.209
		ModCon	18	8.675	19.611	14.550	3.030
	Anterior Femur	MedHigh	7	11.917	14.959	13.800	1.154
		MedLow	3	8.367	13.438	10.734	2.552
		ModCon	18	9.762	22.693	15.579	3.076
	Posterior Femur	MedHigh	25	3.930	19.777	11.699	2.946
		MedLow	28	6.212	19.777	12.564	3.620
On.Circ	Rib	MedHigh	25	0.893	0.937	0.916	0.012
		MedLow	28	0.907	0.938	0.922	0.009

		ModCon	18	0.876	0.931	0.902	0.015
	Anterior Femur	MedHigh	7	0.885	0.938	0.907	0.020
		MedLow	3	0.910	0.927	0.920	0.009
		ModCon	18	0.845	0.895	0.877	0.013
	Posterior Femur	MedHigh	25	0.818	0.938	0.907	0.024
		MedLow	28	0.889	0.941	0.919	0.011
Po.Ar (mm^2)	Rib	MedHigh	25	0.004	0.061	0.018	0.012
		MedLow	28	0.009	0.052	0.025	0.011
		ModCon	18	0.008	0.042	0.020	0.009
	Anterior Femur	MedHigh	7	0.024	0.050	0.032	0.010
		MedLow	3	0.025	0.038	0.031	0.006
		ModCon	18	0.026	0.058	0.038	0.009
	Posterior Femur	MedHigh	25	0.014	0.068	0.038	0.011
		MedLow	28	0.021	0.062	0.033	0.009
Ct.Po (%)	Rib	MedHigh	25	0.750	8.090	3.263	2.187
		MedLow	28	0.369	10.480	3.373	2.261
		ModCon	18	0.272	8.270	2.582	2.275
	Anterior Femur	MedHigh	7	16.519	26.978	22.856	4.271
		MedLow	3	18.065	25.165	21.750	3.557
		ModCon	18	12.348	42.051	28.974	8.137
	Posterior Femur	MedHigh	25	8.747	43.839	23.337	6.756
		MedLow	28	10.535	30.223	21.565	5.093
Ct.Wi (mm)	Rib	MedHigh	11	0.470	1.092	0.837	0.206
		MedLow	10	0.559	1.662	0.953	0.309
		ModCon	9	0.316	0.753	0.492	0.173
%Ct.Ar (%)	Rib	MedHigh	10	27.755	56.992	39.781	9.563
		MedLow	10	20.989	62.378	40.284	14.089
		ModCon	11	15.807	44.948	30.579	10.092

Descriptive results identified higher OPD in modern contemporary individuals for the anterior femur (Medieval high status m = 13.800/mm^2; Medieval low status m = 10.734/mm^2; Contemporary m = 15.579/mm^2) and rib (Medieval high status m = 8.922/mm^2; Medieval low status m = 9.147/mm^2; Contemporary m = 14.550/mm^2). The posterior femur had higher OPD values in the medieval low status individuals (Medieval high status m = 11.699/mm^2; Medieval low status m = 12.564/mm^2) (Table 6.16; Figure 6.5A). On.Circ was highest in medieval low status individuals for the anterior femur (Medieval high status m = 0.907; Medieval low status m = 0.920; Contemporary m = 0.877), posterior femur (Medieval high status m = 0.907; Medieval low status m = 0.919) and rib (Medieval high status m = 0.916; Medieval low status m = 0.922; Contemporary m = 0.902). The lowest On.Circ was recorded for the contemporary individuals in both the anterior femur and the rib (Table 6.16; Figure 6.5B).

Po.Ar in the anterior femur was highest in contemporary individuals and lowest in medieval low status individuals (Medieval high status m = 0.032 mm^2; Medieval low status m = 0.031 mm^2; Contemporary m = 0.038 mm^2). In the posterior femur, Po.Ar was higher in medieval high status individuals (Medieval high status m = 0.038 mm^2; Medieval low status m = 0.033 mm^2). The rib had the lowest overall Po.Ar values, but was highest in medieval low status

individuals and lowest in medieval high status individuals (Medieval high status *m* = 0.018 mm^2; Medieval low status *m* = 0.025 mm^2; Contemporary *m* = 0.020 mm^2) (Table 6.16; Figure 6.5C). In the anterior femur, Ct.Po was highest in the contemporary individuals and lowest in the medieval low status individuals (Medieval high status *m* = 22.856%; Medieval low status *m* = 21.750%; Contemporary *m* = 28.974%). Similarly, the posterior femur had the lowest Ct.Po in the medieval low status individuals (Medieval high status *m* = 23.337%; Medieval low status *m* = 21.565%). The rib had higher Ct.Po values in the medieval low status individuals, and lowest in the contemporary individuals (Medieval high status *m* = 3.263%; Medieval low status *m* = 3.373%; Contemporary *m* = 2.582%). Overall, Ct.Po values were lower in the rib than both femoral aspects (Table 6.16; Figure 6.5D).

Rib Ct.Wi was highest in medieval low status individuals, and lowest in contemporary individuals (Medieval high status *m* = 0.837 mm; Medieval low status *m* = 0.953 mm; Contemporary *m* = 0.492 mm) (Table 6.16; Figure 6.5E). Rib %Ct.Ar was highest in medieval low status individuals, and lowest in contemporary individuals (Medieval high status *m* = 39.781%; Medieval low status *m* = 40.284%; Contemporary *m* = 30.579%) (Table 6.16; Figure 6.5F).

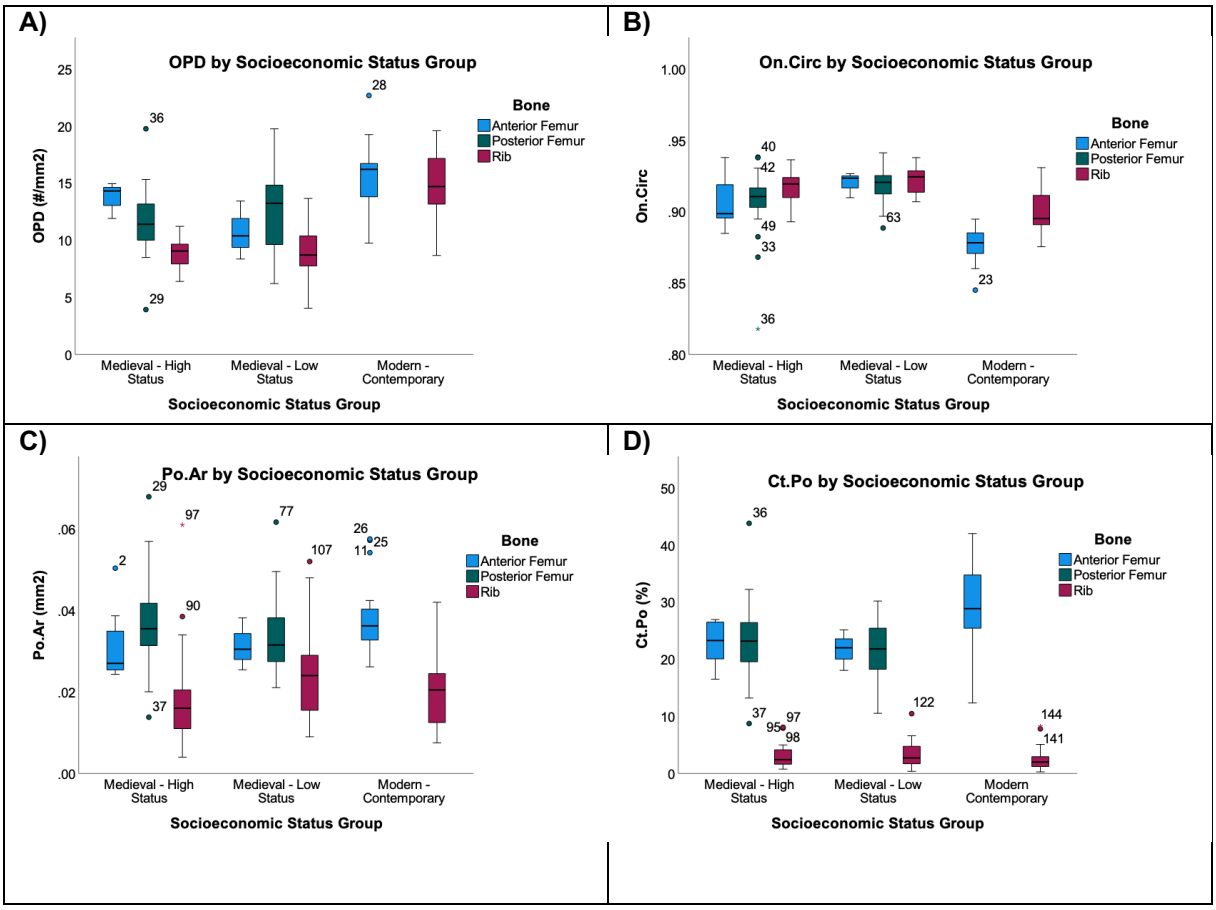

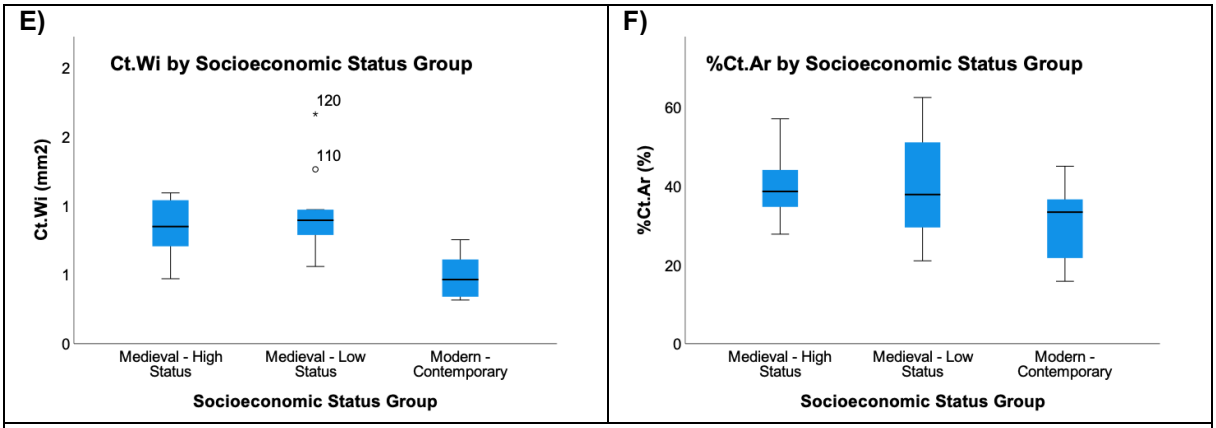

Figure 6.5: Boxplots of key socioeconomic status variables.

A) Osteon Population Density (OPD) by Socioeconomic Status (SES). **B)** Osteon Circularity (On.Circ) by SES. **C)** Porosity Area (Po.Ar) by SES. **D)** Cortical Porosity Area (Ct.Po) by SES. **E)** Cortical Width (Ct.Wi) by SES in the rib. **F)** Percent Cortical Area (%Ct.Ar) by SES in the rib.

6.3.8 Inferential Statistics: Socioeconomic Status Group

Results of the Kruskal-Wallis *H* test indicate that OPD (*H* = 29.392, *p* <0.001), On.Circ (*H* = 18.479, *p* <0.001), Po.Ar (*H* = 7.951, *p* =0.019) and Ct.Wi (*H* = 12.804, *p* = 0.002) are significantly different between SES Groups in the rib. While OPD (*H* = 6.940, *p* = 0.031), On.Circ (*H* = 16.500, *p* <0.001) and Ct.Po (*H* = 6.323, *p* = 0.042) are significantly different between SES Groups in the anterior femur. On.Circ (*H* = 7.238, *p* = 0.007) and Po.Ar (*H* = 4.054, *p* = 0.044) are significantly different between SES Groups in the posterior femur.

Table 6.17: Differences between SES Groups (Kruskal-Wallis).

Variable	Bone	SES Group	*n*. Individuals	Mean Rank	Kruskal-Wallis *H*	*p*-value
OPD	Rib	MedHigh	25	27.80	29.392	**<0.001****
		MedLow	28	28.68		
		ModCon	18	58.78		
	Anterior Femur	MedHigh	7	12.00	6.940	**0.031***
		MedLow	3	4.50		
		ModCon	18	17.14		
	Posterior Femur	MedHigh	25	24.76	0.996	0.318
		MedLow	28	29.00		
On.Circ	Rib	MedHigh	25	36.92	18.479	**<0.001****
		MedLow	28	45.96		
		ModCon	18	19.22		
	Anterior Femur	MedHigh	7	22.00	16.500	**<0.001****
		MedLow	3	25.00		
		ModCon	18	9.83		
	Posterior Femur	MedHigh	25	20.96	7.238	**0.007***
		MedLow	28	32.39		

Po.Ar	Rib	MedHigh	25	27.64	7.951	**0.019***
		MedLow	28	43.64		
		ModCon	18	35.72		
	Anterior Femur	MedHigh	7	10.00	4.264	0.119
		MedLow	3	10.67		
		ModCon	18	16.89		
	Posterior Femur	MedHigh	25	31.52	4.054	**0.044***
		MedLow	28	22.96		
Ct.Po	Rib	MedHigh	25	37.56	2.526	0.283
		MedLow	28	38.86		
		ModCon	18	29.39		
	Anterior Femur	MedHigh	7	9.86	6.323	**0.042***
		MedLow	3	8.00		
		ModCon	18	17.39		
	Posterior Femur	MedHigh	25	29.08	0.858	0.354
		MedLow	28	25.14		
Ct.Wi	Rib	MedHigh	10	17.70	12.804	**0.002****
		MedLow	10	19.80		
		ModCon	9	6.67		
%Ct.Ar	Rib	MedHigh	10	16.80	2.025	0.363
		MedLow	10	16.20		
		ModCon	9	11.67		

* Significance values have been adjusted by the Bonferroni Correction for multiple tests.

Results of the post-hoc pairwise comparisons identified which SES Group pairings were significantly different from each other. For OPD in the rib, the contemporary group was significantly higher than the medieval high status (-30.978, p <0.001) and medieval low status group (-30.099, p <0.001). There was no significant difference between the medieval groups. For OPD in the anterior femur, the contemporary group was significantly higher than the medieval low status (-12.639, p = 0.041), but not from the medieval high status group. Similarly, the contemporary group individuals had significantly higher On.Circ in the rib than the medieval high status (17.698, p = 0.017) and medieval low status groups (26.742, p <0.001). On.Circ was significantly higher in the medieval high (17.698, p = 0.017) and low (17.698, p = 0.017) status individuals than the contemporary individuals. Po.Ar in the rib was significantly higher in the medieval low status individuals than the medieval high status individuals (-16.003, p = 0.014). Once the Bonferroni correction was applied, differences in the anterior femur in Ct.Po were no longer statistically significant. Ct.Wi in the rib was significantly lower in the modern contemporary individuals than both the medieval high status (11.606, p = 0.010) and medieval low status (13.733, p = 0.002) individuals.

Table 6.18: SES Groups: Post-hoc Kruskal-Wallis pairwise comparisons.				
Variable	**Bone**	**SES Group 1 – SES Group 2**	**Test Statistic**	***p*-value***
OPD	Rib	MedHigh – MedLow	-0.879	1.000
		MedHigh – ModCon	-30.978	**<0.001*** **
		MedLow – ModCon	-30.099	**<0.001*** **
	Anterior Femur	MedHigh – MedLow	7.500	0.559
		MedHigh – ModCon	-5.139	0.482
		MedLow – ModCon	-12.639	**0.041***
On.Circ	Rib	MedHigh – MedLow	-9.044	0.334
		MedHigh – ModCon	17.698	**0.017***
		MedLow – ModCon	26.742	**<0.001*** **
	Anterior Femur	MedHigh – MedLow	-3.000	1.000
		MedHigh – ModCon	12.167	**0.003****
		MedLow – ModCon	15.167	**0.009***
Po.Ar	Rib	MedHigh – MedLow	-16.003	**0.014***
		MedHigh – ModCon	-8.082	0.615
		MedLow – ModCon	7.921	0.611
Ct.Po	Anterior Femur	MedHigh – MedLow	1.857	1.000
		MedHigh – ModCon	-7.532	0.119
		MedLow – ModCon	-9.389	0.202
Ct.Wi	Rib	MedHigh – MedLow	-2.127	1.000
		MedHigh – ModCon	11.606	**0.010***
		MedLow – ModCon	13.733	**0.002****

* Significance values have been adjusted by the Bonferroni Correction for multiple tests.

Once OPD, On.Circ, Po.Ar, Ct.Po, Ct.Wi and %Ct.Ar were corrected by stature to account for individual variation in body size, results of the Kruskal-Wallis *H* test changed. These results indicate that OPD ($H = 21.060$, $p < 0.001$), Po.Ar ($H = 8.421$, $p = 0.015$), and Ct.Wi ($H = 10.131$, $p = 0.006$) are significantly different between SES Group in the rib. OPD ($H = 6.107$, $p = 0.047$) and Po.Ar ($H = 7.377$, $p = 0.025$) are significantly different between SES Group in the anterior femur. Po.Ar appears to be the variable most sensitive to changes in SES, with significant differences between SES Group across the rib, anterior and posterior femur. However, it seems to be impacted differently between the bones. In the rib, Po.Ar was highest in the medieval low status group, and lowest in the medieval high status group, while in the anterior femur Po.Ar was highest in the contemporary group and lowest in the medieval high status group. In the posterior femur, Po.Ar was highest in the medieval high status group and lowest in the medieval low status group, however no posterior femur sampling was available from the contemporary group. There was no statistically significant differences between SES groups in On.Circ, Ct.Po or %Ct.Ar.

Table 6.19: Differences between SES Groups (Kruskal-Wallis): Corrected by stature.

Variable	Bone	SES Group	*n*. Individuals	Mean Rank	Kruskal-Wallis *H*	*p*-value
OPD	Rib	MedHigh	25	26.96	21.060	**<0.001****
		MedLow	26	28.27		
		ModCon	15	53.47		
	Anterior Femur	MedHigh	6	10.83	6.107	**0.047***
		MedLow	2	1.50		
		ModCon	15	13.87		
	Posterior Femur	MedHigh	24	23.08	1.269	0.260
		MedLow	26	27.73		
On.Circ	Rib	MedHigh	25	32.76	5.753	0.056
		MedLow	26	39.38		
		ModCon	15	24.53		
	Anterior Femur	MedHigh	6	13.33	0.328	0.849
		MedLow	2	11.00		
		ModCon	15	11.60		
	Posterior Femur	MedHigh	24	21.71	3.123	0.077
		MedLow	26	29.00		
Po.Ar	Rib	MedHigh	25	25.72	8.421	**0.015***
		MedLow	26	41.31		
		ModCon	15	32.93		
	Anterior Femur	MedHigh	6	5.83	7.377	**0.025***
		MedLow	2	10.50		
		ModCon	15	14.67		
	Posterior Femur	MedHigh	24	29.75	3.923	**0.048***
		MedLow	26	21.58		
Ct.Po	Rib	MedHigh	25	35.16	4.639	0.098
		MedLow	26	37.23		
		ModCon	15	24.27		
	Anterior Femur	MedHigh	6	8.50	3.267	0.195
		MedLow	2	8.50		
		ModCon	15	13.87		
	Posterior Femur	MedHigh	24	27.63	0.981	0.322
		MedLow	26	23.54		
Ct.Wi	Rib	MedHigh	11	16.64	10.131	**0.006***
		MedLow	10	18.10		
		ModCon	7	6.00		
%Ct.Ar	Rib	MedHigh	10	17.20	2.503	0.286
		MedLow	10	16.10		
		ModCon	9	11.33		

* Significance values have been adjusted by the Bonferroni Correction for multiple tests.

The contemporary group had significantly higher OPD in the rib than the medieval high status (-26.507, p <0.001) and medieval low status groups (-25.107, p <0.001). In the anterior femur, OPD was statistically significantly higher in the contemporary group than the medieval low status group (-12.367, p = 0.046). Po.Ar was significantly higher in medieval low status individuals than medieval high status individuals in the rib (-15.588, p = 0.011). Po.Ar was significantly lower in medieval high status individuals than in the contemporary individuals at the anterior femur (-8.833, p = 0.021). Ct.Wi in the rib was significantly lower in the

contemporary group than both the medieval high status individuals (10.636, p = 0.022) and medieval low status individuals (12.100, p = 0.009).

Table 6.20: SES Groups: Corrected by Stature: Post-hoc Kruskal-Wallis pairwise comparisons.

Variable	Bone	SES Group 1 – SES Group 2	Test Statistic	*p*-value*
OPD	Rib	MedHigh – MedLow	-1.309	1.000
		MedHigh – ModCon	-26.507	**<0.001*** **
		MedLow – ModCon	-25.107	**<0.001*** **
	Anterior Femur	MedHigh – MedLow	9.333	0.276
		MedHigh – ModCon	-3.033	1.000
		MedLow – ModCon	-12.367	**0.046***
Po.Ar	Rib	MedHigh – MedLow	-15.588	**0.011***
		MedHigh – ModCon	-7.213	0.750
		MedLow – ModCon	8.374	0.535
	Anterior Femur	MedHigh – MedLow	-4.667	1.000
		MedHigh – ModCon	-8.833	**0.021***
		MedLow – ModCon	-4.167	1.000
Ct.Wi	Rib	MedHigh – MedLow	-1.464	1.000
		MedHigh – ModCon	10.636	**0.022***
		MedLow – ModCon	12.100	**0.009***

* Significance values have been adjusted by the Bonferroni Correction for multiple tests.

6.3.9 Hypotheses Results: Socioeconomic Status Group

$H0_a$: Each of the observed variables, OPD, On.Circ, Po.Ar, Ct.Po, Ct.Wi and %Ct.Ar have a similar distribution across the three socioeconomic status (SES) groups; medieval lower class, medieval upper class and contemporary.

Descriptive statistics presented in Table 6.16 and Figure 6.5 suggested mean differences between SES groups, including higher OPD in the contemporary group, in both the anterior femur and rib, while the medieval low status group had the highest OPD in the posterior femur (Figure 6.5A). On.Circ was highest in the medieval low status group, across both femoral aspects and the rib, and the lowest On.Circ values were recorded in the contemporary group in both the anterior femur and rib (Figure 6.5B). Po.Ar and Ct.Po were similar across the medieval groups in the femur and rib, and values of Po.Ar and Ct.Po were both lowest in the contemporary group (Figure 6.5C-D). Both rib Ct.Wi and %Ct.Ar were lowest in the contemporary group and similar in the medieval groups (Figure 6.5E-F).

The Kruskal-Wallis results indicate that the contemporary group had statistically significantly higher OPD in the rib than both the medieval high and low status groups, but there was no difference between the medieval groups. In the anterior femur, OPD was significantly higher in the contemporary group than the medieval low status group, but there was no difference between medieval groups or between the contemporary and medieval high status groups. The

medieval low status group had significantly higher Po.Ar in the rib than the medieval high status group, but in the anterior femur the contemporary group had significantly higher Po.Ar than the medieval high status group. Rib Ct.Wi was significantly lower in the contemporary group compared to both medieval groups (Table 6.20).

These results suggest that there are differences in the targeted variables between SES group, particularly separating the contemporary from medieval groups, and especially in OPD and Ct.Wi, but that these effects manifest differently across bones. This rejects the null hypothesis.

$H0_b$: Each of the observed variables, OPD, On.Circ, Po.Ar and Ct.Po have similar distributions between the rib and posterior femur.

The rib had the most amount of statistically significant differences in the targeted variables between socioeconomic status groups. OPD was statistically significantly higher in the rib for contemporary individuals than both medieval status groups. Additionally, Po.Ar was statistically significantly higher in the medieval low status group than the medieval high status group in the rib. Meanwhile in the anterior femur, OPD was statistically significantly higher in the contemporary than the medieval low status group, and Po.Ar was statistically significantly lower in the medieval high status than contemporary group. There were no statistically significant differences between socioeconomic status groups in any variable at the posterior femur (Table 6.20).

These results demonstrate that the null hypothesis should be rejected as the rib and femur, represented by both the anterior and posterior regions, were differently impacted by the effects of socioeconomic status.

6.4 Research Question 2

Is there a trend of bone quality "deteriorating" in modern individuals to reflect generally more sedentary lifestyles than their medieval ancestral population?

6.4.1 Descriptive Trends

There are three key steps, and thus three hypotheses to test to address this research question. The first tests if there are differences between era (medieval or modern), and the key variables; OPD, On.Circ, On.Ar, %Ct.Ar, Po.Ar and Ct.Po in both the rib and anterior femur separately. The second tests if these differences can be used in order to classify a sample as either medieval or modern using discriminant function analysis (DFA). Finally, the third hypothesis

will test if the differences identified in $H0_a$ and $H0_a$, suggest that there is evidence of a more sedentary lifestyle in modern individuals compared to medieval. Therefore, the null hypotheses for research question 2 are as follows:

$H0_a$: Each of the observed variables, OPD, On.Circ, On.Ar, %Ct.Ar, Po.Ar and Ct.Po have a similar distribution between medieval and modern era individuals.

H0b: Medieval and modern ribs and anterior femora cannot be separated using discriminant function analysis (DFA), based on the variables OPD, On.Circ, On.Ar, Po.Ar and Ct.Po.

$H0_c$: There is no evidence of a more sedentary lifestyle influencing modern individuals as compared to medieval individuals in either observed variable; OPD, On.Circ, On.Ar, %Ct.Ar, Po.Ar and Ct.Po.

Variables observed to assess femoral and rib bone quality in medieval and modern individuals included OPD, On.Circ, On.Ar, Ct.Po, Po.Ar and %Ct.Ar.

Table 6.21: Descriptive statistics for all variables observed in research question 2.

Variable	Bone /Region	Era	*n*.	Min.	Max.	Mean	St.D.
OPD (#/mm^2)	Rib	Medieval	53	4.056	13.672	9.040	1.815
		Modern	18	8.675	19.611	14.550	3.030
	Anterior Femur	Medieval	10	8.367	14.959	12.880	2.128
		Modern	18	9.762	22.693	15.579	3.076
On.Circ	Rib	Medieval	53	0.893	0.938	0.919	0.011
		Modern	18	0.876	0.931	0.902	0.015
	Anterior Femur	Medieval	10	0.885	0.938	0.911	0.018
		Modern	18	0.845	0.895	0.877	0.013
On.Ar (μm^2)	Rib	Medieval	53	11270.171	82811.746	29541.297	11582.575
		Modern	18	15035.562	26510.242	19779.385	3405.972
	Anterior Femur	Medieval	10	24310.345	50365.854	31645.671	8409.016
		Modern	18	26170.213	57.525.000	38280.393	9229.172
Ct.Po (%)	Rib	Medieval	53	0.369	10.480	3.321	2.206
		Modern	18	0.272	8.270	2.582	2.275
	Anterior Femur	Medieval	10	16.519	26.978	22.524	3.906
		Modern	18	12.348	42.051	28.974	8.137
Po.Ar (mm^2)	Rib	Medieval	53	0.004	0.061	0.022	0.012
		Modern	18	0.008	0.042	0.020	0.009
	Anterior Femur	Medieval	10	0.024	0.050	0.032	0.008
		Modern	18	0.026	0.058	0.038	0.009
%Ct.Ar (%)	Rib	Medieval	20	20.989	62.378	40.033	11.722
		Modern	11	15.807	44.948	30.579	10.092

OPD was higher in the modern individuals across the anterior femur (medieval *m* = 12.880/mm^2; modern *m* = 15.579/mm^2) and rib (medieval *m* = 9.040/mm^2; modern *m* =

14.550/mm^2) (Table 6.21; Figure 6.6A). On.Circ was higher in the medieval individuals across the anterior femur (medieval *m* = 0.911; modern *m* = 0.877) and rib (medieval *m* = 0.919; modern *m* = 0.902) (Table 6.21; Figure 6.6B). On.Ar in the anterior femur was higher among modern individuals (medieval *m* = 31,645.671 μm^2; modern *m* = 38,280.393 μm^2), but in the rib On.Ar was higher among medieval individuals (medieval *m* = 29541.297 μm^2; modern *m* = 19,779.385. μm^2) (Table 6.21; Figure 6.6C). Ct.Po was higher among the modern individuals in the anterior femur (medieval *m* = 22.524%; modern *m* = 28.974%), but was higher among medieval individuals in the rib (medieval *m* = 3.321%; modern *m* = 2.582%) (Table 6.21; Figure 6.6D). Po.Ar was higher in the modern individuals in the anterior femur (medieval *m* = 0.032 mm^2; modern *m* = 0.038 mm^2) but higher in the medieval individuals in the rib (medieval *m* = 0.022 mm^2; modern *m* = 0.020 mm^2) (Table 6.21; Figure 6.6E). Rib %Ct.Ar was higher in medieval individuals (medieval *m* = 40.033%; modern *m* = 30.579%) (Table 6.21; Figure 6.6F).

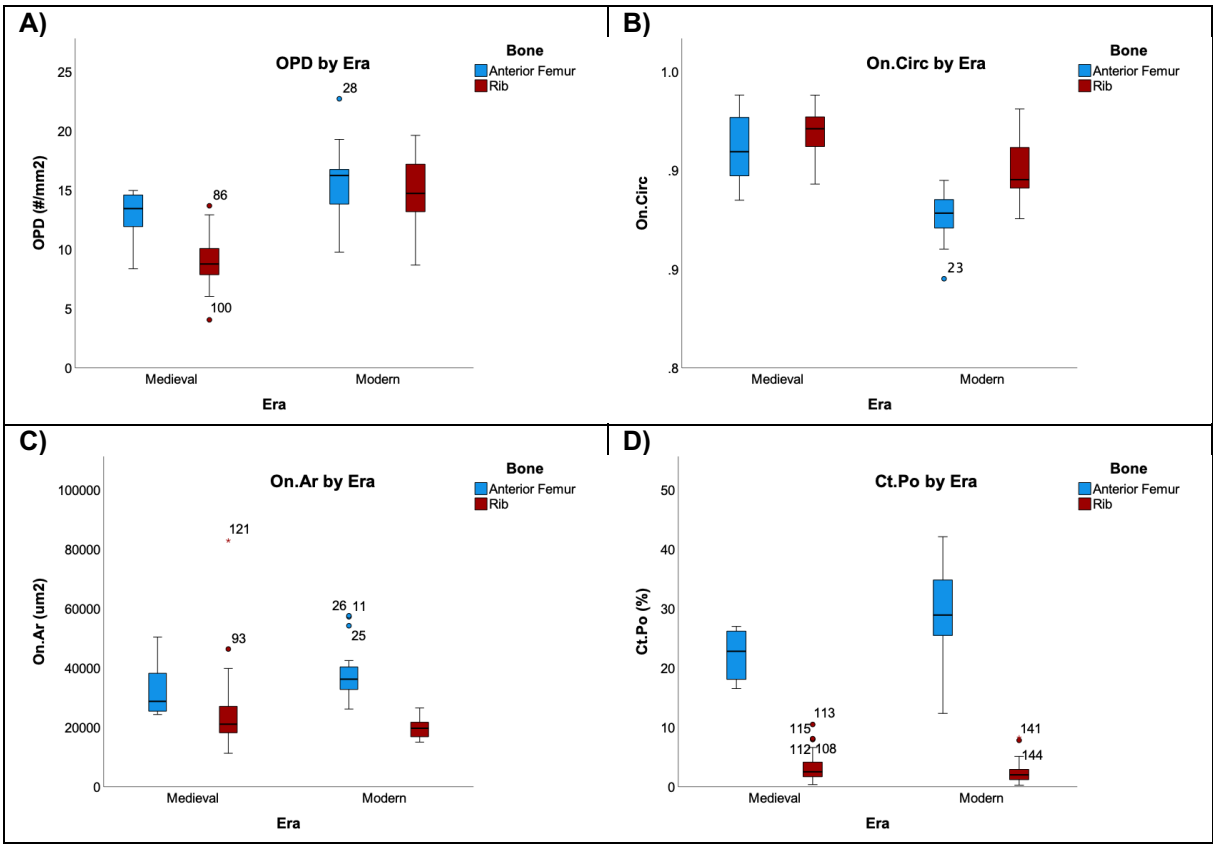

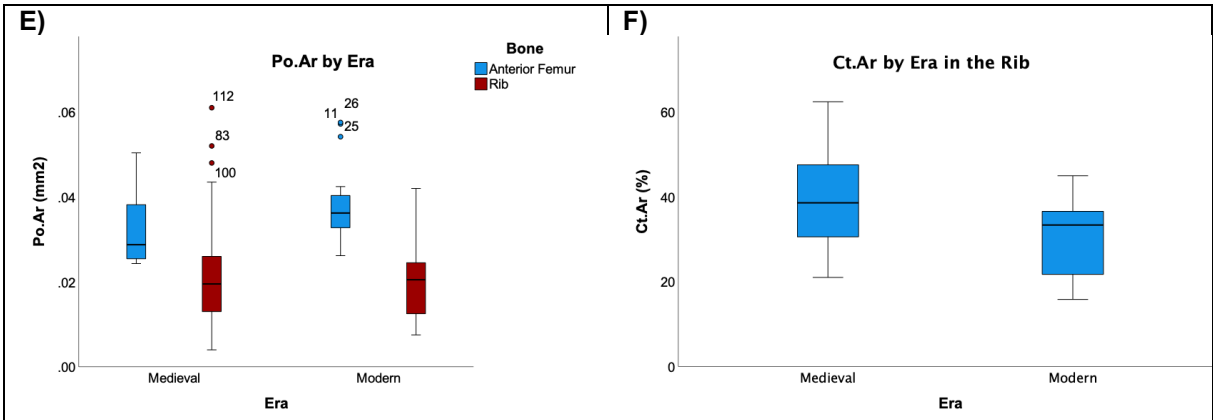

Figure 6.6: Boxplots of key era variables.

A) Osteon population density (OPD) by era. **B)** Mean osteon circularity (On.Circ) by era. **C)** Osteon area (On.Ar) by era. **D)** Cortical porosity (Ct.Po) by era. **E)** Porosity area (Po.Ar) by era. **F)** Cortical area (Ct.Ar) by era.

6.4.2 Inferential Statistics

There was significant difference in OPD between medieval and modern individuals, as observed in both the rib (U = 67.000; z = -5.419, p <0.001) and anterior femur (U = 42.500; z = -2.279, p = 0.023), with modern individuals having statistically significantly higher OPD than the medieval individuals (Table 6.22). On.Circ was also significantly different between medieval and modern individuals in both the rib (U = 175.000; z = -3.993, p <0.001) and anterior femur (U = 6.000; z = -4.027, p <0.001), with the medieval individuals having statistically significantly higher On.Circ than the modern individuals. There was a statistically significant difference in On.Ar between medieval and modern individuals in the anterior femur (U = 47.000; z = -2.062, p = 0.039), with higher On.Ar in the modern individuals than the medieval individuals. %Ct.Ar, Ct.Po and Po.Ar were not statistically significantly different between medieval and modern individuals in the rib, but Ct.Po (U = 38.000; z = -2.493, p = 0.013) and Po.Ar (U = 47.000; z = -2.062, p = 0.039) were significantly different between medieval and modern individuals in the anterior femur, with both Ct.Po and Po.Ar being higher in modern individuals than the medieval individuals (Table 6.22).

Table 6.22: Medieval to Modern bone differences (Mann-Whitney U).

Variable	Bone	Era	*n.* Individuals	Mean Rank	Mann-Whitney *U*	*z*-value	*p*-value
OPD	Rib	Medieval	53	28.26	67.000	-5.419	**<0.001****
		Modern	18	58.78			
	Anterior Femur	Medieval	10	9.75	42.500	-2.279	**0.023***
		Modern	18	17.14			
On.Circ	Rib	Medieval	53	41.70	175.000	-3.993	**<0.001****
		Modern	18	19.22			
	Anterior Femur	Medieval	10	22.90	6.000	-4.027	**<0.001****
		Modern	18	9.83			
On.Ar	Rib	Medieval	53	38.28	356.000	-1.599	0.110
		Modern	18	29.28			
	Anterior Femur	Medieval	10	10.20	47.000	-2.062	**0.039***
		Modern	18	16.89			
Po.Ar	Rib	Medieval	53	36.09	472.000	-0.066	0.947
		Modern	18	35.72			
	Anterior Femur	Medieval	10	10.20	47.000	-2.062	**0.039***
		Modern	18	16.89			
Ct.Po	Rib	Medieval	53	38.25	358.000	-1.573	0.116
		Modern	18	29.39			
	Anterior Femur	Medieval	10	9.30	38.000	-2.493	**0.013***
		Modern	18	17.39			
%Ct.Ar	Rib	Medieval	20	18.20	66.000	-1.817	0.069
		Modern	11	12.00			

* Significance values have been adjusted by the Bonferroni Correction for multiple tests.

Once data were corrected by stature to account for individual body size variation, the results of the Mann-Whitney *U* tests differed (Table 6.23). OPD was significantly higher in modern individuals in the rib (U = 59.000; z = -4.950, p <0.001). On.Circ was significantly higher in the medieval individuals in the anterior femur (U = 18.000; z = -2.771, p = 0.007). There were statistically significant differences between medieval and modern On.Ar in the anterior femur (U = 26.000; z = -2.195, p = 0.028), with higher values in the modern individuals. Po.Ar was similar, with significant differences between medieval and modern individuals in the anterior femur (U = 26.000; z = -2.195, p = 0.028), with higher values in the modern individuals. Rib Ct.Po was significantly different between medieval and modern individuals (U = 254.000; z = -1.966, p = 0.049) with values suggesting a statistically significantly higher percent of porosity area in the rib cortical bone in medieval individuals than the modern. %Ct.Ar could only be measured in the rib, but there were no significant differences between the medieval and modern groups (Table 6.23).

Table 6.23: Medieval to Modern bone differences (Mann-Whitney U): Corrected by stature.

Variable	Bone	Era	*n.* Individuals	Mean Rank	Mann-Whitney *U*	*z*-value	*p*-value
OPD	Rib	Medieval	51	27.16	59.000	-4.950	**<0.001****
		Modern	15	55.07			
	Anterior Femur	Medieval	8	9.25	38.000	-1.420	0.156
		Modern	15	13.47			
On.Circ	Rib	Medieval	51	33.73	371.000	-0.176	0.860
		Modern	15	32.73			
	Anterior Femur	Medieval	8	17.25	18.000	-2.711	**0.007***
		Modern	15	9.20			
On.Ar	Rib	Medieval	51	35.22	295.000	-1.339	0.181
		Modern	15	27.67			
	Anterior Femur	Medieval	8	7.75	26.000	-2.195	**0.028***
		Modern	15	14.27			
Po.Ar	Rib	Medieval	51	33.67	374.000	-0.130	0.897
		Modern	15	32.93			
	Anterior Femur	Medieval	8	7.75	26.000	-2.195	**0.028***
		Modern	15	14.27			
Ct.Po	Rib	Medieval	51	36.02	254.000	-1.966	**0.049***
		Modern	15	24.93			
	Anterior Femur	Medieval	8	8.75	34.000	-1.678	0.093
		Modern	15	13.73			
%Ct.Ar	Rib	Medieval	20	16.55	59.000	-1.461	0.144
		Modern	9	11.56			

* Significance values have been adjusted by the Bonferroni Correction for multiple tests.

6.4.3 Multivariate Statistics

Four discriminant function analyses (DFAs) were performed with the era (medieval or modern) as the dependent variable (Table 6.24 – 6.27). DFAs were run to discriminate medieval from modern contemporary data from the rib (Table 6.24). Linearity, normality, multicollinearity, and singularity assumptions were met for each DFA. Predictor variables included OPD, On.Circ, On.Ar, Po.Ar and Ct.Po for the entire sample ($n = 71$). The assumption of homogeneity for the variance-covariance matrices was met ($p = 0.056$). One significant discriminant function was calculated, with 91.5% successful classification.

Predictor variables included OPD, On.Circ, On.Ar, Po.Ar and Ct.Po for the OA sub-group ($n = 21$). The assumption of homogeneity for the variance-covariance matrices was not met ($p < 0.001$), with cases classified based on separate covariance matrices. One significant discriminant function was calculated with 90.5% successful classification.

Predictor variables included OPD, On.Circ, On.Ar, Po.Ar and Ct.Po for the male sub-group ($n = 45$). The assumption of homogeneity for the variance-covariance matrices was met ($p =$

0.296). One significant discriminant function was calculated, with 91.1% successful classification.

Predictor variables included OPD, On.Circ, On.Ar, Po.Ar and Ct.Po for the female sub-group ($n = 32$). The assumption of homogeneity for the variance-covariance matrices was not met ($p < 0.001$), with cases classified based on separate covariance matrices. One significant discriminant function was calculated, with 96.9% successful classification.

Table 6.24: Medieval to Modern bone: Discriminant Function Analysis of the Rib.

Sub-group		Predictor Variables	*n.*	Eigen-value	Canonical Correlation	Function Chi-square	*p*-value	Loading matrix	Classification
Entire Sample		OPD On.Circ On.Ar Po.Ar Ct.Po	71	1.887	0.808	70.512	**<0.001*** **	0.709 -0.471 -0.150 -0.009 -0.153	91.5%
By Age-At-Death	OA	OPD On.Circ On.Ar Po.Ar Ct.Po	21	3.349	0.878	24.255	**<0.001*** **	0.521 -0.283 -0.143 0.207 -0.193	90.5%
By Sex	M	OPD On.Circ On.Ar Po.Ar Ct.Po	45	2.518	0.846	50.948	**<0.001*** **	0.676 -0.436 -0.034 -0.008 -0.099	91.1%
	F	OPD On.Circ On.Ar Po.Ar Ct.Po	32	1.348	0.758	23.469	**<0.001*** **	-0.825 0.442 0.160 0.038 0.304	96.9%

* Significance values have been adjusted by the Bonferroni Correction for multiple tests.

DFAs were run to discriminate medieval from modern contemporary data from the anterior femur (Table 6.25). Linearity, normality, multicollinearity, or singularity assumptions were met for each DFA. Predictor variables included OPD, On.Circ, On.Ar, Po.Ar and Ct.Po for the entire sample ($n = 28$). The assumption of homogeneity for the variance-covariance matrices was met ($p = 0.306$). The Po.Ar variable failed the tolerance test ($p < 0.001$) and so was removed from analysis. One significant discriminant function was calculated, with 92.9% successful classification.

Predictor variables included OPD, On.Circ, On.Ar, Po.Ar and Ct.Po for the OA sub-group ($n = 20$). The assumption of homogeneity for the variance-covariance matrices was not met

($p \leq 0.000$), with cases classified based on separate covariance matrices. The Po.Ar variable failed the tolerance test ($p < 0.001$) and was removed from analysis. One significant discriminant function was calculated, with 90.0% successful classification.

Predictor variables included OPD, On.Circ, On.Ar, Po.Ar and Ct.Po for the male sub-group ($n = 21$). The assumption of homogeneity for the variance-covariance matrices was not met ($p \leq 0.000$), with cases classified based on separate covariance matrices. The Po.Ar variable failed the tolerance test ($p<0.001$) and so was removed from analysis. One significant discriminant function was calculated, with 100.0% successful classification.

Table 6.25: Medieval to Modern bone: Discriminant Function Analysis of the Anterior Femur.

Sub-Group	Predictor Variables	*n.*	Eigen-value	Canonical Correlation	Function Chi-Square	*p*-value	Loading Matrix	Classification
Entire Sample	OPD	28	1.886	0.808	25.435	**<0.001*** **	0.341	92.9%
	On.Circ						-0.832	
	On.Ar						0.305	
	Po.Ar	*Not included in analysis				* Failed tolerance test <0.001		
	Ct.Po						0.289	
By Age-At-Death OA	OPD	20	0.600	0.612	7.523	0.111	0.200	90.0%
	On.Circ						-0.822	
	On.Ar						0.262	
	Po.Ar	*Not included in analysis				*Failed tolerance test <0.001		
	Ct.Po						0.133	
By Sex M	OPD	21	4.068	0.896	27.591	**<0.001*** **	0.314	100.0%
	On.Circ						-0.804	
	On.Ar						0.291	
	Po.Ar	*Not included in analysis				*Failed tolerance test <0.001		
	Ct.Po						0.384	

* Significance values have been adjusted by the Bonferroni Correction for multiple tests.

DFAs were run to discriminate medieval from modern contemporary data from the rib after controlling for individual body size differences using the stature measurement (Table 6.26). Linearity, normality, multicollinearity, or singularity assumptions were met for each DFA. Predictor variables included OPD, On.Circ, On.Ar, Po.Ar and Ct.Po for the entire sample ($n = 66$). The assumption of homogeneity for the variance-covariance matrices was met ($p = 0.272$). One significant discriminant function was calculated, with 87.9% successful classification.

Predictor variables included OPD, On.Circ, On.Ar, Po.Ar and Ct.Po for the OA sub-group ($n = 18$). The assumption of homogeneity for the variance-covariance matrices was not met ($p <0.001$), with cases classified based on separate covariance matrices. One significant discriminant function was calculated, with 94.4% successful classification.

Predictor variables included OPD, On.Circ, On.Ar, Po.Ar and Ct.Po for the male sub-group (n = 40). The assumption of homogeneity for the variance-covariance matrices was met (p = 0.731). One significant discriminant function was calculated, with 82.5% successful classification.

Predictor variables included OPD, On.Circ, On.Ar, Po.Ar and Ct.Po for the female sub-group (n = 32). The assumption of homogeneity for the variance-covariance matrices was not met (p <0.001), with cases classified based on separate covariance matrices. One significant discriminant function was calculated, with 93.8% successful classification.

Table 6.26: Medieval to Modern bone: Discriminant Function Analysis of the Rib: Corrected by Stature.

Sub-group		Predictor Variables	*n.*	Eigen-value	Canonical Correlation	Function Chi-square	*p*-value	Loading matrix	Classification
Entire Sample		OPD On.Circ On.Ar Po.Ar Ct.Po	66	1.151	0.731	47.102	**<0.001*** **	0.887 -0.017 -0.156 -0.007 -0.239	87.9%
By Age-At-Death	OA	OPD On.Circ On.Ar Po.Ar Ct.Po	18	3.200	0.873	19.374	**0.002** **	0.517 -0.230 -0.167 0.202 -0.235	94.4%
By Sex	M	OPD On.Circ On.Ar Po.Ar Ct.Po	40	1.297	0.751	29.526	**<0.001*** **	0.858 -0.158 -0.017 -0.021 -0.203	82.5%
	F	OPD On.Circ On.Ar Po.Ar Ct.Po	32	1.198	0.738	21.657	**<0.001*** **	0.939 -0.081 -0.169 -0.039 -0.315	93.8%

* Significance values have been adjusted by the Bonferroni Correction for multiple tests.

DFAs were run to discriminate medieval from modern contemporary data from the anterior femur after controlling for individual body size differences using the stature measurement (Table 6.27). Linearity, normality, multicollinearity, or singularity assumptions were met for each DFA. Predictor variables included OPD, On.Circ, On.Ar, Po.Ar and Ct.Po for the entire sample (n = 23). The assumption of homogeneity for the variance-covariance matrices was not met (p = 0.042), with cases classified based on separate covariance matrices. The Po.Ar

variable failed the tolerance test (p <0.001) and was removed from analysis. One significant discriminant function was calculated, with 91.3% successful classification.

Predictor variables included OPD, On.Circ, On.Ar, Po.Ar and Ct.Po for the OA sub-group (n = 17). The assumption of homogeneity for the variance-covariance matrices was not met (p ≤0.000), with cases classified based on separate covariance matrices. The Po.Ar variable failed the tolerance test (p <0.001) and was removed from analysis. One significant discriminant function was calculated, with 82.4% successful classification.

Predictor variables included OPD, On.Circ, On.Ar, Po.Ar and Ct.Po for the male sub-group (n = 17). The female sub-group could not be run due to low case numbers (n = 5). The assumption of homogeneity for the variance-covariance matrices was met (p = 0.124). The Po.Ar variable failed the tolerance test (p<0.001) and was removed from analysis. One significant discriminant function was calculated, with 94.1% successful classification.

Table 6.27: Medieval to Modern bone: Discriminant Function Analysis of the Anterior Femur: Corrected by Stature.

Sub-Group	Predictor Variables	*n.*	Eigen-value	Canonical Correlation	Function Chi-Square	*p*-value	Loading Matrix	Classification
Entire Sample	OPD	23	2.184	0.828	22.003	**<0.001*** **	0.200	91.3%
	On.Circ						-0.476	
	On.Ar						0.342	
	Po.Ar	*Not included in analysis				* Failed tolerance test <0.001		
	Ct.Po						0.182	
By Age-At-Death OA	OPD	17	0.529	0.588	5.518	0.238	0.131	82.4%
	On.Circ						-0.374	
	On.Ar						0.312	
	Po.Ar	*Not included in analysis				*Failed tolerance test <0.001		
	Ct.Po						0.097	
By Sex M	OPD	17	5.442	0.919	24.217	**<0.001*** **	0.211	94.1%
	On.Circ						-0.434	
	On.Ar						0.205	
	Po.Ar	*Not included in analysis				*Failed tolerance test <0.001		
	Ct.Po						0.246	

* Significance values have been adjusted by the Bonferroni Correction for multiple tests.

6.4.4 Hypotheses Results

$H0_a$: Each of the observed variables, OPD, On.Circ, On.Ar, %Ct.Ar, Po.Ar and Ct.Po have a similar distribution between medieval and contemporary era individuals.

Before correcting for individual stature variation, contemporary individuals had statistically significantly higher OPD than medieval individuals at both the rib and anterior femur (U = 42.500; z = -2.279, p = 0.023 (Table 6.22). Medieval individuals had statistically significantly higher On.Circ than contemporary individuals in the rib and anterior femur (Table 6.22). On.Ar was statistically significantly higher in the contemporary group than medieval group in the anterior femur (Table 6.22). %Ct.Ar, Ct.Po and Po.Ar were not statistically significantly different between medieval and contemporary individuals in the rib, but Ct.Po and Po.Ar were both statistically significantly higher in the contemporary individuals than medieval in the anterior femur (Table 6.22).

Once data were corrected to account for individual stature variation, OPD was statistically significantly higher in contemporary individuals in the rib (Table 6.23). On.Circ was statistically significantly higher in the medieval group in the anterior femur (Table 6.23). There were statistically significantly higher On.Ar and Po.Ar in the anterior femur of contemporary individuals (Table 6.23). Rib Ct.Po was statistically significantly higher in medieval individuals than contemporary (Table 6.23). Rib %Ct.Ar was not statistically significantly different between the medieval and contemporary groups (Table 6.23).

These results confirm the rejection of the null hypothesis as there were statistically significant group differences between the medieval and contemporary individuals in almost all variables measured.

$H0_b$: Medieval and modern ribs and anterior femora cannot be separated using discriminant function analysis (DFA), based on the variables OPD, On.Circ, On.Ar, Po.Ar and Ct.Po.

Medieval and modern ribs and anterior femora were successfully separated using DFA, based upon the targeted variables. Medieval and modern ribs could be successfully classified in 91.5% of cases, and when delving into demographic sub-groups, the OA AAD category classification success rate was 90.5%, while the male sub-group was 91.1% and female sub-group was 96.9%. Medieval and modern anterior femora could only be successfully separated by DFA after the removal of Po.Ar which failed the tolerance test (p <0.001). After this, the entire sample could be successfully classified in 92.9% of instances, while the OA AAD category rate was 90.0% and the male sub-group was 100.0%.

After correcting raw values for variation in individual body size using stature measurements, the classification rate for the rib entire sample was 87.9%, OA AAD category sub-group the rate was 94.4%, male sub-group was 82.5% and female sub-group was 93.8%. For the anterior

femur, Po.Ar again failed the tolerance test ($p < 0.001$) and was removed. After this the entire sample could be correctly classified in 91.3% of instances, the OA AAD category sub-group rate was 82.4% and the male sub-group was 94.1%.

These results reject the null hypothesis as medieval and modern ribs and anterior femora were able to be separated using discriminant function analysis (DFA), based on these targeted variables.

$H0_c$: There is no evidence of a more sedentary lifestyle influencing modern individuals as compared to medieval individuals in either observed variable; OPD, On.Circ, On.Ar, %Ct.Ar, Po.Ar and Ct.Po.

If the modern individuals showed evidence for a more sedentary lifestyle influencing their bone microstructures, you would expect to see lower OPD and %Ct.Ar, and an increase in On.Circ, On.Ar, Po.Ar and Ct.Po in the modern sub-group.

Instead, there is a statistically significant increase in OPD in the modern individuals in the rib (Table 6.23), and a non-statistically significant trend in the same direction in the anterior femur (Table 6.22). Additionally, there is a statistically significant decrease in On.Circ in the modern group in the anterior femur (Table 6.23), and a non-statistically significant trend in the same direction in the rib (Table 6.22). Ct.Po was statistically significantly lower in modern individuals in the rib (Table 6.23), but there was a non-significant trend towards higher Ct.Po in the modern group in the anterior femur (Table 6.22).

However, there is a statistically significant increase in On.Ar in the modern group in the anterior femur (Table 6.23), but a non-significant trend towards smaller On.Ar in the modern group in the rib (Table 6.22; 6.23). Similarly, there is a statistically significant increase in Po.Ar in modern individuals in the anterior femur (Table 6.23), but a non-significant trend towards smaller Po.Ar in the modern group in the rib (Table 6.22; 6.23). Rib %Ct.Ar was lower, but not statistically significantly so in the modern individuals (Table 6.22; 6.23).

These results suggest that there are some indications that a more sedentary lifestyle in modern individuals may be influencing some bone microstructural variables, such as On.Ar and Po.Ar, but with differing extent between the rib and anterior femur. Additionally, there are statistically significant differences between medieval and modern groups in OPD, On.Circ and Ct.Po that are not generally expected with a sedentary lifestyle. These results reject the null hypothesis

as they are not all in agreement with expected evidence of a more sedentary lifestyle in modern individuals compared to the medieval group.

6.5 Research Question 3

Is there variation in standardised histological variables between serial cross-sections from the human rib midshaft?

6.5.1 Descriptive Trends

There are two hypotheses to test in order to addresses this research question. The first, tests whether there is a relationship between either targeted variable between the paired serial histological sections of the rib, taken 1cm apart in the rib shaft. The second hypothesis tests if there are group differences between the first and second paired serial histological rib section. Therefore, the null hypotheses for research question 3 are as follows:

$H0_a$: There is no monotonic relationship in either observed variable; Ct.Ar, Ct.Wi, Ct.ArA, Po.Ar, On.Ar, H.Ar, Ct.Po, OPD, Fg.OPD and On.Circ between paired serial histological sections of the rib, approximately 1cm apart in the rib shaft.

H0b: Each of the observed variables; Ct.Ar, Ct.Wi, Ct.ArA, Po.Ar, On.Ar, H.Ar, Ct.Po, OPD, Fg.OPD and On.Circ have a similar distribution between paired serial histological sections of the rib, approximately 1cm apart in the rib shaft.

Variables observed to assess variation between serial rib sections included Ct.Ar, Ct.Wi, Ct.ArA, Po.Ar, On.Ar, Ct.Po, H.Ar, OPD, Fg.OPD and On.Circ.

Table 6.28: Descriptive statistics for all variables observed in research question 3.

Variable	Slide #	*n*.	Min.	Max.	Mean	St.D.
Ct.Ar (mm^2)	Slide 1	48	7.788	43.814	18.793	8.227
	Slide 2	48	6.194	44.946	18.852	8.440
Ct.Wi (mm)	Slide 1	15	0.316	1.206	0.656	0.302
	Slide 2	21	0.360	1.662	0.803	0.312
Ct.ArA (mm^2)	Slide 1	48	7.406	43.128	18.266	8.093
	Slide 2	48	6.194	43.776	18.265	8.251
Po.Ar (mm^2)	Slide 1	48	0.005	0.052	0.018	0.011
	Slide 2	48	0.008	0.091	0.027	0.017
On.Ar (μm^2)	Slide 1	48	11933.318	138179.065	24386.494	19017.569
	Slide 2	48	0.916	55412.091	21848.470	8044.274
Ct.Po (%)	Slide 1	48	0.326	11.200	2.937	2.303
	Slide 2	48	0.217	9.759	3.177	2.307
H.Ar (μm^2)	Slide 1	48	860.955	9494.747	2065.780	1356.914
	Slide 2	48	907.842	4759.323	1880.291	791.712

OPD (#/mm²)	Slide 1	48	6.371	20.344	11.218	3.709
	Slide 2	48	5.851	20.060	10.690	3.266
Fg.OPD (#/mm²)	Slide 1	48	1.500	9.117	4.178	1.953
	Slide 2	48	1.027	9.366	3.862	1.761
On.Circ	Slide 1	48	0.873	0.936	0.912	0.017
	Slide 2	48	0.874	0.938	0.914	0.017

Scatterplots were created to visualise descriptive trends between each variable from serial rib sections (Figure 6.7A-J). The strongest relationships between paired rib section seriations were in Ct.Ar (Figure 6.7A), Ct.Wi (Figure 6.7B), Ct.ArA (Figure 6.7C) and OPD (Figure 6.7H). Very weak correlations between paired rib section seriations were identified in Po.Ar (Figure 6.7D), On.Ar (Figure 6.7E) and H.Ar (Figure 6.7F). Medium correlations between paired rib section seriations were identified in Ct.Po (Figure 6.7G), Fg.OPD (Figure 6.7I) and On.Circ (Figure 6.7J).

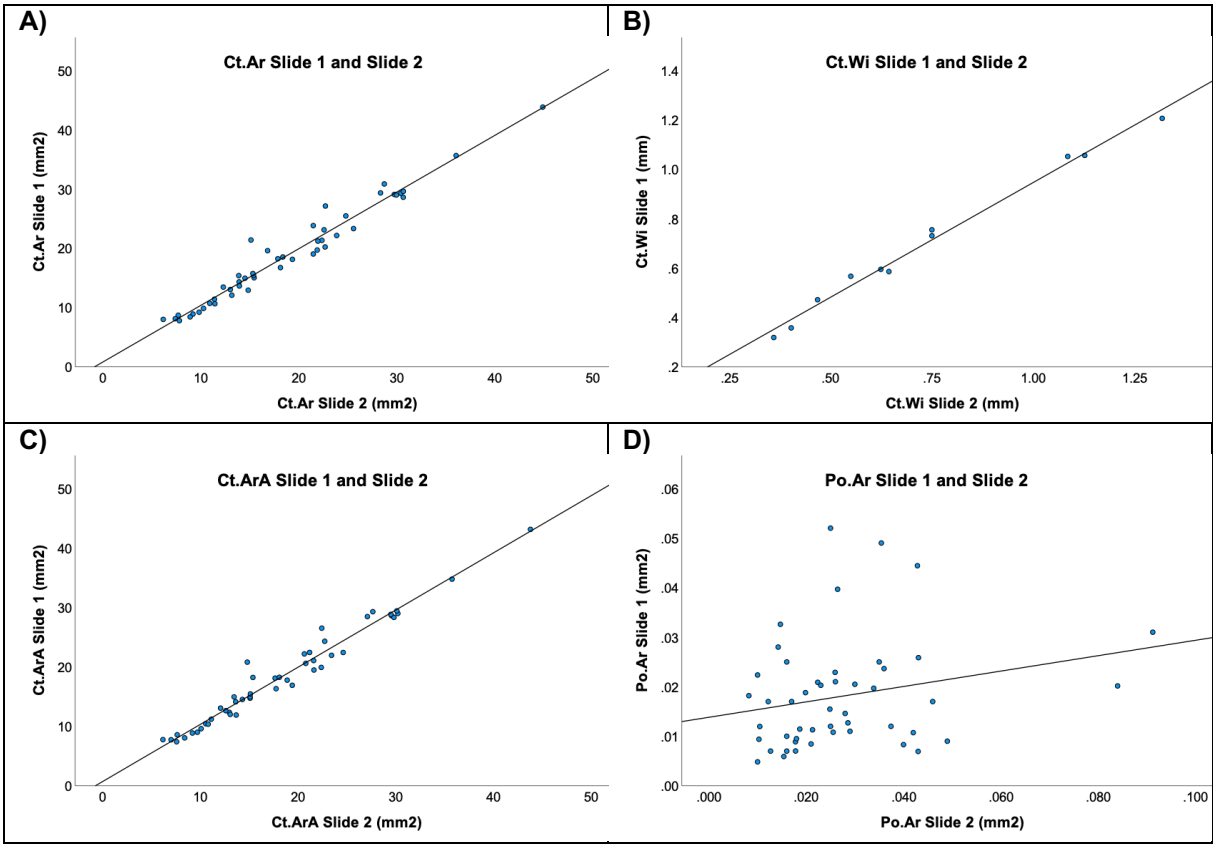

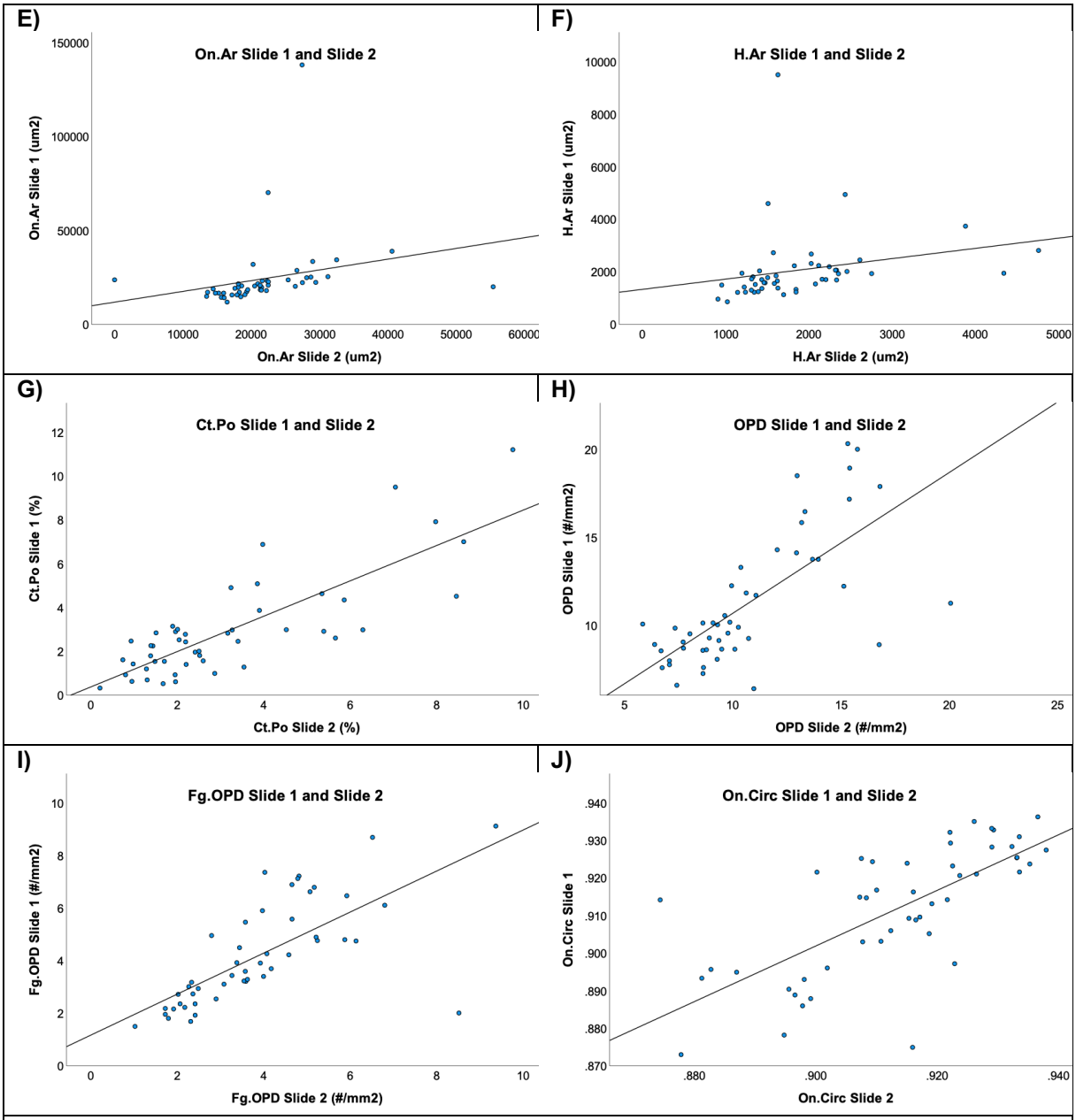

Figure 6.7: Scatterplots of standard rib histology variables.

A) Cortical area (Ct.Ar) of rib slide 1 by Ct.Ar of rib slide 2. **B)** Cortical width (Ct.Wi) of rib slide 1 by Ct.Wi of rib slide 2. **C)** Absolute cortical area (Ct.ArA) of rib slide 1 by Ct.ArA of rib slide 2. **D)** Porosity area (Po.Ar) of rib slide 1 by Po.Ar of rib slide 2. **E)** Osteon area (On.Ar) of rib slide 1 by On.Ar of rib slide 2. **F)** Haversian canal area (H.Ar) of rib slide 1 by H.Ar of rib slide 2. **G)** Cortical porosity area (Ct.Po) of rib slide 1 by Ct.Po of rib slide 2. **H)** Osteon population density (OPD) of rib slide 1 by OPD of rib slide 2. **I)** Fragmentary OPD (Fg.OPD) of rib slide 1 by Fg.OPD of rib slide 2. **J)** Osteon circularity (On.Circ) of rib slide 1 by On.Circ of rib slide 2.

6.5.2 Inferential Statistics

The Spearman's *Rho* results identified statistically significant strong relationships between almost all observed variables in serial rib sections from the same individuals. This included both cross-sectional geometry variables, Ct.Ar (*rho* = 0.971, rho^2 = 0.943, *p* <0.001), Ct.Wi (*rho* = 0.989, rho^2 = 0.978, *p* <0.001), Ct.ArA (*rho* = 0.975, rho^2 = 0.951, *p* <0.001) and Ct.Po (*rho* = 0.731, rho^2 = 0.534, *p* <0.001), and microstructural variables, On.Ar (*rho* = 0.722, rho^2 = 0.521, *p* <0.001), H.Ar (*rho* = 0.595, rho^2 = 0.354, *p* <0.001), OPD (*rho* = 0.718, rho^2 = 0.516, *p* <0.001), Fg.OPD (*rho* = 0.785, rho^2 = 0.616, *p* <0.001) and On.Circ (*rho* = 0.755, rho^2 = 0.570, *p* <0.001). However, there was no correlation between Po.Ar between the serial pairs of rib sections (*rho* = 0.246, rho^2 = 0.061, *p* = 0.092). Much of the variation between paired serial rib sections of Ct.Ar (94.3%), Ct.Wi (97.8%) and Ct.ArA (95.1%) can be explained by the relationship with paired values in the paired rib section. However, the lower rho^2 scores of other variables suggest that other factors are influencing these variables differently between the serial rib sections (Table 6.29).

Table 6.29: Serial rib differences (Spearman's Rho).

Variable	No. of Individuals	Spearman's *Rho*	Spearman's Rho^2	*p*-value
Ct.Ar	48	0.971	0.943	**<0.001****
Ct.Wi	11	0.989	0.978	**<0.001****
Ct.ArA	48	0.975	0.951	**<0.001****
Po.Ar	48	0.246	0.061	0.092
Ct.Po	48	0.731	0.534	**<0.001****
On.Ar	48	0.722	0.521	**<0.001****
H.Ar	48	0.595	0.354	**<0.001****
OPD	48	0.718	0.516	**<0.001****
Fg.OPD	48	0.785	0.616	**<0.001****
On.Circ	48	0.755	0.570	**<0.001****

* Significance values have been adjusted by the Bonferroni Correction for multiple tests.

Wilcoxon Signed Rank test results revealed several statistically significant differences between serial rib slides. Ct.Wi was statistically significantly different between serial pairs of rib histological slides (60.000, *p* = 0.016). This contradicts the results of the Spearman's *Rho* whereby Ct.Wi had a significant correlation between paired rib seriations (*rho* = 0.989, *p*<0.001). Po.Ar was statistically significantly different between serial sections (878.500, *p*<0.001), but this reinforces the results of the Spearman's *Rho*, which showed no correlation between paired rib sections (*rho* = 0.246, *p* = 0.092). OPD was statistically significantly different between serial sections (364.000, *p* = 0.022), which may complement the Spearman's *Rho* results when you consider the low r^2 score (*rho* = 0.719, r^2 = 0.516, *p*<0.001). Similarly, Fg.OPD was statistically significantly different between serial sections (393.000, *p* = 0.045),

which may complement the results of the Spearman's *Rho* results given the low r^2 score (*rho* = 0.785, r^2 = 0.616, p<0.001) (Table 6.30).

Table 6.30: Serial rib differences: Wilcoxon signed rank test results.

Variable	Slide #	*n*. Individuals	Test Statistic	*p*-value
Ct.Ar	1 2	48 48	670.000	0.262
Ct.Wi	1 2	11 11	60.000	**0.016***
Ct.ArA	1 2	48 48	658.000	0.473
Po.Ar	1 2	48 48	878.500	**<0.001*****
Ct.Po	1 2	48 48	681.000	0.340
On.Ar	1 2	48 48	656.000	0.486
H.Ar	1 2	48 48	579.000	0.926
OPD	1 2	48 48	364.000	**0.022***
Fg.OPD	1 2	48 48	393.000	**0.045***
On.Circ	1 2	48 48	692.000	0.286

* Significance values have been adjusted by the Bonferroni Correction for multiple tests.

6.5.3 Hypothesis Results

$H0_a$: There is no monotonic relationship in either observed variable; Ct.Ar, Ct.Wi, Ct.ArA, Po.Ar, On.Ar, H.Ar, Ct.Po, OPD, Fg.OPD and On.Circ between paired serial histological sections of the rib, approximately 1cm apart in the rib shaft.

The Spearman's Rho results identified statistically significant strong relationships between almost all observed variables between the pairs of serial rib sections. Cross-sectional geometry variables with statistically significant strong relationships included Ct.Ar, Ct.Wi, Ct.ArA and Ct.Po, and microstructural variables included On.Ar, H.Ar, OPD, Fg.OPD and On.Circ. The only variable which had no monotonic relationship between the paired serial rib sections was Po.Ar. Further, the majority of the variation between paired serial rib sections of Ct.Ar, Ct.Wi and Ct.ArA can be explained by the relationship with paired values in the paired rib section. However, the lower rho2 scores of other variables, such as Ct.Po, On.Ar, H.Ar, OPD and On.Circ, suggest that other factors are also influencing these variables between one serial rib section and its pair (Table 6.29).

These results suggest that some microstructural variables, particularly porosity, osteon and Haversian canal densities, can change vary between sections. However, variables such as Ct.Ar, Ct.Po, On.Ar, H.Ar and On.Circ may not significantly vary between sections up to 1cm apart along the rib shaft. With several monotonic relationships identified via Spearman's rho testing, the null hypothesis can be rejected.

$H0_b$: Each of the observed variables; Ct.Ar, Ct.Wi, Ct.ArA, Po.Ar, On.Ar, H.Ar, Ct.Po, OPD, Fg.OPD and On.Circ have a similar distribution between paired serial histological sections of the rib, approximately 1cm apart in the rib shaft.

Wilcoxon Signed Rank test results revealed several statistically significant differences between serial rib slide groups 1 and 2. Ct.Wi was statistically significantly different between groups and this contradicted the results of the Spearman's *Rho* whereby Ct.Wi had a significant correlation between paired serial rib sections. Po.Ar was statistically significantly different between serial section groups 1 and 2, but this reinforced the results of the Spearman's *Rho*, which showed no statistically significant correlation between paired rib sections. OPD was statistically significantly different between serial section groups 1 and 2, which may complement the Spearman's *Rho* results when you consider the low r^2 score suggesting additional factors impacting upon this variable outside of the sections pair. Similarly, Fg.OPD was statistically significantly different between serial sections, which may complement the results of the Spearman's *Rho* given the low r^2 score.

These results reject the null hypothesis as there are several statistically significant differences between slide 1 and slide 2 groups.

6.6 Research Question 4

Does cortical bone histology vary between bones of different levels of metabolic activity, such as the femur and the rib?

6.6.1 Descriptive Trends

There are three key steps, and thus three hypotheses to test in order to address this research question. The first tests if osteon and Haversian canal size variables, On.Ar, H.Ar, On.Dm, H.Dm, On.Pm and H.Pm are different between the rib and femur. The second tests if osteon and Haversian canal shape variables, On.Circ, H.Circ, On.Rd, H.Rd, On.AsRa, H.AsRa, On.Sd and H.Sd, are different between the rib and femur. The third hypothesis tests if there are

differences in osteon and Haversian canal growth rates between the rib and femur. Therefore, the null hypotheses for research question 4 are as follows:

$H0_a$: Each of the observed osteon and Haversian canal size variables, On.Ar, H.Ar, On.Dm, H.Dm, On.Pm and H.Pm, have a similar distribution across the rib and the femur.

$H0_b$: There is no difference in the osteon and Haversian canal shape variables, On.Circ, H.Circ, On.Rd, H.Rd, On.AsRa, H.AsRa, On.Sd and H.Sd between the rib and the femur.

$H0_c$: There is no difference in the osteon and Haversian canal growth rates, (1) between osteons and Haversian canals, and (2) between the rib and the femur.

Variables observed to assess osteon and Haversian canal size, shape and rates of growth included On.Ar, H.Ar, On.Dm, H.Dm, On.Pm, H.Pm, On.Circ, H.Circ, On.Rd, H.Rd, On.AsRa, H.AsRa, On.Sd and H.Sd.

Table 6.31: Descriptive statistics for all variables observed in research question 4.

Variable	Bone	*n*.	Min.	Max.	Mean	St.D.
Size Variables						
On.Ar (μm^2)	Rib	71	11270.170	82811.750	22975.309	9663.777
	Anterior Femur	28	24310.350	57525.000	35910.849	9363.851
	Posterior Femur	53	13800.00	67904.760	35055.179	10317.359
H.Ar (μm^2)	Rib	71	881.96	5561.53	1906.994	798.064
	Anterior Femur	28	1309.920	7901.500	3194.852	1536.822
	Posterior Femur	53	1216.330	12541.430	3628.894	2412.230
On.Dm (μm)	Rib	71	137.030	264.080	190.347	24.018
	Anterior Femur	28	200.080	315.550	249.217	32.396
	Posterior Femur	53	161.940	337.240	239.034	33.633
H.Dm (μm)	Rib	71	39.520	80.420	53.158	7.428
	Anterior Femur	28	46.780	106.200	70.688	14.783
	Posterior Femur	53	42.820	125.130	73.301	20.182
On.Pm (μm)	Rib	71	381.710	714.040	522.081	66.352
	Anterior Femur	28	559.810	880.570	686.717	90.156
	Posterior Femur	53	430.160	943.430	661.091	93.469
H.Pm (μm)	Rib	71	108.270	209.290	144.017	19.521
	Anterior Femur	28	128.340	281.200	188.011	37.993
	Posterior Femur	53	121.080	333.640	197.592	52.677
Shape Variables						
On.Circ	Rib	71	0.876	0.938	0.915	0.014
	Anterior Femur	28	0.845	0.938	0.889	0.022
	Posterior Femur	53	0.818	0.969	0.914	0.021
H.Circ	Rib	71	0.852	0.926	0.893	0.016
	Anterior Femur	28	0.842	0.910	0.883	0.018
	Posterior Femur	53	0.854	0.932	0.891	0.015
On.Rd	Rib	71	0.667	0.798	0.748	0.030
	Anterior Femur	28	0.681	0.801	0.745	0.025
	Posterior Femur	53	0.692	0.971	0.761	0.039

H.Rd	Rib	71	0.668	0.816	0.751	0.028
	Anterior Femur	28	0.649	0.807	0.721	0.038
	Posterior Femur	53	0.668	0.918	0.747	0.045
On.AsRa	Rib	71	1.277	1.583	1.382	0.067
	Anterior Femur	28	1.271	1.545	1.391	0.055
	Posterior Femur	53	1.030	1.535	1.355	0.074
H.AsRa	Rib	71	1.246	1.607	1.388	0.069
	Anterior Femur	28	1.278	1.745	1.482	0.112
	Posterior Femur	53	1.089	1.658	1.402	0.107
On.Sd	Rib	71	0.989	1.066	0.996	0.009
	Anterior Femur	28	0.959	0.998	0.980	0.011
	Posterior Femur	53	0.950	1.000	0.992	0.008
H.Sd	Rib	71	0.997	1.000	0.999	0.001
	Anterior Femur	28	0.988	1.000	0.997	0.003
	Posterior Femur	53	0.989	1.000	0.998	0.002

The rib had the smallest values in all variables pertaining to osteon and Haversian canal size, including On.Ar (Figure 6.8A; anterior femur *m* = 35,910.849 μm^2; posterior femur *m* = 35,055.179 μm^2; rib *m* = 22,975.309 μm^2), H.Ar (Figure 6.8B; anterior femur *m* = 3,194.852 μm^2; posterior femur *m* = 3,628.984 μm^2; rib *m* = 1,906.994 μm^2), On.Dm (Figure 6.8C; anterior femur *m* = 249.217 μm; posterior femur *m* = 239.034 μm; rib *m* = 190.347 μm), H.Dm (Figure 6.8D; anterior femur *m* = 106.20 μm; posterior femur *m* = 73.301 μm; rib *m* = 53.158 μm), On.Pm (Figure 6.8E; anterior femur *m* = 686.717 μm; posterior femur *m* = 661.091 μm; rib *m* = 522.081 μm) and H.Pm (Figure 6.8F; anterior femur *m* = 188.011 μm; posterior femur *m* = 197.592 μm; rib *m* = 144.017 μm).

On.Circ was similar in the rib and posterior femur, and lower in the anterior femur (Figure 6.8G; anterior femur *m* = 0.889; posterior femur *m* = 0.914; rib *m* = 0.915). Similarly, H.Circ was similar in the rib and posterior femur, and lower in the anterior femur (Figure 6.8H; anterior femur *m* = 0.883; posterior femur *m* = 0.891; rib *m* = 0.893). On.Rd was the highest in the posterior femur and similar in the anterior femur and rib (Figure 6.8I; anterior femur *m* = 0.745; posterior femur *m* = 0.761; rib *m* = 0.748). H.Rd was the highest in the rib and lowest in the anterior femur (Figure 6.8J; anterior femur *m* = 0.721; posterior femur *m* = 0.747; rib *m* = 0.751). On.AsRa was similar in the anterior femur and rib, and lowest in the posterior femur (Figure 6.8K; anterior femur *m* = 1.391; posterior femur *m* = 1.355; rib *m* = 1.382). H.AsRa was highest in the anterior femur and lowest in the rib (Figure 6.8L; anterior femur *m* = 1.482; posterior femur *m* = 1.402; rib *m* = 1.388). On.Sd was highest in the rib and lowest in the anterior femur (Figure 6.8M; anterior femur *m* = 0.980; posterior femur *m* = 0.992; rib *m* = 0.996). H.Sd was also highest in the rib and lowest in the anterior femur (Figure 6.8N; anterior femur *m* = 0.988; posterior femur *m* = 0.989; rib *m* = 0.997).

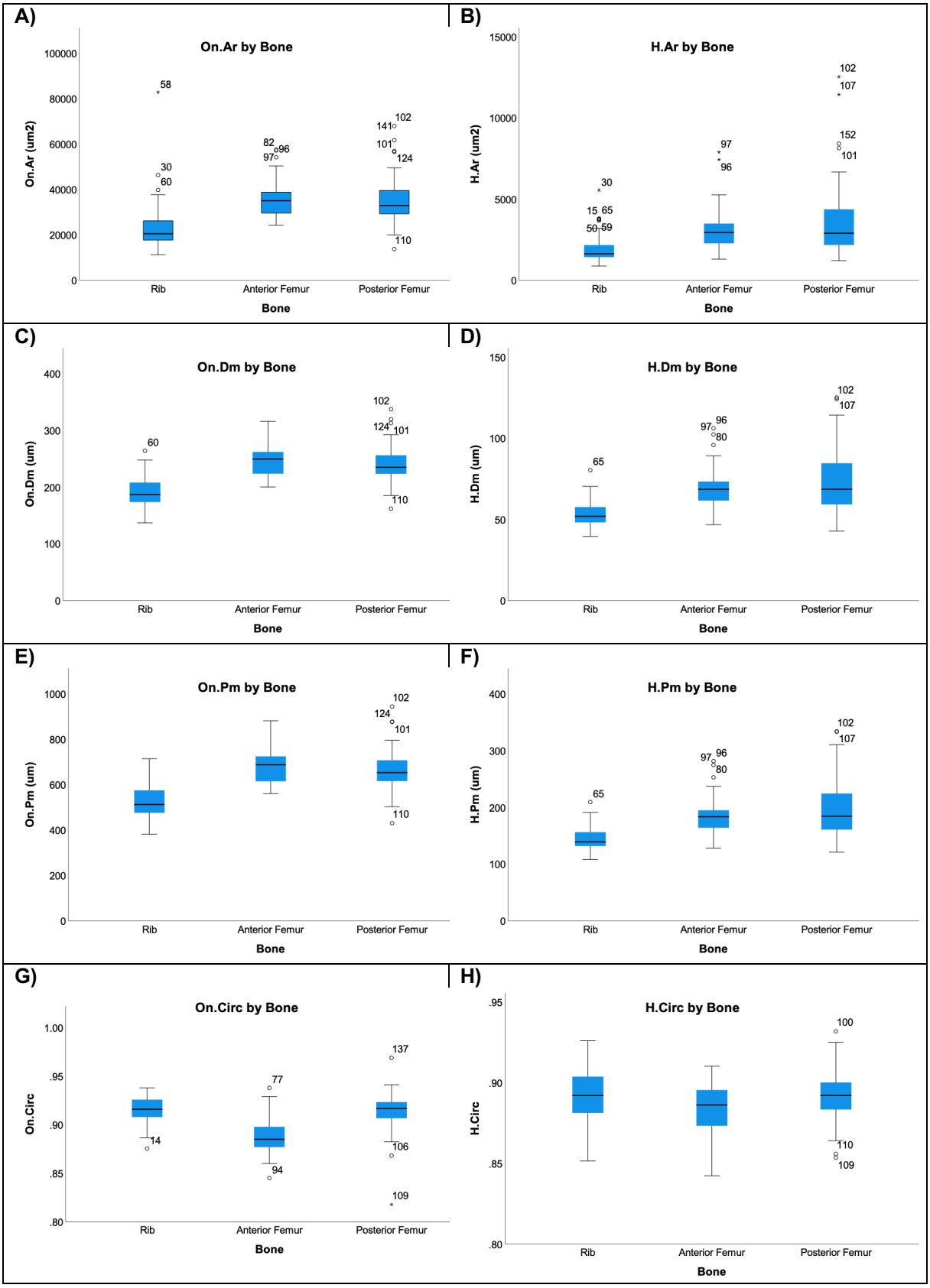
A)
On.Ar by Bone
On.Ar (um2)
100000
80000
60000
40000
20000
0
58
30
60
82
96
97
102
141
101
124
110
Rib
Anterior Femur
Posterior Femur
Bone
B)
H.Ar by Bone
H.Ar (um2)
15000
10000
5000
0
30
15
65
50
59
97
96
102
107
152
101
Rib
Anterior Femur
Posterior Femur
Bone
C)
On.Dm by Bone
On.Dm (um)
400
300
200
100
0
60
102
124
101
110
Rib
Anterior Femur
Posterior Femur
Bone
D)
H.Dm by Bone
H.Dm (um)
150
100
50
0
65
97
96
80
102
107
Rib
Anterior Femur
Posterior Femur
Bone
E)
On.Pm by Bone
On.Pm (um)
1000
800
600
400
200
0
102
124
101
110
Rib
Anterior Femur
Posterior Femur
Bone
F)
H.Pm by Bone
H.Pm (um)
400
300
200
100
0
65
97
96
80
102
107
Rib
Anterior Femur
Posterior Femur
Bone
G)
On.Circ by Bone
On.Circ
1.00
.95
.90
.85
.80
14
77
94
137
106
109
Rib
Anterior Femur
Posterior Femur
Bone
H)
H.Circ by Bone
H.Circ
.95
.90
.85
.80
100
110
109
Rib
Anterior Femur
Posterior Femur
Bone

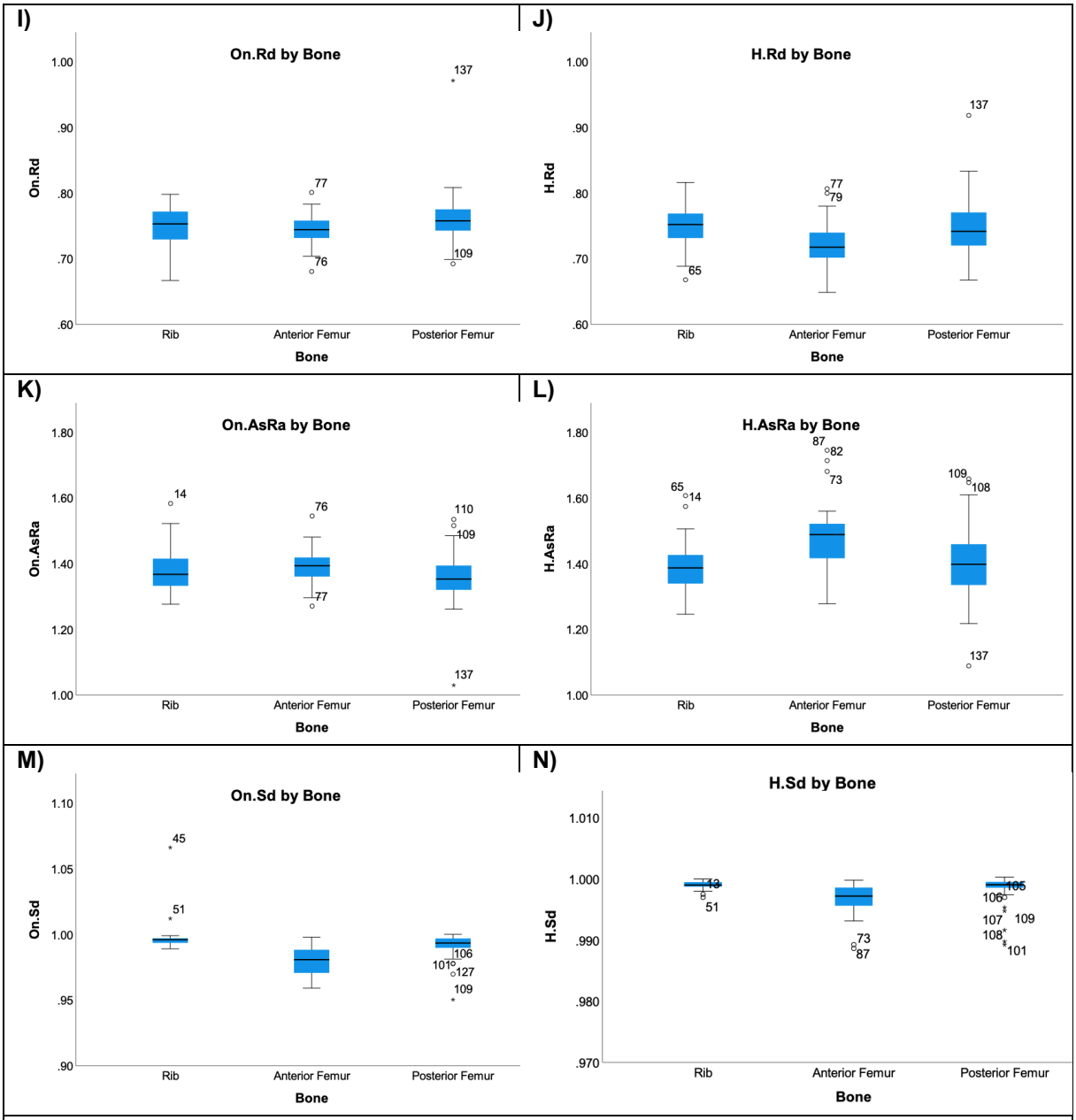

Figure 6.8: Boxplots of key osteon and Haversian canal variables.

A) Osteon area (On.Ar) by bone. **B)** Haversian canal area (H.Ar) by bone. **C)** Osteon diameter (On.Dm) by bone. **D)** Haversian canal diameter (H.Dm) by bone. **E)** Osteon perimeter (On.Pm) by bone. **F)** Haversian canal perimeter (H.Pm) by bone. **G)** Osteon circularity (On.Circ) by bone. **H)** Haversian canal circularity (H.Circ) by bone. **I)** Osteon roundness (On.Rd) by bone. **J)** Haversian canal roundness (H.Rd) by bone. **K)** Osteon aspect ratio (On.AsRa) by bone. **L)** Haversian canal aspect ratio (H.AsRa) by bone. **M)** Osteon solidity (On.Sd) by bone. **N)** Haversian canal solidity (H.Sd) by bone.

As in the whole sample group described in Table 6.31, the rib had the smallest values in all size variables, including On.Ar (posterior femur m = 38,070.239 μm^2; rib m = 19,683.767 μm^2),

H.Ar (posterior femur *m* = 4,822.454 μm^2; rib *m* = 1,759.350 μm^2), On.Dm (posterior femur *m* = 248.333 μm; rib *m* = 179.613 μm), H.Dm (posterior femur *m* = 80.501 μm; rib *m* = 53.014 μm), On.Pm (posterior femur *m* = 688.941 μm; rib *m* = 522.081 μm) and H.Pm (posterior femur *m* = 217.514 μm; rib *m* = 143.291 μm) (Table 6.32).

On.Circ was similar in the rib and posterior femur (posterior femur *m* = 0.914; rib *m* = 0.913). H.Circ was slightly higher in the posterior femur than the rib (posterior femur *m* = 0.898; rib *m* = 0.891). On.Rd was the highest in the posterior femur (posterior femur *m* = 0.769; rib *m* = 0.741). H.Rd was the highest in the posterior femur (posterior femur *m* = 0.750; rib *m* = 0.746). On.AsRa was the highest in the rib (posterior femur *m* = 1.339; rib *m* = 1.394). H.AsRa was the highest in the rib (posterior femur *m* = 1.384; rib *m* = 1.397). On.Sd was the highest in the rib (posterior femur *m* = 0.992; rib *m* = 1.004) (Table 6.32).

Table 6.32: Descriptive statistics for independent sample sub-group observed in research question 4.

Variable	Bone	*n*	Min.	Max.	Mean	St.D.	SW *p*	Skd/ Nor
Size Variables								
On.Ar (μm^2)	Rib	9	11270.17	39804.92	19683.77	8735.03	**0.005****	Skd
	Posterior Femur	7	21868.42	67904.76	38070.24	15082.22	0.222	Nor
H.Ar (μm^2)	Rib	9	1138.05	2352.90	1759.35	420.89	0.590	Nor
	Posterior Femur	7	2181.55	12541.43	4822.45	3668.97	**0.005****	Skd
On.Dm (μm)	Rib	9	137.03	264.08	179.61	37.06	**0.017***	Skd
	Posterior Femur	7	191.74	337.24	248.33	47.00	0.501	Nor
H.Dm (μm)	Rib	9	44.92	59.31	53.01	5.29	**0.017***	Skd
	Posterior Femur	7	60.12	124.14	80.50	22.95	**0.046***	Skd
On.Pm (μm)	Rib	9	381.71	714.04	490.37	98.79	**0.013***	Skd
	Posterior Femur	7	527.47	943.43	688.94	133.70	0.436	Nor
H.Pm (μm)	Rib	9	121.09	160.73	143.29	14.27	0.637	Nor
	Posterior Femur	7	161.14	333.10	217.51	60.31	0.052	Nor
Shape Variables								
On.Circ	Rib	9	0.893	0.930	0.913	0.013	0.540	Nor
	Posterior Femur	7	0.907	0.921	0.914	0.006	0.419	Nor
H.Circ	Rib	9	0.876	0.920	0.891	0.014	0.284	Nor
	Posterior Femur	7	0.885	0.911	0.898	0.011	0.333	Nor
On.Rd	Rib	9	0.702	0.774	0.741	0.029	0.194	Nor
	Posterior Femur	7	0.753	0.791	0.769	0.018	**0.018***	Skd
H.Rd	Rib	9	0.719	0.780	0.746	0.020	0.458	Nor
	Posterior Femur	7	0.725	0.770	0.750	0.017	0.641	Nor

On.AsRa	Rib	9	1.326	1.469	1.394	0.060	0.088	Nor
	Posterior Femur	7	1.294	1.377	1.339	0.035	0.106	Nor
H.AsRa	Rib	9	1.317	1.485	1.397	0.051	0.972	Nor
	Posterior Femur	7	1.335	1.436	1.384	0.039	0.289	Nor
On.Sd	Rib	9	0.991	1.066	1.004	0.024	**<0.001*** **	Skd
	Posterior Femur	7	0.982	0.996	0.992	0.005	0.125	Nor
H.Sd	Rib	9	0.999	1.000	0.999	0.0005	**0.014***	Skd
	Posterior Femur	7	0.999	1.000	0.999	0.0004	**<0.001*** **	Skd

* Significance values have been adjusted by the Bonferroni Correction for multiple tests.

As in the whole sample and independent sample groups, described in Table 6.31 and 6.32, the rib had the smallest values in all variables pertaining to osteon and Haversian canal size, including On.Ar (anterior femur *m* = 35,910.850 μm^2; posterior femur *m* = 34,596.367 μm^2; rib *m* = 23,453.113 μm^2), H.Ar (anterior femur *m* = 3,194.852 μm^2; posterior femur *m* = 3,447.370 μm^2; rib *m* = 1,928.427 μm^2), On.Dm (anterior femur *m* = 249.217 μm; posterior femur *m* = 237.620 μm; rib *m* = 191.905 μm), H.Dm (anterior femur *m* = 70.688 μm; posterior femur *m* = 72.205 μm; rib *m* = 53.179 μm), On.Pm (anterior femur *m* = 656.853 μm; posterior femur *m* = 656.853 μm; rib *m* = 526.685 μm) and H.Pm (anterior femur *m* = 188.011 μm; posterior femur *m* = 194.561 μm; rib *m* = 144.123 μm) (Table 6.33).

On.Circ was similar in the rib and posterior femur, and lower in the anterior femur (anterior femur *m* = 0.889; posterior femur *m* = 0.914; rib *m* = 0.915). Similarly, H.Circ was similar in the rib and posterior femur, and lower in the anterior femur (anterior femur *m* = 0.883; posterior femur *m* = 0.890; rib *m* = 0.893). On.Rd was the highest in the posterior femur and similar in the anterior femur and rib (anterior femur *m* = 0.745; posterior femur *m* = 0.760; rib *m* = 0.749). H.Rd was the highest in the rib and lowest in the anterior femur (anterior femur *m* = 0.721; posterior femur *m* = 0.746; rib *m* = 0.752). On.AsRa was the highest in the anterior femur and the lowest in the posterior femur (anterior femur *m* = 1.391; posterior femur *m* = 1.357; rib *m* = 1.380). H.AsRa was the highest in the anterior femur and the lowest in the rib (anterior femur *m* = 1.482; posterior femur *m* = 1.405; rib *m* = 1.386). On.Sd was the highest in the rib and lowest in the anterior femur (anterior femur *m* = 0.980; posterior femur *m* = 0.991; rib *m* = 0.995) (Table 6.33).

Table 6.33: Descriptive statistics for related sample sub-group observed in research question 4.

Variable	Bone	*n*	Min.	Max.	Mean	St.D.	KS/SW *p*	Skd/ Nor
Size Variables								
On.Ar (μm^2)	Rib	62	14203.43	82811.75	23453.11	9763.71	**<0.001*** **	Skd
	Anterior Femur	28	24310.35	57525.00	35910.85	9363.85	**0.007***	Nor
	Posterior Femur	46	13800.00	61666.67	34596.37	9541.88	0.054	Nor
H.Ar (μm^2)	Rib	62	881.96	5561.53	1928.43	839.02	**<0.001*** **	Skd
	Anterior Femur	28	1309.92	7901.50	3194.85	1536.82	**<0.001*** **	Skd
	Posterior Femur	46	1216.33	11450.90	3447.37	2161.91	**<0.001*** **	Skd
On.Dm (μm)	Rib	62	154.98	247.39	191.91	21.50	0.080	Nor
	Anterior Femur	28	200.08	315.55	249.22	32.40	0.079	Nor
	Posterior Femur	46	161.94	319.30	237.62	31.58	0.433	Nor
H.Dm (μm)	Rib	62	39.52	80.42	53.18	7.72	0.060	Nor
	Anterior Femur	28	46.78	106.20	70.69	14.78	0.054	Nor
	Posterior Femur	46	42.82	125.13	72.21	19.78	**0.007***	Skd
On.Pm (μm)	Rib	62	423.17	682.44	526.69	60.02	**0.016***	Skd
	Anterior Femur	28	559.81	880.57	686.72	90.16	0.063	Skd
	Posterior Femur	46	430.16	876.89	656.85	87.02	0.246	Nor
H.Pm (μm)	Rib	62	108.27	209.29	144.12	20.26	**0.016***	Skd
	Anterior Femur	28	128.34	281.20	188.01	37.99	**0.031***	Skd
	Posterior Femur	46	121.08	333.64	194.56	51.48	**0.007***	Skd
Shape Variables								
On.Circ	Rib	62	0.876	0.938	0.915	0.014	0.058	Nor
	Anterior Femur	28	0.845	0.938	0.889	0.022	0.372	Nor
	Posterior Femur	46	0.818	0.969	0.914	0.022	**<0.001*** **	Skd
H.Circ	Rib	62	0.852	0.926	0.893	0.017	0.200	Nor
	Anterior Femur	28	0.842	0.910	0.883	0.018	0.163	Nor
	Posterior Femur	46	0.854	0.932	0.890	0.016	0.179	Nor
On.Rd	Rib	62	0.667	0.798	0.749	0.030	0.075	Nor
	Anterior Femur	28	0.681	0.801	0.745	0.025	0.810	Nor
	Posterior Femur	46	0.692	0.971	0.760	0.041	**<0.001*** **	Skd
H.Rd	Rib	62	0.668	0.816	0.752	0.029	0.200	Nor
	Anterior Femur	28	0.649	0.807	0.721	0.038	0.229	Nor
	Posterior Femur	46	0.668	0.918	0.746	0.048	**0.027***	Skd

On.AsRa	Rib	62	1.277	1.583	1.380	0.068	**0.012***	Skd
	Anterior Femur	28	1.271	1.545	1.391	0.055	0.535	Nor
	Posterior Femur	46	1.030	1.535	1.357	0.078	**<0.001*****	Skd
H.AsRa	Rib	62	1.246	1.607	1.386	0.071	0.200	Nor
	Anterior Femur	28	1.278	1.745	1.482	0.112	0.084	Nor
	Posterior Femur	46	1.089	1.658	1.405	0.114	0.640	Nor
On.Sd	Rib	62	0.989	1.012	0.995	0.003	**0.002****	Skd
	Anterior Femur	28	0.959	0.998	0.980	0.011	0.330	Nor
	Posterior Femur	46	0.950	1.000	0.991	0.009	**<0.001*****	Skd
H.Sd	Rib	62	0.997	1.000	0.999	0.001	**<0.001*****	Skd
	Anterior Femur	28	0.989	1.000	0.996	0.003	**0.016***	Skd
	Posterior Femur	46	0.989	1.000	0.998	0.002	**<0.001*****	Skd

* Significance values have been adjusted by the Bonferroni Correction for multiple tests.

6.6.2 Inferential Statistics

As the sample size was <50 (rib n = 9, posterior femur n = 7), inferential testing of the independent (unpaired) rib and posterior femur samples were nonparametric, regardless of normal or abnormal distribution. The Mann-Whitney U test results identified statistically significant differences between the rib and posterior femur in all osteon and Haversian canal size variables, including On.Ar (U = 57.000, p = 0.005), H.Ar (U = 62.000, p <0.001), On.Dm (U = 57.000, p = 0.005), H.Dm (U = 63.000, p <0.001), On.Pm (U = 57.000, p = 0.005) and H.Pm (U = 63.000, p <0.001) (Table 6.34).

The rib mean rank was consistently smaller than that of the posterior femur in all size variables, including On.Ar (rib mean rank = 5.670; posterior femur mean rank = 12.140), H.Ar (rib mean rank = 5.110; posterior femur mean rank = 12.860), On.Dm (rib mean rank = 5.670; posterior femur mean rank = 12.140), H.Dm (rib mean rank = 5.000; posterior femur mean rank = 13.000), On.Pm (rib mean rank = 5.670; posterior femur mean rank = 12.140) and H.Pm (rib mean rank = 5.000; posterior femur mean rank = 13.000) (Table 6.34).

Of all of the shape variables, only On.Sd was statistically significantly different between the rib and posterior femur (U = 9.500, p = 0.016), with the rib (mean rank = 10.940) having a statistically significantly higher mean rank than the posterior femur (mean rank = 5.360). H.Circ in the femur and rib had the same mean rank (mean rank = 8.500) and were not statistically significantly different (U = 31.500, p = 1.000). The On.Rd mean rank was the highest in the

posterior femur (posterior femur mean rank = 10.860, rib mean rank = 6.670), but this was not statistically significant (*U* = 44.000, *p* = 0.210). Similarly, the H.Rd mean rank was the highest in the posterior femur (posterior femur mean rank = 9.360, rib mean rank = 7.830), but this was not statistically significant (*U* = 37.500, *p* = 0.536). On.AsRa was higher in the rib (mean rank = 10.220) than the posterior femur (mean rank = 6.290), but this was not statistically significantly different (*U* = 16.000, *p* = 0.114). Similarly, H.AsRa was the highest in the rib (mean rank = 9.110) than the posterior femur (mean rank = 7.710) but this difference was not statistically significant (*U* = 26.000, *p* = 0.606). Conversely, H.Sd was highest in the posterior femur (mean rank = 9.500) than the rib (mean rank = 7.720) but this was not statistically significant (*U* = 38.500, *p* = 0.470) (Table 6.34).

Table 6.34: Mann-Whitney U results: Independent sample sub-group.

Variable	Bone	*n*	Mean Rank	Mann-Whitney *U*	*p*-value
Size Variables					
On.Ar (μm²)	Rib	9	5.670	57.000	**0.005****
	Posterior Femur	7	12.140		
H.Ar (μm²)	Rib	9	5.110	62.000	**<0.001*****
	Posterior Femur	7	12.860		
On.Dm (μm)	Rib	9	5.670	57.000	**0.005****
	Posterior Femur	7	12.140		
H.Dm (μm)	Rib	9	5.000	63.000	**<0.001*****
	Posterior Femur	7	13.000		
On.Pm (μm)	Rib	9	5.670	57.000	**0.005****
	Posterior Femur	7	12.140		
H.Pm (μm)	Rib	9	5.000	63.000	**<0.001*****
	Posterior Femur	7	13.000		
Shape Variables					
On.Circ	Rib	9	8.500	31.500	1.000
	Posterior Femur	7	8.500		
H.Circ	Rib	9	7.110	44.000	0.210
	Posterior Femur	7	10.290		
On.Rd	Rib	9	6.670	48.000	0.091
	Posterior Femur	7	10.860		
H.Rd	Rib	9	7.830	37.500	0.536
	Posterior Femur	7	9.360		
On.AsRa	Rib	9	10.220	16.000	0.114
	Posterior Femur	7	6.290		
H.AsRa	Rib	9	9.110	26.000	0.606
	Posterior Femur	7	7.710		
On.Sd	Rib	9	10.940	9.500	**0.016***
	Posterior Femur	7	5.360		
H.Sd	Rib	9	7.720	38.500	0.470
	Posterior Femur	7	9.500		

*Significance values have been adjusted by the Bonferroni Correction for multiple tests.

Related samples were split into related pairs and related triplets of datapoints. Results of the Friedman's pairwise comparison identified statistically significant differences between the rib, anterior femur and posterior femur across all size variables in triple related samples, including On.Ar (Q = 7.000, p = 0.030), H.Ar (Q = 6.750, p = 0.034), On.Dm (Q = 9.250, p = 0.010), H.Dm (Q = 6.750, p = 0.034), On.Pm (Q = 7.000, p = 0.030), and H.Pm (Q = 6.750, p = 0.034) (Table 6.35). However, in the post-hoc pairwise testing, once the Bonferroni Correction has been applied, statistically significant differences were identified in On.Ar with the rib bring smaller than the anterior femur (-1.250, p = 0.037); in On.Dm with the rib being smaller than the anterior femur (-1.375, p = 0.018), and the posterior femur (-1.250, p = 0.037); and in On.Pm with the rib being smaller than the anterior femur (-1.250, p = 0.037). There was only one statistically significant difference in the shape variables, and that was in H.Sd (Q = 9.172, p = 0.010). In the post-hoc pairwise testing, it was determined that H.Sd in the rib was statistically significantly higher than the anterior femur (1.438, p = 0.012) (Table 6.35).

Table 6.35: Friedman's results: Related sample sub-group: Triple Datapoints.

Variable	Bone	*n*	Mean Rank	Friedman's	*p*-value	Pair	Test Stat.	*p*-value
Size Variables								
On.Ar (μm^2)	Rib	8	1.250	7.000	**0.030***	R – AF	-1.250	**0.037***
	Anterior Femur	8	2.500			R – PF	-1.000	0.137
	Posterior Femur	8	2.250			AF – PF	0.250	1.000
H.Ar (μm^2)	Rib	8	1.250	6.750	**0.034***	R – AF	-1.125	0.073
	Anterior Femur	8	2.380			R – PF	-1.125	0.073
	Posterior Femur	8	2.380			AF – PF	0.000	1.000
On.Dm (μm)	Rib	8	1.130	9.250	**0.010***	R – AF	-1.375	**0.018***
	Anterior Femur	8	2.500			R – PF	-1.250	**0.037***
	Posterior Femur	8	2.380			AF – PF	0.125	1.000
H.Dm (μm)	Rib	8	1.250	6.750	**0.034***	R – AF	-1.125	0.073
	Anterior Femur	8	2.380			R – PF	-1.125	0.073
	Posterior Femur	8	2.380			AF – PF	0.000	1.000
On.Pm (μm)	Rib	8	1.250	7.000	**0.030***	R – AF	-1.250	**0.037***
	Anterior Femur	8	2.500			R – PF	-1.000	0.137
	Posterior Femur	8	2.250			AF – PF	0.250	1.000
H.Pm (μm)	Rib	8	1.250	6.750	**0.034***	R – AF	-1.125	0.073
	Anterior Femur	8	2.380			R – PF	-1.125	0.073
	Posterior Femur	8	2.380			AF – PF	0.000	1.000
Shape Variables								
On.Circ	Rib	8	2.380	1.750	0.417	R – AF	N/A	
	Anterior Femur	8	1.750			R – PF		
	Posterior Femur	8	1.880			AF – PF		
H.Circ	Rib	8	2.630	4.750	0.093	R – AF	N/A	
	Anterior Femur	8	1.750			R – PF		
	Posterior Femur	8	1.630			AF – PF		
On.Rd	Rib	8	2.500	3.250	0.197	R – AF	N/A	
	Anterior Femur	8	1.880			R – PF		
	Posterior Femur	8	1.630			AF – PF		
H.Rd	Rib	8	2.630	5.250	0.072	R – AF	N/A	
	Anterior Femur	8	1.880			R – PF		

	Posterior Femur	8	1.500			AF – PF		
On.AsRa	Rib	8	1.630	2.000	0.368	R – AF		
	Anterior Femur	8	2.060			R – PF	N/A	
	Posterior Femur	8	2.310			AF – PF		
H.AsRa	Rib	8	1.380	5.250	0.072	R – AF		
	Anterior Femur	8	2.130			R – PF	N/A	
	Posterior Femur	8	2.500			AF – PF		
On.Sd	Rib	8	2.310	2.516	0.284	R – AF		
	Anterior Femur	8	1.560			R – PF	N/A	
	Posterior Femur	8	2.130			AF – PF		
H.Sd	Rib	8	2.690	9.172	**0.010***	R – AF	1.438	**0.012***
	Anterior Femur	8	1.250			R – PF	0.625	0.634
	Posterior Femur	8	2.060			AF – PF	-0.812	0.312

*Significance values have been adjusted by the Bonferroni Correction for multiple tests.

As the sample size was <50 (n = 26), inferential testing of the paired rib and anterior femur samples were nonparametric, regardless of normal or abnormal distribution (Table 6.36). Similar to the results of the analysis of the independent samples (Table 6.33), the anterior femur values were the highest in all size variables and these differences were statistically significant, including On.Ar (W = 351.000, p<0.001), H.Ar (W = 343.000, p<0.001), On.Dm (W = 351.000, p<0.001), H.Dm (W = 345.000, p<0.001), On.Pm (W = 351.000, p<0.001) and H.Pm (W = 344.000, p<0.001) (Table 6.36).

Of the shape variables, the rib had the highest On.Circ (W = 15.000, p<0.001), H.Rd (W = 49.000, p<0.001), On.Sd (W = 7.500, p<0.001), and H.Sd (W = 9.500, p<0.001) with these differences being statistically significant. The anterior femur had the highest H.AsRa (W = 319.000, p<0.001), and this difference was also statistically significant (Table 6.36).

Table 6.36: Wilcoxon Signed Rank Test results: Related sample sub-group: Rib/Anterior Femur Pairs.

Variable	Bone	*n*.	Mean	Test Stat.	*p*-value
Size Variables					
On.Ar (μm²)	Rib	26	19717.740	351.000	**<0.001*** **
	Anterior Femur	26	35783.204		
H.Ar (μm²)	Rib	26	1656.337	343.000	**<0.001*** **
	Anterior Femur	26	3220.765		
On.Dm (μm)	Rib	26	184.006	351.000	**<0.001*** **
	Anterior Femur	26	248.904		
H.Dm (μm)	Rib	26	50.616	345.000	**<0.001*** **
	Anterior Femur	26	70.580		
On.Pm (μm)	Rib	26	501.455	351.000	**<0.001*** **
	Anterior Femur	26	686.129		
H.Pm (μm)	Rib	26	137.008	344.000	**<0.001*** **
	Anterior Femur	26	187.652		
Shape Variables					
On.Circ	Rib	26	0.908	15.000	**<0.001*** **

	Anterior Femur	26	0.887		
H.Circ	Rib	26	0.890	119.000	0.151
	Anterior Femur	26	0.883		
On.Rd	Rib	26	0.736	220.000	0.258
	Anterior Femur	26	0.744		
H.Rd	Rib	26	0.750	49.000	**0.001****
	Anterior Femur	26	0.721		
On.AsRa	Rib	26	1.412	134.000	0.292
	Anterior Femur	26	1.394		
H.AsRa	Rib	26	1.390	319.000	**<0.001*****
	Anterior Femur	26	1.483		
On.Sd	Rib	26	0.995	7.500	**<0.001*****
	Anterior Femur	26	0.980		
H.Sd	Rib	26	0.999	9.500	**<0.001*****
	Anterior Femur	26	0.997		

*Significance values have been adjusted by the Bonferroni Correction for multiple tests.

As the sample size was <50 (n = 44), inferential testing of the paired rib and posterior femur samples were nonparametric, regardless of normal or abnormal distribution (Table 6.37). Similar to the results of the analysis of the independent samples (Table 6.33) and rib and anterior femur paired samples, the posterior femur values were the highest in all size variables and these differences were statistically significant, including On.Ar (W = 881.000, p<0.001), H.Ar (W = 839.000, p<0.001), On.Dm (W = 977.000, p<0.001), H.Dm (W = 926.000, p<0.001), On.Pm (W = 973.000, p<0.001) and H.Pm (W = 926.000, p<0.001). Of the shape variables, the rib had the highest H.Circ (W = 297.500, p = 0.034) and On.Sd (W = 202.000, p = 0.003), with these differences being statistically significant (Table 6.37).

Table 6.37: Wilcoxon Signed Rank Test results: Related sample sub-group: Rib/Posterior Femur Pairs.

Variable	Bone	*n*.	Mean	Test Stat.	*p*-value
Size Variables					
On.Ar (μm²)	Rib	44	24968.328	881.000	**<0.001*****
	Posterior Femur	44	34725.89		
H.Ar (μm²)	Rib	44	2069.558	839.000	**<0.001*****
	Posterior Femur	44	3417.655		
On.Dm (μm)	Rib	44	194.427	977.000	**<0.001*****
	Posterior Femur	44	238.043		
H.Dm (μm)	Rib	44	54.597	926.000	**<0.001*****
	Posterior Femur	44	71.784		
On.Pm (μm)	Rib	44	536.232	973.000	**<0.001*****
	Posterior Femur	44	657.872		
H.Pm (μm)	Rib	44	148.372	926.000	**<0.001*****
	Posterior Femur	44	193.534		
Shape Variables					
On.Circ	Rib	44	0.920	347.500	0.085
	Posterior Femur	44	0.914		
H.Circ	Rib	44	0.898	297.500	**0.034***
	Posterior Femur	44	0.891		
On.Rd	Rib	44	0.759	449.000	0.591

	Posterior Femur	44	0.759		
H.Rd	Rib	44	0.757	353.000	0.097
	Posterior Femur	44	0.746		
On.AsRa	Rib	44	1.358	540.500	0.595
	Posterior Femur	44	1.359		
H.AsRa	Rib	44	1.376	604.500	0.201
	Posterior Femur	44	1.402		
On.Sd	Rib	44	0.996	202.000	**0.003****
	Posterior Femur	44	0.991		
H.Sd	Rib	44	0.999	151.000	0.148
	Posterior Femur	44	0.998		

*Significance values have been adjusted by the Bonferroni Correction for multiple tests.

As the sample size was <50 (*n* = 10), inferential testing of the paired anterior and posterior femur samples were nonparametric, regardless of normal or abnormal distribution (Table 6.38). There were no statistically significant differences detected between the paired anterior and posterior femur samples for any size or shape variables (Table 6.38).

Table 6.38: Wilcoxon Signed Rank Test results: Related sample sub-group: Anterior Femur/Posterior Femur Pairs.

Variable	Bone	*n*.	Mean	Test Stat.	*p*-value
Size Variables					
On.Ar (μm^2)	Anterior Femur	10	31645.672	30.000	0.799
	Posterior Femur	10	31719.321		
H.Ar (μm^2)	Anterior Femur	10	3057.868	38.000	0.285
	Posterior Femur	10	4272.791		
On.Dm (μm)	Anterior Femur	10	232.431	24.000	0.721
	Posterior Femur	10	228.872		
H.Dm (μm)	Anterior Femur	10	70.762	36.000	0.386
	Posterior Femur	10	80.588		
On.Pm (μm)	Anterior Femur	10	637.361	24.000	0.721
	Posterior Femur	10	627.985		
H.Pm (μm)	Anterior Femur	10	189.352	36.000	0.386
	Posterior Femur	10	214.927		
Shape Variables					
On.Circ	Anterior Femur	10	0.889	22.500	1.000
	Posterior Femur	10	0.914		
H.Circ	Anterior Femur	10	0.883	24.500	0.760
	Posterior Femur	10	0.890		
On.Rd	Anterior Femur	10	0.745	24.000	0.721
	Posterior Femur	10	0.760		
H.Rd	Anterior Femur	10	0.721	23.000	0.646
	Posterior Femur	10	0.746		
On.AsRa	Anterior Femur	10	1.391	27.000	0.594
	Posterior Femur	10	1.357		
H.AsRa	Anterior Femur	10	1.482	36.000	0.386
	Posterior Femur	10	1.405		
On.Sd	Anterior Femur	10	0.980	34.000	0.506
	Posterior Femur	10	0.992		
H.Sd	Anterior Femur	10	0.997	12.000	0.366
	Posterior Femur	10	0.998		

* Significance values have been adjusted by the Bonferroni Correction for multiple tests.

The Mann-Whitney *U* test was repeated for independent samples after correcting by individual stature to account for differences between individuals in body size (Table 6.39). These results identified statistically significant differences between the rib and posterior femur in all osteon and Haversian canal size variables, with the posterior femur mean ranks being consistently higher than the rib. These values included On.Ar (U = 57.000, p = 0.005), H.Ar (U = 61.000, p <0.001), On.Dm (U = 57.000, p = 0.005), H.Dm (U = 61.000, p <0.001), On.Pm (U = 58.000, p = 0.003) and H.Pm (U = 61.000, p <0.001) (Table 6.39).

Of all of the shape variables, only On.Rd was statistically significantly different between the rib and posterior femur (U = 51.000, p = 0.042), with the posterior femur (mean rank = 11.290) having a statistically significantly higher mean rank than the rib (mean rank = 6.330) (Table 6.39).

Table 6.39: Mann-Whitney U results: Independent sample sub-group: Corrected by Stature.

Variable	Bone	*n*.	Mean Rank	Mann-Whitney *U*	*p*-value
Size Variables					
On.Ar (μm²)	Rib	9	5.670	57.000	**0.005****
	Posterior Femur	7	12.140		
H.Ar (μm²)	Rib	9	5.220	61.000	**<0.001*****
	Posterior Femur	7	12.710		
On.Dm (μm)	Rib	9	5.670	57.000	**0.005****
	Posterior Femur	7	12.140		
H.Dm (μm)	Rib	9	5.220	61.000	**<0.001*****
	Posterior Femur	7	12.710		
On.Pm (μm)	Rib	9	5.560	58.000	**0.003****
	Posterior Femur	7	12.290		
H.Pm (μm)	Rib	9	5.220	61.000	**<0.001*****
	Posterior Femur	7	12.710		
Shape Variables					
On.Circ	Rib	9	7.330	42.000	0.299
	Posterior Femur	7	10.000		
H.Circ	Rib	9	7.220	43.000	0.252
	Posterior Femur	7	10.140		
On.Rd	Rib	9	6.330	51.000	**0.042***
	Posterior Femur	7	11.290		
H.Rd	Rib	9	7.440	41.000	0.351
	Posterior Femur	7	9.860		
On.AsRa	Rib	9	9.000	27.000	0.681
	Posterior Femur	7	7.860		
H.AsRa	Rib	9	8.000	36.000	0.681
	Posterior Femur	7	9.140		
On.Sd	Rib	9	7.890	37.000	0.606
	Posterior Femur	7	9.290		
H.Sd	Rib	9	7.780	38.000	0.491
	Posterior Femur	7	9.430		

* Significance values have been adjusted by the Bonferroni Correction for multiple tests.

The Friedman's pairwise comparison in the triplet rib, anterior and posterior femur samples was repeated after correcting by individual stature to account for differences between individuals in body size (Table 6.40). Results identified statistically significant differences in size between the rib, anterior femur and posterior femur across H.Ar (Q = 8.000, p = 0.018), On.Dm (Q = 7.714, p = 0.021), H.Dm (Q = 8.000, p = 0.018) and H.Pm (Q = 8.000, p = 0.018). Post-hoc pairwise testing indicated that H.Ar is statistically significantly higher in the posterior femur than the rib (-1.429, p = 0.023). On.Dm is statistically significantly higher in the anterior (-1.286, p = 0.048) and posterior femur (-1.286, p = 0.048) than the rib. H.Dm was statistically significantly higher in the posterior femur than the rib (-1.429, p = 0.023) (Table 6.40).

Statistically significant differences were identified between the triplet rib, anterior and posterior femur samples in H.Circ (Q = 8.615, p = 0.013), H.Rd (Q = 8.074, p = 0.018), H.AsRa (Q = 8.000, p = 0.018) and H.Sd (Q = 8.880, p = 0.012). Post-hoc pairwise testing indicated that H.Circ is statistically significantly highest in the rib than the posterior femur (1.429, p = 0.023), H.Rd is statistically significantly highest in the rib than the posterior femur (1.357, p = 0.033), H.AsRa is statistically significantly highest in the posterior femur than the rib (-1.429, p = 0.023) and H.Sd is statistically significantly highest in the rib than anterior femur (1.500, p = 0.015) (Table 6.40).

Table 6.40: Friedman's results: Related sample sub-group: Triple Datapoints: Corrected by Stature.

Variable	Bone	*n*	Mean Rank	Friedman's	*p*-value	Pair	Test Stat.	*p*-value
Size Variables								
On.Ar (μm^2)	Rib	7	1.290	5.429	0.066	R – AF	N/A	
	Anterior Femur	7	2.430			R – PF		
	Posterior Femur	7	2.290			AF – PF		
H.Ar (μm^2)	Rib	7	1.140	8.000	**0.018***	R – AF	-1.143	0.098
	Anterior Femur	7	2.290			R – PF	-1.429	**0.023***
	Posterior Femur	7	2.570			AF – PF	-0.286	1.000
On.Dm (μm)	Rib	7	1.140	7.714	**0.021***	R – AF	-1.286	**0.048***
	Anterior Femur	7	2.430			R – PF	-1.286	**0.048***
	Posterior Femur	7	2.430			AF – PF	0.000	1.000
H.Dm (μm)	Rib	7	1.140	8.000	**0.018***	R – AF	-1.143	0.098
	Anterior Femur	7	2.290			R – PF	-1.429	**0.023***
	Posterior Femur	7	2.570			AF – PF	-0.286	1.000
On.Pm (μm)	Rib	7	1.290	5.429	0.066	R – AF	N/A	
	Anterior Femur	7	2.430			R – PF		
	Posterior Femur	7	2.290			AF – PF		
H.Pm (μm)	Rib	7	1.140	8.000	**0.018***	R – AF	-1.143	0.098
	Anterior Femur	7	2.290			R – PF	-1.429	**0.023***
	Posterior Femur	7	2.570			AF – PF	-0.286	1.000
Shape Variables								
On.Circ	Rib	7	2.430	2.000	0.368	R – AF	N/A	
	Anterior Femur	7	1.860			R – PF		

	Posterior Femur	7	1.710			AF – PF		
H.Circ	Rib	7	2.860	8.615	**0.013***	R – AF	1.143	0.098
	Anterior Femur	7	1.710			R – PF	1.429	**0.023***
	Posterior Femur	7	1.430			AF – PF	0.286	1.000
On.Rd	Rib	7	2.640	4.667	0.097	R – AF		
	Anterior Femur	7	1.790			R – PF	N/A	
	Posterior Femur	7	1.570			AF – PF		
H.Rd	Rib	7	2.860	8.074	**0.018***	R – AF	1.214	0.069
	Anterior Femur	7	1.640			R – PF	1.357	**0.033***
	Posterior Femur	7	1.500			AF – PF	0.143	1.000
On.AsRa	Rib	7	1.430	4.222	0.121	R – AF		
	Anterior Femur	7	2.070			R – PF	N/A	
	Posterior Femur	7	2.500			AF – PF		
H.AsRa	Rib	7	1.140	8.000	**0.018***	R – AF	-1.143	0.098
	Anterior Femur	7	2.290			R – PF	-1.429	**0.023***
	Posterior Femur	7	2.570			AF – PF	-0.286	1.000
On.Sd	Rib	7	2.290	1.412	0.494	R – AF		
	Anterior Femur	7	1.860			R – PF	N/A	
	Posterior Femur	7	1.860			AF – PF		
H.Sd	Rib	7	2.790	8.880	**0.012***	R – AF	1.500	**0.015***
	Anterior Femur	7	1.290			R – PF	0.857	0.326
	Posterior Femur	7	1.930			AF – PF	-0.643	0.687

* Significance values have been adjusted by the Bonferroni Correction for multiple tests.

The Wilcoxon Signed Rank test was repeated for paired rib and anterior femur samples, this time corrected by stature to account for differences in individual body size, results were similar (Table 6.41). The anterior femur consistently had statistically significantly higher means across all size variables than the rib. These variables included On.Ar (W = 253.000, p<0.001), H.Ar (W = 247.000, p<0.001), On.Dm (W = 253.000, p<0.001), H.Dm (W = 249.000, p<0.001), On.Pm (W = 253.000, p<0.001) and H.Pm (W = 248.000, p<0.001) (Table 6.41).

Of the shape variables, the rib had the highest On.Circ (W = 13.000, p<0.001), H.Rd (W = 23.000, p = 0.001) and On.Sd (W = 2.500, p <0.001), with these differences being statistically significant. The anterior femur had the highest H.AsRa (W = 228.000, p<0.001) and H.Sd (W = 7.000, p<0.001), and this difference was also statistically significant (Table 6.41).

Table 6.41: Wilcoxon Signed Rank Test results: Related sample sub-group: Rib/Anterior Femur Pairs: Corrected by stature.

Variable	Bone	*n.*	Mean	Test Stat.	*p*-value
Size Variables					
On.Ar (μm^2)	Rib	22	3949.555	253.000	**<0.001*** **
	Anterior Femur	22	6211.453		
H.Ar (μm^2)	Rib	22	328.936	247.000	**<0.001*** **
	Anterior Femur	22	573.384		
On.Dm (μm)	Rib	22	322.411	253.000	**<0.001*** **
	Anterior Femur	22	428.274		
H.Dm (μm)	Rib	22	89.737	249.000	**<0.001*** **
	Anterior Femur	22	123.130		

On.Pm (μm)	Rib	22	88.541	253.000	**<0.001*** **
	Anterior Femur	22	118.164		
H.Pm (μm)	Rib	22	24.336	248.000	**<0.001*** **
	Anterior Femur	22	32.784		
Shape Variables					
On.Circ	Rib	22	1.539	13.000	**<0.001*** **
	Anterior Femur	22	1.525		
H.Circ	Rib	22	1.502	77.500	0.109
	Anterior Femur	22	1.516		
On.Rd	Rib	22	1.260	115.000	0.420
	Anterior Femur	22	1.277		
H.Rd	Rib	22	1.265	23.000	**0.001** **
	Anterior Femur	22	1.239		
On.AsRa	Rib	22	2.314	82.500	0.401
	Anterior Femur	22	2.376		
H.AsRa	Rib	22	2.325	228.000	**<0.001*** **
	Anterior Femur	22	2.531		
On.Sd	Rib	22	1.672	2.500	**<0.001*** **
	Anterior Femur	22	1.680		
H.Sd	Rib	22	1.679	7.000	**<0.001*** **
	Anterior Femur	22	1.707		

* Significance values have been adjusted by the Bonferroni Correction for multiple tests.

The Wilcoxon Signed Rank test was repeated for paired rib and posterior femur samples to correct by stature to account for differences in individual body size, however results remained similar to those prior to stature correction (Table 6.42). The posterior femur values were the highest in all size variables and these differences were statistically significant, including On.Ar (W = 764.000, p<0.001), H.Ar (W = 740.000, p<0.001), On.Dm (W = 851.000, p<0.001), H.Dm (W = 830.000, p<0.001), On.Pm (W = 845.000, p<0.001) and H.Pm (W = 827.000, p<0.001). Of the shape variables, the rib had the highest H.Circ (W = 204.500, p = 0.043) and On.Sd (W = 80.000, p = 0.006), with these differences being statistically significant (Table 6.42).

Table 6.42: Wilcoxon Signed Rank Test results: Related sample sub-group: Rib/Posterior Femur Pairs: Corrected by stature.

Variable	Bone	*n.*	Mean	Test Stat.	*p*-value
Size Variables					
On.Ar (μm²)	Rib	41	3949.555	764.000	**<0.001*** **
	Posterior Femur	41	5878.138		
H.Ar (μm²)	Rib	41	328.936	740.000	**<0.001*** **
	Posterior Femur	41	588.961		
On.Dm (μm)	Rib	41	322.411	851.000	**<0.001*** **
	Posterior Femur	41	401.035		
H.Dm (μm)	Rib	41	89.737	830.000	**<0.001*** **
	Posterior Femur	41	121.972		
On.Pm (μm)	Rib	41	88.541	845.000	**<0.001*** **
	Posterior Femur	41	110.793		
H.Pm (μm)	Rib	41	24.336	827.000	**<0.001*** **
	Posterior Femur	41	32.869		
Shape Variables					
On.Circ	Rib	41	1.539	254.000	0.089
	Posterior Femur	41	1.529		

H.Circ	Rib	41	1.502	204.500	**0.043***
	Posterior Femur	41	1.492		
On.Rd	Rib	41	1.260	356.500	0.471
	Posterior Femur	41	1.270		
H.Rd	Rib	41	1.265	265.000	0.051
	Posterior Femur	41	1.248		
On.AsRa	Rib	41	2.314	472.500	0.401
	Posterior Femur	41	2.280		
H.AsRa	Rib	41	2.325	548.000	0.128
	Posterior Femur	41	2.355		
On.Sd	Rib	41	1.672	80.000	**0.006***
	Posterior Femur	41	1.660		
H.Sd	Rib	41	1.679	126.000	0.130
	Posterior Femur	41	1.674		

* Significance values have been adjusted by the Bonferroni Correction for multiple tests.

The Wilcoxon Signed Rank test was repeated in the paired anterior and posterior femur samples to correct by stature to control for differences in individual body size, but results didn't change (Table 6.43). There were again no statistically significant differences detected between the paired anterior and posterior femur samples for any size or shape variables (Table 6.43).

Table 6.43: Wilcoxon Signed Rank Test results: Related sample sub-group: Anterior Femur/Posterior Femur Pairs: Corrected by stature.

Variable	Bone	*n*.	Mean	Test Stat.	*p*-value
Size Variables					
On.Ar (μm^2)	Anterior Femur	8	6211.453	25.000	0.327
	Posterior Femur	8	5878.138		
H.Ar (μm^2)	Anterior Femur	8	573.384	24.000	0.401
	Posterior Femur	8	588.961		
On.Dm (μm)	Anterior Femur	8	428.274	21.000	0.674
	Posterior Femur	8	401.035		
H.Dm (μm)	Anterior Femur	8	123.130	23.000	0.484
	Posterior Femur	8	121.972		
On.Pm (μm)	Anterior Femur	8	118.164	21.000	0.674
	Posterior Femur	8	110.793		
H.Pm (μm)	Anterior Femur	8	32.784	22.000	0.575
	Posterior Femur	8	32.869		
Shape Variables					
On.Circ	Anterior Femur	8	1.524	12.500	0.799
	Posterior Femur	8	1.529		
H.Circ	Anterior Femur	8	1.516	4.000	0.345
	Posterior Femur	8	1.492		
On.Rd	Anterior Femur	8	1.277	10.000	0.496
	Posterior Femur	8	1.270		
H.Rd	Anterior Femur	8	1.239	11.500	0.672
	Posterior Femur	8	1.248		
On.AsRa	Anterior Femur	8	2.376	19.500	0.352
	Posterior Femur	8	2.280		
H.AsRa	Anterior Femur	8	2.531	24.000	0.401
	Posterior Femur	8	2.355		
On.Sd	Anterior Femur	8	1.680	5.000	1.000
	Posterior Femur	8	1.660		
H.Sd	Anterior Femur	8	1.707	13.000	0.866
	Posterior Femur	8	1.674		

* Significance values have been adjusted by the Bonferroni Correction for multiple tests.

6.6.3 Multivariate Statistics

Results of the reduced major axis regression (RMA) for the rib samples are presented in Figure 6.9A-N and Table 6.44. Log10(On.Ar) and Log10(H.Ar) consistently had a positive strong relationship, as evidenced in Figure 6.9. This was across the RMA analysis of the entire sample and all sub-analyses taken to account for era, sex and age-at-death of the individuals.

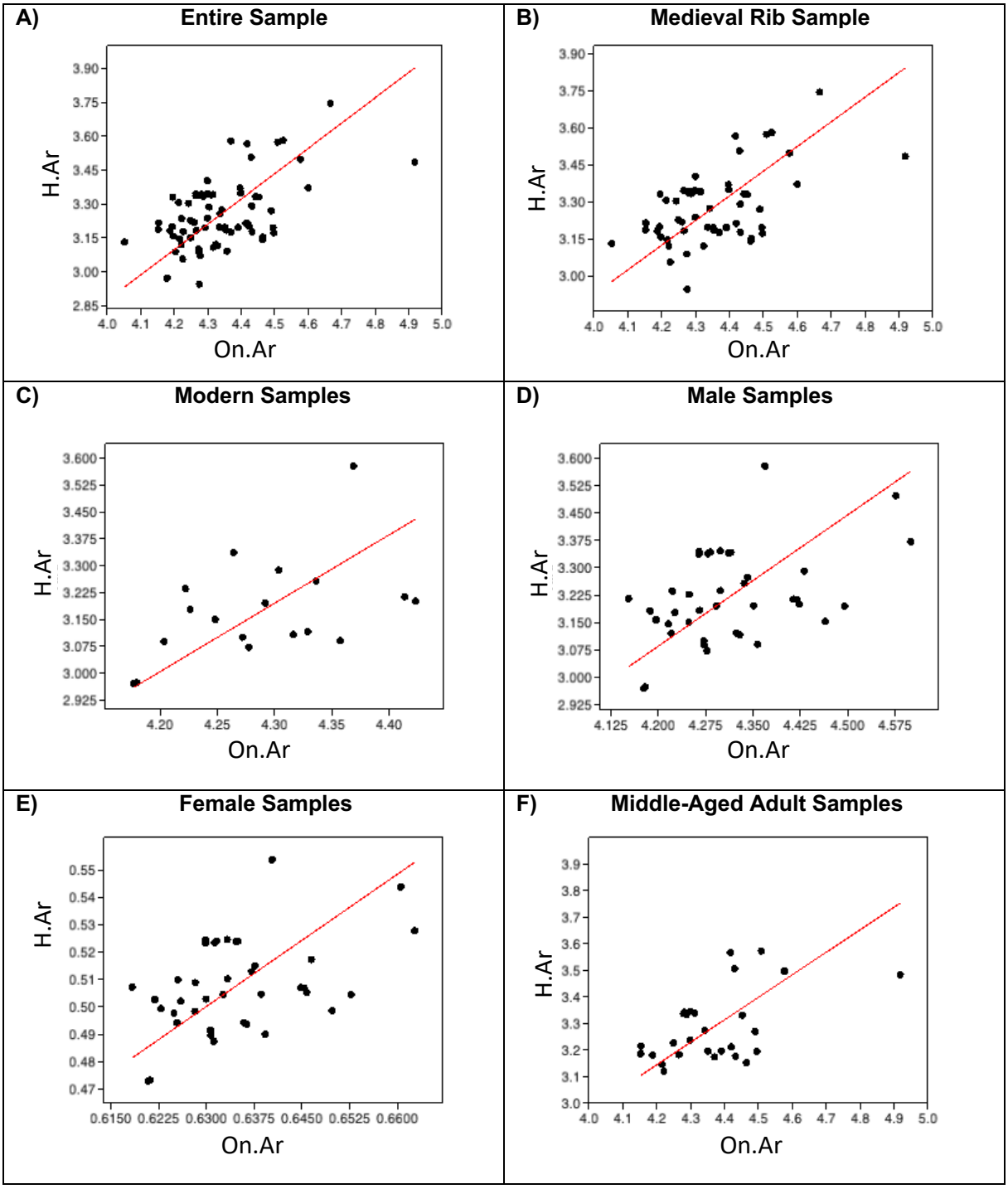

G) Older Adult Samples

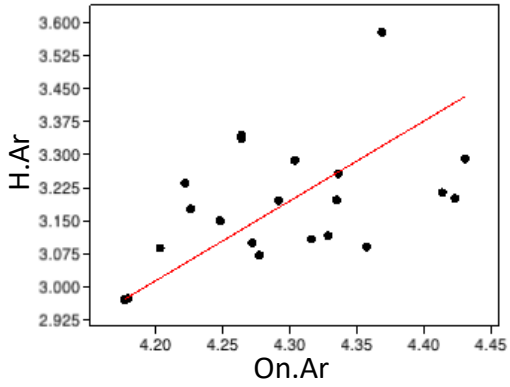

H) Male Middle-Aged Adult Samples

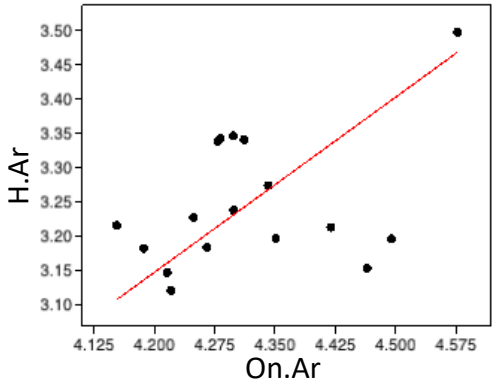

I) Male Older Adult Samples

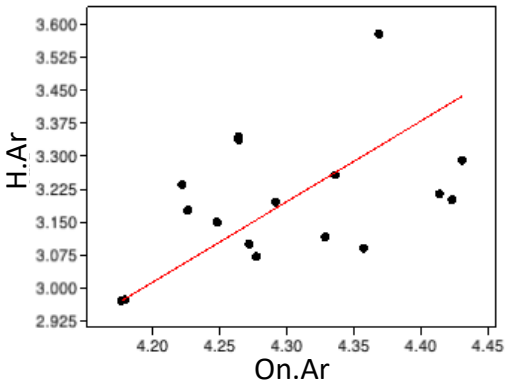

J) Female Middle-Aged Adult Samples

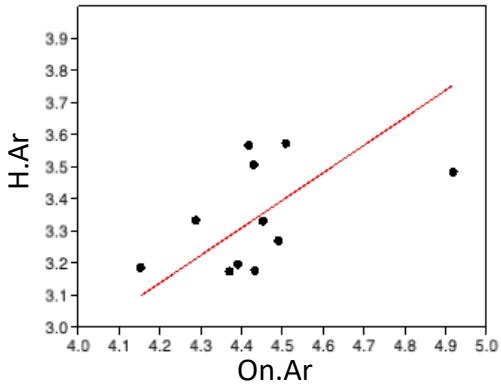

K) Modern Older Adult Samples

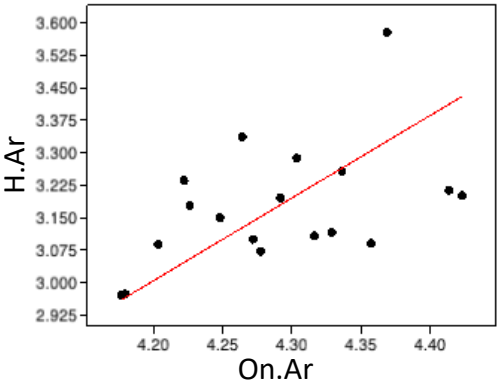

L) Medieval Male Samples

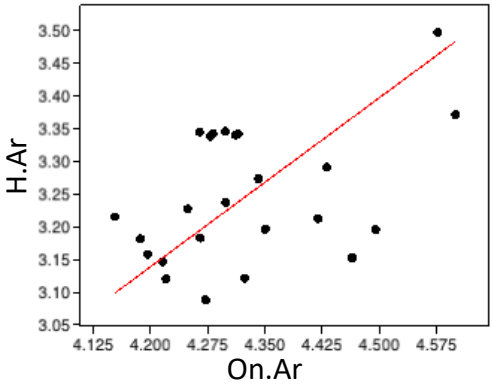

M) Medieval Female Samples

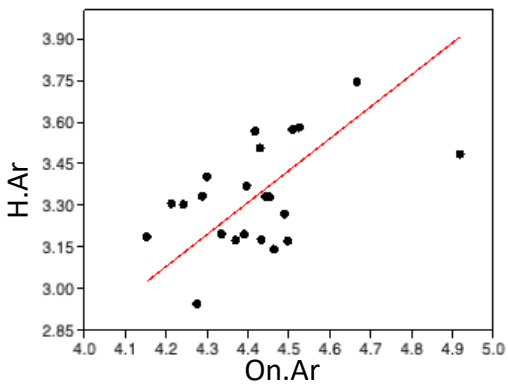

N) Modern Male Samples

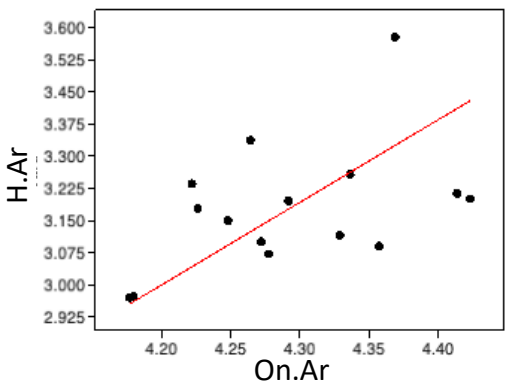

Figure 6.9: Reduced major axis regression plots of the rib data.

A) RMA of entire sample of the rib. **B)** RMA of medieval samples of the rib. **C)** RMA of modern samples of the rib. **D)** RMA of male samples of the rib. **E)** RMA of female samples of the rib. **F)** RMA of middle-aged adult samples of the rib. **G)** RMA of older adult samples of the rib. **H)** RMA of male middle-aged adult samples of the rib. **I)** RMA of male older adult samples of the rib. **J)** RMA of female middle-aged adult samples of the rib. **K)** RMA of modern older adult samples of the rib. **L)** RMA of medieval male samples of the rib. **M)** RMA of medieval female samples of the rib. **N)** RMA of modern male samples of the rib.

Statistically significant isometric growth was identified in the entire sample (b = 1.120, p<0.001), medieval (b = 1.000, p<0.001), male (b = 1.198, p<0.001), middle adult (b = 0.848, p<0.001), male middle adult (b = 0.853, p<0.001), female middle adult (b = 0.858, p = 0.008), medieval middle adult (b = 0.848, p<0.001), medieval male (b = 0.862, p<0.001) and medieval female (b = 1.149, p<0.001) sub-analyses, suggesting that osteon and Haversian canal growth occurs at similar rates within these sub-groups. Statistically significant positive allometric growth was identified in the remaining analyses, including modern (b = 1.907, p<0.001), female (b = 1.609, p<0.001), older adult (b = 1.813, p<0.001), male older adult (b = 1.835, p<0.001), modern older adult (b = 1.907, p<0.001), and modern male (b = 1.926, p<0.001) sub-analyses, suggesting that the Haversian canal growth rate is faster than the osteon growth rate within these sub-groups (Table 6.44).

Table 6.44: Reduced Major Axis Regression Results for the Rib.

***x* = On.Ar y= H.Ar**	***n***	**Slope (*b*)**	**r^2**	**95% CI slope**	**Intercept**	***p*-value**	**Relationship *b* >1: positive allometry *b* = 1: isometric growth *b* <1: negative allometry**
Entire Sample	71	1.120	0.298	0.791, 1.402	-1.605	**<0.001*** **	Isometric growth
Medieval	53	1.000	0.293	0.644, 1.261	-1.074	**<0.001*** **	Isometric growth
Modern	18	1.907	0.226	0.861, 2.810	-5.006	**<0.001*** **	Positive allometry
Males	39	1.198	0.195	0.685, 1.546	-1.947	**<0.001*** **	Isometric growth
Females	25	1.609	0.197	0.933, 2.057	-0.513	**<0.001*** **	Positive allometry
Middle-Aged Adult	28	0.848	0.269	0.326, 1.139	-0.415	**<0.001*** **	Isometric growth
Older Adult	21	1.813	0.209	0.926, 2.573	-4.601	**<0.001*** **	Positive allometry
Males							
Middle-Aged Adult	17	0.853	0.152	0.554, 2.664	-0.437	**<0.001*** **	Isometric growth
Older Adult	17	1.835	0.203	0.859, 2.703	-4.694	**<0.001*** **	Positive allometry

Females							
Middle-Aged Adult	11	0.858	0.216	-1.482, 1.267	-0.462	**0.008***	Isometric growth
Medieval							
Middle-Aged Adult	28	0.848	0.269	0.326, 1.139	-0.415	**<0.001*****	Isometric growth
Males	24	0.862	0.195	0.533, 2.557	-0.480	**<0.001*****	Isometric growth
Females	22	1.149	0.251	0.306, 1.609	-1.746	**<0.001*****	Isometric growth
Modern							
Older Adult	18	1.907	0.226	0.906, 2.866	-5.006	**<0.001*****	Positive allometry
Males	15	1.926	0.223	0.878, 3.004	-5.091	**0.001****	Positive allometry

* Significance values have been adjusted by the Bonferroni Correction for multiple tests.

Results of the RMA for the anterior femur samples are presented in Figure 6.10A-H and Table 6.45. Log10(On.Ar) and Log10(H.Ar) consistently had a positive strong relationship, as evidenced in Figure 6.10. This was across the RMA analysis of the entire sample and all sub-analyses taken to account for era, sex and age-at-death of the individuals.

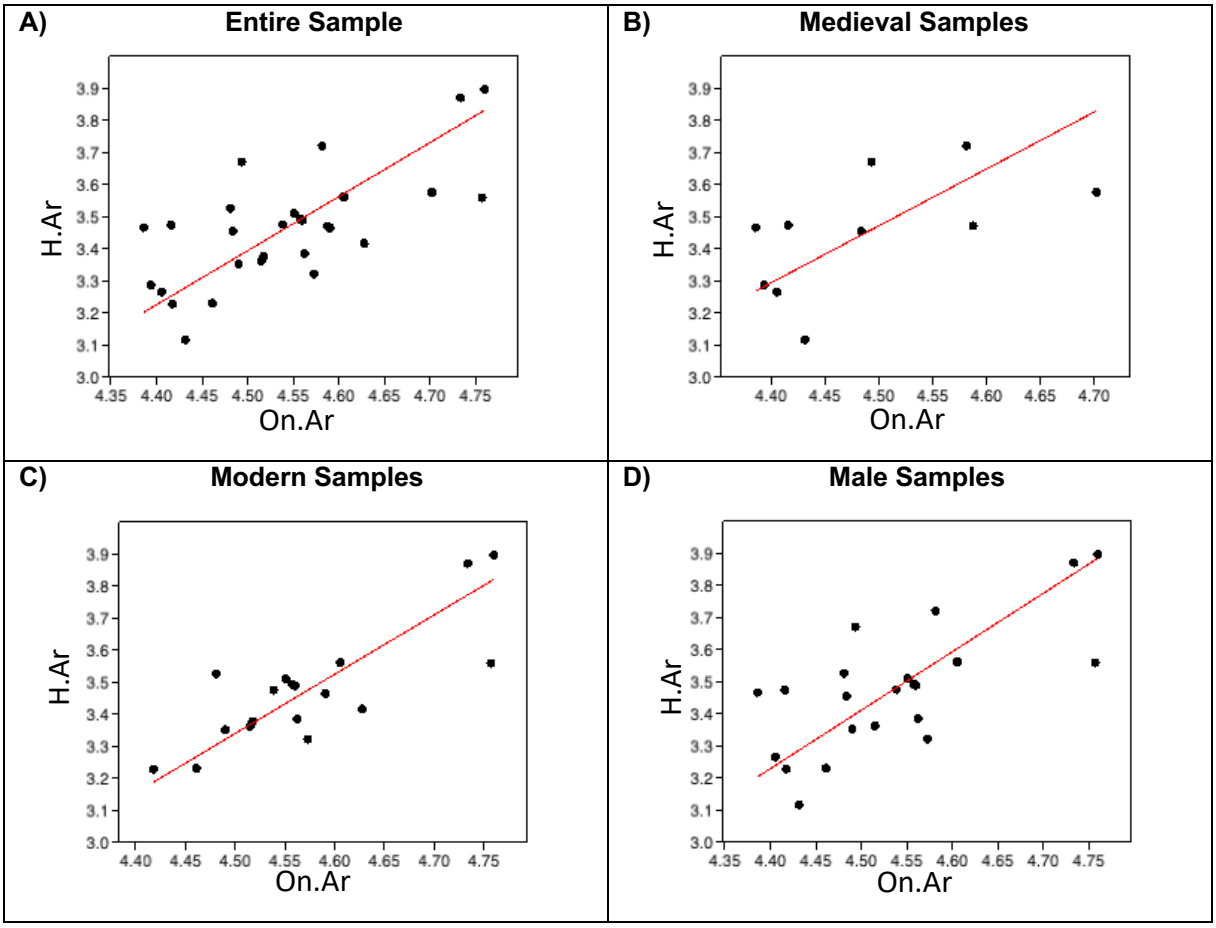

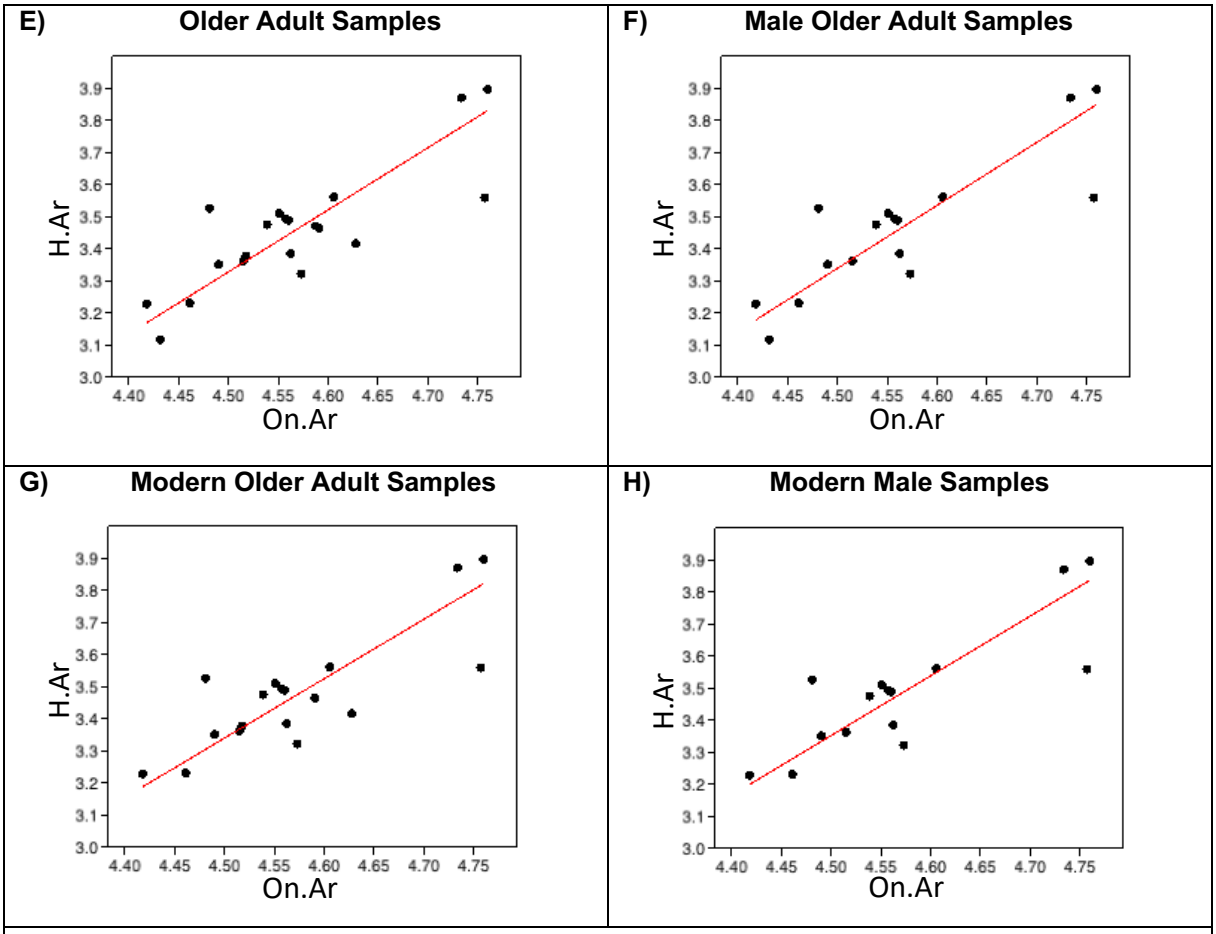

Figure 6.10: Reduced major axis regression plots of the anterior femur data.

A) RMA of entire sample of the anterior femur. **B)** RMA of medieval samples of the anterior femur. **C)** RMA of modern samples of the anterior femur. **D)** RMA of male samples of the anterior femur. **E)** RMA of older adult samples of the anterior femur. **F)** RMA of male older adult samples of the anterior femur. **G)** RMA of modern older adult samples of the anterior femur. **H)** RMA of modern male samples of the anterior femur.

Statistically significant positive allometry was identified in the entire sample (b = 1.683, p<0.001), and all sub-analyses including medieval (b = 1.773, p = 0.009), modern (b = 1.850, p<0.001), males (b = 1.821, p<0.001), older adults (b = 1.932, p<0.001), male older adults (b = 1.961, p<0.001), modern older adults (b = 1.850, p<0.001) and modern males (b = 1.864, p<0.001). This suggests that the Haversian canal growth rate is faster than the osteon growth rate across all sub-groups of the sample within the anterior femur (Table 6.45).

Table 6.45: Reduced Major Axis Regression Results for the Anterior Femur.

x **= On.Ar** **y = H.Ar**	***n.***	**Slope (*b*)**	r^2	**95% CI slope**	**Interce pt**	***p*-value**	**Relationship** ***b*** **>1: positive allometry** ***b*** **= 1: isometric growth** ***b*** **<1: negative allometry**
Entire Sample	28	1.683	0.479	1.244, 2.128	-4.178	**<0.001*** **	Positive allometry
Medieval	10	1.773	0.335	-0.171, 2.668	-4.507	**0.009***	Positive allometry
Modern	18	1.850	0.661	1.414, 2.548	-4.985	**<0.001*** **	Positive allometry
Males	22	1.821	0.502	1.195, 2.333	-4.781	**<0.001*** **	Positive allometry
Older Adults	20	1.932	0.695	1.520, 2.544	-5.364	**<0.001*** **	Positive allometry
Males							
Older Adults	16	1.961	0.727	1.456, 2.561	-5.484	**<0.001*** **	Positive allometry
Modern							
Older Adults	18	1.850	0.661	1.414, 2.548	-4.985	**<0.001*** **	Positive allometry
Males	15	1.864	0.697	1.373, 2.538	-5.035	**<0.001*** **	Positive allometry

* Significance values have been adjusted by the Bonferroni Correction for multiple tests.

Results of the reduced major axis regression (RMA) for the posterior femur samples are presented in Figure 6.11A-H and Table 6.46. Log10(On.Ar) and Log10(H.Ar) consistently had a positive strong relationship, as evidenced in Figure 6.11. This was across the RMA analysis of the entire sample and all sub-analyses taken to account for era, sex and age-at-death of the individuals.

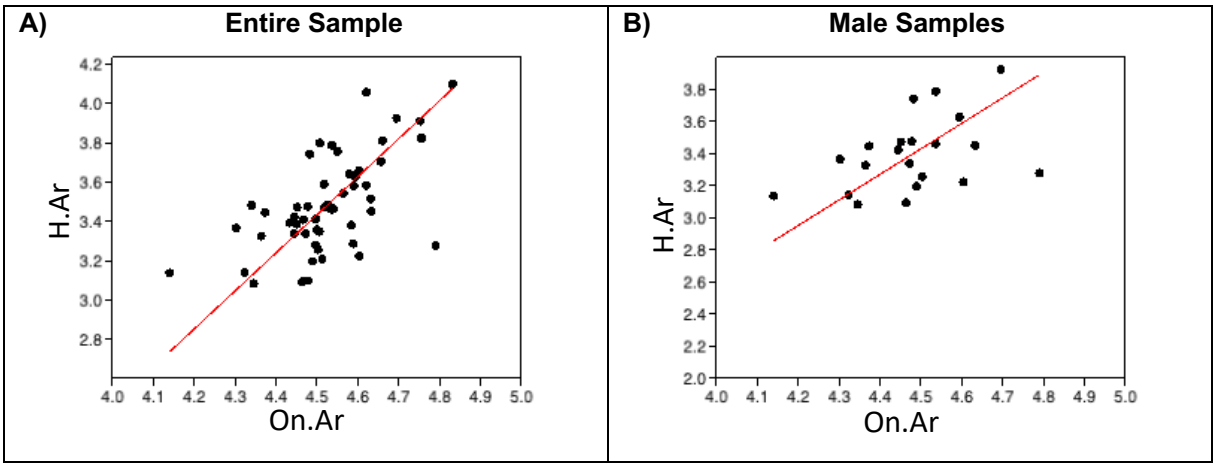

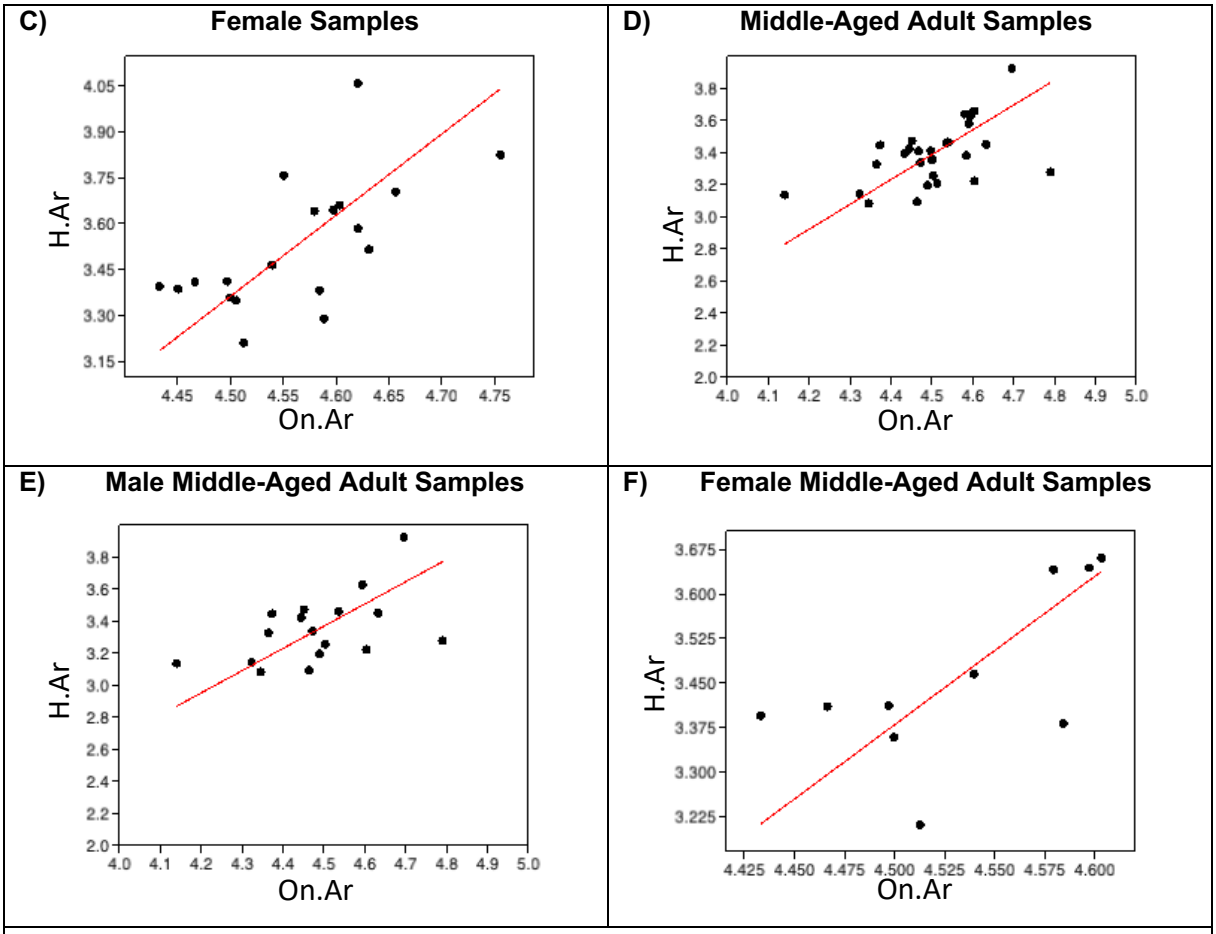

Figure 6.11: Reduced major axis regression plots of the posterior femur data.

A) RMA of entire sample of the posterior femur. **B)** RMA of male samples of the posterior femur. **C)** RMA of female samples of the posterior femur. **D)** RMA of middle-aged adult samples of the posterior femur. **E)** RMA of male middle-aged adult samples of the posterior femur. **F)** RMA of female middle-aged adult samples of the posterior femur.

Statistically significant positive allometry was identified in the entire sample (b = 1.934, p<0.001), and all sub-analyses including males (b = 1.593, p<0.001), females (b = 2.653, p<0.001), middle-aged adults (b = 1.548, p<0.001), male middle-aged adults (b = 1.388, p<0.001) and female middle-aged adults (b = 2.500, p = 0.006). This suggests that the Haversian canal growth rate is faster than the osteon growth rate across all sub-groups of the sample within the posterior femur.

Table 6.46: Reduced Major Axis Regression Results for the Posterior Femur.

***x* = On.Ar y = H.Ar**	***n*.**	**Slope (*b*)**	**r^2**	**95% CI slope**	**Intercept**	***p*-value**	**Relationship *b* >1: positive allometry *b* = 1: isometric growth *b* <1: negative allometry**
Entire Sample	53	1.934	0.379	1.386, 2.336	-5.266	**<0.001*** **	Positive allometry
Males	21	1.593	0.193	0.707, 2.325	-3.736	**<0.001*** **	Positive allometry
Females	19	2.653	0.413	1.009, 3.554	-8.578	**<0.001*** **	Positive allometry
Middle Adult	28	1.548	0.297	0.798, 2.034	-3.576	**<0.001*** **	Positive allometry
Males							
Middle Adult	17	1.388	0.253	0.517, 2.052	-2.874	**<0.001*** **	Positive allometry
Females							
Middle Adult	10	2.500	0.419	0.823, 3.566	-7.812	**0.006***	Positive allometry

* Significance values have been adjusted by the Bonferroni Correction for multiple tests.

6.6.4 Hypotheses Results

$H0_a$: Each of the observed osteon and Haversian canal size variables, On.Ar, H.Ar, On.Dm, H.Dm, On.Pm and H.Pm, have a similar distribution across the rib and the femur.

In the descriptive data, the rib had the smallest values in all variables pertaining to osteon and Haversian canal size (Table 6.31; Figure 6.8) and this was consistent across the sub-samples that were independent (Table 6.32) and related (Table 6.33).

The rib mean rank was consistently statistically significantly smaller than that of the posterior femur in all size variables, including On.Ar, H.Ar, On.Dm, H.Dm, On.Pm and H.Pm in the independent samples group (Table 6.34). In the related sample sets of rib, anterior and posterior femur samples from the same individuals, the rib was statistically significantly smaller than the anterior femur in On.Ar, On.Dm and On.Pm, and statistically significantly smaller than the posterior femur in On.Dm (Table 6.35). In the related sample pairs of rib and anterior femur samples from the same individuals, the rib was statistically significantly smaller in all osteon and Haversian canal size variables (Table 6.36). In the related sample pairs of rib and posterior femur samples from the same individuals, the rib was statistically significantly smaller in all osteon and Haversian canal size variables (Table 6.37). There were no statistically significant differences in osteon or Haversian canal size between the anterior and posterior femur (Table 6.38).

Once correcting by stature to account for individual body size differences, the rib mean rank was consistently statistically significantly smaller than that of the posterior femur in all size variables in the independent samples group (Table 6.39). In the related sample sets of rib, anterior and posterior femur samples from the same individuals, the rib was statistically significantly smaller than the anterior femur in On.Dm, and statistically significantly smaller than the posterior femur in H.Ar, On.Dm, H.Dm and H.Pm (Table 6.40). In the related sample pairs of rib and anterior femur samples from the same individuals, the rib was statistically significantly smaller in all osteon and Haversian canal size variables (Table 6.41). In the related sample pairs of rib and posterior femur samples from the same individuals, the rib was statistically significantly smaller in all osteon and Haversian canal size variables (Table 6.42). There were no statistically significant differences in osteon or Haversian canal size between the anterior and posterior femur (Table 6.43).

These results suggest that osteons and Haversian canals are both of a statistically significantly smaller size in the rib compared to the femur, rejecting the null hypothesis.

$H0_b$: There is no difference in the osteon and Haversian canal shape variables, On.Circ, H.Circ, On.Rd, H.Rd, On.AsRa, H.AsRa and On.Sd, between the rib and the femur.

Descriptive values demonstrated only minimal differences between the rib and femoral regions in all shape values, whether observing descriptives for the entire sample (Table 6.31; Figure 6.8), independent samples (Table 6.32) or related samples (Table 6.33).

Of all of the shape variables in the independent samples, only On.Sd was statistically significantly different between the rib and posterior femur, with the rib having statistically significantly higher On.Sd (Table 6.34). After correcting by stature, the rib had statistically significantly smaller On.Rd than the posterior femur (Table 6.39). In the related sets of rib, anterior and posterior femur samples, only H.Sd was statistically significantly higher in the rib than anterior femur (Table 6.35). After correcting by stature, identified that H.Circ and H.Rd are statistically significantly higher in the rib than posterior femur, H.AsRa is statistically significantly higher in the posterior femur than rib and H.Sd is statistically significantly higher in the rib than anterior femur (Table 6.40). In the paired rib and anterior femur samples, the rib had statistically significantly higher On.Circ, H.Rd, On.Sd and H.Sd, while the anterior femur had statistically significantly higher H.AsRa (Table 6.36). Once stature was corrected for, these statistically significant results remained, with the exception of H.Sd, which was no longer statistically significantly different between the rib and anterior femur (Table 6.41). In the paired rib and posterior femur samples, H.Circ and On.Sd were statistically significantly higher in the

rib (Table 6.37) and these results remained consistent after correcting by stature (Table 6.42). There were no statistically significant differences between the anterior and posterior femur in any shape variables either before (Table 6.38) or after correcting by stature (Table 6.43).

These results confirm there are statistically significant differences in osteon and Haversian canal shape between the femur and rib, rejecting the null hypothesis.

$H0_c$: There is no difference in the osteon and Haversian canal growth rates, (1) between osteons and Haversian canals, and (2) between the rib and the femur.

Results of the RMA demonstrated that the Haversian canal rate of growth is either faster or a similar speed to the osteon rate of growth, but never slower than the osteon (negative allometry) across the rib or either femoral region. As Haversian canals are nested within an osteon, it is not able to grow larger than its paired osteon and maintain a normal osteon morphology, and so the size of the osteon, here represented by On.Ar, acts as a constraint to which the Haversian canal can grow to, here presented by H.Ar.

Additionally, there appear to be different patterns of these rates of growth depending on the bone the osteons and Haversian canals are located in. In the rib, the RMA identified largely isometric growth relationships, with osteons and Haversian canals growing at a similar speed, but with some sub-groups of the samples included having positive allometry whereby the Haversian canals are growing faster than their paired osteons. These sub-groups which demonstrated positive allometric growth include the modern, females, older adults, male older adults, modern older adults and modern males. However, across both the anterior and posterior femur, this relationship was exclusively positive allometry, indicating that Haversian canals were consistently growing faster than their paired osteons. This demonstrates that there is a marked difference in osteonal and Haversian canal rates of growth between the rib and the femur, as well as a difference in the rates of growth between the osteons and Haversian canals themselves. Further, this demonstrates that some demographic sub-groups may be more likely to shift from isometric growth in the rib to positive allometry based on demographic factors.

These results reject the null hypothesis as they confirm differences in osteon and Haversian canal rates of growth between the two paired structures in some bones and demographic sub-groups, as well as differences in rates of growth between the rib and femur.

6.7 Results Summary

6.7.1 Research Question 1

Does human rib and femur histology, and its associated remodelling vary with age-at-death, sex and systemic health and physical activity (both inferred by SES status) in samples of English ancestry?

Key findings from this question include:

- Spearman's *Rho* correlation results indicate there is no relationship between known AAD and either variable, in the rib or femur. However, inferential results demonstrated significant differences between the OA and MA AAD categories from the YA and Adol categories, including OPD, Fg.OPD and Ct.Wi in the rib. There were some trends identifying differences in how AAD bone microstructural changes manifest in OPD, Fg.OPD and Ct.Po between the rib and the femur, but these patterns are inconsistent and, mostly, not statistically significant. However, it does appear that the rib may be more sensitive to changes in microstructural variables with AAD than the femur as it had the most amount of statistically significant differences between AAD categories.

- Some trends were identified during data description, but after inferential testing, no statistically significant differences between males and females was identified in either bone in OPD, Fg.OPD, Ct.Po or Ct.Wi. Only H.Ar in the rib was significantly higher in females than males. As the only significant difference was identified in the rib, it may suggest that the rib is more sensitive to microstructural changes with biological sex than the femur.

- The ModCon SES group is the most significantly different to both medieval SES groups, regardless of their High or Low status, especially for variables such as Ct.Wi in the rib, and OPD in both the rib and anterior femur. Key differences in the trajectories of effects on the rib versus the femur were identified, particularly in porosity variables.

6.7.2 Research Question 2

Is there a trend of bone quality "deteriorating" in modern individuals to reflect generally more sedentary lifestyles?

Key findings from this question include:

- OPD and Ct.Po was significantly different between medieval and modern individuals in the rib. In the anterior femur, there were significant differences in On.Circ, On.Ar and Po.Ar between medieval and modern individuals. %Ct.Ar was not significantly different between the two era groups in either bone. This suggests that there are significant differences between the modern and medieval groups, in all variables except %Ct.Ar.

- These differences included significantly higher OPD and significantly lower Ct.Po in the rib in the modern group. Additionally, there is significantly lower On.Circ and significantly higher On.Ar and Po.Ar in the modern group in the anterior femur. These results suggest that there are some indications that a more sedentary lifestyle in modern individuals may be influencing some bone microstructural variables, such as On.Ar and Po.Ar, but the opposite or no effect in other variables including OPD, %Ct.Ar, On.Circ and Ct.Po.

6.7.3 Research Question 3

Is there variation in standardized histological variables between serial sections from the human rib?

Key findings from this question include:

- The Spearman's *Rho* results identified statistically significant strong relationships between almost all observed variables in serial rib sections from the same individuals, including Ct.Ar, Ct.Wi, Ct.ArA, Ct.Po, On.Ar, H.Ar, OPD, Fg.OPD and On.Circ. However, there was no correlation between Po.Ar between the serial pairs of rib sections.

- This suggests that porosity can change significantly between sections, but other cross-sectional geometry and microstructural variables may not significantly vary between sections up to 1cm apart along the rib shaft.

6.7.4 Research Question 4

A) Are osteon and Haversian canal size smaller in the rib than the femur? B) Do we see more irregular geometric properties like osteon and Haversian canal circularity, aspect ratio, roundness and solidity in the femur as compared to the rib?

Key findings from this question include:

- The rib osteon and Haversian canal values were significantly smaller than those of both the anterior and posterior femur, across all size variables, but no statistically significant difference between osteon or Haversian canal size variables in the anterior versus posterior femur. These results suggest that osteons and Haversian canals are both generally of a smaller size in the rib as compared to the femur.

- There was no difference in the osteon and Haversian shape variables On.Circ, H.Circ, On.Rd, H.Rd, On.AsRa and On.Sd, between the rib and femur. There was a significant difference in H.AsRa between the rib and anterior femoral aspect, and between the anterior and posterior femoral aspects, but no significant difference between the rib and posterior femur. These results suggest that there is no significant difference in most shape variables between the rib and the femur, with the exception of H.AsRa differences between the rib and the anterior femur.

- Results of the RMA demonstrated that the Haversian canal rate of growth is either faster or a similar speed to the osteon rate of growth, but never slower than the osteon (negative allometry) across the rib or either femoral region. In the rib, the RMA identified largely isometric growth relationships, with osteons and Haversian canals growing at a similar speed, but with some sub-groups of the samples included having positive allometry whereby the Haversian canals are growing faster than their paired osteons. However, across both the anterior and posterior femur, this relationship was exclusively positive allometry, indicating that Haversian canals were consistently growing faster than their paired osteons. This demonstrates a marked difference in osteonal and Haversian canal rates of growth between the rib and the femur, as well as a difference in the rates of growth between the osteons and Haversian canals themselves. Further, this demonstrates that some demographic sub-groups may be more likely to shift from isometric growth in the rib to positive allometry based on demographic factors.

Chapter 7 Discussion

This chapter discusses the findings of each research question and contextualises them within the broader literature, including those discussed in Chapter 3: Literature Review.

7.1 Research Question 1

Does human rib and femur histology vary with age-at-death, sex and systemic health and physical activity (as inferred by socioeconomic status) in samples of English ancestry?

This research question addressed not only how age-at-death, biological sex, and systemic health and physical activity affect human rib and femoral histology, but also how these factors affect the rib and femur differently based on the intrinsic differences in the structure and key functions of these two bones. Here, this research question will be broken down by factor, followed by the differences in how the rib and femur respond to these demographic, health and lifestyle factors.

7.1.1 Age-At-Death and Bone Remodelling

For this research question, targeted variables were selected which were most likely to reflect or be sensitive to changes with advancing age. This included osteon population density, fragmentary osteon population density, cortical porosity, and cortical width.

The results of research question one demonstrated that there was no statistically significant correlation between chronological age-at-death and either variable in either bone; total and fragmentary osteon population density, cortical porosity and cortical width, even after correcting for individual stature variation. This result goes against findings by Goliath et al. (2016) who identified a statistically significant strong positive relationship between chronological age-at-death and osteon population density in the femoral midshaft. Other studies have struggled with sample size and acquiring samples from a wide range of ages (e.g., Pedersen et al. 2024). In fact, the individuals in the present study with documented age-at-death were all of an advanced age, at least 59 years of age and older (4.1.1.3 The Donor Samples; Table 4.1), which is a common problem in body donation programs globally (Balta et al. 2022; Fennell and Jones 1992; Jenkin and Keay 2025; McClea and Stringer 2010; Smith et al. 2022). This could have contributed to the lack of correlation between chronological age-at-death and either variable, as differences between the included individuals were not polarising enough, being too close in age-at-death, to document age-related changes.

However, when individuals with estimated age-at-death categories were included in the categorical age-at-death analysis by adding in the medieval individuals to the analysis, some statistically significant differences were identified between age-at-death categories.

Older adults (aged 50+ years) had statistically significantly higher total and fragmentary osteon population density than middle aged adults (35 – 49 years) in the rib. This agrees with literature elsewhere where increasing osteon and fragmentary osteon population densities have increased with advancing age in the rib (Cho et al. 2002; García-Donas et al. 2022; Goliath et al. 2016; Kim et al. 2007; Pavón et al. 2010; Pfeiffer et al. 2016; Stout and Paine 1992). More recently, attention has been given to fragmentary osteon population density as a separate variable, rather than a contribution to general osteon population density calculations in studies of age-related changes (Crowder et al. 2022). This is because of the phenomenon, called the 'asymptote', of osteonal remodelling continuously and indiscriminately throughout life, which leads to the remodelling over of existing osteons, creating fragmentary osteons as only portions of 'older' osteons remain visible (Frost 1987b; Stout and Paine 1994). This phenomenon resulting in such an increase of fragmentary osteons is not generally seen in younger individuals as there are a lower population of osteons in their cortical bone which means a lower chance of osteons being remodelled over (Crowder and Rosella 2007; Stout and Paine 1994).

Middle-aged and young adults (20 – 34 years) had statistically significantly higher cortical width than older adults in the rib. This agrees with literature elsewhere that has identified cortical thinning in older individuals (Agnew and Stout 2012; Dominguez and Agnew 2016; Pfeiffer et al. 2016). Cortical thinning is a well-documented phenomenon in the clinical realm (Chen et al. 2013; Parfitt 1984; Pignolo et al. 2021; Thompson 1980), that occurs with advancing age and is often associated with increased fracture risk and decreasing bone mineral density (Li and Gong 2021; Yadav et al. 2021). This explains the decrease in cortical width in older adults compared to middle and young adults seen in the present results. Further, the lack of statistically significant difference between young and middle-aged adult age-at-death categories, suggests that the cortical thinning phenomenon may not occur until reaching older adult age (50+ years), or perhaps just not to the degree that is recognisable in group mean difference testing. In the clinical literature, cortical thinning is often described as beginning in the third decade of life but escalating in the later fourth to fifth decade (Compston 2001; Farr and Khosla 2015; Khosla 2013; Pignolo et al. 2021). This could explain why there are no statistically significant differences in cortical width between young and middle-aged adults in this sample, but there are statistically significant differences that separate the older age-at-

death category. Like this research, Maggio and Franklin (2021) failed to identify correlations with variables and chronological age-at-death but identified statistically significant differences between age-at-death categories. The most polarising differences were between the younger and older adult age-at-death categories, with fewer differences in between the middle adult category and its neighbouring categories, reinforcing this presence of escalated bone loss with the later fourth to fifth decade of life (Farr and Khosla 2015; Khosla 2013; Maggio and Franklin 2021; Pignolo et al. 2021).

7.1.2 Sex and Bone Remodelling

To observe sex-related changes, targeted microstructural and cross-sectional variables were selected which were most likely to differ between biological sexes. This included osteon population density, fragmentary osteon population density, cortical porosity, cortical width, osteon area and Haversian canal area.

There were no statistically significant differences between males and females in osteon or fragmentary osteon population density, cortical porosity or width, either before or after correcting for individual stature variation. Elsewhere, females have had statistically significantly larger mean osteon population density, inclusive of fragmentary osteons (Fahy et al. 2017), though in some literature this finding was restricted to the rib and not mirrored in the femur, which seemed to be more closely related to body size, perhaps due to its weight-bearing status (Cho and Stout 2011). Literature has identified lower cortical width (Clarke and Khosla 2009; Compston 2001; Handelsman et al. 2018; Stewart et al. 2015) and higher cortical porosity (Cauley et al. 2003; Compston 2001; Khosla and Hofbauer 2017; Krum et al. 2008) in females than males, albeit these differences are more pronounced in individuals of advanced age. This has been associated with menopause in females, whereby estrogen changes result in bone loss, with increasing cortical porosity and cortical thinning as part of bone trabecularisation associated with osteoporosis (Cauley et al. 2003; Compston 2001; Dominguez and Agnew 2016; Khosla and Hofbauer 2017; Krum et al. 2008). These results could demonstrate that cortical width and porosity are more closely aligned with age-related changes rather than sex differences, and with all age-at-death categories pooled together for an analysis of males versus females, the sex-specific changes with ageing are perhaps weakened in the statistical output. Unfortunately, due to sample size restraints, further statistical analysis of sex by age-at-death category was not possible. Future research where sex and age-at-death demographic groups can be analysed separately could better identify sex differences in osteon and fragmentary osteon population density, cortical porosity and width.

Osteon and Haversian canal area were statistically significantly higher in females than males in this research. Contrary to this, Pfeiffer (1998), Pfeiffer et al. (2006) and Stewart et al. (2015) did not find any association with sex or age-at-death with osteon size, though did state that osteon size was frequently larger in female individuals than males. Meanwhile, statistically significantly larger osteons and Haversian canals have been identified in female individuals than their male counterparts by several studies elsewhere (Cho and Stout 2011). Conversely, Britz et al. (2009) and Karydi et al. (2022) found the reverse, with males having statistically significantly higher osteon area than females. Literature consensus to date suggests this could reflect a societal specific mechanical difference, such as gendered roles in physical activity patterns, with females undertaking less physically demanding roles in society and therefore having larger osteons and Haversian canals than males (Burr et al. 1990; Dominguez and Agnew 2016; Mulhern 2000; Mulhern and Van Gerven 1997). For example, Van Oers et al. (2008a; 2008b) found that smaller osteon area was associated with localised higher strain, which could suggest for this research that males have increased amounts of localised strain at the posterior femur than females. However the larger osteon and Haversian canal size in the ribs of females in the present research, is more likely to reflect a systemic and thereby biological difference between the sexes, as the rib is less clouded by gender role influence as it is not impacted by physical activity patterns in the same way that the femur is (Agnew and Stout 2012; Crowder and Rosella 2007; Dominguez and Agnew 2016; Karlson 1998; Paine and Brenton 2006; Seeman et al. 1992; 2000; Stewart et al. 2021; Tommerup et al. 1993). However, gendered access to quality foods has been identified in some populations, particularly in the past, and may conflate sex differences in rib microstructure (Błaszczyk et al. 2021; Dyer 2000; Jotischky 2011; Paine and Brenton 2006; Powell et al. 2001; Van der Veen 2003). This is likely more of an issue for the medieval individuals in this research rather than the contemporary Australians.

Haversian canal area was only statistically significantly higher in females in the posterior femur samples after the correction for individual body size variation was applied. Similarly, osteon area was only statistically significantly higher in females in the rib after individual body size variation correction. This suggests that there is an effect of body size on these variables which must be accounted for in applications of sex estimation from human remains or where observations on sex-differences are being recorded. This effect of body size on osteon and Haversian canal area has been recorded elsewhere in the literature (Britz et al. 2009; Cho and Stout 2011) but has also been disputed (Beresheim et al. 2018).

Finally, there were no statistical differences between males and females in the anterior femur samples. It is important to note that there were only four female anterior femur samples which may in part be why no statistically significant differences were identified as the analysis was underpowered. However, it could also be bone specific. The anterior femur is not particularly susceptible to systemic differences like we see in the rib, but simultaneously, is not as subjected to physical activity and/or biomechanical loading that we see in the posterior femur (Coratella et al. 2020; Fuchs et al. 2009; Monk et al. 2016). Interestingly, while not statistically significant, Haversian canal area was marginally higher in males in the anterior femur samples according to the descriptive data (Table 6.13). Further analysis with a larger anterior femur sample size is needed to investigate this finding.

7.1.3 Socioeconomic Status and Bone Remodelling

To observe changes in bone histology with socio-economic status, targeted variables were selected which were most likely to differ between the medieval high and low status, and contemporary groups. This included osteon population density, osteon circularity, porosity area, cortical porosity, cortical width and cortical area. A key limitation of this part of the analysis is that for the contemporary Australian individuals, there were no posterior femur samples available, and so this portion of the analysis could only look at results from the rib and anterior femur. These results overwhelmingly demonstrated differences between the contemporary socioeconomic status group and the medieval groups, both high and low socioeconomic status groups, with fewer statistically significant differences between the medieval high and low status groups.

Contemporary Australians had statistically significantly higher osteon population density in the rib than both the medieval high and low socioeconomic status individuals, both before and after stature correction. Additionally, the contemporary Australians had statistically significantly higher osteon population density in the anterior femur than the medieval low status individuals, both before and after stature correction. These results suggest that contemporary individuals have a statistically significantly higher cortical bone remodelling rate, deduced by the statistically significantly higher osteon population density, a commonly used proxy for estimating bone remodelling rate (Fahy et al. 2017; Miszkiewicz and Mahoney 2016). Higher bone remodelling rates in the rib in modern versus both the high and low status medieval individuals, are more likely to pertain to systemic rather than physical activity patterns (Agnew and Stout 2012; Crowder and Rosella 2007; Dominguez and Agnew 2016; Karlson 1998; Paine and Brenton 2006; Seeman et al. 1992; 2000; Stewart et al. 2021; Tommerup et al. 1993). While the higher remodelling rate in the anterior femur is more likely to pertain to higher

localised strain and increased biomechanical loading. Higher bone remodelling rates have been associated with higher quality nutrition and better systemic health, and access to health and dental care (Miszkiewicz and Mahoney 2016). However, bone remodelling also increases with advancing age (Mallorie and Shine 2022), which is important to note as the contemporary Australian individuals were all in the older adult age-at-death category. The increased bone remodelling with advancing age occurs due to the balance of resorption and formation in bone turnover becomes imbalanced, with more resorption and less formation (Mallorie and Shine 2022). Another important nuance is that bone remodelling does have an optimal rate, which, when it is surpassed, and bone remodelling occurs too quickly, it has been associated with increased bone fragility and fracture rate, decreased bone mineral density and increased porosity, and increase the development of conditions such as osteoarthritis (Katsimbri 2017; Lin et al. 2022; Mashiba et al. 2010; Odvina et al. 2005; Seeman 2008).

The contemporary Australian group had statistically significantly lower osteon circularity than both the medieval high and low socioeconomic status groups, in both the rib and the femur, but only prior to stature correction application. Less circular osteons are more elongated in shape rather than a perfect circle (Zdilla et al. 2016) and have been attributed to more variable repertoires of physical activity patterns, with angled repetitive activity (Frost 1964; Nareliya Mishra et al. 2022; Skedros 2024; Tommerup et al. 1993). However, here, as the low osteon circularity results were only statistically significant prior to the correction of individual stature variation, suggests there is an effect of body size on osteon circularity. This could be a result of higher stature individuals generally having a higher level of biomechanical load and strain due to heavier bodyweight (Ruff et al. 2006; Skedros 2024; Skedros et al. 2001; 2009).

Porosity area was statistically significantly higher in the anterior femur in the contemporary Australians than the medieval high status group after stature correction was applied. The increased porosity area in the modern contemporary Australians could reflect their advanced age-at-death as compared to the broader range of ages present in the medieval high status group due to the known increase in cortical porosity area with advancing age (Cooper et al. 2016). Another possible explanation could be related to the increased bone remodelling rate in the contemporary Australian group, which temporarily increases local cortical porosity, and could more easily impact a weight-bearing region of bone such as the anterior femur (Hughes et al. 2017). Cortical porosity can be reduced by weight-bearing activities and by optimising physical activity levels, increasing bone density and reducing bone fragility (Warden et al. 2021). Thus, a final alternative also postulated by Miszkiewicz and Mahoney (2016), was that the high status medieval individuals from St Gregory's were more physically active than first

thought, perhaps participating in documented activities such as pilgrim walks to far away Priories or jousting competitions which knights in the high status classes participated in. This could explain the lower cortical porosity area in medieval high status individuals than the contemporary Australians who are generally assumed to lead sedentary Western lifestyles (Australian Bureau of Statistics 2022a).

Additionally, the medieval low status group had statistically significantly higher porosity area than the medieval high status group in the rib, and this was the only statistically significant difference identified between the medieval low and high socioeconomic status groups. This higher porosity area in the rib in the medieval low status group as compared to the medieval high status group, could be a reflection of the poor diet quality the low status individuals were subjected to as compared to the affluent diet enjoyed by the high status individuals, which has been discussed in the literature pertaining to St Gregory's and medieval Britain more broadly (see Section 4.1.2.4; Dyer 2000; Jotischky 2011; Miszkiewicz and Mahoney 2016; Powell et al. 2001; Rogers and Waldron 2001; Serjeantson and Woolgar 2006). As the rib experiences biomechanical loading and strain with respiration rather than physical activity (Crowder and Rosella 2007; Dominguez and Agnew 2016), it would have been difficult for the medieval low status individuals to overcome poor bone health in their rib via the prolonged and strenuous physical activity they undertook as part of their daily occupations (Miszkiewicz and Mahoney 2016).

The contemporary Australians had statistically significantly lower rib cortical width than both medieval high and low status individuals, both before and after stature correction was applied. This suggests that cortical thinning of the rib is more prevalent in contemporary Australians than medieval high and low status groups. However, it is important to note that all contemporary Australians observed in this research were within the older adult age-at-death category (50+ years). The more extensive cortical thinning in the contemporary Australian group could be a reflection of their advanced age-at-death compared to the wider age range present in the medieval sample. As described above (Section 7.1.1), cortical thinning, especially of the rib, has been widely associated with advanced age (Agnew and Stout 2012; Chen et al. 2013; Corrado et al. 2020; Dominguez and Agnew 2016; Ebbesen et al. 1999; Kenkre and Bassett 2018; Li and Gong 2021; Parfitt 1984; Parfitt et al. 1995; Pfeiffer et al. 2016; Pignolo et al. 2021; Thompson 1980; Yadav et al. 2021). Rather than a reflection of socioeconomic status, this could be attributed to the advanced age recorded in the contemporary sample. Further research with a large enough sample size to control for age-at-

death and sex, would perhaps be better at teasing out differences in cortical width with socioeconomic status.

Finally, both the rib and anterior femur were similar in the degree in which they demonstrated statistically significant differences between socioeconomic status. Both demonstrated statistically significant different osteon population densities, osteon circularity and porosity area, while cortical width could only be assessed in the rib due to a lack of full cross-sections of the femur. Overall, the results of this part of research question one demonstrate a vast difference between the contemporary Australian and both medieval groups. Due to the vastly different lifestyles experienced by the contemporary versus medieval individuals, in healthcare, diet, physical labour, it is possible that these differences alone could be masking true relationships of age-at-death and biological sex and bone microstructures and cross-sectional geometry elsewhere in research question one. These differences between contemporary and medieval humans will be further explored, along with the impacts of modern sedentary lifestyles, via research question two.

7.1.4 Differences Between Rib and Femoral Bone Remodelling

The results from research question one demonstrate differences in the way the rib and femur respond to intrinsic and extrinsic factors, including age, biological sex and socioeconomic status. The rib appears to be more sensitive and responsive to intrinsic bone changes, while the posterior and anterior femur respond more so to physical activity, biomechanical loading and strain patterns of behaviour. Of the femoral regions, the posterior femur was more likely to render statistically significant differences between groups, though these may be more so a reflection of patterns of physical activity and biomechanical load than as a result of the intrinsic factors such as age-at-death (lesser physical activity in individuals of advanced age), sex (gendered societal roles) and socioeconomic status (patterns of strenuous physical labour versus sedentary lifestyles). Further, the rib samples demonstrated more statistically significant age-related changes, while the femur was more susceptible to biomechanical loading stress, which could perhaps mask the differences that come with advancing age, sex and even socioeconomic status, of which a large portion of status differences are intrinsically linked with physical activity patterns. Larger sample size within each demographic group, allowing for separate analysis of each sex, age-at-death category and each socioeconomic status group, could facilitate further investigation of these effects on bone microstructure and cross-sectional geometry.

Previous studies have identified that the rib is broadly more sensitive to systemic as opposed to local factors, such as age, sex, general health and nutrition, while the femur is less likely to show microstructural changes with systemic factors, but rather, reflects local patterns in physical activity levels and biomechanical loading repertoires (Agnew and Stout 2012; Crowder and Rosella 2007; Dominguez and Agnew 2016; Karlson 1998; Paine and Brenton 2006; Pedersen et al. 2024; Seeman et al. 1992; 2000; Stewart et al. 2021; Tommerup et al. 1993). This study provides a direct comparison of a modern contemporary Australian population to a well-established and widely-studied medieval British sample to determine where in the bone biology literature the contemporary Australian group resides.

Statistically significant differences between age-at-death categories were only identified in the rib, while no such differences were identified in the posterior femur. The statistically significant results in the anterior femur samples were only rendered prior to correction for individual stature variation, which suggests that body size may have influenced this variation between age-at-death categories rather than being strictly related to changes with advancing age. This is similar to results in the literature, where the rib has been identified as a more suitable bone to observe when interested in age-at-death estimation or age-related changes (Pedersen et al. 2024; Stewart et al. 2021; Tommerup et al. 1993) but disagrees with literature elsewhere that have identified age-related changes in the femur (Ahlqvist and Damsten 1969; Ericksen 1991; Kerley 1965; Lagacé et al. 2019; Maat et al. 2006; Singh and Gunberg 1970; Watanabe et al. 1998).

Sex differences on the surface appear to present similarly between the posterior femur and rib, with statistically significantly larger osteons and Haversian canals in females identified in both bones. However, it is important to look at this contextually. For example, larger osteon and Haversian canal size is also associated with less physical activity, increased sedentism and reduced biomechanical loading pressures (Burr et al. 1990; Dominguez and Agnew 2016; Mulhern 2000; Mulhern and Van Gerven 1997; Van Oers et al. 2008a; 2008b). Thus, seeing larger osteons and Haversian canals in the posterior femur in females could also reflect difference in societal gender roles, with women being historically less likely to partake in physically strenuous, labour-intensive jobs (Jervis 2022; Whittle and Hailwood 2020). The fact that the larger osteon and Haversian canal size was also identified in females in the rib, reinforces that this could also be associated with biological sex differences rather than sex/gender related physical activity patterns. Interestingly, there were no differences at all identified between the sexes in the anterior femur samples. This is not to say that the anterior femur is unaffected by changes with biological sex, but rather that the effects of biomechanical

load and physical activity are so extreme and variable between individuals on this highly biomechanically active bone, that differences with advancing age, sex and general health and nutrition are perhaps clouded in the femur.

These results add to the vast body of literature that demonstrates the rib is poorly equipped in biological terms to overcome detrimental changes due to advancing age with increased physical activity as it is not a weight-bearing bone (Agnew and Stout 2012; Crowder and Rosella 2007; Dominguez and Agnew 2016; Karlson 1998; Paine and Brenton 2006; Pedersen et al. 2024; Seeman et al. 1992; 2000; Stewart et al. 2021; Tommerup et al. 1993). Additionally, elsewhere it has been determined that the anterior femur is less biomechanically loaded than the posterior femur due to fewer origin and insertion points for muscles, tendons and ligaments (Coratella et al. 2020; Fuchs et al. 2009; Monk et al. 2016). As bone does not respond systemically to physical activity and biomechanical loading, but rather adapts locally, bone loss events such as cortical thinning cannot be overcome by physical activity alone as easily as the posterior femur (Biewener and Bertram 1993; Lanyon et al. 1982; Stout et al. 2019). Additionally, the rib has been identified as more susceptible to systemic changes than the femur due to a higher proportion of medullary cavity to cortical bone, and therefore higher surface area contact to medullary and nutrient tissues (Robling and Stout 2003). This may mean it is faster to respond to systemic changes in the body than the femur as it has more exposure to systemic nutrients and is not easily able to increase its own vascularity by osteonal remodelling with physical activity and biomechanical loading as the femur (Agnew and Stout 2012; Crowder and Rosella 2007; Dominguez and Agnew 2016; Tommerup et al. 1993).

7.2 Research Question 2

Is there a trend of bone quality "deteriorating" in contemporary individuals to reflect generally more sedentary lifestyles than their medieval ancestral population?

For this research question, targeted variables were selected which were most likely to reflect or be sensitive to changes with biomechanical load pressures, associated with physical activity. This included osteon population density, osteon circularity, osteon area, porosity area, cortical porosity and cortical area.

7.2.1 Contemporary and Medieval Bone Differences

Contemporary individuals had statistically significantly higher osteon population density in the rib and anterior femur. Osteon circularity was statistically significantly higher in the medieval

individuals in both skeletal elements. Modern individuals had statistically significantly higher osteon area and porosity area in the anterior femur. Cortical porosity was statistically significantly higher in the modern individuals at the anterior femur prior to stature correction, but lower at the rib following stature correction. There was no statistically significant difference in cortical area between medieval and modern groups.

In the rib, the discrimination function analysis (DFA) successfully classified 87.9% of cases as either medieval or contemporary based on osteon population density, circularity, area, porosity area and cortical porosity. Classification success increased when accounting for age-at-death category but decreased in the male sub-group and increased in the female sub-group. In the anterior femur, the DFA successfully classified 91.3% of cases as medieval or contemporary based on osteon population density, circularity, area and cortical porosity. Classification reliability decreased when age-at-death category was accounted for and increased in reliability in the male sub-group.

In humans, DFA has been used elsewhere to separate human remains by sex (Mastrangelo et al. 2011; Šlaus and Tomičić 2005; Šlaus et al. 2013), skeletally mature versus immature individuals (Dolding-Smith 2023) and to separate human from animal bone (Weisleitner et al. 2026). While DFA has also been used to discriminate historical dog breeds from their modern counterparts (Phillips et al. 2009), it has not been used to distinguish past and modern human remains in the available literature. However, this novel application offers significant benefit to disciplinary knowledge and toolkits to not only observe differences between the two groups, but to form classification systems for categorising remains of unknown temporal origin from within the same region. This method could assist bioarchaeologists and forensic anthropologists in methodological improvements, expanding available tools at their disposal.

7.2.2 Contemporary Sedentary Lifestyle

The literature has demonstrated that a more sedentary lifestyle is associated with decreased osteon population density as bone remodelling slows down due to a lack of stimulation from physical activity and biomechanical loading (Miszkiewicz 2016; Raab et al. 1991; Schlecht et al. 2012; Skedros 2005; Skedros et al. 2005; Tommerup et al. 1993). However, here we see that contemporary individuals have statistically significantly higher osteon population density than the medieval group. Additionally, cortical area is expected to be smaller in more sedentary individuals, as bone mineral density decreases and cortical thinning increases (Aloia 1994; Frost 2000; Robling et al. 2006), but in this research there was no statistically significant difference between the medieval and contemporary groups in cortical area. In conjunction with

cortical bone loss, it has been demonstrated in the literature that increased cortical porosity is also associated with more sedentary lifestyles, as trabecularisation of the cortex occurs, increasing bone loss (Burr 2010; Schlecht et al. 2012; Zebaze et al. 2010). However, in this research, contemporary individuals had statistically significantly lower cortical porosity than the medieval group in the rib. Higher osteon circularity has been associated with more sedentary lifestyles, with less directional strain to cause osteonal drift (Frost 1964; Keenan et al. 2017; Nareliya Mishra et al. 2022; Skedros 2024), and also increasing with advancing age (Goliath et al. 2016; Karydi et al. 2022) and with some suggesting it is merely a byproduct of higher osteon population density (Britz et al. 2009; Currey 1964; Goliath 2010). However, in contemporary individuals, a group with older age-at-death ranges recorded than the medieval group, but also with higher osteon population density, we see statistically significantly lower osteon circularity suggesting more variable directional strain and increased osteonal drift. Finally, cortical area reduces with sedentary lifestyles or limb disuse due to the lack of loading pressures to result in cortical bone growth (Burr 2010; Schlecht et al. 2012; Zebaze et al. 2010), but in this research there is no statistically significant difference in percent cortical area between the contemporary and medieval individuals.

Elsewhere, higher osteon area has been associated with sedentism or even disuse of limbs (Schlecht et al. 2012; Van Ooers et al. 2008a; 2008b), which occurs when bone metabolism and remodelling slows due to a lack of stimulation of osteocytic channels and decreased loading pressures to signal bone growth (Skedros et al. 2001; Smit 2022) and reduced blood circulation (Tuckermann and Adams 2021). Here, contemporary individuals have statistically significantly higher osteon area in the anterior femur than medieval individuals, perhaps indicative of a more sedentary lifestyle. Additionally, the literature demonstrates that with increased sedentism or even limb disuse, porosity area and cortical porosity increase (Aloia 1994; Burr 2010; Frost 2000; Robling et al. 2006; Schlecht et al. 2012; Zebaze et al. 2010) due to the slowed bone remodelling which is unable to efficiently remove damaged or old bone tissue, and, in turn, is slow to replace this with new bone. Further increasing porosity is that slowed bone metabolism does not calcify efficiently, leading to the extended presence of woven bone, which is not as strong as lamellar bone due to disorganised and reduced population of collagen fibrils (see 2.3.2 Bone Tissue Types; Clarke 2008; Eriksen et al. 1994). This could help to explain the statistically significantly higher cortical porosity observed in the contemporary Australian anterior femoral samples.

However, cortical porosity results were nuanced. While contemporary individuals had statistically significantly higher cortical porosity in the anterior femur, they also had statistically

significantly lower cortical porosity in the rib. This could be a result of differences in functional adaptations between the femur and rib. For example, as the rib is more reflective of systemic health, the statistically significantly lower cortical porosity in the rib in contemporary individuals could reflect a better-quality diet and nutrition and better general health in contemporary humans than those in medieval Britain. Food in medieval Britain was largely either of poor hygiene and quality with little access to animal protein for low status individuals, or the exact opposite with an oversaturation in animal proteins and fatty cholesterol, leading to protein saturation and skeletal manifestations of diffuse idiopathic skeletal hyperostosis (DISH) believed to be associated with protein rich and fatty cholesterol diets (see Section 4.1.2.4; Dyer 2000; Jotischky 2011; Miszkiewicz and Mahoney 2016; Powell et al. 2001; Rogers and Waldron 2001; Serjeantson and Woolgar 2006). Conversely, contemporary Australians have easier access to sufficient food, though dietary decision-making varies by socio-economic status and age (Abebe et al. 2025; Australian Institute of Health and Welfare 2024b), over 80% of Australians accessed publicly funded primary healthcare in the 2024-2025 financial year (Australian Institute of Health and Welfare 2025) and high hygiene standards which have improved over the 20th century, along with increased availability of vaccines for many communicable diseases (Australian Institute of Health and Welfare 2024c).

7.3 Research Question 3

Is there variation in standardised histological variables between serial cross-sections from the human rib midshaft?

To investigate whether serial sections of the rib could produce statistically significant differences in histological variables, the most commonly assessed histological variables were selected for observation. This included cortical area, cortical width, absolute cortical area, porosity area, osteon area, cortical porosity, Haversian canal area, osteon population density, fragmentary osteon population density, and osteon circularity.

7.3.1 Rib Cross-Sectional Intra-Element Variation

Rib cross-sectional intra-element variation has important implications for sampling techniques and improving understanding of localised bone metabolic variation within a single bone as represented via microstructural (Dominguez et al. 2020) and cross-sectional geometry (Murach et al. 2017) variables. This research question examined relationships between paired histological slides 1cm apart, from the same rib using Spearman's *Rho* correlations and Wilcoxon Signed Rank tests. Statistically significant strong correlations were identified in

cortical area, width and absolute area, suggesting that the values of these variables were similar between the paired slides. There were statistically significant medium strength relationships identified in cortical porosity, osteon area, osteon population density, fragmentary osteon population density and osteon circularity, suggesting some variation between these variables in the paired slides. The weakest, but still statistically significant relationship was identified in Haversian canal area. Finally, there was no statistically significant relationship identified in porosity area between the paired slides.

The Spearman's *Rho* results demonstrate that, generally, cross-sectional geometry variables, such as cortical area, width and absolute area, seem to be most consistent across the shaft of the rib. Elsewhere, cross-sectional geometry properties have been determined critically important for the structural integrity and maximum force a rib can be subjected to without fracture (Charpail et al. 2005; Cormier et al. 2005; Kemper et al. 2007; Murach et al. 2017). Thus, the maintenance of similar cross-sectional geometry measures across the length of the rib could be associated with maintaining cortical stability across the length of the bone. These results suggest that when preparing a sampling strategy with the purposes of examining cross-sectional geometry variables such as cortical area, width and absolute area, to expect less variation in these variables as you traverse the length of your selected bone. However, these results conflict with existing literature by Dominguez et al. (2020) where a significant difference in cortical area was identified between the rib midshaft at both the anterior and posterior aspects. However, Dominguez et al. (2020) compared serial cross-sections at the 25%, 50% and 75% margins of each rib, which means the sections compared in that research were likely further apart than those within this study, which were just 1 cm apart, and could more so reflect changing rib morphology to facilitate soft tissue attachments and curvature.

However, the variables pertaining to microscopic structures such as the area of porosities, osteons and Haversian canals found in a cross-section do vary more widely as you traverse the length of the rib. We know from the literature that osteons are longitudinal structures, visible two-dimensionally in transverse cross-section, and run the length of a bone (Ascenzi et al. 1973; Ascenzi and Bonucci 1967; Ascenzi and Fabry 1959; Ascenzi and Roe 2012; Eriksen et al. 1994; Frost 1964; Weiner and Wagner 1998). It is natural and expected that blood vessels and the circular bone lamina that surround them to ebb and flow throughout the longitudinal axis rather than remaining perfectly parallel (Robling and Stout 1999; Schnitzler and Mesquita 2013; Streeter 2010), which would lead to these variations seen in these results here between paired cross-sections. Finally, with no statistically significant relationship in porosity area identified between the paired sections, porosity of a bone should perhaps not be based on one

cross-section alone. In investigations of bone porosity, it may be more pertinent to examine multiple cross-sections and average results, as porosity can vary widely between sections taken just 1 cm apart. Porosity was defined here as those pertaining to vascularity or resorption, but did not include canaliculi or osteocyte lacunae (as defined by Agnew and Stout 2012; Martin 1984). This means that variation in the porosity area variable seen here, could also be conflated by the ebbs and flows of the vascular Haversian canals as they run longitudinally through the rib shaft. Further investigation of porosities associated with canaliculi or osteocyte lacunae structures is warranted to see if this pattern is consistent among other definitions of porosity.

Interestingly, the results of the Wilcoxon Signed Rank tests identified several statistically significant differences in some variables between paired histological slides, including cortical width, porosity area, osteon population density and fragmentary osteon population density, contradicting some Spearman's *Rho* results. However, it is important to note that the Wilcoxon Signed Rank test does not examine paired samples from the same individuals, but rather, all of the 'slide 1' group versus all of 'slide 2', observing the samples as a group and comparing them to each other (Rosner et al. 2006). As such, these results may be conflated by inter-individual variation in addition to the previously identified intra-individual variation, which could have resulted in these additional variables appearing to be statistically significantly different between the cross-sections. These results should be considered when preparing a sampling strategy and subsequent statistical analysis, as potentially statistically significant differences could be identified in cortical width, porosity area, osteon population density and fragmentary osteon population density, depending on your statistical analysis and sampling methodology.

7.4 Research Question 4

Does cortical bone histology vary between bones of different levels of metabolic activity, such as the femur and the rib?

To investigate osteon and Haversian canal size differences between the femur and rib, variables measured included common size metrics used elsewhere in the literature such as osteon and Haversian canal area, osteon and Haversian canal diameter and osteon and Haversian canal perimeter. Osteon and Haversian canal shape has largely been measured in the literature using osteon and Haversian canal circularity. However, there are three other shape measures commonly employed in other biological disciplines which can add nuance to shape descriptions. These include osteon and Haversian canal roundness, osteon and Haversian canal aspect ratio and osteon and Haversian canal solidity.

7.4.1 Osteon and Haversian Canal Size in the Rib and Femur

7.4.1.1 Rib and femur

The rib has statistically significantly smaller osteons and Haversian canals compared to both the anterior and posterior aspects of the femur. These results contrast with Cho and Stout (2011) who did not identify any statistically significant differences in osteon area between femoral and rib samples from Imperial Romans. However, these results resonate with those of Eleazer and Jankauskas (2016) who identified statistically significantly larger osteon area in femora as compared to their paired ribs in sub-adult skeletons excavated from a Lithuanian cemetery (14-18th century AD). Additionally, these results resonate with Karydi et al. (2022) where osteon area was statistically significantly larger in femora than ribs in a British 19th century sample, though these were not paired from the same individuals. Haversian canal area was also statistically significantly larger in the femur than rib of an individual excavated in the Marshall Islands and believed to have been buried approximately 1720 years ago (Miszkiewicz et al. 2022). Similarly, Mavroudas et al. (2022) and Pederson et al. (2024) both determined that osteon and Haversian canal area were statistically significantly larger in the femur than rib in six contemporary individuals from Texas, USA and 17 contemporary individuals from Queensland, Australia respectively.

To expand upon the reasons for osteon and Haversian canal size differences between the rib and femur, this most likely is largely related to differences in strain load between the two bones. It has been established in the literature that osteon area is indicative of strain level, with smaller osteon size correlating with increased localised strain (Frost 1990; O'Brien et al. 2005; Schlecht 2012; Skedros et al. 2001; 2007; Sobelman et al. 2004; van Oers et al. 2008b). This could cause the production of smaller BMUs during remodelling to reduce cortical porosity in bone regions of higher strain magnitudes (Schlecht 2012), or be due to improved proficiency for smaller osteons to absorb energy with higher strain reducing microdamage to bone structure (O'Brien et al. 2005; Sobelman et al. 2004). However, without controlling for differences in bone size (i.e. femoral size compared to rib size) in the present research, it is difficult to attribute the size differences in osteon area to strain magnitude differences.

The results of this research also agree with Pfeiffer (1998), where the femur rendered statistically significantly larger osteon area than in the rib, in paired samples, but in the St Thomas sample, this difference was not as pronounced as in the Spitalfields sample. Additionally, Haversian canal area was statistically significantly larger in the femur than rib in the Spitalfields sample, but not in the St Thomas sample (Pfeiffer 1998). Interestingly, Pfeiffer

(1998) also found that femoral osteon area had a much large range between minimum and maximum values than the rib, and no difference in Haversian canal area. But in the results of this thesis, osteon area variability was statistically significantly larger in the rib than either femoral region, and Haversian canal area variability was statistically significantly smaller in the rib than either femoral region. Firstly, the increased osteon area variability in the rib could suggest that osteon area is more easily impacted in the rib than the femur due to the lesser extent and variation in pattern of biomechanical loading and increased susceptibility to systemic and metabolic changes (Lanyon et al. 1982; Skedros et al. 2013a; Stewart et al. 2021; Tommerup et al. 1993). Whereas the increased Haversian canal area variability in the femur could relate to the larger variability in biomechanical load patterns between individuals in a weightbearing bone like the femur, impacting upon vascularity requirements dependent on levels and patterns of physical activity (Lanyon et al. 1982; Skedros et al. 2013a; Stewart et al. 2021; Tommerup et al. 1993). Secondly, the differences between the Spitalfields and St Thomas samples could suggest that the degree of this difference in osteon and Haversian canal size between the femur and rib could be dependent on population differences, such as genetic, environmental, societal or behavioural influences (Christian et al. 1989; Dequeker et al. 1987; Havill et al. 2013; Kelly et al. 1990; Norris et al. 2013; Pocock et al. 1987; Seeman et al. 1996; Solomon 1968; Thandrayen et al. 2009). This further demonstrates the importance of exploring these phenomena across populations and geographic regions to better our understanding of human bone metabolism and what influences it.

7.4.1.2 Anterior and posterior femur

The anterior and posterior femur have no statistically significant differences in osteon or Haversian canal size. Zedda et al. (2016) and Maggio and Franklin (2021) also failed to identify statistically significant size differences in osteons between cranial, lateral, caudal or medial regions within equine femora, and between the anterior and posterior midshaft of the human femur respectively. A lack of regional difference in osteon and Haversian canal size suggests that despite regional, topographical differences between, in this case, the anterior and posterior femur in humans, these do not significantly affect the size of osteons and Haversian canals within the microstructure at these regions. Differences in anterior and posterior femoral topography include varying muscle and tendon attachment sites. For example, at the posterior femur midshaft, multiple muscle attachment sites run along the *linea aspera* such as the *adductor longus*, *brevis* and *magnus*, the *vastus lateralis* and *medialis* and the *biceps femoris,* while at the anterior femoral midshaft is the origin site of the *vastus intermedius* and is a thoroughfare for the quadriceps muscle groups (Fuchs et al. 2009). While the posterior femur

is more active than the anterior femur in terms of muscle, tendon and ligament insertion and origin sites, the lack of significant difference in osteon and Haversian canal size between the two regions suggests that either the levels of biomechanical forces are similar despite these differences, *or* the biomechanical forces applied by these soft tissue structures do not overtly influence the microstructures found locally there. However, elsewhere in the literature, entheseal increases in cross-section area have been identified at muscle, tendon and ligament origin and insertion points (Turcotte et al. 2022), suggesting some degree of localised bone response. While entheseal variation in osteocyte lacunae orientation, but not size, has been identified in non-human fossils (Sanchez et al. 2013), site influences on osteon and Haversian canal morphology remains unknown. Further investigation into osteon and Haversian canal size at more localised entheseal regions might be well-placed to answer this question.

However, it is also possible that bone may microstructurally compensate for these differing forces passing through the tissue on a broader scale than the isolated insertion and origin sites. To explore this possibility, it is useful to refer to the four driving principles of bone functional adaptation (see Chapter 2, section 2.8.1.2). Specifically, there are two conflicting principles that could be at play. The first is that bone responds locally to strain and not as a whole entity, which will result in preferential remodelling at the bone surface rather than evenly distributed bone remodelling (Frost 2000; 2001; Lanyon et al. 1982; Stout et al. 2019). However, another bone principle states that bone can become immune to strain loading cycles due to the oversaturation of the osteocyte network, which subsequently overproduces fluids pertaining to overstrain and simultaneously reduces the osteocytic mechano-sensory response (Scheiner et al. 2016). Given the presence of variation in osteocytic orientation, identified at entheseal sites which are subjected to increased strain (Sanchez et al. 2013), it could also suggest that bone sites which are subject to increased strain, such as the posterior as compared to anterior femur, are overloaded, leading to a lack of differences in osteon and Haversian canal size.

7.4.1.3 Paired and unpaired femora and ribs

It is also interesting how these results vary with independent versus related samples, and corrections for stature are applied. In the independent, or unpaired, rib and posterior femur analysis, all size variables were statistically significantly larger in the posterior femur than the rib and these results held true after correcting by individual stature to account for individual body size variation. However, in the related rib, anterior and posterior femur analysis, fewer variables were statistically significantly different. This could be due to the presence of inter-individual variation in the independent samples with individual differences in systemic health

and patterns in physical activity and biomechanical loading, which amplify the inter-bone differences (Okoye and Hosseini 2024). In contrast, when paired samples are examined from the same individual, variations associated with inter-individual differences are controlled for, perhaps reducing the overall size differences in osteon and Haversian canal size between the rib and femur (Okoye and Hosseini 2024). In particular, biomechanical loading differences are most extreme in the independent rib and posterior femur samples as the posterior femur undergoes a much higher biomechanical load compared to the rib, which is extremely susceptible to inter-individual variation due to metabolic and systemic health intrinsic influences (Agnew and Stout 2012; Crowder and Rosella 2007; Dominguez and Agnew 2016; Karlson 1998; Stewart et al. 2021; Tommerup et al. 1993).

7.4.2 Osteon and Haversian Canal Shape in the Rib and Femur

Measures of osteon and Haversian canal shape have largely focused on circularity (Goliath et al. 2016; Karydi et al. 2022; Maggiano et al. 2021; Maggio and Franklin 2021), with other shape measures being employed in other disciplines such as mineral science (Sinkhonde et al. 2022), neurosurgery (Zdilla et al. 2016), or within bone biology, as a measure of porosity shape (Cole et al. 2022). Here, circularity, roundness, aspect ratio and solidity were used to capture shape morphological nuances of osteons and Haversian canals. The key to understanding the biological implications of these results lays in comprehending the way each shape variable is calculated. Circularity measures provide a value between 0-1, with 1 indicating that the shape is a perfect circle (Doube et al. 2010; Zdilla et al. 2016). While roundness is similar to circularity in that it measures how close a structure is to a perfect circle with a value of 0-1, it differs by not being affected by slight trajectory deviations away from a smooth border by not using the area and perimeter measure, but rather the area and major axis of best fit ellipse (Doube et al. 2010; Zdilla et al. 2016). The calculation of aspect ratio focuses on the ratio between the major and minor axes of the best-fit ellipse, which gives a lower-limit of 1, indicative of a perfect circle, with no upper-limit, but the higher the value, the more elongated a structure is (Doube et al. 2010; Zdilla et al. 2016). The final variable measured was solidity, which measures to what degree a shape is convex or concave, with 1 being a totally convex shape or perfect circle, and values closest to 0 being more concave or fragmented (Doube et al. 2010; Zdilla et al. 2016).

In the paired rib and anterior femur samples, osteon circularity and Haversian canal roundness were statistically significantly higher in the rib and Haversian canal aspect ratio was statistically significantly higher in the anterior femur, and these results continued once stature was corrected for. Osteon and Haversian canal solidity were statistically significantly higher in the

rib, but this reversed once individual stature was corrected for. In the paired rib and posterior femur samples, Haversian canal circularity and osteon solidity were statistically significantly higher in the rib and this continued once stature was corrected for. In the paired rib, anterior and posterior femur sample analysis Haversian canal solidity was statistically significantly higher in the rib than the anterior femur and these results remained consistent once stature was corrected for. Haversian canal roundness and circularity were statistically significantly higher in the rib than posterior femur, but only once individual stature had been corrected for. Haversian canal aspect ratio was statistically significantly higher in the posterior femur than the rib, but only after correcting for stature. Finally, in the independent sample analysis, osteon roundness was statistically significantly higher in the posterior femur than the rib, but only once stature was corrected for.

7.4.2.1 Circularity

Circularity was higher in the rib than both the anterior and posterior femur. Thus, in this research, osteons were closer to a perfect circle in the rib than anterior femur and Haversian canals more so in the rib than the posterior femur. Existing literature has determined that osteon circularity increases with advancing age in both the femur and rib (Goliath et al. 2016; Karydi et al. 2022), of which the vast majority of both the contemporary Australian donors and medieval British skeletons, are of advanced age (see Chapter 4: Materials). This suggests that the differences in osteon circularity determined here between the rib and femur are likely downplayed due to the advanced age-at-death of many of the individuals observed. It is also important to note that methods of osteon recording in bone histology are recommended to only include osteons rounded in shape rather than obviously elongated or of irregular morphology to avoid recording osteons sectioned angularly as opposed to transversely (Stout and Crowder 2011). This has likely also downplayed the differences identified here between the rib and femur as non-circular osteons are less likely to have been recorded (see Chapter 5: Methods). Conversely, it is interesting that although elongated and irregularly shaped osteons and Haversian canals were excluded from this analysis, there were still statistically significant differences identified between the rib and femur.

Exploring the differences in osteon and Haversian canal circularity between the rib and femur has not been widely explored in the literature. For example, osteon circularity is often used as a measure when estimating age-at-death, and even using both the rib and the femur, but results are rarely presented in such a way that we can observe intra-skeletal differences (Karydi et al. 2022), or as a secondary part of their analysis, do not identify statistically significant differences between the femur and rib (Britz et al. 2009; Crescimanno & Stout 2012;

Goliath et al. 2016). Elsewhere in the literature, circularity has been applied to other microstructures, such as porosity, rather than osteonal structures (Cole et al. 2022). However, the biomechanical and bone functional adaptation literature describe the femur being associated with a broad biomechanical repertoire, often with repeated angled movements, significant individual variation, and with the maximum level of stress peaking at the femoral midshaft (Frost 1964; Nareliya Mishra et al. 2022). Though the effect of behaviour on osteonal structures has been disputed in some circles (Pfeiffer et al. 2006; Skedros et al. 2007), much of the osteonal structure literature describes patterns in osteon shape varying more widely in the femur due to these broader biomechanical repertoires (Keenan et al. 2017; Skedros 2024). Therefore, a potential explanation for the femur having less circular osteons and Haversian canals than the rib, is that the rib is not subjected to as varied patterns of biomechanical load and strain as the femur (Dominguez and Agnew 2016; Frost 1964; Skedros et al. 2013a; Stewart et al. 2021; Tommerup et al. 1993). Instead, the rib experiences more multi-directional, lower magnitude loads consistent with respiration (Dominguez and Agnew 2016; Frost 1969; Skedros et al. 2013a; Stewart et al. 2021; Tommerup et al. 1993), which would result in more circular osteons and Haversian canals. As the femur is subjected to comparatively higher compressive, higher bending forces and higher longitudinal loading to the rib (Dominguez and Agnew 2016; Frost 1969; Skedros et al. 2013a; Stewart et al. 2021; Tommerup et al. 1993), this could result in less circular osteons and Haversian canals. Additionally, the posterior femur bears significant axial compressive forces (Frost 1964; Nareliya Mishra et al. 2022), which could drive elliptical osteon and Haversian canal formation, reducing circularity (Skedros 2024).

7.4.2.2 Roundness

Roundness has not been explored in the osteon morphology literature, despite perhaps being a useful alternative to circularity to avoid slight deviations in the lamina perimeter when measuring, to look more holistically at the overall shape and to reduce human error during shaky perimeter tracing (Doube et al. 2010; Zdilla et al. 2016). Here, Haversian canal roundness was statistically significantly higher in the rib than anterior and posterior femur in the paired samples analysis, which agrees with the circularity results reported above. Interestingly, Haversian canal roundness results were statistically significant in the paired rib and anterior femur analysis and continued once individual stature variation was controlled for. However, in the triple paired rib, anterior and posterior femur samples analysis, it only reached statistical significance between the rib and posterior femur, but not the anterior femur, and only once individual stature variation had been corrected for. Similarly, in the independent,

unrelated samples, osteon roundness was only statistically significantly higher in the posterior femur than the rib once stature variation was corrected for.

The nuances of these results suggest that Haversian canals are rounder in the rib than the anterior femur and posterior femur, increasingly so if individual body size differences are corrected for. These results demonstrate that Haversian canals in the femur are more elliptical or elongated and this could be a result of the highly compressive and bending forces in the femur (Frost 1964; 1969; Nareliya Mishra et al. 2022; Skedros 2024; Tommerup et al. 1993), causing more elongated Haversian canals (Frost 1964; Skedros 2024). Meanwhile, the rib experiences less axial loading, but more multi-directional, lower magnitude strains with respiration (Agnew and Stout 2012; Crowder and Rosella 2007; Dominguez and Agnew 2016) that perhaps results in an overall more round Haversian canal. This could also be a result of less structural deformation in the rib than femur due to overall less variable biomechanical stress (Crowder and Rosella 2007; Dominguez and Agnew 2016).

Despite osteon circularity being significantly higher in the rib than posterior femur, osteon roundness was statistically significantly higher in the posterior femur than the rib in a seemingly contradictory result. However, rather than being a contradiction of results, these results when interpreted together, could suggest that osteons in the posterior femur are more rounded or circular overall, but have a less smooth and circular lamina border which translates to a significantly more rounded shape (higher roundness values), but significantly less circular border (lower circularity values) due to perimeter deviations (Doube et al. 2010; Zdilla et al. 2016). Alternatively, osteon roundness may not usually be different between the rib and either femoral aspect. Instead, the results from the independent and unrelated samples analysis may just amplify differences in osteon roundness between the rib and femur, due to other, either intrinsic or extrinsic, differences between the individuals which were not able to be accounted for due to the small sample size of that analysis.

7.4.2.3 Aspect Ratio

Similarly to roundness, aspect ratio has not been observed in an osteonal morphology context within the existing literature. However, it can provide additional nuances to shape differences. While osteon aspect ratio was not statistically significantly different between the rib and anterior or posterior femoral aspects, Haversian canal aspect ratio was statistically significantly higher in the anterior and posterior femur than the rib, across paired samples analyses, especially once variation in individual body size differences were controlled for. These results suggest that Haversian canals in the anterior femur are more elongated, with a higher ratio

between the major and minor ellipse axes (Doube et al. 2010; Zdilla et al. 2016). This reinforces results and interpretation of roundness and circularity analyses described above, and likely reflects the strong longitudinal forces acting upon the anterior and posterior femur, elongating the canals dependent on the direction of the applied biomechanical load and stress (Frost 1964; Nareliya Mishra et al. 2022; Skedros 2024; Tommerup et al. 1993). Meanwhile, in contrast, the rib experiences more evenly distributed, multi-directional biomechanical loads (Agnew and Stout 2012; Crowder and Rosella 2007; Dominguez and Agnew 2016), resulting in a more balanced Haversian canal aspect ratio.

7.4.2.4 Solidity

Similarly to roundness and aspect ratio, solidity has also been unexplored in the osteonal morphology literature, but as it differs in its definition from the other three shape measures, it can provide additional context to shape morphology. In the paired rib, anterior and posterior femur samples analysis, Haversian canal solidity was statistically significantly higher in the rib than the anterior femur, which continued once individual stature variation was corrected for. The higher solidity of osteons and Haversian canals in the rib, even after correcting for individual stature, likely reflects the fundamentally different mechanical environments between the axial and appendicular skeleton. The rib cage experiences relatively low, cyclic, and more uniform strains due to respiration, which promotes more regularly shaped, convex microstructures in the cortical bone (Rho et al. 1998; Currey 2002). In contrast, the femoral cortex, particularly the posterior region, undergoes high, variable, and complex mechanical loads during weight-bearing and locomotion, which stimulates bone remodelling that results in more irregular, concave microstructures as a functional adaptation to mechanical stress (Martin et al. 1998; Skedros et al. 2009). This morphological variation in microstructure supports the idea that osteon shape and Haversian canal morphology are directly influenced by local biomechanical demands, rather than reflecting body size or stature differences (Skedros 2024; Zedda and Babosova 2021).

However, in the paired rib and anterior femur samples analysis, osteon and Haversian canal solidity were higher in the rib, but osteon and Haversian canal solidity were higher in the anterior femur once individual stature variation was corrected for, leaving osteon and Haversian canal solidity statistically significantly higher in the anterior femur. In the paired rib and anterior femur sample analysis, initial results indicated that both osteon and Haversian canal solidity were higher in the rib, consistent with its relatively uniform mechanical environment and effects described above. However, once individual variation in stature was accounted for, this pattern reversed, revealing statistically significantly higher osteon and

Haversian canal solidity in the anterior femur. This suggests that body size exerts a confounding influence on bone microstructure measures of the anterior femur in this case, and when controlled, the anterior femur, which is subject to more complex and higher magnitude mechanical loads during locomotion and weight-bearing, exhibits more robust microstructural adaptations. These findings highlight that biomechanical forces and individual morphology interact intricately to shape cortical bone architecture, with stature potentially masking intrinsic differences in remodelling and microstructural solidity between the rib (an axial) and femur (an appendicular site) (Martin et al. 1998; Skedros 2024; Skedros et al. 2001; 2009). Such results underscore the importance of correcting for confounding factors like stature to accurately interpret functional bone adaptation in comparative analyses (Currey 2002; Zedda and Babosova 2021). Further research into differences between the anterior and posterior femur is warranted to explore this finding.

7.4.2.5 Anterior and posterior femur

Finally, it is important to note that there were no statistically significant differences identified in any shape variable between the anterior and posterior femur, suggesting little variation between the two regions. The midshaft of the posterior femur is a key attachment site for several muscles and tendons along the *linea aspera*, including the *adductor longus*, *brevis* and *magnus*, as well as the *vastus lateralis* and *medialis*, and the *biceps femoris* (Fuchs et al. 2009; Monk et al. 2016). While the midshaft of the anterior femur is the origin site of the *vastus intermedius*, but acts more as a thoroughfare for muscle groups, such as the quadriceps, rather than a direct insertion or origin site (Coratella et al. 2020; Fuchs et al. 2009; Monk et al. 2016). The lack of difference in osteon and Haversian canal shape between the two regions suggests that it is not entirely, or perhaps just not significantly, impacted by the biomechanical forces applied by these muscle groups that can influence osteon and Haversian canal morphology. Rather, the bone may compensate for the different forces between the two regions on a ‘larger than local’ scale, resulting in similarly shaped osteons and Haversian canals at the anterior and posterior femur. However, it is noteworthy that there were several results that identified statistically significant differences in osteon and Haversian canal morphology between the rib and either the anterior *or* posterior femur, suggesting some limited variation between the two regions.

In summary, the rib exhibits higher circularity, solidity and roundness in both osteons and Haversian canals than the femur, likely due to the lower and evenly distributed mechanical loading compared to the femur (Agnew and Stout 2012; Crowder and Rosella 2007; Dominguez and Agnew 2016). The anterior femur has lower circularity, solidity and roundness

and higher aspect ratio, with more elongated shaped osteons and Haversian canals, reflecting the highly directional stresses and remodelling activity due to weight-bearing forces (Coratella et al. 2020). The posterior femur has lower Haversian canal circularity, but higher osteon roundness, suggesting bone adaptations to compressive stress, with more elliptical osteons but with relatively smooth outer borders of the shapes overall (Crescimanno and Stout 2012; Maggiano et al. 2021; Maggio and Franklin 2021). These findings align with biomechanical expectations, which require ribs to be flexible yet resilient to undergo respiration, favouring more circular and compact osteons and Haversian canals (Agnew and Stout 2012; Crowder and Rosella 2007; Dominguez and Agnew 2016). While femora, which are subjected to significant biomechanical load, show more elongated and irregularly shaped osteons and Haversian canals as an adaptation to stress (Skedros 2024).

7.4.3 Rates of Osteonal and Haversian Canal Growth in the Rib and Femur

The reduced major axis regression (RMA) found statistically significant differences in rates of osteonal and Haversian canal growth patterns between the rib and femoral regions. The majority of the RMA analysis and sub-group analyses of the paired osteons and Haversian canals in the rib were indicative of isometric growth, which demonstrates that Haversian canal area increases at a proportional rate to osteon area as osteonal size increases (Shingleton 2010). For example, as osteon area doubles in size, the Haversian canal will also double in size. Isometric growth ensures that Haversian canals will remain the same size relative to their osteon, regardless of an osteon increasing size. Thus, there is no preferential allocation of space to the Haversian canal as osteons continue to grow. Biologically speaking, this suggests that osteons maintain a consistent ratio of vascular supply to the surrounding bone matrix across different osteon sizes and based upon bone structural properties outlined by Frost (1964), this reflects a healthy or optimal osteonal structure to support bone health.

However, some of the rib analyses and all femoral RMA results identified a positive allometric scaling relationship between Haversian canals and their paired osteons. A positive allometric relationship indicates that Haversian canal area increases at a proportionally greater rate than osteonal size as the osteon grows (Shingleton 2010). For example, as osteon area doubles in size, the Haversian canal will more than double in size. However, we know from skeletal biology that Haversian canals are nested within osteons and the broaching of the osteonal laminal wall by a Haversian canal is an irregular osteon morphology (Cooper et al. 1966; Parfitt 1983) which were not recorded as part of this study. This suggests that to maintain a regular osteon morphology, Haversian canal area growth, even when faster than its nested osteon, is still constrained by osteon area as it must remain within the outer limits of the osteonal lamellar

wall. Biological interpretation of this result could suggest that larger osteons allocate proportionally more space to their paired Haversian canals, compared to smaller osteons. Additionally, this could reflect bone metabolic adaptation to enhance vascularisation or metabolic requirements in larger osteons, possibly due to increased demands for nutrient delivery or waste removal in larger osteonal structures with a larger number of layers of new bone deposition (Chen et al. 2020).

As the rib demonstrated mostly scaling relationships of isometric growth and both regions of the femur were exclusively positive allometry, this likely reflects differences in the mechanical function and physiological demands of the rib and femur. Mechanically speaking, the rib primarily functions in respiration and protection and is not a weight-bearing bone (Dominguez and Agnew 2016; Frost 1964; Fuchs et al. 2009; Skedros et al. 2013a; Stewart et al. 2021; Tommerup et al. 1993). As ribs are subjected to a relatively low level of mechanical loading, there is likely less need for structural adaptation in osteon and Haversian canal size with increasing osteon area. Rather, there may be more benefit to maintaining a constant osteon-to-Haversian canal ratio (isometrical scaling relationship) to ensure sufficient vascular supply without excessive Haversian canal enlargement, which would, in effect, increase bone porosity and potentially weaken bone, reducing the ribs capacity to perform the protective function it is required to achieve (Chen et al. 2020; Mishra and Knoth-Tate 2008). Additionally, this could also result in a more even distribution of vascularity across the rib, and thus, an even distribution of nutrient supply and waste removal (Chen et al. 2020). Meanwhile, the femur is a heavily weight-bearing bone and is subjected to high levels of mechanical loading (Frost 1964; 1969; Nareliya Mishra et al. 2022; Ruff et al. 2006; Skedros 2024; Skedros et al. 2001; 2009; Tommerup et al. 1993). Thus, larger osteonal area in the femur may require disproportionately larger canals to support increased metabolic demand (Chen et al. 2020), bone remodelling (Martin et al. 1998) and vascularisation (Chen et al. 2020) than the rib. This increased vascularisation would assist in repair and remodelling, due to the continuous stress and microdamage which accumulates in weight-bearing bones such as the femur (Burr et al. 1985; 1998; Frost 1964; Skedros et al. 2001). This demonstrates the benefits of a structural adaptation in the femur for a greater relative increase in Haversian canal size (positive allometric scaling relationship) to help to meet these physiological demands by localised increases in nutrient exchange and waste removal.

Interestingly, the rib did not exclusively demonstrate a scaling relationship of isometric growth amongst all sub-groups. Rather, isometric growth relationships were identified in the entire sample, males, middle-aged adults, middle-aged males, middle-aged females, medieval

middle-aged adults, medieval males, and medieval females, but positive allometry in the modern group, females, older adults, older males, modern older adults and modern males. This could reflect differences in bone remodelling dynamics (Burr et al. 1985; 1998; Martin et al. 1998), metabolic demands related to age and sex (Chen et al. 2020; Choi et al. 2021), and hormonal influences on bone turnover, particularly post-menopausal estrogen decline and age-related changes in remodelling patterns (Seeman 2002; Riggs et al. 2002), rather than a structural adaptation due purely to mechanical loading within these sample sub-groups (Ruff et al. 2006; Skedros 2024; Skedros et al. 2001; 2009).

To interpret the positive allometry result in the rib within the modern sub-group, it is important to consider differences between the medieval and modern sub-groups that could have contributed to the difference in structural adaptation that resulted in the isometric growth versus positive allometry scaling relationships. One key difference in lifestyle between the modern and medieval individuals is the higher levels of physical activity through hard labour experienced by medieval individuals compared to a relatively sedentary lifestyle in modern humans (Nowak and Ogurkowska 2024; Ruff et al. 2006). While there is evidence in the literature that modern humans tend to lead a more sedentary lifestyle, this research has determined that there is inconsistent evidence that modern humans have had a detrimental effect on their bone, with no statistically significant differences identified in osteon area between the modern and medieval individuals in the rib (see research question 2 in Section 7.2). It may be expected to see a scaling relationship of positive allometry in the modern group, due to this increased sedentism, which could lead to reduced mechanical loading, allowing bone adaptation to be driven instead by remodelling than by structural demands (Burr et al. 1985; 1998; Martin et al. 1998; Sugiyama et al. 2012). This would result in increased osteon remodelling and possibly increase the demand for vascular support via larger Haversian canals relative to osteon size (Chen et al. 2020; Choi et al. 2024). In contrast to this, medieval humans likely experienced higher levels of mechanical loading due to more frequent and extreme physically demanding activities, which would make the isometric growth scaling relationship more advantageous, with osteon and Haversian canal growth being proportionate to meet bone structural needs (Ruff et al. 2006; Skedros et al. 2001; Sugiyama et al. 2012).

However, it may also be beneficial to examine the sub-group differences between the modern and medieval individuals. For example, all modern individuals examined in this research were older adults (50+ years). Additionally, modern humans have easier access to higher quality nutrition and more advanced medical care, which prolongs the human lifespan and means that modern older adults are likely of a more advanced age than those of the same age-at-death

category in the medieval sample (Christensen et al. 2019). Therefore, it is important to consider how the effects of advancing age could have influenced the results of the older adult sub-group analyses to adhere to a positive allometric scaling relationship. With increasing age-at-death, we tend to see an increase in vascular networks, due to the osteoporotic trabecularisation of the rib cortices phenomenon, whereby the cortical area is slowly obliterated, increasing the medullary cavity and trabecular bone area (Agnew and Stout 2012; Seeman 2015). This phenomenon could be contributing to these results by individuals of an advanced age having a higher-than-average Haversian canal area, particularly along the cortical/trabecular junction. Future research could assist in identifying if this is the case by looking at regional differences in the scaling relationship within the rib.

A further consideration is that in the rib, positive allometry appeared to be more prevalent in the female than male sub-groups, which could be indicative of a strong hormonal influence on the scaling relationship between Haversian canals and their paired osteons. Estrogen plays a crucial role in bone maintenance by regulating remodelling and preserving bone mass (Khosla 2008; Khosla et al. 2012; Manolagas et al. 2013), and its decline, especially post-menopause, causes increased osteon turnover and remodelling rates (Farlay et al. 2019), which drives an increased need for vascular supply, thus increasing cortical porosity, due to the larger Haversian canals (Agnew and Stout 2012; Martin 1984). Another potential factor that could contribute to female sub-groups being more likely to have a positive allometry scaling relationships, is that the literature has demonstrated that females tend to have thinner cortices than males (Ho-Pham et al. 2018), which could contribute to the need for relatively larger Haversian canals for metabolic support (Ramchand and Seeman 2018). However, it should be stated that the female middle adult group RMA results demonstrated an isometric growth scaling relationship which appears to suggest that age is more influential on the scaling relationship between osteons and Haversian canals than biological sex. In addition, samples from individuals in the medieval sub-groups seem to be more likely to also subscribe to isometric growth scaling relationships between osteons and Haversian canals regardless of biological sex. This is demonstrated by the medieval male and female sub-groups RMA results being isometric growth.

Finally, also of interest is the lack of negative allometry identified in the RMA results across the rib or femur. A negative allometry scaling relationship would indicate that the osteon grows at a faster rate than its paired Haversian canal (Shingleton 2010). This form of scaling relationship could be considered sub-optimal for bone health as osteons may not have sufficient access to nutrient transferral and the bone tissue may have reduced vascularisation

(Mishra and Knothe Tate 2008). Despite this being a sub-optimal scaling relationship, there were several sub-groups in the rib RMA analysis that had slope values <1, but due to the confidence intervals ranging >1, a non-isometric growth scaling relationship could not be ruled out statistically (Shingleton 2010). Interestingly, the sub-groups that came close to a result of negative allometry were middle-aged adults, male middle-aged adults, female middle-aged adults, medieval middle-aged adults and medieval males. A commonality between these groups is they were all medieval individuals represented in these sub-groups as all modern individuals were older adults, as well as largely middle-aged adults, who would have formed the crux of the physical labour workforce (Mays 1991; 2014; Miszkiewicz and Mahoney 2016; Roberts and Cox 2003). This could mean that rather than bone adapting to a borderline negative allometric scaling relationship, that medieval individuals had sub-optimal nutrient supply due to poor systemic health (Gernay 2015; Hanawalt 1977), poor diet and nutrition (Mahoney et al. 2016a; Mays 2021), disease prevalence (DeWitte and Stojanowski 2015) and extremely high levels of physical labour (Dyer 2000; White et al. 2022; Zvi 1981). Further, the entire medieval sample sub-group also included younger and older adult individuals, which could have been enough to push the scaling relationship slope to a 1.000, and into the realm of isometric growth.

In summary, the rib may more commonly demonstrate isometric growth scaling relationships between osteons and their paired Haversian canals due to a more beneficial bone structural adaptation. This is supported by findings that ribs, being metabolically more active and sensitive to hormonal changes, often exhibit isometric or near-isometric scaling to maintain efficient nutrient exchange without compromising structural integrity (Mishra and Knothe Tate 2008). However, some population sub-groups may be more likely to subscribe to positive or borderline negative allometric scaling relationships due to external and internal influences on bone metabolism. This further reinforces that the rib is more susceptible to systemic metabolic change than the femur. While both femoral regions demonstrated exclusive positive allometric scaling relationships between osteons and their paired Haversian canals, likely due to bone structural adaptation to increased biomechanical load and cortical density, with lower cortical porosity.

Chapter 8 Conclusion

This chapter summarises the key findings of this research, describes the limitations and provides next steps for future research. Finally, the research achievements are detailed, describing how far reaching these results are for direct and related disciplines.

8.1 Key Findings

The key findings outlined in this dissertation are outlined here in reference to each research question and sub-question.

8.1.1 Research Question 1

Does human rib and femur histology vary with age-at-death, sex and systemic health and physical activity (as inferred by socioeconomic status) in samples of English ancestry?

8.1.1.1 Age-At-Death

There was no statistically significant correlation between chronological age-at-death and either total or fragmentary osteon population density, cortical porosity or cortical width. However, statistically significant differences were identified between age-at-death categories; young (20 – 34 years), middle-aged (35 – 49 years) and older adults (50+ years). Older adults had statistically significantly higher densities of total and fragmentary osteons than middle-aged adults due to many advanced years of remodelling surpassing the asymptote. Both middle-aged and young adults had statistically significantly higher cortical width than older adults due to bone loss and trabecularisation of cortical bone that occur with advanced age. A key takeaway of these results is that if, due to small sample size, or when using samples with estimated rather than documented age-at-death, looking for group or categorical differences may provide some insights where chronological age-at-death does not.

8.1.1.2 Biological Sex

There were no statistically significant sex differences in total or fragmentary osteon population densities, cortical porosity or width, either before or after correction of body size with stature measurements. However, females only had statistically larger Haversian canals in the posterior femur and osteons only statistically significantly larger in females in the rib after correcting for individual stature variation, which suggests an effect of body size on osteon and Haversian canal size. Additionally, there were no statistically significant sex differences

identified in the anterior femur, which could mean this region of the femur is not ideal for sex difference testing in future studies due to a lack of systemic influence such as in the rib, and the effects due to biomechanical loading and physical activity not being as pronounced as in the posterior femur.

8.1.1.3 Socioeconomic Status

These results overwhelming demonstrated statistically significant differences between the contemporary Australian samples and the medieval samples, with some statistically significant differences also identified between the medieval high and low status sub-samples. Contemporary Australians had statistically significantly high osteon population density then both medieval status groups suggesting faster remodelling rates in the contemporary humans. Contemporary Australians had statistically significantly lower osteon circularity than both medieval sub-samples, suggesting more complex or variable physical activity repertoires, but this difference was not statistically significant after accounting for stature variation, suggesting an effect of body size on osteon circularity. Medieval low status individuals had statistically significantly higher porosity area than medieval high status individuals, perhaps indicating that poor systemic health, lack of access to healthcare and poor nutrition restricted low status medieval people from being able to overcome poor bone health associated with these factors by their increased levels of physical activity and biomechanical loading. Porosity area was statistically significantly higher in the anterior femur of contemporary Australians than the medieval high status sub-sample, perhaps a reflection of the older average age-at-death in the contemporary Australian sample. Additionally, contemporary Australians had statistically significantly lower rib cortical width than both medieval status sub-samples, further increasing the likelihood that the older average age-at-death in the contemporary Australian sample demographics could be influencing these variables that are known to be affected by advancing age such as cortical porosity and cortical width.

8.1.1.4 Femoral versus Rib Responses to Demographic Factors

The rib appears to be more susceptible to bone changes with intrinsic factors such as those due to age-at-death and biological sex, but also some factors associated with socioeconomic status such as poor nutrition and systemic health. Meanwhile, the femur appears less impacted by those intrinsic factors and perhaps is better able to overcome negative impacts from those factors to some extent, with increased biomechanical load and physical activity. For example, statistically significant differences between age-at-death categories were only identified in the rib and not in the posterior femur, while statistically significant differences were only identified

in the anterior femur following correction for individual stature variation, suggesting an effect of body size and therefore possibly biomechanical load on this femoral region. In summary, these results demonstrate that the rib is poorly equipped biologically speaking, to overcome detrimental changes that occur with advancing age, poor nutrition or poor systemic health by increasing, or optimising, physical activity levels as it is not a weight-bearing bone.

8.1.2 Research Question 2

Is there a trend of bone quality "deteriorating" in contemporary individuals to reflect generally more sedentary lifestyles than their medieval ancestral population?

8.1.2.1 Contemporary versus Medieval Bone Differences

Contemporary and medieval bone, even that of ancestrally similar genetic makeup, were so markedly different that they were able to be classified correctly as either contemporary or medieval 87.9% of the time based on osteon population density, circularity, area and cortical porosity. Further, once age-at-death and sex were corrected for, the reliability of discriminant function analysis increased. This confirms that the use of discriminant function analysis could be used to not only observe differences between temporal groups of the same ancestry, but also to develop classification systems for categorising remains of unknown temporal origin within a site.

8.1.2.2 Contemporary Sedentary Lifestyle

Overall, results were not suggestive of a more sedentary lifestyle in contemporary humans than medieval. Osteon population density was higher in contemporary individuals, suggesting a faster remodelling rate, often associated with increased stimulation from physical activity. Further, smaller cortical area has been associated with physical inactivity, as bone mineral density decreases and cortical thinning increases, but here there was no statistically significant difference in cortical area between the contemporary and medieval groups. In conjunction with cortical bone loss, cortical porosity has been associated with sedentism as trabecularisation of the cortex occurs, but contemporary individuals had statistically significantly lower cortical porosity than medieval individuals here. Higher osteon circularity can occur as a result of less directional strain, which causes osteonal drift and results in elongated osteons, however in this research we see statistically significantly less circular osteons in the contemporary group, suggesting higher directional strain and osteonal drift.

8.1.3 Research Question 3

Is there variation in standardised histological variables between serial cross-sections from the human rib midshaft?

Key findings from this research questions determined that cross-sections taken approximately 1cm apart vary more so in their microstructural variables than cross-sectional geometry variables as you traverse the length of the rib midshaft. For example, paired cortical area, width and absolute area data for the two cross-sections had the strongest statistically significant correlations, while the weakest, but still statistically significant correlation was in Haversian canal area. Medium strength statistically significant correlations included cortical porosity, osteon area, total and fragmentary osteon population density and osteon circularity. This suggests that the maintenance of cross-sectional geometry measures across the length of the rib could be associated with maintaining cortical stability, potentially reducing fracture risk. However, the microscopic structure variables tend to vary more widely between cross-sections, even those taken close together, due to the nature of osteonal structures that ebb and flow longitudinally through the length of the rib. Statistical results also determined that paired analysis between two cross-sections is more valuable than treating slides 1 and 2 as categories to look at group differences, and how these statistical tests can present very different results. These results help to inform histological sampling strategy for ribs, as well as overall statistical analysis of such data.

8.1.4 Research Question 4

Does cortical bone histology vary between bones of different levels of metabolic activity, such as the femur and the rib?

8.1.4.1 Osteon and Haversian Canal Size in the Rib and Femur

Osteons and Haversian canals in the rib were consistently statistically significantly smaller than in both the anterior and posterior femur, across all size measures including area, diameter and perimeter. However, there were no statistically significant differences in osteon and Haversian canal size between the anterior and posterior femoral regions, in any size measures.

8.1.4.2 Osteon and Haversian Canal Shape in the Rib and Femur

This research involved both the application of existing measure of osteon shape, circularity, but also adopted novel shape measures from other fields including roundness, aspect ratio and solidity. Results of each shape analysis between the rib and femoral regions were nuanced

and complex, and when contextualised with knowledge of how each of these shape measures function mathematically provide enhanced shape analysis and biological significance. While there were several statistically significant differences in osteon and Haversian canal shape between the rib and femoral regions, there were no such statistically significant differences between the posterior and anterior femur, suggestive of intra-skeletal differences between bones as opposed to regional or localised strain patterns within the femur between the two regions.

8.1.4.3 Rates of Osteonal and Haversian Canal Growth in the Rib and Femur

This research sub-question involved the novel application of a reduced major axis regression (RMA) to compare patterns in rates of growth of osteons and their paired Haversian canals between the rib and femoral regions. While the anterior and posterior femur demonstrated that osteons and Haversian canals adhered to a positive allometric growth rate, with Haversian canals growing faster than their paired osteons, the rib demonstrated largely isometric growth, with both structures growing at a similar rate. However, once sorting into demographic sub-groups, femoral results remained indicative of positive allometry but the rib results were inconsistent. Isometric growth relationships were identified in the entire sample, males, middle-aged adults, middle-aged males, middle-aged females, medieval middle-aged adults, medieval males and medieval females, but positive allometry in the modern group, females, older adults, older males, modern older adults and modern males. Additionally, some sub-groups that continued to demonstrate isometric growth had scores almost suggestive of negative allometry, almost a borderline result. These demographic sub-groups included middle-aged adults, male middle-aged adults, female middle-aged adults, medieval middle-aged adults and medieval males, which interestingly all consisted of medieval individuals as all contemporary individuals were in the older adult age-at-death category. This could reflect a sub-optimal nutrient supply due to poor systemic health, diet and nutrition, disease prevalence and extremely high levels of physical labour in the medieval middle-aged individuals. Lastly, the fact that demographic sub-groups only changed the outcome of the rib results, while femoral results remained indicative of positive allometry further suggests that the rib is not as biologically able to overcome detrimental bone quality as a result of intrinsic factors as the femur.

8.2 Limitations

Limitations of this research can be categorised as pertaining to sample demographics, methodological limitations of histology, skeletal element selection and taphonomy of archaeological samples.

8.2.1 Sample Demographics

Limitations within this study prevented more specific sub-group analysis due to a lack of representation in some population demographics, such as limited age-at-death categories and small numbers of female donors in the modern Australian samples. Future studies may benefit from a larger demographic sample size with even sub-group representation to tease out singular effects of age-at-death, biological sex and general health, nutrition and physical activity levels while accounting for these other factors. Additionally, medieval individuals age-at-death and sex were estimated based on skeletal biological profiling methods, which introduces assumptions to sub-group analysis, conducted where possible given small sample sizes. Finally, the samples observed as part of this research were inconsistent in sampling strategies due to sample availability during a global pandemic and travel restrictions. Some individuals provided paired rib and anterior femur samples only, while others provided rib, anterior and posterior femur samples, and others only one of the three sampling regions was provided. This contributed to a complex dataset and analysis to reduce artificial conflation of results, accurately test paired and unpaired data, and limited the ability to conduct analyses between demographic sub-groups.

8.2.2 Methodological Limitations of Histology

The largest limitation associated with histology is that it is primarily a 2D technique of what are in actuality 3D structures. This limitation has been identified in the field for many years (Hillman 2000), and recently, using advances from the clinical realm, other techniques have been proposed as potential future avenues of histological applications. These include serial sections to construct a 3D model (Ruusuvuori et al. 2022), micro-CT (Lundin et al. 2017) and a variety of other possibilities based on clinical 3D imaging suggested recently (Xu et al. 2025). It is this very limitation that resulted in the development and value of research question three in this study, where serial rib cross-sections were used to characterise changes in microstructural features within the same bone.

8.2.3 Skeletal Element Selection

This research looked at intra-skeletal variation between the rib and the femur, two bones of differing metabolic activity as well as different functional adaptations in their structure. These results and existing literature tell us that other bones will also have different metabolic signatures and different functional adaptations based on their unique form and function within the human skeleton (Amprino and Mariotti 1964; Doblaré and Garcia 2002; Fahy et al. 2017; Frost 2001; Iyo et al. 2004; Frankel and Nordin 2012; Lanyon et al. 1982; Mulhern 2000; Rittweger 2011; Stewart et al. 2021). It is necessary to explore intra-skeletal variation in other elements in order to understand human bone metabolism, structure and function more broadly, particularly with regard to microstructures and cross-sectional geometry measures.

8.2.4 Taphonomy of Archaeological Samples

While the preservation in the contemporary samples was good and did not hinder the visibility of microstructures during data collection (see Schotsmans et al. 2024 for summary), the medieval samples were on occasion difficult to conduct data analysis on due to taphonomical changes. While this has not been formally measured and quantified in the medieval samples like Schotsmans et al. (2024) have conducted on the contemporary samples, it is possible that some structures were undermeasured or underrepresented due to obscuration with taphonomy, or decomposition that occurs with time in human remains (Reid et al. 2024).

8.3 Future Directions

In addition to rectifying the above limitations either through improved distribution of sample demographics, feasibly introducing a 3D histological method, examining additional skeletal elements to expand upon intra-skeletal variation and having access to a larger contemporary sample size to counteract the taphonomical degredation of the medieval samples, there are a few future research avenues that could naturally continue this research.

One future avenue for this research would be to employ a clinical imaging-based study to observe cross-sectional changes with advancing age, sex and socioeconomic status in a living Australian population. Novel methods of artificial intelligence for auto-registration of clinical imaging shows great promise in the clinical realm (Rytky et al. 2024), routinely being employed by clinicians and researchers alike to increase sample size and demographic representation, as well as bone changes throughout the lifespan of individuals (Segal and Li 2022). With clinical imaging techniques improving vastly and with great speed, it is a promising future direction and will mean easier access to multiple bones for intra-skeletal comparisons.

Additionally, this would benefit the bioarchaeology and forensic anthropology disciplines to create a representative large-scale study to ascertain standards in bone cross-sectional geometry in the Australian population.

This is the first time that the relationship between osteons and their paired Haversian canals has been characterised in terms of rates of growth. This novel method for comparing growth rates between these structures would be beneficial to apply to a range of other skeletal elements, even in a single individual, to look at how this relationship differs between other bones in the human skeleton. The susceptibility of the rib to be influenced to sway either to positive allometry or hover in isometric growth, but borderline with negative allometry, suggests that it might be a potential avenue to investigate early bone mineral density loss in vulnerable demographic groups. Currently, bone mineral density is routinely measured in at-risk individuals by densitometry scans of the femoral neck (Chun 2011). These results demonstrate that the rib is more easily impacted by bone loss or sub-optimal bone metabolism and thus, could be an earlier indicator of bone loss than the femoral neck, which when bone mineral density is compromised at that location, can lead to catastrophic joint fracture (Bible et al. 2014; Giannoulis et al. 2016; Mori et al. 2025).

Lastly, diet remains an important but difficult to tease out factor in histological analysis, with the best possible factor associated with diet being socioeconomic status as used here. However, a paired study using bone histology and blood samples to compare serum levels of dietary components such as vitamin D (Center et al. 1999) and calcium (Balk et al. 2017), which are crucial to healthy bone development and metabolism (Bell et al. 2010; Dunlop et al. 2023; Shlisky et al. 2022), would be incredibly valuable to understand dietary impact on bone tissue and give reference to dietary patterns in the past. While this study design was not feasible with this research due to covid-19 travel restrictions hindering sample access, this is potentially an avenue to pursue postdoctorally.

8.4 Research Significance

The findings reported in this thesis have made significant contributions to the disciplines of bioarchaeology, forensic and biological anthropology, and skeletal biology, especially to Australian audiences. The contributions advance our current knowledge of bone remodelling and metabolism with age-at-death, biological sex and socioeconomic status, which is historically associated with restrictions in dietary quality and nutrition access (Bhote 2004; Dyer 2000; Rogers and Waldron 2001), levels of physical activity (Jordan 2001; Zvi 1981) and general health and wellbeing (Covey 2001; Manchester and Roberts 1989; see also

Miszkiewicz and Mahoney 2016). Specifically, this research improves our understanding of how the rib and the femur respond to these factors differently, due to their differing functional adaptations (Agnew and Stout 2012; Crowder and Rosella 2007; Dominguez and Agnew 2016; Karlson 1998; Paine and Brenton 2006; Seeman et al. 1992; 2000; Stewart et al. 2021; Tommerup et al. 1993), and how these factors manifest in their bone microstructure (Baccino et al. 1999; Cho and Stout 2011; Cole et al. 2022; Eleazer and Jankauskas 2016; Fahy et al. 2017; Jowsey 1966; Karydi et al. 2022; Mavroudas et al. 2022; Miszkiewicz et al. 2022; Pedersen et al. 2024; Pfeiffer 1998; Pfeiffer et al. 2006; Reid 1986; Robling and Stout 2003; Stewart et al. 2015). Additionally, typifying key differences in bone histology variables between modern and medieval human bone informs methodological practice of categorising bone based on temporal age of a sample, and demonstrates the vast differences between these two populations of the same ancestry. For the first time, temporal difference in bone microstructure and metabolism has been conducted within a contemporary population and their genetically ancestral counterparts. Furthermore, intra-element variation was characterised between serial cross-sections within the rib, quantifying differences in microstructural and cross-sectional geometry features just one cm apart in the midshaft. In addition, osteonal and Haversian canal morphometrics were measured in the rib and femur, identifying significant size differences and nuanced results around their shape using novel measures of ring-like structures (Doube et al. 2010; Zdilla et al. 2016). Finally, differences in growth rates of osteons and Haversian canals were identified in the femur and rib using novel statistical methods, categorising these scaling relationships within these bones for the first time (Shingleton 2010).

For each of the impacted disciplines, there are real world ramifications associated with these results to improve and hone techniques, broaden understanding of disciplinary knowledge and give rise to future research directions. Firstly, bioarchaeologists, who reconstruct human behaviour from bone histology (Buikstra et al. 2022; Larsen 2002; Roberts and Gowland 2018), can apply the reported differences in manifestation of age-at-death, biological sex and socioeconomic status in the rib and femur to inform their sampling strategies, and broaden disciplinary understanding of how these factors impact upon differently adapted bones. Additionally, bioarchaeologists may be interested in applying similar methods to statistically separate temporal population groups, or groups with different subsistence strategies, using targeted histological variables most impacted by patterns of physical activity and biomechanical loading. The results reported here around intra-element variation inform sampling methods. Lastly, the novel shape measures employed in this research can hopefully provide new ways for a more in-depth analysis of osteon and Haversian canal shape, which can be used to inform on physical activity and biomechanical loading repertoires (Keenan et

al. 2017; Skedros 2024). Circularity has become the constant in the existing literature (Goliath et al. 2016; Karydi et al. 2022; Maggiano et al. 2021; Maggio and Franklin 2021), but the addition of roundness, aspect ratio and solidity from mineral science (Sinkhonde et al. 2022), neurosurgery (Zdilla et al. 2016) or within bone biology as a measure of porosity shape (Cole et al. 2022), can provide further nuances in microstructural shape (Doube et al. 2010) and behaviour interpretations.

Secondly, forensic and biological anthropologists who observe skeletal remains for biological profiling and identification purposes (Biehler-Gomez et al. 2024; Lemos et al. 2024; Pilli et al. 2025; Spradley 2016), may benefit from the reported variation in bone microstructures and cross-sectional geometry measures with advancing age-at-death and biological sex estimation. The outcomes of observing microstructural and geometric change in bone morphology in serial rib cross-sections could also inform forensic and biological anthropology sampling strategies when undertaking estimations of age-at-death and sex using bone histology. Finally, the significant differences identified here in osteon and Haversian canal sizes between the rib and femur could assist in the identification of bone fragments and pave the way for future research to categorise similar measures for other skeletal elements.

Thirdly and finally, the findings in this thesis are all united by knowledge in skeletal biology, the discipline that underpins this research and likely most benefits from these results. These reported findings increase understanding in how the rib and femur respond differently with demographic factors such as age-at-death, biological sex and socioeconomic status. These results widen our understanding of the impacts on bone microstructure and morphology with advancing age and between biological sexes. Temporal changes in bone metabolism between medieval and contemporary humans with the same ancestry have been identified and characterised for the first time in this research. Intra-element variation, even between close serial sections in the midshaft, help to improve understanding of localised microstructural adaptation within skeletal biology (Biewener and Bertram 1993; Lanyon et al. 1982; Stout et al. 2019). The differences in osteonal and Haversian canal morphometrics between the rib and femur provide insight into patterns of bone metabolism in two differently metabolically active bones with differing functional adaptations (Agnew and Stout 2012; Crowder and Rosella 2007; Dominguez and Agnew 2016; Karlson 1998; Paine and Brenton 2006; Seeman et al. 1992; 2000; Stewart et al. 2021; Tommerup et al. 1993). Finally, the differences in growth rates of osteons and their paired Haversian canals, and their scaling relationships, identified a novel way to look at bone metabolism and the relationship between these two microstructures.

8.5 Research Achievements

This dissertation has observed patterns of bone remodelling with age-at-death, biological sex and socio-economic status in the human rib and femur and observed how these factors manifest differently between the rib, posterior and anterior femur.

Additionally, this research has identified differences between modern and medieval human bone, including being the first study to use discriminant function analysis multivariate statistics to separate and categorise medieval and modern cortical bone.

Further, this work characterised intra-elemental variation via serial rib histological sections within the same bone.

Moreover, this research identified significant differences between osteonal and Haversian morphometrics between the rib and femur as well as being the first study to use reduced major axis regression to describe differences in growth rates of osteons and Haversian canals in human femur and rib cortical bone.

Finally, this is the first research to directly compare contemporary Australian human cortical bone to medieval British high and low status individuals.

Chapter 9 References

Aaron JE. 2012. Periosteal sharpey's fibers: a novel bone matrix regulatory system? *Frontiers in Endocrinology* 9(3): 98.

Aaron JE, Makins NB, Sagreiya K. 1987. The microanatomy of trabecular bone loss in normal aging men and women. *Clinical Orthopaedics and Related Research* 215(2): 260-271.

Aaron JE, Rogers J, Kanis JA. 1992. Paleohistology of Paget's disease in two medieval skeletons. *American Journal of Biological Anthropology* 89(3): 325-331.

Abd El-Aziz YM, Sobh MS, Saad HM, Morsy MHE, El-Haroun E, Abass KS, Kari ZA, Mathew RT, Eissa MEH, Eissa E-SH. 2025. Mastering the art of sectioning: a comprehensive guide to slide-microtome technology and histological applications. *Frontiers in Veterinary Science* 12(1): 1635706.

Abdi H. 2007. The Bonferroni and Sidak corrections for multiple comparisons. In: Salkind NJ (ed.). *Encyclopedia of measurement and statistics*, pp. 103-107. Sage: Thousand Oaks, Canada.

Abebe Z, Dickinson K, Mekonnen TC, Reynolds A, Appleton S, Mohammadi L, Eckert DJ, Adams R, Livingstone KM, Melaku YA. 2025. What Do Australians Eat? A Systematic Review of Dietary Patterns and Adverse Health Outcomes. *Nutrition Reviews* 83(10): 1908-1927.

Aboulenain S, Saber AY. 2022. Primary Osteoarthritis. [Updated 2022 Aug 18]. In: *StatPearls* [Internet]. StatPearls Publishing: Treasure Island, Florida; 2025 Jan-. Available from: https://www-ncbi-nlm-nih-gov.virtual.anu.edu.au/books/NBK557808/.

Abrams SA, O'Brien KO, Liang LK, Stuff JE. 1995. Differences in calcium absorption and kinetics between black and white girls aged 5-16 years. *Journal of Bone and Mineral Research* 10(5): 829-833.

Abrams SA, Copeland KC, Gunn SK, Stuff JE, Clarke LL, Ellis KJ. 1999. Calcium absorption and kinetics are similar in 7- and 8-year-old Mexican-American and Caucasian girls despite hormonal differences. *The Journal of Nutrition* 129(3): 666-671.

Absolonova K, Veleminsky P, Dobisikova M, Beran M, Zocova J. 2013. Histological Estimation of Age at Death from the Compact Bone of Burned and Unburned Human Ribs. *Journal of Forensic Sciences* 58(S1): S135-S145.

Abu EO, Horner A, Kusec V, Triffitt JT, Compston JE. 1997. The localization of androgen receptors in human bone. *The Journal of Clinical Endocrinology and Metabolism* 82(10): 3493-3497.

Adejuyigbe B, Kallini J, Chiou D, Kallini JR. 2023. Osteoporosis: Molecular Pathology, Diagnostics, and Therapeutics. *International Journal of Molecular Sciences* 24(19): 14583.

Agnew AM, Stout SD. 2012. Brief communication: Reevaluating osteoporosis in human ribs: The role of intracortical porosity. *American Journal of Biological Anthropology* 148(3): 462-466.

Ahlqvist J, Damsten OA. 1969. Modification of Kerley's Method for the Microscopic Determination of Age in Human Bone. *Journal of Forensic Science* 14(2): 205-212.

Aigner T, McKenna L. 2002. Molecular pathology and pathobiology of osteoarthritic cartilage. *Cellular and Molecular Life Sciences* 59(1): 5-18.

Aina V, Lusvardi G, Annaz B, Gibbon IR, Imrie FE, Malavasi G, Menabue L, Carrato G, Martra G. 2012. Magnesium- and strontium-co-substituted hydroxyapatite: the effects of doped-ions on the structure and chemico-physical properties. *Journal of Materials Science: Materials in Medicine* 23(12): 2867-2979.

Akesson A, Bjellerup P, Lundh T, Lidfeldt J, Nerbrand C, Samsioe G, Samsioe G, Skerfving S, Vahter M. 2006. Cadmium-induced effects on bone in a population-based study of women. *Environmental Health Perspectives* 114(6): 830-834.

Akiva A, Kerschnitzki M, Pinkas I, Wagermaier W, Yaniv K, Fratzyl P, Addadi L, Weiner S. 2016. Mineral formation in the larval zebrafish tail bone occurs via an acidic disordered calcium phosphate phase. *Journal of the American Chemical Society* 138(43): 14481-14487.

Albright F, Smith PH, Richardson AM. 1941. Postmenopausal osteoporosis. *Journal of the American Medical Association* 116(22): 2465-2474.

Alford AI, Kozloff KM, Hankenson KD. 2015. Extracellular matrix networks in bone remodelling. *The International Journal of Biochemistry and Cell Biology* 65(1): 20-31.

Allen NE, Appleby PN, Key TJ, Bueno-de-Mesquita HB, Ros MM, Kiemeney LALM, Tjønneland A, Roswall N, Overvad K, Weikert S, Boeing H, Chang-Claude J, Teucher B, Panico S, Sacerdote C, Tumino R, Palli D, Sieri S, Peeters P, Quirós JR, Jakszyn P, Molina-Montes E, Chirlaque M-D, Ardanaz E, Dorronsoro M, Khaw K-T, Wareham N, Ljungberg B, Hallmans G, Ehrnström R, Ericson U, Gram IT, Parr CL, Trichopoulou A, Karapetyan T, Dilis V, Clavel-Chapelon F, Boutron-Ruault M-C, Fagherrazzi G, Romieu I, Gunter MJ, Riboli E. 2013. Macronutrient intake and risk of urothelial cell carcinoma in the European prospective investigation into cancer and nutrition. *International Journal of Cancer* 132(3): 635-644.

Aloia JF. 1994. The gain and loss of bone in the human life cycle. *Advances in Nutritional Research* 9(1): 1-33.

Amiche MA, Albaum JM, Tadrous M, Pechlivanoglou P, Lévesque LE, Adachi JD, Cadarette SM. 2016. Fracture risk in oral glucocorticoid users: a Bayesian meta-regression leveraging control arms of osteoporosis clinical trials. *Osteoporosis International* 27(5): 1709-1718.

Aminoff M, Daroff RB. 2003. *Encyclopedia of the Neurological Sciences*. Academic Press: San Diego.

Ammann P, Rizzoli R. 2003. Bone strength and its determinants. *Osteoporosis International* 14(S3): 13-18.

Amprino R, Marotti G. 1964. A topographic quantitative study of bone formation and reconstruction. In: Blackwood H (ed.). *Bone and Tooth*, pp. 21-33. Pergamon Press: London.

An YH, Martin KL. 2003. *Handbook of Histology Methods for Bone and Cartilage*. Humana Press: Totowa, New York.

Anderson T. 1994. Medieval example of cleft lip and palate from St. Gregory's Priory, Canterbury. *The Cleft Palate-Craniofacial Journal* 31(6): 466-472.

Anderson T. 1996. Paracondylar process: Manifestation of an occipital vertebra. *International Journal of Osteoarchaeology* 6(2): 195-201.

Anderson T. 2002. Congenital conditions and neoplastic disease in British palaeopathology. In: Cox M, Mays S (eds.). *Human Osteology: In Archaeology and Forensic Science*, pp. 199-226. Cambridge University Press: Cambridge.

Anderson T, Andrews J. 2001. The Human Remains. In: Hicks M, Hicks A (eds.). *St Gregory's Priory, Northgate, Canterbury: Excavations 1988-1991*, pp. 338-370. Canterbury Archaeological Trust: Great Britain.

Anderson T, Carter AR. 1995. The first archaeological case of Madelung's deformity? *International Journal of Osteoarchaeology* 5(2): 168-173.

Anderson T, Thomas TG. 1997. A possible case of Arthrogryposis Multiplex from Medieval Canterbury. *International Journal of Osteoarchaeology* 7(2): 181-185.

Andrews RE, Shah KM, Wilkinson JM, Gartland A. 2011. Effects of cobalt and chromium ions at clinically equivalent concentrations after metal-on-metal hip replacement on human osteoblasts and osteoclasts: implications for skeletal health. *Bone* 49(4): 717-723.

Andronowski JM, Pratt IV, Cooper DML. 2017. Occurrence of osteon banding in adult human cortical bone. *American Journal of Biological Anthropology* 164(3): 635-642.

Appelman-Dijkstra NM, Papapoulos SE. 2018. Paget’s disease of bone. *Best Practice and Research: Clinical Endocrinology and Metabolism* 32(5): 657-668.

Armiento AR, Alini M, Stoddart MJ. 2019. Articular fibrocartilage - Why does hyaline cartilage fail to repair? *Advanced Drug Delivery Reviews* 146(1): 289-305.

Ascenzi A, Bonucci E. 1967. The tensile properties of single osteons. *The Anatomical Record* 158(4): 375-386.

Ascenzi A, Bonucci E. 1968. The compressive properties of single osteons. *The Anatomical Record* 161(3): 377-391.

Ascenzi A, Bonucci E. 1972. The shearing properties of single osteons. *The Anatomical Record* 172(3): 499-510.

Ascenzi A, Bonucci E, Simkin A. 1973. An approach to the mechanical properties of single osteonic lamellae. *Journal of Biomechanics* 6(3): 227-235.

Ascenzi A, Fabry C. 1959. Technique for dissection and measurement of refractive index of osteones. *The Journal of Biophysical and Biochemical Cytology* 6(1): 139-142.

Ascenzi M-G, Roe AK. 2012. The osteon: the micromechanical unit of compact bone. *Frontiers in Bioscience* 17(4): 1551-1581.

Astolphi RD, de Seixas Alves MT, Evison MP, Francisco RA, Guimarães MA, Iwamura ESM. 2019. The impact of burial period on compact bone microstructure: Histological analysis of matrix loss and cell integrity in human bones exhumed from tropical soil. *Forensic Science International* 298(1): 384-392.

Aszmann OC. 2000. The life and work of Theodore Schwann. *Journal of Reconstructive Microsurgery* 16(1): 291-295.

Aubourg G, Rice SJ, Bruce-Wootton P, Loughlin J. 2021. Genetics of osteoarthritis. *Osteoarthritis and Cartilage* 30(5): 636-649.

Aufderheide A. 2003. *The scientific study of mummies*. Cambridge University Press: Cambridge.

Aufderheide A, Rodríguez-Martín C. 1998. *The Cambridge encyclopedia of human paleopathology*. Cambridge University Press: Cambridge.

Austin AE. 2017. The cost of a commute: a multidisciplinary approach to osteoarthritis in New Kingdom Egypt. *International Journal of Osteoarchaeology* 27(4): 537-550.

Austin G, Ferguson JJA, Eslick S, Oldmeadow C, Wood LG, Garg ML. 2024. Bone mineral density and body composition in Australians following plant-based diets vs. regular meat diets. *Frontiers in Nutrition* 21(11): 1411003.

Australian Bureau of Statistics. 2021. *Cultural diversity: Census*, ABS Website, viewed 13 September 2025, <https://www-abs-gov-au.virtual.anu.edu.au/statistics/people/people-and-communities/cultural-diversity-census/latest-release>

Australian Bureau of Statistics. 2022a. *Physical activity*, ABS Website, viewed 26 July 2025, <https://www-abs-gov-au.virtual.anu.edu.au/statistics/health/health-conditions-and-risks/physical-activity/latest-release>.

Australian Bureau of Statistics. 2022b. *Chronic Obstructive Pulmonary Disease*, ABS Website, viewed 29 March 2024, <20>.

Australian Bureau of Statistics. 2023. *Dietary supplements*, ABS Website, viewed 29 March 2024, <https://www-abs-gov-au.virtual.anu.edu.au/statistics/health/food-and-nutrition/dietary-supplements/latest-release>.

Australian Institute of Health and Welfare. 2024a. *Osteoporosis and minimal trauma fractures*, AIHW Website, viewed 29 March 2024, <https://www.aihw.gov.au/reports/chronic-musculoskeletal-conditions/osteoporosis>.

Australian Institute of Health and Welfare. 2024b. *Diet*. AIHW Website, last accessed 26 July 2025, <https://www.aihw.gov.au/reports/food-nutrition/diet>.

Australian Institute of Health and Welfare. 2024c. *Infectious and communicable diseases.* AIHW Website, last accessed 26 July 2025, <https://www.aihw.gov.au/reports/australias-health/infectious-and-communicable-diseases>.

Australian Institute of Health and Welfare. 2025. *Medicare-subsidised GP, allied health and specialist health care across local areas.* AIHW Website, last accessed 26 July 2025, <https://www.aihw.gov.au/reports/primary-health-care/medicare-subsidised-gp-allied-health-specialist>.

Azzouzi H, Ichchou L. 2022. Schmorl's nodes: demystification road of endplate defects: A critical review. *Spine Deformity* 10(3): 489-499.

Baccino E, Ubelaker DH, Hayek LA, Zerilli A. 1999. Evaluation of Seven Methods of Estimating Age at Death from Mature Human Skeletal Remains. *Journal of Forensic Sciences* 44(5): 931-936.

Bach-Gansmo FL, Bruel A, Jensen MV, Ebbesen EN, Birkedal H, Thomsen JS. 2016. Osteocyte lacunar properties and cortical microstructure in human iliac crest as a function of age and sex. *Bone* 91(1): 11-19.

Bach-Gansmo FL, Weaver JC, Jensen MH, Leemreize H, Mader KS, Stampanoni M, Brüel A, Thomsen JS, Birkedal H. 2015. Osteocyte lacunar properties in rat cortical bone: Differences between lamellar and central bone. *Journal of Structural Biology* 191(1): 59-67.

Baek K, Park H-J, Baek J-H, Kim H-R. 2017. Isoproterenol Increases RANKL Expression in a ATF4/NFATc1-Dependent Manner in Mouse Osteoblastic Cells. *International Journal of Molecular Sciences* 18(10): 2204.

Bagur AC, Mautalen CA. 1992. Risk for developing osteoporosis in untreated premature menopause. *Calcified Tissue International* 51(1): 4-7.

Bai P, Sun Y, Jin J, Hou J, Li R, Zhang Q, Wang Y. 2011. Disturbance of the OPG/RANK/RANKL pathway and systemic inflammation in COPD patients with emphysema and osteoporosis. *Respiratory Research* 12(1): 157.

Bala Y, Farlay D, Boivin G. 2013. Bone mineralization: from tissue to crystal in normal and pathological contexts. *Osteoporosis International* 24(8): 2153-2166.

Balk EM, Adam GP, Langberg VN, Earley A, Clark P, Ebeling PR, Mithal A, Rizzoli R, Zerbini F, Pierroz DD, Dawson-Hughes B, The International Osteoporosis Foundation Calcium Steering Committee. 2017. Global dietary calcium intake among adults: a systematic review. *Osteoporosis International* 28(12): 3315-3324.

Balta JY, Venne G, Noël GPJC. 2022. 10 tips on working with human body donors in medical training and research. *Anatomical Sciences International* 97(3): 307-312.

Bancroft JD, Gamble M. 2002. *Theory and Practice of Histological Techniques*. Churchill Livingstone: London.

Barbero S, Raynaud D. 2023. The Perfect Eye - Das perfekte Auge: the Influence of a Presupposition from Kepler to Helmholtz. *Sudhoffs Archiv* 107(1): 27-54.

Barellus P. 1665. *De vero telescopii inventore, cum brevi omnium conspiciliorum historia – Observationum microcospicarum centuria*. Adriaan Vlacq: The Hague.

Barlow F. 1979. *The English Church, 1066-1154: A History of the Anglo-Norman Church, vol. 2*. Longman Publishing: Michigan, USA.

Barrett JM, McKinnon C, Callaghan JP. 2020. Cervical spine joint loading with neck flexion. *Ergonomics* 63(1): 101-108.

Barton PS, Reboldi A, Dawson BM, Ueland M, Strong C, Wallman JF. 2020. Soil chemical markers distinguishing human and pig decomposition islands: A preliminary study. *Forensic Science, Medicine and Pathology* 16(4): 605-612.

Bass SL, Saxon L, Daly RM, Turner CH, Robling AG, Seeman E, Stuckey S. 2002. The Effect of Mechanical Loading on the Size and Shape of Bone in Pre-, Peri-, and Postpubertal Girls: A Study in Tennis Players. *Journal of Bone and Mineral Research* 17(12): 2274-2280.

Bassett JHD, Gogakos A, White JK, Evans H, Jacques RM, van der Spek AH, Sanger Mouse Genetics Project, Ramirez-Solis R, Ryder E, Sunter D, Boyde A, Campbell MJ, Croucher PI. 2012. Rapid-Throughput Skeletal Phenotyping of 100 Knockout Mice Identifies 9 New Genes That Determine Bone Strength. *PLoS Genetics* 8(8): e1002858.

Bassett JHD, Nordström K, Boyde A, Howell PGT, Kelly S, Vennström B, Williams GR. 2007. Thyroid status during skeletal development determines adult bone structure and mineralization. *Molecular Endocrinology* 21(8): 1893-1904.

Beauchesne P, Saunders S. 2006. A test of the revised Frost's "rapid manual method" for the preparation of bone thin sections. *International Journal of Osteoarchaeology* 16(1): 82-87.

Bell LS. 2012. Histotaphonomy. In: Crowder C, Stout S (eds.). *Bone histology. An Anthropological Perspective*, pp. 241-251. CRC Press: Boca Raton.

Bell TD, Demay MB, Burnett-Bowie S-A M. 2010. The Biology and Pathology of Vitamin D Control in Bone. *Journal of Cellular Biochemistry* 111(1): 7-13.

Bellahcène A, Castronovo V, Ogbureke KU, Fisher LW, Fedarko NS. 2008. Small integrin-binding ligand N-linked glycoproteins (SIBLINGs): multifunctional proteins in cancer. *Nature Reviews: Cancer* 8(3): 212-226.

Ben-Hur H, Thole HH, Mashiah A, Insler V, Berman V, Shezen E, Elias D, Zuckerman A, Ornoy A. 1997. Estrogen, progesterone and testosterone receptors in human fetal

cartilaginous tissue: Immunohistochemical studies. *Calcified Tissue International* 60(6): 520-526.

Berendsen AD, Olsen BR. 2015. Bone development. *Bone* 80(1): 14-18.

Beresheim AC, Pfeiffer S, Alblas A. 2018. The Influence of Body Size and Bone Mass on Cortical Bone Histomorphometry in Human Ribs. *The Anatomical Record* 301(10): 1788-1796.

Bernard P. 2003. Dimerization of SOX9 is required for chondrogenesis, but not for sex determination. *Human Molecular Genetics* 12(14): 1755-1765.

Bertelloni S, Baroncelli GI, Battini R, Perri G, Saggese G. 1995. Short-term effect of testosterone treatment on reduced bone density in boys with constitutional delay of puberty. *Journal of Bone and Mineral Research* 10(10): 1488-1495.

Bertram JE, Swartz SM. 1991. "The "Law of Bone Transformation: A Case of Crying Wolff?" *Biological Reviews of the Cambridge Philosophical Society* 66(3): 245-273.

Bevelaqua FA, Hasselbacher P, Schumacher HR. 1976. Scurvy and hemarthrosis. *Journal of the American Medical Association* 235(17): 1874-1876.

Bhattacharya S, Khanna V, Kohli R. 2009. Cleft lip: The historical perspective. *Indian Journal of Plastic Surgery* 42(Suppl.): S4-S8.

Bhattarai HK, Shrestha S, Rokka K, Shakya R. 2020. Vitamin D, Calcium, Parathyroid Hormone, and Sex Steroids in Bone Health and Effects of Aging. *Journal of Osteoporosis* 17(1): 9324505.

Bhote T. 2004. *Medieval feasts and banquets: food, drink, and celebration in the Middle Ages*. The Rosen Publishing Group: New York.

Bhutta BS, Alghoula F, Berim I. 2022. Hypoxia. In: *StatPearls* [Internet]. StatPearls Publishing: Treasure Island, Florida; 2024 Jan-. Available from: <https://www-ncbi-nlm-nih-gov.virtual.anu.edu.au/books/NBK482316/>.

Bible JE, Wegner A, McClure DJ, Kadakia RJ, Richards JE, Bauer JM, Mir HR. 2014. One-year mortality after acetabular fractures in elderly patients presenting to a level-1 trauma center. *Journal of Orthopaedic Trauma* 28(3): 154-159.

Biehler-Gomez L, Giordano G, Sardanelli F, Di Candia D, Cattaneo C. 2024. Towards an integrative approach to the biological profile. *Legal Medicine* 71(1): 102499.

Bier EE, Inzana JA, Sudu TJ, Shu L, Puzas JE, Money RA. 2015. Effects of combined exposition to lead and high fat diet on bone quality in juvenile mice. *Environmental Health Perspectives* 123(10): 935-943.

Biewener AA, Bertram JEA. 1993. “Mechanical Loading and Bone Growth in Vivo.” In: Hall BK (ed.). *Bone*, *7th vol*, pp. 1-36. Boca Raton: Florida, USA.

Biewener AA, Bertram JEA. 1994. Structural response of growing bone to exercise and disuse. *Journal of Applied Physiology* 76(2): 946-955.

Biller BM, Saxe V, Herzog DB, Rosenthal DI, Holzman S, Klibanski A. 1989. Mechanisms of osteoporosis in adult and adolescent women with anorexia nervosa. *The Journal of Clinical Endocrinology and Metabolism* 68(3): 548-554.

Biondi NL, Tiwari V, Varacallo MA. 2024. Enchondroma. In: *StatPearls* [Internet]. StatPearls Publishing: Treasure Island, Florida; 2025 Jan-. Available from: <https://www-ncbi-nlm-nih-gov.virtual.anu.edu.au/books/NBK536938/>.

Bishak YK, Payahoo L, Osatdrahimi A, Nourazarian A. 2015. Mechanisms of cadmium carcinogenicity in the gastrointestinal act. *Asian Pacific Journal of Cancer Prevention* 16(1): 9-21.

Bland JM, Altman DG. 1986. Statistical methods for assessing agreement between two methods of clinical measurement. *The Lancet* 1(8476): 307-310.

Błaszczyk D, Beaumont J, Krzyszowski A, Poliński D, Drozd-Lipińska A, Wrzesińska A, Wrzesiński J. 2021. Social status and diet. Reconstruction of diet of individuals buried in some early medieval chamber graves from Poland by carbon and nitrogen stable isotopes analysis. *Journal of Archaeological Science: Reports* 38(1): 103103.

Blau S, Sterenberg J, Weeden P, Urzedo F, Wright R, Watson C. 2018. Exploring non-invasive approaches to assist in the detection of clandestine human burials: developing a way forward. *Forensic Sciences Research* 3(4): 304-326.

Bliziotes M, Sibonga JD, Turner RT, Orwoll E. 2006. Periosteal Remodelling at the Femoral Neck in Nonhuman Primates. *Journal of Bone and Mineral Research* 21(7): 1060-1067.

Boivin G, Bala Y, Doublier A, Farlay D, Ste-Marie L, Meunier P, Delmas PD. 2008. The role of mineralization and organic matrix in the microhardness of bone tissue from controls and osteoporotic patients. *Bone* 43(3): 532-538.

Bolamperti S, Villa I, Rubinacci A. 2022. Bone remodelling: an operational process ensuring survival and bone mechanical competence. *Bone Research* 10(1): 48.

Bone K, Seary P. 2015. The Western Barrack Block of the Royal Calvary Barracks, Canterbury. *Archaeologia Cantiana* 136(1): 71-86.

Bonewald LF. 2011. The amazing osteocyte. *The Journal of Bone and Mineral Research* 26(2): 229-238.

Bonewald LF, Johnson ML. 2008. Osteocytes, mechanosensing and Wnt signaling. *Bone* 42(4): 606-615.

Bonewald LF, Mundy GR. 1990. Role of transforming growth factor-beta in bone remodelling. *Clinical Orthopaedics and Related Research* 1(250): 261-276.

Bonferroni CE. 1936. Teoria statistica delle classi e calcolo delle probabilit `a. *Pubblicazioni del R Istituto Superiore di Scienze Economiche e Commerciali di Firenze* 8(1): 3-62.

Bonjour J-P, Theintz G, Buchs B, Slosman D, Rizzoli R. 1991. Critical years and stages of puberty for spinal and femoral bone mass accumulation during adolescence. *The Journal of Clinical Endocrinology and Metabolism* 73(3): 555-563.

Boskey AL, Moore DJ, Amling M, Canalis E, Delany AM. 2003. Infrared Analysis of the Mineral and Matrix in Bones of Osteonectin-Null Mice and Their Wildtype Controls. *Journal of Bone and Mineral Research* 18(6): 1005-1011.

Both J, Wu T, Bras J, Schaap GR, Baas F, Hulsebos TJM. 2012. Identification of Novel Candidate Oncogenes in Chromosome Region 17p11.2-p12 in Human Osteosarcoma. *PLoS One* 7(1): e30907.

Bourrin S, Ammann P, Bonjour JP, Rizzoli R. 2000. Dietary protein restriction lowers plasma insulin-like growth factor I (IGF-I), impairs cortical bone formation, and induces osteoblastic resistance to IGF-I in adult female rats. *Endocrinology* 141(9): 3149-3155.

Boyde A, Hordell MH. 1968. Scanning electron microscopy of lamellar bone. *Zeitschrift fur Zellforschung und Mikroskopische Anatomie* 93(2): 213-231.

Boyde A, Jones SJ. 1968. Scanning electron microscopy of cementum and sharpey fibre bone. *Zeitschrift fur Zellforschung und Mikroskopische Anatomie* 92(4): 536-548.

Boyden LM, Mao J, Belsky J, Mitzner L, Farhi A, Mitnick MA, Wu D, Insogna K, Lifton RP. 2002. High Bone Density Due to a Mutation in LDL-Receptor–Related Protein 5. *New England Journal of Medicine* 346(20): 1513-1521.

Boyle WJ, Simonet WS, Lacey DL. 2003. Osteoclast differentiation and activation. *Nature* 423(1): 337-342.

Bozic B, Loncar G, Prodanovic N, Radojicic Z, Cvorovic V, Dimkovic S, Popovic-Brkic V. 2010. Relationship between high circulating adiponectin with bone mineral density and bone metabolism in elderly males with chronic heart failure. *Journal of Cardiac Failure* 16(4): 301-307.

Bracegirdle B. 2002. The history of staining. In: Horobin R, Kiernan J (eds.). *Conn's Biological Stains 10th edition,* pp.15-22. Taylor and Francis: Oxfordshire.

Braun M, Palacios C, Wigertz K, Jackman LA, Bryant RJ, McCabe LD, Martin BR, McCabe GP, Peacock M, Weaver CM. 2007. Racial differences in skeletal calcium retention in adolescent girls with varied controlled calcium intakes. *American Journal of Clinical Nutrition* 85(6): 1657-1663.

Brayda-Bruno M, Albano D, Cannella G, Galbusera F, Zerbi A. 2018. Endplate lesions in the lumbar spine: a novel MRI-based classification scheme and epidemiology in low back pain patients. *European Spine Journal* 27(11): 2854-2861.

Brennan-Olsen SL, Page RS, Berk M, Riancho JA, Leslie WD, Wilson SG, Saban KL, Janusek L, Pasco JA, Hodge JM, Quirk SE, Hyde NK, Hosking SM, Williams LJ. 2016. DNA methylation and the social gradient of osteoporotic fracture: A conceptual model. *Bone* 84(1): 204-212.

Brickley M, Ives R. 2008. *The Bioarchaeology of Metabolic Bone Disease*. Academic Press, Elsevier: Oxford.

Bridges PS. 1990. Skeletal evidence of changes in subsistence activities between the Archaic and Mississippian time periods in Northwestern Alabama. In: Powell ML, Bridges PS, Mires AM (eds.). *What mean these bones: studies in southeastern bioarchaeology,* pp. 89-101. The University of Alabama Press: Tuscaloosa.

Britz HM, Thomas CD, Clement JG, Cooper DM. 2009. The relation of femoral osteon geometry to age, sex, height and weight. *Bone* 45(1): 77-83.

Bromage TG, Hogg RT, Lacruz RS, Hou C. 2012. Primate enamel evinces long period biological timing and regulation of life history. *Journal of Theoretical Biology* 305(1): 131-144.

Bromage TG, Idaghdour Y, Lacruz RS, Crenshaw TD, Ovsiy O, Rotter B, Hoffmeier K, Schrenk F. 2016a. The Swine Plasma Metabolome Chronicles 'Many Days' Biological Timing and Functions Linked to Growth. *PLOS One* 11(1): e0145919.

Bromage TG, Janal MN. 2014. The Havers-Halberg oscillation regulates primate tissue and organ masses across the life-history continuum. *Biological Journal of the Linnean Society* 112(4): 649-656.

Bromage TG, Juwayeyi YM, Katris JA, Gomez S, Ovsiy O, Goldstein J, Janal MN, Hu B, Schrenk F. 2016b. The scaling of human osteocyte lacuna density with body size and metabolism. *Comptes Rendus Palevol* 15(1-2): 32-39.

Bromage TG, Juwayeyi YM, Smolyar I, Hu B, Gomez S, Chisi J. 2011. Enamel-calibrated lamellar bone reveals long period growth rate variability in humans. *Cells Tissues Organs* 194(2-4): 124-130.

Bromage TG, Lacruz RS, Hogg R, Goldman HM, McFarlin SC, Warshaw J, Dirks W, Perez-Ochoa A, Smolyar I, Enlow DH, Boyd A. 2009. Lamellar bone is an incremental tissue

reconciling enamel rhythms, body size, and organismal life history. *Calcified Tissue International* 84(5): 388-404.

Bruno AG, Burkhart K, Allaire B, Anderson DE, Bouxsein ML. 2017. Spinal loading patterns from biomechanical modelling explain the high incidence of vertebral fractures in the thoracolumbar region. *Journal of Bone and Mineral Research* 32(6): 1282-1290.

Bryant RJ, Wastney ME, Martin BR, Wood O, McCabe GP, Morshidi M, Smith DL, Peacock M, Weaver CM. 2003. Racial differences in bone turnover and calcium metabolism in adolescent females. *Journal of Clinical Endocrinology and Metabolism* 88(3): 1043-1047.

Brzóska MM, Rogalska J, Galazyn-Sidorczuk M, Jurczuk M, Roszczenko A, Kulikowska-Karpińska E, Monioszko-Jakoniuk J. 2007. Effect of zinc supplementation on bone metabolism in male rats chronically exposed to cadmium. *Toxicology* 237(1-3): 89-103.

Buchanan JR, Hospodar P, Myers C, Leuenberger P, Demers LM. 1988a. Effect of excess endogenous androgens on bone density in young women. *The Journal of Clinical Endocrinology and Metabolism* 67(5): 937-943.

Buchanan JR, Myers C, Lloyd T, Leuenberger P, Demers LM. 1988b. Determinants of peak trabecular bone density in women: The role of androgens, estrogen, and exercise. *Journal of Bone and Mineral Research* 3(6): 673-680.

Buehler. 2019. *Safety Data Sheet: EpoxiCure II Resin*, Buehler Website, viewed 13 Jan 2022, <https://www.buehler.com/assets/SDS/US/1350306_A_EpoxiCure-2-Resin_EN.PDF>.

Buenzli PR, Sims NA. 2015. Quantifying the osteocyte network in the human skeleton. *Bone* 75(1): 144-150.

Buikstra JE, DeWitte SN, Agarwal SC, Baker BJ, Bartelink EJ, Berger E, Blevins KE, Bolhofner K, Boutin AT, Brickley MB, Buzon MR, de la Cova C, Goldstein L, Gowland R, Grauer AL, Gregoricka LA, Halcrow SE, Hall SA, Hillson S, Kakaliouras AM, Klaus HD, Knudson KJ, Knüsel CJ, Larsen CS, Martin DL, Milner GR, Novak M, Nystrom KC, Pacheco-Forés SI, Prowse TL, Robbins Schug G, Roberts CA, Rothwell JE, Santos AL, Stojanowski C, Stone AC, Stull KE, Temple DH, Torres CM, Toyne JM, Tung TA,

Ullinger J, Wiltschke-Schrotta K, Zakrzewski SR. 2022. Twenty-first century bioarchaeology: Taking stock and moving forward. *American Journal of Biological Anthropology* 178(S74): 54-114.

Buikstra JE, Ubelaker DH. 1994. *Standards for data collection from human skeletal remains. Research series no. 44.* Arkansas Archeological Survey Research Series: Fayetteville.

Burch D, Sheerin F. 2005. Parkinson's disease. *Lancet* 365(9459): 622-627.

Burr DB. 2010. Cortical bone: a target for fracture prevention? *Lancet* 375(9727): 1672-1673.

Burr DB. 2014. Repair Mechanisms for Microdamage in Bone. *Journal of Bone and Mineral Research* 29(12): 2534-2536.

Burr DB, Martin RB. 1993. Calculating the probability that microcracks initiate resorption spaces. *Journal of Biomechanics* 26(4-5): 613-616.

Burr DB, Martin RB, Schaffler MB, Radin EL. 1985. Bone remodelling in response to in vivo fatigue microdamage. *Journal of Biomechanics* 18(3): 189-200.

Burr DB, Robling AG, Turner CH. 2002. Effects of biomechanical stress on bones in animals. *Bone* 30(5): 781-786.

Burr DB, Ruff CB, Thompson DD. 1990. Patterns of skeletal histologic change through time: comparison of an archaic Native American population with modern populations. *The Anatomical Record* 226(3): 307-313.

Burr DB, Turner CH, Naick P, Forwood MR, Ambrosius W, Sayeed Hasan M, Pidaparti R. 1998. Does microdamage accumulation affect the mechanical properties of bone? *Journal of Biomechanics* 31(4): 337-345.

Burton J. 2005. The Convent and the Community: Cause Papers as a Source for Monastic History. In: Hoskins P, Brooke C, Dobson B (eds.). *The Foundations of Medieval English Ecclesiastical History: Studies Presented to David Smith*, pp. 63-76. The Boydell Press: Woodbridge.

Caetano-Lopes J, Canhão H, Fonseca JE. 2007. Osteoblasts and bone formation. *Acta Reumatologica Portuguesa* 32(2): 103-110.

Callis GM. 2002. Bone. In: Bancroft JD, Gamble M (eds.). *Theory and Practice of Histological Techniques*, pp. 269-301. Churchill Livingstone: London.

Canalis E, Raisz LG. 1978. Effect of sex steroids on bone collagen synthesis in vitro. *Calcified Tissue Research* 25(1): 105-110.

Cannata-Andía JB, Martín-Carro B, Martín-Vírgala J, Rodríguez-Carrio J, Bande-Fernández JJ, Cristina Alonso-Montes C, Carrillo-López N. 2020. Chronic Kidney Disease – Mineral and Bone Disorders: Pathogenesis and Management. *Calcified Tissue International* 108(4): 410-422.

Carlson DS, Armelagos GJ, van Gerven DP. 1974. Factors influencing the etiology of cribra orbitalia in prehistoric Nubia. *Journal of Human Evolution* 3(5): 405-406.

Carrascosa A, Audi L, Ferrandez MA, Ballabriga A. 1990. Biological effects of androgens and identification of specific dihydrotestosterone-binding sites in cultured human fetal epiphyseal chondrocytes. *The Journal of Clinical Endocrinology and Metabolism* 70(1): 134–140.

Castoldi E, Cappella A, Gibelli D, Sforza C, Cattaneo C. 2018. The Difficult Task of Diagnosing Prostate Cancer Metastases on Dry Bone. *Journal of Forensic Sciences* 63(3): 672-682.

Cauley JA, Robbins J, Chen Z, Cummings SR, Jackson RD, LaCroix AZ, LeBoff M, Lewis CE, McGowan J, Neuner J, Pettinger M, Stefanick ML, Wactawski-Wende J, Watts NB; Women's Health Initiative Investigators. 2003. Effects of estrogen plus progestin on risk of fracture and bone mineral density: the Women's Health Initiative randomized trial. *Journal of the American Medical Association* 290(13): 1729-1738.

Center JR, Nguyen TV, Sambrook PN, Eisman JA.1999. Hormonal and biochemical parameters in the determination of osteoporosis in elderly men. *The Journal of Clinical Endocrinology and Metabolism* 84(10): 3626-3635.

Chahal S, Kumar A, Hussian FSJ. 2019. Development of biomimetic electrospun polymeric biomaterials for bone tissue engineering. A review. *Journal of Biomaterials Science: Polymer Edition* 30(14): 1308-1355.

Chang B, Liu X. 2022. Osteon: Structure, Turnover, and Regeneration. *Tissue Engineering Part B Reviews* 28(2): 261-278.

Chang H, Knothe Tate ML. 2012. Concise review: the periosteum: tapping into a reservoir of clinically useful progenitor cells. *Stem Cells Translational Medicine* 1(6): 480-491.

Chantler S, Dickie K, Goedecke JH, Levitt NS, Lambert EV, Evans J, Joffe Y, Micklesfield LK. 2012. Site-specific differences in bone mineral density in black and white premenopausal South African women. *Osteoporosis International* 23(2): 533-542.

Chapuy MC, Arlot ME, Duboeuf F, Brun J, Crouzet B, Arnaud S, Delmas PD, Meunier PJ. 1992. Vitamin D3 and Calcium to Prevent Hip Fractures in Elderly Women. *The New England Journal of Medicine* 327(23): 1637-1642.

Charpail E, Trosseille X, Petit P, Laporte S, Lavaste F, Vallancien G. 2005. Characterization of PMHS ribs: a new test methodology. *Stapp Car Crash Journal* 49(1): 183-198.

Chen H, Zhang SM, Hernán MA, Willett WC, Ascherio A. 2003. Weight loss in Parkinson's disease. *Annals of Neurology* 53(5): 676-679.

Chen H, Zhou X, Fujita H, Onozuka M, Kubo K-Y. 2013. Age-Related Changes in Trabecular and Cortical Bone Microstructure. *International Journal of Endocrinology,* doi: 10.1155/2013/213234.

Chen J, Hendriks M, Chatzis A, Ramasamy SK, Kusumbe AP. 2020. Bone vasculature and bone marrow vascular niches in health and disease. *Journal of Bone and Mineral Research* 35(11): 2103-2120.

Cheng SY, Levy AR, Lefaivre KA, Guy P, Kuramoto L, Sobolev B. 2011. Geographic trends in incidence of hip fractures: a comprehensive literature review. *Osteoporosis International* 22(10): 2575-2586.

Chen Y-H, Lo RY. 2017. Alzheimer's disease and osteoporosis. *Tzu Chi Medical Journal* 29(3): 138-142.

Ching K, Houard X, Berenbaum F, Wen C. 2021. Hypertension meets osteoarthritis: revisiting the vascular aetiology hypothesis. *Nature Reviews: Rheumatology* 17(9): 533-549.

Cho H. 2012. The histology laboratory and principles of microscope instrumentation. In: Crowder C, Stout D (eds.). *Bone Histology: An Anthropological Perspective*, pp. 341-375. Taylor & Francis Group: Boca Raton, Florida.

Cho H, Stout SD. 2011. Age-associated bone loss and intraskeletal variability in the Imperial Romans. *Journal of Anthropological Sciences* 89(1): 109-125.

Cho H, Stout SD, Bishop TA. 2006. Cortical bone remodelling rates in a sample of African American and European American descent groups from the American Midwest: Comparisons of age and sex in ribs. *American Journal of Biological Anthropology* 130(2): 214-226.

Cho H, Stout SD, Madsen RW, Streeter MA. 2002. Population-Specific Histological Age-Estimating Method: A Model for Known African-American and European-American Skeletal Remains. *Journal of Forensic Sciences* 47(1): 12-18.

Choi A, Umemoto A, Mizuno M, Park-Min KH. 2024. Bone metabolism: an underappreciated player. *npj Metabolic Health and Disease* 2(1): 12.

Choi KH, Lee JH, Lee DG. 2021. Sex-related differences in bone metabolism in osteoporosis observational study. *Medicine (Baltimore)* 100(21): e26153.

Christensen K, Doblhammer G, Rau R, Vaupel JW. 2019. Ageing populations: the challenges ahead. *The Lancet* 374(9696): 1196-1208.

Christian JC, Yu PL, Slemenda CW, Johnston CC. 1989. Heritability of bone mass: A longitudinal study in aging male twins. *The American Journal of Human Genetics* 44(3): 429-433.

Chun KJ. 2011. Bone Densitometry. *Seminars in Nuclear Medicine* 41(3): 220-228.

Citron JT, Ettinger B, Genant HK. 1995. Spinal bone mineral loss in estrogen-replete, calcium-replete premenopausal women. *Osteoporosis International* 5(4): 228-233.

Clark E. 1982. Some aspects of social security in Medieval England. *Journal of Family History* 7(4): 307-320.

Clark GR, Duncan EL. 2015. The genetics of osteoporosis. *British Medical Bulletin* 113(1): 73-81.

Clarke B. 2008. Normal Bone Anatomy and Physiology. *Clinical Journal of the American Society of Nephrology* 3(Suppl 3): S131-S139.

Clarke BL, Khosla S. 2009. Androgens and bone. *Steroids* 74(3): 296-305.

Clarke PC. 1901. The Dean and Chapter's old water supply. *Kentish Gazette*, originally published in *The Star*, 2nd December 1807.

Clegg NW, Reed CG. 1994. The economic decline of the church in Medieval England. *Explorations in Economic History* 31(2): 261-280.

Cole ME, Gosman JH, Stout SD. 2023. Current concepts in bone biology. In: Larsen CS (ed.). *A Companion to Biological Anthropology, 2nd edition*, pp. 527-543. Wiley Blackwell: New Jersey, USA.

Cole ME, Stout SD, Dominguez VM, Agnew AM. 2022. Pore Extractor 2D: An ImageJ toolkit for quantifying cortical pore morphometry on histological bone images, with application to intraskeletal and regional patterning. *American Journal of Biological Anthropology* 179(3): 365-385.

Coleman R, Body JJ, Aapro M, Hadji P, Herrstedt J, The ESMO Guidelines Working Group. 2014. Bone health in cancer patients: ESMO Clinical Practice Guidelines. *Annals of Oncology* 25(Suppl 3): 123-137.

Colnot C. 2009. Skeletal cell fate decisions within periosteum and bone marrow during bone regeneration. *Journal of Bone and Mineral Research* 24(2): 274-282.

Compston JE. 2001. Sex steroids and bone. *Physiological Reviews* 81(1): 419-447.

Congiu T, Pazzaglia UE. 2011. The Sealed Osteons of Cortical Diaphyseal Bone. Early Observations Revisited With Scanning Electron Microscopy. *The Anatomical Record* 294(2): 193-198.

Connor M, Belcher WR, Dabbs GR, Falsetti A, Forbes SL, Gocha TP, Harris J, Hughes S, Listi G, Mavroudas S, Polonitza A, Reck SI, Steadman D, Ward J, Wescott DJ, Yim A-D,

Zedjlik K. 2024. From a small plot in Knoxville to a worldwide footprint: An overview of human decomposition facilities. *Forensic Anthropology* 7(4): 267-281.

Cooke KM, Mahoney P, Miszkiewicz JJ. 2022. Secondary osteon variants and remodelling in human bone. *The Anatomical Record* 305(6): 1299-1315.

Cooper C, Atkinson EJ, O'Fallon WM, Melton LJ. 1992. Incidence of clinically diagnosed vertebral fractures: a population-based study in Rochester, Minnesota, 1985-1989. *Journal of Bone and Mineral Research* 7(2): 221-227.

Cooper DML, Kawalilak CE, Harrison K, Johnston BD, Johnston JD. 2016. Cortical Bone Porosity: What Is It, Why Is It Important, and How Can We Detect It? *Current Osteoporosis Reports* 14(5): 187-198.

Cooper RR, Milgram JW, Robinson RA. 1966. Morphology of the Osteon: An Electron Microscopic Study. *The Journal of Bone and Joint Surgery* 48(7): 1239-1271.

Coratella G, Longo S, Borrelli M, Doria C, Cè E, Esposito F. 2020. Vastus intermedius muscle architecture predicts the late phase of the knee extension rate of force development in recreationally resistance-trained men. *Journal of Science and Medicine in Sport* 23(11): 1100-1104.

Cormier JM, Stitzel JD, Duma SM, Matsuoka F. 2005. Regional variation in the structural response and geometrical properties of human ribs. *Annual Proceedings of the Association for the Advancement of Automotive Medicine* 49(1): 153-170.

Corrado A, Cici D, Rotondo C, Maruotti N, Cantatore FP. 2020. Molecular Basis of Bone Aging. *International Journal of Molecular Sciences* 21(10): 3679.

Corral-Gudino L, Borao-Cengotita-Bengoa M, Del Pino-Montes J, Ralston S. 2013. Epidemiology of Paget’s disease of bone: a systematic review and meta-analysis of secular changes. *Bone* 55(2): 347-352.

Coulson-Thomas YM, Coulson-Thomas VJ, Norton AL, Gesteira TF, Cavalheiro RP, Meneghetti MC, Martins JR, Dixon RA, Nader HB. 2015. The identification of proteoglycans and glycosaminoglycans in archaeological human bones and teeth. *PloS One* 10(6): e0131105.

Courtney MG, Roberts J, Quintero Y, Godde K. 2023. Childhood Family Environment and Osteoporosis in a Population-Based Cohort Study of Middle-to Older-Age Americans. *JBMR Plus* 7(5): e10735.

Covey H. 2001. People with leprosy (Hansen's disease) during the Middle Ages. *The Social Science Journal* 38(1): 315-321.

Cox G, Sealy J. 1997. Investigating identity and life histories: isotopic analysis and historical documentation of slave skeletons found on the cape town foreshore, South Africa. *International Journal of Historical Archaeology* 1(3): 207e224.

Crescimanno A, Stout SD. 2012. Differentiating fragmented human and nonhuman long bone using osteon circularity. *Journal of Forensic Sciences* 57(2): 287-294.

Crowder C. 2013. *Estimation of age at death using cortical bone histomorphometry*. US Department of Justice: New York.

Crowder C, Dominguez VM, Heinrich J, Pinto D, Mavroudas S. 2022. Analysis of histomorphometric variables: Proposal and validation of osteon definitions. *Journal of Forensic Sciences* 67(1): 80-91.

Crowder C, Rosella L. 2007. Assessment of intra- and intercostal variation in rib histomorphometry: its impact on evidentiary examination. *Journal of Forensic Sciences* 52(2): 271-276.

Crowder C, Stout D. 2011. *Bone Histology: An Anthropological Perspective*. Taylor & Francis Group: Boca Raton, Florida.

Cunningham C, Scheuer L, Black SM. 2016. *Developmental juvenile osteology*. Elsevier: Amsterdam.

Currey JD. 1964. Some effects of ageing in human Haversian systems. *Journal of Anatomy* 98(1): 69-75.

Currey JD. 2002. *Bones*. Princeton University Press: New Jersey, USA.

Currey JD, Dean MN, Shahar R. 2017. Revisiting the links between bone remodelling and osteocytes: insights from across phyla: What is bone remodelling for? *Biological Reviews of the Cambridge Philosophical Society* 92(3): 1702-1719.

Cusabio Technology LLC. 2024. *Structure-Osteocyte.jpg*, Cusabio Website, viewed 04 August 2024, <https://www.cusabio.com/statics/images/Structure-Osteocyte.jpg>.

Dalle Carbonare L, Valenti MT, Giannini S, Gallieni M, Stefani F, Ciresa R, Politi C, Fusaro M. 2021. Bone Biopsy for Histomorphometry in Chronic Kidney Disease (CKD): State-of-the-Art and New Perspectives. *Journal of Clinical Medicine* 10(19): 4617.

Danford CJ, Trivedi HD, Bonder A. 2020. Bone Health in Patients with Liver Diseases. *Journal of Clinical Densitometry* 23(2): 212-222.

Daniel M, Martin AD, Drinkwater DT. 1992. Cigarette smoking, steroid hormones, and bone mineral density in young women. *Calcified Tissue International* 50(4): 300-305.

Darrah TH, Campbell ME, Prustman-Pfeiffer JJ, Poreda RJ, Hannigan RE. 2013. Trace Element Composition of Modern Human Bone. In: Censi P, Darrah T, Erel Y (eds.). *Medical Geochemistry*, pp. 167-191. Springer: Dordrecht.

Datta HK, Ng WF, Walker JA, Tuck SP, Varanasi SS. 2008. The cell biology of bone metabolism. *Journal of Clinical Pathology* 61(5): 577-587.

Dawson BM, Barton PS, Wallman JF. 2020. Contrasting insect activity and decomposition of pigs and humans in an Australian environment: A preliminary study. *Forensic Science International* 316: 110515.

Dawson H. 2014. *Unearthing late Medieval children: health, status and burial practice in southern England*. Archaeopress: Oxford.

Dawson H, Brown KR. 2013. Exploring the relationship between dental wear and status in late medieval subadults from England. *American Journal of Biological Anthropology* 150(3): 433-441.

Dawson-Hughes B, Harris SS, Krall EA, Dallal GE. 1997. Effect of calcium and vitamin D supplementation on bone density in men and women 65 years of age or older. *The New England Journal of Medicine* 337(10): 670-676.

de Boer HH, Van der Merwe AE. 2016. Diagnostic dry bone histology in human paleopathology. *Clinical Anatomy* 29(7): 831-843.

de Boer HH, Van der Merwe AE, Maat GJR. 2013. The diagnostic value of microscopy in dry bone palaeopathology: A review. *International Journal of Paleopathology* 3(2): 113-121.

de Gruchy YA, Faillace KE, Van de Vijver K, Schotsmans EMJ, Seifert J, Bricking A, Nederbragt AJ, Madgwick R. 2024. Bone of contention: Intra-element variability in remodelling of human femora based on histomorphometric and isotope analyses. *PLOS One* 19(6): e0305089.

Delany AM, Amling M, Priemel M, Howe C, Baron R, Canalis E. 2000. Osteopenia and decreased bone formation in osteonectin-deficient mice. *Journal of Clinical Investigation* 105(7): 915-923.

De Leon-Oliva D, Barrena-Blázquez S, Jiménez-Álvarez L, Fraile-Martinez O, García-Montero C, López-González L, Torres-Carranza D, García-Puente LM, Carranza ST, Álvarez-Mon MÁ, Álvarez-Mon M, Diaz R, Ortega MA. 2023. The RANK-RANKL-OPG System: A Multifaceted Regulator of Homeostasis, Immunity, and Cancer. *Medicina (Kaunas)* 59(10): 1752.

Dempster DW, Compston JE, Drezner MK, Glorieux FH, Kanis JA, Malluche H, Meunier PJ, Ott SM, Recker RR, Parfitt AM. 2013. Standardized nomenclature, symbols, and units for bone histomorphometry: a 2012 update of the report of the ASBMR Histomorphometry Nomenclature Committee. *Journal of Bone and Mineral Research* 28(1): 2-17.

Dennerstein L, Spencer-Gardner C, Gotts G, Brown JB, Smith MA, Burrows GD. 1985. Progesterone and the premenstrual syndrome: A double-blind crossover trial. *British Medical Journal* 290(6482): 1617-1621.

Denton J. 2008. Slices of mummy: a histologist's perspective. In: David R (ed.). *Egyptian mummies and modern science,* pp. 71-82. Cambridge University Press: Cambridge.

Deo A, Forbes SL, Stuart BH, Ueland M. 2019. Profiling the seasonal variability of decomposition odour from human remains in a temperate Australian environment. *Australian Journal of Forensic Sciences* 52(6): 654-664.

Department of Agriculture, Fisheries and Forestry. 2015. *Biosecurity Act, Act No. 61, C2025C00015*, Federal Register of Legislation Website, viewed 10 September 2025, <https://www.legislation.gov.au/C2015A00061/latest/versions>.

Designua. 2014. *Osteon-development-and-structure-osteoblast-osteocyte-and-osteoclast.jpg,* Shutterstock Website, viewed 17 August 2024, <https://www.shutterstock.com/da/image-illustration/osteon-development-structure-osteoblast-osteocyte-osteoclast-186714569>.

Dequeker J, Nijs J, Verstraeten A, Geusens P, Gevers G. 1987. Genetic determinants of bone mineral content at the spine and radius: A twin study. *Bone* 8(4): 207-209.

DeWitte SN, Stojanowski CM. 2015. The osteological paradox 20 years later: past perspectives, future directions. *Journal of Archaeological Research* 23(4): 397-450.

Dey A, Bomans PH, Müller FA, Will J, Frederik PM, de With G, Sommerdijk NAJM. 2010. The role of prenucleation clusters in surface-induced calcium phosphate crystallization. *Nature Materials* 9(12): 1010-1014.

Dhanwal DK, Cooper C, Dennison EM. 2010. Geographic Variation in Osteoporotic Hip Fracture Incidence: The Growing Importance of Asian Influences in Coming Decades. *Journal of Osteoporosis* 2010: 757102.

Diamantis A, Beloukas AI, Kalogeraki AM, Magiorkinis E. 2013. A brief chronicle of cytology: From Janssen to Papanicolaou and beyond. *Diagnostic Cytopathology* 41(6): 555-564.

Ding D, Lawson KD, Kolbe-Alexander TL, Finkelstein EA, Katzmarzyk PT, van Mechelen W, Pratt M. 2016. The economic burden of physical inactivity: a global analysis of major non-communicable diseases. *The Lancet* 388(10051): 1311-1324.

Ding D, Rogers K, van der Ploeg H, Stamatakis E, Bauman AE. 2015. Traditional and Emerging Lifestyle Risk Behaviors and All-Cause Mortality in Middle-Aged and Older Adults: Evidence from a Large Population-Based Australian Cohort. *PLoS Medicine* 12(12): e1001917.

Dixon JE, Rodin A, Murby B, Chapman MG, Fogelman I. 1989. Bone mass in hirsute women with androgen excess. *Clinical Endocrinology* 30(3): 271-277.

Doblaré M, Garcia JM. 2002. Anisotropic bone remodelling model based on a continuum damage-repair theory. *Journal of Biomechanics* 35(1): 1-17.

Dolding-Smith, JAM. 2023. *Maturation of the Modern Human Skeleton*. Doctor of Philosophy (PhD) thesis submitted to the University of Kent. Available from: <https://kar.kent.ac.uk/100671/>.

Dominguez VM, Agnew AM. 2016. Examination of Factors Potentially Influencing Osteon Size in the Human Rib. *The Anatomical Record* 299(3): 313-324.

Dominguez VM, Crowder CM. 2012. The utility of osteon shape and circularity for differentiating human and non-human Haversian bone. *American Journal of Biological Anthropology* 149(1): 84-91.

Dominguez VM, Harden AL, Wascher M, Agnew AM. 2020. Rib Variation at Multiple Locations and Implications for Histological Age Estimation. *Journal of Forensic Sciences* 65(6): 2108-2111.

Dong P, Haupert S, Hesse B, Langer M, Gouttenoire P-J, Bousson V, Peyrin F. 2014. 3D osteocyte lacunar morphometric properties and distributions in human femoral cortical bone using synchrotron radiation micro-CT images. *Bone* 60(1): 172-185.

Doube M, Kłosowski M, Arganda-Carreras I, Cordelières FP, Dougherty RP, Jackson JS, Schmid B, Hutchinson JR, Shefelbine SJ. 2010. BoneJ: Free and extensible bone image analysis in ImageJ. *Bone* 47(6): 1076-1079.

Drake MT. 2014. Osteoporosis and Cancer. *Current Osteoporosis Reports* 11(3): 163-170.

Drapeau MS, Streeter MA. 2006. Modelling and remodelling responses to normal loading in the human lower limb. *American Journal of Biological Anthropology* 129(3): 403-409.

Drew ER, Mahoney P, Miszkiewicz JJ. 2021. Osteocyte lacuno-canalicular microstructure across the midshaft femur in adult males from Medieval England. *International Journal of Osteoarchaeology* 31(2): 176-187.

Ducy P, Desbois C, Boyce B, Pinero G, Story B, Dunstan C, Smith E, Bonadio J, Goldstein S, Gundberg C, Bradley A, Karsenty G. 1996. Increased bone formation in osteocalcin-deficient mice. *Nature* 382(6590): 448-452.

Dudhia J. 2005. Aggrecan, aging and assembly in articular cartilage. *Cellular and Molecular Life Sciences* 62(19-20): 2241-2256.

Dunlop E, Boorman JL, Hambridge TL, McNeill J, James AP, Kiely M, Nowson CA, Rangan A, Cunningham J, Adorno P, Atyeo P, Black LJ. 2023. Evidence of low vitamin D intakes in the Australian population points to a need for data-driven nutrition policy for improving population vitamin D status. *Journal of Human Nutrition and Dietetics* 36(1): 203-215.

Dyer C. 2000. *Everyday life in Medieval England*. Cambridge University Press: Cambridge.

Ebbesen EN, Thomsen JS, Beck-Nielsen H, Nepper-Rasmussen HJ, Mosekilde L. 1999. Age- and gender-related differences in vertebral bone mass, density, and strength. *Journal of Bone and Mineral Research* 14(8): 1394-1403.

Elders PJM, Netelenbos JC, Lips P, van Ginkel FC, van der Stelt PF. 1988. Accelerated vertebral bone loss in relation to the menopause: a cross-sectional study on lumbar bone density in 286 women of 46 to 55 years of age. *Bone and Mineral* 5(1): 11-19.

Eleazer CD, Jankauskas R. 2016. Mechanical and Metabolic Interactions in Cortical Bone Development. *American Journal of Biological Anthropology* 160(2): 317-333.

Elliott AC, Woodward WA. 2007. *Statistical Analysis Quick Reference Guidebook*. SAGE Publications: California.

Emaus N, Berntsen GKR, Joakimsen RM, Fønnebø V. 2005. Longitudinal Changes in Forearm Bone Mineral Density in Women and Men Aged 25–44 Years. *American Journal of Epidemiology* 162(7): 633-643.

Emaus N, Berntsen GKR, Joakimsen R, Fonnebø V. 2006. Longitudinal Changes in Forearm Bone Mineral Density in Women and Men Aged 45–84 Years: The Tromsø Study, a Population-based Study. *American Journal of Epidemiology* 163(5): 441-449.

Emmanual J, Hornbeck C, Bloebaum RD. 1987. A polymethyl methacrylate method for large specimens of mineralized bone with implants. *Stain Technology* 62(6): 401-410.

Engström A, Michaëlsson K, Vater M, Julin B, Wolk A, Äkesson A. 2012. Associations between dietary cadmium exposure and bone mineral density and risk of osteoporosis and fractures among women. *Bone* 50(6): 1372-1378.

Erben RG. 1996. Trabecular and endocortical bone surfaces in the rat: modelling or remodelling. *The Anatomical Record* 246(1): 39-46.

Erben RG. 1997. Embedding of bone samples in methylmethacrylate: An improved method suitable for bone histomorphometry, histochemistry and immunohistochemistry. *The Journal of Histochemistry and Cytochemistry* 45(2): 307-313.

Ericksen MF. 1980. Patterns of microscopic bone remodelling in three Aboriginal American populations. In: Browman DL (ed.). *Early Native Americans*, 239-270. Mouton: The Hague.

Ericksen MF. 1991. Histologic Estimation of Age at Death Using the Anterior Cortex of the Femur. *American Journal of Biological Anthropology* 84(2): 171-179.

Eriksen EF, Axelrod DW, Melsen F. 1994. *Bone histomorphometry*. Raven Press: New York.

Eriksen EF, Eghbali-Fatourechi GZ, Khosla S. 2007. Remodelling and Vascular Spaces in Bone. *Journal of Bone and Mineral Research* 22(1): 1-6.

Evans FG. 1976. Mechanical properties and histology of cortical bone from younger and older men. *The Anatomical Record* 185(1): 1-12.

Everts V, Delaissé JM, Korper W, Jansen DC, Tigchelaar-Gutter W, Saftig P, Beertsen W. 2002. The Bone Lining Cell: Its Role in Cleaning Howship's Lacunae and Initiating Bone Formation. *Journal of Bone and Mineral Research* 17(1): 77-90.

Eyre DR, Weis MA, Wu JJ. 2006. Articular cartilage collagen: an irreplaceable framework? *European Cells and Materials* 12(1): 57-63.

Fahy GE, Deter C, Pitfield R, Miszkiewicz JJ, Mahoney P. 2017. Bone deep: Variation in stable isotope ratios and histomorphometric measurements of bone remodelling within adult humans. *Journal of Archaeological Science* 87(1): 10-16.

Fain O. 2005. Musculoskeletal manifestations of scurvy. *Joint, Bone, Spine* 72(2): 124-128.

Farlay D, Bala Y, Rizzo S, Bare S, Lappe JM, Recker R, Boivin G. 2019. Bone remodelling and bone matrix quality before and after menopause in healthy women. *Bone* 128(1): 115030.

Farr JN, Khosla S. 2015. Skeletal changes through the lifespan—from growth to senescence. *Nature Reviews: Endocrinology* 11(9): 513-521.

Fatima M, Scholes CJ, Zhong E, Kohan L. 2019. Towards a Dynamic Model of the Kangaroo Knee for Clinical Insights into Human Knee Pathology and Treatment: Establishing a Static Biomechanical Profile. *Biomimetics* 4(3): 52.

Fazeli PK, Horowitz MC, MacDougald OA, Scheller EL, Rodeheffer MS, Rosen CJ, Klibanski A. 2013. Marrow fat and bone--new perspectives. *The Journal of Clinical Endocrinology and Metabolism* 98(3): 935-945.

Fennell S, Jones DG. 1992. The bequest of human bodies for dissection: a case study in the Otago Medical School. *The New Zealand Medical Journal* 105(946): 472-474.

Ferrari C, Possemato N, Pipitone N, Manger B, Salvarani C. 2015. Rheumatic manifestations of scurvy. *Current Rheumatology Reports* 17(4): 26.

Figueroa CA, Rosen CJ. 2020. Parkinson's disease and osteoporosis: basic and clinical implications. *Expert Review of Endocrinology and Metabolism* 15(3): 185-193.

Finck H, Hart AR, Jennings A, Welch AA. 2014. Is there a role for vitamin C in preventing osteoporosis and fractures? A review of the potential underlying mechanisms and current epidemiological evidence. *Nutrition Research Reviews* 27(2): 268-283.

Finkelman RD, Butler WT. 1985. Appearance of dentin gamma-carboxyglutamic acid-containing proteins in developing rat molars in vitro. *Journal of Dental Research* 64(7): 1008-1015.

Finkelstein JS, Klibanski A, Neer RM, Doppelt SH, Rosenthal DI, Segre GV, Crowley WF. 1989. Increases in bone density during treatment of men with idiopathic hypogonadotropic hypogonadism. *The Journal of Clinical Endocrinology and Metabolism* 69(4): 776-783.

Finkelstein JS, Klibanski A, Neer RM, Greenspan SL, Rosenthal DI, Crowley WF. 1987. Osteoporosis in men with idiopathic hypogonadotropic hypogonadism. *Annals of Internal Medicine* 106(3): 354-361.

Finkelstein JS, Neer RM, Biller BMK, Crawford JD, Klibanski A. 1992. Osteopenia in men with a history of delayed puberty. *The New England Journal of Medicine* 326(9): 600-604.

Finkelstein JS, Sowers M, Greendale GA, Lee M-LT, Neer RM, Cauley JA, Ettinger B. 2002. Ethnic Variation in Bone Turnover in Pre- and Early Perimenopausal Women: Effects of Anthropometric and Lifestyle Factors. *The Journal of Clinical Endocrinology and Metabolism* 87(7): 3051-3056.

Floyd AD. 2002. Quantitative data from microscopic specimens. In: Bancroft JD, Gamble M (eds.). *Theory and Practice of Histological Techniques,* pp. 729-747. Churchill Livingstone: London.

Forbes SL. 2017. Body farms. *Forensic Science, Medicine and Pathology* 13(4): 477-479.

Forwood MR. 2008. Physical activity and bone development during childhood: insights from animal models. *Journal of Applied Physiology* 105(1): 334-341.

Francescone MA, Levitt J. 2005. Scurvy masquerading as leukocytoclastic vasculitis: a case report and review of the literature. *Cutis* 76(4): 261-266.

Frankel VH, Nordin M. 2012.Biomechanics of Bone. In: Nordin, M, Frankel VH (eds.). *Basic Biomechanics of the Musculoskeletal System, 4th edition,* pp. 24-59. Lippincott Williams and Wilkins: Baltimore.

Franz-Odendaal TA, Hall BK, Witten PE. 2006. Buried alive: how osteoblasts become osteocytes. *Developmental Dynamics* 235(1): 176-190.

Frenkel B, Hong A, Baniwal SK, Coetzee GA, Ohlsson C, Khalid O, Gabet Y. 2010. Regulation of Adult Bone Turnover by Sex Steroids. *Journal of Cellular Physiology* 224(2): 305-310.

Frere SS, Hassall MWC, Tomlin RSO. 1990. Roman Britain in 1989. *Britannia* 21(1): 303-378.

Friedman MA, Bailey AM, Rondon MJ, McNerny EM, Sahar ND, Kohn DH. 2016. Calcium- and Phosphorus-Supplemented Diet Increases Bone Mass after Short-Term Exercise and Increases Bone Mass and Structural Strength after Long-Term Exercise in Adult Mice. *PLOS One* 11(3): e0151995.

Frost HM. 1958. Preparation of thin undecalcified bone sections by rapid manual method. *Stain Technology* 33(6): 273-277.

Frost HM. 1960. Micropetrosis. *The Journal of Bone and Joint Surgery* 42-A: 144-150.

Frost HM. 1962. Interlamellar thickness in human bone. *Clinical Orthopaedics and Related Research* 24(1): 198-205.

Frost HM. 1964. *The laws of bone structure*. CC Thomas: Springfield, Illinois.

Frost HM. 1969. Tetracycline-based histological analysis of bone remodelling. *Calcified Tissue Research* 3(1): 211-237.

Frost HM. 1987a. Bone ‘mass’ and the ‘mechanostat’: A proposal. *The Anatomical Record* 219(1): 1-9.

Frost HM. 1987b. Secondary osteon population densities: An algorithm for estimating the missing osteons. *American Journal of Biological Anthropology* 30(S8): 239-254.

Frost HM. 1990. Skeletal structural adaptations to mechanical usage (SATMU): 2. Redefining Wolff's law: the remodelling problem. *The Anatomical Record* 226(4): 414-422.

Frost HM. 1997. Why do marathon runners have less bone than weight lifters? A vital-biomechanical view and explanation. *Bone* 20(3): 183-189.

Frost HM. 2000. The Utah paradigm of skeletal physiology: what is it? *Journal of Bone and Mineral Metabolism* 18(6): 305-316.

Frost HM. 2001. From Wolff's law to the Utah paradigm: insights about bone physiology and its clinical applications. *The Anatomical Record* 262(4): 398-419.

Fuchs RK, Warden SJ, Turner CH. 2009. Bone anatomy, physiology and adaptation to mechanical loading. In: Planell JA, Best SM, Lacroix D, Merolli A (eds.). *Bone Repair Biomaterials*, pp. 25-68. Woodhead Publishing: Cambridge.

Fulgoni VL, Chu Y-F, O'Shea M, Slavin JL, DiRienzo MA. 2015. Oatmeal consumption is associated with better diet quality and lower body mass index in adults: the National Health and Nutrition Examination Survey (NHANES), 2001-2010. *Nutrition Research* 35(12): 1052-1059.

Fulzele K, Lai F, Dedic C, Saini V, Uda Y, Shi C, Tuck P, Aronson JL, Liu X, Spatz JM, Wein MN, Pajevic PD. 2017. Osteocyte-Secreted Wnt Signaling Inhibitor Sclerostin Contributes to Beige Adipogenesis in Peripheral Fat Depots. *Journal of Bone and Mineral Research* 32(2): 373-384.

Gaffney-Stomberg, E. 2019. The Impact of Trace Minerals on Bone Metabolism. *Biological Trace Element Research* 188(1): 26-34.

Gaimster DRM, Margeson S, Hurley M. 1990. Medieval Britain and Ireland in 1989. *Medieval Archaeology* 34(1): 162-253.

Gallagher JC. 2013. Vitamin D Insufficiency and Deficiency. In: Roden CJ (ed.). *Primer on the Metabolic Bone Diseases and Disorders of Mineral Metabolism*, pp. 624-631. John Wiley & Sons, Inc.: Ames, USA.

Gao H, Wei X, Liao J, Wang R, Xu J, Liu X, Pan X, Li Z, Li Z, Xia Y, Wang Q. 2015. Lower Bone Mineral Density in Patients with Parkinson's Disease: A Cross-Sectional Study from Chinese Mainland. *Frontiers in Aging Neuroscience* 7(1): 203.

García-Donas JG, Dalton A, Chaplin I, Kranioti EF. 2017. A revised method for the preparation of dry bone samples used in histological examination: Five simple steps. *HOMO* 68(4): 283-288.

García-Donas JG, Dyke J, Paine RR, Nathena D, Kranioti EF. 2016. Accuracy and sampling error of two age estimation techniques using rib histomorphometry on a modern sample. *Journal of Forensic and Legal Medicine* 38(1): 28-35.

García-Donas JG, Paine RR, Bonicelli A, Kranioti EF. 2022. Age Estimation for Two Mediterranean Populations: Rib Histomorphometry Applied to Forensic Identification and Bone Remodelling Research. *International Journal of Legal Medicine* 136(5): 1469-1481.

Garland A. 1993. An introduction to the histology of exhumed mineralized tissue. In: Grupe G, Garland A (ed.). *Histology of ancient human bone: methods and diagnosis,* pp. 1-16. Springer-Verlag: Berlin.

Garn SM, Sullivan TV, Decker SA, Larkin FA, Hawthorne VM. 1992. Continuing bone expansion and increasing bone loss over a two-decade period in men and women from a total community sample. *American Journal of Human Biology* 4(1): 57-67.

Garnero P. 2012. The contribution of collagen crosslinks to bone strength. *BoneKey Reports* 1(1): 182.

Garnero P. 2015. The Role of Collagen Organization on the Properties of Bone. *Calcified Tissue International* 97(3): 229-240.

Garnsey P. 1999. The people of Isola Sacra. In: Rossi PF, Bondioli L, Geusa G, Macchiarelli R (eds.). *Digital Archives of Human Paleobiology*. E-LISA Sas: Milan.

Gaudio A, Pennisi P, Bratengeier C, Torrisi V, Lindner B, Mangiafico RA, Pulvirenti I, Hawa G, Tringali G, Fiore CE. 2010. Increased sclerostin serum levels associated with bone formation and resorption markers in patients with immobilization-induced bone loss. *The Journal of Clinical Endocrinology and Metabolism* 95(5): 2248-2253.

GBD. 2017. Disease and Injury Incidence and Prevalence Collaborators. Global, regional, and national incidence, prevalence, and years lived with disability for 354 diseases and injuries for 195 countries and territories, 1990-2017: a systematic analysis for the Global Burden of Disease Study 2017. *The Lancet* 392(10159): 1789-1858.

Gegenbaur C. 1864. *Untersuchungen zur vergleichenden anatomie der wirbelthiere.* W. Engelmann: Leipzig, Germany.

Gentles I. 1980. The Sales of Bishops' Lands in the English Revolution, 1646-1660. *The English Historical Review* 95(376): 573-596.

Genung EF. 1942. The Development of the Compound Microscope. *Bulletin of the History of Medicine* 12(4): 575-594.

George RL, Zejdlik K, Messer DL, Passalacqua NV. 2022. The John A. Williams Human Skeletal Collection at Western Carolina University. *Forensic Sciences* 2(2): 362-370.

Gernay MJC. 2015. *Health in urban late medieval North-West Europe: A bioarchaeological study of Caen, Canterbury and Ghent.* Doctor of Philosophy (PhD) thesis submitted to Durham University. Available from: <http://etheses.dur.ac.uk/11433/>.

Giangreco A, Hoste E, Takai Y, Rosewell I, Watt FM. 2012. Epidermal Cadm1 Expression Promotes Autoimmune Alopecia via Enhanced T Cell Adhesion and Cytotoxicity. *Journal of Immunology* 188(3): 1514-1522.

Giannoulis D, Calori GM, Giannoudis PV. 2016. Thirty-day mortality after hip fractures: Has anything changed? *European Journal of Orthopaedic Surgery* 26(4): 365-370.

Glastre C, Braillon P, David L, Cochat P, Meunier P, Delmas PD. 1990. Measurement of bone mineral content of the lumbar spine by dual energy x-ray absorptiometry in normal children: Correlations with growth parameters. *The Journal of Clinical Endocrinology and Metabolism* 70(5): 1330-1333.

Glauert AM, Glauert RH. 1958. Araldite as an embedding medium for electron microscopy. *The Journal of Biophysical and Biochemical Cytology* 4(2): 191-194.

Glauert AM, Rocers GE, Glauert HR. 1956. A new embedding medium for electron microscopy. *Nature* 178(1): 803.

Gocha TP, Agnew AM. 2016. Spatial variation in osteon population density at the human femoral midshaft: histomorphometric adaptations to habitual load environment. *Journal of Anatomy* 228(5): 733-745.

Gocha TP, Mavroudas SR, Wescott DJ. 2022. The Texas State Donated Skeletal Collection at the Forensic Anthropology Center at Texas State. *Forensic Sciences* 2(1): 7-19.

Goh JC, Mech AM, Lee EH, Ang EJ, Bayon P, Pho RW. 1992. Biomechanical study on the load-bearing characteristics of the fibula and the effects of fibular resection. *Clinical Orthopaedics and Related Research* 279(1): 223-228.

Goliath JR. 2010. *Variation in osteon circularity and its impact on estimating age at death.* Masters (MA) thesis submitted to Ohio State University. Available from: <https://etd.ohiolink.edu/acprod/odb_etd/etd/r/1501/10?clear=10&p10_accession_num=osu1273762376>.

Goliath JR, Stewart MC, Stout SD. 2016. Variation in osteon histomorphometrics and their impact on age-at-death estimation in older individuals. *Forensic Science International* 262(1): 282.e1-282.e6.

Goltzman D. 2018. Functions of vitamin D in bone. *Histochemistry and Cell Biology* 149(4): 305–312.

Goodman AH, Armelagos GJ. 1985. Factors affecting the distribution of enamel hypoplasias within the human permanent dentition. *American Journal of Biological Anthropology* 68(4): 479-493.

Goodman AH, Martin DL. 2002. Reconstructing health profiles from skeletal remains. In: Steckel RH, Rose JC (eds.). *The Backbone of History: Health and Nutrition in the Western Hemisphere*, pp. 11-60. Cambridge University Press: New York.

Goodman AH, Rose JC. 1990. Assessment of systemic physiological perturbations from dental enamel hypoplasias and associated histological structures. *American Journal of Biological Anthropology* 33(S11): 59-110.

Goren HP. 2023. An investigation of the inter and intra post-mortem microstructural change seen in an experimental series of pigs exposed to a marine environment. *Journal of Forensic and Legal Medicine* 99(1): 102588.

Gosman JH. 2011. Growth and development: Morphology, mechanisms and abnormalities. In: Crowder C, Stout S (eds.). *Bone Histology: An Anthropological Perspective,* pp. 23-44. CRC Press: Boca Raton.

Graf W. 1949. Preserved histological structures in Egyptian mummy tissues and ancient Swedish skeletons. *Acta Anatomica* 8(3): 236-250.

Grandhi RR, Thornton-Trump AB, Doigei CE.1986. Influence of dietary calcium-phosphorus levels on certain mechanical, physical and histological properties and chemical

composition of bones in gilts and second litter sows. *Canadian Journal of Animal Science* 66(2): 495-503.

Grant SFA, Reid DM, Blake G, Herd R, Fogelman I, Ralston SH. 1996. Reduced bone density and osteoporosis associated with a polymorphic Sp1 binding site in the collagen type I α 1 gene. *Nature Genetics* 14(2): 203-205.

Griffin RC, Donlon D. 2009. Patterns in dental enamel hypoplasia by sex and age at death in two archaeological populations. *Archives of Oral Biology* 54(S1): S93-S100.

Grizzo FMF, Alarcão ACJ, Dell'Agnolo CM, Pedroso RB, Santos TS, Vissoci JRN, Pinheiro MM, Carvalho MDB, Pelloso SM. 2020. How does women's bone health recover after lactation? A systematic review and meta-analysis. *Osteoporosis International* 31(3): 413-427.

Grupe G, Garland A. 1993. *Histology of ancient human bone: methods and diagnosis.* Springer Berlin: Heidelberg.

Grynpas MD, Omelon S. 2007. Transient precursor strategy or very small biological apatite crystals? *Bone* 41(2): 162-164.

Guan Z, Yuan W, Jia J, Zhang C, Zhu J, Huang J, Zhang W, Fan D, Leng H, Li Z, Xu Y, Song C. 2023. Bone mass loss in chronic heart failure is associated with sympathetic nerve activation. *Bone* 166: 116596.

Gubbiotti MA, Neill T, Iozzo RV. 2017. A current view of perlecan in physiology and pathology: a mosaic of functions. *Matrix Biology* 57-58(1): 285-298.

Guichelaar MMJ, Malinchoc M, Sibonga J, Clarke BL, Hay JE. 2002. Bone metabolism in advanced cholestatic liver disease: analysis by bone histomorphometry. *Hepatology* 36(4):895-903.

Guo EX, Hu YJ, Dinescu AT. 2020. Bone Structure and Function. In: Zaidi M (ed.). *Encyclopedia of Bone Biology,* pp. 233-246. Academic Press: London.

Gupta HS, Seto J, Wagermaier W, Zaslansky P, Boesecke P, Fratzl P. 2006. Cooperative deformation of mineral and collagen in bone at the nanoscale. *Proceedings of the National Academy of Sciences* 103(47): 17741-17746.

Haapasalo H, Kontulainen S, Sievänen H, Kannus P, Järvinen M, Vuori I. 2000. Exercise-induced bone gain is due to enlargement in bone size without a change in volumetric bone density: A peripheral quantitative computed tomography study of the upper arms of male tennis players. *Bone* 27(3): 351-357.

Habibah TU, Amlani DV, Brizuela M. 2022. Hydroxyapatite Dental Material. In: *StatPearls* [Internet]. StatPearls Publishing: Treasure Island, Florida; 2024 Jan-. Available from: <https://www-ncbi-nlm-nih-gov.virtual.anu.edu.au/books/NBK513314/>.

Hadley KB, Newman SM, Hunt JR. 2010. Dietary zinc reduces osteoclast resorption activities and increases markers of osteoblast differentiation, matrix maturation, and mineralization in the long bones of growing rats. *Journal of Nutritional Biochemistry* 21(4): 297-303.

Hagström E, Ingelsson E, Sundström J, Hellman P, Larsson TE, Berglund L, Melhus H, Held C, Michaëlsson K, Lind L, Arnlöv J. 2010. Plasma parathyroid hormone and risk of congestive heart failure in the community. *European Journal of Heart Failure* 12(11): 1186-1192.

Hakki SS, Dundar N, Kayis SA, Hakki EE, Hamurcu, Kerimoglu U, Baspinar N, Basovou A, Nielsen FH. 2013. Boron enhances strength and alters mineral composition of bone in rabbits fed a high energy diet. *Journal of Trace Element Research in Medicine and Biology* 27(2): 148-153.

Hall BK. 2003. Evo-Devo: evolutionary developmental mechanisms. *International Journal of Developmental Biology* 47(7-8): 491-495.

Hall BK. 2005. *Bones and Cartilage: Developmental and Evolutionary Skeletal Biology*. Elsevier Academic Press: San Diego, California, USA.

Hall BK, Miyake T. 1992. The membranous skeleton: The role of cell condensations in vertebrate skeletogenesis. *Anatomy and Embryology* 186(2): 107-124.

Han L, Frank EH, Greene JJ, Lee HY, Hung HHK, Grodzinsky AJ, Ortiz C. 2011. Time-dependent nanomechanics of cartilage. *Biophysical Journal* 100(7): 1846-1854.

Han ZH, Palnitkar S, Rao DS, Parfitt AM, Nelson D. 1996. Effect of ethnicity and age or menopause on the structure and geometry of iliac bone. *Journal of Bone and Mineral Research* 11(12): 1967-1975.

Hanawalt B. 1977. Childrearing among the lower classes of late medieval England. *The Journal of Interdisciplinary History* 8(1): 1-22.

Handelsman DJ, Hirschberg AL, Bermon S. 2018. Circulating testosterone as the hormonal basis of sex differences in athletic performance. *Endocrine Reviews* 39(5): 803-829.

Harper WV. 2016. Reduced Major Axis Regression. *Wiley StatsRef*. doi: 10.1002/9781118445112.stat07912.

Hart NH, Newton RU, Tan J, Rantalainen T, Chivers P, Siafarikas A, Nimphius S. 2020. Biological basis of bone strength: anatomy, physiology and measurement. *Journal of Musculoskeletal and Neuronal Interactions* 20(3): 347-371.

Harvey B. 2002. *Living and Dying in England 1140-1540: The Monastic Experience*. Oxford University Press: Oxford.

Hauge EM, Qvesel D, Eriksen EF, Mosekilde L, Melsen F. 2001. Cancellous Bone Remodelling Occurs in Specialized Compartments Lined by Cells Expressing Osteoblastic Markers. *Journal of Bone and Mineral Research* 16(9): 1575-1582.

Havers C. 1691. *Osteologia nova, or, Some new observations of the bones, and the parts belonging to them, with the manner of their accretion, and nutrition, communicated to the Royal Society in several discourses to which is added a fifth discourse of the cartilages.* Samuel Smith: London.

Havill LM, Allen MR, Harris JAK, Levine SM, Coan HB, Mahaney MC, Nicolella DP. 2013. Intracortical Bone Remodelling Variation Shows Strong Genetic Effects. *Calcified Tissue International* 93(5): 472-480.

Hawkey DE, Merbs CF. 1995. Activity-induced musculoskeletal stress markers (MSM) and subsistence strategy changes among ancient Hudson Bay Eskimos. *International Journal of Osteoarchaeology* 5(4): 324-338.

Haynes W. 2013. Bonferroni Correction. In: Dubitzky W, Wolkenhauer O, Cho KH, Yokota H (eds.). *Encyclopedia of Systems Biology,* p. 154. Springer: New York, NY.

Haywood L, McWilliams DF, Pearson CI, Gill SE, Ganesan A, Wilson D, Walsh DA. 2003. Inflammation and angiogenesis in osteoarthritis. *Arthritis and Rheumatology* 48(8): 2173-2177.

Hedges REM, Clement JG, Thomas CDL, O'Connell TC. 2007. Collagen turnover in the adult femoral mid-shaft: modeled from anthropogenic radiocarbon tracer measurements. *American Journal of Biological Anthropology* 133(2): 808-816.

Hedges, REM, Millard AR, Pike AWG. 1995. Measurements and relationships of diagenetic alteration of bone from three archaeological sites. *Journal of Archaeological Science* 22(2): 201-209.

Hemmatian H, Bakker AD, Klein-Nulend J, van Lenthe GH. 2017. Aging, Osteocytes, and Mechanotransduction. *Current Osteoporosis Reports* 15(1): 401-411.

Henry JP, Bordoni B. 2023. Histology, Osteoblasts. [Updated 2023 May 1]. In: *StatPearls* [Internet]. StatPearls Publishing: Treasure Island, Florida; 2024 Mar-. Available from: <https://www-ncbi-nlm-nih-gov.virtual.anu.edu.au/books/NBK557792/>.

Hernigou P, Hosny GA, Scarlat M. 2024. Evolution of orthopaedic diseases through four thousand three hundred years: from ancient Egypt with virtual examinations of mummies to the twenty-first century. *International Orthopaedics* 48(3): 865-884.

Hert J, Lisková M, Landa J. 1971. Reaction of bone to mechanical stimuli. 1. Continuous and intermittent loading of tibia in rabbit. *Folia Morphologica* 19(3): 290-300.

Hewadikaram KA, Goff ML. 1991. Effect of Carcass Size on Rate of Decomposition and Arthropod Succession Patterns. *The American Journal of Forensic Medicine and Pathology* 12(3): 235-240.

Hicks M, Hicks A. 2001a. The Archaeological Site. In: Hicks M, Hicks A (eds.). *St Gregory's Priory, Northgate, Canterbury: Excavations 1988-1991*, pp. 1-150. Canterbury Archaeological Trust: Great Britain.

Hicks M, Hicks A (eds.). 2001b. *St Gregory's Priory, Northgate, Canterbury: Excavations 1988-1991*. Canterbury Archaeological Trust: Great Britain.

High WB. 1987. Effects of Orally Administered Prostaglandin E-2 on Cortical Bone Turnover in Adult Dogs: A Histomorphometric Study. *Bone* 8(6): 363-373.

Hillier ML, Bell LS. 2007. Differentiating human bone from animal bone: a review of histological methods. *Journal of Forensic Sciences* 52(2): 249-263.

Hillman H. 2000. Limitations of clinical and biological histology. *Medical Hypotheses* 54(4): 553-564.

Hillson S, Bond S. 1997. Relationship of enamel hypoplasia to the pattern of tooth crown growth: A discussion. *American Journal of Biological Anthropology* 104(1): 89-103.

Hilton RC, Ball J, Benn RT. 1976. Vertebral end-plate lesions (Schmorl's nodes) in the dorsolumbar spine. *Annals of the Rheumatic Diseases* 35(2): 127-132.

Hirschmann JV, Raugi GJ. 1999. Adult scurvy. *Journal of the American Academy of Dermatology* 41(6): 895-906.

Ho-Pham LT, Ho-Le TP, Mai LD, Do TM, Doan MC, Nguyen TV. 2018. Sex-difference in bone architecture and bone fragility in Vietnamese. *Nature Scientific Reports* 8(1): 7707.

Holcombe SA, Huang Y. 2023. Cross-sectional properties of rib geometry from an adult population. *Frontiers in Bioengineering and Biotechnology* 22(11): 1158242.

Holcombe SA, Kang Y-S, Derstine BA, Wang SC, Agnew AM. 2019. Regional maps of rib cortical bone thickness and cross sectional geometry. *Journal of Anatomy* 235(5): 883-891.

Holecki M, Zahorska-Markiewicz B, Janowska J, Mizia-Stec K, Zak-Gołab A, Olszanecka-Glinianowicz M, Wojaczyńska-Stanek K, Nieszporek T, Wiecek A. 2007. Osteoprotegerin--does it play a protective role in the pathogenesis of bone loss in obese perimenopausal women? *Endokrynologia Polska* 58(1): 7-10.

Holick MF. 2002. Sunlight and vitamin D: Both good for cardiovascular health. *Journal of General Internal Medicine* 17(9): 733-735.

Holt JC. 1972. Politics and property in early Medieval England. *Past and Present* 57(1): 3-52.

Hooke R. 1665. *Micrographia, or, Some physiological descriptions of minute bodies made by magnifying glasses with observations and inquiries thereupon*. Jo Martyn: London.

Hopwood PR, Butterfield RM. 1990. The locomotor apparatus of the crus and pes of the Eastern Gray Kangaroo, Macropus giganteus. *Australian Journal of Zoology* 38(4): 397-413.

Horobin RW. 2002. Theory of staining and its practical implications. In: Bancroft JD, Gamble M (eds.). *Theory and Practice of Histological Techniques*, pp. 109-138. Churchill Livingstone: London.

Hsia AW, Collette NM, Christiansen BA. 2017. Osteophyte Formation and the Effect of Mechanical Loading: Comparisons to Fracture Healing. *Osteoarthritis and Cartilage* 25(S1): S305-S306.

Hsu C-Y, Chen L-R, Chen K-H. 2020. Osteoporosis in Patients with Chronic Kidney Diseases: A Systemic Review. *International Journal of Molecular Sciences* 21(18): 6846.

Hu Z, Yang K, Hu Z, Li M, Wei H, Tang Z, Chen B, Su C, Cai D, Xu J. 2021. Determining the association between hypertension and bone metabolism markers in osteoporotic patients. *Medicine* 100(24): e26276.

Hughes JM, Popp KL, Yanovich R, Bouxsein ML, Matheny RW. 2017. The role of adaptive bone formation in the etiology of stress fracture. *Experimental Biology and Medicine* 242(9): 897-906.

Hughes-Austin JM, Pereira RC, Jorgetti V, Salusky IB, Ix JH. 2025. Static histomorphometry parameters can identify bone turnover status in children and adults with chronic kidney disease. *Bone* 190(1): 117329.

Hui SL, Johnston CC, Mazess RB. 1985. Bone mass in normal children and young adults. *Growth* 49(1): 34-43.

Hui SL, Slemenda CW, Johnston CC, Appledorn CR. 1987. Effects of age and menopause on vertebral bone density. *Bone and Mineral* 2(2): 141-146.

Huijbregts PA. 2001. Osteoporosis: Epidemiology, histology, bone remodelling, and classification. *Journal of Manual and Manipulative Therapy* 9(3): 134-142.

Hull BB. 1989. Religion, afterlife and property rights in the high Middle Ages. *Studies in Economic Analysis* 12(1): 3-21.

Hunt CD. 2012. Dietary boron: progress in establishing essential roles in human physiology. *Journal of Trace Elements in Medicine and Biology* 26(2-3): 157-160.

Ismail AA, Cooper C, Felsenberg D, Varlow J, Kanis JA, Silman AJ, O'Neill TW. 1999. Number and type of vertebral deformities: epidemiological characteristics and relation to back pain and height loss. European Vertebral Osteoporosis Study Group. *Osteoporosis International* 9(3): 206-213.

Ito A, Hagiyama M, Oonuma J. 2008. Nerve-mast cell and smooth muscle-mast cell interaction mediated by cell adhesion molecule-1, CADM1. *Journal of Smooth Muscle Research* 44(2): 83-93.

Iyo T, Maki Y, Sasaki N, Nakata M. 2004. Anisotropic viscoelastic properties of cortical bone. *Journal of Biomechanics* 37(9): 1433-1437.

Jackson RD, LaCroix AZ, Gass M, Wallace RB, Robbins J, Lewis CE, Bassford T, Beresford SA, Black HR, Blanchette P, Bonds DE, Brunner RL, Brzyski RG, Caan B, Cauley JA, Chlebowski RT, Cummings SR, Granek I, Hays J, Heiss G, Hendrix SL, Howard BV, Hsia J, Hubbell FA, Johnson KC, Judd H, Kotchen JM, Kuller LH, Langer RD, Lasser NL, Limacher MC, Ludlam S, Manson JE, Margolis KL, McGowan J, Ockene JK, O'Sullivan MJ, Phillips L, Prentice RL, Sarto GE, Stefanick ML, Van Horn L, Wactawski-Wende J, Whitlock E, Anderson GL, Assaf AR, Barad D; Women's Health Initiative Investigators. 2006. Calcium plus vitamin D supplementation and the risk of fractures. *New England Journal of Medicine* 354(7): 669-683.

Jacobs K. 1992. Estimating femur and tibia length from fragmentary bones: An evaluation of Steele's (1970) method using a prehistoric European sample. *American Journal of Biological Anthropology* 89(3): 333-345.

Jamieson JA, Tailor CG, Weiler HA. 2006. Marginal zinc deficiency exacerbates bone lead accumulation and high dietary zinc attenuates lead accumulation at the expense of bone density in growing rats. *Toxicological Sciences* 92(1): 286-294.

Jankauskas R. 1994. Variability of vertebral column measurements in Lithuanian paleopopulation. *International Journal of Anthropology* 9(1): 137-151.

Jankauskas R. 1998. History of human tuberculosis in Lithuania: possibilities and limitations of paleoosteological evidences. *Bulletins et Mémoires de la Société d'Anthropologie de Paris* 10(3-4): 357-374.

Jankauskas R, Urbanavičius A. 1998. Diseases in European historical populations and their effects on individuals and society. *Collegium Antropologicum* 22(2): 465-476.

Jankowska EA, Jakubaszko J, Cwynar A, Majda J, Ponikowska B, Kustrzycka-Kratochwil D, Reczuch K, Borodulin-Nadzieja L, Banasiak W, Poole-Wilson PA, Ponikowski P. 2009. Bone mineral status and bone loss over time in men with chronic systolic heart failure and their clinical and hormonal determinants. *European Journal of Heart Failure* 11(1): 28-38.

Jantz LM, Jantz RL. 2008. The Anthropology Research Facility: The Outdoor Laboratory of the Forensic Anthropology Center, University of Tennessee. In: Warren MW, Walsh-Haney HA, Freas L (eds.). *The Forensic Anthropology Laboratory*, pp. 7-22. CRC Press: Boca Raton.

Javaheri B, Pitsillides AA. 2019. Aging and Mechanoadaptive Responsiveness of Bone. *Current Osteoporosis Reports* 17(6): 560-569.

Jay D, K.A. Waller KA. 2014. The biology of lubricin: near frictionless joint motion. *Matrix Biology* 39(1): 17-24.

Jenkin RA, Keay KA. 2025. Body donor programs in Australia and New Zealand: Current status and future opportunities. *Anatomical Sciences Education* 18(3): 301-328.

Jeong HM, Kim DJ. 2019. Bone Diseases in Patients with Chronic Liver Disease. *International Journal of Molecular Sciences* 20(17): 4270.

Jervis B. 2022. Becoming Through Milling: Challenging Linear Economic Narratives in Medieval England. *Cambridge Archaeological Journal* 32(2): 281-294.

Jha S, Chapman M, Roszko K. 2019. When low bone mineral density and fractures is not osteoporosis. *Current Osteoporosis Reports* 17(5): 324-332.

Jiang J, Zhang M, Meng H, Cui X, Yang Y, Yuan L, Su C, Wang J, Zhang L. 2020. Demographic and motivational factors affecting the whole-body donation programme in Nanjing, China: a cross-sectional survey. *BMJ Open* 10(1): e035539.

Jiménez G, Cobo-Molinos J, Antich C & López-Ruiz E. 2018. Osteoarthritis: Trauma vs Disease. In: Oliveira J, Pina S, Reis R, San Roman J (eds.). *Osteochondral Tissue Engineering: Advances in Experimental Medicine and Biology*, pp. 63-83. Springer: Cham.

Johnson K, Goding J, Van Etten D, Sali A, Hu S-I, Farley D, Krug H, Hessle L, Millán JL, Terkeltaub R. 2003. Linked Deficiencies in Extracellular PPi and Osteopontin Mediate Pathologic Calcification Associated With Defective PC-1 and ANK Expression. *Journal of Bone and Mineral Research* 18(6): 994-1004.

Johnson NA, Sultana RN, Brown WJ, Bauman AE, Gill T. 2021. Physical activity in the management of obesity in adults: A position statement from Exercise and Sport Science Australia. *Journal of Science and Medicine in Sport* 24(12): 1245-1254.

Jones G, Nguyen T, Sambrook P, Kelly PJ, Eisman JA. 1994. Progressive loss of bone in the femoral neck in elderly people: Longitudinal findings from the Dubbo osteoporosis epidemiology study. *BMJ* 309(6956): 691-695.

Jordan WC. 2001. *Europe in the High Middle Ages*. Penguin Books: London.

Jotischky A. 2011. *A Hermit's Cookbook: Monks, Food and Fasting in the Middle Ages*. Continuum International Publishing Group: London.

Jowsey J. 1960. Age changes in human bone. *Clinical Orthopaedics and Related Research* 17: 210-218.

Jowsey J. 1966. Studies of Haversian systems in man and some animals. *Journal of Anatomy* 100(4): 857-864.

Judd MA, Roberts CA. 1999. Fracture trauma in a medieval British farming village. *American Journal of Biological Anthropology* 109(2): 229-243.

Jüppner H, Abou-Samra A, Freeman M, Kong X, Schipani E, Richards J, Kolakowski L, Hock J, Potts J, Kronenberg H, Segre GV. 1991. A G protein-linked receptor for parathyroid hormone and parathyroid hormone-related peptide. *Science* 254(5034): 1024-1026.

Kaifu Y, Kasai K, Townsend GC, Richards LC. 2003. Tooth wear and the “design” of the human dentition: A perspective from evolutionary medicine. *American Journal of Biological Anthropology* 122(S37): 47-61.

Kalamajski S, Aspberg A, Lindblom K, Heinegard D, Oldberg A. 2009. Asporin competes with decorin for collagen binding, binds calcium and promotes osteoblast collagen mineralization. *The Biochemical Journal* 423(1): 53-59.

Kalkwarf HJ, Specker BL. 1995. Bone mineral loss during lactation and recovery after weaning. *Obstetrics and Gynecology* 86(1): 26-32.

Kalia LV, Lang AE. 2015. Parkinson's disease. *The Lancet* 386(9996): 896-912.

Kanazawa I, Yamamoto M, Yamaguchi T, Yano S, Sugimoto T. 2007. A case of magnesium deficiency associated with insufficient parathyroid hormone action and severe osteoporosis. *Endocrine Journal* 54(6): 935-940.

Karlson KA. 1998. Rib Stress Fractures in Elite Rowers: A case series and proposed mechanism. *The American Journal of Sports Medicine* 26(4): 516-519.

Karydi C, García-Donas JG, Tsiminikaki K, Bonicelli A, Moraitis K, Kranioti EF. 2022. Estimation of Age-at-Death Using Cortical Bone Histomorphometry of the Rib and Femur: A Validation Study on a British Population. *Biology* 11(11): 1615.

Katsimbri P. 2017. The biology of normal bone remodelling. *European Journal of Cancer Care* 26(6): e12740.

Ke Y, Hu H, Zhang J, Yuan L, Li T, Feng Y, Wu Y, Fu X, Wang M, Gao Y, Huo W, Chen Y, Zhang W, Wang L, Li X, Pang J, Zheng Z, Hu F, Zhang M, Sun L, Zhao Y, Lu J, Hu D. 2023. Alcohol Consumption and Risk of Fractures: A Systematic Review and Dose–

Response Meta-Analysis of Prospective Cohort Studies. *Advances in Nutrition* 14(4): 599-611.

Keenan KE, Mears CS, Skedros JG. 2017. Utility of osteon circularity for determining species and interpreting load history in primates and nonprimates. *Journal of Biological Anthropology* 162(4): 657-681.

Keenleyside A. 1998. Skeletal evidence of health and disease in pre-contact Alaskan eskimos and Aleuts. *American Journal of Biological Anthropology* 107(1): 51-70.

Kelly PJ, Eisman JA, Sambrook PN. 1990. Interaction of genetic and environmental influences on peak bone density. *Osteoporosis International* 1(1): 56-60.

Kelly P, Keely N, Bright S, Yassin B, Ana G, Fayne D, Zisterer D, Meegan M. 2017. Novel Selective Estrogen Receptor Ligand Conjugates Incorporating Endoxifen-Combretastatin and Cyclofenil-Combretastatin Hybrid Scaffolds: Synthesis and Biochemical Evaluation. *Molecules* 22(9): 1440.

Kemper AR, McNally C, Pullins CA, Freeman LJ, Duma SM, Rouhana SM. 2007. The biomechanics of human ribs: material and structural properties from dynamic tension and bending tests. *Stapp Car Crash Journal* 51(1): 235-273.

Kenkre JS, Bassett J. 2018. The bone remodelling cycle. *Annals of Clinical Biochemistry* 55(3): 308-327.

Kenny AM, Boxer R, Walsh S, Hager WD, Raisz LG. 2006. Femoral bone mineral density in patients with heart failure. *Osteoporosis International* 17(9): 1420-1427.

Kerley ER. 1965. The Microscopic Determination of Age in Human Bone. *American Journal of Biological Anthropology* 23(2): 149-163.

Kerley ER, Ubelaker DH. 1978. Revisions in the Microscopic Method of Estimating Age at Death in Human Cortical Bone. *American Journal of Biological Anthropology* 49(4): 545-546.

Kerschnitzki M, Wagermaier W, Roschger P, Seto J, Shahar R, Duda GN, Mundlos S, Fratzl P. 2011. The organization of the osteocyte network mirrors the extracellular matrix orientation in bone. *Journal of Structural Biology* 173(2): 303-311.

Khosla S. 2008. Estrogen and bone: Insights from estrogen-resistant, aromatase-deficient, and normal men. *Bone* 43(3): 414-417.

Khosla S. 2013. Pathogenesis of age related bone loss in humans. *The Journals of Gerontology Series A Biological Sciences and Medical Sciences* 68(10): 1226-1235.

Khosla S, Hofbauer LC. 2017. Osteoporosis treatment: recent developments and ongoing challenges. *The Lancet Diabetes and Endocrinology* 5(11): 898-907.

Khosla S, Oursler MJ, Monroe DG. 2012. Estrogen and the skeleton. *Trends in Endocrinology and Metabolism* 23(11): 576-581.

Kim JM, Lin C, Stavre Z, Greenblatt MB, Shim JH. 2020. Osteoblast-Osteoclast Communication and Bone Homeostasis. *Cells* 9(9): 2073.

Kim S-H, Chung S-K, Bahk Y-W, Park Y-H, Lee S-Y, Sohn H-S. 1999. Whole-body and pinhole bone scintigraphic manifestations of Reiter's syndrome: distribution patterns and early and characteristic signs. *European Journal of Nuclear Medicine* 26(2): 163-170.

Kim SW, Lu Y, Williams EA, Lai F, Lee JY, Enishi T, Balani DH, Ominsky MS, Ke HZ, Kronenberg HM, Wein MN. 2017. Sclerostin Antibody Administration Converts Bone Lining Cells Into Active Osteoblasts. *Journal of Bone and Mineral Research* 32(5): 892-901.

Kim Y-S, Kim D-I, Park D-K, Lee J-H, Chung N-E, Lee W-T, Han S-H. 2007. Assessment of Histomorphological Features of the Sternal End of the Fourth Rib for Age Estimation in Koreans. *Journal of Forensic Sciences* 52(6): 1237-1242.

Kimura T. 1985. Bipedal and quadrupedal walking of primates: comparative dynamics. In: Kondo O, Ishida H, Kimura T, Okada M, Yamazaki N, Prost JH (eds.). *Primate Morphophysiology, Locomotor Analyses and Human Bipedalism*, pp. 81-104. University of Tokyo Press: Tokyo.

Kirby DJ, Young MF. 2018. Isolation, production, and analysis of small leucine-rich proteoglycans in bone. *Methods in Cell Biology* 143(1): 281-296.

Kleerekoper M, Nelson DA, Peterson EL, Flynn MJ, Pawluszka AS, Jacobsen G, Wilson P. 2009. Reference data for bone mass, calciotropic hormones, and biochemical markers

of bone remodelling in older (55-75) postmenopausal white and black women. *Journal of Bone and Mineral Research* 9(8): 1267-1276.

Klein-Hitpass L, Schwerk C, Kahmann S, Vassen L. 1998. Targets of activated steroid hormone receptors: Basal transcription factors and receptor interacting proteins. *Journal of Molecular Medicine* 76(7): 490-496.

Klein-Nulend J, Bakker AD, Bacabac RG, Vatsa A, Weinbaum S. 2013. Mechanosensation and transduction in osteocytes. *Bone* 54(2): 182-190.

Knobel Z, Ueland M, Nizio KD, Patel D, Forbes SL. 2019. A comparison of human and pig decomposition rates and odour profiles in an Australian environment. *Australian Journal of Forensic Sciences* 51(5): 557-572.

Knowles AK. 1983. 'Acute Traumatic Lesions'. In: Hart GD (ed.) *Disease in Ancient Man: An international symposium*, pp. 61-83. Irwin Clarke: Toronto.

Knowles D, Brooke CNL (eds.). 1951. *The Monastic Constitutions of Lanfranc*. Clarendon Press: London.

Kobayashi S, Takahashi HE, Ito A, Saito N, Nawata M, Horiuchi H, Ohta H, Ito A, Iorio R, Yamamoto N, Takaoka K. 2003. Trabecular minimodelling in human iliac bone. *Bone* 32(2): 163-169.

Konigsberg LW, Hens SM. 1998. Use of ordinal categorical variables in skeletal assessment of sex from the cranium. *American Journal of Biological Anthropology* 107(1): 97-112.

Krabbe S, Christiansen C, Rødbro P, Transbøl I. 1979. Effect of puberty on rates of bone growth and mineralisation: With observations in male delayed puberty. *Archives of Disease in Childhood* 54(12): 950-953.

Kraft MD. 2015. Phosphorus and Calcium: A Review for the Adult Nutrition Support Clinician. *Nutrition in Clinical Practice* 30(1): 21-33.

Kranioti EF, Michopoulou E, Tsiminikaki K, Bonicelli A, Kalochristianakis M, Xhemali B, Paine RR, García-Donas JG. 2020. Bone histomorphometry of the clavicle in a forensic sample from Albania. *Forensic Science International* 313: 110335.

Krishnan Y, Grodzinsky AJ. 2018. Cartilage diseases. *Matrix Biology* 71-72(1): 51-69.

Kronenberg HM. 2003. Developmental regulation of the growth plate. *Nature* 423(6937): 332-336.

Krönig G. 1887. Diagnostische Beitrag zur Hertz-Und Lungenpathologie. *Berlin Klin Wschr* 24(1): 961-967.

Krum SA, Miranda-Carboni GA, Hauschka PV, Carroll JS, Lane TF, Freedman LP, Brown M. 2008. Estrogen protects bone by inducing Fas ligand in osteoblasts to regulate osteoclast survival. *The EMBO Journal* 27(3): 535-545.

Kubiak K, Klimczak A, Dzikl L, Modranka R, Malinowska K. 2010. Influence of copper (II) complex on the activity of selected oxidative enzymes. *Polski Merkuriusz Lekarski* 28(163): 22-25.

Kulak CAM, Dempster DW. 2010. Bone histomorphometry: a concise review for endocrinologists and clinicians. *Archives of Endocrinology and Metabolism* 54(2): 87-98.

Kumar S, Chandnani A, Aung NH, Shahid S, Bukhari D, Shahzad S, Kumar B, Memon S. 2021. Alzheimer's Disease and Its Association With Bone Health: A Case-Control Study. *Cureus* 13(3): e13772.

Lad SE, McGraw WS, Daegling DJ. 2019. Haversian remodelling corresponds to load frequency but not strain magnitude in the macaque (Macaca fascicularis) skeleton. *Bone* 127(1): 571-576.

Lagacé F, Schmitt A, Martrille L, Benassi J, Adalian P. 2020. Using histomorphometry for human and nonhuman distinction: A test of four methods on fresh and archaeological fragmented bones. *Forensic Science International* 313(1): 110369.

Lagacé F, Verna E, Adalian P, Baccino E, Martrille L. 2019. Testing the accuracy of a new histomorphometric method for age-at-death estimation. *Forensic Science International* 296(1): 48-52.

Lambert PM. 1993. Health in prehistoric populations of the santa barbara Channel Islands. *American Antiquity* 58(3): 509-522.

Lambrick G. 1985. Further excavations at the second site of the Dominican Priory, Oxford. *Oxoniensa* 50(1): 188-201.

Langen UH, Pitulescu ME, Kim JM, Enriquez-Gasca R, Sivaraj KK, Kusumbe AP, Singh A, Di Russo J, Bixel MG, Zhou B, Sorokin L, Vaquerizas JM, Adams RH. 2017. Cell-matrix signals specify bone endothelial cells during developmental osteogenesis. *Nature Cell Biology* 19(3): 189-201.

Langlois K, Greene-Finestone L, Little J, Hidiroglou N, Whiting S. 2010. Vitamin D status of Canadians as measured in the 2007 to 2009 Canadian Health Measures Survey. *Health Reports* 21(1): 47-55.

Lanyon LE, Baggott D. 1976. Mechanical function as an influence on the structure and form of bone. *The Journal of Bone and Joint Surgery* 58-B(4): 436-443.

Lanyon LE, Goodship AE, Pye CJ, MacFie JH. 1982. Mechanically Adaptive Bone Remodelling. *Journal of Biomechanics* 15(3): 141-154.

Lanyon LE, Rubin CT. 1984. Static versus dynamic loads as an influence on bone remodelling. *Journal of Biomechanics* 17(12): 897-905.

Larsen CS. 1997. Stress and deprivation during the years of growth and development and adulthood. In: Larsen CS (ed.). *Bioarchaeology: Interpreting behaviour from the human skeleton*, pp. 6-63. Cambridge University Press: United Kingdom.

Larsen CS. 2002. Bioarchaeology: The Lives and Lifestyles of Past People. *Journal of Archaeological Research* 10(2): 119-166.

Larsen CS, Ruff CB. 1990. Biomechanical adaptation and behavior on the Prehistoric Georgia Coast. In: Powell ML, Bridges PS, Mires AM (eds.). *What mean these bones: studies in southeastern bioarchaeology,* pp. 102-113. The University of Alabama Press: Tuscaloosa.

Lauderdale DS, Thisted RA, Goldberg J. 1998. Is geographic variation in hip fracture rates related to current or former region of residence? *Epidemiology* 9(5): 574-577.

Lazenby RA, Pfeiffer SK. 1993. Effects of a nineteenth century below-knee amputation and prosthesis on femoral morphology. *International Journal of Osteoarchaeology* 3(1): 19-28.

Lee HY, Han L, Roughley PJ, Grodzinsky AJ, Ortiz C. 2013. Age-related nanostructural and nanomechanical changes of individual human cartilage aggrecan monomers and their glycosaminoglycan side chains. *Journal of Structural Biology* 181(3): 264-273.

Lee TC, Taylor D. 1999. Bone Remodelling: Should We Cry Wolff? *Irish Journal of Medical Science* 168(2): 102-105.

Lee W, Ko KR, Kim H, Lee DS, Nam I-J, Lim S, Kim S. 2018. Dehydrodiconiferyl Alcohol Inhibits Osteoclast Differentiation and Ovariectomy-Induced Bone Loss through Acting as an Estrogen Receptor Agonist. *Journal of Natural Products* 81(6): 1343-1356.

Lemos YV, Furtado AN, Lima AZ, Dionísio AS, Araújo RM, Cunha E. 2024. Human identification by medical findings in a forensic anthropology context. *Forensic Sciences Research* 9(3): owae041.

Li BB, Yu SF. 2007. In vitro study of the effects of copper ion on osteoclastic resorption in various dental mineralized tissues. *Chinese Journal of Stomatology* 42(2): 110-113.

Li C, Fennessy P. 2021. The periosteum: a simple tissue with many faces, with special reference to the antler-lineage periostea. *Biology Direct* 16(1): 17.

Li J, Gong H. 2021. Fatigue behavior of cortical bone: a review. *Acta Mechanica Sinica* 37(3): 516-526.

Li X, Ominsky MS, Niu Q-T, Sun N, Daugherty B, D'Agostin D, Kurahara C, Gao Y, Cao J, Gong J, Asuncion F, Barrero M, Warmington K, Dwyer D, Stolina M, Morony S, Sarosi I, Kostenuik PJ, Lacey DL, Simonet WS, Ke HZ, Paszty C. 2008. Targeted Deletion of the Sclerostin Gene in Mice Results in Increased Bone Formation and Bone Strength. *Journal of Bone and Mineral Research* 23(6): 860-869.

Li Y, Gao H, Zhao L, Wang J. 2022. Osteoporosis in COPD patients: Risk factors and pulmonary rehabilitation. *The Clinical Respiratory Journal* 16(7): 487-496.

Liang B, Feng Y. 2012. The association of low bone mineral density with systemic inflammation in clinically stable COPD. *Endocrine* 42(1): 190-195.

Liao K-M, Shen C-W, Chiu K-L, Lu C-H, Fang C-W, Chen C-Y. 2024. Epidemiology of Osteoporosis in Patients with Chronic Obstructive Pulmonary Disease in Taiwan. *Journal of Epidemiology and Global Health* 14(1): 213-222.

Liguori S, Moretti A, Paoletta M, Gargiulo F, Barra G, Gimigliano F, Iolascon G. 2024. Bone involvement in the early stages of Parkinson's disease: a case–control study. *Journal of International Medical Research* 52(3): 3000605241237880.

Lim JS, Jin S-H, Kim SB, Lee J-I. 2012. Effect of bisphosphonates on bone mineral density and fracture prevention in gastric cancer patients after gastrectomy. *Journal of Clinical Gastroenterology* 46(8): 669-674.

Lin C, Chen Z, Guo D, Zhou L, Lin S, Li C, Li S, Wang X, Lin B, Ding Y. 2022. Increased expression of osteopontin in subchondral bone promotes bone turnover and remodelling, and accelerates the progression of OA in a mouse model. *Aging* 14(1): 253-271.

Lin Y, Xiao L, Zhang Y, Li P, Wu Y, Lin Y. 2019. MiR-26b-3p regulates osteoblast differentiation via targeting estrogen receptor α. *Genomics* 111(5): 1089-1096.

Lin X, Patil S, Gao YG, Qian A. 2020. The Bone Extracellular Matrix in Bone Formation and Regeneration. *Frontiers in Pharmacology* 26(11): 757.

Lindsay R, Cosman F, Zhou H, Bostrom MP, Shen VW, Cruz JD, Nieves JW, Dempster DW. 2006. A Novel Tetracycline Labeling Schedule for Longitudinal Evaluation of the Short-Term Effects of Anabolic Therapy With a Single Iliac Crest Bone Biopsy: Early Actions of Teriparatide. *Journal of Bone and Mineral Research* 21(3): 366-373.

Lips P, van Schoor NM, Bravenboer N. 2013. Vitamin D-Related Disorders. In: Rosen CJ (ed.). *Primer on the Metabolic Bone Diseases and Disorders of Mineral Metabolism*, pp. 613-623. John Wiley and Sons, Inc.: Ames, USA.

Liu L-F, Shen W-J, Ueno M, Patel S, Kraemer FB. 2011. Characterization of age-related gene expression profiling in bone marrow and epididymal adipocytes. *BMC Genomics* 12(1): 212.

Locklin R. 1999. Effects of TGFβ and BFGF on the differentiation of human bone marrow stromal fibroblasts. *Cell Biology International* 23(3): 185-194.

Logan CY, Nusse R. 2004. The WNT Signaling Pathway in Development and Disease. Annual *Review of Cell and Developmental Biology* 20(1): 781-810.

Lohmander LS, Roos H, Dahlberg L, Hoerrner LA, Lark MW. 1994. Temporal patterns of stromelysin-1, tissue inhibitor, and proteoglycan fragments in human knee joint fluid after injury to the cruciate ligament or meniscus. *Journal of Orthopaedic Research* 12(1): 21-28.

Loncar G, Cvetinovic N, Lainscak M, Isaković A, von Haehling S. 2020. Bone in heart failure. *Journal of Cachexia, Sarcopenia and Muscle* 11(2): 381-393.

Looker AC, Dawson-Hughes B, Calvo MS, Gunter EW, Sahyoun NR. 2002. Serum 25-hydroxyvitamin D status of adolescents and adults in two seasonal subpopulations from NHANES III. *Bone* 30(5): 771-777.

Loro LM, Sayre J, Roe TF, Goran MI, Kaufman FR, Gilsanz V. 2000. Early identification of children predisposed to low peak bone mass and osteoporosis later in life. *The Journal of Clinical Endocrinology and Metabolism* 85(10): 3908-3918.

Loskutova N, Honea R, Vidoni E, Brooks W, Burns JM. 2009. Bone Density and Brain Atrophy in Early Alzheimer's Disease. *Journal of Alzheimer's Disease* 18(4): 777-785.

Lovejoy CO. 1985. Dental wear in the Libben population: Its functional pattern and role in the determination of adult skeletal age at death. *American Journal of Biological Anthropology* 68(1): 47-56.

Lovejoy CO, Meindl RS, Pryzbeck TR, Mensforth RP. 1985. Chronological metamorphosis of the auricular surface of the ilium: A new method for the determination of adult skeletal age at death. *American Journal of Biological Anthropology* 68(1): 15-28.

Lu B, Jiao Y, Wang Y, Dong J, Wei M, Cui B, Sun Y, Wang L, Zhang B, Chen Z, Zhao Y. 2017. A FKBP5 mutation is associated with Paget's disease of bone and enhances osteoclastogenesis. *Experimental and Molecular Medicine* 49(5): e336.

Lucas R, Ramos E, Oliveira A, Monjardino T, Barros H. 2012. Low-grade systemic inflammation and suboptimal bone mineral density throughout adolescence: a prospective study in girls. *Clinical Endocrinology* 77(5): 665-671.

Luft JH. 1961. Improvements in epoxy resin embedding methods. *The Journal of Biophysical and Biochemical Cytology* 9(2): 409-414.

Lundin EL, Stauber M, Papageorgiou P, Ehrbar M, Ghayor C, Weber FE, Tanner C, Goksel O. 2017. Automatic registration of 2D histological sections to 3D microCT volumes: Trabecular bone. *Bone* 105(1): 173-183.

Luo GB, Ducy P, McKee MD, Pinero GJ, Loyer E, Behringer RR, Karsenty G. 1997. Spontaneous calcification of arteries and cartilage in mice lacking matrix GLA protein. *Nature* 386(6620): 78-81.

Luong S, Forbes SL, Wallman JF, Roberts RG. 2018. Monitoring the extent of vertical and lateral movement of human decomposition products through sediment using cholesterol as a biomarker. *Forensic Science International* 285(1): 93-104.

Luyten FP, Tylzanowski P, Lories RJ. 2009. Wnt signaling and osteoarthritis. *Bone* 44(4): 522-527.

Lynnerup N, Thomsen JL, Frohlich B. 1998. Intra- and inter-observer variation in histological criteria used in age at death determination based on femoral cortical bone. *Forensic Science International* 91(3): 219-230.

Maat GJR, Maes A, Aarents MJ, Nagelkerke NJ. 2006. Histological Age Prediction from the Femur in a Contemporary Dutch Sample. The Decrease of Nonremodeled Bone in the Anterior Cortex. *Journal of Forensic Sciences* 51(2): 230-237.

Maat GJR, Van Den Bos RPM, Aarents MJ. 2001. Manual preparation of ground sections for the microscopy of natural bone tissue: Update and modification of Frost's rapid manual method? *International Journal of Osteoarchaeology* 11(5): 366-374.

MacDonald BT, Tamai K, He X. 2009. Wnt/β-Catenin Signaling: Components, Mechanisms, and Diseases. *Developmental Cell* 17(1): 9-26.

MacDonald HM, Mavroeidi A, Barr RJ, Black AJ, Fraser WD, Reid DM. 2008. Vitamin D status in postmenopausal women living at higher latitudes in the UK in relation to bone health, overweight, sunlight exposure and dietary vitamin D. *Bone* 42(5): 996-1003.

Mackie EJ, Ahmed YA, Tatarczuch L, Chen K-S, Mirams M. 2008. Endochondral ossification: How cartilage is converted into bone in the developing skeleton. *The International Journal of Biochemistry and Cell Biology* 40(1): 46-62.

Mackie EJ, Tatarczuch L, Mirams M. 2011. The skeleton: a multi-functional complex organ. The growth plate chondrocyte and endochondral ossification. *Journal of Endocrinology* 211(2): 109-121.

MacLennan WJ. 1999. History of arthritis and bone rarefaction evidence from paleopathology onwards. *Scottish Medical Journal* 44(1):18-20.

Madeiros DM, Stoecker B, Plattner A, Jennings D, Haub M. 2004. Iron deficiency negatively affects vertebrae and femurs of rats independently of energy intake and body weight. *Journal of Nutrition* 134(11): 3061-3067.

Maggiano IS, Maggiano CM, Clement JG, Thomas CDL, Carter Y, Cooper DML. 2016. Three-dimensional reconstruction of Haversian systems in human cortical bone using synchrotron radiation-based micro-CT: morphology and quantification of branching and transverse connections across age. *Journal of Anatomy* 228(5): 719-732.

Maggiano IS, Maggiano CM, Cooper DML. 2021. Osteon circularity and longitudinal morphology: Quantitative and qualitative three-dimensional perspectives on human Haversian systems. *Micron* 140(1): 102955.

Maggio A. 2022. *Quantitative histological approaches to forensic identification of human and non-human bone in an Australian context.* Doctoral (PhD) thesis submitted to the University of Western Australia. Available from: <https://research-repository.uwa.edu.au/en/publications/quantitative-histological-approaches-to-forensic-identification-o>.

Maggio A, Flavel A, Franklin D. 2019. A simplified and inexpensive method for the preparation of fresh or fixed bone samples for forensic histological examination. *Australian Journal of Forensic Sciences* 51(S1): s193-s196.

Maggio A, Franklin D. 2019. Histomorphometric age estimation from the femoral cortex: A test of three methods in an Australian population. *Forensic Science International* 303(1): 109950.

Maggio A, Franklin D. 2021. An examination of histomorphometric relationships in the anterior and posterior human femoral cortex. *Journal of Bone and Mineral Metabolism* 39(4): 649-660.

Mahoney P, Miszkiewicz JJ, Chapple S, Le Luyer M, Schlecht SH, Stewart TJ, Griffiths RA, Deter C, Guatelli-Steinberg D. 2018. The biorhythm of human skeletal growth. *Journal of Anatomy* 232(1): 26-38.

Mahoney P, Miszkiewicz JJ, Pitfield R, Deter C, Guatelli-Steinberg D. 2017. Enamel biorhythms of humans and great apes: the Havers-Halberg Oscillation hypothesis reconsidered. *Journal of Anatomy* 230(2): 272-281.

Mahoney P, Miszkiewicz JJ, Pitfield R, Schlecht SH, Deter C, Guatelli-Steinberg D. 2016a. Biorhythms, deciduous enamel thickness, and primary bone growth: a test of the Havers-Halberg Oscillation hypothesis. *Journal of Anatomy* 228(6): 919-928.

Mahoney P, Schmidt CW, Deter C, Remy A, Slavin P, Johns SE, Miszkiewicz JJ, Nystrom P. 2016b. Deciduous enamel 3D microwear texture analysis as an indicator of childhood diet in medieval Canterbury, England. *Journal of Archaeological Science* 66(1): 128-136.

Majumdar SR, Ezekowitz JA, Lix LM, Leslie WD. 2012. Heart failure is a clinically and densitometrically independent risk factor for osteoporotic fractures: population-based cohort study of 45,509 subjects. *The Journal of Clinical Endocrinology and Metabolism* 97(4): 1179-1186.

Mallorie A, Shine B. 2022. Normal bone physiology, remodelling and its hormonal regulation. *Surgery (Oxford)* 40(3): 163-168.

Mallouchou M, Katikas L, Stathopoulou E, Papaioannou N, Varagka N, Nakos B. 2020. Mapping Cheshire Cats' Leg: A histological approach of cortical bone tissue through modern GIS technology. *Anatomical Sciences International* 95(1): 104-125.

Manchester K, Roberts C. 1989. The palaeopathology of leprosy in Britain: A review. *World Archaeology* 21(2): 265-272.

Manolagas SC. 2000. Birth and death of bone cells: Basic regulatory mechanisms and implications for the pathogenesis and treatment of osteoporosis. *Endocrine Reviews* 21(2): 115-137.

Manolagas SC, O'Brien CA, Almeida M. 2013. The role of estrogen and androgen receptors in bone health and disease. *Nature Reviews Endocrinology* 9(12): 699-712.

Mansour A, Mezour MA, Badran Z, Tamimi F. 2017. Extracellular Matrices for Bone Regeneration: A Literature Review. *Tissue Engineering Part A* 23(23-24): 1436-1451.

Marhoff-Beard SJ, Forbes SL, Green H. 2018. The validation of 'universal' PMI methods for the estimation of time since death in temperate Australian climates. *Forensic Science International* 291(1): 158-166.

Marinovich R, Soenjaya Y, Wallace GQ, Zuskov A, Dunkman A, Foster BL, Ao M, Bartman K, Lam V, Rizkalla A, Beier F, Somerman MJ, Holdsworth DW, Soslowsky LJ, Lagugné-Labarthet F, Goldberg HA. 2016. The role of bone sialoprotein in the tendon-bone insertion. *Matrix Biology* 52-54(1): 325-338.

Mariotti V, Facchini F, Belcastro MG. 2007. The study of entheses: proposal of a standardised scoring method for twenty-three entheses of the postcranial skeleton. *Collegium Antropologicum* 31(1): 291-313.

Marks SC, Odgren PR. 2002. Structure and Development of the Skeleton. In: Bilezikian JP, Raisz LG, Rodan GA (eds.). *Principles of Bone Biology, 2nd edition,* pp. 3-15. Elsevier: United Kingdom.

Martin DL, Armelagos GJ. 1979. Morphometrics of compact bone: an example from Sudanese Nubia. *American Journal of Biological Anthropology* 51(4): 571-578.

Martin DL, Armelagos GJ. 1985. Skeletal remodelling and mineralization as indicators of health: an example from prehistoric Sudanese Nubia. *Journal of Human Evolution* 14(5): 527-537.

Martin RB. 1984. Porosity and specific surface of bone. *Critical Reviews in Biomedical Engineering* 10(3): 179-222.

Martin RB. 2007. Targeted bone remodelling involves BMU steering as well as activation. *Bone* 40(6): 1574-1580.

Martin RB, Burr DB, Sharkey NA. 1998. *Skeletal Tissue Mechanics*. Springer: New York.

Martin RB, Burr DB, Sharkey NA, Fyhrie DP. 2015. *Skeletal Tissue Mechanics, 2nd edition.* Springer: New York, USA.

Martin TJ, Sims NA. 2005. Osteoclast-derived activity in the coupling of bone formation to resorption. *Trends in Molecular Medicine* 11(2): 76-81.

Mashiba T, Hirano T, Turner CH, Forwood MR, Johnston CC, Burr DB. 2010. Suppressed Bone Turnover by Bisphosphonates Increases Microdamage Accumulation and Reduces Some Biomechanical Properties in Dog Rib. *Journal of Bone and Mineral Research* 15(4): 613-620.

Mastrangelo P, De Luca S, Alemán I, Botella MC. 2011. Sex assessment from the carpals bones: Discriminant function analysis in a 20th century Spanish sample. *Forensic Science International* 206(1-3): 216.e1-216.e10.

Matković V, Kostial K, Šimonović I, Buzina R, Brodarec A, Nordin BEC. 1979. Bone status and fracture rates in two regions of Yugoslavia. *The American Journal of Clinical Nutrition* 32(3): 540-549.

Matsuo H, Tsurumoto T, Maeda J, Saiki K, Okamoto K, Ogami-Takamura K, Kondo H, Tomita M, Yonekura A, Osaki M. 2019. Investigating interindividual variations in cortical bone quality: analysis of the morphotypes of secondary osteons and their population densities in the human femoral diaphysis. *Anatomical Science International* 94(1): 75-85.

Mauras N, Haymond MW, Darmaun D, Vieira NE, Abrams SA, Yergey AL. 1994. Calcium and protein kinetics in prepubertal boys: Positive effects of testosterone. *The Journal of Clinical Investigation* 93(3): 1014-1019.

Mavroudas SR, Meckel LA, Gocha TP, Goldstein JZ, Garza SL. 2022. The Effects of Experimental Whole-Body Burning on Histological Age-at-Death Estimation from Human Cortical Bone and Dental Cementum. *Biology* 11(11): 1569.

Mayall A. 1890. A description of Bernardino Marzoli's achromatic objective. *Journal of the Royal Microscopical Society* 1890(1): 420-422.

Mays SA. 1991. *The medieval burials from the Blackfriars Friary, School Street, Ipswich, Suffolk (excavated 1983-85), AML Report 16/91.* Historic England: Suffolk, UK.

Mays SA. 2014. The palaeopathology of scurvy in Europe. *International Journal of Paleopathology* 5(1): 55-62.

Mays SA. 2021. *The Archaeology of Human Bones, 3rd edition*. Routledge: Cambridge.

Mazess RB. 1982. On aging bone loss. *Clinical Orthopaedics and Related Research* 165(1): 239-252.

Mazess RB, Barden HS, Ettinger M, Johnston C, Dawson-Hughes B, Baran D, Powell M, Notelovitz M. 1987. Spine and femur density using dual-photon absorptiometry in US white women. *Bone and Mineral* 2(3): 211-219.

McBride SH, Evans SF, Knothe Tate ML. 2011. Anisotropic mechanical properties of ovine femoral periosteum and the effects of cryopreservation. *Journal of Biomechanics* 44(10): 1954-1959.

McCarthy EF. 2016. The histology of metabolic bone disease. *Diagnostic Histopathology* 22(10): 378-383.

McClea K, Stringer MD. 2010. The profile of body donors at the Otago School of Medical Sciences—has it changed? *The New Zealand Medical Journal* 123(1312): 9-17.

McClung MR, Grauer A, Boonen S, Bolognese MA, Brown JP, Diez-Perez A, Langdahl BL, Reginster J-Y, Zanchetta JR, Wasserman SM, Katz L, Maddox J, Yang Y-C, Libanati C, Bone HG. 2014. Romosozumab in Postmenopausal Women with Low Bone Mineral Density. *New England Journal of Medicine* 370(5): 412-420.

Meakin LB, Price JS, Lanyon LE. 2014. The Contribution of Experimental in Vivo Models to Understanding the Mechanisms of Adaptation to Mechanical Loading in Bone. *Frontiers in Endocrinology* 5(1): 154.

Megyesi M, Nawrocki SP, Haskell NH. 2005. Using accumulated degree-days to estimate the postmortem interval from decomposed human remains. *Journal of Forensic Sciences* 50(3): 618-626.

Meiggs R. 1973. *Roman Ostia*. Oxford University Press: Oxford.

Melrose J, Shu C, Whitelock JM, Lord MS. 2016. The cartilage extracellular matrix as a transient developmental scaffold for growth plate maturation. *Matrix Biology* 52-54(1): 363-383.

Melton LJ, Lane AW, Cooper C, Eastell R, O'Fallon WM, Riggs BL. 1993. Prevalence and incidence of vertebral deformities. *Osteoporosis International* 3(3): 113-119.

Mendelow H, Hamilton JB. 1950. A new technique for rapid freezing and dehydration of tissues for histology and histochemistry. *The Anatomical Record* 107(4): 443-451.

Menetrier P. 1886. Cancer primitif du poumon. *Bulletin de la Société vaudoise des sciences naturelles* 61(1): 643-647.

Menzies JK. 2021. *The Taphonomy of Human and Non-Human Skeletal Remains in Australian Conditions and the Implications for Post-Mortem Interval Research*. Doctoral (PhD) dissertation submitted to the University of Sydney. Available from: <https://ses.library.usyd.edu.au/handle/2123/25534>.

Merle B, Garnero P. 2012. The multiple facets of periostin in bone metabolism. *Osteoporosis International* 23(4): 1199-1212.

Mertens MT, Gertner E. 2011. Rheumatic manifestations of scurvy: a report of three recent cases in a major urban center and a review. *Seminars in Arthritis and Rheumatism* 41(2): 286-290.

Milch RA, Rall DP, Tobie JE. 1958. Fluorescence of Tetracycline Antibiotics in Bone. *The Journal of Bone and Joint Surgery* 40-A(4): 897-910.

Millard AR. 2001. The deterioration of bone. In: Brothwell DR, Pollard AM (eds.). *Handbook of Archaeological Sciences*, pp. 637-647. John Wiley & Sons: Chichester.

Miller AC, Cake MA, Warburton NM. 2017. The fibular meniscus of the kangaroo as an adaptation against external tibial rotation during saltatorial locomotion. *Journal of Anatomy* 231(6): 931-938.

Miller PD. 2008. The role of bone biopsy in patients with chronic renal failure. *Clinical Journal of the American Society of Nephrology* 3(Suppl3): S140-S150.

Mishra P, Pandey CM, Singh U, Gupta A, Sahu C, Keshri A. 2019. Descriptive Statistics and Normality Tests for Statistical Data. *Annals of Cardiac Anaesthesia* 22(1): 67-72.

Mishra S, Knothe Tate ML. 2008. Comparative study of bone micro-architecture of some mammalian bones. *The Palaeobotanist* 57(1-3): 299-302.

Miszkiewicz JJ. 2014. *Ancient human bone histology and behaviour*. Doctoral (PhD) Dissertation submitted to the University of Kent, Canterbury, UK.

Miszkiewicz JJ. 2015a. Linear Enamel Hypoplasia and Age-at-Death at Medieval (11th–16th Centuries) St. Gregory's Priory and Cemetery, Canterbury, UK. *International Journal of Osteoarchaeology* 25(1): 79-87.

Miszkiewicz JJ. 2015b. Histology of a Harris line in a human distal tibia. *Journal of Bone and Mineral Metabolism* 33(4): 462-466.

Miszkiewicz JJ. 2016. Investigating histomorphometric relationships at the human femoral midshaft in a biomechanical context. *Journal of Bone and Mineral Metabolism* 34(2): 179-192.

Miszkiewicz JJ, Buckley HR, Feldman M, Kiko L, Carlhoff S, Naegele K, Bertolini E, Dias Guimarães NR, Walker MM, Powell A, Posth C, Kinaston RL. 2022a. Female bone physiology resilience in a past Polynesian Outlier community. *Nature Scientific Reports* 12(1): 18857.

Miszkiewicz JJ, Mahoney P. 2016. Ancient Human Bone Microstructure in Medieval England: Comparisons between Two Socio-Economic Groups. *The Anatomical Record* 299(1): 42-59.

Miszkiewicz JJ, Mahoney P. 2017. Human bone and dental histology in an archaeological context. In: Thompson T, Errricksen D (eds.). *Imaging Human Remains: Another Dimension*, pp. 29-43. Elsevier: Academic Press.

Miszkiewicz JJ, Mahoney P. 2019. Histomorphometry and cortical robusticity of the adult human femur. *Journal of Bone and Mineral Metabolism* 37(1): 90-104.

Miszkiewicz JJ, Matisoo-Smith EA, Weisler MI. 2022b. Behavior and intra-skeletal remodelling in an adult male from 1720 BP Ebon Atoll, Marshall Islands, eastern Micronesia. *The Journal of Island and Coastal Archaeology* 17(3): 445-459.

Miszkiewicz JJ, Rider C, Kealy S, Vrahnas C, Sims NA, Vongsvivut J, Tobin MJ, Bolunia MJLA, De Leon AS, Peñalosa AL, Pagulayan PS, Soriano AV, Page R, Oxenham MF. 2020. Asymmetric midshaft femur remodelling in an adult male with left sided hip joint ankylosis, Metal Period Nagsabaran, Philippines. *International Journal of Paleopathology* 31(1): 14-22.

Miszkiewicz JJ, Stewart TJ, Naseri R, Sołtysiak A. 2022c. The lifestyles of Bronze Age Zagros highlanders at Deh Dumen, Iran: Insights from midshaft femur cross-sectional geometry and histology. *Archaeometry* 64(5): 1270-1287.

Miszkiewicz JJ, Valentin F, Vrahnas C, Sims NA, Vongsvivut J, Tobin MJ, Clark G. 2021. Bone loss markers in the earliest Pacific Islanders. *Nature: Scientific Reports* 11(1): 3981.

Miyamoto K, Sugiyama S, Hosoe H, Iinuma N, Suzuki Y, Shimizu K. 2009. Postsurgical recurrence of osteophytes causing dysphagia in patients with diffuse idiopathic skeletal hyperostosis. *European Spine Journal* 18(11): 1652-1658.

Mizokami A, Kawakubo-Yasukochi T, Hirata M. 2017. Osteocalcin and its endocrine functions. *Biochemical Pharmacology* 132(1): 1-8.

Monier-Faugere M, Langub MC, Malluche HH. 1998. Bone biopsies: A modern approach. In: Avioli LV, Krane SM (eds.). *Metabolic bone diseases and clinically related disorders, 3rd edition,* pp. 237-273. Academic Press: San Diego.

Monk AP, Oldenrijk JV, Riley ND, Gill RHS, Murray DW. 2016. Biomechanics of the lower limb. *Surgery (Oxford)* 34(9): 427-435.

Moorehead C, Prudnikova K, Marcolongo M. 2019. The regulatory effects of proteoglycans on collagen fibrillogenesis and morphology investigated using biomimetic proteoglycans. *Journal of Structural Biology* 206(2): 204-215.

Moreira CA, Dempster DW. 2019. Histomorphometric Analysis of Bone Remodelling. In: Bilezikian JP, Martin TJ, Clemens TL, Rosen C (eds.). *Principles of Bone Biology, 4th edition,* pp. 445-467. Elsevier: United Kingdom.

Mori Y, Tarasawa K, Tanaka H, Mori N, Fushimi K, Fujimori K, Aizawa T. 2025. Does total hip arthroplasty in elderly patients with femoral neck fractures reduce complications? A Japanese DPC study. *Journal of Orthopaedic Surgery* 30(3): 507-512.

Morrison NA, Qi JC, Tokita A, Kelly PJ, Crofts L, Nguyen TV, Sambrook PN, Eisman JA. 1994. Prediction of bone density from vitamin D receptor alleles. *Nature* 367(6460): 284-287.

Mow VC, Ratcliffe A, Poole AR. 1992. Cartilage and diarthrodial joints as paradigms for hierarchical materials and structures. *Biomaterials* 13(2): 67-97.

Mulhern DM. 2000. Rib remodelling dynamics in a skeletal population from Kulubnarti, Nubia. *American Journal of Biological Anthropology* 111(4): 519-530.

Mulhern DM, Jones EB. 2005. Test of revised method of age estimation from the auricular surface of the ilium. *American Journal of Biological Anthropology* 126(1): 61-65.

Mulhern DM, Ubelaker DH. 2001. Differences in osteon banding between human and nonhuman bone. *Journal of Forensic Sciences* 46(2): 220-222.

Mulhern DM, Van Gerven DP. 1997. Patterns of femoral bone remodelling dynamics in a Medieval Nubian population. *American Journal of Biological Anthropology* 104(1): 133-146.

Murach MM, Kang Y-S, Goldman SD, Schafman MA, Schlecht SH, Moorhouse K, Bolte JH, Agnew AM. 2017. Rib Geometry Explains Variation in Dynamic Structural Response: Potential Implications for Frontal Impact Fracture Risk. *Annals of Biomedical Engineering* 45(9): 2159-2173.

Myszka A, Piontek J, Tomczyk J, Lisowska-Gaczorek A, Zalewska M. 2020. Relationships between osteoarthritic changes (osteophytes, porosity, eburnation) based on historical skeletal material. *Annals of Human Biology* 47(3): 262-272.

Naba A, Clauser KR, Ding H, Whittaker CA, Carr SA, Hynes RO. 2016. The extracellular matrix: tools and insights for the “omics” era. *Matrix Biology* 49(1): 10-24.

Nareliya Mishra R, Kumar Singh M, Kumar V. 2022. Biomechanical Analysis of Human Femur using Finite Element Method: A Review Study. *Materials Today: Proceedings* 56(1): 384-389.

Neagu TP, Ţigliş M, Cocoloş I, Jecan CR. 2016. The relationship between periosteum and fracture healing. *Romanian Journal of Morphology and Embryology* 57(4): 1215-1220.

New South Wales Government. 2018. *Anatomy Act 1977, No. 126*. Last updated 15 June 2018. Available from: <https://legislation.nsw.gov.au/view/html/inforce/current/act-1977-126>.

Ng L, Grodzinsky AJ, Patwari P, Sandy J, Plaas A, Ortiz C. 2003. Individual cartilage aggrecan macromolecules and their constituent glycosaminoglycans visualized via atomic force microscopy. *Journal of Structural Biology* 143(3): 242-257.

Nganvongpanit K, Siengdee P, Buddhachat K, Brown JL, Klinhom S, Pitakarnnop T, Angkawanish T, Thitaram C. 2017. Anatomy, histology and elemental profile of long bones and ribs of the Asian elephant (Elephas maximus). *Anatomical Science International* 92(4): 554-568.

Nicolau R, Pereira L, Terroso G, Vaz C, Brito I, Frazão J. 2025. The role of bone histomorphometry in the management of metabolic bone disease. *ARP Rheumatology* 4(1): 37-43.

Nielsen FH, Stoecker B. 2009. Boron and fish oil have different beneficial effects on strength and trabecular microarchitecture of bone. *Journal of Trace Element Research in Medicine and Biology* 23(3): 195-203.

Nilas L, Gotfredsen A, Hadberg A, Christiansen C. 1988. Age-related bone loss in women evaluated by the single and dual photon technique. *Bone and Mineral* 4(1): 95-103.

Nolet PS, Friedman L, Brubaker D. 1999. Paracondylar process: a rare cause of craniovertebral fusion: a case report. *Journal of the Canadian Chiropractic Association* 43(4): 229-235.

Norris SA, Micklesfield LK, Pettifor JM. 2013. Ethnic Differences in Bone Acquisition. In: Rosen CJ (ed.). *Primer on the Metabolic Bone Diseases and Disorders of Mineral Metabolism, 8th edition,* pp. 135-141. John Wiley & Sons, Inc.: Ames, USA.

Nowak A, Ogurkowska M. 2024. Bone health and physical activity: The complex mechanism. *Aging and Disease* 15(5): 1316-1330.

O'Brien FJ, Hardiman DA, Hazenberg JG, Mercy MV, Mohsin S, Taylor D, Lee TC. 2005. The behaviour of microcracks in compact bone. *European Journal of Morphology* 42(1-2): 71-79.

Odvina CV, Zerwekh JE, Rao DS, Maalouf N, Gottschalk FA, Pak CYC. 2005. Severely Suppressed Bone Turnover: A Potential Complication of Alendronate Therapy. *The Journal of Clinical Endocrinology and Metabolism* 90(3): 1294-1301.

Ogden JA. 1987. The development and growth of the musculo-skeletal system. In: Albright JA, Brands R (eds.). *Scientific Basis of Orthopaedics*, pp. 41-103. Appleton-Century-Crofts: New York.

Okoye K, Hosseini S. 2024. Understanding the Different Types of Statistical Data Analysis and Methods. In: Okoye K, Hosseini S (eds.). *R Programming*, pp. 109-130. Springer: Mexico.

Olsen BR. 1995. New insights into the function of collagens from genetic analysis. *Current Opinion in Cell Biology* 7(5): 720-727.

Olsen BR. 1997. Collagen IX. *The International Journal of Biochemistry and Cell Biology* 29(4): 555-558.

Oostra R-J, Gelderman T, Groen WJM, Uiterdijk HG, Cammeraat ELH, Krap T, Wilk LS, Lüschen M, Morriën WE, Wobben F, Duijst WLJM, Aalders MCG. 2020. Amsterdam Research Initiative for Sub-surface Taphonomy and Anthropology (ARISTA) - A taphonomic research facility in the Netherlands for the study of human remains. *Forensic Science International* 317: 110483.

Orcan F. 2020. Parametric or Non-parametric: Skewness to Test Normality for Mean Comparison. *International Journal of Assessment Tools in Education* 7(2): 255-265.

Ortner DJ (ed.). 2003. *Identification of pathological conditions in human skeletal remains, 2nd edition.* Elsevier Academic Press: USA.

Ortner DJ, Aufderheide AC. 1991. *Human paleopathology: current syntheses and future options.* Smithsonian Institution Press: USA.

Ortona E, Pagano MT, Capossela L, Malorni W. 2023. The Role of Sex Differences in Bone Health and Healing. *Biology* 12(7): 993.

Orwoll ES. 2003. Toward an Expanded Understanding of the Role of the Periosteum in Skeletal Health. *Journal of Bone and Mineral Research* 18(6): 949-954.

Ouchi N, Parker JL, Lugus JJ, Walsh K. 2011. Adipokines in inflammation and metabolic disease. *Nature Reviews Immunology* 11(2): 85-97.

Owen N, Bauman A. 1992. The Descriptivte Epidemiology of a Sedentary Lifestyle in Adult Australians. *International Journal of Epidemiology* 21(2): 305-310.

Paine RR. 2007. How to equip a basic histological lab for the anthropological assessment of human bone and teeth. *Journal of Anthropological Sciences* 85(1): 213-219.

Paine RR, Brenton BP. 2006. Dietary Health Does Affect Histological Age Assessment: An Evaluation of the Stout and Paine (1992) Age Estimation Equation Using Secondary Osteons from the Rib. *Journal of Forensic Sciences* 51(3): 489-492.

Paine RR, Godfrey LR. 1997. The scaling of skeletal microanatomy in non-human primates. *Journal of Zoology* 241(4): 803-821.

Paiva KBS, Granjeiro JM. 2017. Matrix Metalloproteinases in Bone Resorption, Remodelling, and Repair. *Progress in Molecular Biology and Translational Science* 148(1): 203-303.

Paracuellos P, Kalamajski S, Bonna A, Bihan D, Farndale RW, Hohenester E. 2017. Structural and functional analysis of two small leucine-rich repeat proteoglycans, fibromodulin and chondroadherin. *Matrix Biology* 63(1): 106-116.

Parelman M, Stoecker B, Baker A, Medeiros D. 2006. Iron restriction negatively affects bone in female rats and mineralization of hFOB osteoblast cells. *Experimental Biology and Medicine* 231(4): 378-386.

Parfitt AM. 1983. The Physiologic and Clinical Significance of Bone Histomorphometric Data. In: Recker RR (ed.). *Bone Histomorphometry: Techniques and Interpretation*, pp. 143-223. CRC Press: London.

Parfitt AM. 1984. Age-related structural changes in trabecular and cortical bone: Cellular mechanisms and biomechanical consequences. *Calcified Tissue International* 36(Suppl 1): S123–S128.

Parfitt AM. 1990. Bone-forming cells in clinical conditions. In: Hall BK (ed.). *Bone: The Osteoblast and Osteocyte*, pp. 351-429. Telford Press and CRC Press: Boca Raton, Florida.

Parfitt AM, Drezner MK, Glorieux FH, Kanis JA, Malluche H, Meunier PJ, Ott SM, Recker RR. 1987. Bone histomorphometry: standardization of nomenclature, symbols, and units. *Journal of Bone and Mineral Research* 2(6): 595-610.

Parfitt AM, Villanueva AR, Foldes J, Rao DS. 1995. Relations between histologic indices of bone formation: Implications for the pathogenesis of spinal osteoporosis. *Journal of Bone and Mineral Research* 10(3): 466-473.

Parfitt AM. 2001a. The Bone Remodelling Compartment: A Circulatory Function for Bone Lining Cells. *Journal of Bone and Mineral Research* 16(9): 1583-1585.

Parfitt AM. 2001b. Skeletal Heterogeneity and the Purposes of Bone Remodelling: Implications for the Understanding of Osteoporosis. In: Marcus R, Feldman D, Kelsey J (eds.). *Osteoporosis, 2nd edition,* pp. 433-447. Elsevier: United Kingdom.

Parfitt AM. 2002a. Targeted and nontargeted bone remodelling: relationship to basic multicellular unit origination and progression. *Bone* 30(1): 5-7.

Parfitt AM. 2002b. Misconceptions (2): turnover is always higher in cancellous than in cortical bone. *Bone* 30(6): 807-809.

Parsons TJ, Prentice A, Smith EA, Cole TJ, Compston JE. 1996. Bone mineral mass consolidation in young British adults. *Journal of Bone and Mineral Research* 11(2): 264-274.

Pasiakos SM, Margolis LM, Orr JS. 2015. Optimized dietary strategies to protect skeletal muscle mass during periods of unavoidable energy deficit. *FASEB Journal* 29(4): 1136-1142.

Pavón MV, Cucina A, Tiesler V. 2010. New Formulas to Estimate Age at Death in Maya Populations Using Histomorphological Changes in the Fourth Human Rib. *Journal of Forensic Sciences* 55(2): 473-477.

Payne JA, King EW, Beinhart G. 1968. Arthropod Succession and Decomposition of Buried Pigs. *Nature* 219(5159): 1180-1181.

Pazzaglia UE, Sibilia V, Congiu T, Pagani F, Ravanelli M, Zarattini G. 2015. Setup of a bone aging experimental model in the rabbit comparing changes in cortical and trabecular bone: Morphological and morphometric study in the femur. *Journal of Morphology* 276(7): 733-747.

Pazzola G, Possemato N, Germanò G, Salvarani C. 2013. Scurvy mimicking spondyloarthritis in a young man. *Clinical and Experimental Rheumatology* 31(5): 795.

Pbroks13. 2008. *Bone cross-section.svg*. Available from: <https://commons.wikimedia.org/wiki/File:Bone_cross-section.svg>.

Peck JJ, Stout SD. 2007. Intraskeletal variability in bone mass. *American Journal of Biological Anthropology* 132(1): 89-97.

Pecsi EL, Bronchti G, Crispino F, Forbes SL. 2020. Perspectives on the establishment of a canadian human taphonomic facility: The experience of REST[ES]. *Forensic Science International: Synergy* 2(1): 287-292.

Pedersen LT, Miszkiewicz J, Cheah LC, Willis A, Domett KM. 2024. Age-dependent change and intraskeletal variability in secondary osteons of elderly Australians. *Journal of Anatomy* 244(6): 1078-1092.

Peris P, Parés A, Guañabens N, Pons F, Martínez de Osaba MJ, Caballería J, Rodés J, Muñoz-Gómez J. 1992. Reduced spinal and femoral bone mass and deranged bone mineral metabolism in chronic alcoholics. *Alcohol and Alcoholism* 27(6): 619-625.

Perry HM, Horowitz M, Morley JE, Fleming S, Jensen J, Caccione P, Miller DK, Kaiser FE, Sundarum M. 1996. Aging and bone metabolism in African American and Caucasian women. *Journal of Clinical Endocrinology and Metabolism* 81(3): 1108-1117.

Pettit AR, Chang MK, Hume DA, Raggatt L-J. 2008. Osteal macrophages: A new twist on coupling during bone dynamics. *Bone* 43(6): 976-982.

Pfeiffer S. 1998. Variability in Osteon Size in Recent Human Populations. *American Journal of Biological Anthropology* 106(2): 219-227.

Pfeiffer S, Cameron ME, Sealy J, Beresheim AC. 2019. Diet and adult age-at-death among mobile foragers: A synthesis of bioarcheological methods. *American Journal of Biological Anthropology* 170(1): 131-147.

Pfeiffer S, Crowder C, Harrington L, Brown M. 2006. Secondary osteon and Haversian canal dimensions as behavioral indicators. *American Journal of Biological Anthropology* 131(4): 460-468.

Pfeiffer S, Heinrich J, Beresheim A, Alblas M. 2016. Cortical Bone Histomorphology of Known-Age Skeletons from the Kirsten Collection, Stellenbosch University, South Africa. *American Journal of Biological Anthropology* 160(1): 137-147.

Phenice TW. 1969. A newly developed visual method of sexing the os pubis. *American Journal of Biological Anthropology* 30(2): 297-301.

Phillips C, Baxter IL, Nussbaumer M. 2009. The Application of Discriminant Function Analysis to Archaeological Dog Remains as an Aid to the Elucidation of Possible Affinities with Modern Breeds. *Archaeofauna* 18(1): 51-64.

Pignolo RJ, Law SF, Chandra A. 2021. Bone Aging, Cellular Senescence, and Osteoporosis. *Journal of Bone and Mineral Research Plus* 5(4): e10488.

Pilli E, Palamenghi A, Cattaneo C. 2025. Forensic skeletal and molecular anthropology face to face: Combining expertise for identification of human remains. *Annals of the New York Academy of Sciences* 1550(1): 77-107.

Pirok DJ, Ramser JR, Takahashi H, Villanueva AR, Frost HM. 1966. Normal histological, tetracycline and dynamic parameters in human, mineralized bone sections. *Henry Ford Hospital Medical Journal* 14(2): 195-218.

Pitfield R, Deter C, Mahoney P. 2019. Bone histomorphometric measures of physical activity in children from medieval England. *American Journal of Biological Anthropology* 169(4): 730-746.

Pocock NA, Eisman JA, Hopper JL, Yeates MG, Sambrook PN, Eberl S. 1987. Genetic determinants of bone mass in adults: A twin study. *Journal of Clinical Investigation* 80(3): 706-710.

Poopedi MA, Norris SA, Pettifor JM. 2011. Factors influencing the vitamin D status of 10-year-old urban South African children. *Public Health Nutrition* 14(2): 334-339.

Poulton R, Woods H. 1984. *Excavations on the site of the Dominican Friary at Guildford in 1974 and 1978.* Surrey Archaeological Society Research: Guildford, UK.

Powell A, Serjeantson D, Smith P. 2001. Food consumption and disposal: The animal remains. In: Hicks M, Hicks A. (eds.). *St Gregory's Priory, Northgate, Canterbury Excavations 1988-1991*, pp. 289-333. Canterbury Archaeological Trust: Great Britain.

Prince RL, Devine A, Dhaliwal SS, Dick IM. 2006. Effects of calcium supplementation on clinical fracture and bone structure: results of a 5-year, double-blind, placebo-controlled trial in elderly women. *Archives of Internal Medicine* 166(8): 869-875.

Prior JC. 2018. Progesterone for the prevention and treatment of osteoporosis in women. *Climacteric* 21(4): 366-374.

Prior JC, Vigna YM, Schechter MT, Burgess AE. 1990. Spinal Bone Loss and Ovulatory Disturbances. *New England Journal of Medicine* 323(18): 1221-1227.

Prowse TL, Schwarcz HP, Saunders SR, Macchiarelli R, Bondioli L. 2004. Isotopic paleodiet studies of skeletons from the Imperial Roman-age cemetery of Isola Sacra, Rome, Italy. *Journal of Archaeological Science* 31(3): 259-272.

Qiu S, Fyhrie DP, Palnitkar S, Rao DS. 2003. Histomorphometric assessment of Haversian canal and osteocyte lacunae in different-sized osteons in human rib. *The Anatomical Record* 272(2): 520-525.

Qiu S, Rao DS, Palnitkar S, Parfitt AM. 2002. Relationships Between Osteocyte Density and Bone Formation Rate in Human Cancellous Bone. *Bone* 31(6): 709-711.

Quekett JA. 1848. *Practical Treatise on the use of the Microscope*. Hippolyte Bailliere: London.

Raab DM, Crenshaw TD, Kimmel DB, Smith EL. 1991. A histomorphometric study of cortical bone activity during increased weight-bearing exercise. *Journal of Bone and Mineral Research* 6(7): 741-749.

Rabey KN, Green DJ, Taylor AB, Begun DR, Richmond BG, McFarlin SC. 2015. Locomotor activity influences muscle architecture and bone growth but not muscle attachment site morphology. *Journal of Human Evolution* 78(1): 91-102.

Rajakumar K, Fernstrom JD, Holick MF, Janosky JE, Greenspan SL. 2008. Vitamin D status and response to Vitamin D(3) in obese vs. non-obese African American children. *Obesity* 16(1): 90-95.

Ralston SH. 2021. Bone structure and metabolism. *Medicine* 49(9): 567-571.

Ramchand SK, Seeman E. 2018. The Influence of Cortical Porosity on the Strength of Bone During Growth and Advancing Age. *Current Osteoporosis Reports* 16(5): 561-572.

Recker RR, Davies KM, Hinders SM, Heaney RP, Stegman MR, Kimmel DB. 1992. Bone gain in young adult women. *JAMA* 268(17): 2403-2408.

Reid RAG, Jans MME, Chesson LA, Taylor RJ, Berg GE. 2024. The influence of taphonomy on histological and isotopic analyses of treated and untreated buried modern human bone. *Journal of Archaeological Science* 161(1): 105901.

Reid SA. 1986. A study of lamellar organisation in juvenile and adult human bone. *Anatomy and Embryology* 174(3): 329-338.

Rho JY, Kuhn-Spearing L, Zioupos P. 1998. Mechanical properties and the hierarchical structure of bone. *Medical Engineering and Physics* 20(2): 92-102.

Richards JB, Kavvoura FK, Rivadeneira F, Styrkársdóttir U, Estrada K, Halldórsson BV, Hsu Y-H, Zillikens MC, Wilson SG, Mullin BH, Amin N, Aulchenko YS, Cupples LA, Deloukas P, Demissie S, Hofman A, Kong A, Karasik D, van Meurs JB, Oostra BA, Pols HAP, Sigurdsson G, Thorsteinsdottir U, Soranzo N, Williams FMK, Zhou Y, Ralston SH, Thorleifsson G, van Duijn CM, Kiel DP, Stefansson K, Uitterlinden AG, Ioannidis JPA, Spector TD, for the GEFOS (Genetic Factors for Osteoporosis) Consortium. 2009. Collaborative meta-analysis: associations of 150 candidate genes with osteoporosis and osteoporotic fracture. *Annals of Internal Medicine* 151(8): 528-537.

Richardson KC, Jarett L, Finke EH. 1960. Embedding in epoxy resins for ultrathin sectioning in electron microscopy. *Stain Technology* 35(6): 313-323.

Richman EA, Ortner DJ, Schulter-Ellis FP. 1979. Differences in intracortical bone remodelling in three aboriginal American populations: Possible dietary factors. *Calcified Tissue International* 28(3): 209-214.

Riggs BL, Khosla S, Melton LJ. 2002. Sex steroids and the construction and conservation of the adult skeleton. *Endocrine Reviews* 23(3): 279-302.

Riggs BL, Wahner HW, Dunn WL, Mazess RB, Offord KP, Melton LJ. 1981. Differential changes in bone mineral density of the appendicular and axial skeleton with aging: Relationship to spinal osteoporosis. *Journal of Clinical Investigation* 67(2): 328-335.

Riggs BL, Wahner HW, Seeman E, Offord KP, Dunn WL, Mazess RB, Johnson KA, Melton LJ. 1982. Changes in bone mineral density of the proximal femur and spine with aging. Differences between the postmenopausal and senile osteoporosis syndromes. *The Journal of Clinical Investigation* 70(4): 716-723.

Rigotti NA, Nussbaum SR, Herzog DB, Neer RM. 1984. Osteoporosis in women with anorexia nervosa. *The New England Journal of Medicine* 311(25): 1601-1606.

Ringer P, Colo G, Fässler, Grashoff C. 2017. Sensing the mechano-chemical properties of the extracellular matrix. *Matrix Biology* 64(1): 6-16.

Rittweger J. 2011. Bone Physiology. In: Cardinale M, Newton R, Nosaka K (eds.). *Strength and conditioning: Biological principles and practical applications*, pp. 29-44. John Wiley & Sons Portland: Oregan, USA.

Rivera F, Lahr MM. 2017. New evidence suggesting a dissociated etiology for cribra orbitalia and porotic hyperostosis. *American Journal of Biological Anthropology* 164(1): 76-96.

Robb J. 1998. The interpretation of skeletal muscle sites: a statistical approach. *International Journal of Osteoarchaeology* 8(5): 363-377.

Roberts CA, Cox M. 2003. *Health and Disease in Britain: From Prehistory to the Present Day*. Sutton Publishing: London.

Roberts CA, Gowland R. 2018. Bioarchaeology. In: Callan H (ed.). *The International Encyclopedia of Anthropology*, pp. 385-398. Springer Verlag: Durham, UK.

Roberts CA, Manchester K. 2005. *The Archaeology of Disease*. Sutton Publishing: London.

Roberts CA, Mays S. 2011. Study and restudy of curated skeletal collections in bioarchaeology: a perspective on the UK and the implications for future curation of human remains. *International Journal of Osteoarchaeology* 21(5): 626-630.

Robling AG, Castillo AB, Turner CH. 2006. Biomechanical and molecular regulation of bone remodelling. *Annual Review of Biomedical Engineering* 8(1): 455-498.

Robling AG, Stout SD. 1999. Morphology of the drifting osteon. *Cells, Tissues, Organs* 164(4): 192-204.

Robling AG, Stout SD. 2003. Histomorphology, geometry, and mechanical loading in past populations. In: Agarwal SC, Stout SD (eds.). *Bone Loss and Osteoporosis: An Anthropological Perspective*, pp. 189-205. Kluwer Academic/Plenum Publishers: New York.

Robling AG, Stout SD. 2008. Histomorphometry of human cortical bone: applications to age estimations. In: Katzenberg M, Saunders SR (eds.). *Biological anthropology of the human skeleton*, pp. 149-182. New York: Wiley-Liss.

Rodin A, Murby B, Smith MA, Caleffi M, Fentiman I, Chapman MG, Fogelman I. 1990. Premenopausal bone loss in the lumbar spine and neck of femur: A study of 225 Caucasian women. *Bone* 11(1): 1-5.

Roesler H. 1987. The History of Some Fundamental Concepts in Bone Biomechanics. *Journal of Biomechanics* 20(11-12): 1025-1034.

Rogers J, Waldron T. 2001. DISH and the monastic way of life. *International Journal of Osteoarchaeology* 11(5): 357-365.

Rolvien T, Krause M, Jeschke A, Yorgan T, Püschel K, Schinke T, Busse B, Demay MB, Amling M. 2017. Vitamin D regulates osteocyte survival and perilacunar remodelling in human and murine bone. *Bone* 103(1): 78-87.

Roodman GD. 2004. Mechanisms of Bone Metastasis. *The New England Journal of Medicine* 350(16): 1655-1664.

Rosa N, Moura MFSF, Olhero S, Simoes R, Magalhães FD, Torres Marques A, Ferreira JPS, Reis AR, Carvalho M, Parente M. 2022. Bone: An Outstanding Composite Material. *Applied Sciences* 12(7): 3381.

Rose DC, Agnew AM, Gocha TP, Stout SD, Field JS. 2012. Technical note: The use of geographic information systems software for the spatial analysis of bone microstructure. *American Journal of Biological Anthropology* 148(4): 648-654.

Rosen CJ, Klibanski A. 2009. Bone, fat, and body composition: evolving concepts in the pathogenesis of osteoporosis. *The American Journal of Medicine* 122(5): 409-414.

Rosenthal DI, Mayo-Smith W, Hayes CW, Khurana JS, Biller BM, Neer RM, Klibanski A. 1989. Age and bone mass in premenopausal women. *Journal of Bone and Mineral Research* 4(4): 533-538.

Rosner B, Glynn RJ, Lee M-L T. 2006. The Wilcoxon signed rank test for paired comparisons of clustered data. *Biometrics* 62(1): 185-192.

Ross MH, Pawlina W. 2011. *Histology: a text and atlas: with correlated cell and molecular biology*. Wolters Kluwer/Lippincott Williams & Wilkins Health: Philadelphia.

Rosset EM, Bradshaw AD. 2016. SPARC/osteonectin in mineralized tissue. *Matrix Biology* 52-54(1): 78-87.

Rothschild BM, Panza RK. 2007. Lack of bone stiffness/strength contribution to osteoarthritis-evidence for primary role of cartilage damage. *Rheumatology* 46(2): 246-249.

Rott J, Toepfer ET, Bartosova M, Kolevica A, Heuser A , Rabe M, Behets G, D'Haese PC, Eichwald V, Jugold M, Damgov I, Zarogiannis SG, Shroff R, Eisenhauer A, Schmitt CP. 2022. Nutritional Calcium Supply Dependent Calcium Balance, Bone Calcification and Calcium Isotope Ratios in Rats. *International Journal of Molecular Sciences* 23(14): 7796.

Roux, W. 1885. Beitrage Zur Morphologie Der Funktionnellen Anspassung. *Archive of Journal of Anatomy and Physiology* 9(1): 120-158.

Rubin CT, Lanyon LE. 1984. Regulation of bone formation by applied loads. *The Journal of Bone and Joint Surgery* 66(3): 397-402.

Rubin CT, Turner AS, Müller R, McLeod K, Lin W, Qin YX. 2002. Quantity and Quality of Trabecular Bone in the Femur are Enhanced by a Strongly Anabolic, Noninvasive Mechanical Intervention. *Journal of Bone and Mineral Research* 17(2): 349-357.

Ruff C. 1992. Biomechanical analyses of archaeological human skeletal samples. In: Saunders SR, Kanzenberg M (eds.). *Skeletal biology of past peoples: research methods, second edition,* pp. 183-206. Wiley-Liss: New York.

Ruff CB, Hayes WC. 1983a. Cross-sectional geometry of Pecos Pueblos femora and tibiae - a biomechanical investigation: I. Method and general patterns of variation. *American Journal of Biological Anthropology* 60(3): 359-381.

Ruff CB, Hayes WC. 1983b. Cross-sectional geometry of Pecos Pueblos femora and tibiae - a biomechanical investigation: II. Sex, age, and side differences. *American Journal of Biological Anthropology* 60(3): 383-400.

Ruff CB, Hayes WC. 1988. Sex differences in age-related remodelling of the femur and tibia. *Journal of Orthopaedic Research* 6(6): 886-896.

Ruff CB, Holt B, Trinkaus E. 2006. Who's afraid of the big bad Wolff?: "Wolff's law" and bone functional adaptation. *American Journal of Biological Anthropology* 129(4): 484-498.

Ruffer MA. 1921. *Studies in the Palaeopathology of Egypt*. The University of Chicago Press: Chicago, Illinois.

Ruusuvuori P, Valkonen M, Kartasalo K, Valkonen M, Visakorpi T, Nykter M, Latonen L. 2022. Spatial analysis of histology in 3D: quantification and visualization of organ and tumor level tissue environment. *Heliyon* 8(1): 1e08762.

Rytky SJO, Tiulpin A, Finnilä MAJ, Karhula SS, Sipola A, Kurttila V, Valkealahti M, Lehenkari P, Joukainen A, Kröger H, Korhonen RK, Saarakkala S, Niinimäki J. 2024. Clinical super-resolution computed tomography of bone microstructure: Application in musculoskeletal and dental imaging. *Annals of Biomedical Engineering* 52(5): 1255-1269.

Sacco JE, Tarasuk V. 2009. Health Canada's proposed discretionary fortification policy is misaligned with the nutritional needs of Canadians. *Journal of Nutrition* 139(10): 1980-1986.

Sadeghi N, Oveisi MR, Nahnat B, Hajimahmoodi M, Behzad M, Behfar A, Sadeghi F, Saadatmand S. 2014. The relationship between bone health and plasma zinc, copper, lead and cadmium concentration in osteoporotic women. *Journal of Environmental Health Science and Engineering* 12(1): 125.

Safadi FF, Barbe MF, Abdelmagid SM, Rico MC, Aswad RA, Litvin J, Popoff SN. Bone Structure, Development and Bone Biology. In: Khurana, J. (ed). *Bone Pathology*, pp. 1-50. Humana Press: Philadelphia, USA.

Saito M, Marumo K. 2015. Effects of Collagen Crosslinking on Bone Material Properties in Health and Disease. *Calcified Tissue International* 97(3): 242-261.

Samuel M, Blows J. 2001. The Finds. In: Hicks M, Hicks A (eds.). *St Gregory's Priory, Northgate, Canterbury: Excavations 1988-1991*, pp. 151-186. Canterbury Archaeological Trust: Great Britain.

Sanchez S, Dupret V, Tafforeau P, Trinajstic KM, Roll B, Gouttenoire P-J, Wretman L, Zylberberg L, Peyrin F, Ahlberg PE. 2013. 3D microstructural architecture of muscle attachments in extant and fossil vertebrates revealed by synchrotron microtomography. *PLoS One* 8(2): e56992.

Sanderson JB. 1994. *Biological Microtechnique*. Bios Scientific Publishers: Oxford.

Santos L, Elliott-Sale KJ, Sale C. 2017. Exercise and bone health across the lifespan. *Biogerontology* 18(6): 931-946.

Sarkar M, Bhardwaj R, Madabhavi I, Khatana J. 2015. Osteoporosis in Chronic Obstructive Pulmonary Disease. *Clinical Medicine Insights: Circulatory, Respiratory and Pulmonary Medicine* 9(1): 5-21.

Schaffler MB, Kennedy OD. 2012. Osteocyte signaling in bone. *Current Osteoporosis Research* 10(2): 118-125.

Scheiner S, Pivonka P, Hellmich C. 2016. Poromicromechanics Reveals That Physiological Bone Strains Induce Osteocyte-Stimulating Lacunar Pressure. *Biomechanics and Modelling in Mechanobiology* 15(1): 9-28.

Scherft JP. 1978. The lamina limitans of the organic bone matrix: formation in Vitro. *Journal of Ultrastructure Research* 64(2): 173-181.

Schett G, Rudwaleit M. 2010. Can we stop progression of ankylosing spondylitis? *Best Practice and Research Clinical Rheumatology* 24(3): 363-371.

Scheuer L, Black SM. 2000. *Developmental juvenile osteology*. Academic Press: San Diego, CA.

Schindelin J, Arganda-Carreras I, Frise E, Kaynig V, Longair M, Pietzsch T, Preibisch S, Rueden C, Saalfeld S, Schmid B, Tinevez J-Y, White DJ, Hartenstein V, Eliceiri K, Tomancak P, Cardona A. 2012. Fiji: an open-source platform for biological-image analysis. *Nature Methods* 9(7): 676-682.

Schlecht SH. 2012. Understanding entheses: bridging the gap between clinical and anthropological perspectives. *The Anatomical Record* 295(8): 1239-1251.

Schlecht SH, Pinto DC, Agnew AM, Stout SD. 2012. Brief communication: The effects of disuse on the mechanical properties of bone: What unloading tells us about the adaptive nature of skeletal tissue. *American Journal of Biological Anthropology* 149(4): 599-605.

Schnitzler CM, Mesquita JM. 2013. Cortical porosity in children is determined by age dependent osteonal morphology. *Bone* 55(2): 476-486.

Schotsmans EMJ, Van de Voorde W, Forbes SL. 2020. TSD Estimation in the Advanced Stages of Decomposition. In: Hayman J, Oxenham M (eds.). *Estimation of the Time Since Death: Current Research and Future Trends*, pp. 81-108. Academic Press: London.

Schotsmans EMJ, Stuart B, Stewart TJ, Thomas P, Miszkiewicz JJ. 2024. Unravelling taphono-myths. First large-scale study of histotaphonomic changes and diagenesis in bone from modern surface depositions. *PLoS One* 19(9): e0308440.

Schultz M. 2001. Paleohistopathology of Bone: A new approach to the study of ancient diseases. *American Journal of Biological Anthropology* 116(S33): 106-147.

Seckl JR. 2004. 11beta-hydroxysteroid dehydrogenases: changing glucocorticoid action. *Current Opinion in Pharmacology* 4(6): 597-602.

Sedlin ED. 1964. The ratio of cortical area to total cross-section area in rib diaphyses: A quantitative index of osteoporosis. *Clinical Orthopaedics* 36(1): 161-168.

Seeman E. 2002. Pathogenesis of bone fragility in women and men. *The Lancet* 359(9320): 1841-1850.

Seeman E. 2008. Modelling and Remodelling: The Cellular Machinery Responsible for the Gain and Loss of Bone's Material and Structural Strength. In: Bilezikian JP, Raisz LG, Martin TJ (eds.). *Principles of Bone Biology, 3rd edition,* pp. 3-28. Academic Press: United Kingdom.

Seeman E. 2015. Growth and Age-Related Abnormalities in Cortical Structure and Fracture Risk. *Endocrinology and Metabolism (Seoul)* 30(4): 419-428.

Seeman E, Szmukler GI, Formica C, Tsalamandris C, Mestrovic R. 1992. Osteoporosis in anorexia nervosa: The influence of peak bone density, bone loss, oral contraceptive use, and exercise. *Journal of Bone and Mineral Research* 7(12): 1467-1474.

Seeman E, Hopper JL, Young NR, Formica C, Goss P, Tsalamandris C. 1996. Do genetic factors explain associations between muscle strength, lean mass, and bone density? A twin study. *American Journal of Physiology* 270(2Pt1): E320-E327.

Seeman E, Karlsson MK, Duan Y. 2000. On Exposure to Anorexia Nervosa, the Temporal Variation in Axial and Appendicular Skeletal Development Predisposes to Site-Specific Deficits in Bone Size and Density: A Cross-Sectional Study. *Journal of Bone and Mineral Research* 15(11): 2259-2265.

Segal NA, Li S. 2022. WBCT and its evolving role in OA research and clinical practice. *Osteoarthritis Imaging* 2(3-4): 100083.

Šereikienė I, Jankauskas R. 2002. Late medieval Lithuanian children growth (according to palaeo-osteological material of 14th-17th CC. Alytus burial ground. *Anthropologie* 40(2): 157-163.

Šereikienė I, Jankauskas R. 2004. Lithuanian children's growth in the past: an updated medieval sample. *Papers on Anthropology* 13(1): 226-238.

Serjeantson D, Woolgar CM. 2006. Fish Consumption in Medieval England. In: Woolgar CM, Serjeantson D, Waldron T (eds.). *Food in Medieval England*, pp. 102-130. Oxford University Press: Oxford.

Shapovalov V, Musiienko A. 2021. Senile osteoporosis: Modern view of the problem. *Pain, Joints, Spine* 11(3): 118-125.

Shaw CN, Stock JT. 2009a. Intensity, repetitiveness, and directionality of habitual adolescent mobility patterns influence the tibial diaphysis morphology of athletes. *American Journal of Biological Anthropology* 140(1): 149-159.

Shaw CN, Stock JT. 2009b. Habitual throwing and swimming correspond with upper limb diaphyseal strength and shape in modern human athletes. *American Journal of Biological Anthropology* 140(1): 160-172.

Shean B, Messinger L, Papworth M. 1993. Observations of Differential Decomposition on Sun Exposed v. Shaded Pig Carrion in Coastal Washington State. *Journal of Forensic Sciences* 38(4): 938-949.

Shekaran A, García AJ. 2011. Extracellular matrix-mimetic adhesive biomaterials for bone repair. *Journal of Biomedical Materials Research* 96A(1): 261-272.

Shingleton A. 2010. Allometry: The Study of Biological Scaling. *Nature Education Knowledge* 3(10): 1-7.

Shlisky J, Mandlik R, Askari S, Abrams S, Belizan JM, Bourassa MW, Cormick G, Driller-Colangelo A, Gomes F, Khadilkar A, Owino V, Pettifor JM, Rana ZH, Roth DE, Weaver C. 2022. Calcium deficiency worldwide: prevalence of inadequate intakes and associated health outcomes. *Annals of the New York Academy of Sciences* 1512(1): 10-28.

Shore RM, Chesney RW. 2013a. Rickets: Part I. *Pediatric Radiology* 43(2): 140-151.

Shore RM, Chesney RW. 2013b. Rickets: Part II. *Pediatric Radiology* 43(2): 152-172.

Siminoski K, Lee K-C, Jen H, Warshawski R, Matzinger MA, Shenouda N, Charron M, Coblentz C, Dubois J, Kloiber R, Nadel H, O'Brien K, Reed M, Sparrow K, Webber C, Lentle B, Ward LM; STOPP Consortium. 2012. Anatomical distribution of vertebral fractures: comparison of pediatric and adult spines. *Osteoporosis International* 23(7): 1999-2008.

Singh A, Gill G, Kaur H, Amhmed M, Jakhu H. 2018. Role of osteopontin in bone remodelling and orthodontic tooth movement: a review. *Progress in Orthodontics* 19(1): 18.

Singh IJ, Gunberg DL. 1970. Estimation of Age at Death in Human Males from Quantitative Histology of Bone Fragments. *American Journal of Biological Anthropology* 33(3): 373-381.

Singh IJ, Tonna EA, Gandel CP. 1974. A Comparative Histological Study of Mammalian Bone. *Journal of Morphology* 144(4): 421-437.

Singh V, Dhasmana S, Mohammad S, Singh N. 2010. The odontomes: Report of five cases. *National Journal of Maxillofacial Surgery* 1(2): 157-160.

Sinkhonde D, Rimbarngaye A, Kone B, Cooper Herring T. 2022. Representativity of morphological measurements and 2-d shape descriptors on mineral admixtures. *Results in Engineering* 13(3): 100368.

Skedros JG. 2005. Osteocyte lacuna population densities in sheep, elk and horse calcanei. *Cells Tissues Organs* 181(1): 23-37.

Skedros JG. 2024. Biomechanical Foundations of Histological Analysis in Limb Bones: The Crucial Role of Load-Complexity Categorization and Collagen Fiber Orientation Analysis When Interpreting Bone Adaptation. In: Stout SD, Crowder C (eds.). *Bone Histology: A Biological Anthropological Perspective, 2nd edition*, pp. 150-224. Imprint CRC Press: New York.

Skedros JG, Grunander TR, Hamrick MW. 2005. Spatial Distribution of Osteocyte Lacunae in Equine Radii and Third Metacarpals: Considerations for Cellular Communication, Microdamage Detection and Metabolism. *Cells Tissues Organs* 180(4): 215-236.

Skedros JG, Henrie TR, Doutre MS, Bloebaum RD. 2018. Sealed osteons in animals and humans: low prevalence and lack of relationship with age. *Journal of Anatomy* 232(5): 824-835.

Skedros JG, Hunt KJ, Bloebaum RD. 2004. Relationships of loading history and structural and material characteristics of bone: development of the mule deer calcaneus. *Journal of Morphology* 259(3): 281-307.

Skedros JG, Keenan KE, Cooper DML, Bloebaum RD. 2014. Histocompositional organization and toughening mechanisms in antler. *Journal of Structural Biology* 187(2): 129-148.

Skedros JG, Keenan KE, Williams TJ, Kiser CJ. 2013b. Secondary osteon size and collagen/lamellar organization (“osteon morphotypes”) are not coupled, but potentially adapt independently for local strain mode or magnitude. *Journal of Structural Biology* 181(2): 95-107.

Skedros JG, Kiser CJ, Mendenhall SD. 2011. A weighted osteon morphotype score outperforms regional osteon percent prevalence calculations for interpreting cortical bone adaptation. *American Journal of Biological Anthropology* 144(1): 41-50.

Skedros JG, Knight AN, Clark GC, Crowder CM, Dominguez VM, Qiu S, Mulhern DM, Donahue SW, Busse B, Hulsey BI, Zedda M, Sorenson SM. 2013a. Scaling of Haversian canal surface area to secondary osteon bone volume in ribs and limb bones. *American Journal of Biology Anthropology* 151(2): 230-244.

Skedros JG, Mason MW, Bloebaum RD. 1994. Differences in osteonal micromorphology between tensile and compressive cortices of a bending skeletal system: Indications of potential strain-specific differences in bone microstructure. *The Anatomical Record* 239(4): 405-413.

Skedros JG, Mason MW, Bloebaum RD. 2001. Modelling and remodelling in a developing artiodactyl calcaneus: A model for evaluating Frost's Mechanostat hypothesis and its corollaries. *The Anatomical Record* 263(2): 167-185.

Skedros JG, Mendenhall SD, Kiser CJ, Winet H. 2009. Interpreting cortical bone adaptation and load history by quantifying osteon morphotypes in circularly polarized light images. *Bone* 44(3): 392-403.

Skedros JG, Sorenson SM, Jenson NH. 2007. Are Distributions of Secondary Osteon Variants Useful for Interpreting Load History in Mammalian Bones? *Cells Tissues Organs* 185(4): 285-307.

Skedros JG, Su SC, Bloebaum RD. 1997. Biomechanical implications of mineral content and microstructural variations in cortical bone of horse, elk, and sheep calcanei. *The Anatomical Record* 249(3): 297-316.

Skedros JG, Sybrowsky CL, Parry TR, Bloebaum RD. 2003. Regional differences in cortical bone organization and microdamage prevalence in Rocky Mountain mule deer. *The Anatomical Record* 274(1): 837-850.

Skopyk AD, Forbes SL, LeBlanc HN. 2021. Recognizing the Inherent Variability in Dipteran Colonization and Decomposition Rates of Human Donors in Sydney, Australia. *Journal of Clinical and Health Sciences* 6(1): 102-119.

Šlaus M, Bedić Ž, Strinović D, Petrovečki V. 2013. Forensic Anthropology Population Data: Sex determination by discriminant function analysis of the tibia for contemporary Croats. *Forensic Science International* 226(1-3): 302.e1-302.e4.

Šlaus M, Tomičić Ž. 2005. Discriminant function sexing of fragmentary and complete tibiae from medieval Croatian sites. *Forensic Science International* 147(2-3): 147-152.

Smit TH. 2022. Finite Element Models of Osteocytes and Their Load-Induced Activation. *Current Osteoporosis Reports* 20(1): 127-140.

Smith CF, Munro R, Davies DC, Wilkinson T, Shaw H, Claridge K, Llewellyn S, Mc Ateer P, Ward S, Farsides T. 2022. Understanding beliefs, preferences and actions amongst potential body donors. *Anatomical Sciences Education* 16(2): 224-236.

Smith EP, Boyd J, Frank GR, Takahashi H, Cohen RM, Specker B, Williams TC, Lubahn DB, Korach KS. 1994. Estrogen resistance caused by a mutation in the estrogen-receptor gene in a man. *New England Journal of Medicine* 331(16): 1056-1061.

Smith MR. 2007. Obesity and Sex Steroids during Gonadotropin-Releasing Hormone Agonist Treatment for Prostate Cancer. *Clinical Cancer Research* 13(1): 241-245.

Snoddy AM, Miszkiewicz J, Cooke K, Petchey P, Buckley H. 2022. Bone remodelling changes in an individual with tuberculosis-induced, left-sided remoroacetabular joint destruction, from nineteenth-century Milton, New Zealand. *Bioarchaeology International* 6(3): 161-174.

Sobelman OS, Gibeling JC, Stover SM, Hazelwood SJ, Yeh OC, Shelton DR, Martin RB. 2004. Do microcracks decrease or increase fatigue resistance in cortical bone? *Journal of Biomechanics* 37(9): 1295-1303.

Solomon L. 1968. Osteoporosis and fracture of the femoral neck in the South African Bantu. *Journal of Bone and Joint Surgery* 50(1): 2-13.

Sowers MR, Clark MK, Hollis B, Wallace RB, Jannausch M. 1992. Radial bone mineral density in pre- and perimenopausal women: A prospective study of rates and risk factors for loss. *Journal of Bone and Mineral Research* 7(6): 647-657.

Sözen T, Özışık L, Başaran NÇ. 2017. An overview and management of osteoporosis. *European Journal of Rheumatology* 4(1): 46-56.

Spradley MK. 2016. Metric Methods for the Biological Profile in Forensic Anthropology: Sex, Ancestry, and Stature. *Academic Forensic Pathology* 6(3): 391-399.

Šromová V, Sobola D, Kaspar P. 2023. A Brief Review of Bone Cell Function and Importance. *Cells* 12(21): 2576.

Stein KWH, Werner J. 2013. Preliminary Analysis of Osteocyte Lacunar Density in Long Bones of Tetrapods: All Measures Are Bigger in Sauropod Dinosaurs. *PLoS One* 8(10): e77109.

Stěpán JJ, Tesarová A, Havránek T, Jodl J, Formánková J, Pacovský V. 1985. Age and sex dependency of the biochemical indices of bone remodelling. *International Journal of Clinical Chemistry* 151(3): 273-283.

Stern AR, Nicolella DP. 2013. Measurement and estimation of osteocyte mechanical strain. *Bone* 54(2): 191-195.

Stewart MC, Goliath JR, Stout SD, Hubbe M. 2015. Intraskeletal Variability of Relative Cortical Area in Humans. *The Anatomical Record* 298(9): 1635-1643.

Stewart TJ, Louys J, Miszkiewicz JJ. 2021. Intra-skeletal vascular density in a bipedal hopping macropod with implications for analyses of rib histology. *Anatomical Sciences International* 96(3): 386-399.

Stock JT, Shaw CN. 2007. Which measures of diaphyseal robusticity are robust? A comparison of external methods of quantifying the strength of long bone diaphyses to cross-sectional geometric properties. *American Journal of Biological Anthropology* 134(3): 412-423.

Stockwell R. 1967. The cell density of human articular and costal cartilage. *Journal of Anatomy* 101(4): 753-763.

Stout SD. 1976. *Histomorphometric Analysis of Archaeological Bone*. Doctoral (PhD) dissertation submitted to Washington University, St. Louis, Missouri, USA.

Stout SD, Cole ME, Agnew AM. 2019. “Histomorphology: Deciphering the Metabolic Record.” In: Buikstra JE (ed.). *Ortner’s Identification of Pathological Conditions in Human Skeletal Remains, 3rd edition,* pp. 91-167. Academic Press: San Diego.

Stout SD, Crowder C. 2011. Bone remodelling, histomorphology, and histomorphometry. In: Crowder C, Stout S (eds.). *Bone Histology: An Anthropological Perspective*, *1st edition,* pp. 1-21. CRC Press: Boca Raton.

Stout SD, Dietze WH, Işcan MY, Loth SR. 1994. Estimation of Age at Death Using Cortical Histomorphometry of the Sternal End of the Fourth Rib. *Journal of Forensic Science* 39(3): 778-784.

Stout SD, Lueck R. 1995. Bone remodelling rates and skeletal maturation in three archaeological skeletal populations. *American Journal of Biological Anthropology* 98(2): 161-171.

Stout SD, Paine RR. 1992. Brief Communication: Histological Age Estimation Using Rib and Clavicle. *American Journal of Biological Anthropology* 87(1): 111-115.

Stout SD, Paine RR. 1994. Brief communication: Bone remodelling rates: A test of an algorithm for estimating missing osteons. *American Journal of Biological Anthropology* 93(1): 123-129.

Stout SD, Teitelbaum SL. 1976. Histomorphometric determination of formation rates of archaeological bone. *Calcified Tissue Research* 21(3): 163-169.

Streeter M. 2010. A Four-Stage Method of Age at Death Estimation for Use in the Subadult Rib Cortex. *Journal of Forensic Sciences* 55(4): 1019-1024.

Streeter M. 2011. Histological age-at-death estimation. In: Crowder C, Stout S (eds.). *Bone Histology: An Anthropological Perspective, 1st edition*, pp. 134-152. CRC Press: Boca Raton.

Streicher C, Heyny A, Andrukhova O, Haigl B, Slavic S, Schüler C, Kollmann K, Kantner I, Sexl V, Kleiter M, Hofbauer LC, Kostenuik PJ, Erben RG. 2017. Estrogen Regulates Bone Turnover by Targeting RANKL Expression in Bone Lining Cells. *Scientific Reports* 7(1): 6460.

Stroud G, Kemp RL. 1993. *Cemeteries of the Church and Priory of St Andrew, Fishergate.* York Archaeological Trust 12/2: York.

Sucuoglu H, Ornke NI, Caglar C. 2015. Arthrogryposis Multiplex Congenita: Multiple Congenital Joint Contractures. *Case Reports in Medicine* 2015:379730. PMID: 26604929.

Sugiyama T, Meakin LB, Browne WJ, Galea GL, Price JS, Lanyon LE. 2012. Bones' adaptive response to mechanical loading is essentially linear between the low strains associated with disuse and the high strains associated with the lamellar/woven bone transition. *Journal of Bone and Mineral Research* 27(8): 1784-1793.

Sumpter G. 2008. *Lady Chapels and the Manifestation of Devotion to Our Lady in Medieval England*. Doctoral (PhD) dissertation submitted to the University of Leicester. Available from: <https://www.proquest.com/dissertations-theses/lady-chapels-manifestation-devotion-our-medieval/docview/1461742723/se-2?accountid=8330>.

Suzuki T, Kajita Y, Katsumata S, Matsuzaki H, Suzuki K. 2015. Zinc deficiency increases serum concentration of parathyroid hormone through a decrease in serum calcium and induces bone fragility in rats. *Journal of Nutritional Science and Vitaminology* 61(5): 382-390.

Syddall HE, Evandrou M, Dennison EM, Cooper C, Sayer AA. 2012. Social inequalities in osteoporosis and fracture among community dwelling older men and women: findings from the Hertfordshire Cohort Study. *Archives of Osteoporosis* 7(0): 37-48.

Taichman RS. 2005. Blood and bone: two tissues whose fates are intertwined to create the hematopoietic stem-cell niche. *Blood* 105(7): 2631-2639.

Takebe K, Nakagawa A, Minami H, Kanazawa H, Hirohata K. 1984. Role of the fibula in weight-bearing. *Clinical Orthopaedics and Related Research* 184(1): 289-292.

Tan L, Wang Y, Zhou L, Shi Y, Zhang F, Liu L, Nie S. 2014. Parkinson's Disease and Risk of Fracture: A Meta-Analysis of Prospective Cohort Studies. *PLoS One* 9(4): e94379.

Tang Y, Wu X, Lei W, Pang L, Wan C, Shi Z, Zhao L, Nagy TR, Peng X, Hu J, Feng X, Hul WV, Wan M, Cao X. 2009. TGF-β1–induced migration of bone mesenchymal stem cells couples bone resorption with formation. *Nature Medicine* 15(7): 757-765.

Teitelbaum SL, Ross FP. 2003. Genetic regulation of osteoclast development and function. *Nature Reviews Genetics* 4(8): 638-649.

Tepelenis K, Papathanakos G, Kitsouli A, Troupis T, Barbouti A, Vlachos K, Kanavaros P, Kitsoulis P. 2021. Osteochondromas: An Updated Review of Epidemiology, Pathogenesis, Clinical Presentation, Radiological Features and Treatment Options. *In Vivo* 35(2): 681-691.

Terrovitis J, Zotos P, Kaldara E, Diakos N, Tseliou E, Vakrou S, Kapelios C, Chalazonitis A, Nanas S, Toumanidis S, Kontoyannis D, Karga E, Nanas J. 2012. Bone mass loss in chronic heart failure is associated with secondary hyperparathyroidism and has prognostic significance. *European Journal of Heart Failure* 14(3): 326-332.

Thandrayen K, Norris SA, Pettifor JM. 2009. Fracture rates in urban South African children of different ethnic origins: The Birth to Twenty Cohort. *Osteoporosis International* 20(1): 47-52.

Theilmann JM. 1987. Medieval pilgrims and the origins of tourism. *Journal of Popular Culture* 20(4): 93-102.

Theintz G, Buchs B, Rizzoli R, Slosman D, Clavien H, Sizonenko PC, Bonjour JP. 1992. Longitudinal monitoring of bone mass accumulation in healthy adolescents: Evidence for a marked reduction after 16 years of age at the levels of lumbar spine and femoral neck in female subjects. *The Journal of Clinical Endocrinology and Metabolism* 75(4): 1060-1065.

Thermo Scientific. 2015. *DPX Mounting Media: Instructions for Use*. Available online: <https://assets.thermofisher.com/TFS-Assets/APD/manuals/DPX%20Mounting%20Media%20IFU%20EN.pdf>.

Thomas TA. 2017. Theodor Schwann: A Founding Father of Biology and Medicine. *Current Medical Issues* 15(4): 299-301.

Thompson DD. 1980. Age changes in bone mineralization, cortical thickness, and Haversian canal area. *Calcified Tissue International* 31(1): 5-11.

Thompson DD, Gunness-Hey M. 1981. Bone mineral-osteon analysis of Yupik-Inupiaq skeletons. *American Journal of Biological Anthropology* 55(1): 1-7.

Thompson DD, Salter EM, Laughlin WS. 1981. Bone core analysis of Baffin Island skeletons. *Arctic Anthropology* 18(1): 87-96.

Tommerup LJ, Raab DM, Crenshaw TC, Smith EL. 1993. Does Weight-Bearing Exercise Affect Non-Weight-Bearing Bone? *Journal of Bone and Mineral Research* 8(9): 1053-1058.

Tomsová J, Schierová Z. 2016. Skeletal material from Deir El-Medina in the Egyptological Collection of the Hrdlička Museum of Man in Prague. *Annals of the Náprstek Museum* 37(1): 41-69.

Tremblay MS, Colley RC, Saunders TJ, Healy GN, Owen N. 2010. Physiological and health implications of a sedentary lifestyle. *Applied Physiology, Nutrition, and Metabolism* 35(6): 725-740.

Tresguerres FGF, Torres J, López-Quiles J, Hernández G, Vega JA, Tresguerres IF. 2020. The osteocyte: A multifunctional cell within the bone. *Annals of Anatomy* 227: 151422.

Tsai TL, Pan WH, Chung YT, Wu TN, Tseng YC, Liou SH, Wang SL. 2016. Association between urinary lead and bone health in a general population from Taiwan. *Journal of Exposure Science and Environmental Epidemiology* 26(5): 481-487.

Tu X, Delgado-Calle J, Condon KW, Maycas M, Zhang H, Carlesso N, Taketo MM, Burr DB, Plotkin LI, Bellido T. 2015. Osteocytes mediate the anabolic actions of canonical Wnt/β-catenin signaling in bone. *Proceedings of the National Academy of Sciences* 112(5): E478–E486.

Tuckermann J, Adams RH. 2021. The endothelium–bone axis in development, homeostasis and bone and joint disease. *Nature Reviews Rheumatology* 17(10): 608-620.

Turcotte CM, Rabey KN, Green DJ, McFarlin SC. 2022. Muscle attachment sites and behavioral reconstruction: An experimental test of muscle-bone structural response to habitual activity. *American Journal of Biological Anthropology* 177(1): 63-82.

Turner CH. 1998. Three Rules for Bone Adaptation to Mechanical Stimuli. *Bone* 23(5): 399-407.

Turner CH. 2006. Bone Strength: Current Concepts. *Annals of the New York Academy of Sciences* 1068(1): 429-446.

Ubara Y, Fushimi T, Tagami T, Sawa N, Hoshino J, Yokota M, Katori H, Takemoto F, Hara S. 2003. Histomorphometric features of bone in patients with primary and secondary hypoparathyroidism. *Kidney International* 63(5): 1809-1816.

Ubara Y, Tagami T, Nakanishi S, Sawa N, Hoshino J, Suwabe T, Katori H, Takemoto F, Hara S, Takaichi K. 2005. Significance of minimodelling in dialysis patients with adynamic bone disease. *Kidney International* 68(2): 833-839.

Ubelaker DH, Pap I. 1998. Skeletal evidence for health and disease in the iron age of northeastern Hungary. *International Journal of Osteoarchaeology* 8(4): 231-251.

Uda Y, Azab E, Sun N, Shi C, Pajevic PD. 2017. Osteocyte Mechanobiology. *Current Osteoporosis Reports* 15(4): 318-325.

Udagawa N, Koide M, Nakamura M, Nakamichi Y, Yamashita T, Uehara S, Kobayashi Y, Furuya Y, Yasuda H, Fukuda C, Tsuda E. 2021. Osteoclast differentiation by RANKL and OPG signaling pathways. *Journal of Bone and Mineral Metabolism* 39(1): 19-26.

Ueland M, Collins S, Maestrini L, Forbes SL, Luong S. 2021b. Fresh vs. frozen human decomposition – A preliminary investigation of lipid degradation products as biomarkers of post-mortem interval. *Forensic Chemistry* 24(1): 100335.

Ueland M, Forbes SL, Stuart BH. 2018. Seasonal variation of fatty acid profiles from textiles associated with decomposing pig remains in a temperate Australian environment. *Forensic Chemistry* 11(1): 120-127.

Ueland M, Forbes SL, Stuart BH. 2019. Understanding clothed buried remains: the analysis of decomposition fluids and their influence on clothing in model burial environments. *Forensic Science, Medicine and Pathology* 15(1): 3-12.

Ueland M, Harris S, Forbes SL. 2021a. Detecting volatile organic compounds to locate human remains in a simulated collapsed building. *Forensic Science International* 323(1): 110781.

Uitterlinden AG, Burger H, Huang Q, Yue F, McGuigan FEA, Grant SFA, Hofman A, van Leeuwen JPTM, Pols HAP, Ralston SH. 1998. Relation of alleles of the collagen type Iα1 gene to bone density and the risk of osteoporotic fractures in postmenopausal women. *New England Journal of Medicine* 338(15): 1016-1021.

University of Technology Sydney. 2017. *The Australian Facility for Taphonomic Experimental Research (AFTER)*. University of Technology Sydney Website, Australian University, last accessed 29 March 2024. Available from: <https://www.uts.edu.au/about/faculty-science/after-facility/our-facility>.

Unsworth A, Dowson D, Wright V. 1975. Some new evidence on human joint lubrication. *Annals of the Rheumatic Diseases* 34(4): 277-285.

Vajda EG, Kneissel M, Muggenburg B, Miller SC. 1999. Increased intracortical bone remodelling during lactation in beagle dogs. *Biology of Reproduction* 61(6): 1439-1444.

van der Veen M. 2003. When is food a luxury? *World Archaeology* 34(3): 405-427.

van Gerven DP, Sheridan SG, Adams WY. 1995. The health and nutrition of a medieval nubian population: the impact of political and economic change. *American Anthropology* 97(3): 468-480.

van Gulick L, Saby C, Morjani H, Beljebbar A. 2019. Age-related changes in molecular organization of type I collagen in tendon as probed by polarized SHG and Raman microspectroscopy. *Scientific Reports* 9(1): 7280.

van Hove RP, Nolte PA, Vatsa A, Semeins CM, Salmon PL, Smit TH, Klein-Nulend J. 2009. Osteocyte morphology in human tibiae of different bone pathologies with different bone mineral density--is there a role for mechanosensing? *Bone* 45(2): 321-329.

van Oers RFM, Ruimerman R, van Rietbergen B, Hilbers PA, Huiskes R. 2008a. Relating osteon diameter to strain. *Bone* 43(3): 476-482.

van Oers RFM, Ruimerman R, Tanck E, Hilbers PAJ, Huiskes R. 2008b. A unified theory for osteonal and hemi-osteonal remodelling. *Bone* 42(2): 250-259.

Varlet V, Joye C, Forbes SL, Grabherr S. 2020. Revolution in death sciences: body farms and taphonomics blooming. A review investigating the advantages, ethical and legal aspects in a Swiss context. *International Journal of Legal Medicine* 134(5): 1875-1895.

Varma S, Orgel JPRO, Schieber JD. 2016. Nanomechanics of Type I Collagen. *Biophysical Journal* 111(1): 50-56.

Vass AA. 2011. The elusive universal post-mortem interval formula. *Forensic Science International* 204(1-3): 34-40.

Verborgt O, Gibson GJ, Schaffler MB. 2000. Loss of osteocyte integrity in association with microdamage and bone remodelling after fatigue in vivo. *Journal of Bone and Mineral Research* 15(1): 60-67.

Verhaar HJ, Damen CA, Duursma SA, Scheven BA. 1994. A comparison of the action of progestins and estrogen on the growth and differentiation of normal adult human osteoblast-like cells in vitro. *Bone* 15(3): 307-311.

Vidoli GM, Beasley MM, Meadows Jantz L, Bennett Devlin J, Wolfe Steadman D. 2017. The Future of Taphonomic Research. In: Hayman J, Oxenham M (eds.). *Estimation of the Time Since Death: Current Research and Future Trends*, pp. 251-262. Academic Press: London.

Villa C, Lynnerup N. 2010. Technical Note: A Stereological Analysis of the Cross-Sectional Variability of the Femoral Osteon Population. *American Journal of Biological Anthropology* 142(3): 491-496.

Villanueva AR. 1988. A new Goldner's one-step trichrome stain for identification of osteoid seams, bone and cells in undecalcified, plastic embedded sections of bone. *Journal of Histotechnology* 11(4): 249-251.

Vlashi R, Zhang X, Wu M, Chen G. 2023. Wnt signaling: Essential roles in osteoblast differentiation, bone metabolism and therapeutic implications for bone and skeletal disorders. *Genes and Diseases* 10(4): 1291-1317.

Von Hagens G. 1979. Impregnation of soft biological specimens with thermosetting resins and elastomers. *The Anatomical Record* 194(2): 247-255.

Voss SC, Forbes SL, Dadour IR. 2020. The Soil Environment and Forensic Entomology. In: Byrd JH, Tomberlin JK (eds.). *Forensic Entomology: The Utility of Arthropods in Legal Investigations 3rd edition*, pp. 269-286. CRC Press: Boca Raton.

Voss SC, Spafford H, Dadour IR. 2009. Annual and seasonal patterns of insect succession on decomposing remains at two locations in Western Australia. *Forensic Science International* 193(1-3): 26-36.

Wachsmuth L, Söder S, Fan Z, Finger F, Aigner T. 2006. Immunolocalization of matrix proteins in different human cartilage subtypes. *Histology and Histopathology* 21(5): 477-485.

Wagner DO, Aspenberg P. 2011. Where did bone come from? An overview of its evolution. *Acta Orthopaedica* 82(4): 393-398.

Wakely J, Anderson T, Carter A. 1995. A Multidisciplinarian Case Study of Prostatic(?) Carcinoma from Mediaeval Canterbury. *Journal of Archaeological Science* 22(4): 469-477.

Waldron T. 2008. *Palaeopathology*. Cambridge University Press: Cambridge.

Waldron T. 2019. Joint Disease. In: Buikstra JE (ed.). *Ortner's Identification of Pathological Conditions in Human Skeletal Remains 3rd edition*, pp. 719-748. Elsevier Academic Press: Arizona.

Walker MM, Oxenham MF, Vlok M, Matsumura H, Thi Mai Huong N, Hiep Trinh H, Minh TT, Miszkiewicz JJ. 2023a. Human femur morphology and histology variation with ancestry and behaviour in an ancient sample from Vietnam. *Annals of Anatomy* 247(1): 152054.

Walker MM, Oxenham MF, Vlok M, Matsumura H, Thi Mai Huong N, Hiep Trinh H, Minh TT, Miszkiewicz JJ. 2023b. Primary bone retention in a young adult male with limb disuse: a bioarchaeological case study. *Historical Biology: An International Journal of Paleobiology* 35(2): 235-241.

Walker PL, Bathurst RR, Richman R, Gjerdrum T, Andrushko VA. 2009. The causes of porotic hyperostosis and cribra orbitalia: a reappraisal of the iron-deficiency-anemia hypothesis. *American Journal of Biological Anthropology* 139(2): 109-125.

Wallace JM. 2019. Skeletal Hard Tissue Biomechanics. In: Burr DB, Allen MR (eds.). *Basic and Applied Bone Biology, 2nd edition,* pp. 125-140. Elsevier Academic Press: London.

Wang H, Leng Y, Gong Y. 2018. Bone Marrow Fat and Hematopoiesis. *Frontiers in Endocrinology* 28(9): 694.

Wang Q, Alén M, Nicholson P, Lyytikäinen A, Suuriniemi M, Helkala E, Suominen H, Cheng S. 2005. Growth Patterns at Distal Radius and Tibial Shaft in Pubertal Girls: A 2-Year Longitudinal Study. *Journal of Bone and Mineral Research* 20(6): 954-961.

Wang Q, Cheng S, Alén M, Seeman E. 2009. Bone's Structural Diversity in Adult Females Is Established before Puberty. *The Journal of Clinical Endocrinology and Metabolism* 94(5): 1555-1561.

Ward J. 2006. *Women in England in the Middle Ages*. Bloomsbury Academic: London.

Ward SW (ed.). 1990. *Excavations at Chester. The lesser medieval religious houses sites investigated 1964-83, Grosvenor Museum Archaeological Excavation and Survey Reports, No. 6.* Chester Archaeological Society: Chester, UK.

Warden SJ, Edwards WB, Willy RW. 2021. Preventing bone stress injuries in runners with optimal workload. *Current Osteoporosis Reports* 19(3): 298-307.

Warming L, Hassager C, Christiansen C. 2002. Changes in Bone Mineral Density with Age in Men and Women: A Longitudinal Study. *Osteoporosis International* 13(2): 105-112.

Watanabe Y, Konishi M, Shimada M, Ohara H, Iwamoto S. 1998. Estimation of Age from the Femur of Japanese Cadavers. *Forensic Science International* 98(1-2): 55-65.

Watson CJ, Ueland M, Schotsmans EMJ, Sterenberg J, Forbes SL, Blau S. 2020. Detecting grave sites from surface anomalies: A longitudinal study in an Australian woodland. *Journal of Forensic Sciences* 66(2): 479-490.

Weaver CM, McCabe LD, McCabe GP, Braun M, Martin BR, Dimeglio LA, Peacock M. 2008. Vitamin D status and calcium metabolism in adolescent black and white girls on a range of controlled calcium intakes. *Journal of Clinical Endocrinology and Metabolism* 93(10): 3907-3914.

Webster SSJ. 2005. The past, present, and future of bone morphometry: its contribution to an improved understanding of bone biology. *Journal of Bone and Mineral Metabolism* 23(Suppl): 1-10.

Wein MN. 2017. Bone Lining Cells: Normal Physiology and Role in Response to Anabolic Osteoporosis Treatments. *Current Molecular Biology Reports* 3(3): 79-84.

Weiner S, Wagner HD. 1998. The material bone: Structure-mechanical function relations. *Annual Review of Materials Science* 28(1): 271-298.

Weinmann CR, Sicher H. 1947. *Bone and bones: Fundamentals of bone biology*. Henry Kimpton: London.

Weisleitner K, Wöss C, Kampik L, Wolfgang Huck C, Arora R, Brunner A, Zelger B, Schirmer M, Pallua JD. 2026. Rapid forensic differentiation of human and animal bones using handheld near-infrared spectroscopy and deep learning. *Spectrochimica Acta Part A: Molecular and Biomolecular Spectroscopy* 344(1): 126657.

Weiss EP. 2005. Humeral cross-sectional morphology from 18th century Quebec prisoners of war: limits to activity reconstruction. *American Journal of Biological Anthropology* 126(3): 311-317.

Weiss EP, Jordan RC, Frese EM, Albert SG, Villareal DT. 2017. Effects of weight loss on lean mass, strength, bone, and aerobic capacity. *Medicine and Science in Sports and Exercise* 49(1): 206-217.

Wen LP, Chen JP, Duan LL, Li SZ. 2018. Vitamin K-dependent proteins involved in bone and cardiovascular health. *Molecular Medicine Reports* 18(1): 3-15.

Wescott DJ. 2015. Sexual Dimorphism in Auricular Surface Projection and Postauricular Sulcus Morphology. *Journal of Forensic Sciences* 60(3): 679-685.

White SD, Mahoney P, Deter C. 2022. Socioeconomic status and survival in medieval Canterbury. *Journal of Archaeological Science: Reports* 46(1): 103686.

White TD, Folkens PA. 2005. *The Human Bone Manual*. Elsevier Academic Press: Burlington, MA.

Whittle J, Hailwood M. 2020. The gender division of labour in early modern England. *The Economic History Review* 73(1): 3-32.

Williams A, Cassella JP, Pringle JK. 2020. The Ethical Considerations for Creating a Human Taphonomy Facility in the United Kingdom. In: Squires K, Errickson D, Márquez-Grant N (eds.). *Ethical Approaches to Human Remains*, pp. 367-384. Springer Link: Switzerland.

Williams D. 1994. *Guide to Cleaner Technologies: Cleaning and Degreasing Process Changes*. DIANE Publishing: Washington.

Williams FMK, Manek NJ, Sambrook PN, Spector TD, Macgregor AJ. 2007. Schmorl's Nodes: Common, Highly Heritable, and Related to Lumbar Disc Disease. *Arthritis Care and Research* 57(5): 855-860.

Wilsman NJ, Farnum CE, Leiferman EM, Fry M, Barreto C. 1996. Differential growth by growth plates as a function of multiple parameters of chondrocytic kinetics. *Journal of Orthopaedic Research* 14(6): 927-936.

Wilson A, Neilsen P, Berry R, Seckiner D, Mallett X. 2020. Quantifying human post-mortem movement resultant from decomposition processes. *Forensic Science International: Synergy* 2(1): 248-261.

Wilson AK, Bhattacharyya MH, Miller S, Mani A, Sacco-Gibson N. 1998. Ovariectomy-induced changes in aged beagles: histomorphometry of rib cortical bone. *Calcified Tissue International* 62(3): 237-243.

Wilson DM, Hurst JG. 1959. Medieval Britain in 1958. *Medieval Archaeology* 3(1): 295-326.

Wolff J. 1986. *The Law of Bone Remodelling*. Springer: Berlin, Heidelberg.

Wong AK, Beattie KA, Bhargava A, Cheung M, Webber CE, Chettle DR, Papaioannou A, Adachi JD, Canadian Multicentre Osteoporosis Study (CaMOS) Research Group. 2015. Bone lead (Pb) content at the tibia is associated with thinner distal tibia cortices and lower volumetric bone density in postmenopausal women. *Bone* 79(1): 58-64.

Wood JW, Milner GR, Harpending HC, Weiss KM, Cohen MN, Eisenberg LE, Hutchinson DL, Jankauskas R, Cesnys G, Česnys G, Katzenberg MA, Lukacs JR, McGrath JW, Abella Roth E, Ubelaker DH, Wilkinson RG. 1992. The Osteological Paradox: Problems of Inferring Prehistoric Health from Skeletal Samples. *Current Anthropology* 33(4): 343-370.

Wortsman J, Matsuoka LY, Chen TC, Lu Z, Holick MF. 2000. Decreased bioavailability of vitamin D in obesity. *The American Journal of Clinical Nutrition* 72(3): 690-693.

Xu X, Su J, Zhu R, Li K, Zhao X, Fan J, Mao F. 2025. From morphology to single-cell molecules: High-resolution 3D histology in biomedicine. *Molecular Cancer* 24(1): 63.

Yadav RN, Uniyal P, Sihota P, Kumar S, Dhiman V, Goni VG, Sahni D, Bhadada SK, Kumar N. 2021. Effect of ageing on microstructure and fracture behavior of cortical bone as determined by experiment and Extended Finite Element Method (XFEM). *Medical Engineering and Physics* 93(1): 100-112.

Yao W, Jee WSS, Zhou H, Lu J, Cui L, Setterberg R, Liang T, Ma YF. 1999. Anabolic effect of prostaglandin E2 on cortical bone of aged male rats comes mainly from modelling dependent bone gain. *Bone* 25(6): 697-702.

Yerlikaya FH, Onmaz DE. 2022. Inflammation and Bone Turnover Markers in Adult Obesity. *Journal of Clinical Densitometry* 25(4): 470-474.

Yin R, Lord EL, Cohen JR, Buser Z, Lao L, Zhong G, Wang JC. 2015. Distribution of Schmorl nodes in the lumbar spine and their relationship with lumbar disk degeneration and range of motion. *Spine* 40(1): E49-E53.

Yoshizawa S, Brown A, Brchowsky A, Sfeir C. 2014. Magnesium ion stimulation of bone marrow stromal cells enhances osteogenic activity, stimulating the effect of magnesium alloy degradation. *Acta Biomaterialia* 10(6): 2834-2342.

Young DR, Niklowitz WJ, Brown RJ, Jee WSS. 1986. Immobilization-associated osteoporosis in primates. *Bone* 7(2): 109-117.

Youngs SM, Clark J. 1981. Medieval Britain in 1980. *Medieval Archaeology* 25(1): 166-228.

Zdilla MJ, Hatfield SA, McLean KA, Cyrus LM, Laslo JM, Lambert HW. 2016. Circularity, solidity, axes of a best fit ellipse, aspect ratio, and roundness of the foramen ovale: a morphometric analysis with neurosurgical considerations. *Journal of Craniofacial Surgery* 27(1): 222-228.

Zebaze RMD, Ghasem-Zadeh A, Bohte A, Iuliano-Burns S, Mirams M, Price RI, Mackie EJ, Seeman E. 2010. Intracortical remodelling and porosity in the distal radius and post-mortem femurs of women: a cross-sectional study. *The Lancet* 375(9727): 1729-1736.

Zebaze RMD, Jones A, Knackstedt M, Maalouf G, Seeman E. 2007. Construction of the Femoral Neck During Growth Determines Its Strength in Old Age. *Journal of Bone and Mineral Research* 22(7): 1055-1061.

Zedda M, Babosova R. 2021. Does the osteon morphology depend on the body mass? A scaling study on macroscopic and histomorphometric differences between cow (Bos taurus) and sheep (Ovis aries). *Zoomorphology* 140(1): 169-181.

Zedda M, Lepore G, Biggio GP, Gadau GP, Mura S, Farina V. 2016. Morphology, morphometry and spatial distribution of secondary osteons in equine femur. *Anatomia, Histologia, Embryologia* 44(5): 328-332.

Zehra U, Flower L, Robson-Brown K, Adams MA, Dolan P. 2017. Defects of the vertebral end plate: implications for disc degeneration depend on size. *Spine* 17(5): 727-737.

Zelenchuk LV, Hedge AM, Rowe PS. 2015. Age dependent regulation of bone-mass and renal function by the MEPE ASARM-motif. *Bone* 79(1): 131-142.

Zengin A, Pye SR, Cook MJ, Adams JE, Rawer R, Wu FCW, O'Neill TW, Ward KA. 2017. Associations of muscle force, power, cross-sectional muscle area and bone geometry in older UK men. *Journal of Cachexia, Sarcopenia and Muscle* 8(4): 598-606.

Zhumkhawala A-A, Gleason JM, Cheetham TC, Niu F, Loo RK, Dell RM, Jacobsen SJ, Chien GW. 2013. Osteoporosis management program decreases incidence of hip fracture in patients with prostate cancer receiving androgen deprivation therapy. *Urology* 81(5): 1010-1015.

Zijlstra WP, Bulstra SK, Van Raay JJ, Van Leeuven BM, Kuijer R. 2012. Cobalt and chromium ions reduce human oseoblast-like cell activity in vitro, reduce the OPG to RANKL ratio, and induce oxidative stress. *Journal of Orthopaedic Research* 30(5): 740-747.

Zofková I, Davis M, Blahos J. 2017. Trace elements have beneficial, as well as detrimental effects on bone homeostasis. *Physiological Research* 66(3): 391-402.

Zofková I, Nemcikova P, Matucha P. 2013. Trace elements and bone health. *Clinical Chemistry and Laboratory Medicine* 51(8): 1555-1561.

Zvi R. 1981. Family, land and the village community in later Medieval England. Past and Present 93(1): 3-36.

Zylberberg L. 2004. New data on bone matrix and its proteins. *Comptes Rendus Palevol* 3(6-7): 591-604.